AD-A071 337 TEXAS UNIV AT AUSTIN DEPT OF MECHANICAL ENGINEERING F/G 16/2
SUPERSONIC FLOW MEASUREMENTS IN THE BODY VORTEX WAKE OF AN OGIV--ETC(U)
NOV 78 W L OBERKAMPF, T J BARTEL F08635-77-C-0049

UNCLASSIFIED AFATL-TR-78-127 NL

1 OF 4
AD A071337



LEVEL II

AFATL-TR-78-127

Supersonic Flow Measurements in the Body Vortex Wake of an Ogive Nose Cylinder

UNIVERSITY OF TEXAS AT AUSTIN
DEPARTMENT OF MECHANICAL ENGINEERING
AUSTIN, TEXAS 78712

AD A071337

NOVEMBER 1978

DDC
RECEIVED
JUL 18 1979
A

FINAL REPORT FOR PERIOD JANUARY 1977-SEPTEMBER 1978

DDC FILE COPY

Approved for public release; distribution unlimited

Air Force Armament Laboratory
AIR FORCE SYSTEMS COMMAND ★ UNITED STATES AIR FORCE ★ EGLIN AIR FORCE BASE, FLORIDA

79 07 17 058

1. REPORT NUMBER AFATL-TR-78-127	2. GOVT ACCESSION NO.
4. TITLE (and Subtitle) SUPERSONIC FLOW MEASUREMENTS IN THE BODY VORTEX WAKE OF AN OGIVE NOSE CYLINDER,	5. TYPE OF REPORT & PERIOD COVERED Final Report, January 1977-September 1978 6. PERFORMING ORG. REPORT NUMBER
7. AUTHOR(s) W. L. Oberkampf T. J. Bartel	8. CONTRACT OR GRANT NUMBER(s) F08635-77-C-0049
9. PERFORMING ORGANIZATION NAME AND ADDRESS University of Texas at Austin Department of Mechanical Engineering Austin, Texas 78712	10. PROGRAM ELEMENT, PROJECT, TASK AREA & WORK UNIT NUMBERS Program Element 61102F ~~JON~~ 2307E103
11. CONTROLLING OFFICE NAME AND ADDRESS Air Force Armament Laboratory Armament Development and Test Center Eglin Air Force Base, Florida 32542	12. REPORT DATE November 1978 13. NUMBER OF PAGES 301
14. MONITORING AGENCY NAME & ADDRESS (if different from Controlling Office) 302 p.	15. SECURITY CLASS. (of this report) Unclassified 15a. DECLASSIFICATION/DOWNGRADING SCHEDULE

16. DISTRIBUTION STATEMENT (of this Report)

Approved for public release; distribution unlimited

17. DISTRIBUTION STATEMENT (of the abstract entered in Block 20, if different from Report)

18. SUPPLEMENTARY NOTES

Available in DDC

19. KEY WORDS (Continue on reverse side if necessary and identify by block number)

Missile Aerodynamics
Guided Missiles
Aerodynamic Characteristics of Missiles
Aerodynamic Vortex Measurements
Body Vortex Wake of Missiles
Wind Tunnel Experiment
Supersonic Missiles
Aerodynamic Interference on Missiles

20. ABSTRACT (Continue on reverse side if necessary and identify by block number)

This report covers an experimental investigation of the symmetric body vortex wake of a circular cylinder in supersonic flow. Flow field measurements were made in the cross-flow plane at various axial body stations for angles of attack from 10 to 25 degrees. Data were obtained for two Reynolds numbers at a freestream Mach number of 2 and for one Reynolds number at a freestream Mach number of 3. A conical pressure probe was used to measure total pressure, Mach number, and three orthogonal velocity components at a large number of grid points in each of the survey planes. The pitch and yaw

DD FORM 1 JAN 73 1473 EDITION OF 1 NOV 65 IS OBSOLETE

UNCLASSIFIED
SECURITY CLASSIFICATION OF THIS PAGE (When Data Entered)

403 806

LB

angles of the probe were manipulated in the wind tunnel in order to minimize any probe interference effects on the body vortex. A new experimental technique was used which involved the interaction of a theoretical predictive technique, a computer driven probe, and real time data quality optimization. Results are presented for the distribution of total pressure, Mach number, cross-flow velocity field, and axial velocity component in the cross-flow plane. These quantities are further processed to infer the position of the primary body vortex in the cross-flow plane, local circulation distribution in the cross-flow plane, vortex core size, wake height, and total circulation in the cross-flow plane.

PREFACE

This work was conducted by the University of Texas at Austin, Austin, Texas, and was sponsored by the Air Force Armament Laboratory (AFATL/DLDL) under Air Force Contract No. F08635-77-C-0049. The contract monitor for AFATL was Dr. Donald C. Daniel (DLDL). The experiment was conducted at the Arnold Engineering Development Center (AEDC), Arnold Air Force Station, Tennessee. The experimental results were obtained by ARO, Inc. (a subsidiary of Sverdrup & Parcel and Associates, Inc.), contract operator of AEDC. The experiment was conducted in the von Kármán Gas Dynamics Facility of AEDC from 23 June 1977 to 8 July 1977, under Project No. V41A-R7A. The manuscript was submitted for publication on 17 November 1978.

The authors would like to thank Dr. Donald C. Daniel, Aerodynamics Research Manager, of the Air Force Armament Laboratory for his comments and suggestions during the investigation. We also thank the Project Engineers for our experiment, Mr. Bill Martindale and Mr. Terry Penny, ARO, Inc., AEDC, for their efforts.

This report has been reviewed by the Information Office (OI) and is releasable to the National Technical Information Service (NTIS). At NTIS, it will be available to the general public, including foreign nations.

This technical report has been reviewed and is approved for publication.

FOR THE COMMANDER

Gerald P. D'Arcy, Colonel, USAF
Chief, Guns, Rockets, and Explosives Division

Accession For
NTIS GRA&I
DDC TAB
Unannounced
Justification
By
Distribution/
Availability Codes
Dist. | Avail and/or special
A

(The reverse of this page is blank)

TABLE OF CONTENTS

Section	Title	Page
I	INTRODUCTION	1
II	DESCRIPTION OF EXPERIMENT	3
	II-1 Equipment	3
	II-2 Calibration of Probe	7
	II-3 Flow Field Surveys	8
III	DATA PROCESSING	13
	III-1 Data Reduction	13
	III-2 Final Data Set	19
	III-3 Uncertainty Analysis	22
	III-4 Calculated Flow Quantities	26
IV	RESULTS AND DISCUSSION	33
	IV-1 Results for $M_\infty = 1.95$, $R_d = .48 \times 10^6$	33
	IV-2 Results for $M_\infty = 2.$ and $R_d = 1.75 \times 10^6$	43
	IV-3 Results for $M_\infty = 3.01$ and $R_d = 1.70 \times 10^6$	52
V	CONCLUSIONS AND RECOMMENDATIONS	62
REFERENCES		65
APPENDICES		
A	Two-Dimensional Surface Construction Software	203
B	Final Data Set	205
C	P_o and U_c Contour Plots	260

LIST OF FIGURES

Figure	Title	Page
1	VKF Tunnel A (from Reference 22)	76
2	Schematic of Model and Sting	77
3	Cross-Section of the Probe	78
4	Photograph of Probe Tip	79
5	Schematic of Probe and Strut Assembly	80
6	Wind Tunnel Installation	81
7	Body Coordinate System	82
8	Typical Survey Grid and Subgrids	83
9	Data Acquisition Process Diagram	84
10	Pressure Tap and Flow Angle Definitions	85
11	Data Reduction Flow Chart	86
12	Frequency Distribution of α_{vt} for Final Data	87
13	Frequency Distribution of Change in Local Mach Number for Repeat Data	88
14	Truncated Frequency Distribution of Change in Local Mach Number	89
15	Sample Contours of Total Pressure and Magnitude of Cross-Flow Velocity	90
16	U_c/U_∞ in Vortex Coordinate System	91
17	Local Circulation in Vortex Coordinate System	91
18	Typical Variation of w/U_∞ Along Angle of Attack Plane	92
19	Comparison of Integration Sweep Pattern on Streamlines ($M_\infty = 2.00$, $R_d = 1.75 \times 10^6$, $\alpha_b = 15°$, $x/d = 10.$)	93
20	Streamlines for $M_\infty = 2.00$, $R_d = 1.75 \times 10^6$, $\alpha_b = 20°$ and $x/d = 6$	94
21	Cross-Flow Plane Vector Plot for $M_\infty = 1.95$, $R_d = .48 \times 10^6$ and $\alpha_b = 10°$	95

LIST OF FIGURES (CONTINUED)

Figure	Title	Page
22	Cross-Flow Plane Vector Plot for $M_\infty = 1.95$, $R_d = .48 \times 10^6$ and $\alpha_b = 15°$	96
23	Cross-Flow Plane Vector Plot for $M_\infty = 1.95$, $R_d = .48 \times 10^6$ and $\alpha_b = 20°$	97
24	Cross-Flow Plane Vector Plot for $M_\infty = 1.95$, $R_d = .48 \times 10^6$ and $\alpha_b = 25°$	98
25	Total Pressure in Cross-Flow Plane for $M_\infty = 1.95$, $R_d = .48 \times 10^6$ and $\alpha_b = 10°$	99
26	Total Pressure in Cross-Flow Plane for $M_\infty = 1.95$, $R_d = .48 \times 10^6$ and $\alpha_b = 15°$	100
27	Total Pressure in Cross-Flow Plane for $M_\infty = 1.95$, $R_d = .48 \times 10^6$ and $\alpha_b = 20°$	101
28	Total Pressure in Cross-Flow Plane for $M_\infty = 1.95$, $R_d = .48 \times 10^6$ and $\alpha_b = 25°$	102
29	Mach Number in Cross-Flow Plane for $M_\infty = 1.95$, $R_d = .48 \times 10^6$ and $\alpha_b = 10°$	103
30	Mach Number in Cross-Flow Plane for $M_\infty = 1.95$, $R_d = .48 \times 10^6$ and $\alpha_b = 15°$	104
31	Mach Number in Cross-Flow Plane for $M_\infty = 1.95$, $R_d = .48 \times 10^6$ and $\alpha_b = 20°$	105
32	Mach Number in Cross-Flow Plane for $M_\infty = 1.95$, $R_d = .48 \times 10^6$ and $\alpha_b = 25°$	106
33	Magnitude of Cross-Flow Velocity for $M_\infty = 1.95$, $R_d = .48 \times 10^6$ and $\alpha_b = 10°$	107
34	Magnitude of Cross-Flow Velocity for $M_\infty = 1.95$, $R_d = .48 \times 10^6$ and $\alpha_b = 15°$	108
35	Magnitude of Cross-Flow Velocity for $M_\infty = 1.95$, $R_d = .48 \times 10^6$ and $\alpha_b = 20°$	109
36	Magnitude of Cross-Flow Velocity for $M_\infty = 1.95$, $R_d = .48 \times 10^6$ and $\alpha_b = 25°$	110

LIST OF FIGURES (CONTINUED)

Figure	Title	Page
37	Axial Velocity in Cross-Flow Plane for $M_\infty = 1.95$, $R_d = .48 \times 10^6$ and $\alpha_b = 10°$	111
38	Axial Velocity in Cross-Flow Plane for $M_\infty = 1.95$, $R_d = .48 \times 10^6$ and $\alpha_b = 15°$	112
39	Axial Velocity in Cross-Flow Plane for $M_\infty = 1.95$, $R_d = .48 \times 10^6$ and $\alpha_b = 20°$	113
40	Axial Velocity in Cross-Flow Plane for $M_\infty = 1.95$, $R_d = .48 \times 10^6$ and $\alpha_b = 25°$	114
41	Local Circulation in Cross-Flow Plane for $M_\infty = 1.95$, $R_d = .48 \times 10^6$ and $\alpha_b = 10°$	115
42	Local Circulation in Cross-Flow Plane for $M_\infty = 1.95$, $R_d = .48 \times 10^6$ and $\alpha_b = 15°$	116
43	Local Circulation in Cross-Flow Plane for $M_\infty = 1.95$, $R_d = .48 \times 10^6$ and $\alpha_b = 20°$	117
44	Local Circulation in Cross-Flow Plane for $M_\infty = 1.95$, $R_d = .48 \times 10^6$ and $\alpha_b = 25°$	118
45	Vortex Center Location in the Cross-Flow Plane for $M_\infty = 1.95$ and $R_d = .48 \times 10^6$	119
46	Schlieren Photograph for $M_\infty = 1.95$, $R_d = .48 \times 10^6$ and $\alpha_b = 10°$	121
47	Schlieren Photograph for $M_\infty = 1.95$, $R_d = .48 \times 10^6$ and $\alpha_b = 15°$	122
48	Schlieren Photograph for $M_\infty = 1.95$, $R_d = .48 \times 10^6$ and $\alpha_b = 20°$	123
49	Schlieren Photograph for $M_\infty = 1.95$, $R_d = .48 \times 10^6$ and $\alpha_b = 25°$	124
50	Vortex Core Radii for $M_\infty = 1.95$ and $R_d = .48 \times 10^6$	125
51	Angular Orientation of Vortex Core for $M_\infty = 1.95$ and $R_d = .48 \times 10^6$	126

LIST OF FIGURES (CONTINUED)

Figure	Title	Page
52	Total Circulation in the Survey Grids for $M_\infty = 1.95$ and $R_d = .48 \times 10^6$	127
53	Streamlines in the Cross-Flow Plane for $M_\infty = 1.95$, $R_d = .48 \times 10^6$ and $\alpha_b = 15°$	128
54	Cross-Flow Plane Vector Plot for $M_\infty = 2.$, $R_d = 1.75 \times 10^6$ and $\alpha_b = 10°$	129
55	Cross-Flow Plane Vector Plot for $M_\infty = 2.$, $R_d = 1.75 \times 10^6$ and $\alpha_b = 15°$	130
56	Cross-Flow Plane Vector Plot for $M_\infty = 2.$, $R_d = 1.75 \times 10^6$ and $\alpha_b = 20°$	131
57	Cross-Flow Plane Vector Plot for $M_\infty = 2.$, $R_d = 1.75 \times 10^6$ and $\alpha_b = 25°$	132
58	Total Pressure in Cross-Flow Plane for $M_\infty = 2.$, $R_d = 1.75 \times 10^6$ and $\alpha_b = 10°$	133
59	Total Pressure in Cross-Flow Plane for $M_\infty = 2.$, $R_d = 1.75 \times 10^6$ and $\alpha_b = 15°$	134
60	Total Pressure in Cross-Flow Plane for $M_\infty = 2.$, $R_d = 1.75 \times 10^6$ and $\alpha_b = 20°$	135
61	Total Pressure in Cross-Flow Plane for $M_\infty = 2.$, $R_d = 1.75 \times 10^6$ and $\alpha_b = 25°$	136
62	Mach Number in Cross-Flow Plane for $M_\infty = 2.$, $R_d = 1.75 \times 10^6$ and $\alpha_b = 10°$	137
63	Mach Number in Cross-Flow Plane for $M_\infty = 2.$, $R_d = 1.75 \times 10^6$ and $\alpha_b = 15°$	138
64	Mach Number in Cross-Flow Plane for $M_\infty = 2.$, $R_d = 1.75 \times 10^6$ and $\alpha_b = 20°$	139
65	Mach Number in Cross-Flow Plane for $M_\infty = 2.$, $R_d = 1.75 \times 10^6$ and $\alpha_b = 25°$	140
66	Magnitude of Cross-Flow Velocity for $M_\infty = 2.$, $R_d = 1.75 \times 10^6$ and $\alpha_b = 10°$	141

LIST OF FIGURES (CONTINUED)

Figure	Title	Page
67	Magnitude of Cross-Flow Velocity for M_∞ = 2., $R_d = 1.75 \times 10^6$ and α_b = 15°	142
68	Magnitude of Cross-Flow Velocity for M_∞ = 2., $R_d = 1.75 \times 10^6$ and α_b = 20°	143
69	Magnitude of Cross-Flow Velocity for M_∞ = 2., $R_d = 1.75 \times 10^6$ and α_b = 25°	144
70	Axial Velocity in Cross-Flow Plane for M_∞ = 2., $R_d = 1.75 \times 10^6$ and α_b = 10°	145
71	Axial Velocity in Cross-Flow Plane for M_∞ = 2., $R_d = 1.75 \times 10^6$ and α_b = 15°	146
72	Axial Velocity in Cross-Flow Plane for M_∞ = 2., $R_d = 1.75 \times 10^6$ and α_b = 20°	147
73	Axial Velocity in Cross-Flow Plane for M_∞ = 2., $R_d = 1.75 \times 10^6$ and α_b = 25°	148
74	Local Circulation in Cross-Flow Plane for M_∞ = 2., $R_d = 1.75 \times 10^6$ and α_b = 10°	149
75	Local Circulation in Cross-Flow Plane for M_∞ = 2., $R_d = 1.75 \times 10^6$ and α_b = 15°	150
76	Local Circulation in Cross-Flow Plane for M_∞ = 2., $R_d = 1.75 \times 10^6$ and α_b = 20°	151
77	Local Circulation in Cross-Flow Plane for M_∞ = 2., $R_d = 1.75 \times 10^6$ and α_b = 25°	152
78	Vapor Screen Photograph for M_∞ = 2.0, $R_d = 1.58 \times 10^6$, α_b = 25°, and x/d = 6	153
79	Vapor Screen Photograph for M_∞ = 2.0, $R_d = 1.58 \times 10^6$, α_b = 25°, and x/d = 9	154
80	Vortex Center Location in the Cross-Flow Plane for M_∞ = 2. and $R_d = 1.75 \times 10^6$	155
81	Schlieren Photograph for M_∞ = 2., $R_d = 1.75 \times 10^6$ and α_b = 10°	157

LIST OF FIGURES (CONTINUED)

Figure	Title	Page
82	Schlieren Photograph for $M_\infty = 2.$, $R_d = 1.75 \times 10^6$ and $\alpha_b = 15°$	158
83	Schlieren Photograph for $M_\infty = 2.$, $R_d = 1.75 \times 10^6$ and $\alpha_b = 20°$	159
84	Schlieren Photograph for $M_\infty = 2.$, $R_d = 1.75 \times 10^6$ and $\alpha_b = 25°$	160
85	Vortex Core Radii for $M_\infty = 2.$ and $R_d = 1.75 \times 10^6$	161
86	Angular Orientation of Vortex Core for $M_\infty = 2.$, and $R_d = 1.75 \times 10^6$	162
87	Total Circulation in the Survey Grids for $M_\infty = 2.$ and $R_d = 1.75 \times 10^6$	163
88	Streamlines in the Cross-Flow Plane for $M_\infty = 2.$, $R_d = 1.75 \times 10^6$ and $\alpha_b = 15°$	164
89	z-Coordinate of Secondary Nose Vortex for $M_\infty = 2.$ and $R_d = 1.75 \times 10^6$	165
90	Cross-Flow Plane Vector Plot for $M_\infty = 3.01$, $R_d = 1.70 \times 10^6$ and $\alpha_b = 10°$	166
91	Cross-Flow Plane Vector Plot for $M_\infty = 3.01$, $R_d = 1.70 \times 10^6$ and $\alpha_b = 15°$	167
92	Cross-Flow Plane Vector Plot for $M_\infty = 3.01$, $R_d = 1.70 \times 10^6$ and $\alpha_b = 20°$	168
93	Cross-Flow Plane Vector Plot for $M_\infty = 3.01$, $R_d = 1.70 \times 10^6$ and $\alpha_b = 25°$	169
94	Total Pressure in Cross-Flow Plane for $M_\infty = 3.01$, $R_d = 1.70 \times 10^6$ and $\alpha_b = 10°$	170
95	Total Pressure in Cross-Flow Plane for $M_\infty = 3.01$, $R_d = 1.70 \times 10^6$ and $\alpha_b = 15°$	171
96	Total Pressure in Cross-Flow Plane for $M_\infty = 3.01$, $R_d = 1.70 \times 10^6$ and $\alpha_b = 20°$	172
97	Total Pressure in Cross-Flow Plane for $M_\infty = 3.01$, $R_d = 1.70 \times 10^6$ and $\alpha_b = 25°$	173

LIST OF FIGURES (CONTINUED)

Figure	Title	Page
98	Mach Number in Cross-Flow Plane for M_∞ = 3.01, $R_d = 1.70 \times 10^6$ and α_b = 10°	174
99	Mach Number in Cross-Flow Plane for M_∞ = 3.01, $R_d = 1.70 \times 10^6$ and α_b = 15°	175
100	Mach Number in Cross-Flow Plane for M_∞ = 3.01, $R_d = 1.70 \times 10^6$ and α_b = 20°	176
101	Mach Number in Cross-Flow Plane for M_∞ = 3.01, $R_d = 1.70 \times 10^6$ and α_b = 25°	177
102	Magnitude of Cross-Flow Velocity for M_∞ = 3.01, $R_d = 1.70 \times 10^6$ and α_b = 10°	178
103	Magnitude of Cross-Flow Velocity for M_∞ = 3.01, $R_d = 1.70 \times 10^6$ and α_b = 15°	179
104	Magnitude of Cross-Flow Velocity for M_∞ = 3.01, $R_d = 1.70 \times 10^6$ and α_b = 20°	180
105	Magnitude of Cross-Flow Velocity for M_∞ = 3.01, $R_d = 1.70 \times 10^6$ and α_b = 25°	181
106	Axial Velocity in Cross-Flow Plane for M_∞ = 3.01, $R_d = 1.70 \times 10^6$ and α_b = 10°	182
107	Axial Velocity in Cross-Flow Plane for M_∞ = 3.01, $R_d = 1.70 \times 10^6$ and α_b = 15°	183
108	Axial Velocity in Cross-Flow Plane for M_∞ = 3.01, $R_d = 1.70 \times 10^6$ and α_b = 20°	184
109	Axial Velocity in Cross-Flow Plane for M_∞ = 3.01, $R_d = 1.70 \times 10^6$ and α_b = 25°	185
110	Local Circulation in Cross-Flow Plane for M_∞ = 3.01, $R_d = 1.70 \times 10^6$ and α_b = 10°	186
111	Local Circulation in Cross-Flow Plane for M_∞ = 3.01, $R_d = 1.70 \times 10^6$ and α_b = 15°	187
112	Local Circulation in Cross-Flow Plane for M_∞ = 3.01, $R_d = 1.70 \times 10^6$ and α_b = 20°	188

LIST OF FIGURES (CONCLUDED)

Figure	Title	Page
113	Local Circulation in Cross-Flow Plane for M_∞ = 3.01, R_d = 1.70 x 10^6 and α_b = 25°	189
114	Vortex Center Location in the Cross-Flow Plane for M_∞ = 3.01 and R_d = 1.7 x 10^6	190
115	Schlieren Photograph for M_∞ = 3.01, R_d = 1.7 x 10^6 and α_b = 10°	192
116	Schlieren Photograph for M_∞ = 3.01, R_d = 1.7 x 10^6 and α_b = 15°	193
117	Schlieren Photograph for M_∞ = 3.01, R_d = 1.7 x 10^6 and α_b = 20°	194
118	Schlieren Photograph for M_∞ = 3.01, R_d = 1.7 x 10^6 and α_b = 25°	195
119	Vortex Core Radii for M_∞ = 3.01 and R_d = 1.7 x 10^6	196
120	Angular Orientation of Vortex Core for M_∞ = 3.01 and R_d = 1.7 x 10^6	197
121	Total Circulation in the Survey Grids for M_∞ = 3.01 and R_d = 1.7 x 10^6	198
122	Ratio of Body Vortex Circulation to Total Circulation	199
123	Streamlines in the Cross-Flow Plane for M_∞ = 3.01, R_d = 1.7 x 10^6 and α_b = 15°	200
124	Wake Height in the Cross-Flow Plane for x/d = 10	201
125	z-Coordinate of Secondary Nose Vortex for M_∞ = 3.01 and R_d = 1.7 x 10^6	202

LIST OF TABLES

Table	Title	Page
1	CTS ATTITUDE AND POSITION UNCERTAINTIES	67
2	PROBE CALIBRATION FREESTREAM CONDITIONS	67
3	SURVEY FREESTREAM CONDITIONS	68
4	FLOW FIELD SURVEY CONDITIONS	68
5	QUANTITY OF SURVEY DATA	69
6	NUMBER OF GRID POINTS IN FINAL DATA SET	70
7	PERCENT FREESTREAM UNCERTAINTIES	71
8	REPEATABILITY STATISTICS FOR FLOW FIELD DATA	72
9	COMBINED REPEATABILITY STATISTICS FOR THE EXPERIMENT	74
10	RATIO OF PRIMARY VORTEX CIRCULATION TO VORTEX CORE CIRCULATION	75
B-1	FINAL DATA SET FOR $M_\infty = 1.95$, $R_d = .48 \times 10^6$, $\alpha_b = 10°$, $x/d = 8$	206
B-2	FINAL DATA SET FOR $M_\infty = 1.95$, $R_d = .48 \times 10^6$, $\alpha_b = 10°$, $x/d = 11$	207
B-3	FINAL DATA SET FOR $M_\infty = 1.95$, $R_d = .48 \times 10^6$, $\alpha_b = 10°$, $x/d = 14$	208
B-4	FINAL DATA SET FOR $M_\infty = 1.95$, $R_d = .48 \times 10^6$, $\alpha_b = 15°$, $x/d = 7$	210
B-5	FINAL DATA SET FOR $M_\infty = 1.95$, $R_d = .48 \times 10^6$, $\alpha_b = 15°$, $x/d = 10$	211
B-6	FINAL DATA SET FOR $M_\infty = 1.95$, $R_d = .48 \times 10^6$, $\alpha_b = 15°$, $x/d = 13$	213
B-7	FINAL DATA SET FOR $M_\infty = 1.95$, $R_d = .48 \times 10^6$ $\alpha_b = 20°$, $x/d = 6$	215
B-8	FINAL DATA SET FOR $M_\infty = 1.95$, $R_d = .48 \times 10^6$ $\alpha_b = 20°$, $x/d = 8.5$	216
B-9	FINAL DATA SET FOR $M_\infty = 1.95$, $R_d = .48 \times 10^6$ $\alpha_b = 20°$, $x/d = 11$	218

LIST OF TABLES (CONTINUED)

Table	Title	Page
B-10	FINAL DATA SET FOR M_∞ = 1.95, R_d = .48 x 10^6, α_b = 25°, x/d = 6	220
B-11	FINAL DATA SET FOR M_∞ = 1.95, R_d = .48 x 10^6, α_b = 25°, x/d = 9	222
B-12	FINAL DATA SET FOR M_∞ = 2., R_d = 1.75 x 10^6, α_b = 10°, x/d = 8	224
B-13	FINAL DATA SET FOR M_∞ = 2., R_d = 1.75 x 10^6, α_b = 10°, x/d = 11	225
B-14	FINAL DATA SET FOR M_∞ = 2., R_d = 1.75 x 10^6, α_b = 10°, x/d = 14	226
B-15	FINAL DATA SET FOR M_∞ = 2., R_d = 1.75 x 10^6, α_b = 15°, x/d = 7	228
B-16	FINAL DATA SET FOR M_∞ = 2., R_d = 1.75 x 10^6, α_b = 15°, x/d = 10	229
B-17	FINAL DATA SET FOR M_∞ = 2., R_d = 1.75 x 10^6, α_b = 15°, x/d = 13	231
B-18	FINAL DATA SET FOR M_∞ = 2., R_d = 1.75 x 10^6, α_b = 20°, x/d = 6	233
B-19	FINAL DATA SET FOR M_∞ = 2., R_d = 1.75 x 10^6, α_b = 20°, x/d = 8.5	234
B-20	FINAL DATA SET FOR M_∞ = 2., R_d = 1.75 x 10^6, α_b = 20°, x/d = 11	236
B-21	FINAL DATA SET FOR M_∞ = 2., R_d = 1.75 x 10^6, α_b = 25°, x/d = 6	238
B-22	FINAL DATA SET FOR M_∞ = 2., R_d = 1.75 x 10^6, α_b = 25°, x/d = 9	240
B-23	FINAL DATA SET FOR M_∞ = 3.01, R_d = 1.70 x 10^6, α_b = 10°, x/d = 8	242
B-24	FINAL DATA SET FOR M_∞ = 3.01, R_d = 1.70 x 10^6, α_b = 10°, x/d = 11	243
B-25	FINAL DATA SET FOR M_∞ = 3.01, R_d = 1.70 x 10^6, α_b = 10°, x/d = 14	244
B-26	FINAL DATA SET FOR M_∞ = 3.01, R_d = 1.70 x 10^6, α_b = 15°, x/d = 7	246

LIST OF TABLES (CONCLUDED)

Table	Title	Page
B-26	FINAL DATA SET FOR M_∞ = 3.01, R_d = 1.70 x 10^6, α_b = 15°, x/d = 7	246
B-27	FINAL DATA SET FOR M_∞ = 3.01, R_d = 1.70 x 10^6, α_b = 15°, x/d = 10	247
B-28	FINAL DATA SET FOR M_∞ = 3.01, R_d = 1.70 x 10^6, α_b = 15°, x/d = 13	249
B-29	FINAL DATA SET FOR M_∞ = 3.01, R_d = 1.70 x 10^6, α_b = 20°, x/d = 6	251
B-30	FINAL DATA SET FOR M_∞ = 3.01, R_d = 1.70 x 10^6, α_b = 20°, x/d = 8.5	252
B-31	FINAL DATA SET FOR M_∞ = 3.01, R_d = 1.70 x 10^6, α_b = 20°, x/d = 11	254
B-32	FINAL DATA SET FOR M_∞ = 3.01, R_d = 1.70 x 10^6, α_b = 25°, x/d = 6	256
B-33	FINAL DATA SET FOR M_∞ = 3.01, R_d = 1.70 x 10^6, α_b = 25°, x/d = 9	258

LIST OF SYMBOLS

d	Model base diameter
h	Circulation contour size (square h x h, h = .0375d)
M, M_L	Local Mach number
P_{avg}	$(P_2 + P_3 + P_4 + P_5)/4$
P_1	Probe total pressure (pitot pressure)
P_{1c}	Probe total pressure corrected for angle of attack
P_2, P_3, P_4, P_5	Probe surface pressures (see Figure 3-1)
P_o	Local total pressure (upstream of probe normal shock)
P'_o	Total pressure downstream of a normal shock occurring in the freestream
P	Static pressure
q_∞	Dynamic pressure $(1/2\rho_\infty U_\infty^2)$
R_d	Reynolds number based on model diameter $(\rho_\infty U_\infty d/\mu)$
T_o	Total temperature
u,v,w	Velocity components in body axis system (see Figure 2-7)
U_c	Magnitude of cross-flow velocity $(\sqrt{v^2 + w^2}$
U_p, V_p, W_p	Velocity components in probe axis system (see Figure 3-1)
U_T, V_T, W_T	Velocity components in wind tunnel axis system
U_∞, U_i	Freestream speed
V_{TL}	Magnitude of local total velocity (see Figure 3-1)
x,y,z	Body coordinate system (see Figure 2-7)
$\bar{x}$	Statistical mean of population $(\Sigma\, x_i/n)$
X_p, Y_p, Z_p	Probe coordinate system (see Figure 3-1)
y_v, z_v	Coordinates of the primary vortex center
z_s	Coordinate of the secondary nose vortex
z_w	Coordinate of the free stagnation point

α_b	Angle of attack of the body
α_{CTS}, β_{CTS}	Pitch and yaw angles of the CTS in wind tunnel axis system
α_v, β_v	Pitch and yaw angles of local flow in the probe axis system (see Figure 3-1)
α_{vT}	Total angle of attack of local flow in the probe axis system (see Figure 3-1)
β	Ratio of primary vortex circulation to vortex core circulation
Γ	Local circulation in the cross-flow plane (using contour h x h)
Γ_p	Primary vortex circulation
Γ_t	Total circulation in the survey grid
σ	Standard deviation of population ($\sqrt{\Sigma x_i^2/(n-1)}$
ψ	Stream function in the cross-flow plane

Subscript

∞	Freestream condition

SECTION I

INTRODUCTION

During the last several years there has been renewed interest in aerodynamics of missiles at high angle of attack. This interest has been brought about by atmospheric flight requirements such as high maneuverability and high launch angle of attack. Nonlinear forces and moments which come into existence at high incidence angles have caused a number of flight stability and controllability problems on both missiles and aircraft. Many of the nonlinear forces and moments produced by a body or attached lifting surfaces are caused by the existence of the vortex wake on the leeside of the body. At angles of attack above about 10 degrees symmetric vortices form on the leeside of the body and grow in strength along the body. If the angle of attack or body length is increased, the symmetric wake develops along the body into an asymmetric multiple vortex wake. The present investigation is concerned with the symmetric body vortex wake in supersonic flow.

The pioneering work in body vortex flow measurements was conducted by Jorgensen and Perkins (Reference 1) in 1955. They conducted pitot pressure surveys and a limited number of downwash velocity measurements using a pitot-survey rake and two-hole conical pressure probe in supersonic flow. The model used by Jorgensen and Perkins was a circular cylinder body 7.3 calibers long with a three caliber tangent ogive nose. Mello (Reference 2) conducted a more complete investigation at Mach No. 2 using a cone cylinder body. Total pressure surveys and cross-flow velocity measurements were made using a four-hole conical probe. Although his was the more extensive study of the symmetric vortex wake in supersonic flow, very little information was given concerning experimental procedure, data reduction procedure, or data accuracy. Beyond

these early investigations there have been no detailed measurements of the supersonic body vortex wake. In subsonic flow, body vortex wake surveys have been conducted by Tinling and Allen (Reference 3), Fiechter (Reference 4), and Grosche (Reference 5) using conical probes. Limited wake surveys using a laser anemometer in subsonic flow have been conducted recently by Fidler, Nielsen, and Schwind (Reference 6), Yanta and Wardlaw (Reference 7), and Owen (Reference 8).

The present paper describes an extensive experimental investigation of the symmetric body vortex wake of a circular cylinder body in supersonic flow. Total pressure, Mach number, and three dimensional velocity component measurements were made at various survey planes on the leeside of the body. Measurements were made at a nominal Mach number of 2 for two Reynolds numbers and at Mach number 3 for one Reynolds number. The high Reynolds number condition ($R_d = 1.75 \times 10^6$) represented a factor of four increase over previously published data for supersonic flow. Flow field surveys were made at three positions along the body for angles of attack of 10, 15, and 20 degrees and two body positions for an angle of attack of 25 degrees for each freestream condition. The measurements were made using a five-hole conical pressure probe which could be manipulated by computer in angular orientation and position in the wind tunnel. This was done in order to reduce the angle of attack of the probe with respect to local flow and thereby reduce probe interference on the wake. A new experimental technique was used which involved the interaction of the theoretical model of the measured flow, the computer driven probe, and real time data quality optimization. This experiment is the most comprehensive investigation of the symmetric body vortex wake to date.

SECTION II

DESCRIPTION OF EXPERIMENT

The experiment was conducted in Supersonic Tunnel A of the von Kármán Gas Dynamics Facility (VKF) of the Arnold Engineering Development Center (AEDC), Arnold Air Force Station, Tennessee. Wake flow measurements on a two caliber tangent ogive nose model were made with a pressure probe. Measurements were made for two Reynolds numbers at Mach 2 and one Reynolds number at Mach 3. Portions of Section II of this report are taken from a brief description of the experiment given in Reference 9.

1. Equipment

a. Wind Tunnel

Tunnel A is a continuous flow, closed-circuit, variable density wind tunnel with an automatically driven flexible-plate nozzle and a 1.02 m by 1.02 m (40 in. by 40 in.) test section. The tunnel can be operated at Mach numbers from 1.5 to 6 at maximum stagnation pressures from 200 to 1380 kPA (29 to 200 psia), respectively, and stagnation temperatures up to 416°K (750°R) for $M_\infty = 6$. The tunnel is equipped with a model injection system which allows removal of the model from the test section while the tunnel remains in operation. A cross-section view of the tunnel and model injection system is illustrated in Figure 1.

A Schlieren flow visualization apparatus was available at the wind tunnel. A large number of Schlieren photographs were taken during the experiment.

b. Model and Sting

The model was a circular cylinder with a 2 caliber long tangent ogive nose and a 13 caliber long body. The diameter was 76.2 mm (3 in.) and the total length was 1143 mm (45 in.). Figure 2 gives important dimensions of

the body and sting. The model was designed at The University of Texas at Austin and was fabricated at Eglin AFB. The model was composed of three parts: a nose machined from a solid piece of type 303 stainless steel and two body pieces fabricated from thick-walled tube type 321 stainless steel. The nose was machined on a numerical controlled lathe with one ten thousandths of an inch increment and examined on an optical comparator. Extreme care was taken during all handling stages to prevent any damage to the nose tip. Although the model had two body pieces to change the fineness ratio of the model, during the present experiment this option was not exercised.

The sting was fabricated from PH 13-8 Mo stainless steel and heat treated to condition H 1000. The model was attached to the sting with a tapered joint in body #1. This resulted in a rigid support system. A small hole was center drilled through the entire length of the sting to allow for onboard instrumentation.

c. Probe

Wake flow measurments were made with a biconic shaped pressure probe with a diameter of 3.17 mm (0.125 in.) at the union of the two cones and a 20-degree semi-apex angle of the tip cone. The probe was fabricated with four static pressure orifices on the cone surface (equally spaced 90 degrees apart) and a total pressure orifice at the apex of the cone. A cross-section view of the probe is shown in Figure 3. The tip cone expanded to match a 5-degree semi-apex angle conical frustum. A highly magnified view of the tip cone is shown in Figure 4.

The probe was supported by a double offset wedge-shaped support strut. The strut was fabricated from type 304 SS and attached to the probe with solder. The double offset arrangement was required to meet the angular and translational requirements of the test. A drawing of the probe and strut

assembly is shown in Figure 5. The probe and strut assembly were designed and fabricated at AEDC-VKF.

d. Model and Probe Support Systems

The model was supported by an offset sting and strut assembly attached to the main model support system. The model was manually set at the nominal angle of attack while it was external to the tunnel flow; i.e., retracted by the model injection system. Then the model was injected into the tunnel flow field and the angle of attack adjusted via an electrical motor drive.

The flow-field probe strut was supported by the Captive Trajectory System (CTS) which consists of a model support with computer controlled electro-mechanical drive systems for six degrees of freedom. A photograph of the model and probe installation is shown in Figure 6. The axial and vertical motions (x' and z') are obtained using linear drive units while lateral motion (y') is achieved by rotating the roll-pitch-yaw support arm about the vertical support axis and compensating for the resulting yaw (η') with the forward yaw mechanism. The yaw (ψ') and pitch (α') motion are obtained through two knuckle joints with axes 90 degrees to each other (the pitch axis is upstream of the yaw axis). The most upstream motion of the system is the roll mechanism, which was not used during this test.

e. Instrumentation

Tunnel A stilling chamber pressure was measured with a 103, 414, 1030, or a 3070 kPa (15, 60, 150, or a 300 psi) differential transucer referenced to a near vacuum. Based on periodic comparisons with secondary standards, the uncertainty ($\pm$ 2 σ deviation) of these transucers was estimated to be within $\pm$ 0.2 percent of reading or $\pm$ 0.10 kPa (0.015 psi), whichever is greater. Stilling chamber temperature was measured with a copper-constantan thermocouple with an uncertainty of $\pm$ 1.7°K ($\pm$ 3°F) based on repeat calibration.

The six degrees of freedom motions of the CTS were sensed by potentiometers and recorded by a multiplex analog-to-digital converter. The uncertainty in each movement and the model attitude and postion are given in Table 1. The uncertainties in model postion is the root-mean-square (RMS) value of the combined uncertainties in the motions required to obtain the position.

Deflection of the support strut by pressure loading was analyzed by finite element numerical techniques. The deflections in the x' and z' directions were found to be negligible; however, under typical loading conditions, the deflection of the strut in the y' direction was estimated to be $\pm$ 0.01 mm (0.04 in.). Combining the loading deflection with the position uncertainty in Table 1 yields a RMS uncertainty of $\pm$ 0.02 mm (0.09 in.). Angular deflections will be discussed in Section III-3.

The probe surface pressures were measured with 103 kPa (15 psi) transducers referenced to a near vacuum. The probe total pressure was measured with a similar 172 kPA (25 psi) transducer. These transducers were calibrated before each tunnel entry over a range of 0 to 103 kPa (0 to 15 psi). A linear least squares curve fit was then used to determine a single scale factor for each transducer. The precision of these measurements was $\pm$ 0.08 kPa (0.012 psi) for the 103 kPa (15 psi) transducer and $\pm$ 0.14 kPa (0.020 psi) for the 172 kPa (25 psi) transducer. The pressure transducers were located inside the CTS strut assembly in order to minimize the length of tubing to the probe; i.e., minimize pressure lag.

The model angle of attack was measured with an onboard Schaevitz gravity sensing transducer. The model angle was adjusted while at the freestream conditions until it was within $\pm$ 0.05 degree of the required angle.

2. Calibration of Probe

a. Freestream and Angular Conditions

The various freestream conditions at which probe calibration data were acquired are tabulated in Table 2. Although the flow field was to be measured at nominal freestream Mach numbers of 2 and 3, the probe was also calibrated at Mach numbers of 1.5 and 4 because these extremes in local Mach number were expected in the flow field data. The freestream Reynold number was chosen to be a nominal average of the test Reynolds numbers. Prior to the present probe calibration, data were taken in a range of Reynolds and Mach numbers with an identical probe. It was concluded that the calibration data was not a function of Reynolds number in the test range.

Data were taken for α_v and β_v ranging from - 20 to + 20 degrees at each freestream condition. The specific angles of α_v and β_v used in the calibration were all combinations of 0, $\pm$ 1, $\pm$ 2, $\pm$ 4, $\pm$ 6, $\pm$ 8, $\pm$ 10, $\pm$ 12.5, $\pm$ 15, $\pm$ 20 degrees.

b. Procedure

At each freestream condition the CTS was used to position the probe through a series of pitch and sideslip angles. Normally, this was accomplished at a single location in the tunnel. This reduced any uncertainty due to tunnel flow angularity in the calibration tables. Thus, the calibration data contained only instrumentation uncertainties. However, at some extreme combinations of α_v and β_v, the probe had to be positioned away from this location to preclude any part of the CTS penetrating the safety "envelope" in the tunnel. This safety feature was designed such that if any part of the CTS went through an imaginary boundary, indicating that it was very close to the tunnel wall, the CTS would automatically cease operation. The calibration data were used to construct the calibration tables discussed in Section III-1-a.

Pressure lag due to the length of tubing connecting the probe and pressure transducer was checked during the probe calibration and flow field surveys. A time delay was set between the instant the probe attained the required spacial and angular location and that instant at which the pressure measurement was recorded. The registered time delay depended on freestream Reynolds number and Mach number and was predicted by a previously developed analytical technique. These predictions were verified several times during the experiment in order to be certain no error was introduced due to incomplete pressure stabilization.

3. Flow Field Surveys

The general strategy for surveying the flow field was to use the manipulating probe in such a way that interference of the probe on the body vortex wake was minimized. Minimizing interference was effected by minimizing the angle of attack of the probe with respect to the local flow it was sensing. One approach which was considered was to electrically feed-back the probe surface pressure differences and null the local angle of attack of the probe at each survey point. This approach was rejected because of the excessive wind tunnel time required. The approach taken was to use theoretically predicted values of local velocity in the wake and program the CTS computer to align the probe using these predicted values.

a. Freestream Conditions and Survey Locations

A summary of wind tunnel freestream conditions is presented in Table 3. Table 4 shows the model angles of attack and axial grid locations where data were taken at each freestream condition.

The cone probe was positioned by the CTS during the flow field probing phase at a series of grid points in the model cross-flow plane; i.e., the y-z plane shown in Figure 7. Data were taken in the right-half cross-flow

plane as the axial body stations were chosen such that the vortex wake would be symmetric at the survey locations. Two or three axially located grids were surveyed, depending on the angle of attack. The nominal grid point spacing was 5.71 mm (0.225 in.). The size of each grid in the y and z directions depended on axial location, model angle of attack, and freestream condition.

b. Procedure

The flow field survey procedure consisted of three phases: pre-test, primary survey, and secondary survey. The pre-test phase provided an initial estimate of the flow field so that the CTS could be positioned. The theoretically predicted probe angles were obtained utilizing the flow field model discussed in References 10 and 11. These computations were performed on a CDC 6600 at The University of Texas at Austin. Each survey grid was then divided into subgrids where constant probe orientation angles were specified. A sample survey grid indicating the subgrids is shown in Figure 8. Each subgrid, indicated as a dashed rectangle in the figure, contained from 1 to 42 grid points depending on the local gradient of the cross-flow velocity in the survey plane. The probe angles and size of the subgrids were chosen so that the local probe angle of attack was minimized over the entire subgrid. This was done because as the angle of attack of the probe increases, the accuracy of the data decreases for the following three reasons. First, the pitot pressure begins to deviate significantly from the total pressure behind the shock wave of the cone probe. Second, the average value of the surface pressures from the cone begins to approach the pitot pressure making calculation of Mach number inaccurate. Third, the probability of probe interference on the vortex flow greatly increases. Thus, the objective in design of the subgrids was to keep the probe angle of attack less than 10 degrees.

The primary survey phase consisted of using the theoretical probe angles to position the CTS so that flow field data could be acquired. Positioning of the probe through the subgrids was controlled by the VKF CDC-1604B computer which automatically recorded all the data input at each grid point.

Before the data acquisition could be initiated, several CTS reference points had to be established. At freestream conditions the model was injected and its angle of attack adjusted to $\pm$ 0.05 degree of the nominal value. Deflections of one to two degrees were noted as the model entered the tunnel. A reference location, necessary at each tunnel entry so that the computer could orient the CTS movement relative to the model, was then established. Known locations were scribed on the model and the probe tip was manually positioned using a high resolution scope. This established an axial-vertical reference point. A lateral point was obtained with a light sensing phototransceiver. A reflected signal from the probe tip was used to locate the model centerline.

After these initializations were made, the flow-field acquisition began. The axial location sequence used was to go from the most aft body station to the most forward station. A Schlieren photograph was taken at each group, where a group is defined as a column of points in the z-direction within a subgrid. Several times during the experiment, the probe was run through a series of pitch and sideslip angles in the tunnel freestream to verify the probe calibration.

The third phase of the flow field survey consisted of a new type of computer-wind tunnel interaction, employed to allow real-time analysis of the data. Immediately after a subgrid was surveyed the probe pressure data were transmitted to the AEDC IBM 370/165 computer where it was processed. Local

flow properties, angle of attack of the probe, and local flow circulation were calculated and then transmitted back to the wind tunnel area (see Section III-1 for data reduction procedure). These data were scanned for two characteristics. First, if the angle of attack of the probe at any grid point was larger than 20 degrees (the probe half-angle), then the grid point was repeated. The CTS computer was immediately reprogrammed using the pitch and yaw angles of the first data which would set the probe at near zero angle of attack for that grid point. As it was easier to repeat an entire group instead of a single point, a significant number of additional grid points were repeated. Second, local flow circulation data were scanned to ensure that the survey grids were of optimum size and shape. For example, on certain survey planes the circulation data showed that significant circulation passed through the top of the grids. The CTS computer was then immediately reprogrammed so as to add rows of data points to the top of the existing grids. This strategy is surprisingly similar to adjustment of boundary conditions in computational fluid dynamics.

In the event that the flow field measurements had differed greatly from the predicted values of the theoretical model (References 10 and 11), another type of computer-wind tunnel interaction would have been activated. Utilizing the flow measurements, the flow model would have been modified via a teletype linkup with the CDC 6400/6600 computer system at The University of Texas at Austin. The flow model was programmed and stored on disk so that it could be modified by the time sharing mode of the system. The CTS computer would have been reprogrammed using the revised flow angles from the theory. This contingency procedure was not used because experimental flow field measurements were generally near the predicted values and only a small percent of survey points were repeated because of large angle of attack of the probe. Shown

in Figure 9 is a schematic of the interplay between the flow field measurements and the various computer systems.

A summary of the quantity of the data is presented in Table 5. The number of repeat points for each grid is also given. The number of repeat points per grid generally increased as the angle of attack of the body increased and for the high Reynolds number Mach 2 and Mach 3 conditions. This was due to reduced accuracy of the theoretical flow model for these conditions.

SECTION III

DATA PROCESSING

This section will discuss the techniques used to process the probe pressure data. These include determining local flow parameters using the calibration data from Section II-2 and computing flow quantaties from the cross-flow plane parameters. Also included is an uncertainty analysis of the data.

The initial data reduction phase, utilizing the calibration data, was performed at AEDC-VKF using an IBM 370/165 computer. This phase will be discussed in Section III-1. The remainder of the numerical processing was executed at The University of Texas at Austin on a CDC 64/6600 computer system and will be discussed in Sections III-2 to III-4.

1. Data Reduction

A procedure was developed to reduce the cone probe survey data to the following flow quantities: local Mach number, total pressure, and flow angles α_v and β_v. The strategy was to rearrange the calibration data to allow these quantities to be calculated. This procedure was devised by Martindale (Reference 9).

a. Construction of Calibration Tables

The form of the calibration data (discussed in Section II-2) consisted of the pressure differences $(P_4 - P_2)/P_1$ and $(P_5 - P_3)/P_1$, and the average cone surface pressure, P_{avg}/P_1, as functions of local flow angles and Mach number (see Figure 10). The survey data, however, consisted of the pressure differences, pitot pressure, and average cone surface pressure. To obtain the local flow parameters, the functional dependence of the calibration data was interchanged such that the local flow angles and Mach number were functions of the pressure valves.

The calibration data showed that the local Mach number was primarily a function of P_{avg}/P_1 and secondarily a function of α_v and β_v. Local flow angles, α_v and β_v, were determined to be primarily a function of the in-plane* differential pressure, secondarily a function of the out-of-plane differential pressure, and finally a function of local Mach number. The functional relationships just described are summarized as follows where the arguments are in decreasing order of importance:

$$\alpha_v = f[(P_4 - P_2)/P_1;\ (P_5 - P_3)/P_1;\ M_L]$$

$$\beta_v = f[(P_5 - P_3)/P_1;\ (P_4 - P_2)/P_1;\ M_L]$$

$$M_L = f(P_{avg}/P_1;\ \alpha_v;\ \beta_b).$$

Noting the mutual dependence of the flow angles and Mach numbers, the data reduction procedure was inherently an iterative technique.

Several calibration tables were incorporated in the data reduction procedure. The first set were from tables for the flow angles, one for each of the calibration Mach numbers, where the independent parameters are the pressure differences. A cubic spline interpolation method was used to transform the original calibration data from the form

$$(P_4 - P_2)/P_1 = f(\alpha_v;\ \beta_v)$$

$$(P_5 - P_3)/P_1 = f(\alpha_v;\ \beta_v)$$

to the form

$$\alpha_v = f[(P_4 - P_2)/P_1;\ \ (P_5 - P_3)/P_1]$$

$$\beta_v = f[(P_5 - P_3)/P_1;\ \ (P_4 - P_2)/P_1]$$

---

*The "in-plane" is herein defined as the pitch and yaw plane for α_v and β_v, respectively. This is not to be confused with the angle of attack plane.

for each Mach number. These tables were constructed from the present probe calibration phase; that is, α_v and β_v varying from - 20 to + 20 degrees.

To extend the range of the tables, the data from a previous probe calibration phase was utilized. This previous cone probe had the same dimensions and tolerances as the present one and was calibrated over a range of $\pm$ 40 degrees. It was found that the previous probe data for the pitch plane $(P_4 - P_2)/P_1$ and α_v, essentially matched the present data in the range of $\pm$ 20 degrees. Therefore, the calibration tables were extended to $\pm$ 40 degrees in α_v. The sideslip plane data $(P_5 - P_3)/P_1$ and β_v, did not agree with the present probe data. As a result, the calibration tables were simply extrapolated to provide estimates for β_v values greater than 20 degrees. However, only a very small percentage of the survey data had a β_v greater than 20 degrees and these points were subsequently repeated.

An additional, intermediate, calibration table required the introduction of a new parameter, the total angle of attack (α_{vT}), where

$$\alpha_{vT} \equiv \mathrm{Tan}^{-1}\sqrt{\mathrm{Tan}^2(\alpha_v) + [\,\mathrm{Tan}^2(\beta_v)\,/\cos^2(\alpha_v)]}\,.$$

Using the present calibration data plus the previous probe's high α_{vT} data, a table was constructed of the form:

$$P_{avg}/P_1 = f(\alpha_{vT};\ M_L)\ .$$

The final series of calibration tables were constructed of the form:

$$P_{avg}/P_1 = f(\alpha_v;\ \beta_v;\ M_L)\ .$$

Although this table was used for only those data with α_v and β_v less than 20 degrees, values at α_v and β_v of 25 degrees, extrapolated from the present probe data, were included. These additional data were used to set the end

conditions of cubic spline interpolation technique. Also, to set the end conditions, a two dimensional table of P_{avg}/P_1 as functions of α_v and β_v was generated for Mach 5. These data were extrapolated from the Mach 4 calibration data using theoretical values for a cone at an angle of attack. It was found that this technique significantly increased the accuracy of the subsequent interpolation.

b. Calculate Reduced Quantities

An initial approximation was made in order to begin the iterative data reduction procedure. The first approximation was to estimate α_{vT} using an average surface pressure difference. This was accomplished by effecting a single quadratic curve fit for all Mach numbers. The form of the quadratic is

$$\alpha_{vT} = A_1\overline{\Delta P} + A_2\overline{\Delta P}^2$$

where $\overline{\Delta P} = \sqrt{[(P_4 - P_2)/P_1]^2 + [(P_5 - P_3)/P_1]^2}$.

This fit gave a value of α_{vT} within approximately $\pm$ 2.5 degrees for Mach numbers between 1.5 and 4.

Using this value of α_{vT}, a local Mach number was calculated from the calibration table of P_{avg}/P_1 as a function of α_{vT} and M_L. A double interpolation scheme was performed to determine M_L from α_{vT} and P_{avg}/P_1. The first was a cubic spline interpolation for P_{avg}/P_1 as a function of α_{vT} using the known value of α_{vT}. This reduced the functional dependence of the calibration table to the form

$$P_{avg}/P_1 = f(M_L) \quad .$$

This curve was logarithmic in nature; therefore, a cubic spline interpolation, performed in the log-log domain, resulted in a local Mach number. The use of the log-log space reduced the effect of arbitrary end conditions on the spline interpolation.

Using this value of M_L and the pressure differences, the flow angles, α_v and β_v, were determined. Due to the different functional dependence, a linear interpolation was used for the out-of-plane pressure differences followed by a cubic spline interpolation for the in-plane data. For example, to determine α_v, a linear fit was performed on the $(P_5 - P_3)/P_1$ data and a cubic spline on the $(P_4 - P_2)/P_1$ calibration data. A cubic spline interpolation between the calibration Mach numbers was then effected.

Figure 11 is an overview flow chart of the data reduction procedure. Shown are the major steps, discussed above, and the convergence procedure. It was determined that two iteration cycles gave adequate convergence.

Using the local Mach number and flow angles, the local velocity components were computed assuming the total temperature was constant in the flow and $\gamma = 1.4$. With these assumptions,

$$T_L/T_\infty = (1 + 0.2 \times M_\infty^2)/(1 + 0.2 \times M_L^2) \qquad \text{and}$$

$$V_{TL}/U_\infty = M_L/M_\infty \times C/C_\infty = M_L/M_\infty \times \sqrt{T_L/T_\infty} \ .$$

The total velocity (V_{VT}) was resolved into velocity components with respect to the probe support axis by the following equations (see Fig. 10):

$$U_p/U_\infty = V_{TL}/U_\infty \times \cos(\alpha_v) \times \cos(-\beta_v)$$

$$V_p/U_\infty = V_{TL}/U_\infty \times \sin(-\beta_v)$$

$$W_p/U_\infty = V_{TL}/U_\infty \times \sin(\alpha_v) \times \cos(-\beta_v) \ .$$

These components were then transformed to the wind tunnel axis system using the standard vector transformations (see, for example, Reference 12).

$$U_T/U_\infty = U_p/U_\infty \times \cos(\alpha_{CTS}) \times \cos(\beta_{CTS}) - V_p/V_\infty \times \sin(\beta_{CTS})$$

$$+ W_p/V \times \sin(\alpha_{CTS}) \times \cos(\beta_{CTS})$$

$$V_T/U_\infty = U_p/U_\infty \times \cos(\alpha_{CTS}) \times \sin(\beta_{CTS}) + V_p/U_\infty \times \cos(\beta_{CTS})$$

$$+ W_p/V_\infty \times \sin(\alpha_{CTS}) \times \sin(\beta_{CTS})$$

$$W_T/U_\infty = U_p/U_\infty \times \sin(\alpha_{CTS}) + W_p/U_\infty \times \cos(\alpha_{CTS}) .$$

The velocity components in wind tunnel coordinates were transformed to the model axis system by the following equations:

$$u/U_\infty = U_T/V_T \times \cos(\alpha_B) - W_T/U_\infty \times \sin(\alpha_B)$$

$$v/U_\infty = V_T/U_\infty$$

$$w/U_\infty = U_T/U_\infty \times \sin(\alpha_B) + W_T/U_\infty \times \cos(\alpha_B) .$$

The local static pressure was computed from the Rayleigh pitot equation. Pitot pressure was corrected for total angles of attack greater than 20-degrees by the following equation derived from a curve fit of both previous and present calibration data:

$$P_{1c}/P'_0 = (P_1/P'_0)/[0.76355 + 0.022084 \times \alpha_{vT} - (5.1307 \times 10^{-4}) \times \alpha_{vT}^2]$$

$$(\text{for} \quad 20° < \alpha_{vT} < 45°) .$$

Finally, the local total pressure to freestream total pressure ratio, P_0/P_{0_∞}, was calculated using the following equation (Reference 13):

$$P_o/P_{o_\infty} = P_{1c}/P'_o \times f(M_\infty)/f(M_L)$$

where $$f(M) = P_{t_2}/P_{t_1} = [6M^2/(M^2 + 5)]^{3.5} \times [6/(7M^2 - 1)]^{2.5} .$$

2. Final Data Set

This section will discuss the strategy utilized in determining a final data set; that is, a set containing one survey point per grid position. The original data consisted of various types of repeat data; in some cases there were four flow field measurements at a single grid position. The initial data set consisted of 6,233 points. This was reduced to 5,341 points in the final data set.

a. Repeat Data

Approximately 14 percent of the survey data taken consisted of repeat points. The repeat data consisted of three types of points: (1) precision points, i.e., the point was repeated with identical pitch and sideslip angles of the probe, (2) points where the probe was manipulated to reduce the probe angle of attack below 20 degrees, and (3) points where the probe angle was changed even though the original probe angle of attack was less than 20 degrees. Type three points were generated because an entire group was usually repeated to reduce the total angle of any constituent points.

The following procedure was developed to obtain a data set which contained only one measurement per grid point. For type one and three repeat points the point with the lowest angle of attack of the probe was always retained in the final data. For type two points, generally the point with the lowest total angle was also retained. In instances where the repeat data had significant differences in total pressure or Mach number, additional parameters were evaluated. Contour plots of total pressure and local Mach

number and cross-flow vector plots were obtained to aid in determining which repeat point would be included in the final data. The criterion was to obtain a consistent data set; that is, inclusion of the measurement which yielded consistency of total pressure and cross-flow velocity with the surrounding points and based on the physics of the flow.

A total of eight non-repeat points was discarded in two grids due to obvious probe interference: seven points at $M_\infty = 2.0$, $R_d = 1.75 \times 10^6$, $\alpha_b = 20°$ and $x/d = 6$ and one point at $M_\infty = 3.01$, $R_d = 1.70 \times 10^6$, $\alpha_b = 25°$ and $x/d = 6$. These regions are indicated by dashed lines in the cross-flow plane vector plots, total pressure contours, magnitude of cross-flow contours (see Appendix C), and the final data set (see Appendix B).

b. Special Data

Two types of special data were considered: (1) survey points with very low local Mach number and (2) missing data points. Type one points with local Mach numbers less than 1.2 were discarded because it was judged that the calibration table could not be accurately extrapolated below this Mach number. These points occurred near the model and no attempt was made to numerically generate data for these points.

There were twelve type two points: eight deleted points (see Section III-a) and four points at Mach 3, $\alpha_b = 15°$ and $x/d = 10$ which were missed during the survey acquisition due to a programming error. In order to eliminate a "hole" in the data from these few points, five flow parameters, P_0/P_{0_∞}, M_L, u, v, and w, were numerically generated at these points. A two dimensional quadratic least-squares interpolation method was utilized for each of the five parameters in the cross-flow plane. These points are enclosed by dashed lines in the cross-flow vector plots, total pressure contours,

cross-flow velocity contours, and tabulation of the final data set.

c. Final Data

Table 6 shows the quantity of final data. Indicated in the table are the number of final data points per survey grid and those points with a total angle of attack of the probe greater than 20 degrees. There are two grids with an abnormally high number of points greater than 20 degrees. The first, at Mach 2 and high R_d, was the result of inability to obtain certain yaw and sideslipe angles due to excessive aerodynamic loading on the CTS. The CTS could not be positioned at the particular combinations of yaw and sideslip angles needed to reduce the angle of attack of the probe. The second grid, at Mach 3, was the result of wind tunnel time constraints. This was the last grid surveyed in the experiment.

Figure 12 is a plot of frequency of occurrence vs. total angle of attack of the probe using the final data set. The average angle in this final data set was 8.2 degrees. The most probable angle, that is, the most frequent angle, is between 4 and 5 degrees. This figure is a graphic illustration of the probe angle of attack quality of the data. It illustrates the success of the procedure to reduce large α_{VT}.

Appendix B contains the final data set in tabular form. Each table is arranged in a format corresponding to the cross-flow plane. The location on the printed page is analogous to the physical location in the cross-flow plane at which the data were measured (see Figure 8). The large blank region on the left portion of the page is the positive-y, positive-z quadrant of the body. At each location in the table, the value of P_o/P_{o_∞}, M_L, u/U_∞, v/U_∞, and w/U_∞ are printed.

3. Uncertainty Analysis

The purpose of this section is to provide a means for evaluation of the accuracy of the quantitative data, determined from the previous section. A traditional method in experiments is to analyze the influence of random measurement bias and their propagative effects in the final computed quantities. However, the unique testing procedure of the present experiment allowed a statistical analysis based on repeated samples to be performed. In this approach, the repeat data are used to determine the uncertainty.

a. Error Propagation

An evaluation of the influence of random measurement by the Taylor series method of error propagation is presented (from Reference 9). Systematic bias is included in the instrumentation precision values stated in Section II-1-e. Uncertainties in the basic tunnel parameters P_o and T_o and the two-sigma deviation in Mach number, determined from test section flow calibration, were used to estimate uncertainties in the other freestream properties. These results are shown in Table 7.

The following discussion is limited to data in the range of the present probe calibration; i.e., M_L between 1.5 and 4 and $|\alpha_v|$ and $|\beta_v|$ less than 20 degrees. To calculate the precision of M_L, an uncertainty of P_{avg}/P_1 was first obtained using the pressure transducer precision values and the Taylor series method of error propagation. Then using the slope of Mach number versus P_{avg}/P_1, the precision of Mach number was obtained. This value ranged from within the tunnel Mach number uncertainty, $\pm$ 0.02 to $\pm$ 0.03, at high values of P_1 and low values of Mach number, to $\pm$ 0.10 at low values of P_1 and high values of Mach number.

Several factors other than pressure instrument precision enter into the flow angle uncertainty. These include tunnel flow nonuniformity and

deflection of the probe support. Based on these considerations, an estimate of the precision of α_v and β_v measurements was made by computing the difference between the calculated and indicated values for the probe verification data. That is, the data which was taken during periodic pitch and sideslip sweeps in the tunnel freestream. A two-sigma value of $\pm$ 0.8 degree is indicated for both α_v and β_v.

Based on comparisons of the calculated and known values of the velocity components for the verification data, the estimated precision of the velocity ratios, u/U_∞, v/U_∞ and w/U_∞ is 0.02 for the case of minimum Mach number uncertainty. This value increases to approximately 0.04 when Mach number uncertainty approaches 0.1.

b. Statistical Analysis

A statistical analysis was performed using the repeat data as the sample space. As stated before, the repeat data consisted of three types of points: (1) precision points, i.e., the point was repeated with the probe pitch and sideslip angles constant, (2) points where the probe was manipulated to reduce the probe angle of attack below 20 degrees, and (3) points where the probe angle of attack was changed even though the original measurement was made with a total angle of attack less than 20 degrees. The use of the actual data in the statistics yields a dynamic analysis, that is, an analysis which considers the flow field in the results. The error propagation method is a static analysis, using only the uncertainties in the instrumentation and calibration. The type of measured flow field has no effect on the uncertainty in an error propagation analysis.

The distribution of the total probe angle of attack of the final data is shown in Figure 12. Since some of the type 2 data had large angles which

were subsequently reduced below 20 degrees, an upper bound on α_{vT} was used for statistical purposes. Therefore, only repeat points which had an α_{vT} less than 23 degrees (three standard deviations from the average total probe angle of attack) were utilized in the statistical analysis. 99.2 percent of the final data had total probe angles of attack less than the 23 degrees statistical limit.

Statistical sample spaces were created for each of the three freestream conditions using the following parameters: total pressure, local Mach number, and u, v, and w velocity components. A precision data sample space consisted of only type one points while the accuracy repeat space included the type two and three points. The statistical parameter was the absolute change in the quantity (e.g., local Mach number) between data points at the same y and z location in a survey grid. Figure 13 shows distributions from the local Mach number parameter at each of the three freestream conditions. Comparing Figure 13a and b, it is clearly seen that the effect of higher Reynolds number is to widen the distribution. Comparing Figure 13b and c, one observes that Mach number also expands the distribution.

A standard deviation of each distribution was determined using zero as the sample mean; that is, $\sigma = \sqrt{\Sigma x_i^2/(n - 1)}$. The justification for using zero as the mean is as follows. Figure 13 uses the absolute change in the sample parameter as the statistical data point. If a different, arbitrary statistical point were defined using the first minus the second parameter, one would expect it to be normally distributed with its mean at zero. That is, there is an equal probability of the statistical point being positive or negative. Any fixed bias will be subtracted out, leaving only the random uncertainty. Therefore, Figure 13 represents a folded distribution about the zero point.

To reduce the bias of the random scatter at the high end of the distribution, the distribution was truncated at its two sigma point, shown in Figure 13. A new distribution was then determined for each of the five parameters. The new Mach number distributions are shown in Figure 14 as typical of the five parameters. The figure shows the relationship between the standard deviation and the frequency distribution. Also shown on the figure is the average value, that is, the average change in the statistical parameter based on local Mach number. This average is not the value used to determine the standard deviation. Approximately 79, 66, and 74 percent of the statistical data is between zero and the average value for Mach 2 Low R_d, Mach 2 High R_d, and Mach 3, respectively.

Table 8 is a summary of the statistical data after the two sigma truncation process. Shown are the average value of the parameter and the standard deviation based on a zero mean. The precision repeat statistics contain only the uncertainties of the instrumentation. Their standard deviation show that the fluctuations were random in nature because σ is larger than the average sample value. The sample average is, therefore, a measure of the uncertainty in the data due to instrumentation effects. This measure of the data repeatability would correspond to those previous experimental investigations where a fixed probe or survey rake was used. The accuracy repeat statistics in Table 8 include the instrumentation effects discussed above and probe interference effects. Comparing the precision and accuracy repeat statistics clearly demonstrates that probe interference dominates measurement uncertainty. This analysis is not possible with the error propagation method. The average sample value of each parameter is, therefore, a realistic estimate of the accuracy of the present results. The standard

deviation is a measure of the scatter of the sample data about the zero point.

Several important conclusions can be drawn from Table 8. The first is that the effect of Reynolds number had significant effect on the uncertainty of the data. Comparing the results for both Reynolds numbers at Mach 2, it is noted that the higher Reynolds number data had standard deviations approximately twice the lower Reynolds data. The effects of Mach number, comparing Mach 2 high R_d and Mach 3, are somewhat inconsistent. The Mach 3 uncertainty is noticeably higher for local Mach number, but no conclusion can be based on the other parameters. The statistics also indicate that the v and w velocity components have larger uncertainties than the u component. This is due to the magnitude of u velocity being much larger than the magnitude of the v and w velocities. Therefore, a small absolute uncertainty has more effect on the v and w components. A final conclusion is that the statistics clearly indicate the requirement of a manipulating probe when measuring flow fields with large velocity gradients such as the body vortex.

Table 9 shows the combined statistics for the experiment. A statistical sample space containing all the statistical data used in Table 8 for a given parameter was created. The average parameter and the standard deviation based on a zero mean for each parameter were then calculated. The data shown in Table 9 represent the experiment averaged statistical results and quantifies experimental uncertainty.

4. Calculated Flow Quantities

This section presents the numerical techniques utilized to calculate the various quantities implied by the velocity and pressure field in the cross-flow plane. Examples of the present data will be given for illustration purposes in this section. Complete findings will be discussed in Section IV.

a. Vortex Centers

A graphical procedure was devised to determine the vortex center. In the core of the body vortex, the total pressure, P_o/P_{o_∞}, and the magnitude of the cross-flow velocity, U_c/U_∞, decrease because of the "solid body" type rotational motion. At the center of the core, the total pressure and cross-flow velocity attain a local minimum. Therefore, the primary vortex location was determined by analyzing the variation of P_o/P_{o_∞} and U_c/U_∞ in the cross-flow plane. For each of the cross-flow planes measured, contour line plots of P_o/P_{o_∞} and U_c/U_∞ were generated. A two-dimensional quadratic interpolation scheme was used for the data in the cross-flow plane to generate the contours.* Figure 15 shows an example of the plots. The small grid marks in Figure 15 are the locations in the cross-flow plane where measurements were made. The vortex center is located at the minimum concentric contour and is indicated on the figure by a solid dot. A graphical procedure was utilized due to slight experimental scatter in the data. A computer search method could have been employed; however, the results would have been suspect.

b. Core Size

The core size is a rather nebulous quantity to determine precisely. The procedure used on the present data was to measure the size of the core from plots of magnitude of cross-flow velocity versus radial coordinate in a vortex orientated coordinate system. That is, an (r', ϕ) coordinate system was numerically constructed with the origin at the center of the vortex and angular coordinates measured from a line parallel to the Y axis. Using this vortex orientated coordinate system, U_c/U_∞ vs. r' were plotted for various

---

*CPS-1, a software package from Unitech, Inc., Austin, Texas, was used to generate the contours.

angles ϕ. Figure 16 shows a typical plot of U_c/U_∞ vs. r'/d.

To obtain these plots, several numerical procedures were required. First, U_c/U_∞ was calculated at each grid point in a given cross-flow plane. A two dimensional numerical surface was then generated from this data; that is, a continuous surface of U_c/U_∞ as a function of y and z. See Appendix A for a discussion of the surface generation software.

Figure 16 illustrates very clearly the solid body type rotation of the concentrated vortex. The vortex radii is herein defined to be the r' corresponding to the maximum value of U_c/U_∞ for all ϕ. An analysis of this data, along with comparisons of the total pressure contours, shows that the core is elliptical in nature. As a result, two vortex core dimensions were measured: a minor and major axis. The angular orientation of these orthogonal axes was determined such that the core radius of the minor axis was the smallest and the major axis was the largest for all lines passing through the vortex center. For example, Figure 16 shows the line passing through the vortex center at ϕ equal 15 degrees indicates the minor radius while at ϕ equal 105 degrees shows the major radius.

c. Local Circulation

Local circulation, Γ, was calculated in each of the cross-flow survey planes using the cross-flow velocity data $\vec{V}_c = v\vec{j} + w\vec{k}$. Using the definition of circulation on a square contour with side h, one has

$$\Gamma(y,z) \equiv \oint \vec{V} \cdot \vec{ds} = \int_{y,z}^{y+h,z} v\,dy - \int_{y,z+h}^{y+h,z+h} v\,dy + \int_{y+h,z}^{y+h,z+h} w\,dz - \int_{y,z}^{y,z+h} w\,dz ,$$

where Γ is positive counterclockwise. In order to compute $\Gamma(y,z)$, assuming 2-D flow in the cross-flow plane, several numerical procedures were necessary.

As regions of high velocity gradients existed in the flow, the data mesh was too coarse to accurately calculate Γ directly. Therefore, continuous surfaces were numerically generated for $v(y,z)$ and $w(y,z)$ in the cross-field plane using the software described in Appendix A. Local circulation was then calculated on a square contour with side $h = 0.0375d$; i.e., one-half of the survey grid size.

A cubic polynomial approximation was derived and used to carry out the numerical integration indicated above. This approximation used the function value and the derivative at the endpoints of the segmented contour. Let 'a' be the left endpoint and 'a + h' be the right. Then, the approximation of $\int_a^{a+h} f dx$ is

$$\int_a^{a+h} f dx = Ah + Bh^2/2 + Ch^3/3 + Dh^4/4 + O(h^4)$$

where $A = f(a)$

$B = f'(a)$

$C = (f'(a+h) - f'(a))/2h - 1.5\ D\ h$

$D = (2f(a) - 2f(a+h) + hf'(a) + hf'(a+h))/h^3$.

This technique yielded improved results when compared to linear integration methods because of large gradients in the cross-flow velocity near the vortex sheet. See Reference 21 for a complete description on the mesh size evaluation and integration technique.

d. Concentrated and Sheet Circulation

The calculation of the primary vortex, Γ_p, and sheet, Γ_s, circulation was carried out. The segregation of total circulation in the cross-flow plane into Γ_p and Γ_s is rather arbitrary because the vortex sheet blends smoothly into the vortex core. Also, the distribution of circulation does

not coincide with the U_c/U_∞ distribution used to define the vortex core size. This is illustrated by comparing a plot of circulation in a vortex coordinate system, Figure 17, with the U_c/U_∞ distribution, Figure 16. Both figures are for the same cross-flow plane and freestream condition.

The following procedure was devised in order to define Γ_p and Γ_s. First, a ratio of the core circulation, Γ_p, and the circulation inside the defined core ellipse, Γ_e, was determined. This ratio, β, was calculated using a line integral of Γ along the major and minor axes. Beta was taken as the ratio of the integral of the local circulation along a given axis at two radii from the vortex center to the integral using the core radius. That is,

$$\beta = \frac{\int_{-2r}^{2r} \Gamma \, dr'}{\int_{-r}^{r} \Gamma \, dr'} \quad .$$

The two betas, calculated for each axis using Simpson integration, were then averaged to give the final beta. This procedure was utilized to reduce the influence of the feeding sheet on the calculation of β. An average beta was calculated for each cross-flow plane (see Table 10).

Γ_e was then calculated using a 2-D Simpson integration in the vortex coordinate system. All integrations were performed on a continuous 2-D surface construction of Γ using the software discussed in Appendix A. Then, Γ_p was calculated from

$$\Gamma_p = \beta \times \Gamma_e \quad .$$

Finally, the sheet circulation, Γ_s, was simply taken as

$$\Gamma_s = \Gamma_t - \Gamma_p$$

where Γ_t is the total circulation in the survey grid. Γ_t was calculated using a summing process on the Γ mesh discussed in Section III-4-c.

e. Recirculation Height

The recirculation height of the wake, defined as the z distance in the angle of attack plane were the w velocity is zero, was calculated from the data. An example of the variation of w in the angle of attack plane is shown in Figure 18. The circulation height is shown as the point where w changes from negative to positive. The small circles on the velocity line indicate survey data values and the plotting symbol on the line of zero w indicates the top of the survey grid.

f. Streamlines

Numerically generated streamlines in the cross-flow plane were used to qualitatively evaluate effects of Reynolds and Mach number. The stream function requires that the three dimensional continuity equation, $\partial v/\partial y + \partial w/\partial z = - \partial u/\partial x$, be reduced to a two-dimensional form requiring $\partial u/\partial x = 0$. Qualitative analysis of the present data for $\partial u/\partial x$, however, indicate that it is generally not zero throughout the survey grid. An axial velocity defect (i.e., $u/U_\infty < \cos\alpha_b$) was usually measured in the core region of the body vortex. As a result, the $\partial u/\partial x$ behaves as a source term in the cross-flow continuity equation. The magnitude of this term varied for different freestream conditions, but the largest values occurred at the forward body stations and then diminished along the body due to viscous dissipation. This trend is illustrated by observing perspective views of the u velocity component in the cross-flow plane.

The streamlines were numerically generated from the nondimensionalized defining equation

$$\psi_B - \psi_A = \int_A^B w/U_\infty \, d(y/d) - \int_A^B v/U_\infty \, d(z/d) \ .$$

A cubic integration method, similar to the one used in circulation calculations (Section III-4-c), was utilized with mesh size h = 0.0375d. It was found that the integration sweep pattern had significant effect on the stream function plots due to the source term in the continuity equation. Figure 19 illustrates the dramatic difference in the plots on the same cross-flow plane. The numerical procedure used to generate Figure 19a was to arbitrarily set the streamline value at the top survey grid point on the center line to unity and then calculate the line integrals by sweeping in the positive y, negative z directions. The procedure used in Figure 19b was to use the same initialization but sweep first along the top of the grid in the positive y direction to the boundary. Then the sweep process was in the negative z, negative y direction. The effect of the continuity source term on Figure 19a is not readily noticed due to the sweep direction. The different sweep pattern of Figure 19b, however, causes significant apparant mass flow through the angle of attack plane.

Figure 20 illustrates a cross-flow plane and freestream condition where the first integration sweep pattern gives erroneous results. The effect of the continuity source term is clearly seen in the region of the feeding sheet. This cross-flow plane was a more forward station than the preceding figure and, therefore, the velocity defect was larger. In conclusion, the integration sweep procedure and axial location have a significant effect on numerically generated streamlines. The streamlines shown in Section IV utilize the first sweep pattern and the grids are chosen such that the magnitude of $\partial u/\partial x$ is minimized.

SECTION IV

RESULTS AND DISCUSSION

The results from the experiment will be presented in this section in the following order: first, $M_\infty = 1.95$ $R_d = 0.48 \times 10^6$, second, $M_\infty = 2.00$ $R_d = 1.75 \times 10^6$, and third, $M_\infty = 3.01$ $R_d = 1.70 \times 10^6$. The results and physical interpretation will be given concurrently. For each freestream condition the basic flow parameters, such as cross-flow velocity and local total pressure, will be presented first, then inferred parameters, such as vortex center and circulation, will be presented. Tabular form of the final data set is given in Appendix B.

1. Results for $M_\infty = 1.95$ and $R_d = 0.48 \times 10^6$

Figures 21 through 24 show the cross-flow velocity field, $\vec{V}_c = v\vec{j} + w\vec{k}$, for $\alpha_b = 10$, 15, 20 and 25 degrees for all of the body stations surveyed. The base of the vector is the location at which the measurement was made in the cross-flow plane. Every cross-flow vector in this report is plotted according to the same scale which is shown in part (a) of each figure. The magnitude of the vector is measured from the base of the arrow to the tip of the head. If only the arrow head is plotted, then the magnitude is so small that little significance should be given to the direction implied by the arrow head.

For $\alpha_b = 10$ degrees (Figure 21) only slight rotational motion of the vortex can be seen. At $\alpha_b = 15$ degrees (Figure 22) the vortex is readily identified for x/d = 7 as a well organized, nearly circular motion. Farther down the body at x/d = 13 (Figure 22c) the vortex center moves far from the body and shows little rotational motion. At $\alpha_b = 20$ degrees (Figure 23) the vortex develops from a strong circular rotation at x/d = 6 to a clearly defined elliptical rotation at x/d = 11. The highly elliptical nature of

the body vortex has been suggested from vapor screen photographs, e.g., Jones and O'Hare (Reference 14) and Jorgensen (Reference 15), but has not been measured before. In incompressible flow the measurements of Grosche (Reference 5) show that this elliptical nature of the body vortex does not exist. At α_b = 25 degrees (Figure 24) the vortex is elliptical even at x/d = 6. At x/d = 9 (Figure 24b) the elliptical nature has become so dominant that the flow hardly recirculates on the upper position of the ellipse.

A perspective plot* of the local total pressure in the cross-flow plane for α_b = 10, 15, 20 and 25 degrees for all of the body stations is shown in Figures 25 through 28. The perspective view is from above the three-dimensional surface of $P_0(y,z)/P_{0_\infty}$ and looking in the positive y and negative z direction. The positive y and positive z quadrant of the body can be seen inside the arc of the body surface bounded by the coordinate axes. The "blank" region in the upper right position of the plot represents the quadrant of the body and also grid points near the body surface where data were not obtained. Lines hidden from the viewer are plotted as dashed lines. The surface of the perspective plot is numerically constructed by connecting the measured data points with straight lines. The largest and smallest values in the grid are noted on the dependent variable axis, but the scale, i.e., units/length of each dependent variable, e.g., P_0/P_{0_∞}, is constant for all of the perspective plots.

Examing the surface of local total pressure in Figure 25 it can be seen that even at an angle of attack of 10 degrees, a well defined body vortex is implied by the loss in total pressure. Figure 26 shows the total

---

*All of the perspective plots were generated using CPS-1.

pressure distribution for α_b = 15 degrees. The loss in total pressure in the cross-flow plane is confined to two regions; first, the core region of the body vortex, and second, the vortex feeding sheet. The core region is nearly circular for the foward body stations with the loss in P_o restricted to a relatively small region with large gradients. The vortex feeding sheet can be seen as a valley of low total pressure leaving the crest of the body and proceeding in roughly the positive z-direction. The total pressure in the sheet is usually lowest near the body surface and then increases moving away from the body. For α_b = 20 degrees (Figure 27) it can be seen that a large loss in total pressure occurs in the angle of attack plane, i.e., the z-axis, for x/d = 8.5 and 11. This loss in P_o is due to an embedded strong shock wave which lies near the leeside body surface. By comparing its y location for x/d = 8.5 to that for x/d = 11 it is concluded that it lies at a slight angle to the surface. For α_b = 25 degrees (Figure 28) this same shock wave occurs at both x/d = 6 and 9 but it is much weaker. Note that at x/d = 9 (Figure 28b) the region of low total pressure associated with the body vortex stretches more than a body diameter from the surface.

A perspective plot of the local Mach number in the cross-flow plane for α_b = 10, 15, 20 and 25 degrees for all of the body stations is shown in Figures 29 through 32. For α_b = 10 and 15 degrees (Figures 29 and 30) the local Mach number varies little in the vortex wake. A local minimum in Mach number occurs in the body vortex core, but this is not prominent. The lowest Mach numbers typically occur in the vortex sheet near the body surface. For α_b = 20 degrees (Figure 31) the Mach number distribution shows a new characteristic as compared to α_b = 10 and 15 degrees. The

rotational motion of the vortex causes an increase in the magnitude of cross-flow velocity toward the body in the angle of attack plane, i.e., the z-axis. At x/d = 6 (Figure 31a) only a moderate acceleration occurs along the z-axis because of the low strength of the vortex. At x/d = 8.5 (Figure 31b) a strong acceleration toward the body occurs. The Mach number increases from 1.8 at the top of the grid to 2.7, then an embedded shock wave drops the Mach number to 2.0. The loss in total pressure associated with the embedded shock wave was discussed in the preceding paragraph. At x/d = 11 (Figure 31) the embedded wave remains but its strength is diminished. For α_b = 25 degrees (Figure 32) a similar phenomenon occurs, but much sooner along the body. The very rapid acceleration which occurred at x/d = 8.5 for α_b = 20 degrees, now occurs at x/d = 6. The reason for this is the stronger body vortex forming from the increased cross-flow velocity. By x/d = 9 (Figure 32b) the embedded shock has essentially dissipated. It is believed that this is due to growth of the rotational flow associated with the vortex core spreading into the angle of attack plane.

Figures 33 through 36 show perspective plots of the nondimensional cross-flow velocity, i.e., $\sqrt{v^2 + w^2}/U_\infty$, for α_b = 10, 15, 20, and 25 degrees for all of the body stations. The most prominent feature which can be seen in the figures is the vortex core. The vortex core is generally characterized as a solid body rotation with near zero cross-flow velocity at the center of the core. If the flow precisely conformed to this model then the core would appear as a symmetric depression in the surface of U_c/U_∞. From Figures 33 through 36 it is clearly seen that this model is fairly accurate for α_b = 10 and 15 degrees, but not for α_b = 20 and 25 degrees. At the higher angles of attack the depression in the surface becomes elliptical,

e.g., Figure 36a, and then farther down the body, e.g., Figure 36b, the depression becomes a long trough. Another noteworthy feature for α_b = 20 and 25 degrees is the discontinuity which occurs along the z-axis. This is due to the embedded shock wave discussed earlier. The cross-flow velocity component U_c essentially is the normal velocity component to the shock wave. As a result, it suffers a large drop as the fluid crosses the wave.

A perspective plot of the axial velocity component in the cross-flow plane for α_b = 10, 15, 20 and 25 degrees for all of the body stations is shown in Figures 37 through 40. For α_b = 10 degrees (Figure 37) the u/U_∞ surface is flat except in the vortex core and vortex sheet. In these regions a velocity defect occurs, i.e., $u/U_\infty < \cos\alpha_b$. For α_b = 15 and 20 degrees (Figures 38 and 39) the axial velocity defect in the core essentially disappears. The region between the vortex core and the angle of attack plane attains a slightly higher axial velocity than the region outboard of the vortex. For α_b = 25 degrees (Figure 40) this characteristic becomes more prominent. At x/d = 6 (Figure 40a) the fluid inboard of the vortex core and the fluid between the core and the body achieves a nondimensional velocity of 1.06 while the fluid outboard of the core and vortex sheet is 0.86. The distribution shown in Figure 40a also shows the rapid increase in the axial velocity in the angle of attack plane as the body is approached. The magnitude of the cross-flow velocity, U_c, showed the same large increase for this case (Figure 36a). For x/d = 9 (Figure 40b), the axial velocity distribution simply displays two plateaus; one outboard of the viscous flow at a level of u/U_∞ = 0.86, and one inboard at a level of 1.02.

A perspective plot of the local circulation in the cross-flow plane for α_b = 10, 15, 20, and 25 degrees for all of the body stations is shown

in Figure 41 through 44. In all of the perspective plots of circulation the quadrant of the coordinate system is displaced from the survey grid by 0.01875d, that is, one-half of the circulation contour size. The reason for this is that the circulation value at the intersection of the straight lines on the surface is the value associated with a contour integration square of 0.0375d on a side centered on the surface point.

For α_b = 15 degrees and x/d = 7 (Figure 42a) the vorticity is very concentrated in the core region just above the body surface. The vortex sheet is identified as the narrow ridge extending from the crest of the body into the peak of vorticity in the core. Outside the core and sheet the vorticity is uniformly zero. For α_b = 15 degrees and x/d = 10 and 13 (Figures 42b and 42c) the highly concentrated vorticity of the vortex core and vortex sheet begins to diffuse due to the action of viscosity. For α_b = 20 degrees (Figure 43) the same general characteristics exist, except they are more pronounced. Note that after separation near the crest of the body the local vorticity increases along the sheet and then quickly decreases near the vortex core. Considering the two-dimensional Impulse Flow Analogy for bodies of revolution, this could be due to the local convective acceleration of the vortex sheet as it approaches the vortex core. For the aft body stations at α_b = 20 and 25 degrees (Figures 43 and 44) the vorticity is clearly seen to diffuse over a large region of the leeside. These plots quantitatively illustrate the "vortex cloud" suggested by vapor screen photographs of previous investigators (see, for example, Jones and O'Hare (Reference 14) and Jorgensen (Reference 15)). For α_b = 25 degrees and x/d = 9 (Figure 44b) the low values of circulation which occur near the top of the grid possibly indicate a secondary nose vortex. This

vortex was conclusively detected for M_∞ = 2 and 3 for high Reynolds number and will be discussed later.

Probably the most important parameter of the body vortex is its location in the cross-flow plane. Not only is it a difficult parameter to theoretically predict, but it is also the crucial element needed to determine the load distribution imposed on a wing or fin immersed in this flow. The body vortex location was determined using contour plots of total pressure and magnitude of cross-flow velocity (see Section III-4-a). All contour plots are given in Appendix C and the vortex center, if one could be defined, is denoted by a dot.

Figure 45 shows the location of the vortex center in the cross-flow plane versus x/d for α_b = 10, 15, 20 and 25 degrees. In order to be able to interpret all of the data on one graph the ordinate for each angle of attack is displaced by 0.5d. As can be seen from Figure 45 the y and z coordinates of the body vortex demonstrate an almost linear variation with axial distance. The vortex path down the body is essentially in a plane which is slightly tilted toward the z-axis. The present data compare closely with the previous data of Jorgensen and Perkins (Reference 1) and Mello (Reference 2) even though the nose shapes of each model were different. Jorgensen and Perkins used a three caliber tangent ogive nose and Mello used a 15 degree half-angle cone. Two slight differences in the three data sets are evident. First, z_v/d (Figure 45a) at α_b = 20 degrees for Jorgensen and Perkins and Mello indicates that a constant value is attained near x/d = 10. Certain Schlieren photographs of Thomson and Morrison (Reference 16) suggest that the vortices maintain a nearly constant z height shortly before they "break-away" into the asymmetric wake pattern.

The earlier development of the symmetric wake along the body would be expected with the models of Jorgensen and Perkins and Mello because of their sharper noses. Second, the y_v/d data (Figure 45b) of Mello show that the vortex of the cone cylinder is located slightly farther from the angle of attack plane.

Some investigators have suggested that a Schlieren photograph of the vortex wake flow could be used to determine the z-coordinate of the vortex center. They have speculated that the vortex center should be characterized on a Schlieren photograph as a sharp contrast between a light and dark region. This is based on the argument that a large change in the density gradient occurs on a line passing through the vortex center. Figures 46 through 49 show the z-coordinate of the vortex center taken from Figure 45a plotted to scale directly on the Schlieren photograph for α_b = 10, 15, 20 and 25 degrees. Examining photographs for α_b = 10 and 15 degrees (Figures 46 and 47) it is seen that the boundary between light and dark regions occurs precisely on the vortex center. For α_b = 20 degrees (Figure 48) it is seen that for axial stations less than about x/d = 8 the sharp contrast again marks the vortex center. Beyond x/d $\approx$ 8 the sharp contrast degrades and local regions of light and dark appear on both sides of the vortex center. For α_b = 25 degrees (Figure 49) the sharp contrast between light and dark disappears beyond about x/d = 4. Why the sharp contrast disappears along the body and how it is related to angle of attack is not known. The present authors suggest that as the vortex becomes stronger it convects "lumps" of fluid in a spiral path down the body. These lumps of fluid have differing densities and, consequently, cause regions of light and dark to appear on both sides of the vortex center. As a Schlieren photograph is an analog integrator

along the light beam path, these light and dark regions in front of and behind the vortex mitigate the sharp contrast. From the comparisons given in Figures 46 through 49 it can be concluded that when a sharp contrast does exist, the body vortex center is located along the boundary; when a sharp contrast does not exist, the center is roughly located in the "gray" region between the uniform light and dark.

The vortex core radii versus axial location for α_b = 10 and 15 degrees are shown in Figure 50. The minor axis of the vortex core, r_y, and the major axis of the vortex core, r_z, were defined as the radial location at which $\partial U_c/\partial r' = 0$ along the y' and z' axes (see Section III-4-b for more description). Although this is a precise mathematical definition, plots of U_c/U_∞ versus r'/d required some interpretation in order to obtain the vortex core dimensions. Figure 50 shows that for α_b = 10 degrees the vortex core is very nearly circular. For α_b = 15 degrees the core is clearly elliptic with the major axis roughly 60 percent larger than the minor axis. For angles of attack of 20 and 25 degrees the vortex core becomes so elongated in the z' direction that the major axis of the core could not be determined with confidence. Figure 50 shows that the core size grows slightly with angle of attack. The magnitude of $\partial r_z/\partial \alpha_b$ is larger than $\partial r_y/\partial \alpha_b$ because of the development of a trough in U_c discussed in Figures 33 through 36.

Figure 51 shows the angular orientation of the minor axis, y', of the vortex core versus x/d for α_b = 10 and 15 degrees. For α_b = 10 degrees, the minor axis of the vortex is aligned with the y-axis of the body coordinate system. For α_b = 15 degrees and x/d = 7 the minor axis of the vortex is rotated 45 degrees counter-clockwise from the y-axis. As the vortex moves down the body for α_b = 15 degrees, its angular orientation approaches 15 degrees.

The total circulation in the survey grid versus body length for α_b = 10, 15, 20 and 25 degrees is shown in Figure 52 along with data of Mello (Reference 2). The flagged symbols in Figure 52 denote that the height of the survey grid was not large enough such that near zero vorticity existed on the top boundary (see, for example, Figure 43). Consequently, the flagged symbols are a lower bound on the total circulation in the cross-flow plane. The variation of total circulation with body length is remarkably linear for all angles of attack. The agreement between the present results and those of Mello are fairly good. This might not be expected considering the very rough grid spacing and the lack of numerical data fitting by Mello.

As pointed out in Section III-4-f, numerically constructed streamlines in the cross-flow plane assume that $\partial u/\partial x = 0$. By examining Figures 37 through 40 it is easily seen that this is not precisely true. The angle of attack which best satisfies this assumption for each body station is α_b = 15 degrees and x/d = 7, 10 and 13. The growth in size of the body vortex is most clearly demonstrated in this presentation format. Comparing the shape of the streamline ψ = 1.03 for x/d = 7 (Figure 53a) to that of x/d = 10 and 13 (Figures 53b and 53c) clarifies a vortex phenomenon mentioned earlier. The angular orientation of the vortex core changes significantly from x/d = 7 to that for x/d = 10 and 13. For the forward body station the body vortex lies very near the body and, as a result, the vortex feeding sheet and body vortex conform more closely to the inviscid flow streamlines about a cylinder. Farther down the body the vortex moves farther from the body, gains strength, and no longer is as strongly influenced by the body. The major axis of the core then becomes nearly aligned with z-axis of the body.

2. Results for $M_\infty = 2.$ and $R_d = 1.75 \times 10^6$

The cross-flow velocity field for α_b = 10, 15, 20 and 25 degrees for all body stations is shown in Figures 54 through 57. The two small rectangular regions marked by the dashed lines in Figure 56a denote that the vectors within the region were not experimentally measured. They were obtained by means of quadratic, two-dimensional, interpolation from the surrounding field. This was done because it was clear from comparing various measured parameters at these points to the surrounding points that the data were not reliable. This was probably due to interference of the probe or strut on the vortex core. For the condition of α_b = 20 degrees and x/d = 6 the vortex is very small and concentrated and inserting a probe in this type flow represents the worst case for probe interference.

Comparing the cross-flow velocity fields for Mach 2 high Reynods number (Figures 54 through 57) with those for Mach 2 low Reynolds number (Figures 21 through 24), one observes certain differences. For α_b = 20 degrees and high Reynolds number the elliptical nature of the body vortex still exists but is not as well defined as the low Reynolds number condition. Also at α_b = 20 degrees the path of vortex sheet is different between the two Reynolds numbers. The location of the vortex sheet can be estimated by noting the large change in w-component of velocity across the sheet. A large increase in w-component of velocity from the left side to the right side of the sheet will yield a large positive value of circulation. For α_b = 20 degrees the sheet bends noticeably outward for the high Reynolds number, while it takes a vertical path for the low Reynolds number.

Figures 58 through 61 show perspective plots of the local total pressure in the cross-flow plane for α_b = 10, 15, 20 and 25 degrees for all

body stations. Comparing Figures 58 through 61 with the low Reynolds number data (Figures 25 through 28), the "roughness" of the total pressure surface for the high Reynolds number is apparent. The roughness is due primarily to a relatively large number of weak embedded shock waves which apparently do not occur at the lower Reynolds number. For α_b = 25 degrees, these waves can clearly be seen on the vapor screen photographs shown in Figures 78 and 79. The photographs are for freestream conditions of M_∞ = 2., R_d = 1.58 x 10^6, α_b = 25 degrees, and x/d = 6 and 9, respectively. The air flow is from left to right, the laser source is on the right, and the camera is positioned upstream of body station x/d = 6 looking partially downstream. Figures 78 and 79 are the only vapor screen photographs taken during the experiment.

At α_b = 15 degrees a cross-flow embedded shock, outboard of the body vortex, is evident at x/d = 7 and 10 (Figures 59a and b). For α_b = 20 degrees and x/d = 6 (Figure 60a) two cross-flow shocks are seen near the crest of the body. Comparing Figures 59 and 60 with Figures 26 and 27 it is concluded that the cross-flow shocks near the body crest do not exist for the low Reynolds number condition. This could be explained by a leeward movement of the separation point due to a change in the boundary layer from laminar to turbulent between the two Reynolds numbers. For the low Reynolds number the separation point is near the crest of the body, thereby the flow does not continue to expand around the body but simply proceeds downstream. For the high Reynolds number the separation point has moved leeward, thereby requiring the flow to make a compressive turn around the vortex sheet. This explanation is supported by comparing the low and high cross-flow Reynolds numbers, 0.16 x 10^6 and 0.60 x 10^6, respectively, with

the critical cross-flow Reynolds number of 0.40×10^6. If one uses the Reynolds number definition of Lamont and Hunt, (Reference 17) $R_d/\sin\alpha_b$, however, one obtains the values of 1.40×10^6 and 5.12×10^6, respectively, for α_b = 20 degrees. These values suggest that both the high and low Reynolds number conditions exhibit turbulent separation.

The strong embedded shock through the angle of attack plane which occurred for the low Reynolds number (Figure 27) also can be seen at α_b = 20 degrees, x/d = 8.5 and 11 (Figures 60b and c). The strength of the wave is larger, however, and decays faster for the high Reynolds number condition. This wave can be seen between the body vortices on the vapor screen photograph for α_b = 25 degrees and x/d = 6 (Figure 78). The region between the vortices becomes darker as the body is approached because of the rapidly decreasing static temperature brought about by the increasing Mach number. The sharp change from dark to light near the body marks the embedded shock wave. For x/d = 9 the vapor screen photograph (Figure 79) varifies that the shock wave essentially dissipates as shown by Figure 61b.

A perspective plot of the Mach number in the cross-flow plane for α_b = 10, 15, 20 and 25 degrees for all of the body stations is shown in Figures 62 through 65. The high Reynolds number measurements for Mach number compare qualitatively with those for low Reynolds number (Figures 29 through 32). One feature which is more noticeable at the high Reynolds number is the downstream recompression of the wake for α_b = 20 degrees and x/d = 11 (Figure 64c). This embedded shock wave can be seen on both of the vapor screen photographs (Figures 78 and 79) as the change from dark to light occurring outboard and slightly downstream of each body vortex. On the Mach number surface, Figure 64c, and total pressure surface, Figure 60c,

it appears as a slight drop in the level of the surface. This shock wave serves to recompress the portion of the fluid which is not trapped within the body vortex. That is, the fluid which is external to the cross-flow plane dividing streamline must turn downstream away from the plane of symmetry. The fluid internal to the dividing streamline turns toward the plane of symmetry and takes a spiral path down the leeside of the body.

An interesting feature of the Mach number distribution shown in Figure 65a are two points of very low Mach number just above the vortex. Examining Figure 61a it is observed that the total pressure of these points is also lower than the surrounding field. After looking through all of the survey planes of data it was found that this feature occurred at other angles of attack, body stations, and freestream conditions. The feature was always very small, i.e., usually one grid point, and it occurred above the primary body vortex; commonly on the very top row of grid points. Examining the Schlieren photographs for the corresponding angle of attack and flow conditions showed that there indeed was a flow disturbance at that location. Figure 64 shows the Schlieren photograph taken during the data acquisition for α_b = 25 degrees condition. A small but distinctive streak can be seen above the body vortex. It appears to emanate from the body surface near the tangency point of the ogive nose. Reviewing the open literature for documentation of this feature it was found that Werle (Reference 18) and Hsieh (Reference 19) suggested the existence of such a phenomenon. Using dye injection technique in a water tunnel Werle suggested that a secondary nose vortex pops off the surface and proceeds downstream above the body vortices. Using the surface oil flow technique at transonic speeds Hsieh suggested the same phenomenon. Hsieh's oil flows indicated that the vortex

lifted off the surface near the nose-body juncture and that it rotated in opposite rotational sense from the body vortex. The present data confirm the existence of such a vortex and document its location in the wake. Other angles of attack and freestream conditions for which this vortex was detected will be pointed out in later sections.

Figures 66 through 69 show perspective plots of the magnitude of the cross-flow velocity for α_b = 10, 15, 20, and 25 degrees for all of the body stations. Comparing the high Reynolds number measurements with the low Reynolds number data (Figures 33 through 36), certain differences are noted. For α_b = 10 degrees and 15 degrees the gradients of cross-flow velocity in the vortex core are somewhat sharper for the high Reynolds number. For α_b = 20 degrees, the discontinuity due to the shock between the vortices is stronger for the low Reynolds number than for the high Reynolds number. For α_b = 25 degrees high Reynolds number (Figure 69), the cross-flow plane shocks near the body crest and the secondary nose vortex are distinguishable. The free stagnation point in the cross-flow plane occurs on the z-axis at the point where the cross-flow velocity passes through zero. As the body is approached from this point the acceleration of the fluid toward the body is evident. The stagnation point was captured at both Reynolds numbers for all of the angles of attack and body stations except α_b = 25 degrees, x/d = 9. Judging from Figures 36b and 69b, it appears that the grid height was substantially less than needed.

The axial velocity component in the cross-flow plane for α_b = 10, 15, 20 and 25 degrees for all body stations is shown in Figures 70 through 73. For α_b = 10 and 15 degrees the most notable difference between the high Reynolds number and the low Reynolds number data (Figures 37 through 40)

is the sharper gradient of axial velocity near the vortex core and vortex sheet. The minimum value of u/U_∞ in the survey grid is consistently lower in the high Reynolds number data. The velocity defects in the core and the sheet are more severe and they persist farther down the body. For α_b = 20 degrees (Figure 72) the distributions show that the axial velocity defects have essentially disapperard by x/d = 8.5. Only at x/d = 6 is there a significant velocity defect in the core and vortex sheet. At an angle of attack of 25 degrees (Figure 73), for both high and low Reynolds numbers, the situation has reversed: a velocity excess exists in the core and the region between the core and the z-axis, whereas a uniform velocity defect exists outboard of the vortex. A slight velocity defect also exists in the vortex sheet. The large velocity defect above the vortex for x/d = 6 (Figure 73a) marks the secondary nose vortex.

Figures 74 through 77 show the local circulation in the cross-flow plane for α_b = 10, 15, 20 and 25 degrees for all of the body stations. For α_b = 10 and 15 degrees the high Reynolds number condition clearly shows, as expected, higher concentrations of circulation and larger total circulation compared to the low Reynolds number condition (Figures 41 and 42). Note the large negative circulation which occurs for the high Reynolds number at each of the first body stations. These negative values occur underneath the vortex sheet, between the primary separation* point near the crest of the body and a secondary separation point near the leeward generator. They are caused by one of two secondary vortices which lie very near the surface. Boersen (Reference 20) has obtained outstanding quality surface oil flow photographs which show the direction of rotation of these

*Separation refers to three dimensional separation; that is, convergence of body surface streamlines.

secondary vortices. The first vortex past the primary separation point rotates (looking from the rear of the body) in the counterclockwise direction and its mate, slightly to the left on the surface, rotates in the clockwise direction. The vortex with the clockwise rotation produces the large negative values of circulation seen for certain α_b's and x/d's. Another feature noted at α_b = 15 and 20 degrees (Figures 75 and 76), particularly α_b = 20 degrees, is the extremely rapid drop in vorticity along the vortex sheet near the body for the first body station. At the second and third body stations it has essentially disappeared. This feature is not clearly understood. One possible suggestion is that the negative circulation of the separation bubble protrudes into the positive circulation of the vortex sheet from the primary separation thereby cancelling vorticity.

The location of the vortex center in the cross-flow plane versus x/d for α_b = 10, 15, 20 and 25 degrees is shown in Figure 80. For α_b = 10 degrees it can be seen that the height of the vortex above the body is the same for both Reynolds numbers (Figures 45a and 80a) but the vortex is positioned farther outboard for the high Reynolds number (Figure 80b) as compared to the lower Reynolds number (Figure 45b). For $\alpha_b \geq 15$ degrees the y location of the vortex for both Reynolds numbers is identical, but the z coordinate shows significantly different trends with x/d for the two Reynolds numbers. For $\alpha_b \geq 15$ degrees the high Reynolds number vortex is farther from the body for the low x/d and closer to the body for large x/d. That is, the divergence angle between the vortex path and the body axis is lower at the high Reynolds number than at the low Reynolds number. This Reynolds number effect could have a significant impact on the forces and

moments produced by the fins on a finned body of revolution. For fins of small span a change in vortex position of .2d would produce, for example, sizable changes in force and moment variation with roll angle.

Figures 81 through 84 show the Schlieren photographs for α_b = 10, 15, 20 and 25 degrees along with the z-coordinate of the vortex center taken from Figure 80a. Comparing these photographs with those for the low Reynolds number, Figures 46 to 49, it is seen that the boundary between the light and dark more clearly marks the vortex center at the high Reynolds number. This is simply attributed to the higher air density of the flow in the wind tunnel. The secondary nose vortex can be clearly seen at α_b = 25 degrees, Figure 84, as mentioned previously, but it can also be seen at α_b = 20 degrees, Figure 83. For α_b = 20 degrees the secondary nose vortex appears as a light streak as compared to the dark streak at α_b = 25 degrees.

The vortex core radii and the angular orientation of the minor axis versus the axial location for α_b = 10 and 15 degrees are shown in Figures 85 and 86, respectively. The vortex core radii measured for high Reynolds number are almost identical to those for low Reynolds number (Figure 50). For α_b = 10 degrees the vortex orientation is identical for both low and high Reynolds numbers (Figures 51 and 86). For α_b = 15 degrees, high Reynolds number, the vortex orientation rotates clockwise down the body but not to the same extent as the low Reynolds number condition.

Figure 87 shows the total circulation in the survey grid versus body length for α_b = 10, 15, 20 and 25 degrees. One would expect that the high Reynolds number condition would yield higher values of total circulation than the low Reynolds number condition. This supposition is supported by

comparing Figure 52 and 87, except for one condition. For α_b = 10 and . 15 dgrees, data for the second and third body stations show that the high Reynolds number condition consistently yielded higher total circulation than the low Reynolds number. For α_b = 10 and 15 degress at the first body station, however, the circulation at the low Reynolds number is larger than that at the high Reynolds number. The reason for this exception is the negative circulation contributed by the secondary surface vortex which occurs at the high Reynolds number but not at the low Reynolds number. For α_b = 20 and 25 degrees no conclusion comparing high and low Reynolds can be made because certain grids did not capture all of the circulation. Another point should be made in interpreting the total circulation data in Figures 52 and 87. Each data point plotted is the total circulation in the interior of a particular survey grid. As the local circulation is non-zero on the boundary facing the body surface for every grid, then one must be careful in interpreting the results. The fact that the boundaries facing the body are the same (within one or two grids points) at a given angle of attack and body station allows one to make valid conclusions concerning effects of freestream conditions. However, one must not think that the data plotted in Figures 52 and 87 is the total circulation in the cross-flow plane.

The streamlines for α_b = 15 degrees and x/d = 7, 10 and 13 are shown in Figure 88. Comparing these streamlines with those for the low Reynolds number condition (Figure 53) the change in shape of the body vortex is clearly observed. The vortex flow associated with the high Reynolds number is significantly more elliptical than that of the low Reynolds number. This characteristic of the vortex wake cannot be seen in the cross-flow velocity field (Figures 22 and 55), but is distinct in a stream function

field. The reason for the elliptic shaped vortex at the high Reynolds number is not understood.

Figure 89 shows the z-coordinates of the secondary nose vortex versus x/d for α_b = 20 and 25 degrees. Schlieren photograph measurements of this vortex were made because the secondary nose vortex was detected only on certain survey grids and because of questions concerning interference of the probe on the small vortex. Figure 89 compares the Schlieren data and the survey data. The single data point for which the nose vortex was clearly detected in the survey regions is for α_b = 25 degrees, x/d = 6. The agreement of the survey data point and the Schlieren data is poor. Also shown in Figure 89 is the height of the individual survey grids. Comparing this with the nose vortex path from the Schlieren photographs clearly shows that it should have been detected on every grid for α_b = 20 and 25 degrees. Two possible reasons for errors exist in the survey data. First, the small nose vortex, roughly .1d in diameter, passed between the survey grid points and, as a result, it was not detected. Second, the large size of the probe compared to nose vortex caused the nose vortex to move or possibly burst. The Schlieren data in Figure 89 were measured from several photographs of the same flow field condition and are repeatable to within an error band of .05d.

3. Results for M_∞ = 3.01 and $R_d = 1.70 \times 10^6$

The cross-flow velocity field for α_b = 10, 15, 20 and 25 degrees for all body stations is shown in Figures 90 to 93. Two regions of interpolated data are noted in the vector fields: α_b = 15 degrees, x/d = 10 (Figure 91b) and α_b = 25 degrees, x/d = 6 (Figure 93a). The interpolated data for α_b = 15 degrees was not caused by probe interference, but by a programming error in the CTS; the points were simply skipped. The interpolated point at

α_b = 25 degrees is believed to be caused by interference.

Comparing the Mach 3 results (Figures 90 through 93) with those for Mach 2 high Reynolds number (Figures 55 through 58), important differences are noted even at an angle of attack of only 15 degrees. Very little rotational motion characteristic of the body vortex is noted at Mach 3 for the aft body stations of α_b = 15 degrees (Figure 91) and all of the body stations for α_b = 20 and 25 degrees (Figures 92 and 93). For α_b = 25 degrees (Figure 93) the cross-flow vector field clearly shows that a body vortex is essentially nonexistent for this freestream Mach number. The wake flow has none of the characteristics of a shed lifting vortex, but looks very much like the tear-drop wake of a circular cylinder perpendicular to a supersonic stream. Indeed, the cross-field Mach number for M_∞ = 3 and α_b = 25 degrees is 1.27. Lift on the cylinder is generated from very high pressure on the windward surface and not from leeward low pressure caused by a vortex wake. Reexamining the cross-flow vector field for Mach 2, α_b = 25 degrees, x/d = 9 (Figure 57b), the transformation of the wake into a teardrop shape can be seen.

Figures 94 through 97 show a perspective plot of the local total pressure in the cross-flow plane for α_b = 10, 15, 20 and 25 degrees for all of the body stations. The survey grids associated with Figures 95c, 96b, 96c and 97b do not have complete rows of grid points. These missing points were not surveyed in order to conserve wind tunnel time and because little of interest occurred there. As the CPS-1 perspective plotting routine uses a rectangular format, these unspecified survey points were automatically set at the lowest value in the grid.

For all of the angles of attack and body stations the nondimensional total pressure in the vortex core is extremely low; roughly one-tenth of

the freestream value (Figures 94 through 97). The minimum values of total pressure in the core for Mach 2 high Reynolds number (Figures 58 through 61) were a factor of two or three times larger. Not only is the total pressure in the wake quite low, but for α_b = 20 and 25 degrees this characteristic spreads over a large portion of the leeside flow. For example, at α_b = 20 degrees, x/d = 6 (Figure 96a) P_o/P_{o_∞} drops to 0.04 in the core and then rises very sharply in the angle of attack plane to roughly 0.7. At α_b = 20 degrees, x/d = 8.5 (Figure 96b) the total pressure ratio rises to only about 0.6 in a narrow ridge on the angle of attack plane. At α_b = 20 degrees, x/d = 11 (Figure 96c) the low total pressure region spans a region roughly 0.4d on each side of the angle of attack plane and extends 1.5d above the body. Also note the loss in total pressure associated with the secondary nose vortex on α_b = 15 degrees, x/d = 10 and 13 (Figures 95b and c), α_b = 20 degrees, x/d = 6 and 8.5 (Figures 96a and b), and α_b = 25 degrees, x/d = 6 (Figure 97a). Even though the height of the survey planes at Mach 3 were about the same as for Mach 2, the secondary nose vortex was detected at more body stations for Mach 3. The effect of Mach number on this vortex was to force it lower into the wake, i.e., closer to the body. Because of the size of the secondary nose vortex compared to the size of the cone probe it is doubtful that the total pressure, or any of the other measured quantities, meet the accuracy estimates discussed in Section III-3.

A perspective plot of the Mach number distribution in the cross-flow plane for α_b = 10, 15, 20 and 25 degrees for all of the body stations is shown in Figures 98 through 101. Several qualitative differences can be seen comparing the Mach 3 perspectives and the Mach 2 high Reynolds number perspectives (Figures 62 through 65). Significant acceleration of

the fluid toward the body in the angle of attack plane begins to occur at α_b = 15 degrees (Figure 99) for Mach 3 as compared to α_b = 20 degrees (Figure 64) for Mach 2. At α_b = 20 degrees, x/d = 6, Mach 2 (Figure 64a) the Mach number varies in the angle of attack plane from 1.98 to 2.38, while for Mach 3 it varies from 2.74 to 4.29. For α_b = 25 degrees (Figure 101) note the striking changes in Mach number which occur near the vortex core. In the inviscid flow just outside the core the Mach number is near 4 and in the core it is near 2. Changes of this magnitude do not occur for a freestream Mach number of 2. At x/d = 6 (Figure 101a) the high Mach number near the angle of attack plane only occurs along a very narrow ridge. At x/d = 9 (Figure 101b) these large variations in Mach number have been dissipated by viscosity. The location of the embedded cross-flow shock from the crest of the body has changed from M_∞ = 2, as would be expected. For M_∞ = 3 it appears to originate further past the crest of the body than what was observed for M_∞ = 2. However, this is difficult to determine from comparing Figures 65a and 101a because the decrease in the shock wave angle for M_∞ = 3 has changed substantially the path of the embedded wave through the cross-flow plane. The path of the embedded wave can be seen in Figure 101a as a drop-off in Mach number whose angle is roughly 60 degrees from the y-axis. The trace of other embedded waves higher in the wake can be seen in both Figure 101a and 101b.

Figures 102 through 105 show the perspective plot of the magnitude of the cross-flow velocity for α_b = 10, 15, 20 and 25 degrees for all of the body stations. This sequence of figures clearly shows the deterioration of the rotational motion about the body vortex as the angle of attack and

body length are increased. For example, at α_b = 10 degrees, x/d = 7 (Figure 103a) some degree of rotational motion exists about the core. At x/d = 10 (Figure 103b) only a small ridge of cross-flow velocity exists in the northwest direction from the vortex. At x/d = 13 (Figure 103c) this ridge has essentially disappeared, as it is replaced by a trough which extends northwesterly toward the free stagnation point in the cross-flow plane. The development of a trough of U_c represents decay of the body vortex and the development of a shear layer in the wake. This characteristic develops sooner along the body as the angle of attack increases, see for example, Figures 104 and 105.

The axial velocity component in the cross-flow plane for α_b = 10, 15, 20 and 25 degrees for all of the body stations is shown in Figures 106 through 109. For α_b = 10 and 15 degrees the perspective plots of the axial velocity show that there are no qualitative differences compared to the Mach 2 high Reynolds number data (Figures 70 and 71). For α_b = 20 degrees, however, some differences between the Mach 2 (Figure 72) and Mach 3 (Figure 108) begin to appear. For Mach 3 a velocity defect in the core occurs for the first body station and farther down the body a defect occurs where one would commonly locate the vortex sheet. For α_b = 25 degrees at Mach 3 (Figure 109), an axial velocity defect occurs along the development of the shear layer and is well marked at x/d = 9. Mach 2, on the other hand, has a velocity excess over a large region near the angle of attack plane and a defect outboard of the region.

Figures 110 through 113 give the local circulation in the cross-flow plane for α_b = 10, 15, 20 and 25 degrees for all of the body stations. Comparing the Mach 3 data for α_b = 15 degrees (Figure 111) with that for

Mach 2 (Figure 75) it is seen that the transition from core concentrated vorticity to a diffused vortex cloud occurs earlier along the body for Mach 3. At x/d = 13 (Figure 111c) note that a semblance of high core vorticity cannot be found for Mach 3. At the last body station for α_b = 20 and 25 degrees (Figures 112c and 113b) the cylinder wake has none of the vorticity characteristics of the body vortex wake but shows a viscous shear layer character. One observes that almost all of the vorticity is contained in a ridge extending from the crest of the body toward the top corner of the survey grid on the z-axis. For α_b = 25 degrees, x/d = 6 (Figure 113a) the negative circulation of the secondary nose vortex can be seen on the edge of the survey grid roughly three grid points from the z-axis. The negative circulation point near the nose vortex on the z-axis has not been explained.

The location of the vortex center in the cross-flow plane versus x/d for α_b = 10 and 15 degrees is shown in Figure 114. Comparing the z coordinates of the vortex for Mach 3 with that for Mach 2 (Figure 80a) shows that they are essentially identical. That is, when a body vortex is defined, the freestream Mach number had no effect on the height of the vortex in the wake. Comparing the y-coordinate for the two Mach numbers reveals that for α_b = 10 degrees the y-coordinates are identical, but for α_b = 15 degrees there is a measurable difference. For Mach 3 (Figure 114b) the vortex is closer to the angle of attack plane at the forward body stations and then shifts outboard slightly as it moves down the body. For α_b = 20 and 25 degrees at Mach 3 the vortex location could not be measured because a center could not be located on contour plots of P_o and U_c. Contours of P_o and U_c are not closed as one would expect for a vortex center but are

nearly parellel lines extending from the crest of the body toward the downstream direction in the cross-flow plane.

Figures 115 through 118 show the Schlieren photographs for α_b = 10, 15, 20 and 25 degrees along with the z-coordinate of the vortex center taken from Figure 114a. For α_b = 10 and 15 degrees (Figures 115 and 116) the sharp contrast between the dark and light regions below and above the vortex indicate the existence of a well defined vortex over the exposed portion of the body. For α_b = 20 and 25 degrees (Figures 117 and 118) the Schlieren photographs show that the body vortex probably does not exist beyond x/d $\approx$ 5 and 4, respectively. This is consistent with the flow field survey data. The secondary nose vortex can be distinguished on the photographs for α_b = 20 and 25 degrees. It is not as prominent, however, as on the Mach 2 high Reynolds number Schlieren photographs. For α_b = 15 degrees the nose vortex cannot be seen on the Schlieren photograph (Figure 116) but it was detected on the survey grids; see for example, Figures 95 and 99.

The vortex core radii and the angular orientation of the minor axis versus axial location for α_b = 10 and 15 degrees are shown in Figures 119 and 120, respectively. The data for the vortex core radii show that, when the vortex core exists, the core is circular. This is somewhat surprising as the elliptic distortion of the core would seem to be the precursor of the shear layer development. The orientation of the y'-axis of the vortex for Mach 3 (Figure 120) is negative for the first body station as compared to zero for Mach 2. The orientation at the first body station for α_b = 15 degrees for Mach 3 is also less than at Mach 2.

Figure 121 shows the total circulation in the survey grid versus body length for α_b = 10, 15, 20 and 25 degrees. Comparing this figure with that

for Mach 2 high Reynolds number (Figure 87), it is seen that for α_b = 10 and 15 degrees the Mach number change had little effect on total circulation in the field. For α_b = 20 and 25 degrees the data indicate that the Mach 2 wake contains significantly more circulation than the Mach 3 wake. This characteristic could be related to the change in the wake from a vortex cloud to a shear layer for Mach 2 and 3, respectively. To obtain an indication of the relationship of total circulation to angle of attack of the body, a least squares fit of the data was calculated. Using the total circulation data interpolated for x/d = 8 and 11 and α_b = 10, 15, and 20 degrees, a fit of Γ_t versus $\sin^m \alpha_b$ was effected. The values of m where 2.82, 2.33 and 1.90 for M_∞ = 1.95 and R_d = 0.48 x 10^6, M_∞ = 2.00 and R_d = 1.75 x 10^6, and M_∞ = 3.01 and R_d = 1.70 x 10^6, respectively. The correlation coefficients for the power fits were approximately 0.99, indicating that the plot of log Γ_t versus log sin α_b is very close to linear. The fit of the data demonstrates that the total circulation grows with angle of attack at a substantially lower rate as the Reynolds number and Mach number increases.

In certain theoretical approaches, see for example, References 10 and 11, the division of total vorticity between the vortex sheet and primary body vortex is needed from experimental data. The definition of what portion of the total vorticity is attributed to the primary body vortex, Γ_p, versus the vortex sheet, and the asscciated numerical procedures were discussed in Section III-4-d. Figure 122 shows the ratio of primary body vortex circulation to total circulation as a function of the parameter α_b x/d for all three freestream conditions. Also plotted in the figure are the data of Mello (Reference 2). The parameter α_b x/d was

chosen because it yielded a good correlation of the data for each of the freestream conditions, angles of attack, and body stations. Comparing the present data with that of Mello, it is clear that the present measurements demonstrate that a much smaller portion of the total circulation is located in the concentrated vortex than previously measured. That is, the present measurements show that the vorticity in the sheet is typically larger than that in the vortex core. In comparing the present data with that of Mello it must be mentioned that this new insight could be due in part to the definitions of core and sheet vorticity. The definitions used by Mello were not given in Reference 2, so a comparison with definitions given in Section III-4-d cannot be made.

Figure 123 shows the cross-flow plane streamlines for α_b = 15 degrees and x/d = 7, 10 and 13. Comparing this figure with that for Mach 2 high Reynolds number (Figure 88) one obtains a graphic indication of the effects of compressibility in the cross-flow plane. The vortex is significantly elongated in the streamwise direction for Mach 3. The body vortex produces little diversion of the external flow for Mach 3, but simply provides a streamlining of the cylinder wake. The very slow rotational speed of the vortex for Mach 3 can be concluded from the number of streamlines enclosing the body vortex. This lack of flow rotation is not due to less circulation than Mach 2, as can be seen from comparing Figures 87 and 121, but it is due to the lack of organized vorticity.

From the streamline plot for Mach 3 (Figure 123) one obtains the distinct impression that the height of the wake is substantially larger for Mach 3 compared to Mach 2. A means of quantifying the wake height is shown in Figure 124. The figure plots the attachment point on the z-axis of the dividing streamline in the cross-flow plane versus angle

of attack of the body for a ten caliber long body. Present data for high Reynolds number Mach 2 and Mach 3 are shown along with the incompressible flow data of Grosche (Reference 5). As is clear from the figure, the change in wake height from Mach 2 to Mach 3 is minimal up to an α_b of 20 degrees. The impression of a very long wake is simply due to the narrowing of the wake. Comparing the wake height of the present data to that of incompressible flow, the elongation of the wake due to cross-flow compressibility is demonstrated. Interpolating the data in Figure 124 at an angle of attack of 20 degrees permits one to conclude that significant compressibility effects already occur for a freestream Mach number of unity.

Figure 125 shows the z-coordinate of the secondary nose vortex versus x/d for α_b = 20 and 25 degrees. For $x/d < 6$ at α_b = 20 degrees and $x/d < 5$ at α_b = 25 degrees the secondary nose vortex at both Mach 2 (see Figure 89) and Mach 3 have virtually the same height in the wake. Beyond these axial locations, the nose vortex for Mach 3 deviates more quickly away from the body compared to Mach 2. For example, at α_b = 25 degrees for Mach 3 the nose vortex is trailing downstream at nearly the direction of the freestream flow. The existence of the secondary nose vortex for α_b = 15 degrees for Mach 3 is suggested on certain perspective plots at the three axial body stations, see for example, Figures 95 and 99. Its path was not given as part of Figure 125, however, because it could not be seen on the Schlieren photograph, Figure 116.

SECTION V

CONCLUSIONS AND RECOMMENDATIONS

The following conclusions and recommendations are drawn from the present investigation:

1. The experimental technique of strong interaction between theory and data acquisition was successful. Using theoretical predictions both before and during the experiment to improve the data acquisition process should be expanded in the future.
2. The technique of mainpulating a flow field survey probe in order to reduce probe interference was used successfully. This technique could be extended by minimizing the need for manual review of the data during data acquisition. Initially established optimization criteria could be programmed on a computer which surveyed the data, computations made for probe manipulation, and then commands issued to reposition the probe.
3. Because of probe interference that was detected when the probe angle of attack was large for initial measurements at a grid point, the sensitivity of body vortex flow to probe intrusion was demonstrated. For vortex flows that are more sensitive, such as asymmetric vortex shedding at very high angle of attack, the present technique is not recommended. A laser anemometer system should give the most reliable data for the asymmetric vortex wake.
4. Even at a 10-degree angle of attack the data show a well defined body vortex of significant size and strength. Attached lifting surfaces, such as fins, immersed in this vortex would show many of the non-linear forces and moments normally associated with higher angles of attack.

5. For M_∞ = 2 and α_b = 20 degrees the body vortex evolved down the length of the body from a circular shape to a strongly elliptical shape. This is contrary to body vortex development in incompressible flow where the large circular vortices cause a large diversion of the flow around the vortex.

6. The measured distribution of circulation in the cross-flow plane for Mach 2 shows that for α_b = 10 and 15 degrees and $x/d < 10$ the circulation is generally restricted to the vortex core and the vortex sheet. For α_b = 20 and 25 degrees the vorticity is diffused in the cross-flow plane to the extent that it could be described as a vortex cloud.

7. The present data for location of the body vortex in the cross-flow plane compare well with previous data of Jorgensen and Perkins (Reference 1) and Mello (Reference 2). As these previous investigators used different pointed nose shapes than the present model, one can conclude that vortex position is not sensitive to this parameter.

8. The concentration of vorticity along the vortex feeding sheet is a maximum near the body and then decreases near the vortex core. For certain cases, an extremely rapid decrease and then increase in sheet vorticity is observed near the body.

9. Measurements of an elliptic shaped body vortex core are presented for α_b = 10 and 15 degrees. For α_b = 20 and 25 degrees the core is so elongated in the z-direction that core dimensions cannot be defined.

10. For the high Reynolds number Mach 2 condition the body vortex does not move away from the body as rapidly as for the low Reynolds number condition.

11. A secondary nose vortex was found above the primary body vortex for certain freestream conditions and angles of attack. Although

quantitative measurements of strength of the nose vortex were not obtained because of the size of the nose vortex, it is not believed significant with regard to missile flight dynamics.

12. The primary body vortex position in the cross-flow plane was measured for $M_\infty = 3$ at $\alpha_b = 10$ and 15 degrees. For $\alpha_b = 20$ and 25 degrees cross-flow compressibility distorts the body vortex to an extent that a body vortex cannot be defined. Local circulation in the cross-flow plane for $\alpha_b = 20$ and 25 degrees shows that the vorticity is primarily located in a shear layer originating near the crest of the body and extending downstream. This elongated reverse flow region causes the wake to look like that behind a circular cylinder perpendicular to a supersonic stream.

13. Although the wake is distorted due to compressibility, the wake height for Mach 2 and 3 are roughly the same for $\alpha_b \leq 20$ degrees.

14. The total circulation in the wake for $\alpha_b \leq 15$ degrees did not change between Mach 2 and Mach 3. For $\alpha_b \geq 20$ degrees the measurements indicate that the Mach 2 wake contains significantly more circulation than the Mach 3 wake.

15. The theoretical technique used for predicting the wake flow in the present experiment was generally accurate for freestream Mach number 2, but was not reliable for Mach 3. The relatively large cross-flow Mach numbers for $M_\infty = 3$ violated one of the critical assumptions in the theory. Different theoretical techniques, such as finite difference codes, should be developed to predict slender body wakes with high cross-flow Mach number.

REFERENCES

1. Jorgensen, L. H., and E. W. Perkins, "Investigation of Some Wake Vortex Characteristics of an Inclined Ogive-Cylinder Body at Mach No. 2," NACA Report 1371, May, 1955.

2. Mello, J. F., "Investigation of Normal Force Distributions and Wake Vortex Characteristics of Bodies of Revolution at Supersonic Speeds," J. Aero. Sci., Vol. 26, March 1959, p. 155-168.

3. Tinling, B.E., and C. Q. Allen, "An Investigation of the Normal Force and Vortex Wake Characteristics of an Ogive Cylinder," NASA TN D-1297, April, 1962.

4. Fiechter, M., "Uber Wirbelsysteme an Schlanken Rotationskorpern und Ihren Einfluss uaf die Aerodynamischen Beiwerte," Deutsch-Franzosisches Forschungsinstitut, Saint-Louis (I.S.L.) Bericht 10/66, 1966.

5. Grosche, F. R., "Wind Tunnel Investigation of the Vortex System Near an Inclined Body of Revolution With and Without Wings," AGARD-CP-71-71, Aerodynamic Interference, Jan. 1971.

6. Fidler, J. E., J. N. Nielsen, and R. G. Schwind, "An Investigation of Slender-Body Wake Vortices," AIAA 15th Aerospace Sciences Meeting, AIAA Paper No. 77-7, Los Angeles, Calif., Jan. 1977.

7. Yanta, W. J., and A. B. Wardlaw, "Laser Doppler Velocimeter Measurements of Leeward Flowfields on Slender Bodies at Larger Angle of Attack," AIAA 10th Fluid and Plasmadynamics Conf., AIAA Paper No. 77-660, Albuquerque, New Mexico, June, 1977.

8. Owen, F. K., "Wake Vortex Measurements of Bodies at High Angle of Attack," AIAA 16th Aerospace Sciences Meeting, AIAA Paper No. 78-23, Huntsville, Ala., Jan. 1978.

9. Martindale, W. R. and T. R. Penney, "AFATL High Alpha Aerodynamics," Arnold Engineering Development Center/VKF, Project No. V41A-R7A, July 1977.

10. Oberkampf, W. L., and J. D. Nicolaides, "Aerodynamics of Finned Missiles at High Angle of Attack," AIAA Journal, Vol. 9, No. 12, December 1971, p. 2378-2384.

11. Oberkampf, W. L., "Prediction of Roll Moments on Finned Bodies in Supersonic Flow," J. of Spacecraft and Rockets, Vol. 12, No. 1, January 1975, p. 17-21.

12. Trimmer, L. L. and E. L. Clark, "Transformation of Axes Systems by Matrix Methods and Application to Wind Tunnel Data Reduction," AEDC-TDR-63-224, Oct. 1963.

13. "Equations, Tables, and Charts for Compressible Flow," by Ames Research Staff, NACA-Rept.-1135, 1953, p. 7.

14. Jones, J. H., and J. E. O'Hare, "Flow Visualization Photographs of a Yawed Tangent Ogive Cylinder at Mach Number 2," Arnold Engr. Development Center, AEDC-TR-73-45, March, 1973.

15. Jorgensen, L. H., "Predictions of Static Aerodynamic Characteristics for Slender Bodies Alone and With Lifting Surfaces to Very High Angles of Attack," NASA TR-R-474, Sept. 1977.

16. Thomson, K. D. and D. F. Morrison, "The Spacing, Position and Strength of Vortices in the Wake of Slender Cylindrical Bodies at Large Incidence," J. Fluid Mechanics, Vol. 50, Part 4, p. 751-783, 1971.

17. Lamont, P. J. and B. L. Hunt, "Pressure and Force Distributions on a Sharp-Nosed Circular Cylinder at Large Angles of Inclination to a Uniform Subsonic Stream," J. of Fluid Mechanics, Vol. 76, part 3, 1976, pp. 519-559.

18. Werle, H., "Separation on Axisymmetrical Bodies at Low Speed," La Recherche Aeronautique, No. 90, Sept.-Oct., 1962.

19. Hsieh, T., "An Investigation of Separated Flows About a Hemisphere-Cylinder at Incidence in the Mach Number Range from 0.6 to 1.5," AIAA 15th Aerospace Sciences Meeting, AIAA Paper No. 77-179, Los Angeles, Calif., January, 1977.

20. Boersen, S. J., "Reynolds Number Effects on Pressure and Normal Force Distributions Along Conically Pointed Circular Cylinder at Freestream Mach Number 2.3," National Aerospace Lab. NLR, Report NLR-TR-75124-U, The Netherlands, 1975.

21. Bartel, T. J., "Supersonic Flow Measurements in the Body Vortex Wake of an Ogive Nose Cylinder," Univ. of Texas at Austin, M.S. Thesis, Dec. 1978.

22. "Test Facilities Handbook," Arnold Engineering Development Center, Arnold AFS, Tenn., May 1974.

TABLE 1. CTS ATTITUDE AND POSITION UNCERTAINTIES

Motion	Drive System Uncertainty	Model Attitude and Position Uncertainty
x'	$\pm$ 0.001 mm (0.005 in.)	$\pm$ 0.013 mm (0.050 in.)
y'	---	$\pm$ 0.020 mm (0.080 in.)
z'	$\pm$ 0.001 mm (0.005 in.)	$\pm$ 0.015 mm (0.060 in.)
α'	$\pm$ 0.05 deg.	$\pm$ 0.10 deg.
ψ'	$\pm$ 0.05 deg.	$\pm$ 0.10 deg.
ϕ'	$\pm$ 0.20 deg.	$\pm$ 0.20 deg.
η'	$\pm$ 0.03 deg.	---

The yaw angles ψ' and η' are used to obtain both yaw angle and lateral displacement.

TABLE 2. PROBE CALIBRATION FREESTREAM CONDITIONS

M_∞	$R_d \times 10^{-6}$
1.51	1.00
2.00	.85
3.01	.75
4.02	1.55

TABLE 3. SURVEY FREESTREAM CONDITIONS

M_∞	$R_d \times 10^{-6}$	P_o kPa (PSIA)	T_o °R (°K)	P_o' kPa (PSIA)	P_∞ kPa (PSIA)	V_∞ M/Sec (Ft/Sec)	q_∞ kPa (PSIA)
1.95	0.48	60.0 (8.7)	347 (624)	44.8 (6.5)	8.34 (1.21)	548.6 (1800)	22.1 (3.2)
2.00	1.75	211.0 (30.6)	328 (590)	152.4 (22.1)	27.02 (3.92)	514.0 (1775)	75.8 (11.0)
3.01	1.70	337.8 (49.0)	321 (578)	109.6 (15.9)	9.03 (1.31)	644.6 (2115)	57.2 (8.3)

TABLE 4. FLOW FIELD SURVEY CONDITIONS

M_∞	$R_d \times 10^{-6}$	α_b(deg)	x/d
2.00	1.75	10	8,11,14
2.00	1.75	15	7,10,13
2.00	1.75	20	6,8.5,11
2.00	1.75	25	6,9
1.95	.48	10	8,11,14
1.95	.48	15	7,10,13
1.95	.48	20	6,8.5,11
1.95	.48	25	6,9
3.01	1.70	10	8,11,14
3.01	1.70	15	7,10,13
3.01	1.70	20	6,8.5,11
3.01	1.70	25	6,9

TABLE 5. QUANTITY OF SURVEY DATA

α_b (deg)	x/d	$M_\infty = 1.95$, $R_d = 0.48 \times 10^6$		$M_\infty = 2.00$, $R_d = 1.75 \times 10^6$		$M_\infty = 3.01$, $R_d = 1.70 \times 10^6$	
		Pts. Per Grid	Repeat Pts.	Pts. Per Grid	Repeat Pts.	Pts. Per Grid	Repeat Pts.
10	8	78	21	77	0	78	19
10	11	128	0	128	0	128	0
10	14	179	0	179	14	158	55
15	7	98	16	97	22	98	23
15	10	168	11	167	42	163	20
15	13	224	9	223	6	205	44
20	6	129	40	120	38	127	29
20	8.5	213	32	189	72	201	40
20	11	261	36	222	31	234	28
25	6	168	49	147	24	146	18
25	9	213	53	188	28	195	63
		1859	267	1737	279	1733	339

TABLE 6. NUMBER OF GRID POINTS IN FINAL DATA SET

	α_b (deg.)	x/d	No. of pts. per grid	No. of final data pts. with $\lvert\alpha_{VT}\rvert > 20°$
M_∞ = 1.95 and R_d = 0.48 x 10^6	10	8	78	0
	10	11	128	0
	10	14	179	0
	15	7	98	1
	15	10	168	0
	15	13	224	0
	20	6	129	0
	20	8.5	213	2
	20	11	261	0
	25	6	168	2
	25	9	213	0
			1859	5
M_∞ = 2.00 and R_d = 1.75 x 10^6	10	8	77	0
	10	11	128	0
	10	14	179	0
	15	7	97	1
	15	10	167	4
	15	13	223	2
	20	6	127	12
	20	8.5	189	1
	20	11	222	1
	25	6	147	56
	25	9	188	10
			1744	87
M_∞ = 3.01 and R_d = 1.70 x 10^6	10	8	78	1
	10	11	128	0
	10	14	158	0
	15	7	98	1
	15	10	167	0
	15	13	205	0
	20	6	127	0
	20	8.5	201	0
	20	11	234	0
	25	6	147	33
	23	9	195	5
			1738	40

TABLE 7. PERCENT FREESTREAM UNCERTAINTIES

Calibration M_∞	M_∞	P_o	T_o	p_∞	q_∞	R_d
1.5	1.7	0.2	0.5	3.6	0.4	0.9
2.0	0.8	↓	↓	2.5	0.9	1.0
3.0	0.6	↓	↓	2.6	1.4	1.2
4.0	0.5	↓	↓	2.4	1.5	1.2

TABLE 8. REPEATABILITY STATISTICS FOR FLOW FIELD DATA

Statistics*		$M_\infty = 1.95$, $R_d = 0.48 \times 10^6$	$M_\infty = 2.00$, $R_d = 1.75 \times 10^6$	$M_\infty = 3.01$, $R_d = 1.70 \times 10^6$
α_{VT}	avg (deg.)	7.8	8.0	8.8
$P_o/P_{o\infty}$				
Precision Pts:	$\bar{x}$	.009	.011	.005
	σ	.012	.016	.006
	n	66	66	97
Accuracy Pts:	$\bar{x}$	.032	.075	.069
	σ	.045	.113	.108
	n	94	144	161
M				
Precision Pts:	$\bar{x}$	.012	.017	.007
	σ	.019	.034	.011
	n	72	70	106
Accuracy Pts:	$\bar{x}$	.029	.080	.172
	σ	.043	.117	.265
	n	95	143	159
u/U_∞				
Precision Pts:	$\bar{x}$	.002	.002	.001
	σ	.003	.003	.001
	n	69	64	103
Accuracy Pts:	$\bar{x}$	.010	.019	.027
	σ	.013	.030	.042
	n	97	149	157
v/U_∞				
Precision Pts:	$\bar{x}$	.003	.004	.001
	σ	.005	.005	.001
	n	67	67	103
Accuracy Pts.	$\bar{x}$	.017	.025	.026
	σ	.021	.036	.035
	n	97	145	163

TABLE 8. (CONCLUDED)

Statistics*		$M_\infty = 1.95$, $R_d = 0.48 \times 10^6$	$M_\infty = 2.00$ $R_d = 1.75 \times 10^6$	$M_\infty = 3.01$, $R_d = 1.70 \times 10^6$
w/U_∞				
Precision Pts:	$\bar{x}$	.006	.005	.002
	σ	.010	.007	.003
	n	70	65	104
Accuracy Pts:	$\bar{x}$	.019	.049	.045
	σ	.026	.075	.058
	n	96	142	163

* $\bar{x}$ is defined as the average of the sample space, σ is the standard deviation based on a zero mean, and n is the number of points in the sample space.

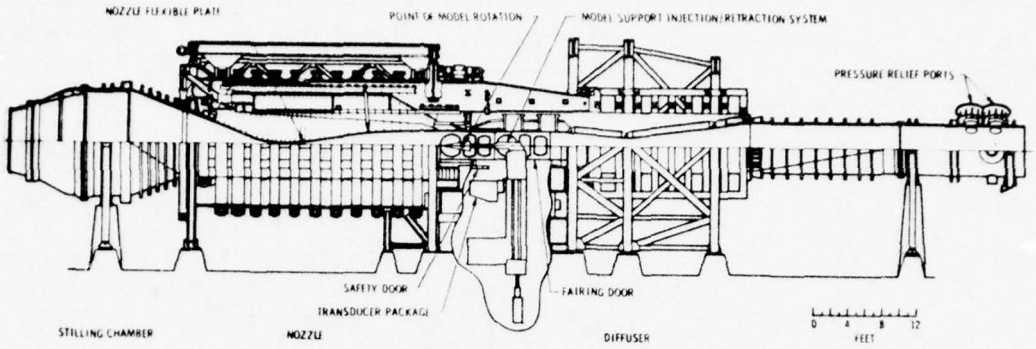
TABLE 9. COMBINED REPEATABILITY STATISTICS FOR THE EXPERIMENT*

Measured Parameter	Precision repeat data		Accuracy repeat data	
	$\bar{x}$	σ	$\bar{x}$	σ
$P_o/P_{o\infty}$	.008	.011	.062	.099
M	.012	.022	.105	.183
u/U_∞	.002	.002	.020	.033
v/U_∞	.002	.004	.023	.032
w/U_∞	.004	.009	.040	.059

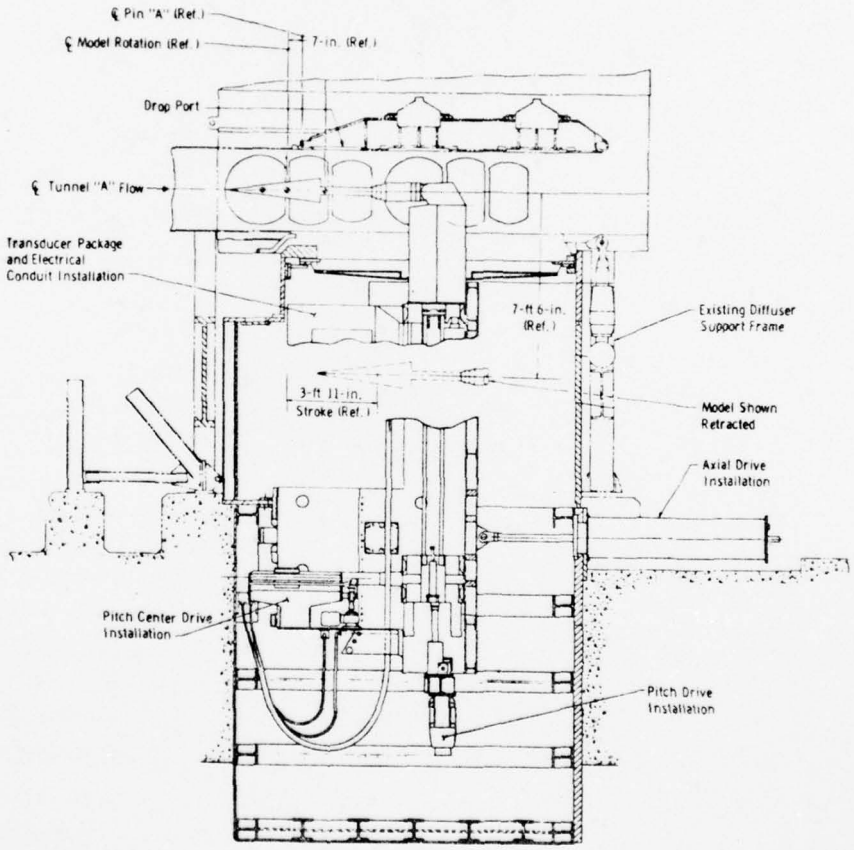
* $\bar{x}$ is the average of the sample space and σ is the standard deviation based on a zero mean.

TABLE 10. RATIO OF PRIMARY VORTEX CIRCULATION TO VORTEX CORE CIRCULATION

α_b (deg.)	x/d	M_∞= 1.95, R_d = 0.48 x 10^6	M_∞= 2.00, R_d = 1.75 x 10^6	M_∞= 3.01, R_d = 1.70 x 10^6
10	8	1.28	1.25	1.27
10	11	1.34	1.19	1.17
10	14	1.28	1.25	1.17
15	7	1.22	1.12	n/a
15	10	1.27	1.17	n/a
15	13	1.28	1.26	n/a

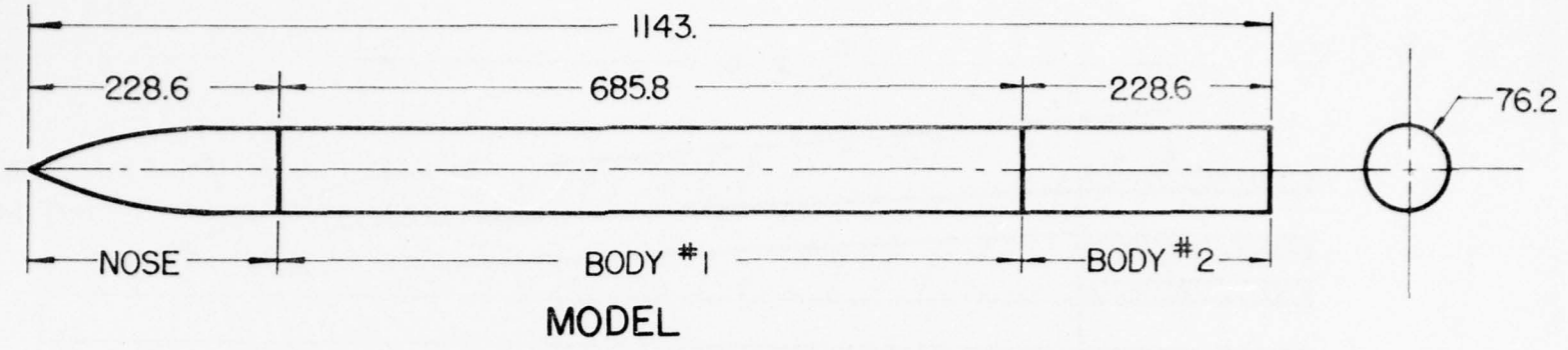


(a) Tunnel A Assembly



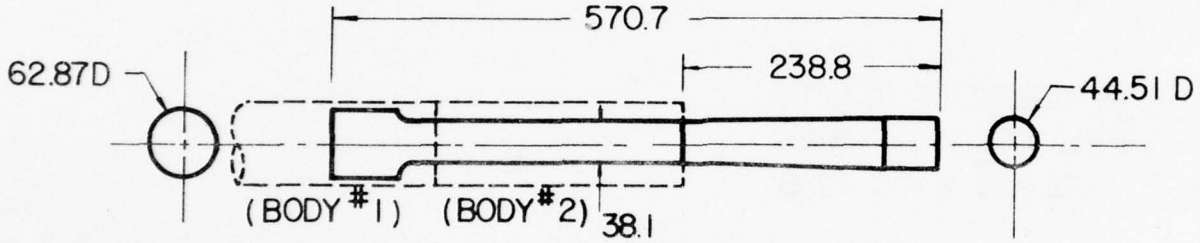
(b) Tunnel A Model Injection System

Figure 1. VKF Tunnel A (from Reference 22)



MODEL

ALL UNITS IN mm



STING

Figure 2. Schematic of Model and Sting

ALL DIMENSIONS IN mm
EXCEPT AS NOTED

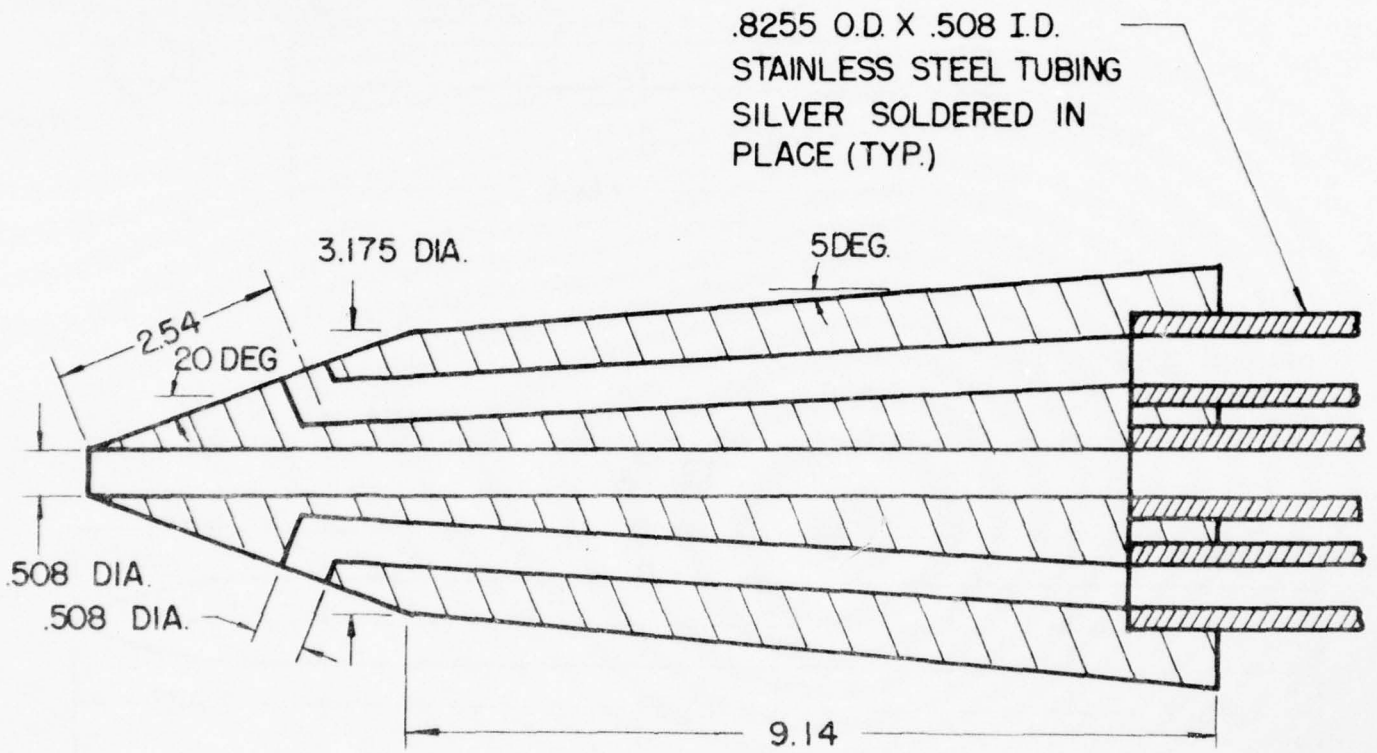
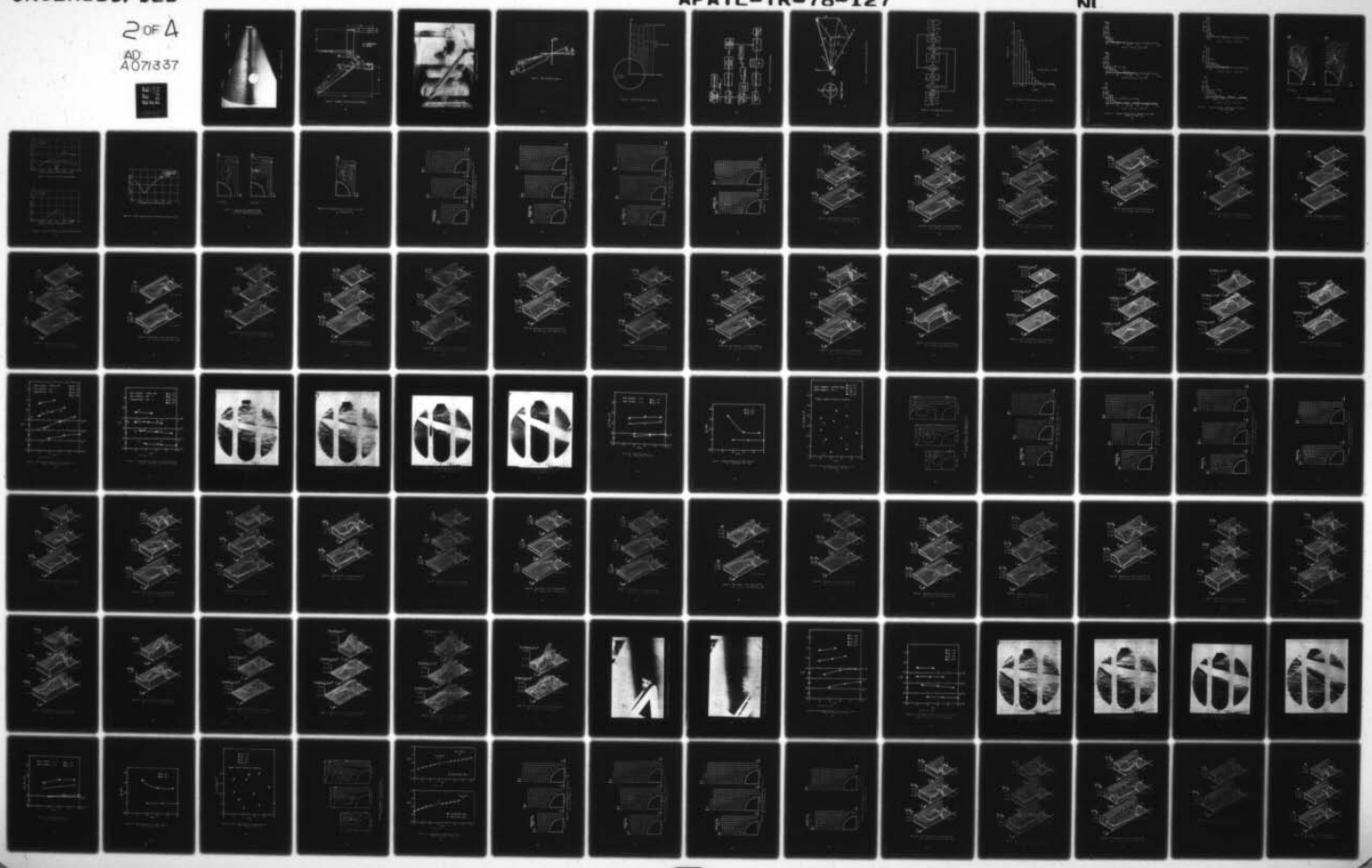


Figure 3 Cross-Section of the Probe

AD-A071 337 TEXAS UNIV AT AUSTIN DEPT OF MECHANICAL ENGINEERING F/G 16/2
SUPERSONIC FLOW MEASUREMENTS IN THE BODY VORTEX WAKE OF AN OGIV--ETC(U)
NOV 78 W L OBERKAMPF, T J BARTEL F08635-77-C-0049

UNCLASSIFIED AFATL-TR-78-127 NL

2 OF 4
AD A071337



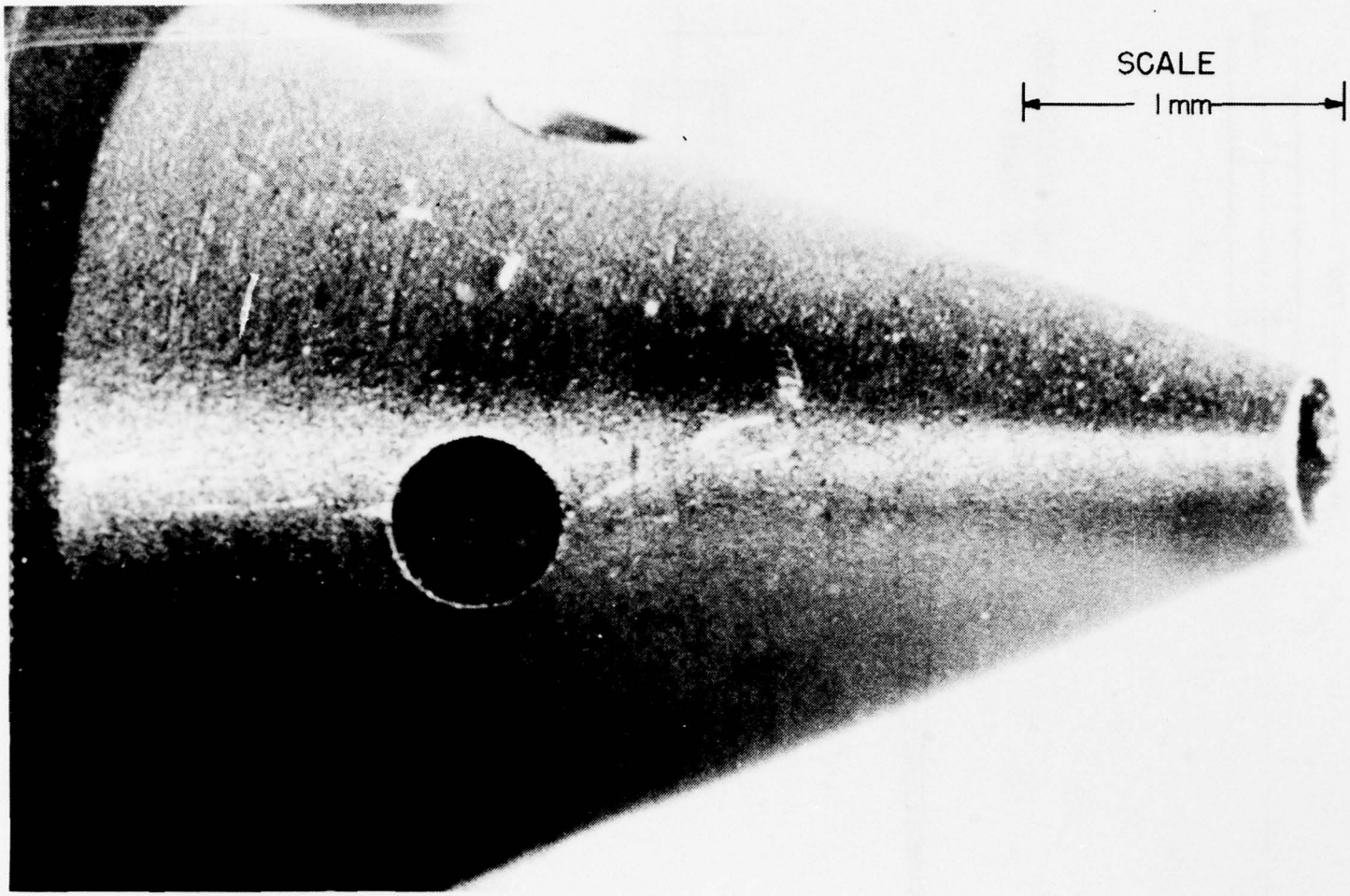


Figure 4. Photograph of Probe Tip

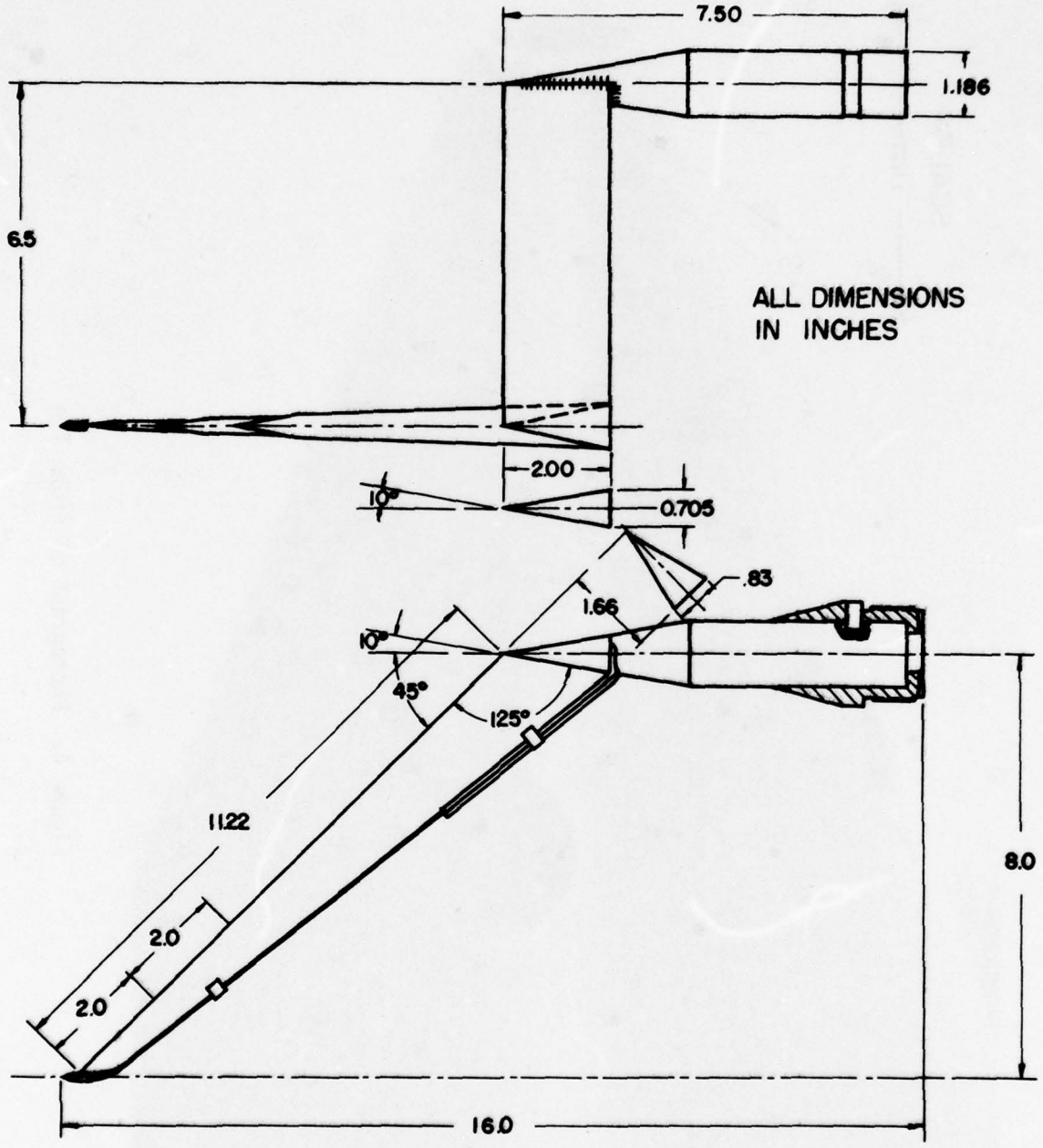


Figure 5. Schematic of Probe and Strut Assembly

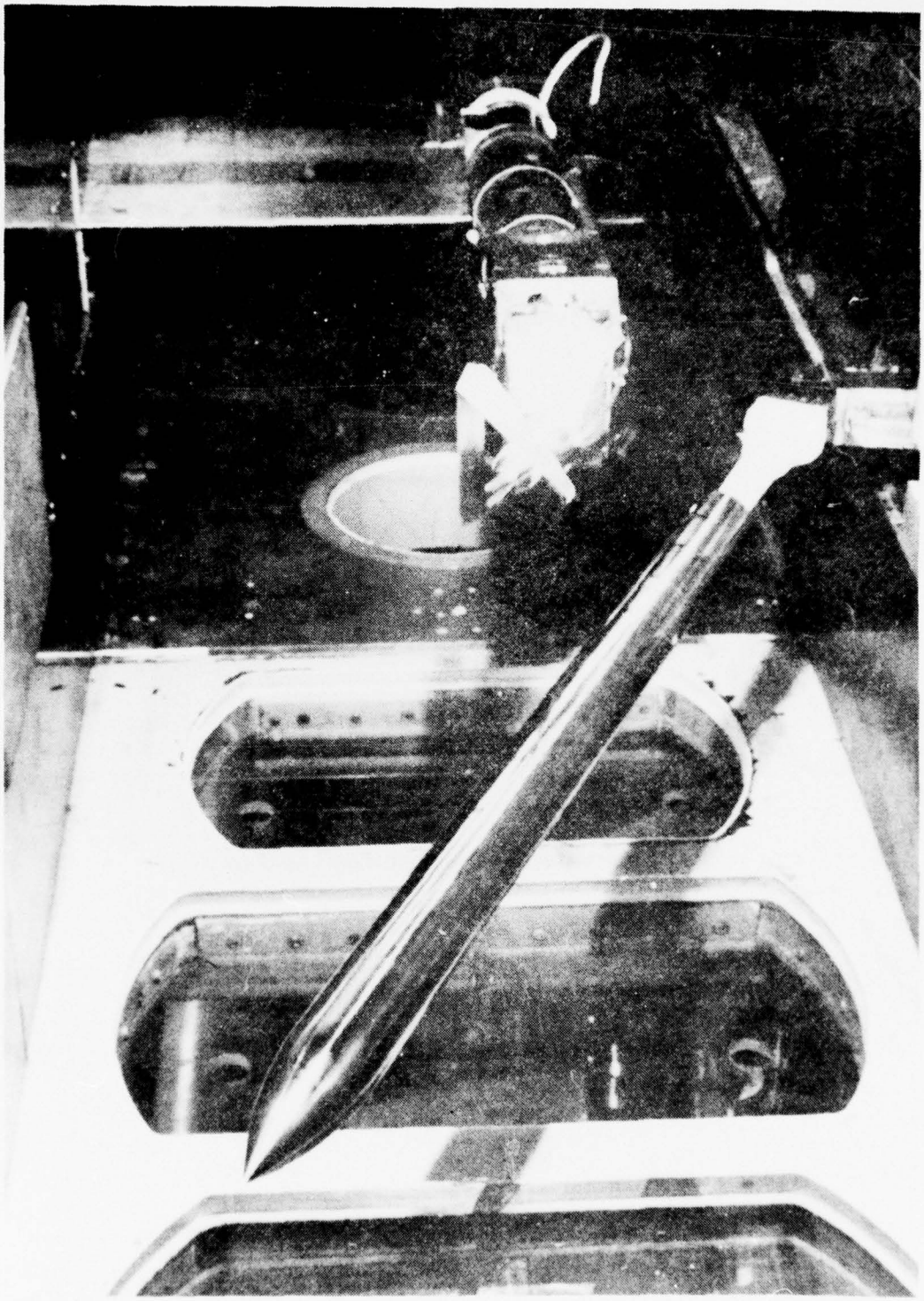


Figure 6. Wind Tunnel Installation

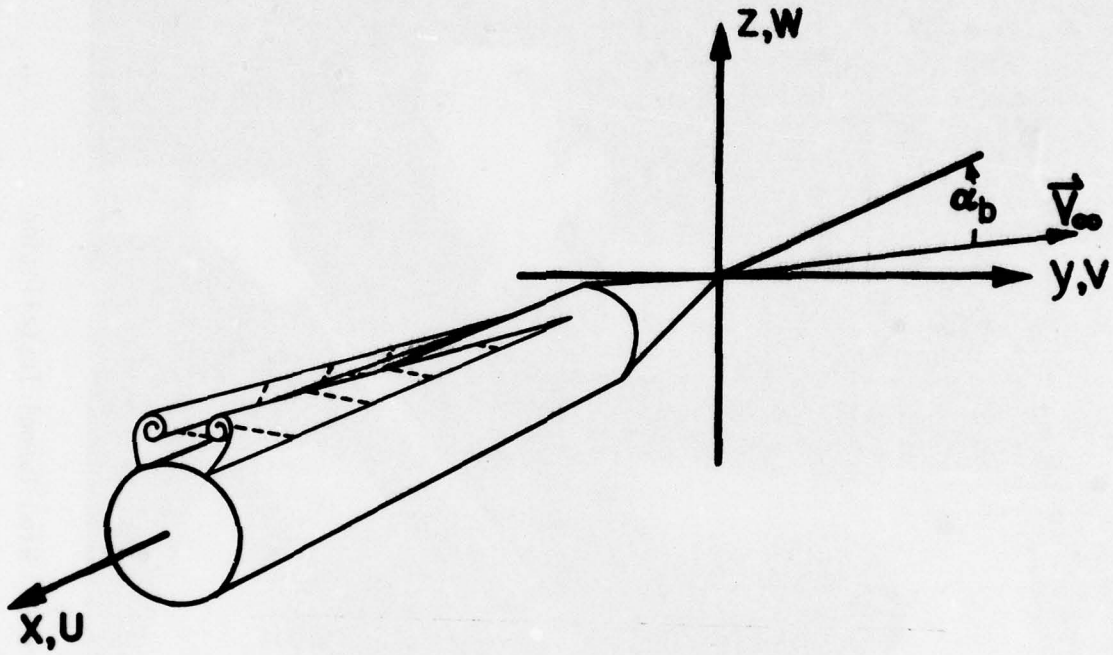


Figure 7. Body Coordinate System

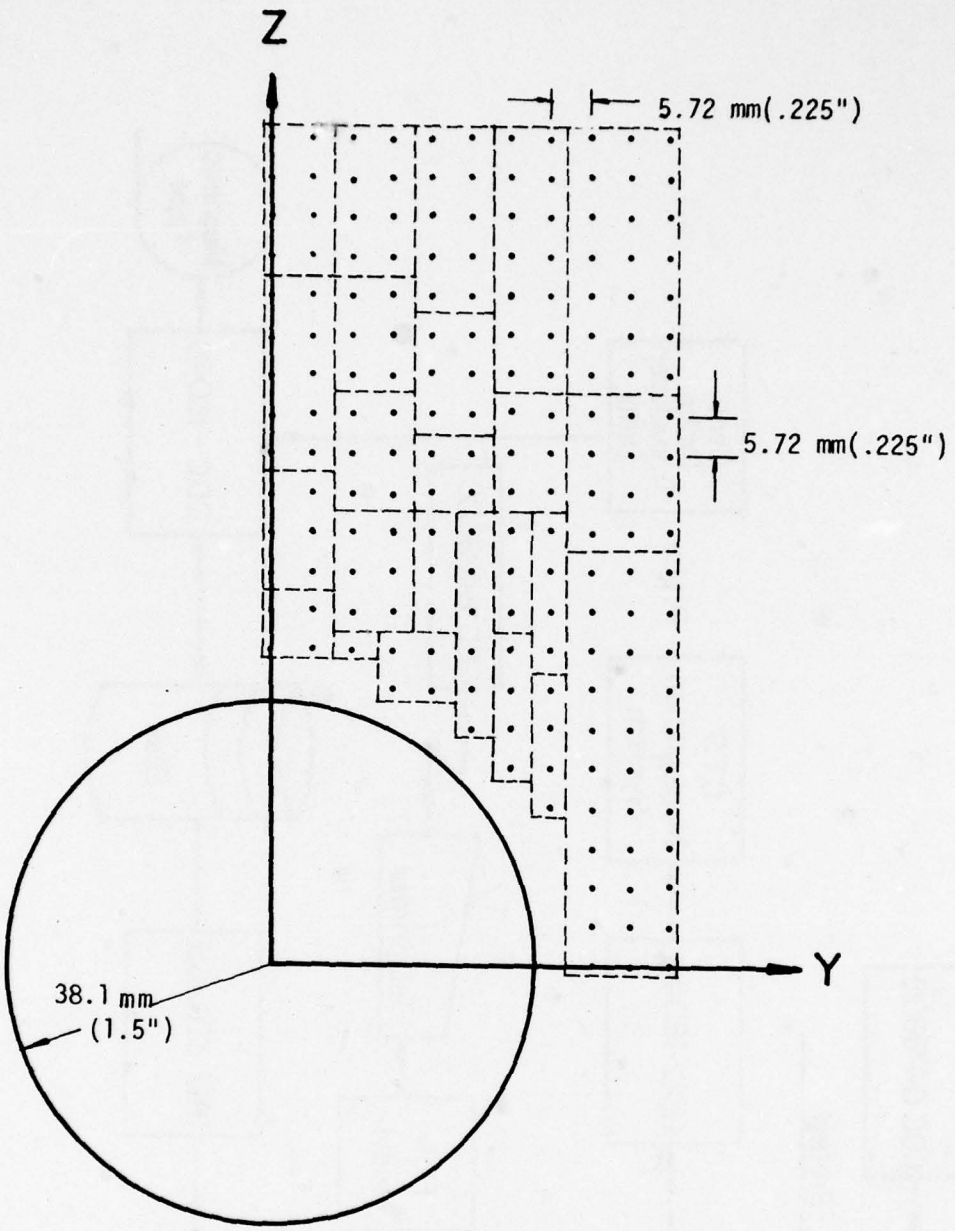


Figure 8. Typical Survey Grid and Subgrids

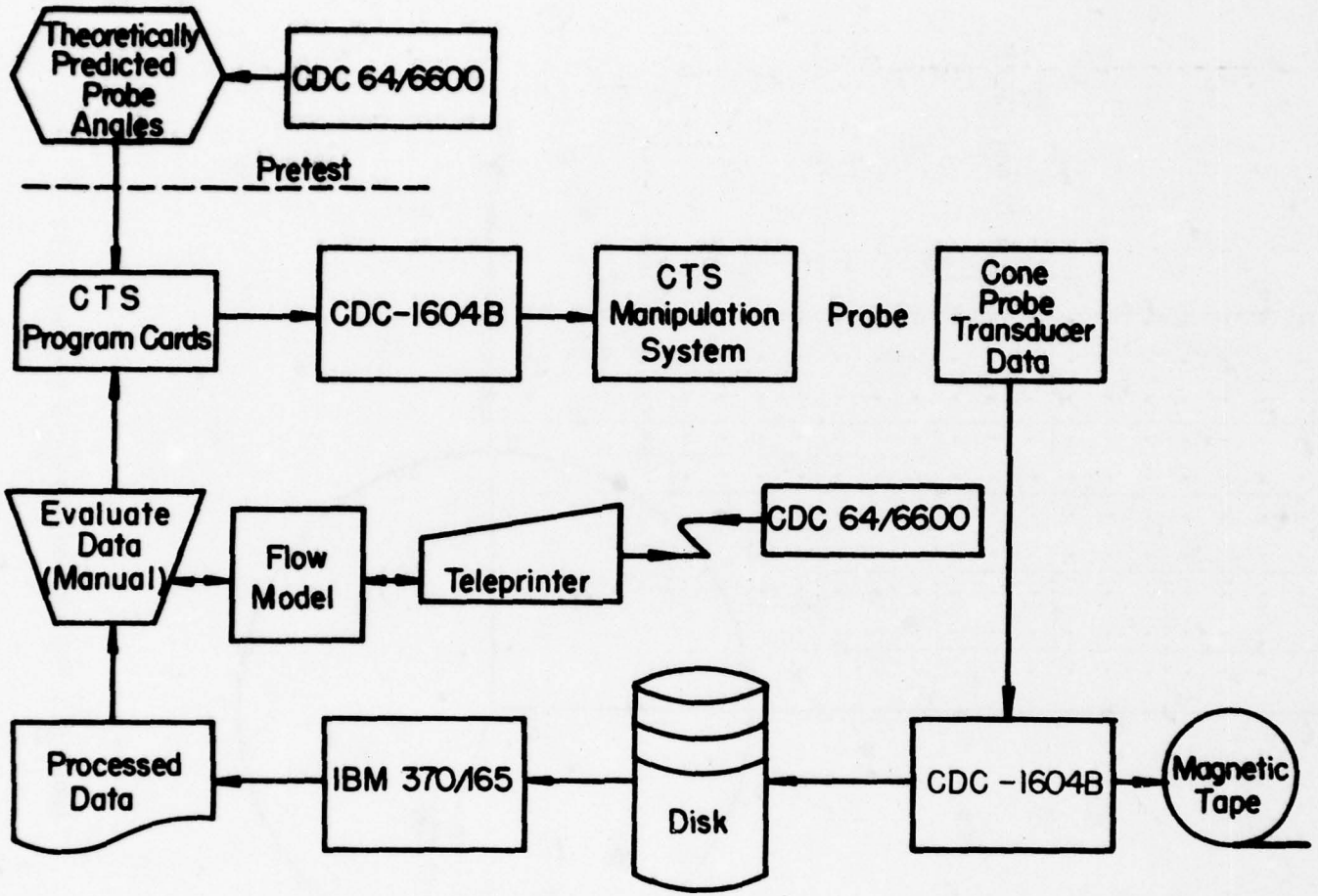


Figure 9. Data Acquisition Process Diagram

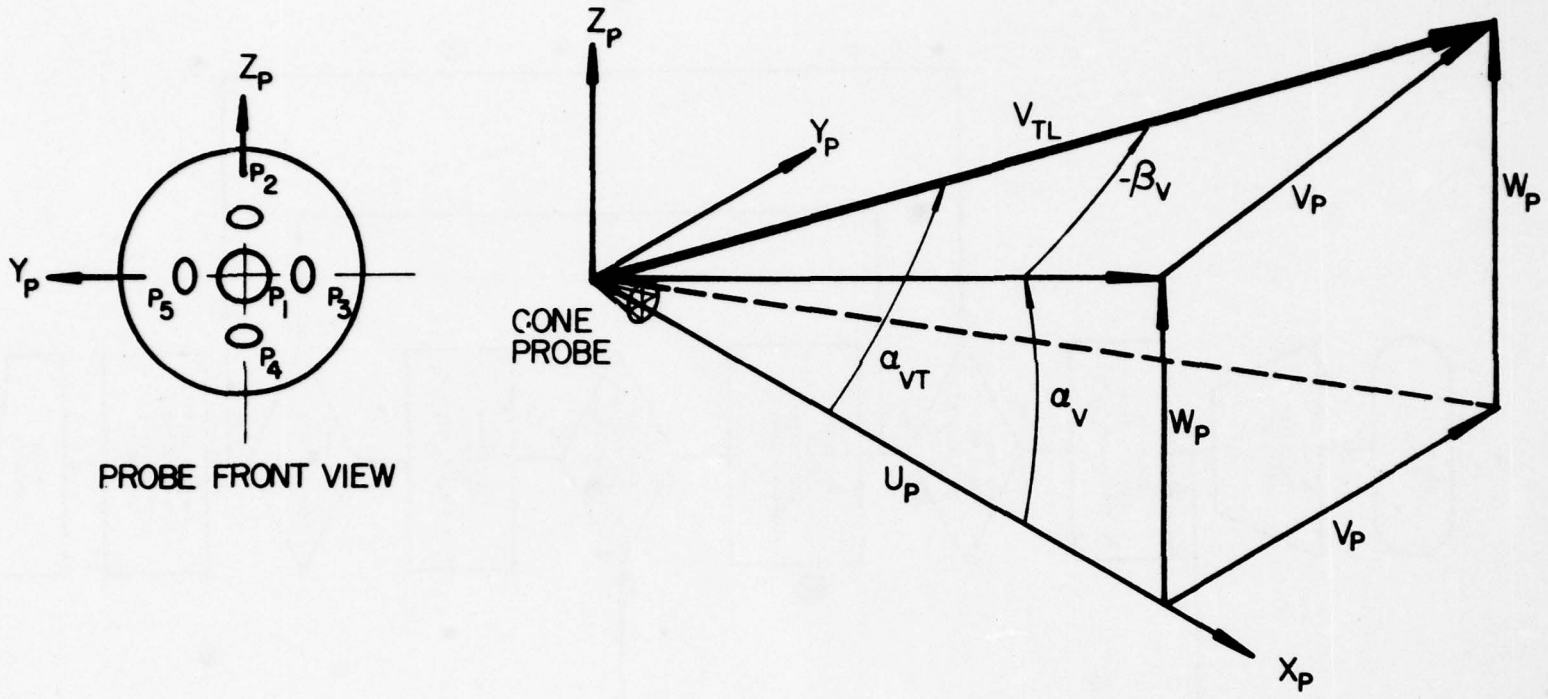


Figure 10. Pressure Tap and Flow Angle Definitions

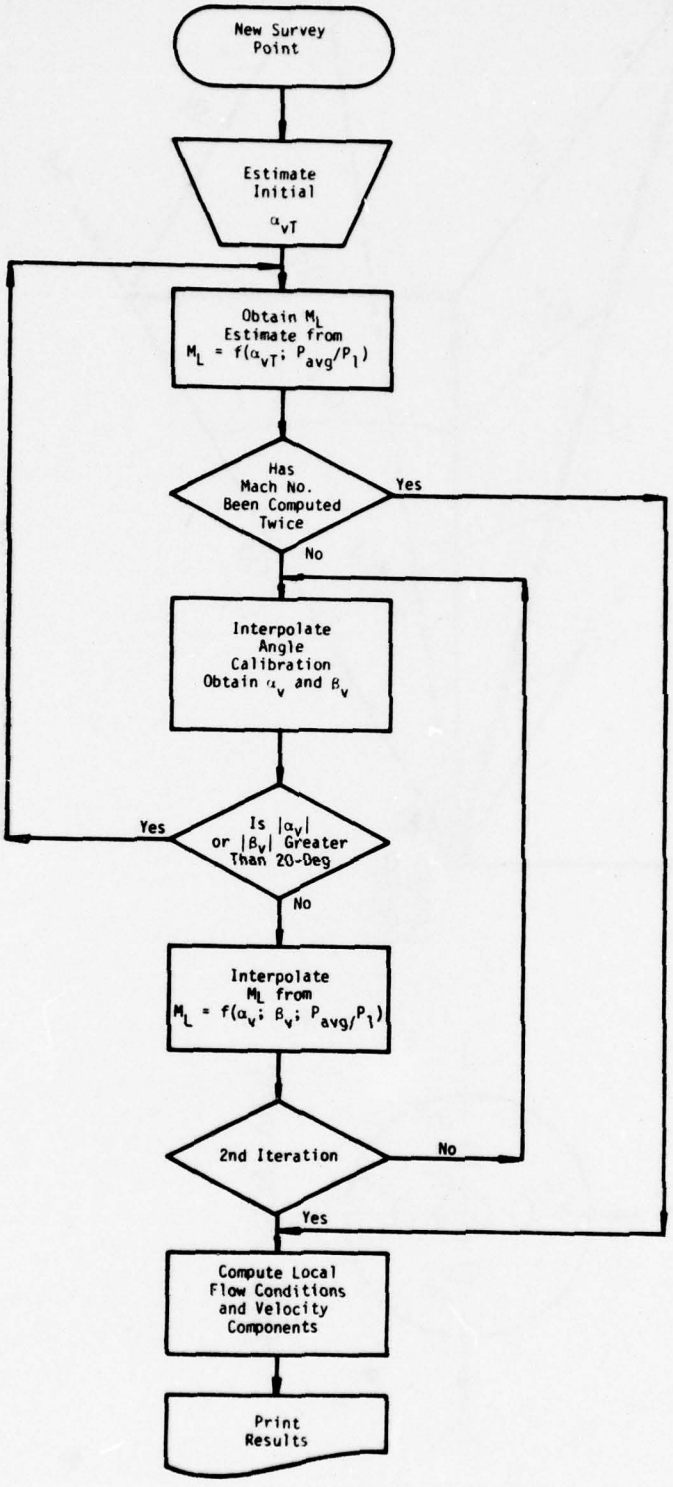


Figure 11. Data Reduction Flow Chart

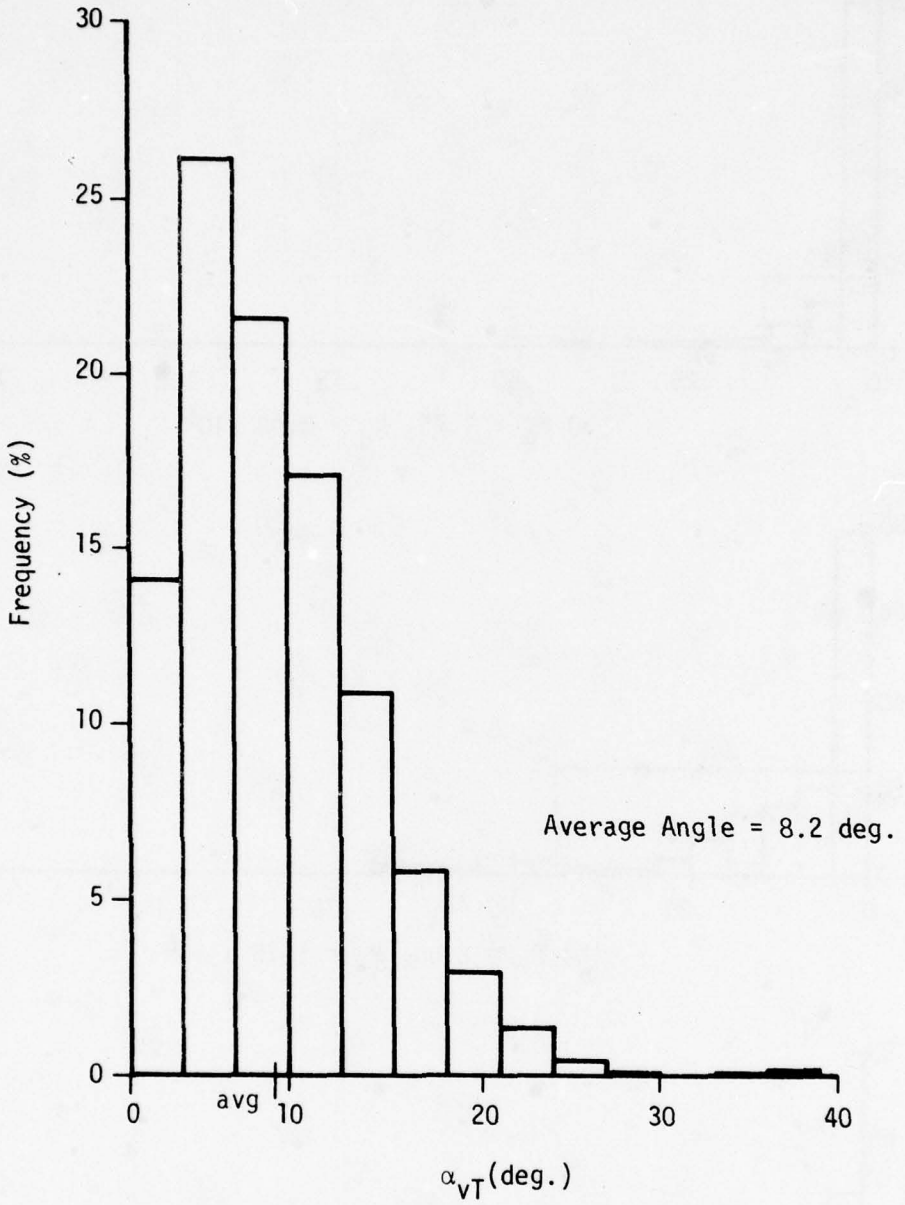
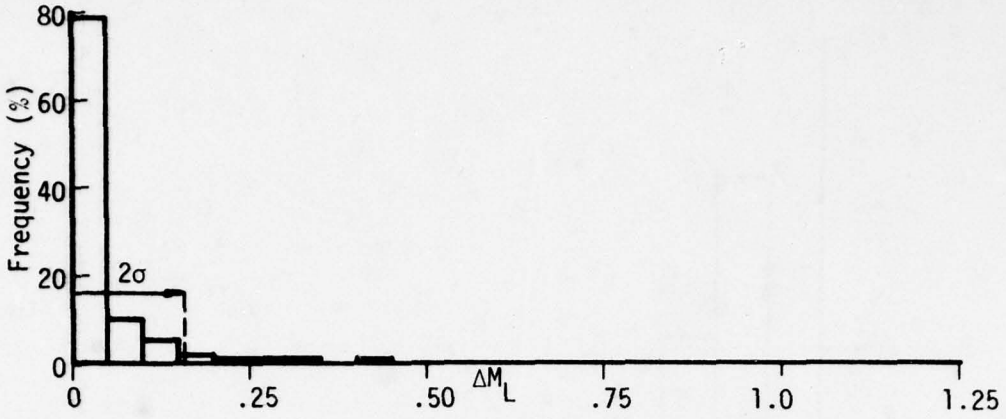
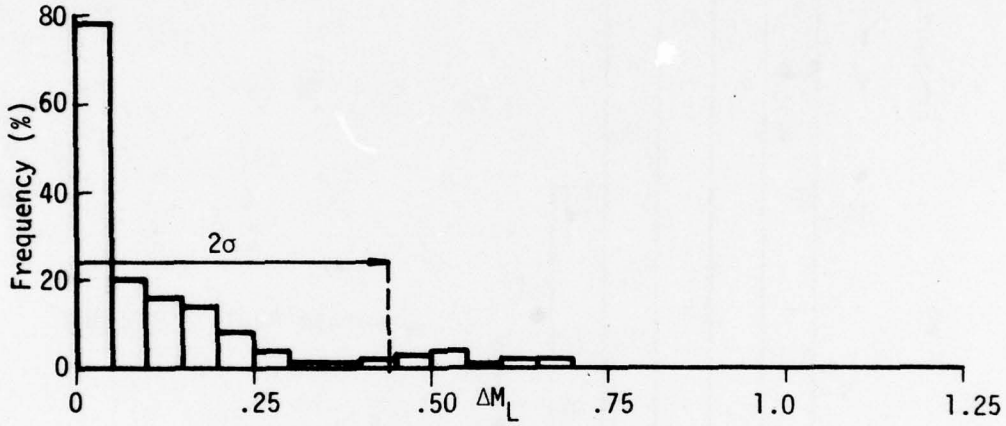


Figure 12. Frequency Distribution of α_{vT} for Final Data



(a) $M_\infty = 1.95$, $R_d = 0.48 \times 10^6$



(b) $M_\infty = 2.00$, $R_d = 1.75 \times 10^6$



(c) $M_\infty = 3.01$, $R_d = 1.70 \times 10^6$

Figure 13. Frequency Distribution of Change in Local Mach Number for Repeat Data

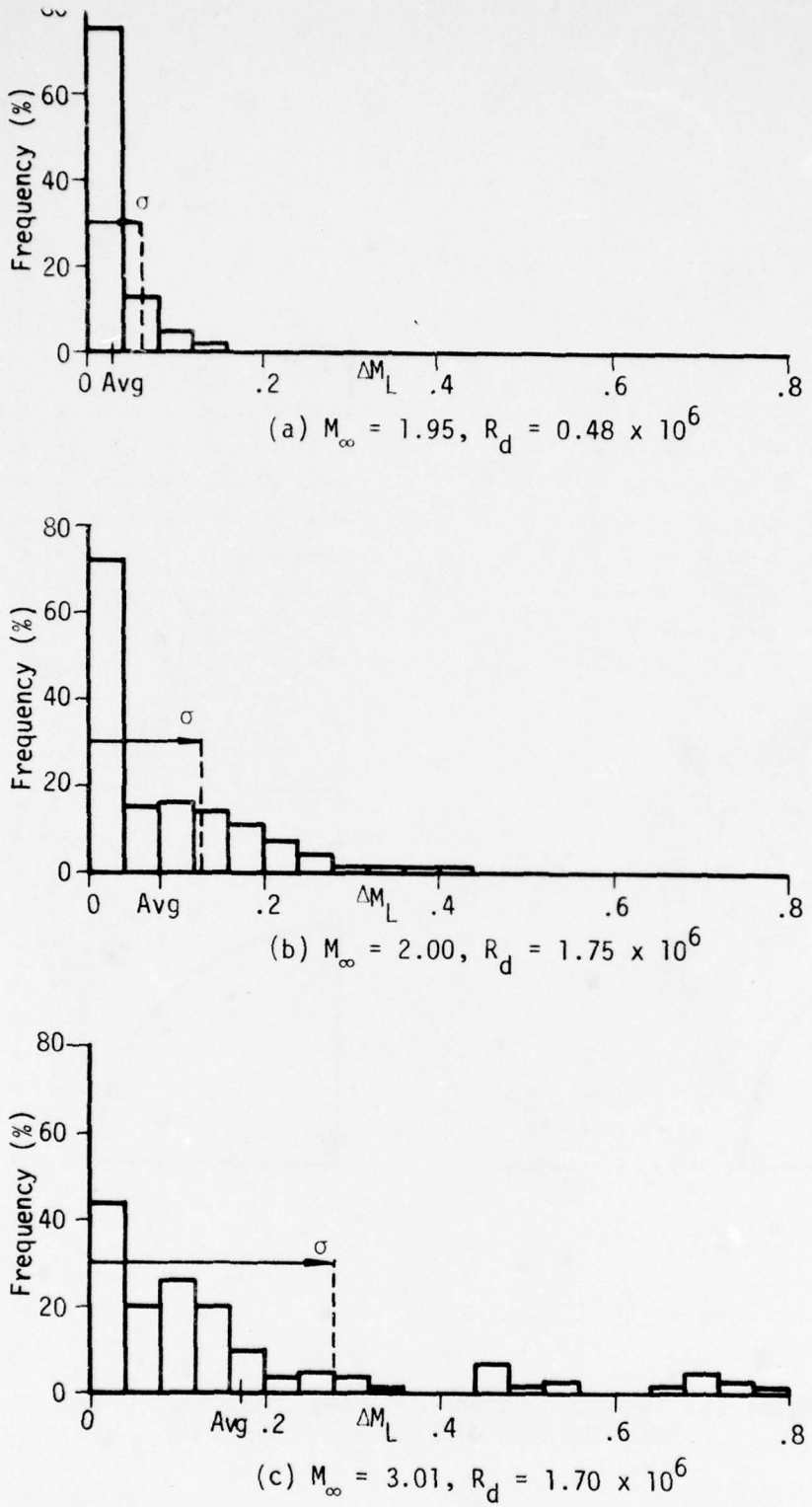
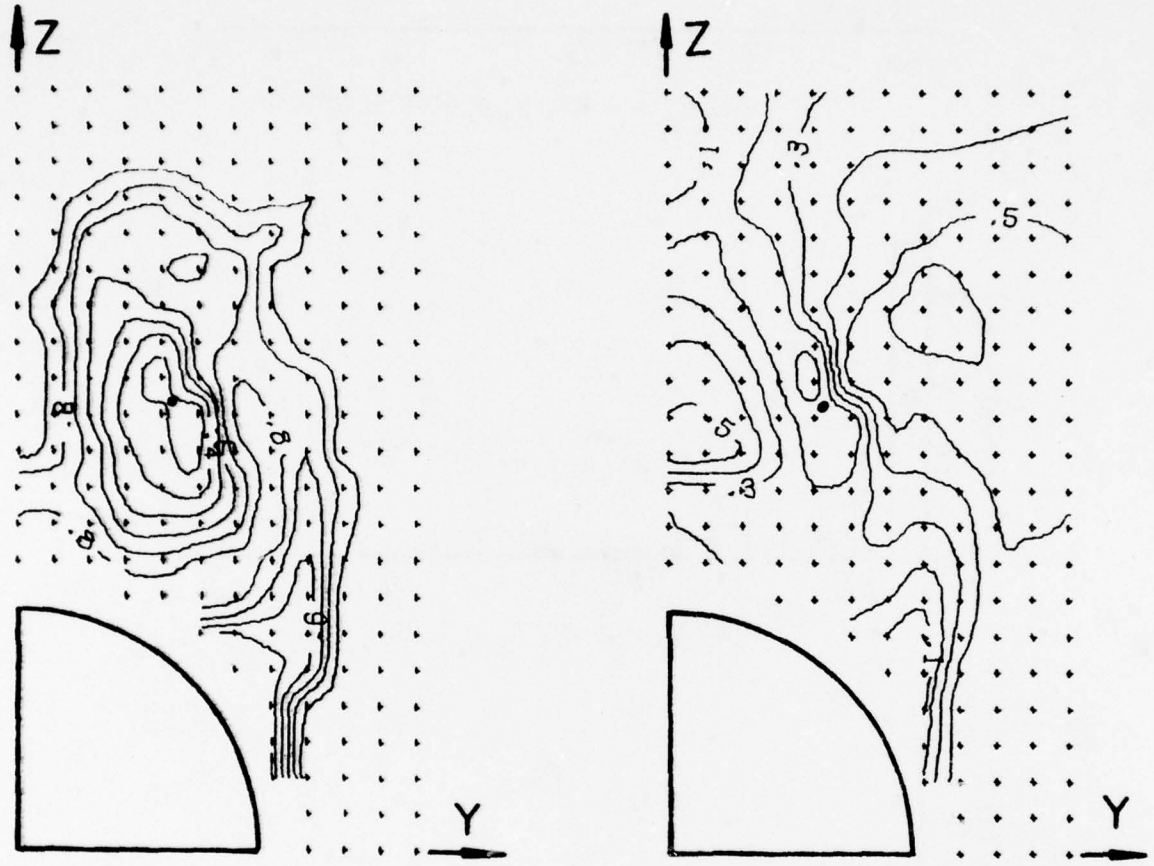


Figure 14. Truncated Frequency Distribution of Change in Local Mach Number



(a) $P_o/P_{o\infty}$

(b) U_c/U_∞

Figure 15. Sample Contours of Total Pressure and Magnitude of Cross-Flow Velocity

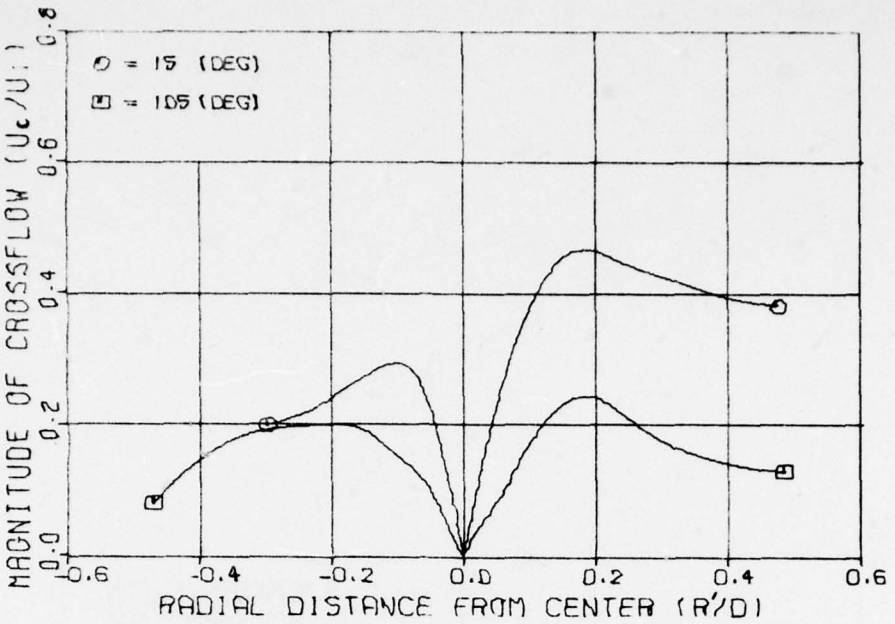


Figure 16. U_c/U_∞ in Vortex Coordinate System

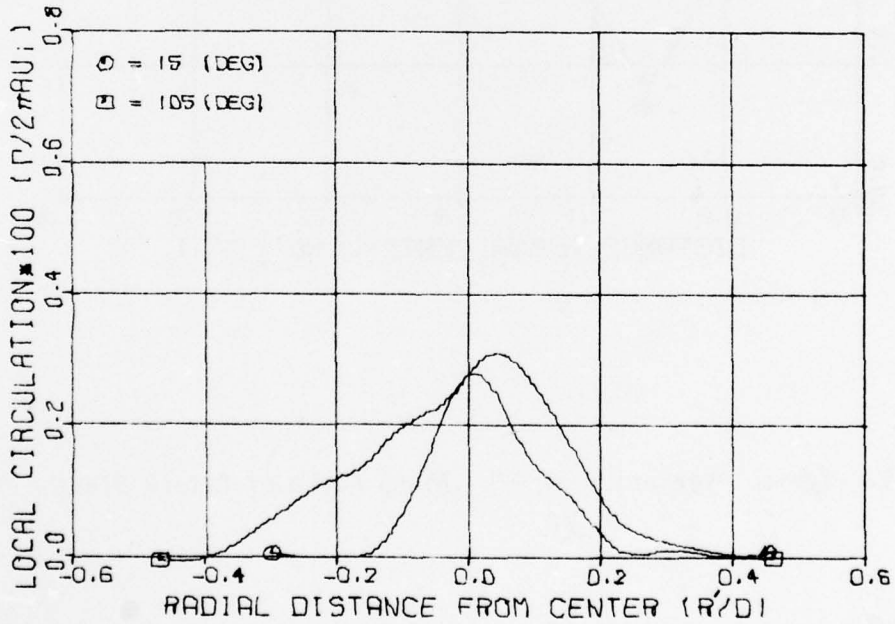


Figure 17. Local Circulation in Vortex Coordinate System

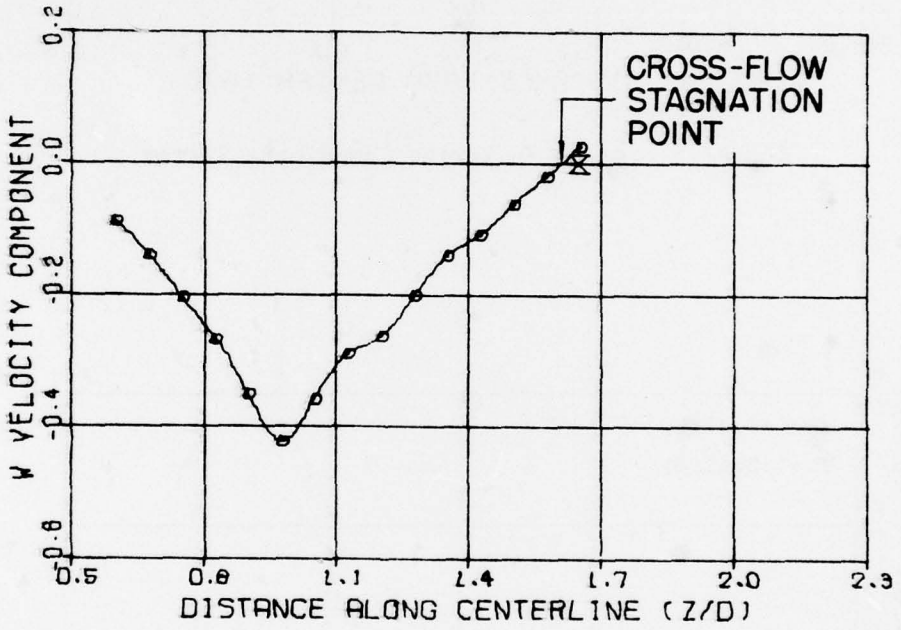
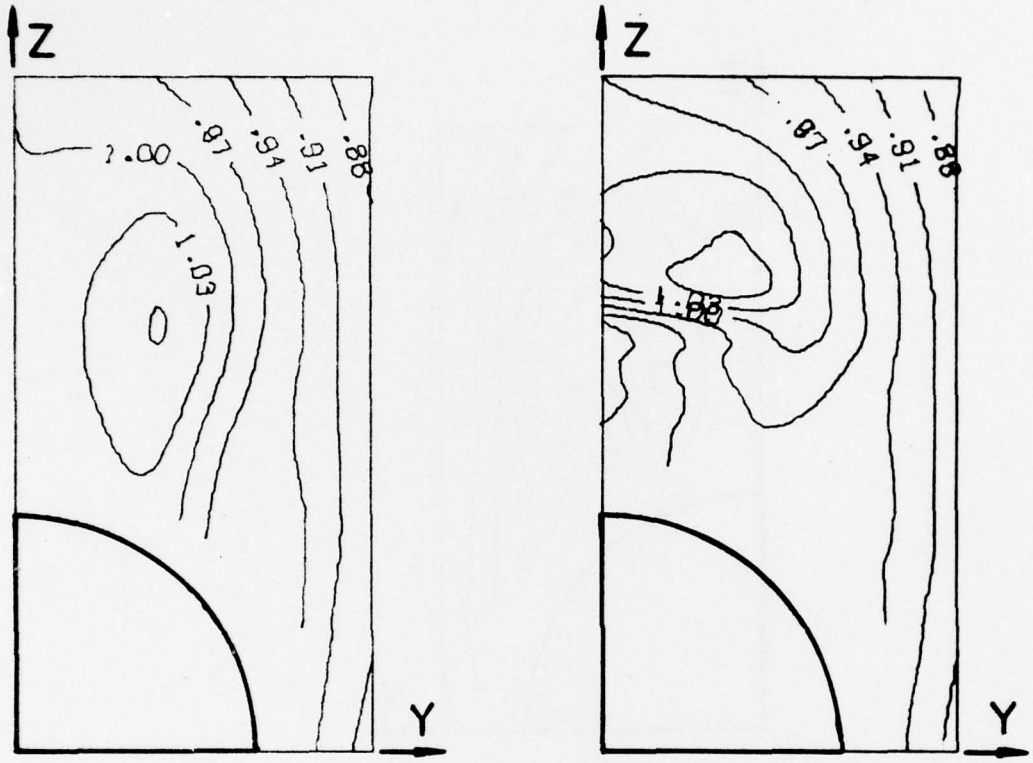


Figure 18. Typical Variation of w/U_∞ Along Angle of Attack Plane



(a) Pattern 1

(b) Pattern 2

Figure 19. Comparison of Integration Sweep Pattern on Streamlines (M_∞= 2.00, R_d = 1.75 x 10^6, α_b = 15, x/d = 10.)

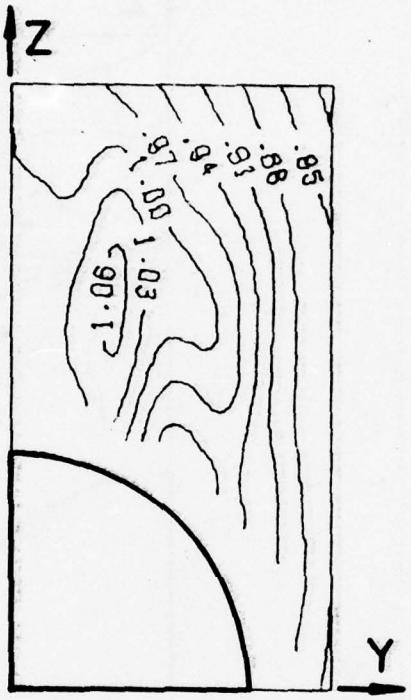


Figure 20. Streamlines for $M_\infty = 2.00$, $R_d = 1.75 \times 10^6$, $\alpha_b = 20$ and $x/d = 6$.

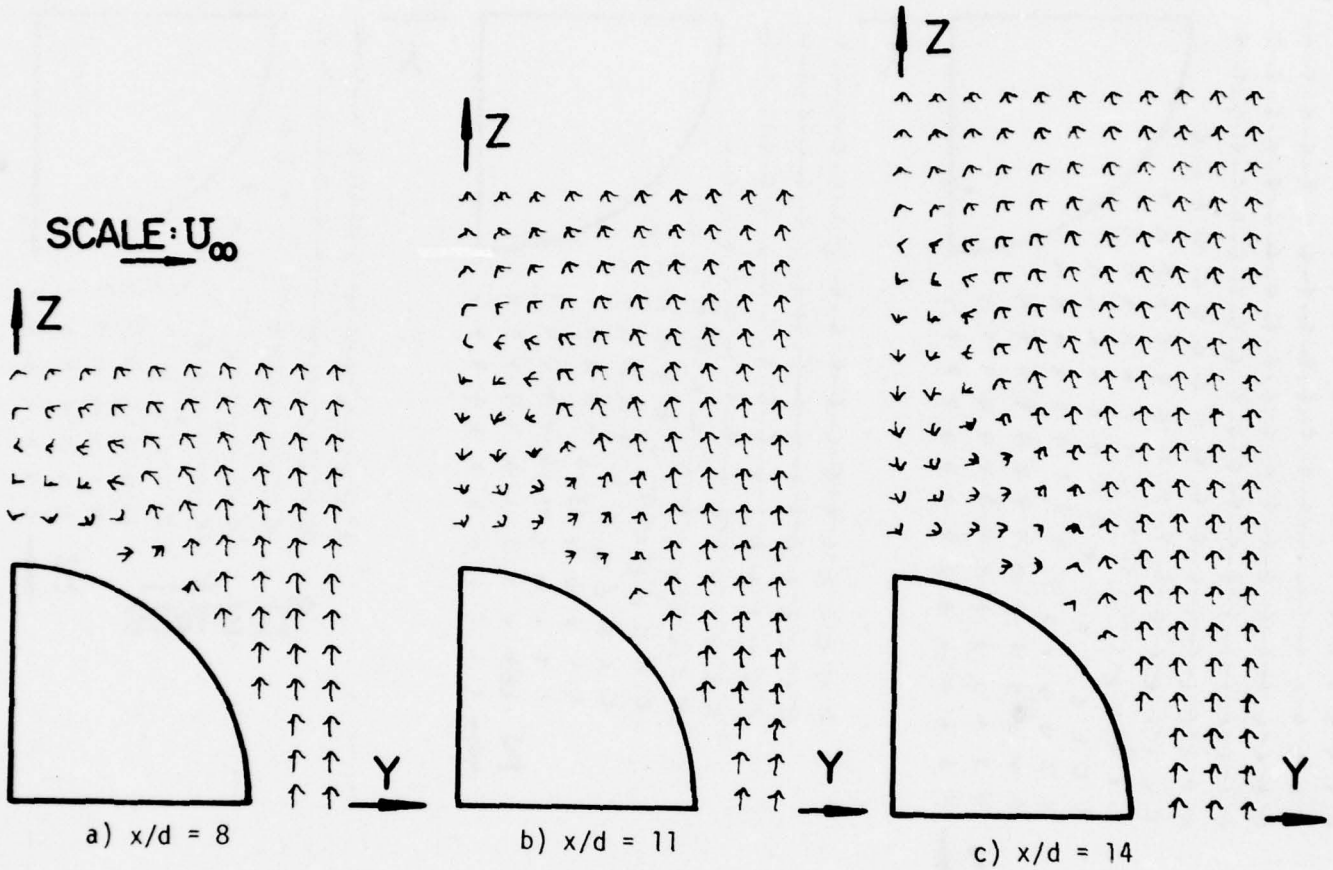


Figure 21. Cross-Flow Plane Vector Plot for $M_\infty = 1.95$, $R_d = .48 \times 10^6$ and $\alpha_b = 10°$

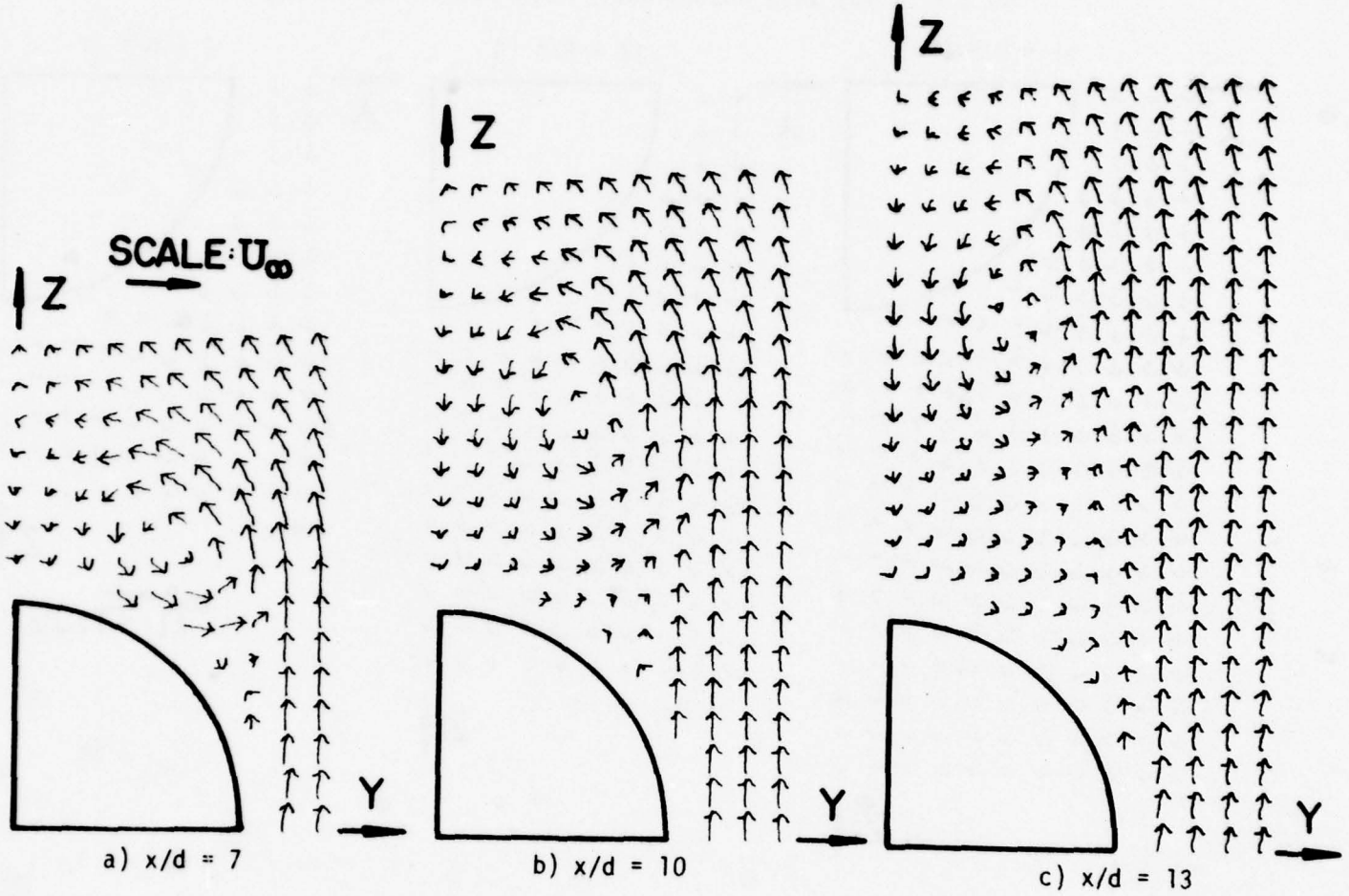


Figure 22. Cross-Flow Plane Vector Plot for M_∞ = 1.95, R_d = .48 x 10^6 and α_b = 15°.

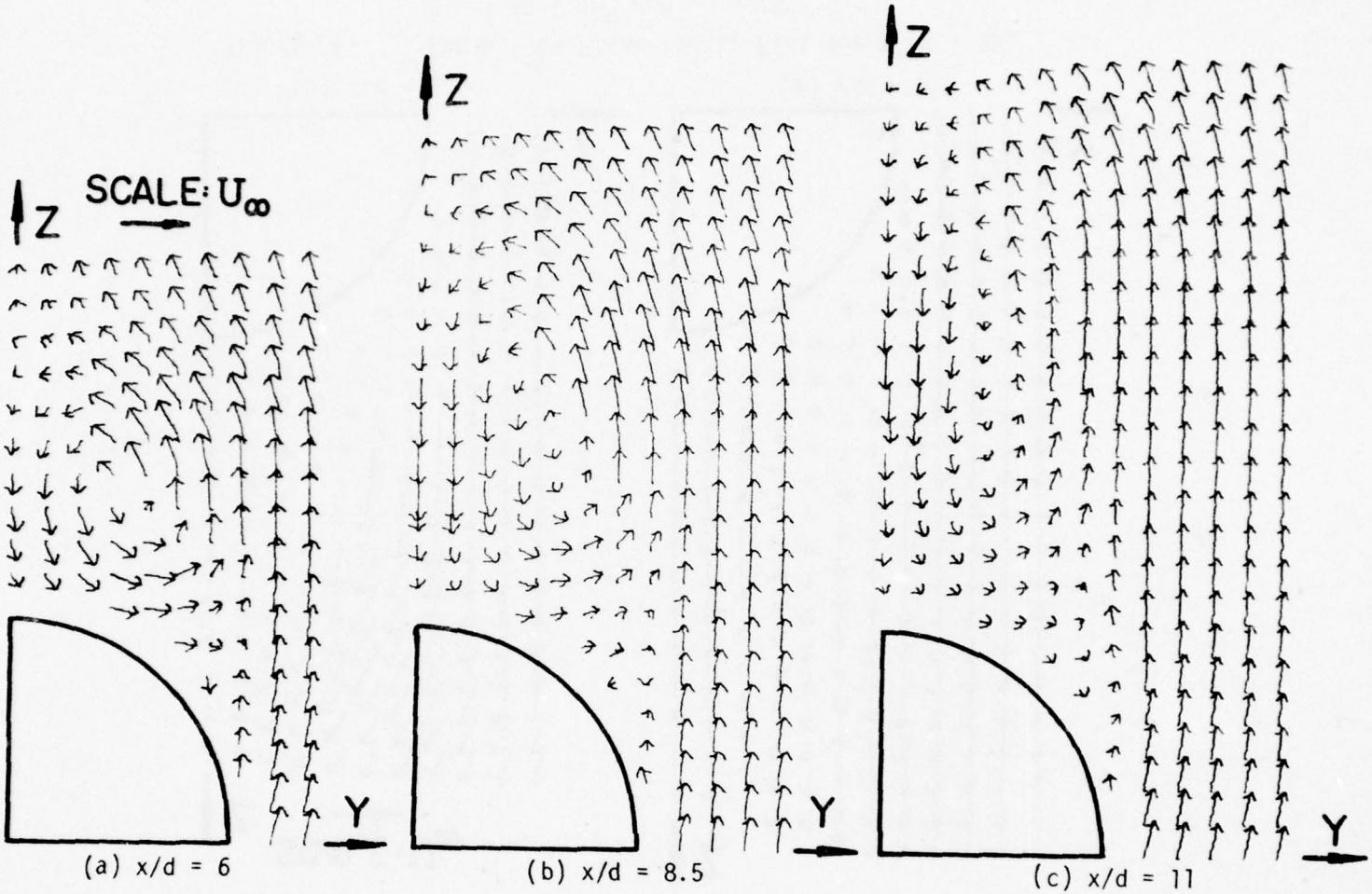
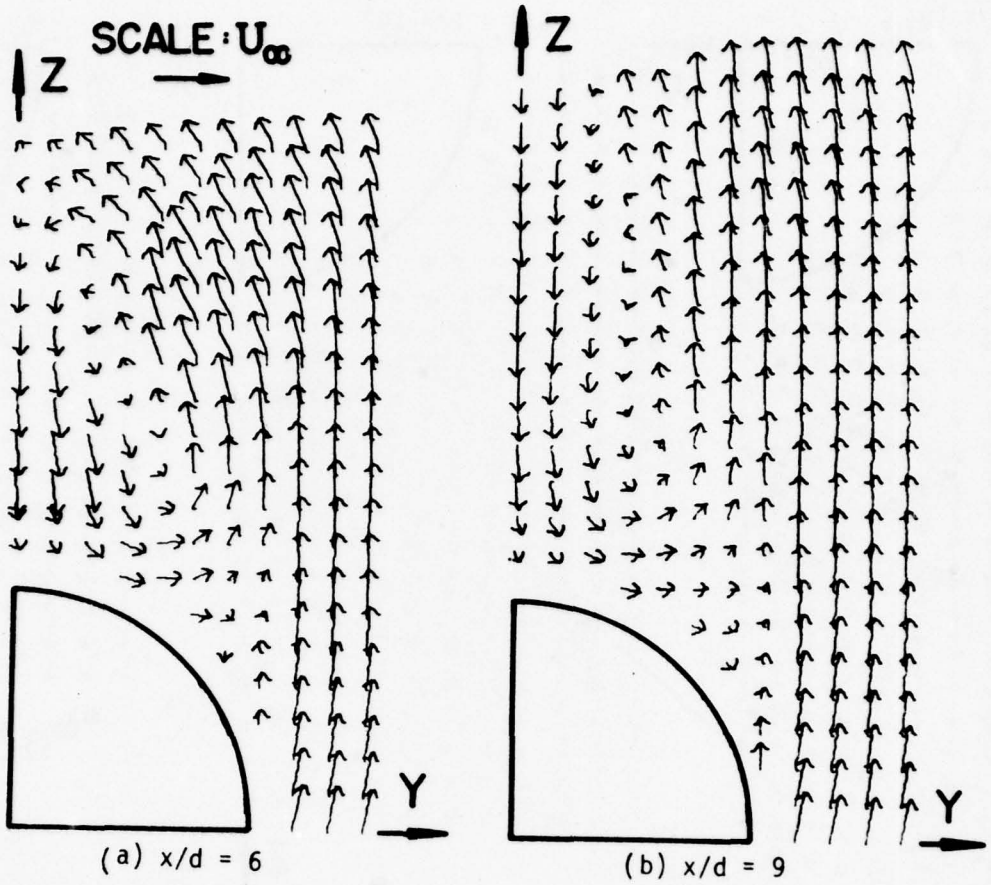


Figure 23. Cross-Flow Plane Vector Plot for M_∞ = 1.95, R_d = .48 x 10^6 and α_b = 20°.



(a) x/d = 6 (b) x/d = 9

Figure 24. Cross-Flow Plane Vector Plot for $M_\infty = 1.95$, $R_d = .48 \times 10^6$ and $\alpha_b = 25°$.

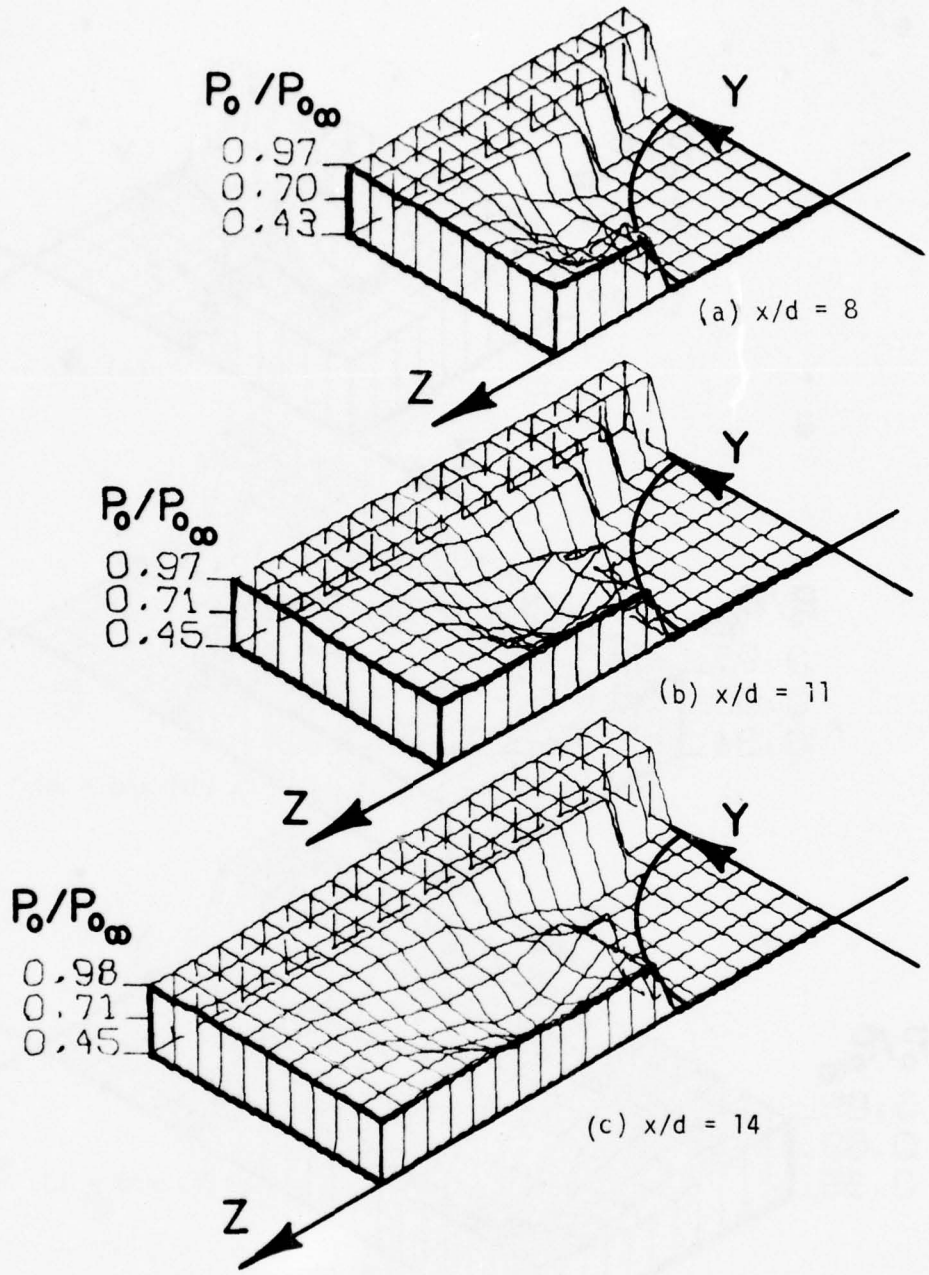


Figure 25. Total Pressure in Cross-Flow Plane for $M_\infty = 1.95$, $R_d = .48 \times 10^6$ and $\alpha_b = 10°$.

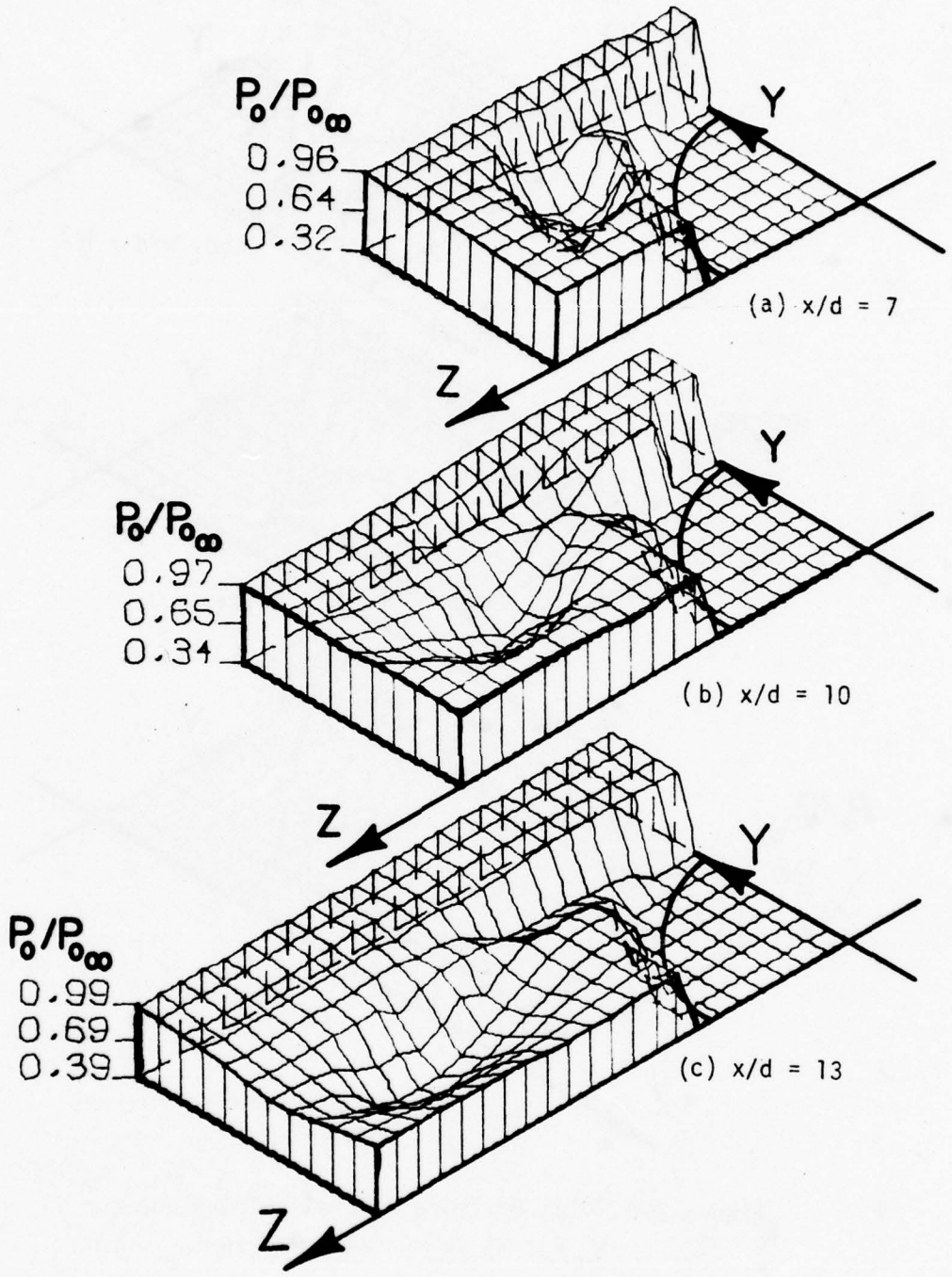


Figure 26. Total Pressure in Cross-Flow Plane for $M_\infty = 1.95$, $R_d = .48 \times 10^6$ and $\alpha_b = 15°$.

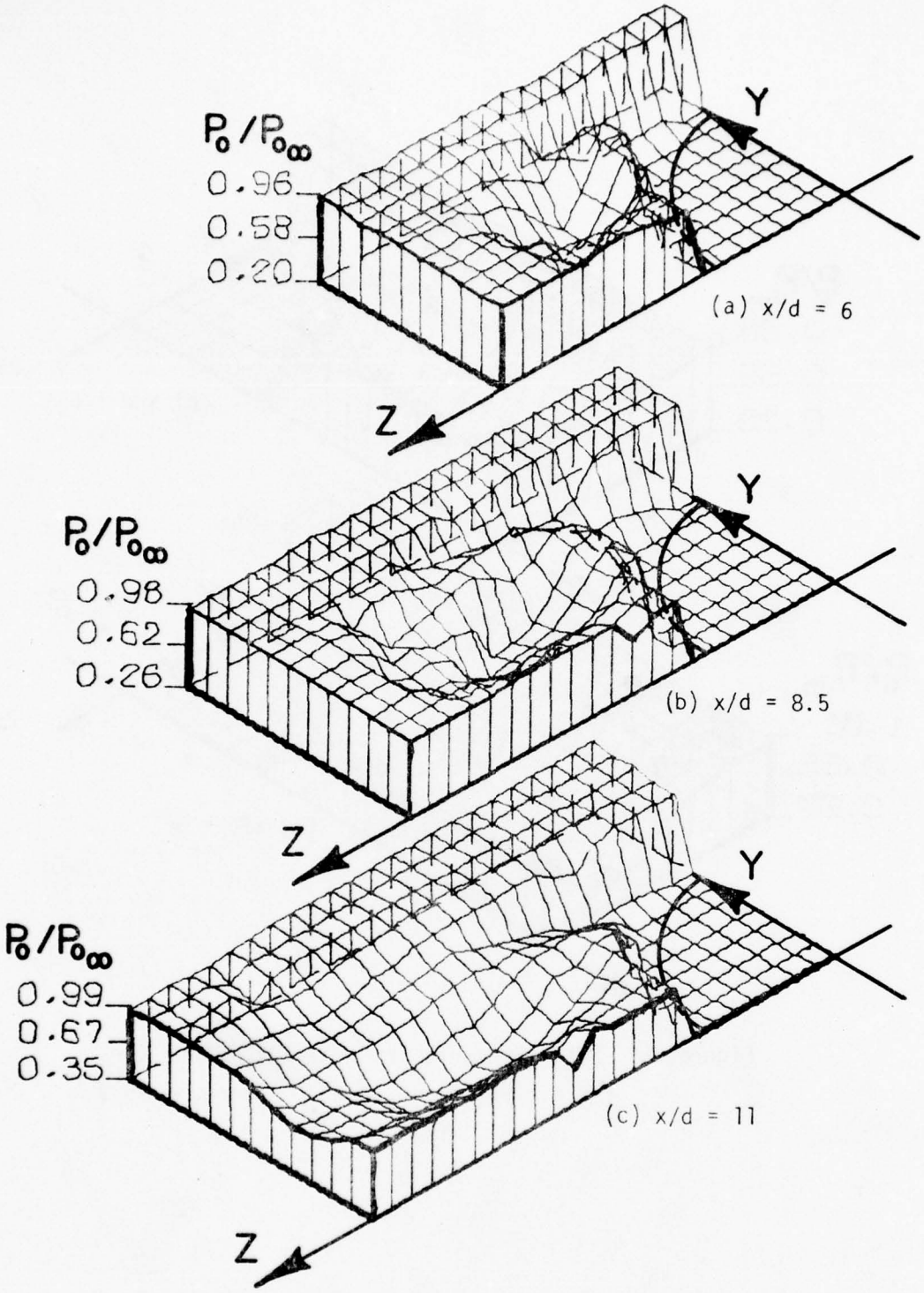


Figure 27. Total Pressure in Cross-Flow Plane for $M_\infty = 1.95$, $R_d = .48 \times 10^6$ and $\alpha_b = 20°$.

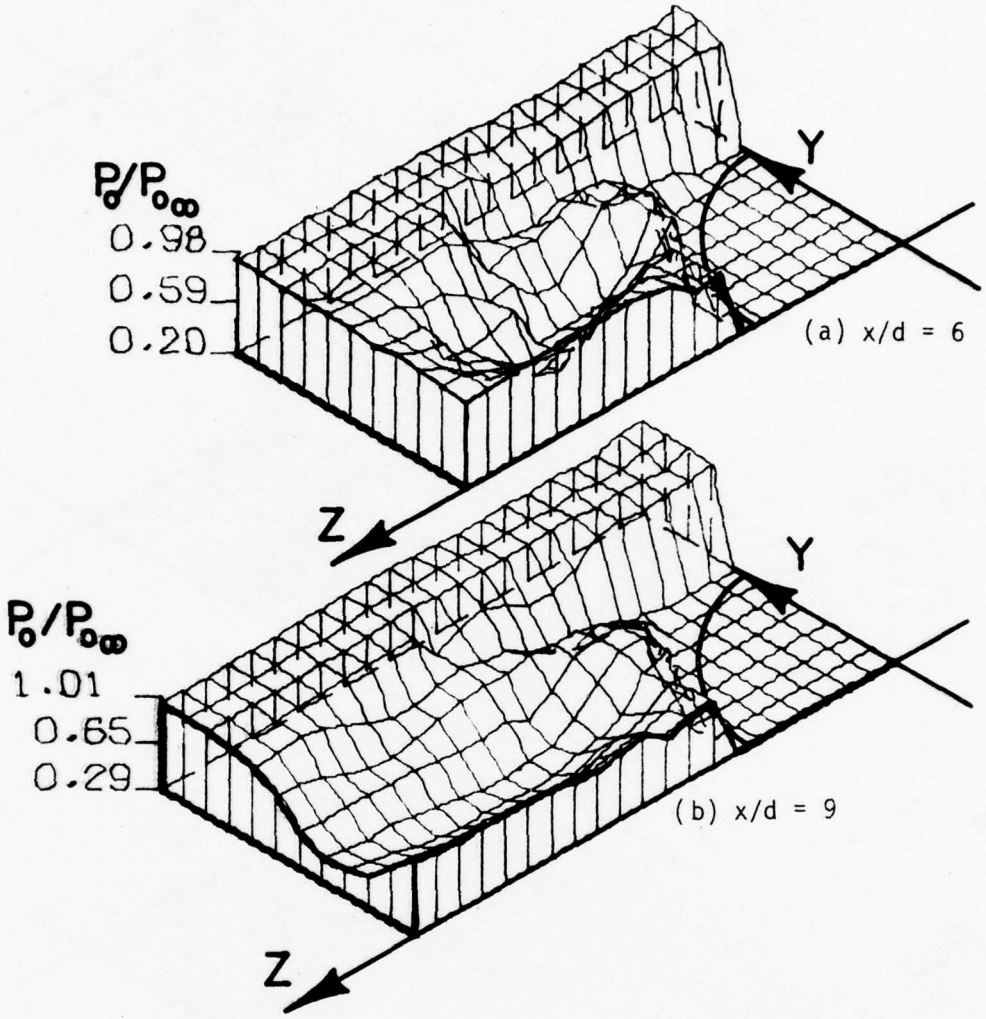


Figure 28. Total Pressure in Cross-Flow Plane for $M_\infty = 1.95$, $R_d = .48 \times 10^6$ and $\alpha_b = 25°$.

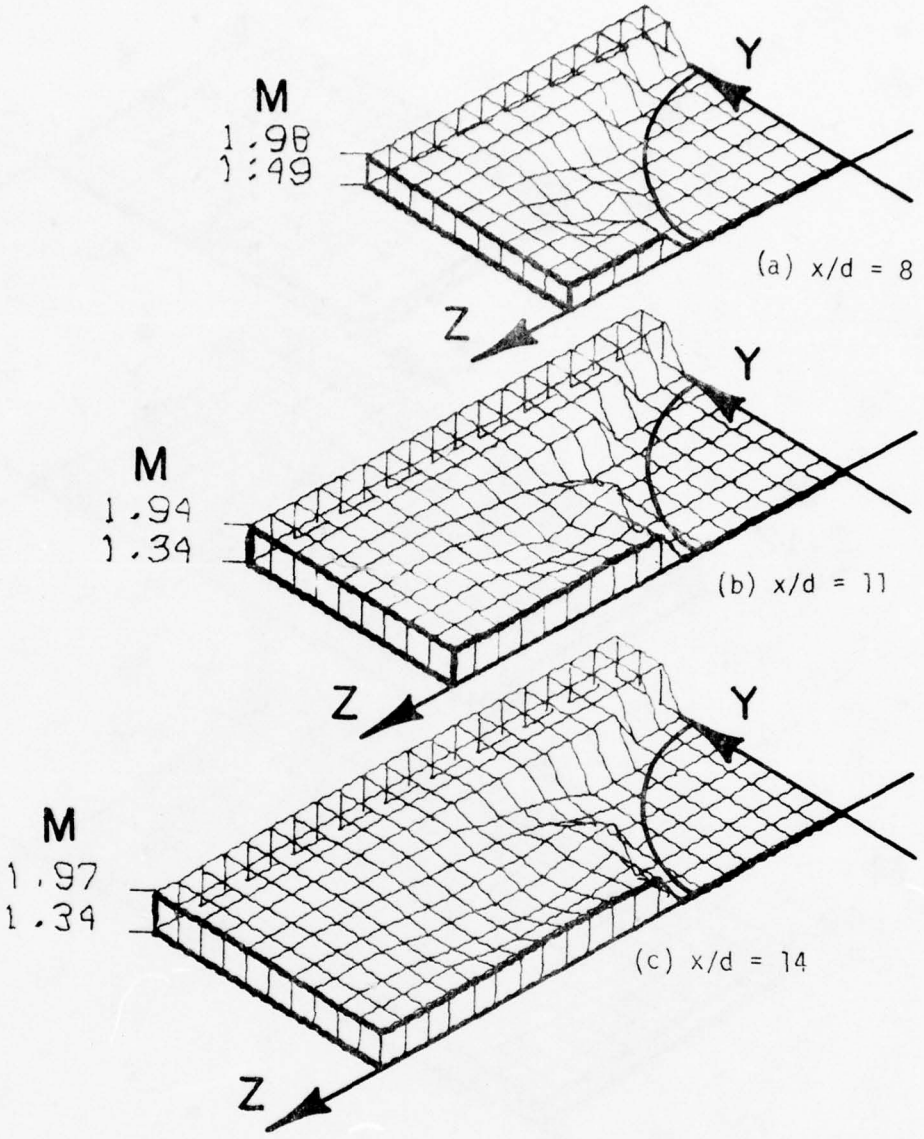


Figure 29. Mach Number in Cross-Flow Plane for $M_\infty = 1.95$, $R_d = .48 \times 10^6$ and $\alpha_b = 10°$.

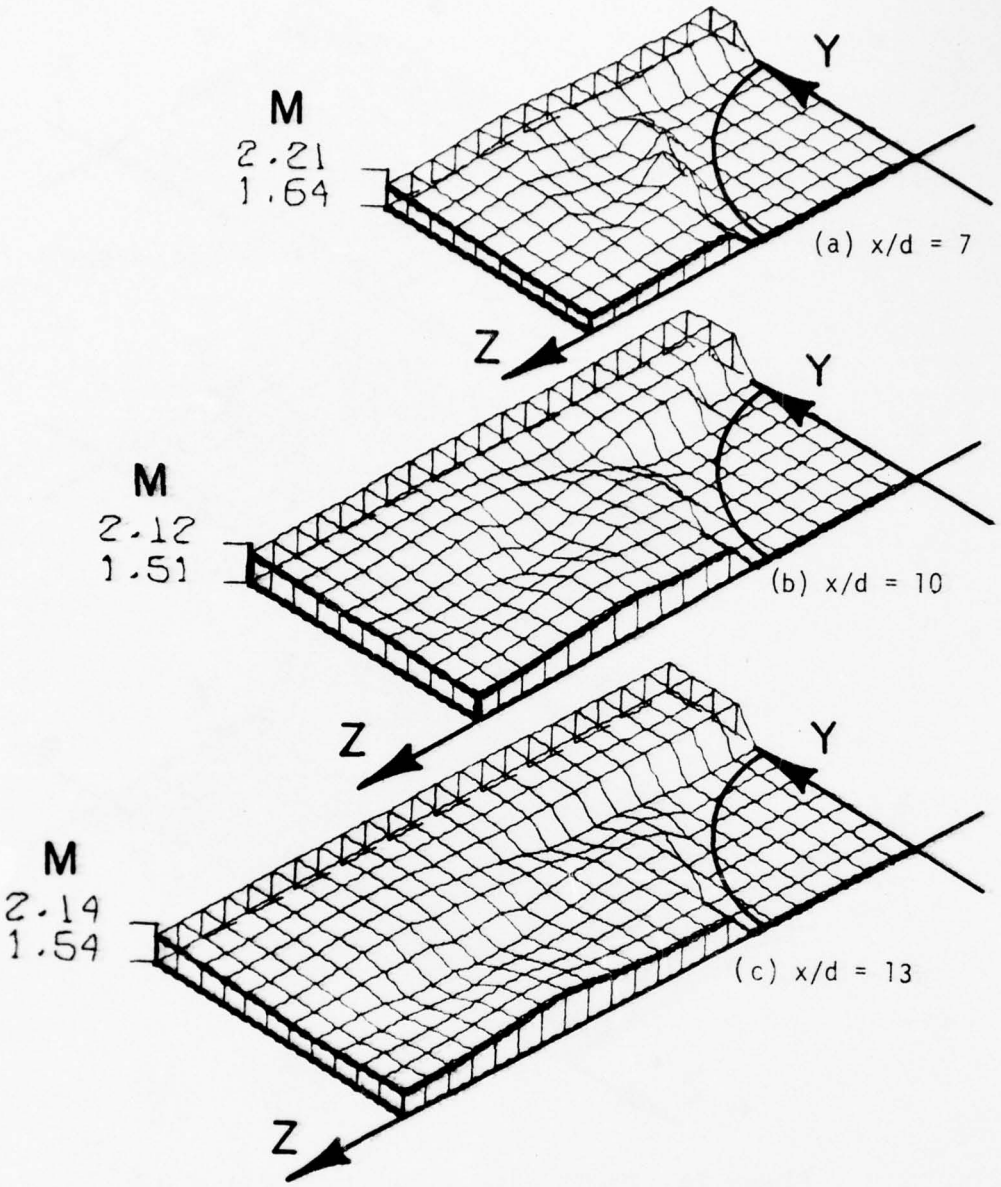


Figure 30. Mach Number in Cross-Flow Plane for $M_\infty = 1.95$, $R_d = .48 \times 10^6$ and $\alpha_b = 15°$.

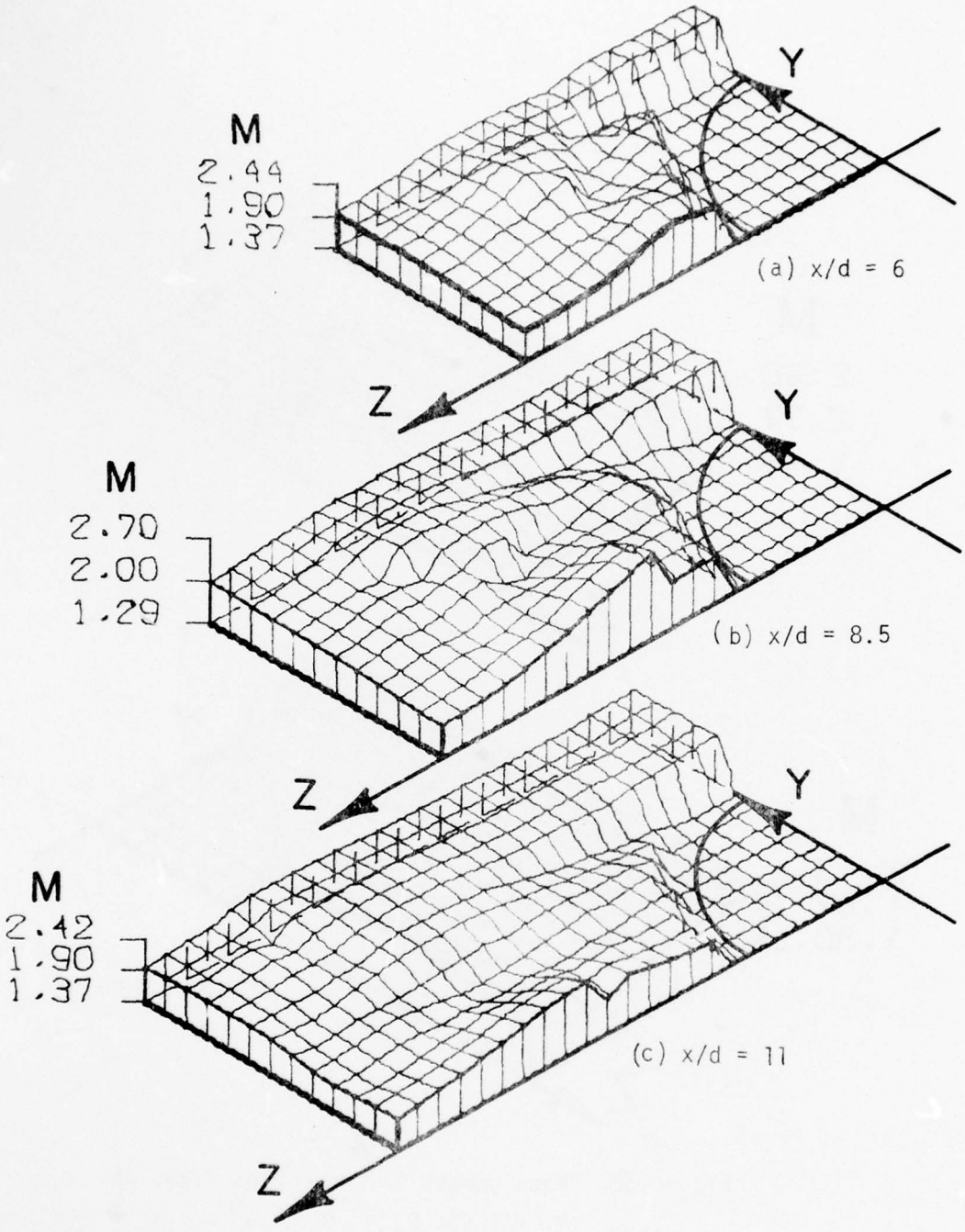


Figure 31. Mach Number in Cross-Flow Plane for $M_\infty = 1.95$, $R_d = .48 \times 10^6$ and $\alpha_b = 20°$.

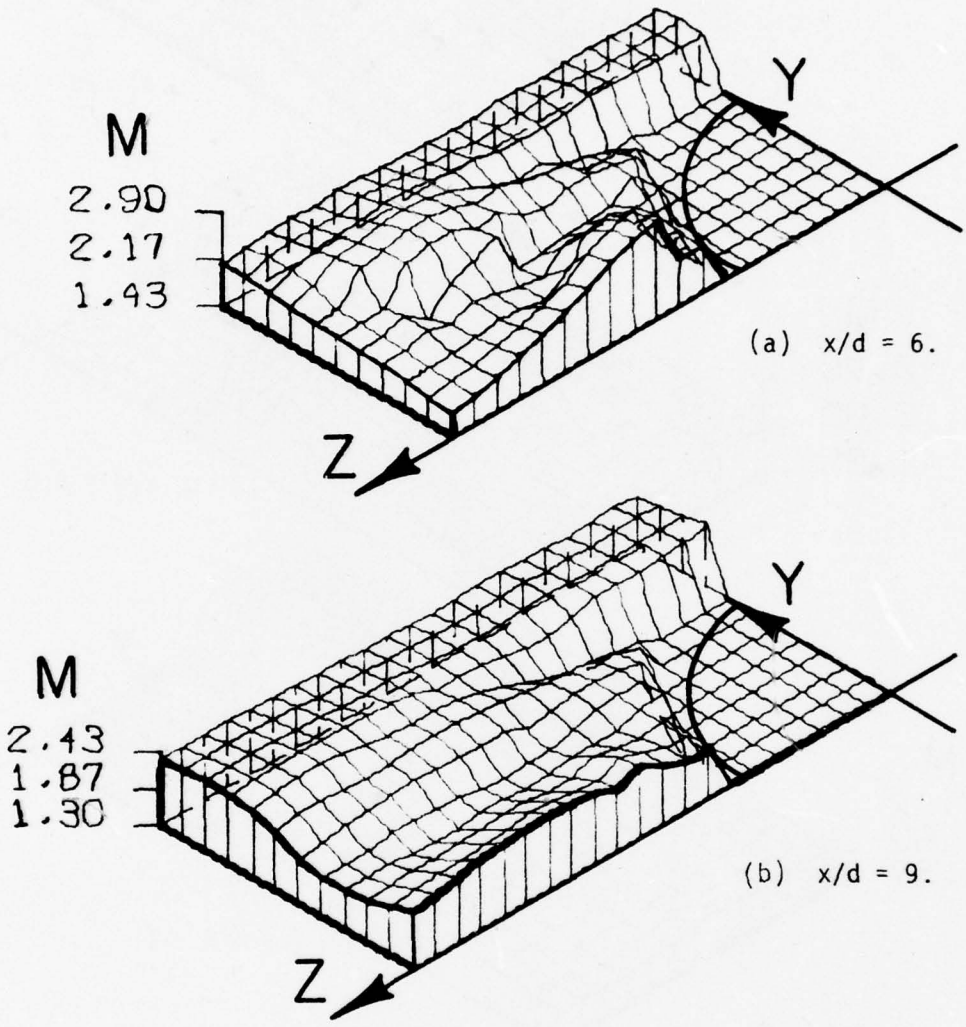


Figure 32. Mach Number in Cross-Flow Plane for $M_\infty = 1.95$, $R_d = .48 \times 10^6$ and $\alpha_b = 25°$.

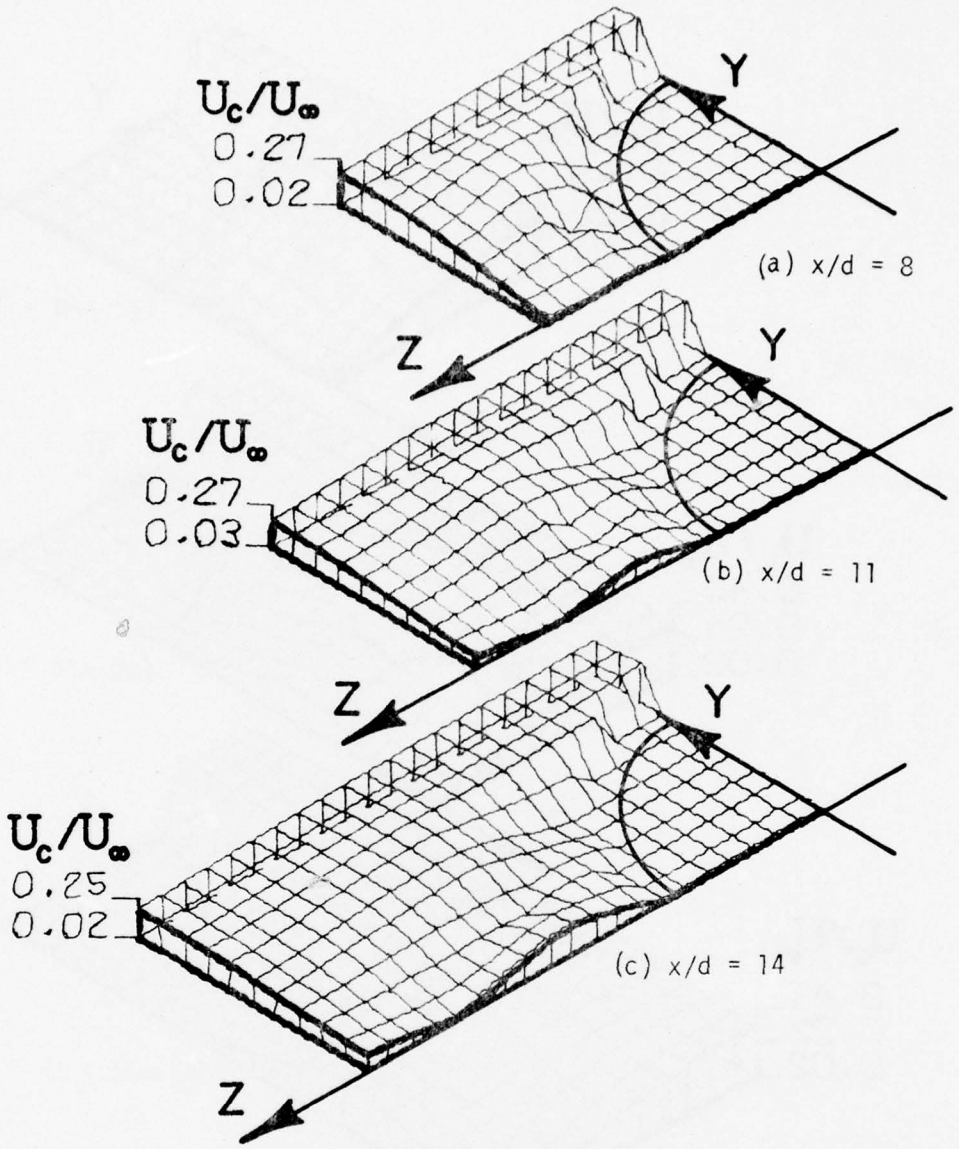


Figure 33. Magnitude of Cross-Flow Velocity for $M_\infty = 1.95$, $R_d = .48 \times 10^6$ and $\alpha_b = 10°$.

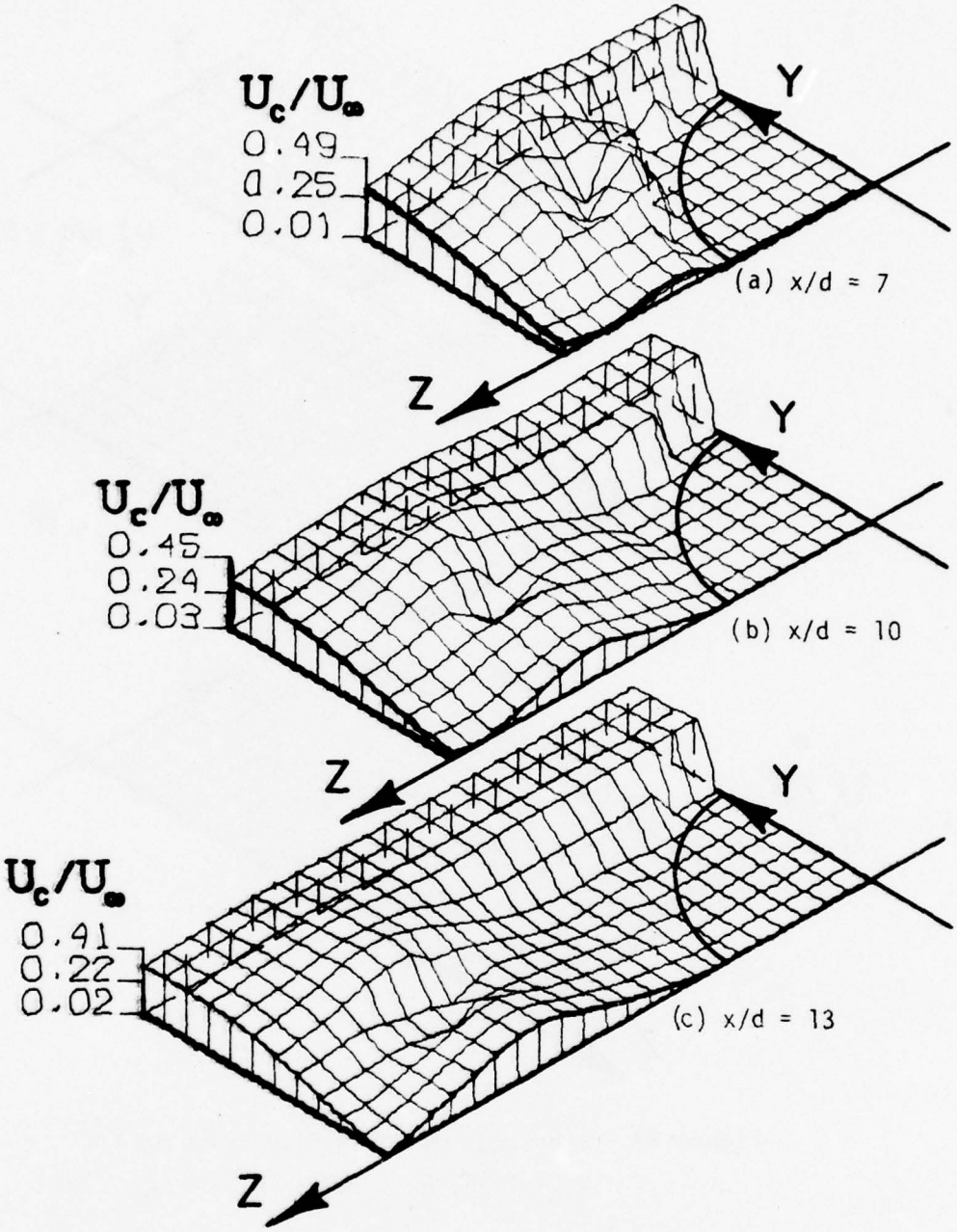


Figure 34. Magnitude of Cross-Flow Velocity for $M_\infty = 1.95$, $R_d = .48 \times 10^6$ and $\alpha_b = 15^c$.

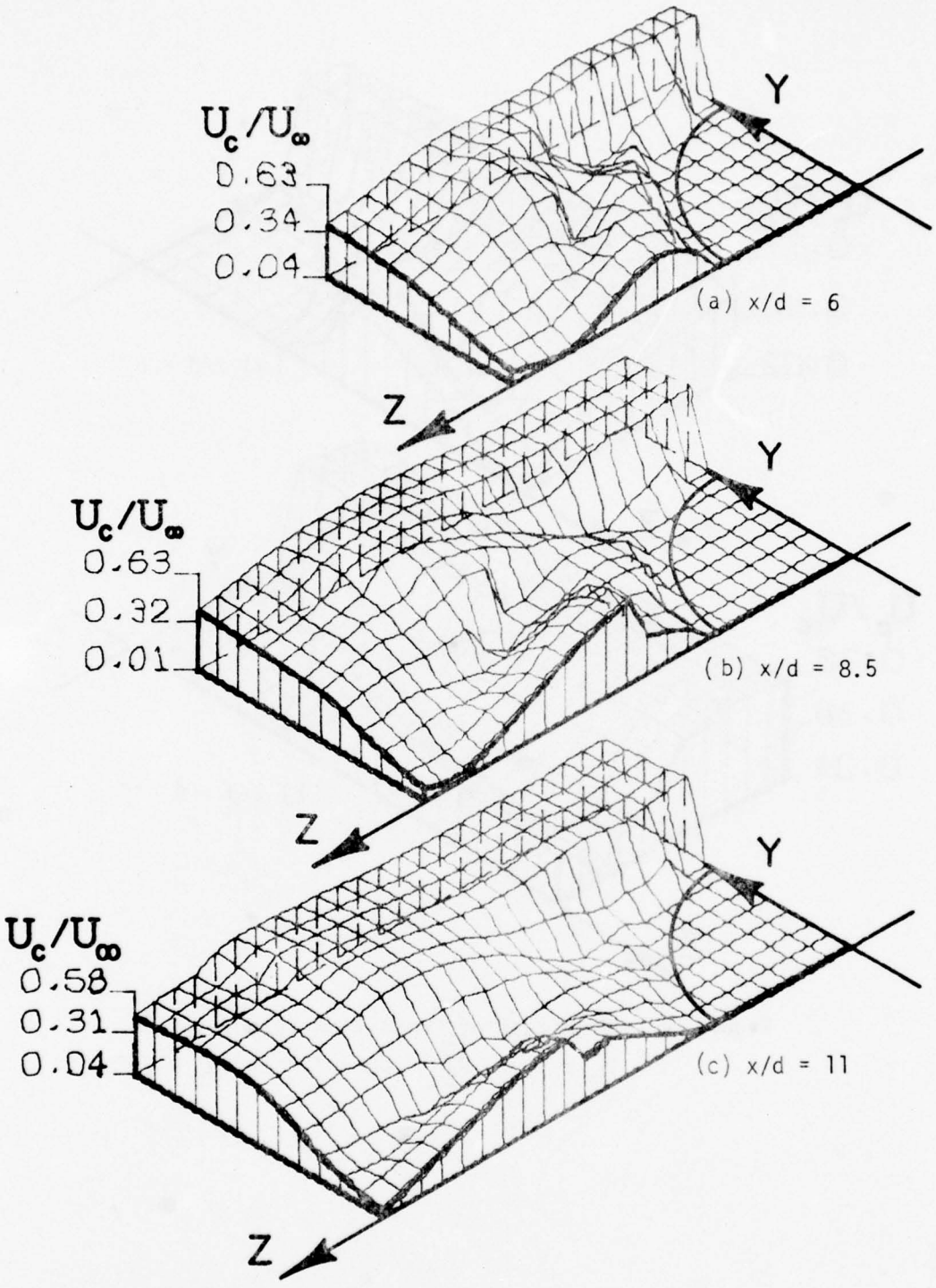


Figure 35. Magnitude of Cross-Flow Velocity for $M_\infty = 1.95$, $R_d = .48 \times 10^6$ and $\alpha_b = 20°$.

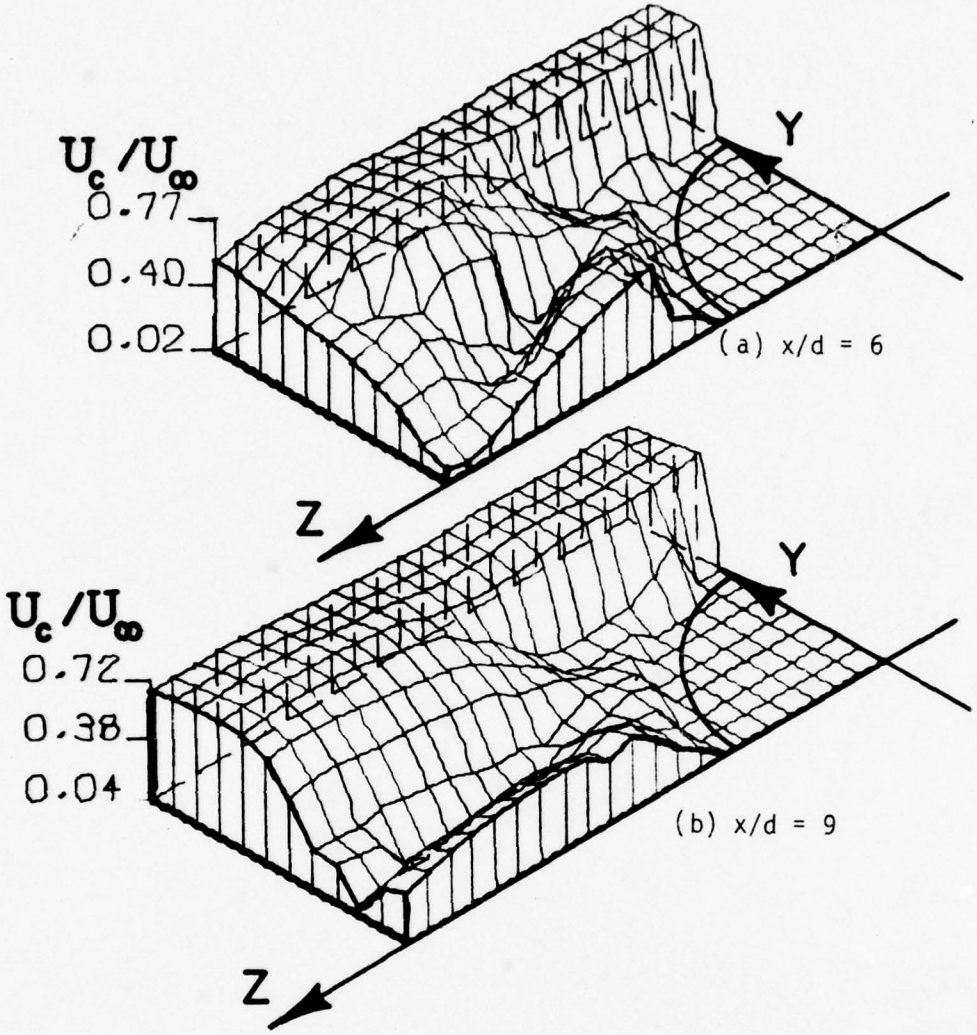


Figure 36. Magnitude of Cross-Flow Velocity for $M_\infty = 1.95$, $R_d = .48 \times 10^6$ and $\alpha_b = 25°$.

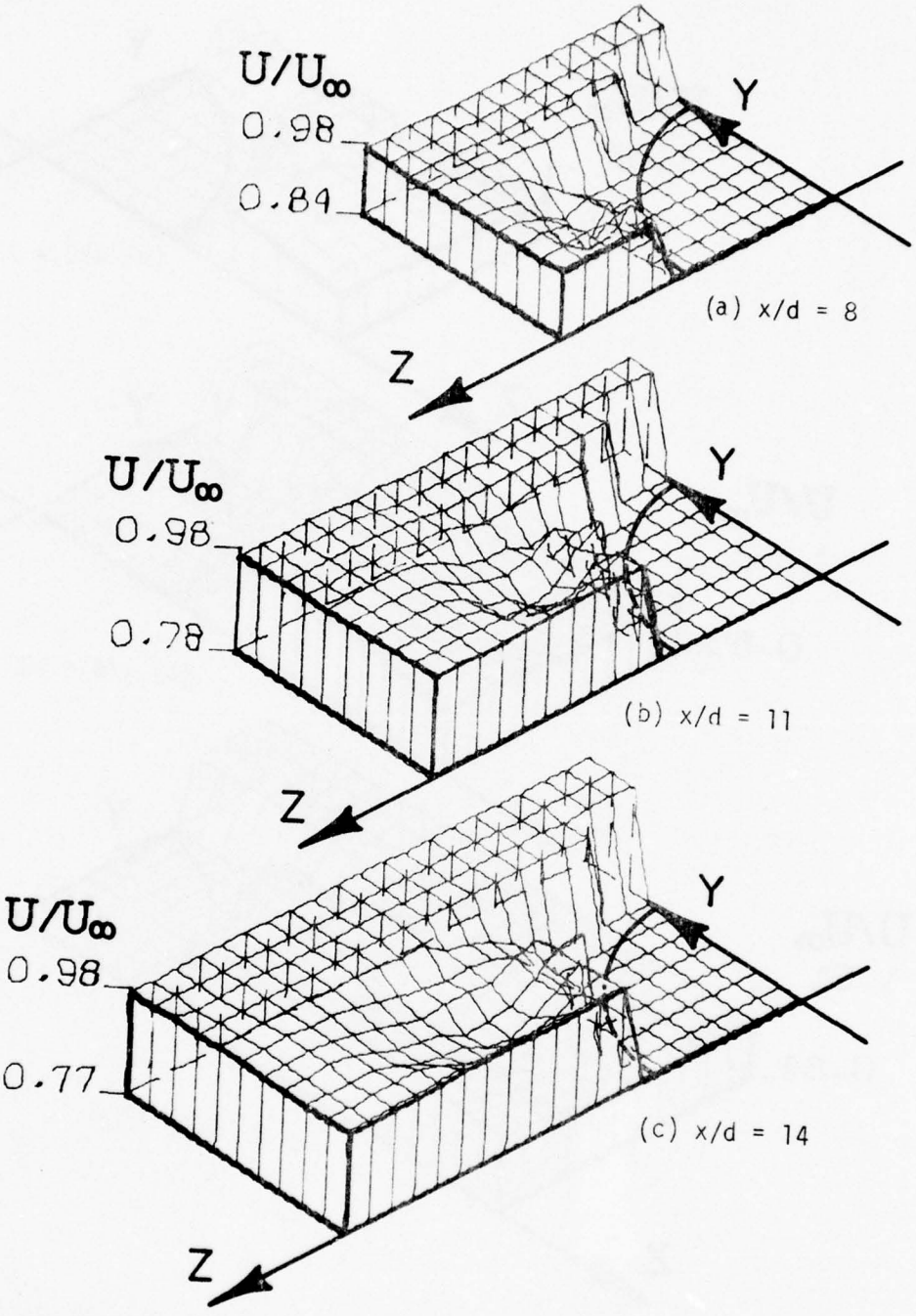


Figure 37. Axial Velocity in Cross-Flow Plane for $M_\infty = 1.95$, $R_d = .48 \times 10^6$ and $\alpha_b = 10°$.

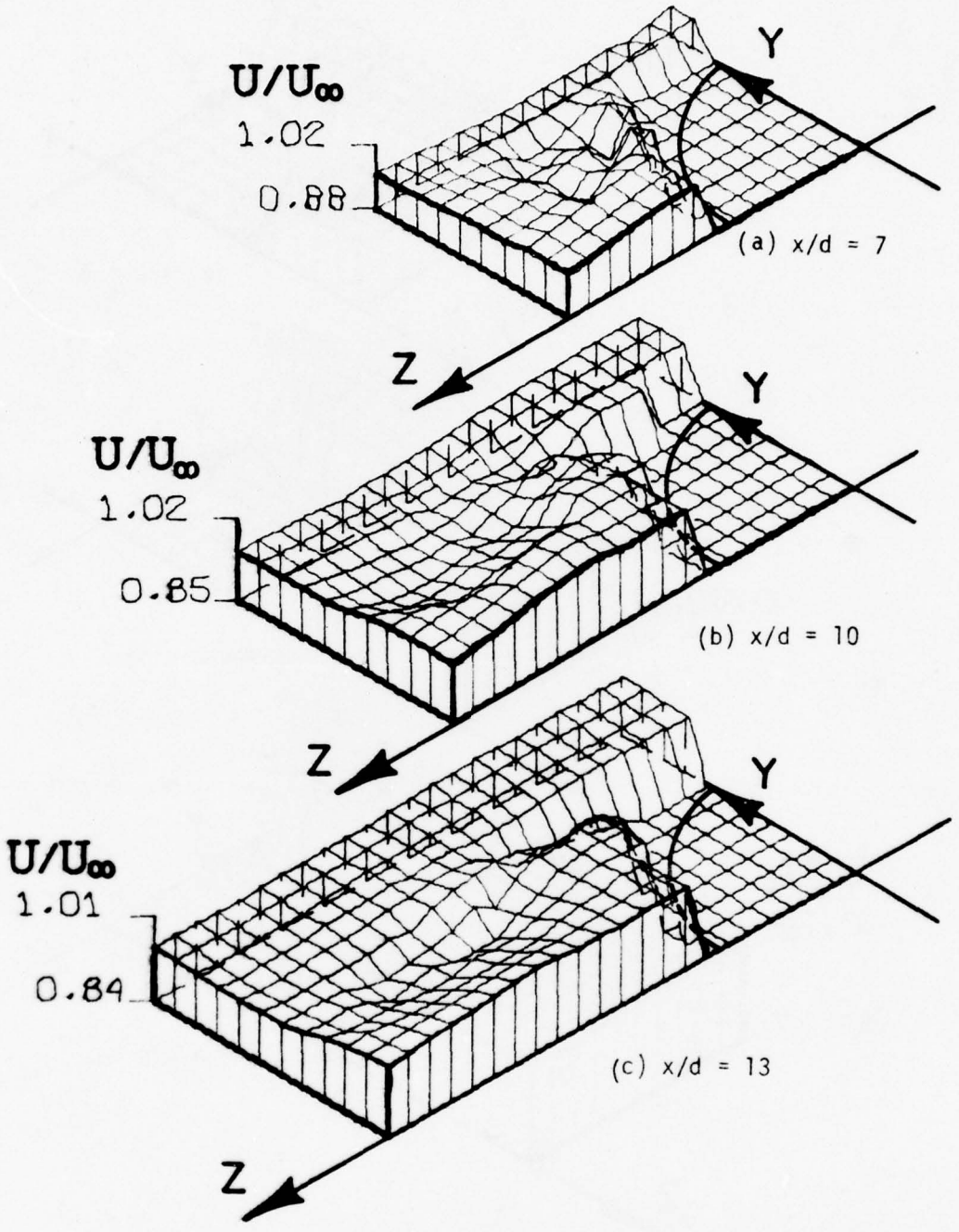


Figure 38. Axial Velocity in Cross-Flow Plane for $M_\infty = 1.95$, $R_d = .48 \times 10^6$ and $\alpha_b = 15°$.

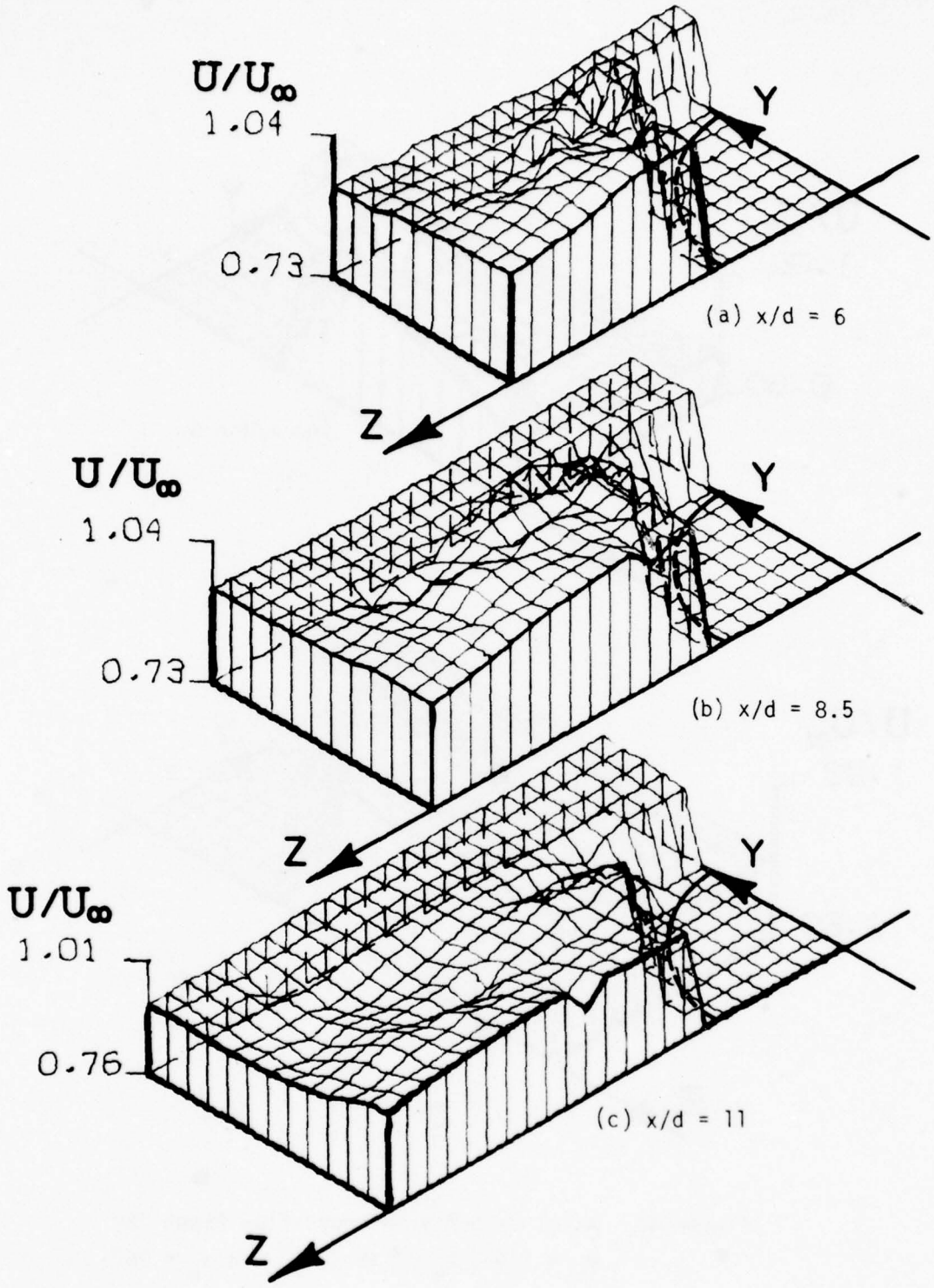


Figure 39. Axial Velocity in Cross-Flow Plane for $M_\infty = 1.95$, $R_d = .48 \times 10^6$ and $\alpha_b = 20°$.

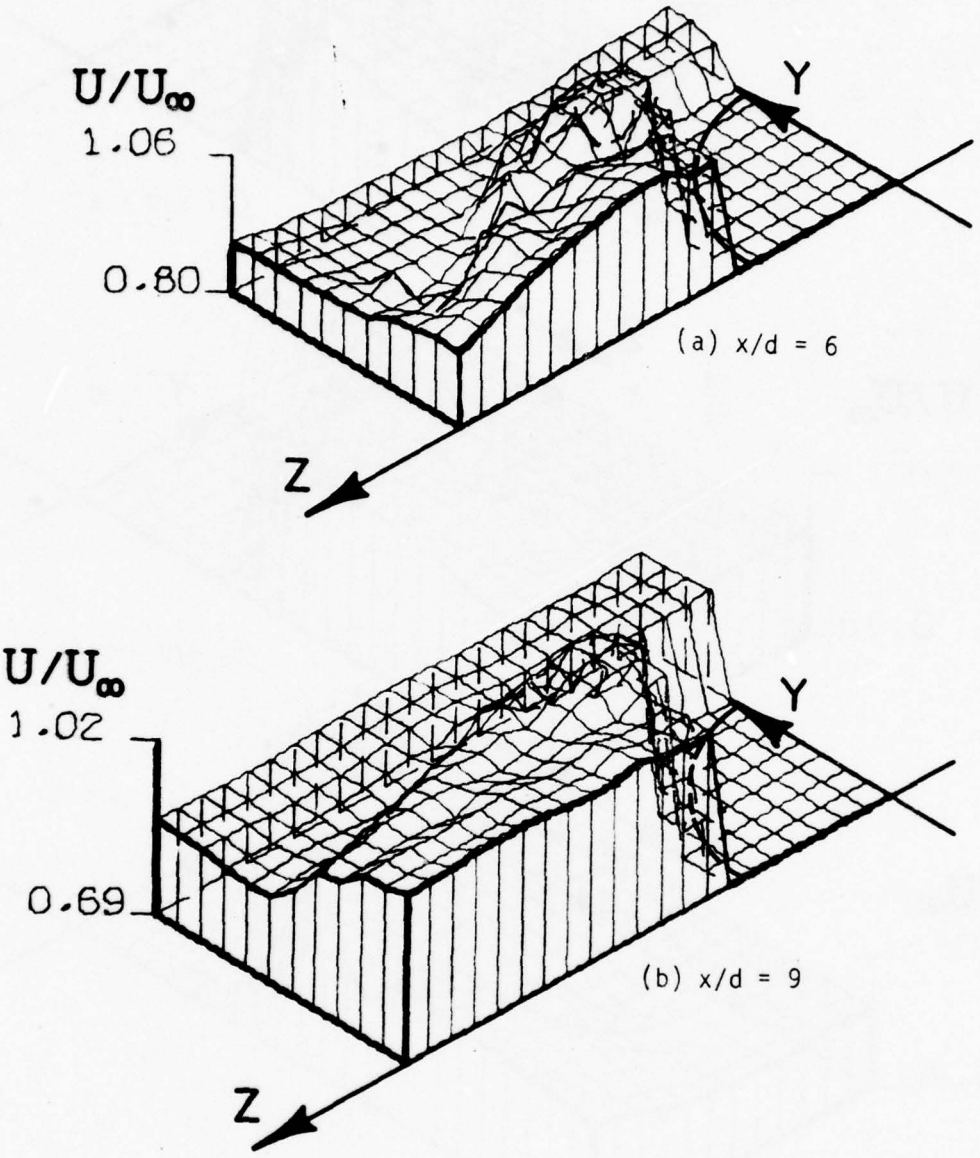


Figure 40. Axial Velocity in Cross-Flow Plane for $M_\infty = 1.95$, $R_d = .48 \times 10^6$ and $\alpha_b = 25°$.

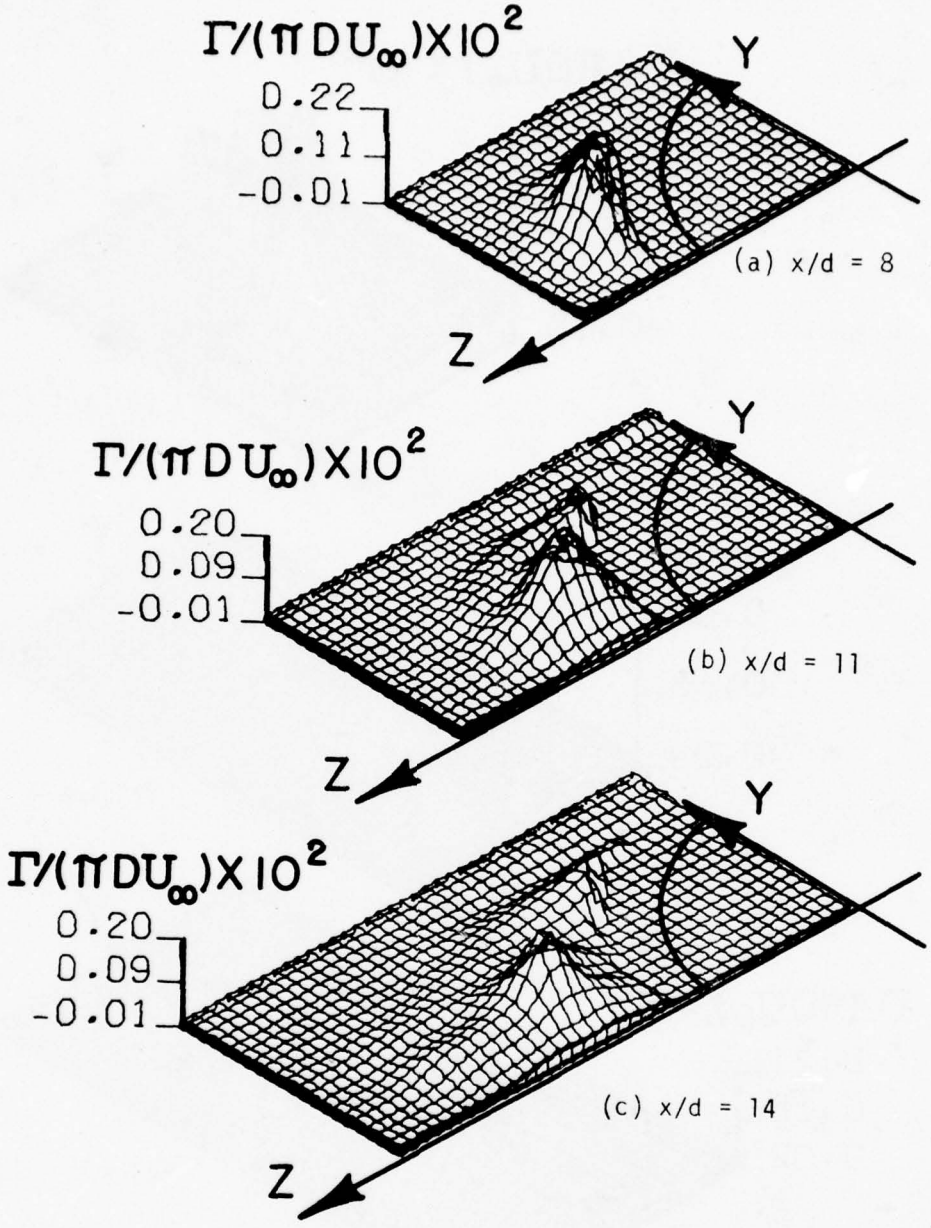


Figure 41. Local Circulation in Cross-Flow Plane for $M_\infty = 1.95$, $R_d = .48 \times 10^6$ and $\alpha_b = 10°$.

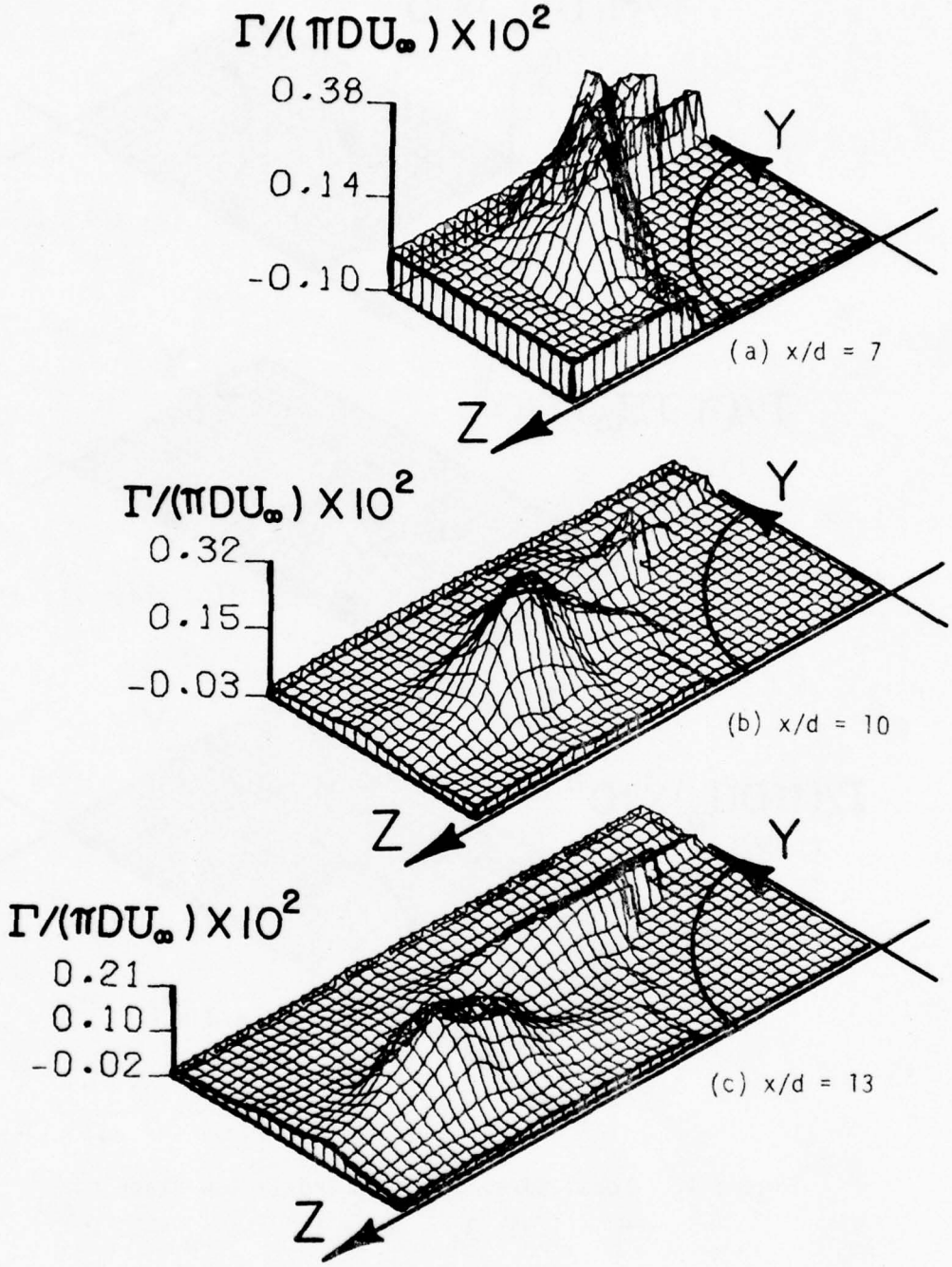


Figure 42. Local Circulation in Cross-Flow Plane for $M_\infty = 1.95$, $R_d = .48 \times 10^6$ and $\alpha_b = 15°$.

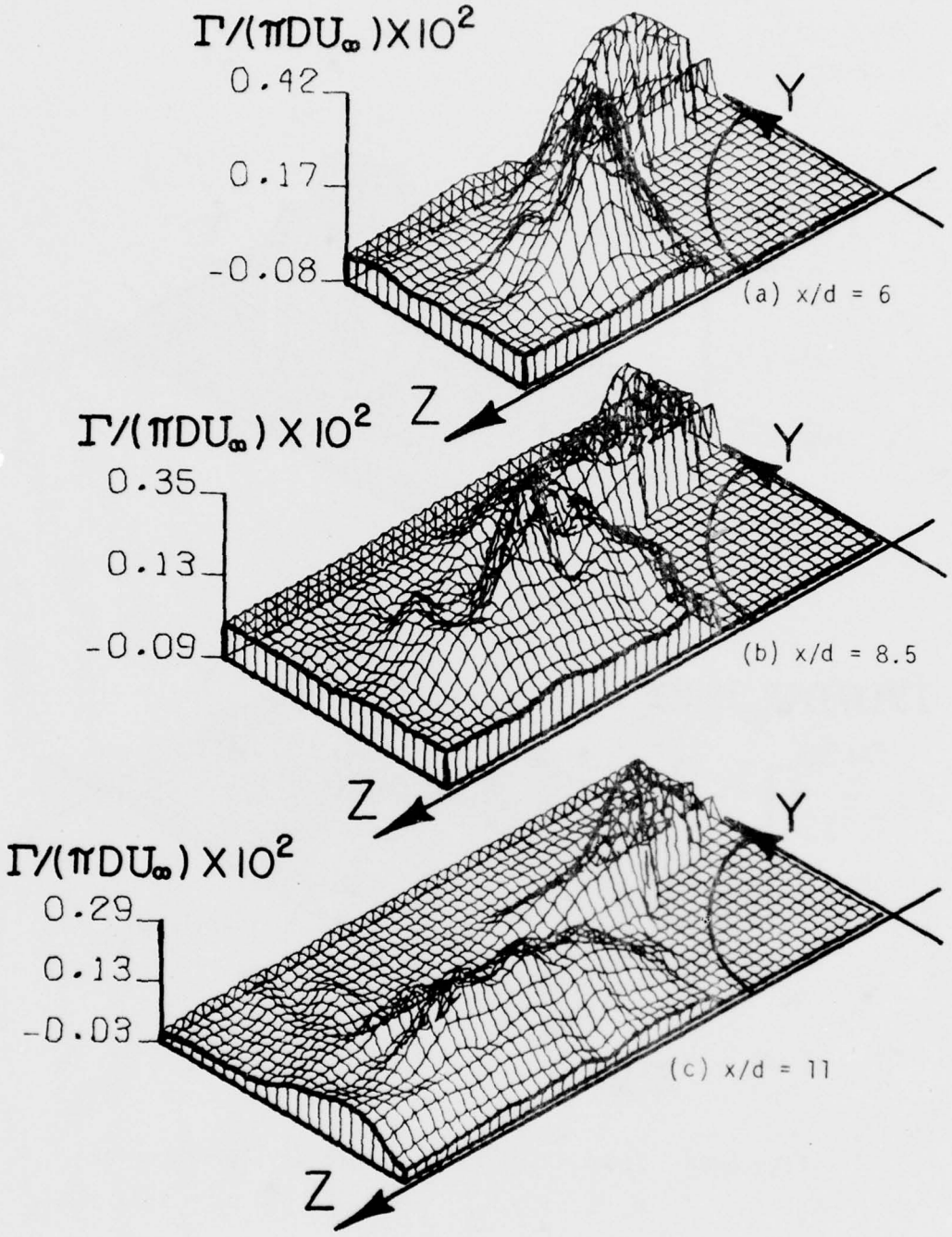


Figure 43. Local Circulation in Cross-Flow Plane for $M_\infty = 1.95$, $R_d = .48 \times 10^6$ and $\alpha_b = 20°$.

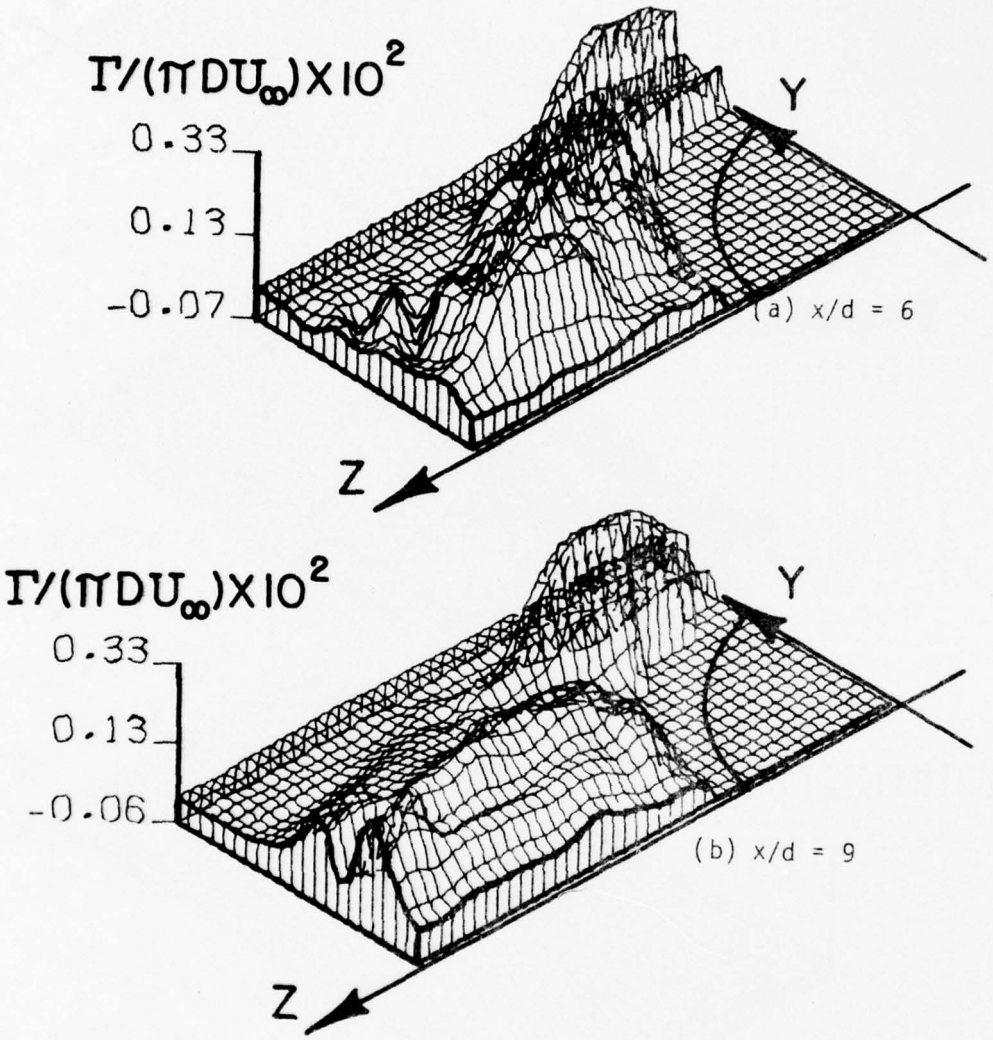
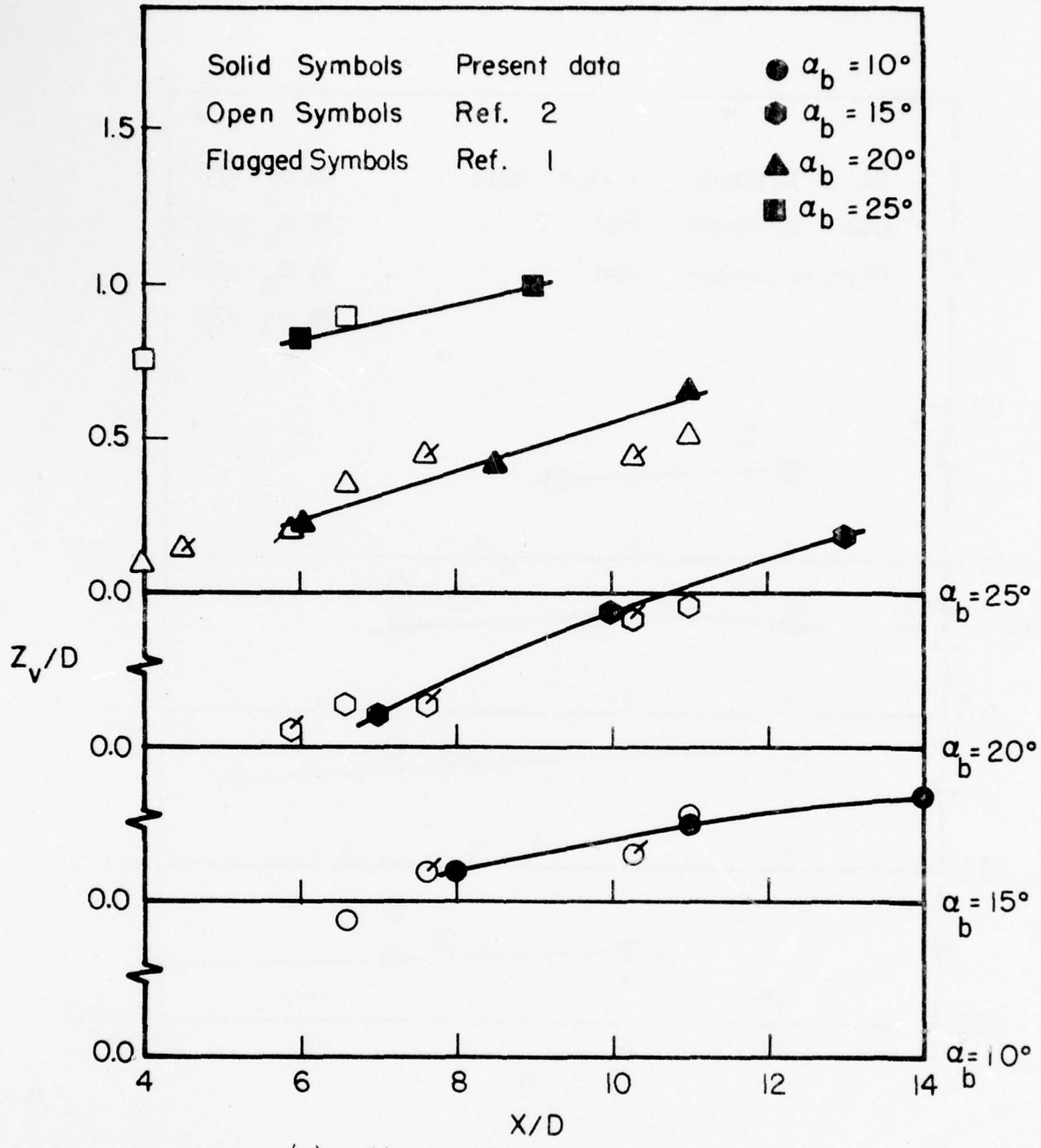
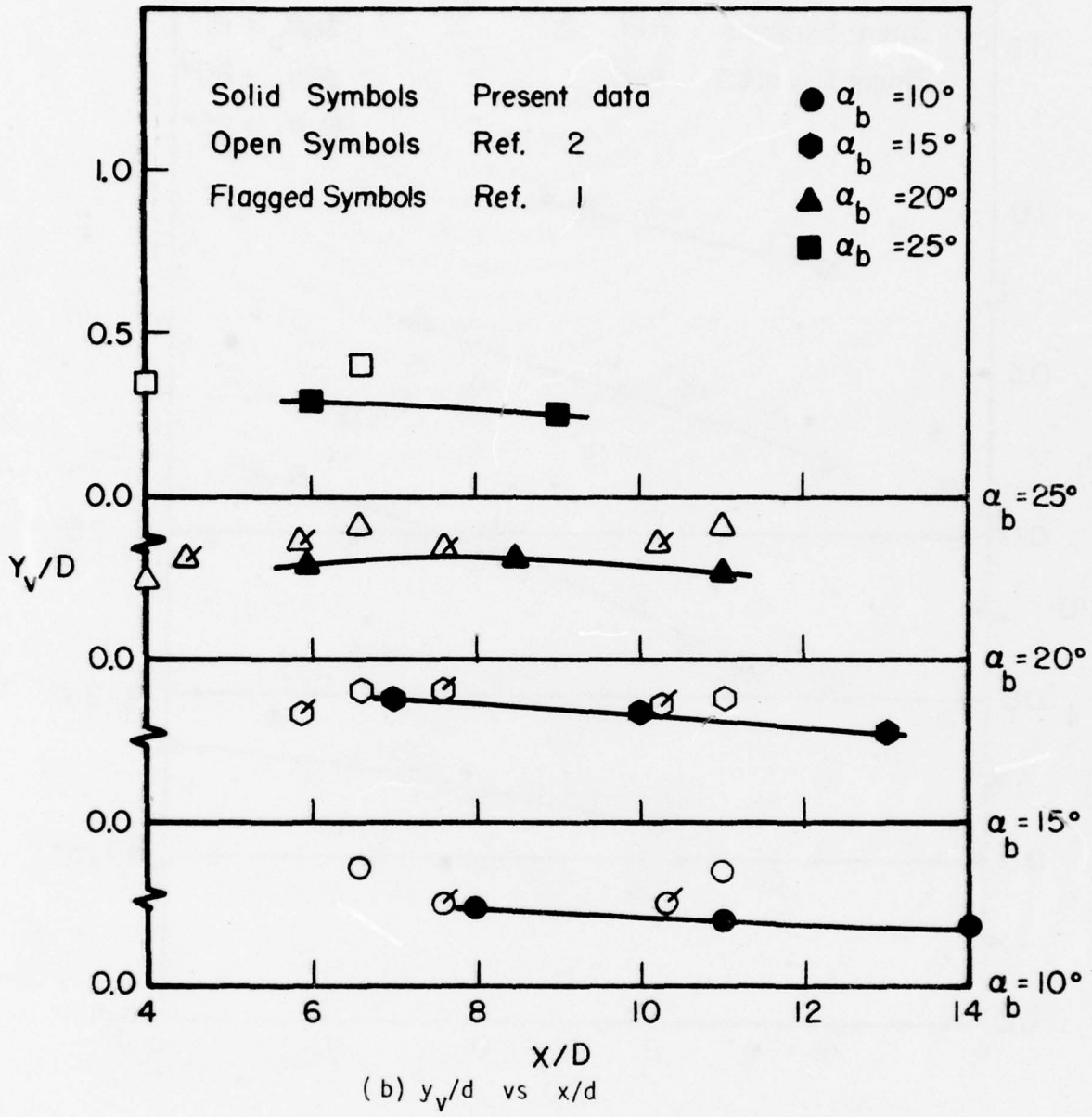


Figure 44. Local Circulation in Cross-Flow Plane for $M_\infty = 1.95$, $R_d = .48 \times 10^6$ and $\alpha_b = 25°$.



(a) z_v/d vs x/d

Figure 45. Vortex Center Location in the Cross-Flow Plane for M_∞ = 1.95 and R_d = .48 x 10^6



(b) y_v/d vs x/d

Figure 45. Vortex Center Location in the Cross-Flow Plane for M_∞ = 1.95 and R_d = .48 x 10^6 (Concluded).

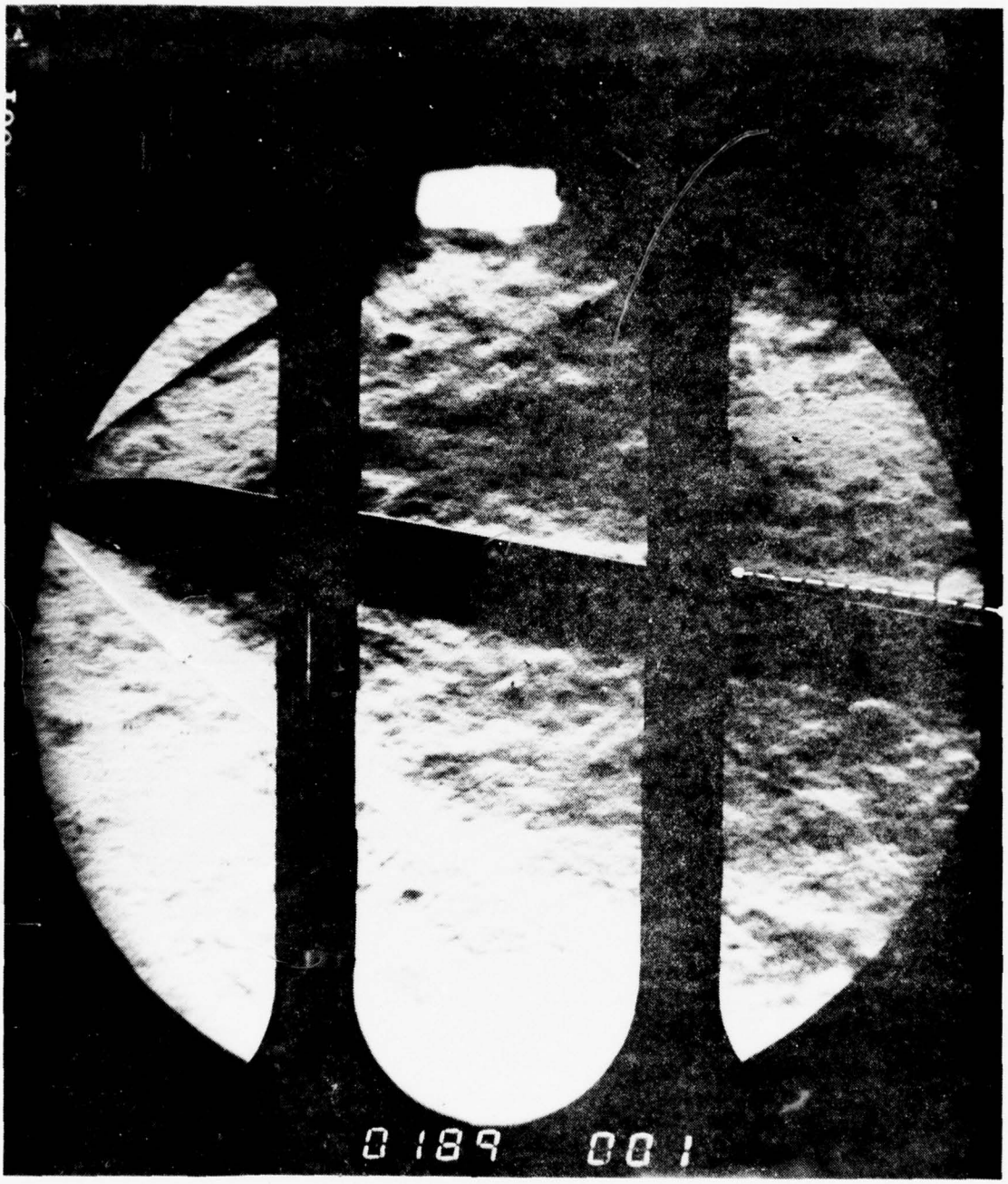


Figure 46. Schlieren Photograph for $M_\infty = 1.95$, $R_d = 0.48 \times 10^6$ and $\alpha_b = 10^\circ$

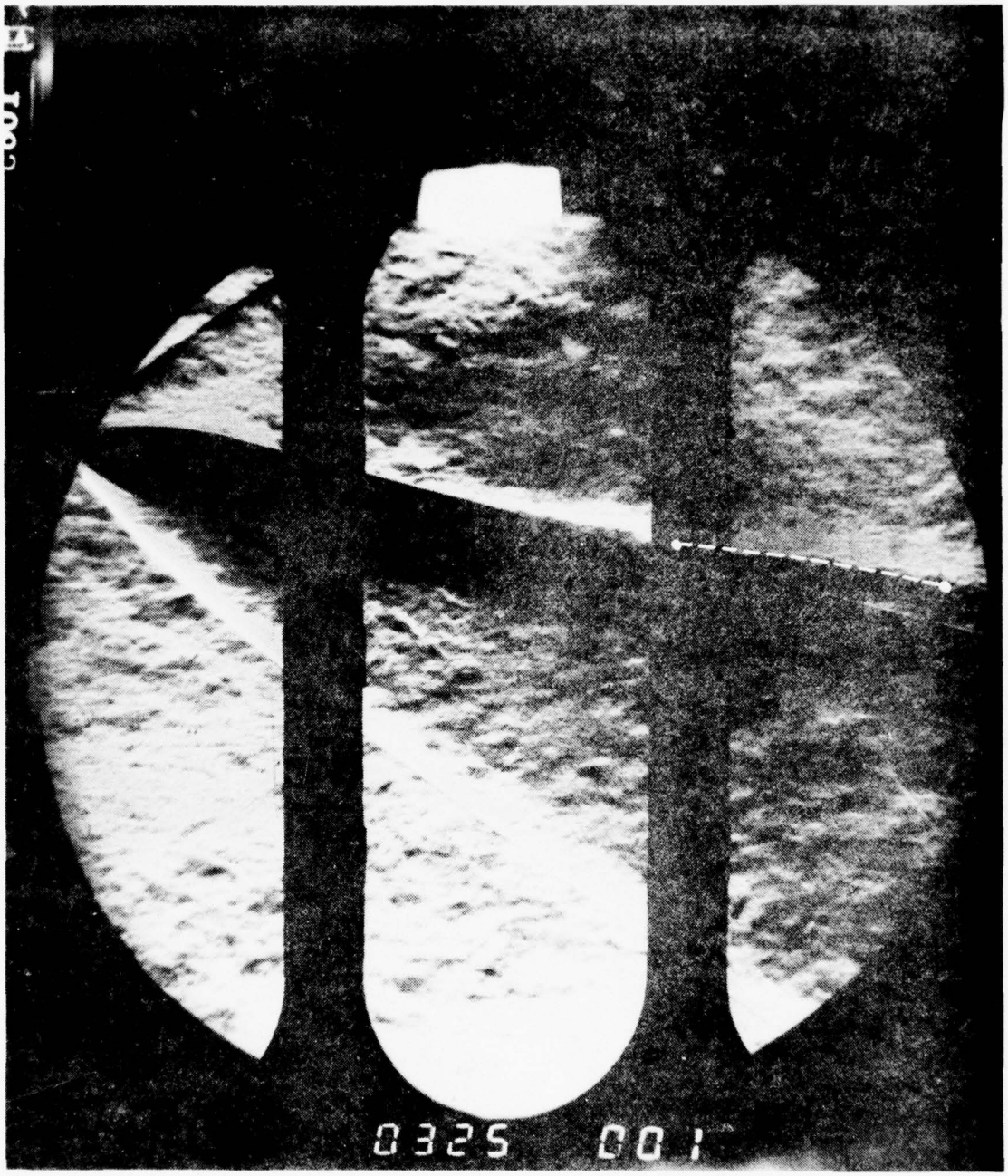


Figure 47. Schlieren Photograph for $M_\infty = 1.95$, $R_d = 0.48 \times 10^6$ and $\alpha_b = 15^\circ$



Figure 48. Schlieren Photograph for $M_\infty = 1.95$, $R_d = 0.48 \times 10^6$ and $\alpha_b = 20^\circ$

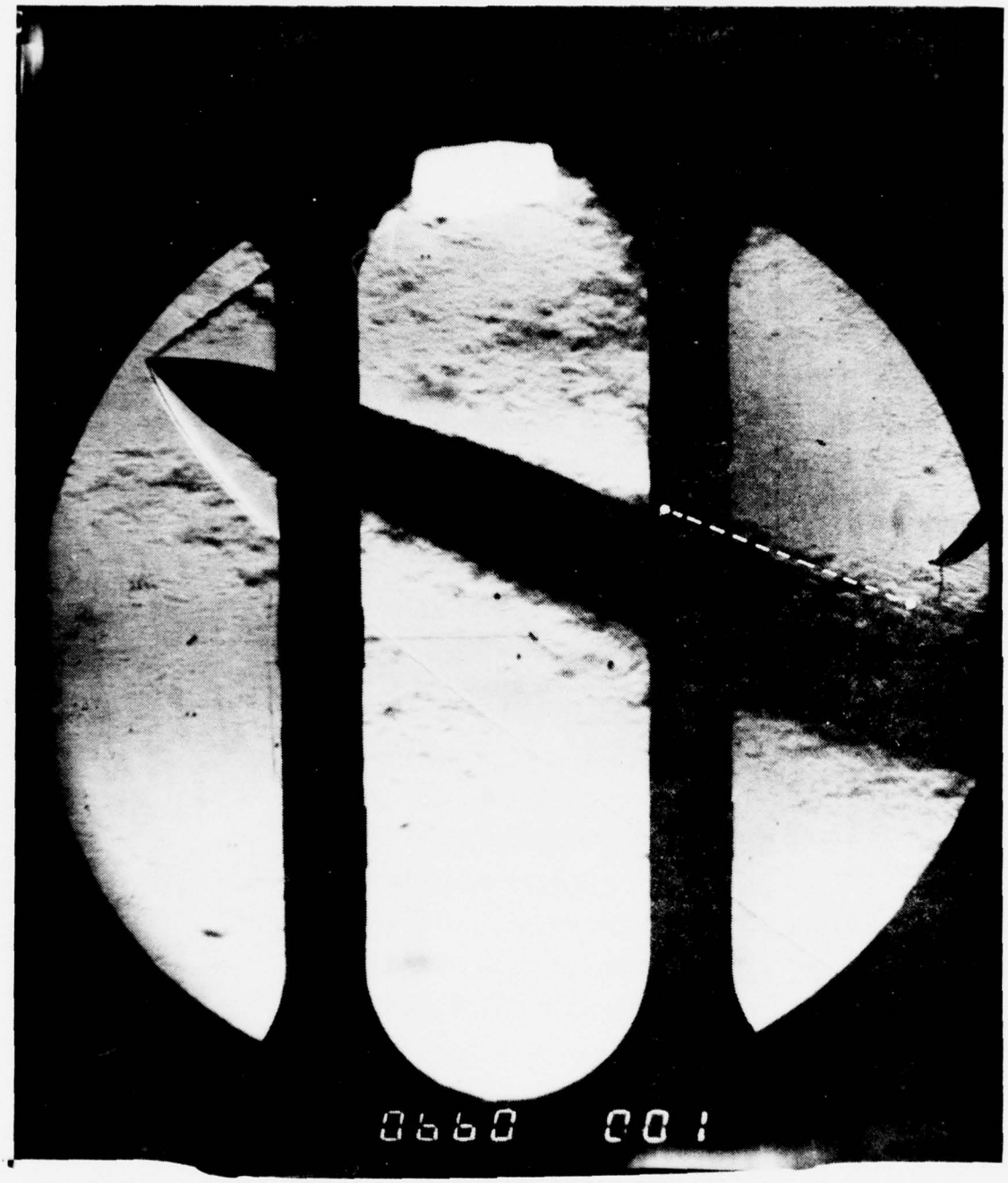


Figure 49. Schlieren Photograph for $M_\infty = 1.95$, $R_d = 0.48 \times 10^6$ and $\alpha_b = 25^\circ$

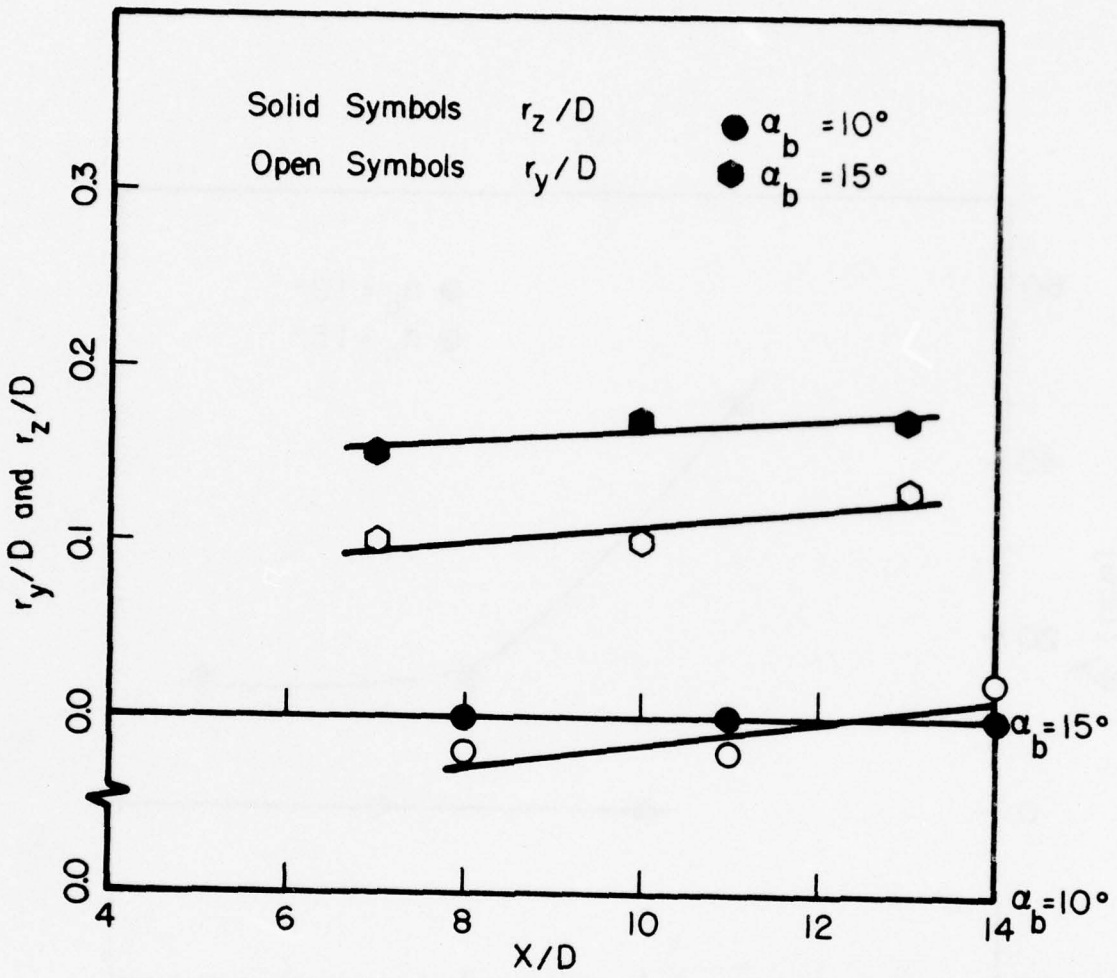


Figure 50. Vortex Core Radii for
M_∞ = 1.95 and R_d = .48 x 10^6

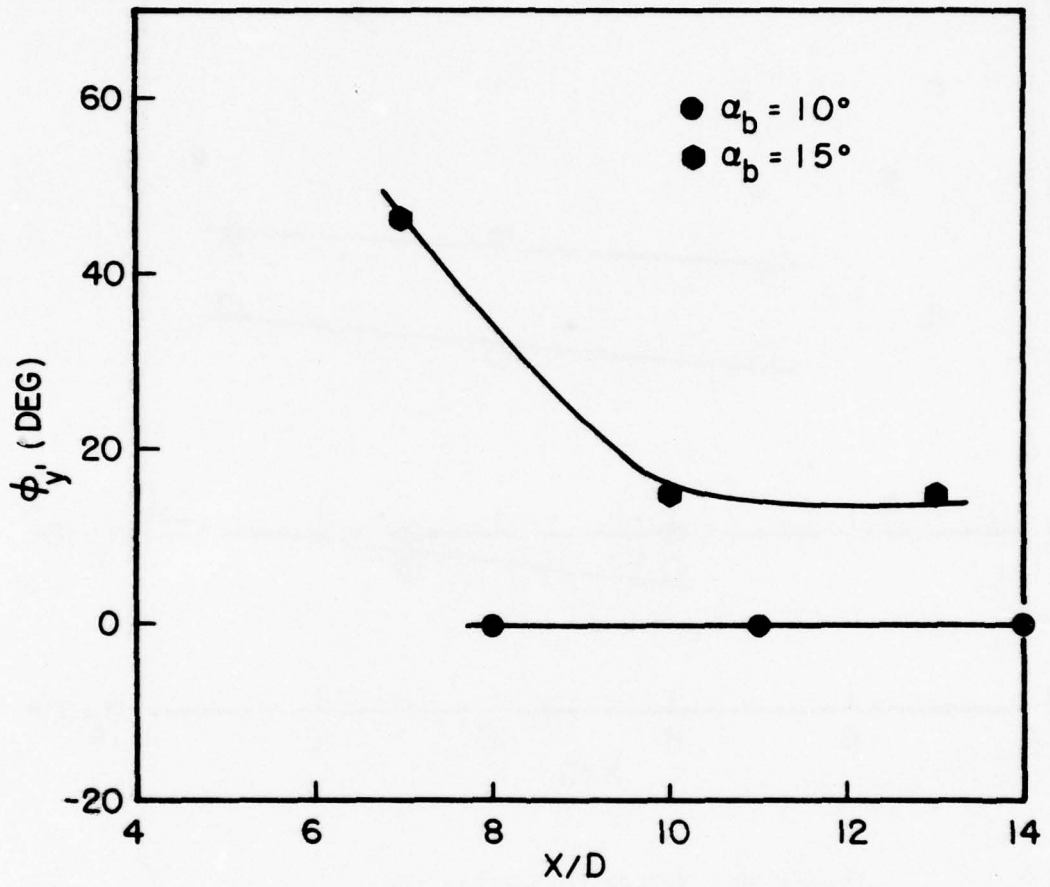


Figure 51. Angular Orientation of Vortex Core for M_∞ = 1.95 and R_d = .48 x 10^6

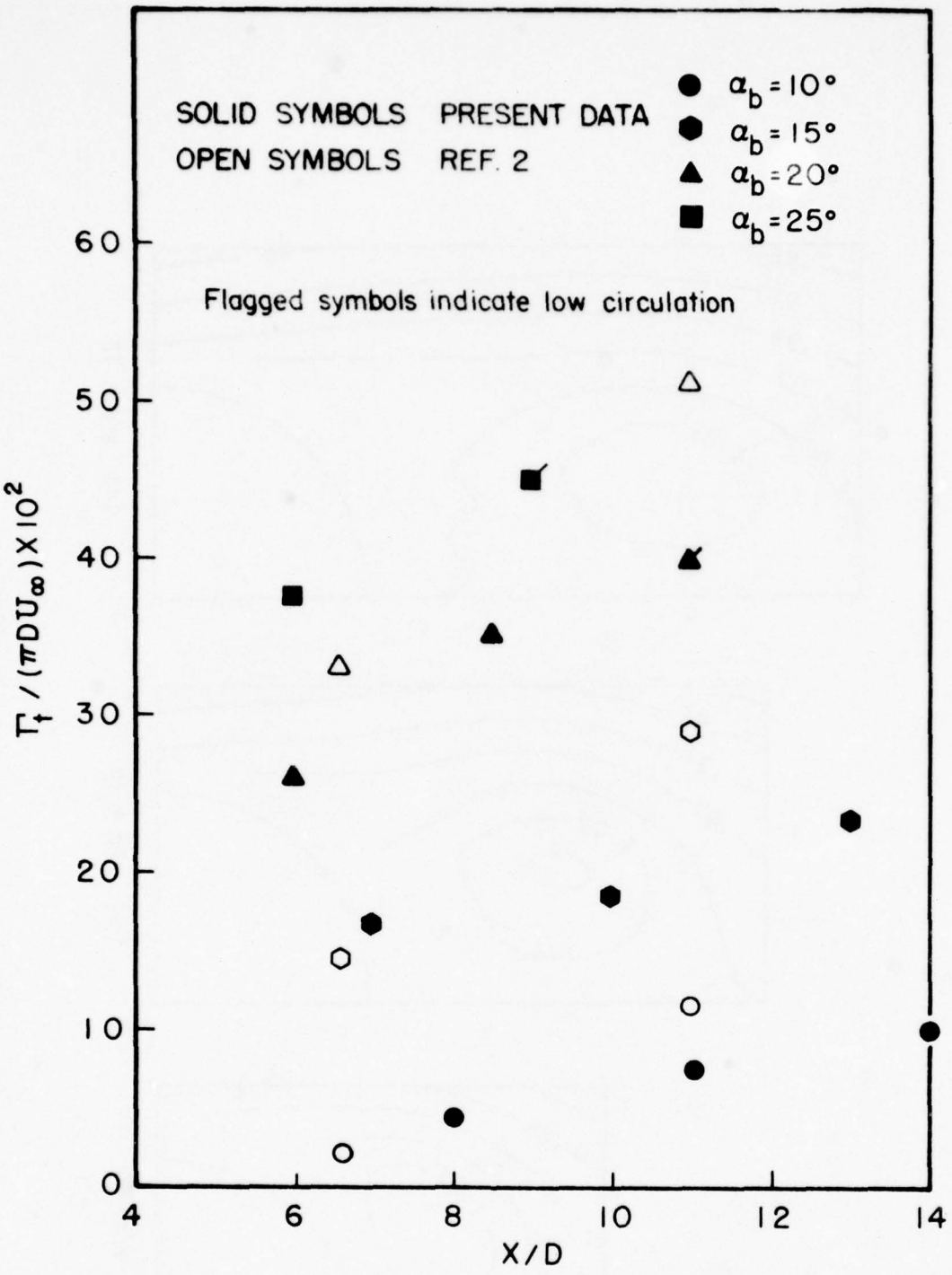
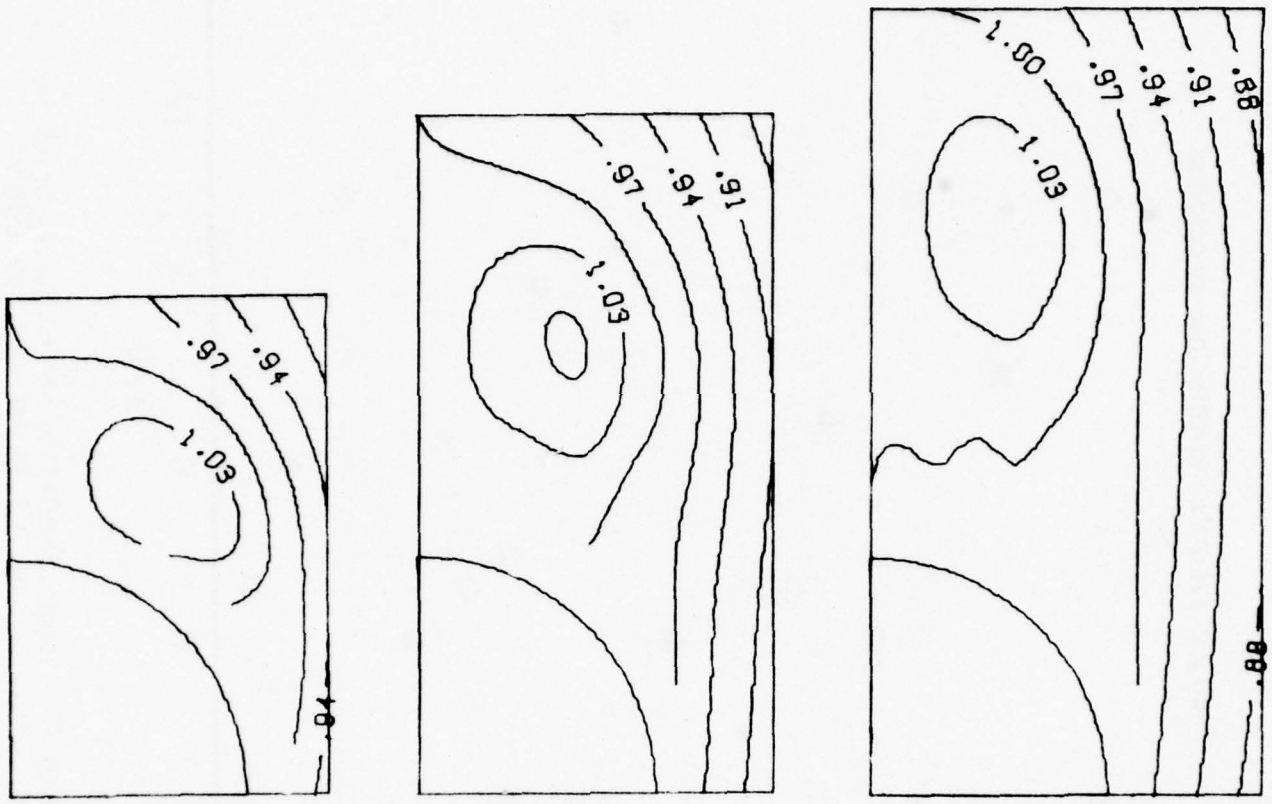


Figure 52. Total Circulation in the Survey Grids for $M_\infty = 1.95$ and $R_d = .48 \times 10^6$



(a) x/d = 7 (b) x/d = 10 (c) x/d = 13

Figure 53. Streamlines in the Cross-Flow Plane for M_∞ = 1.95, R_d = .48 x 10^6 and α_b = 15°

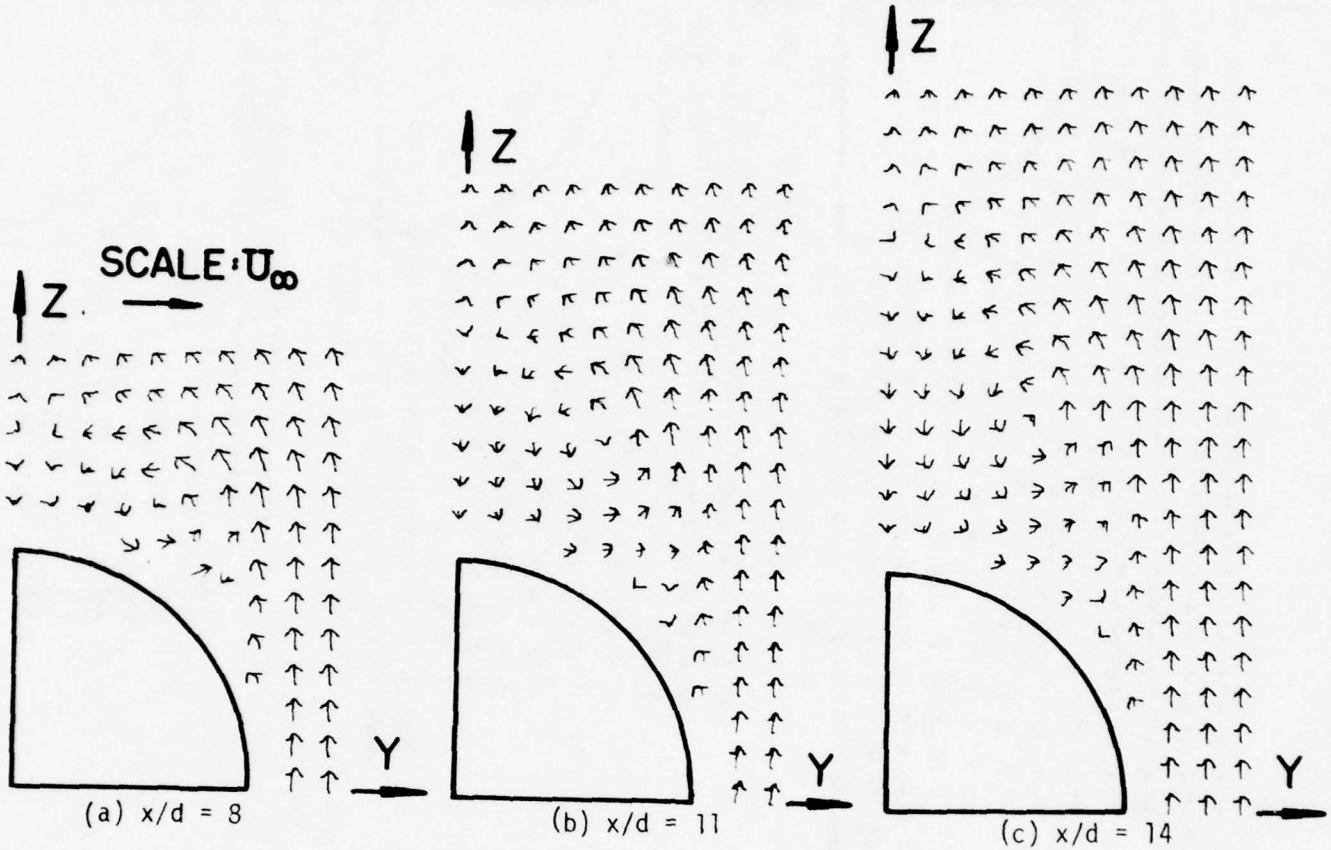


Figure 54. Cross-Flow Plane Vector Plot for M_∞ = 2., R_d = 1.75 x 10^6 and α_b = 10°.

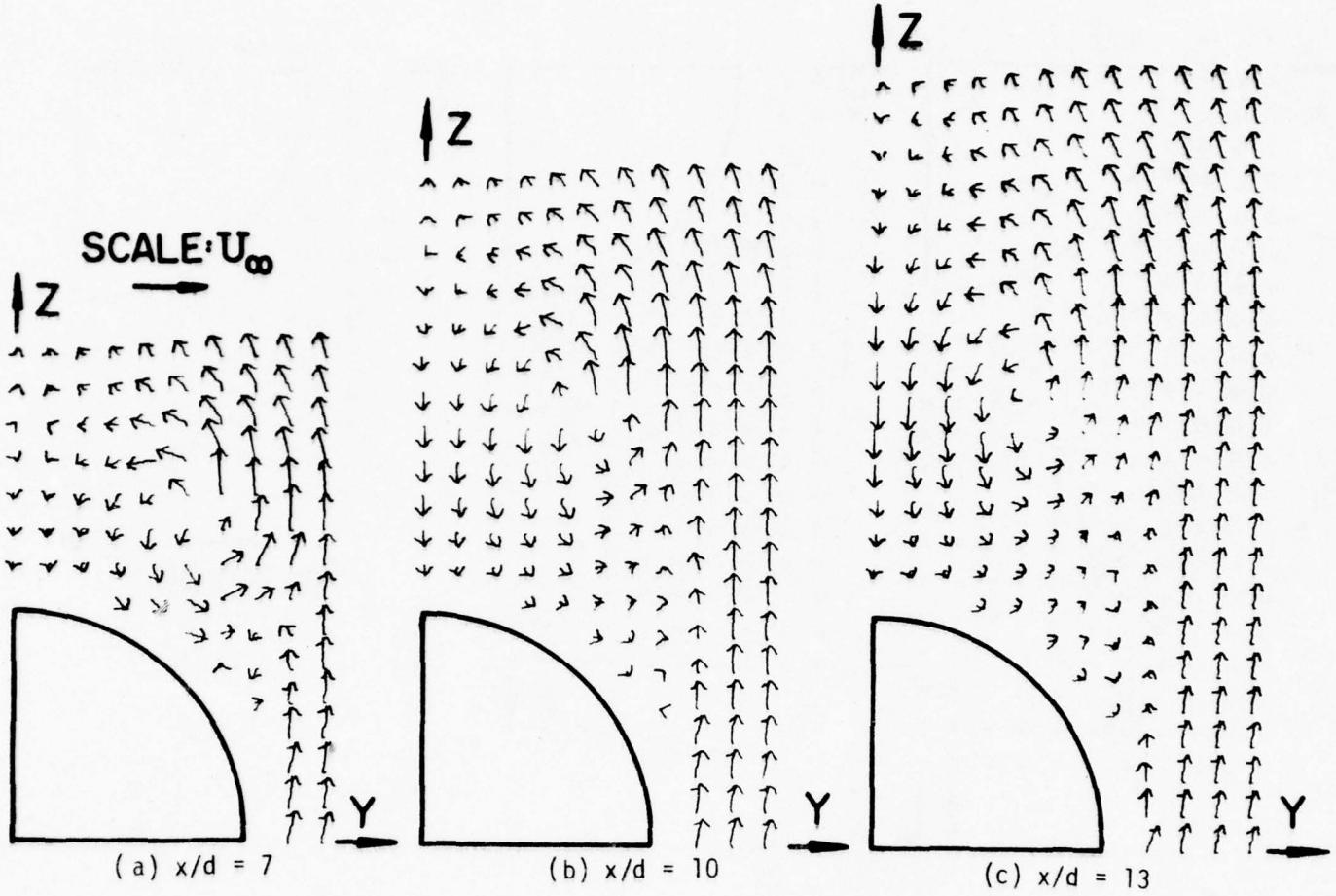
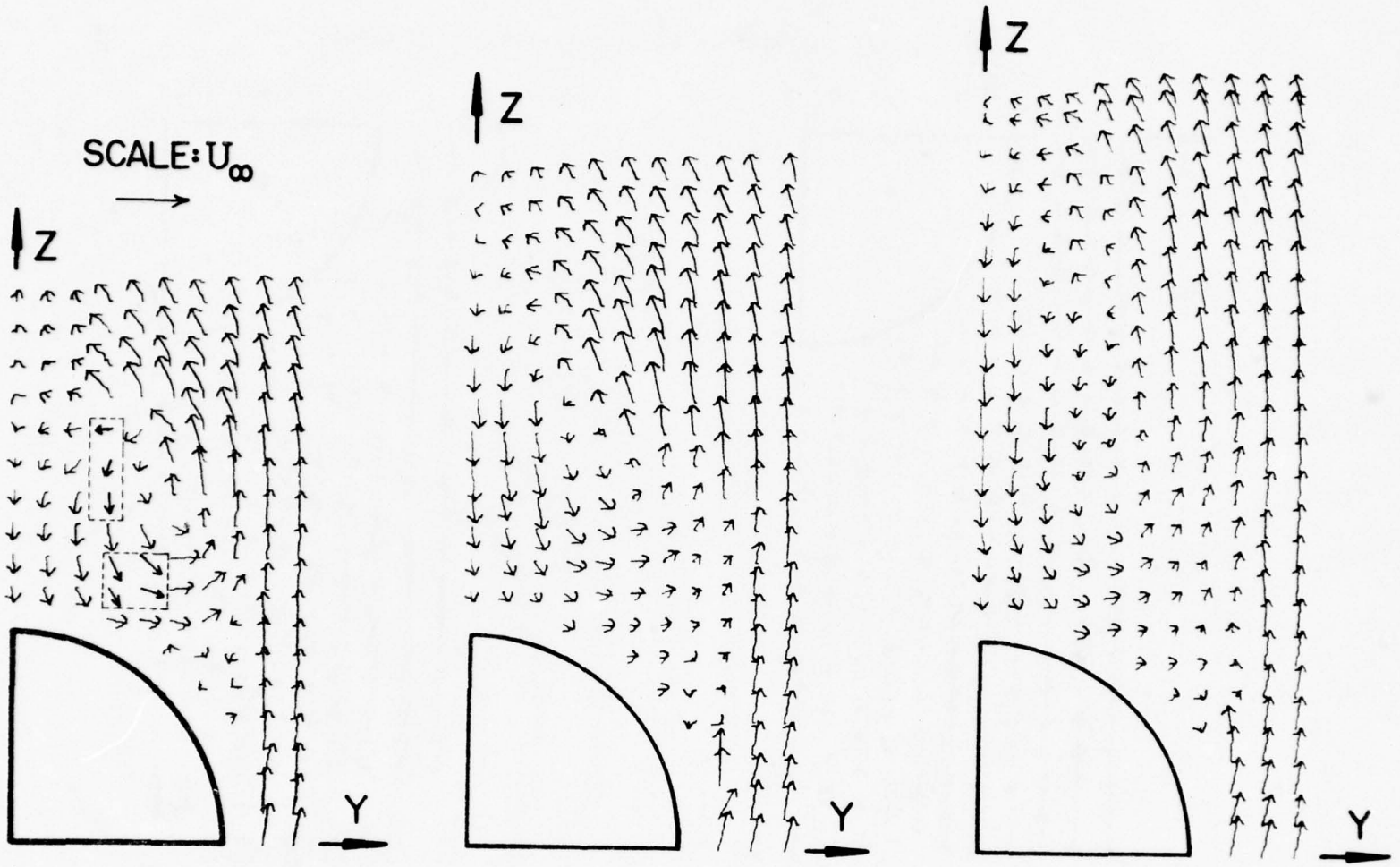
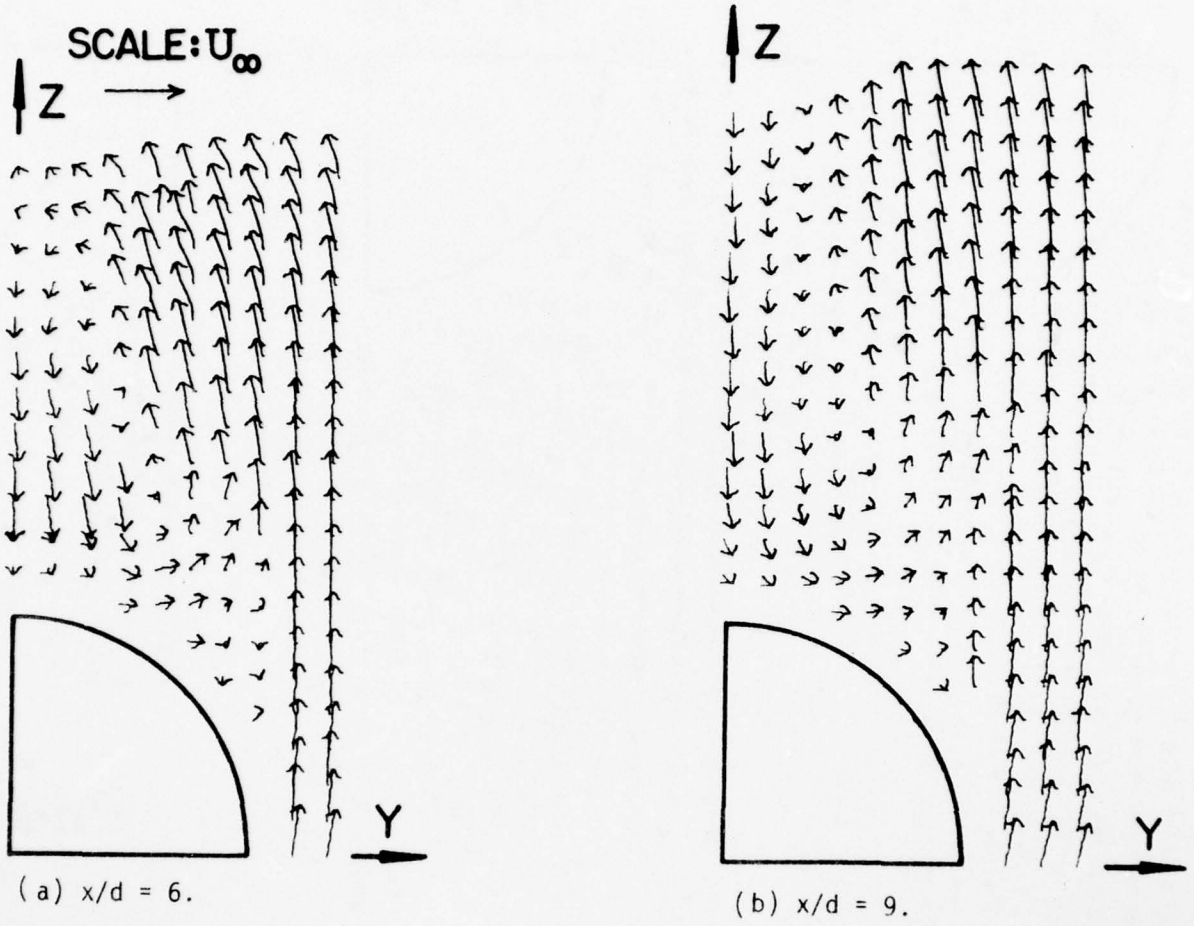


Figure 55. Cross-Flow Plane Vector Plot for $M_\infty = 2.$, $R_d = 1.75 \times 10^6$ and $\alpha_b = 15°$.



(a) x/d = 6. (b) x/d = 8.5 (c) x/d = 11.

Figure 56. Cross-Flow Plane Vector Plot for M_∞ = 2., R_d = 1.75 x 10^6 and α_b = 20°.



(a) x/d = 6.

(b) x/d = 9.

Figure 57. Cross-Flow Plane Vector Plot for $M_\infty = 2.$, $R_d = 1.75 \times 10^6$ and $\alpha_b = 25°$.

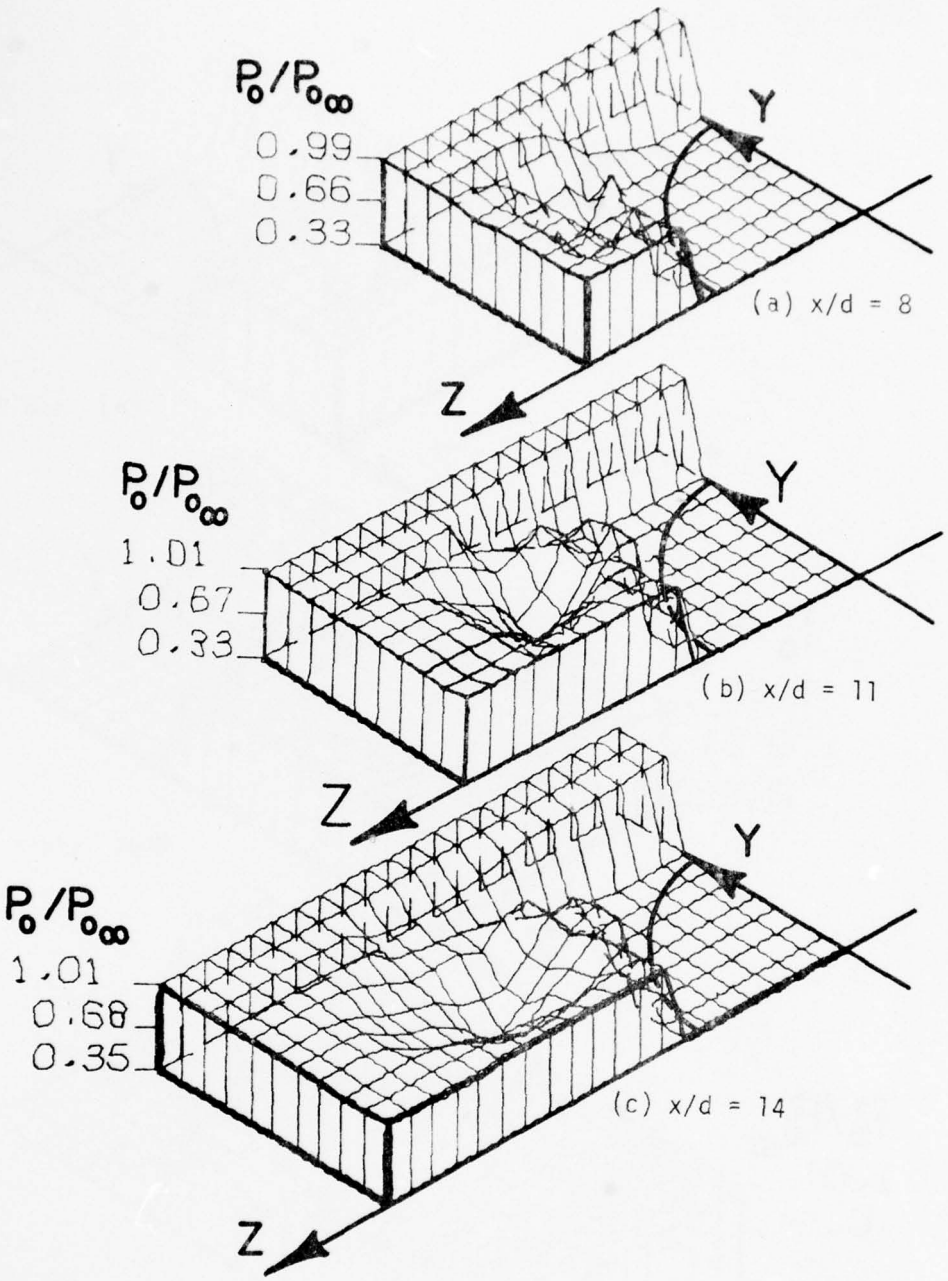


Figure 58. Total Pressure in Cross-Flow Plane for $M_\infty = 2.$, $R_d = 1.75 \times 10^6$ and $\alpha_b = 10°$.

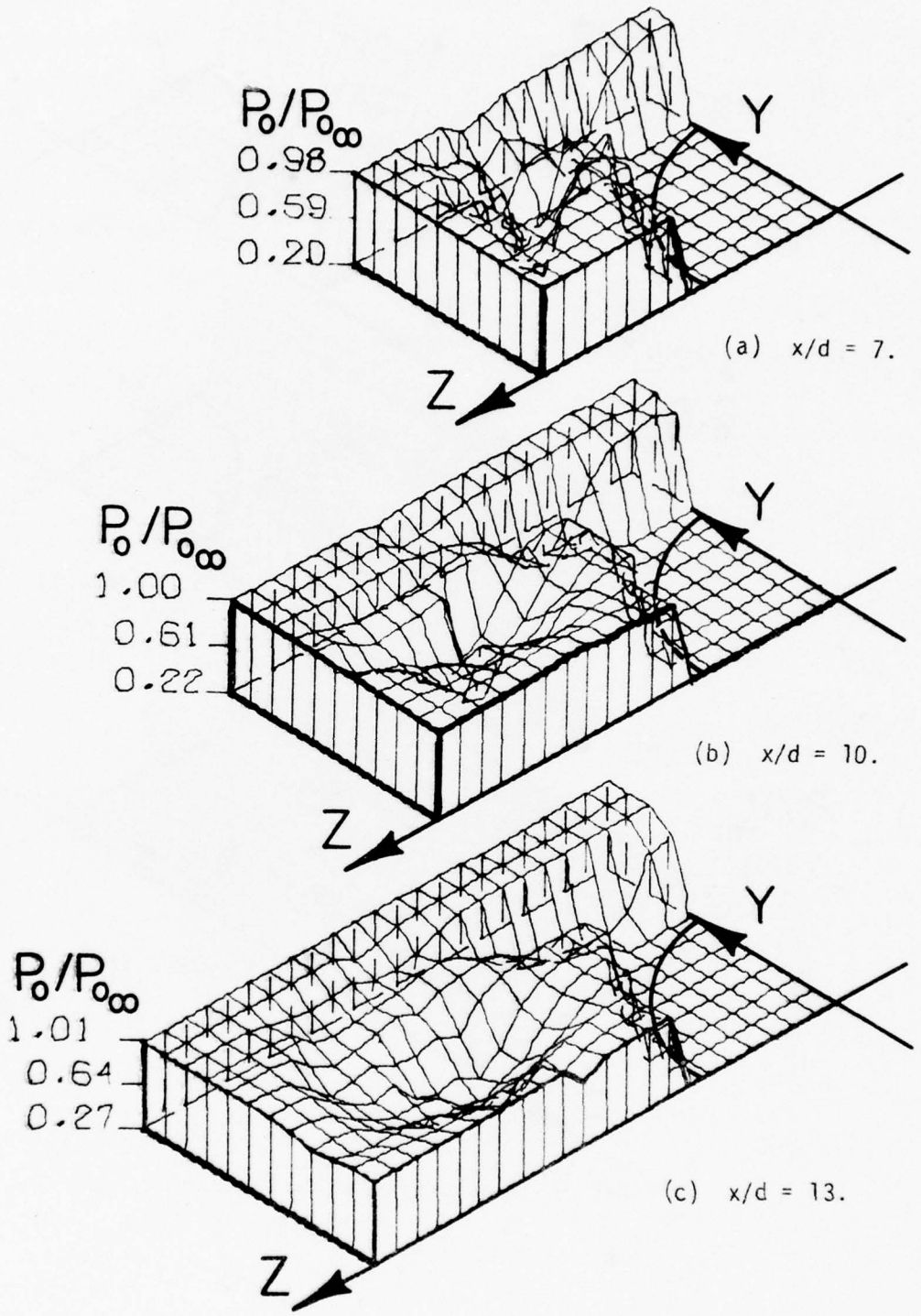


Figure 59. Total Pressure in Cross-Flow Plane for $M_\infty = 2.$, $R_d = 1.75 \times 10^6$ and $\alpha_b = 15°$.

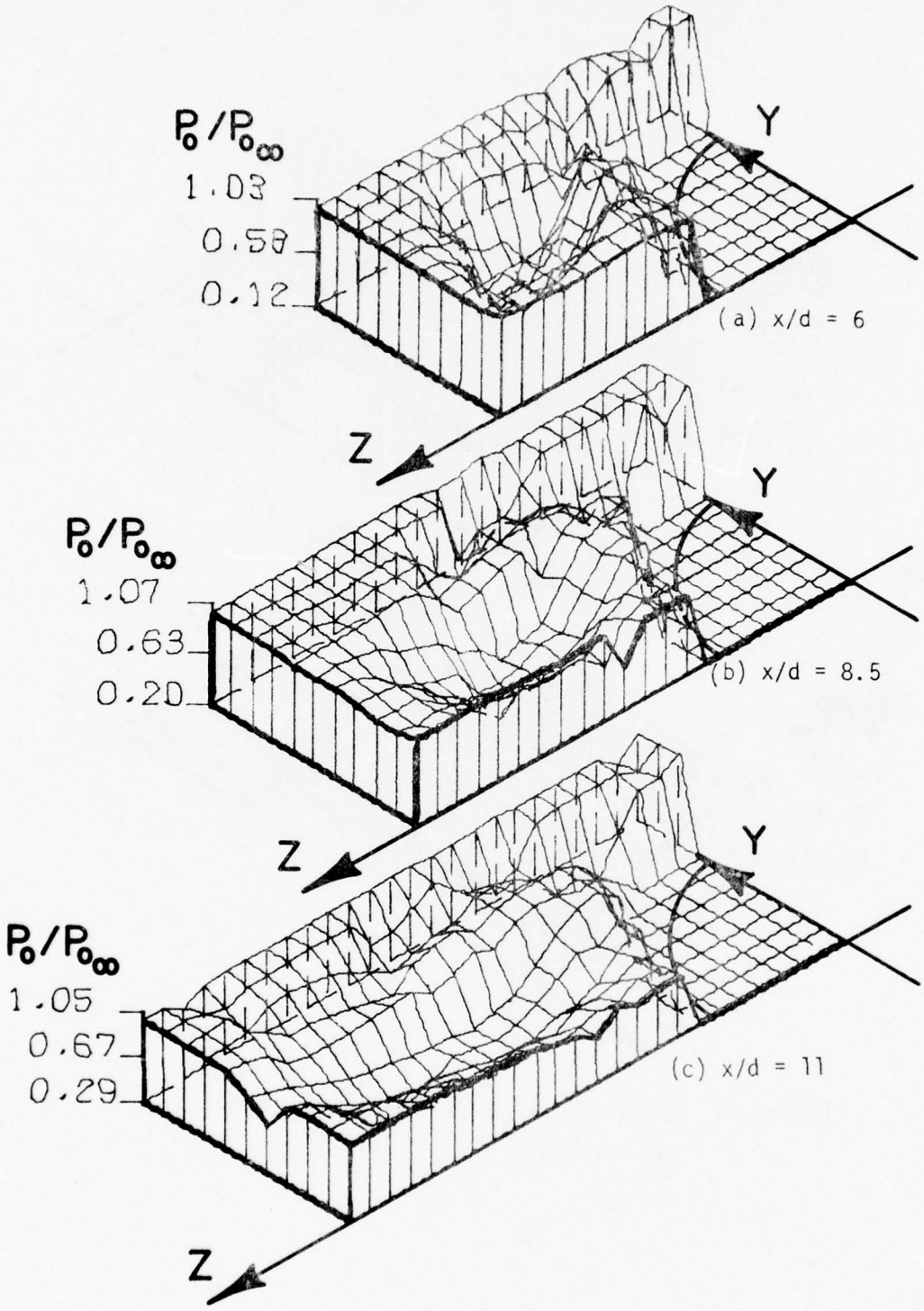


Figure 60. Total Pressure in Cross Flow-Plane for $M_\infty = 2.$, $R_d = 1.75 \times 10^6$ and $\alpha_b = 20°$.

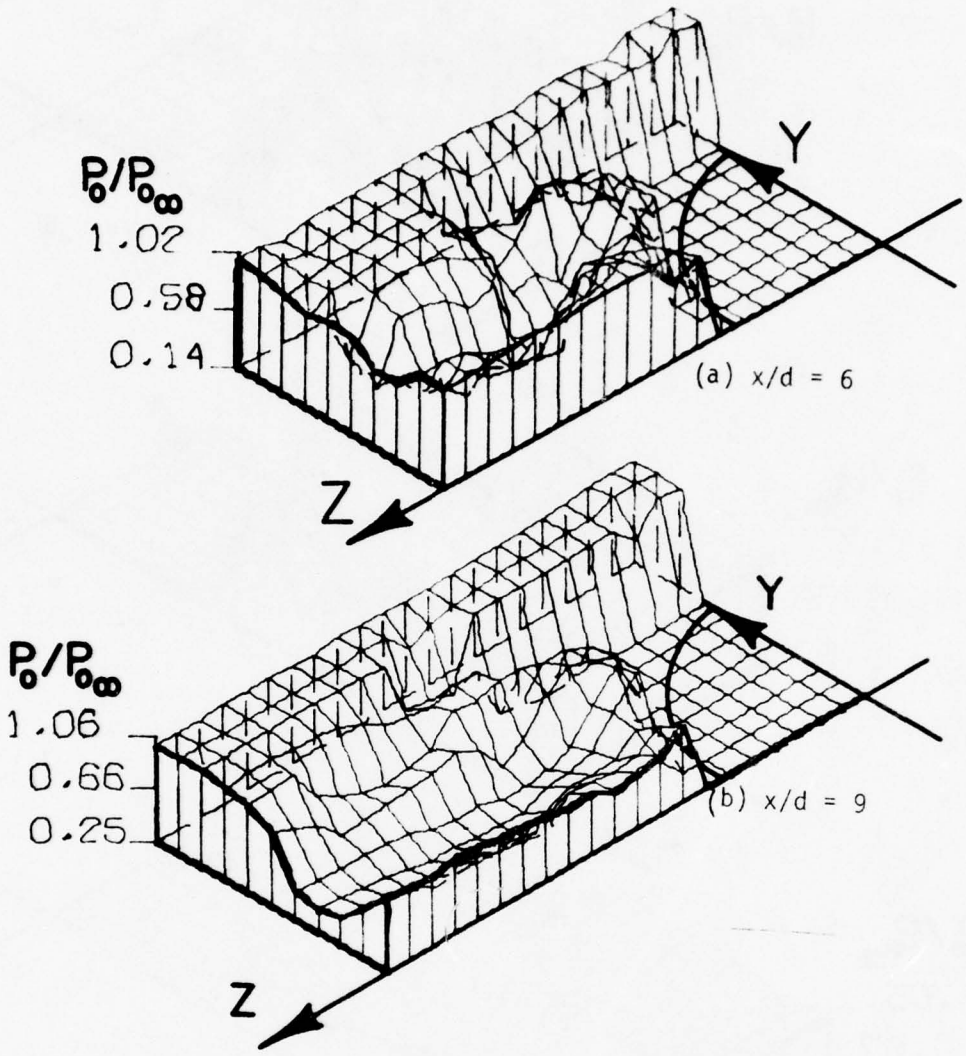


Figure 61. Total Pressure in Cross-Flow Plane for $M_\infty = 2.$, $R_d = 1.75 \times 10^6$ and $\alpha_b = 25°$.

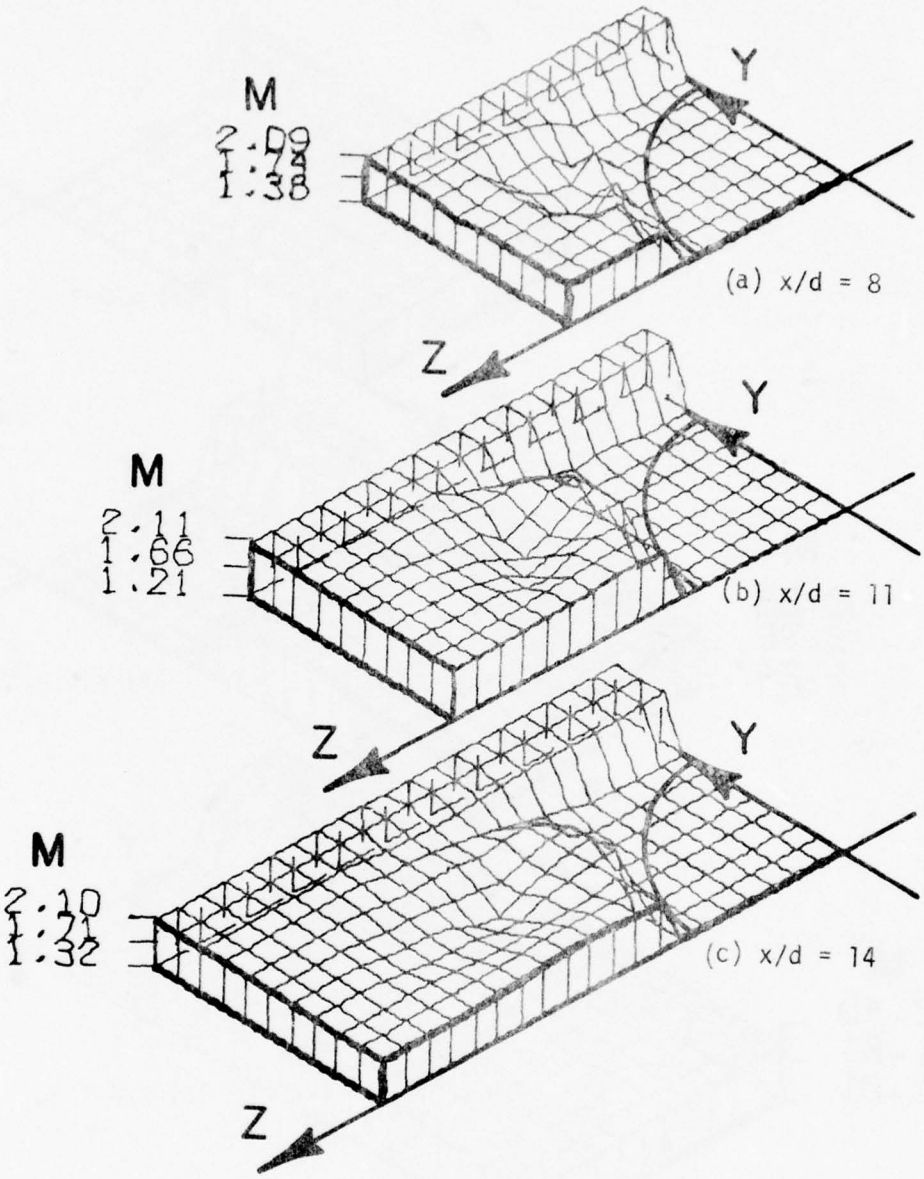


Figure 62. Mach Number in Cross-Flow Plane for $M_\infty = 2.$, $R_d = 1.75 \times 10^6$ and $\alpha_b = 10°$.

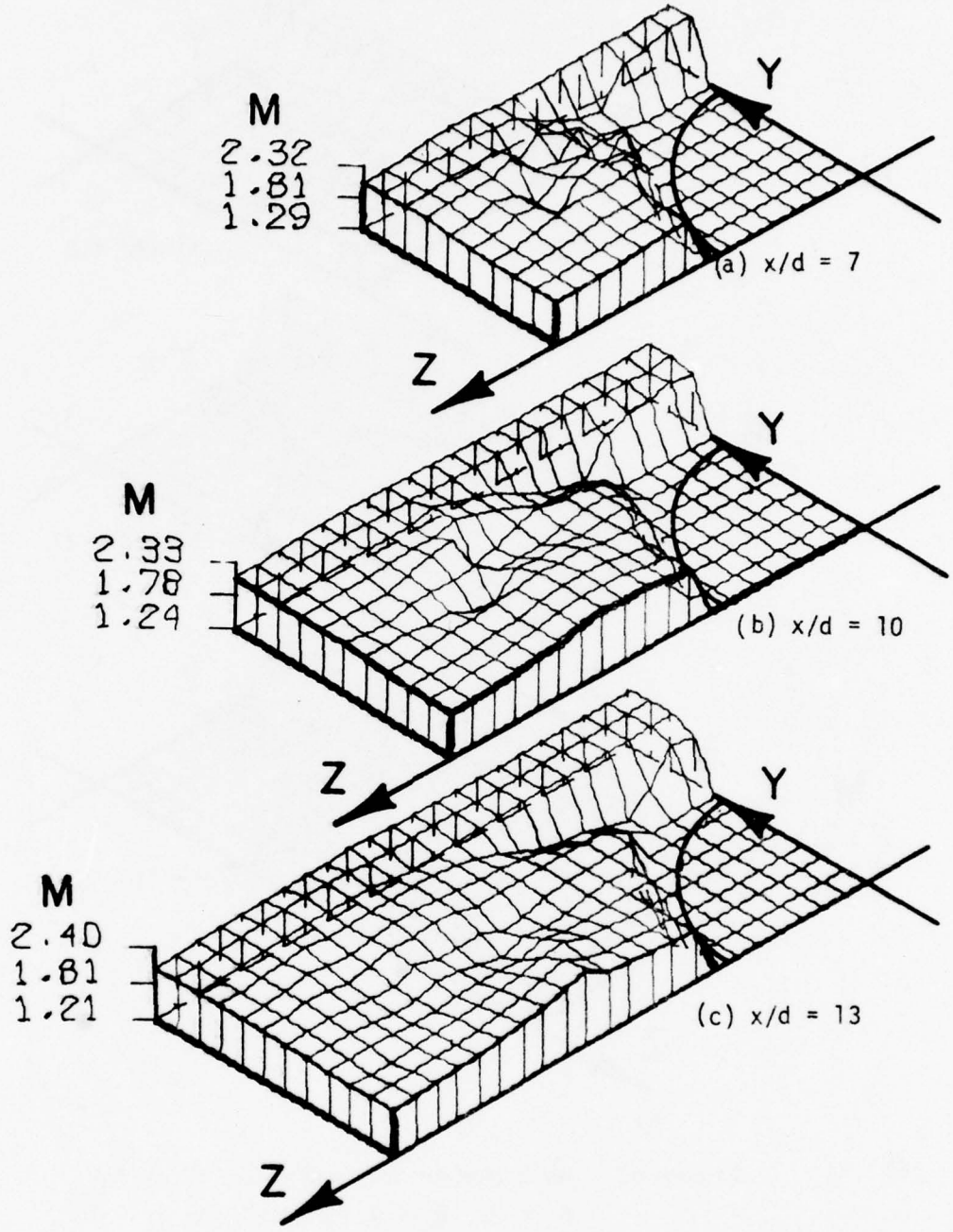


Figure 63. Mach Number in Cross-Flow Plane for $M_\infty = 2.$, $R_d = 1.75 \times 10^6$ and $\alpha_b = 15°$.

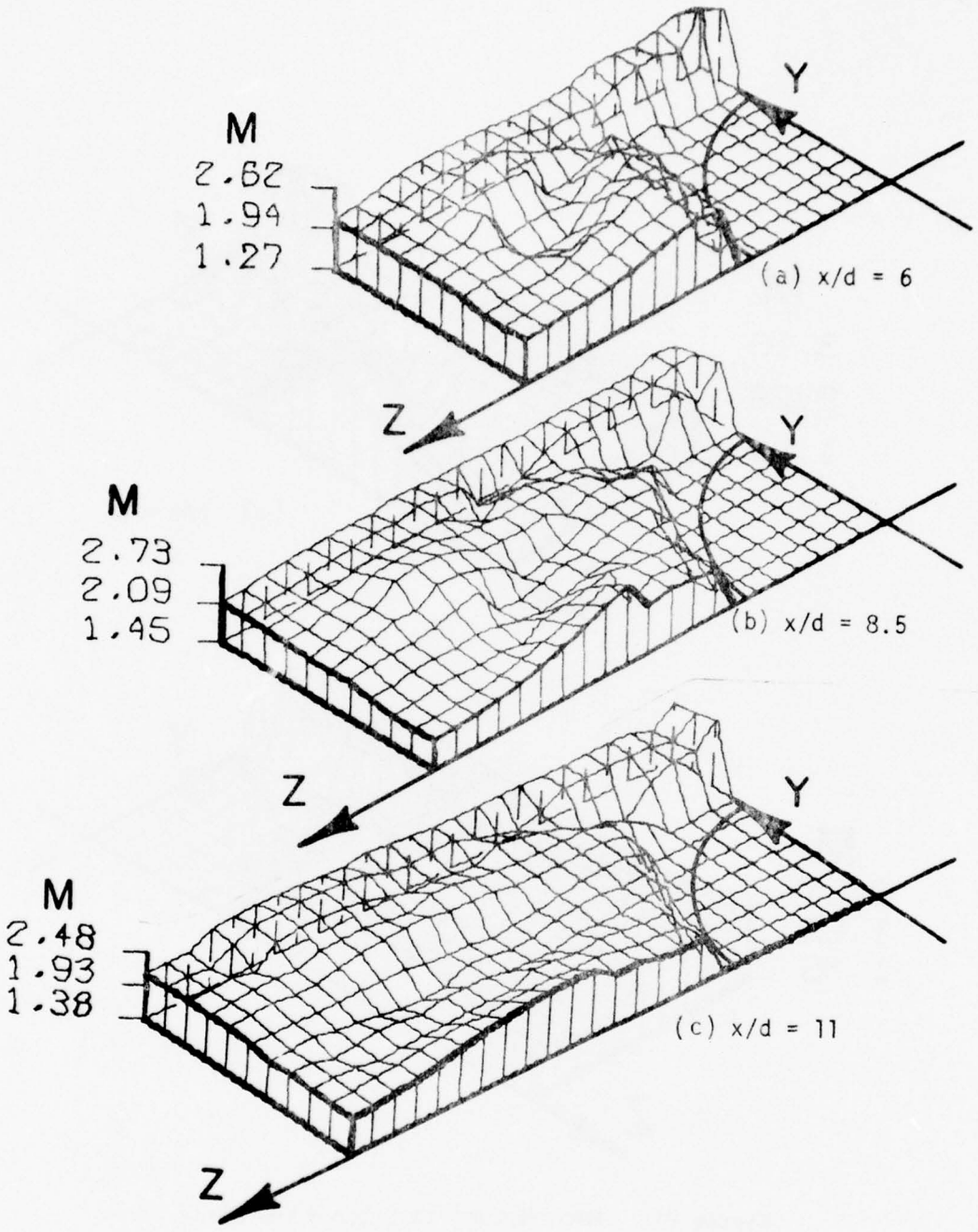
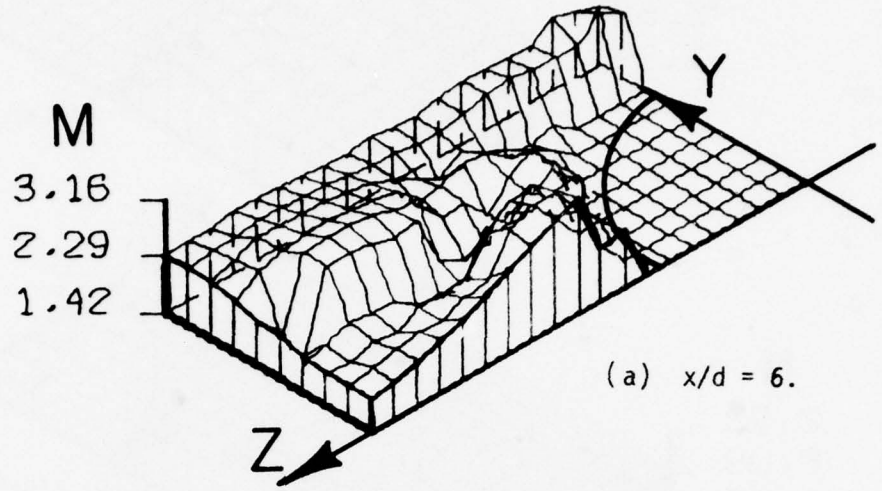


Figure 64. Mach Number in Cross-Flow Plane for $M_\infty = 2.$, $R_d = 1.75 \times 10^6$ and $\alpha_b = 20°$.



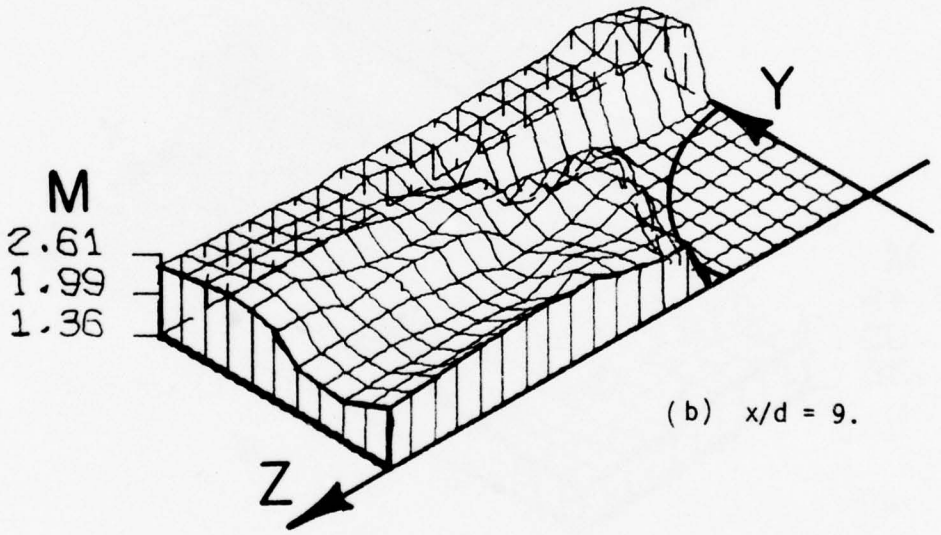


Figure 65. Mach Number in Cross-Flow Plane for $M_\infty = 2.$, $R_d = 1.75 \times 10^6$ and $\alpha_b = 25°$.

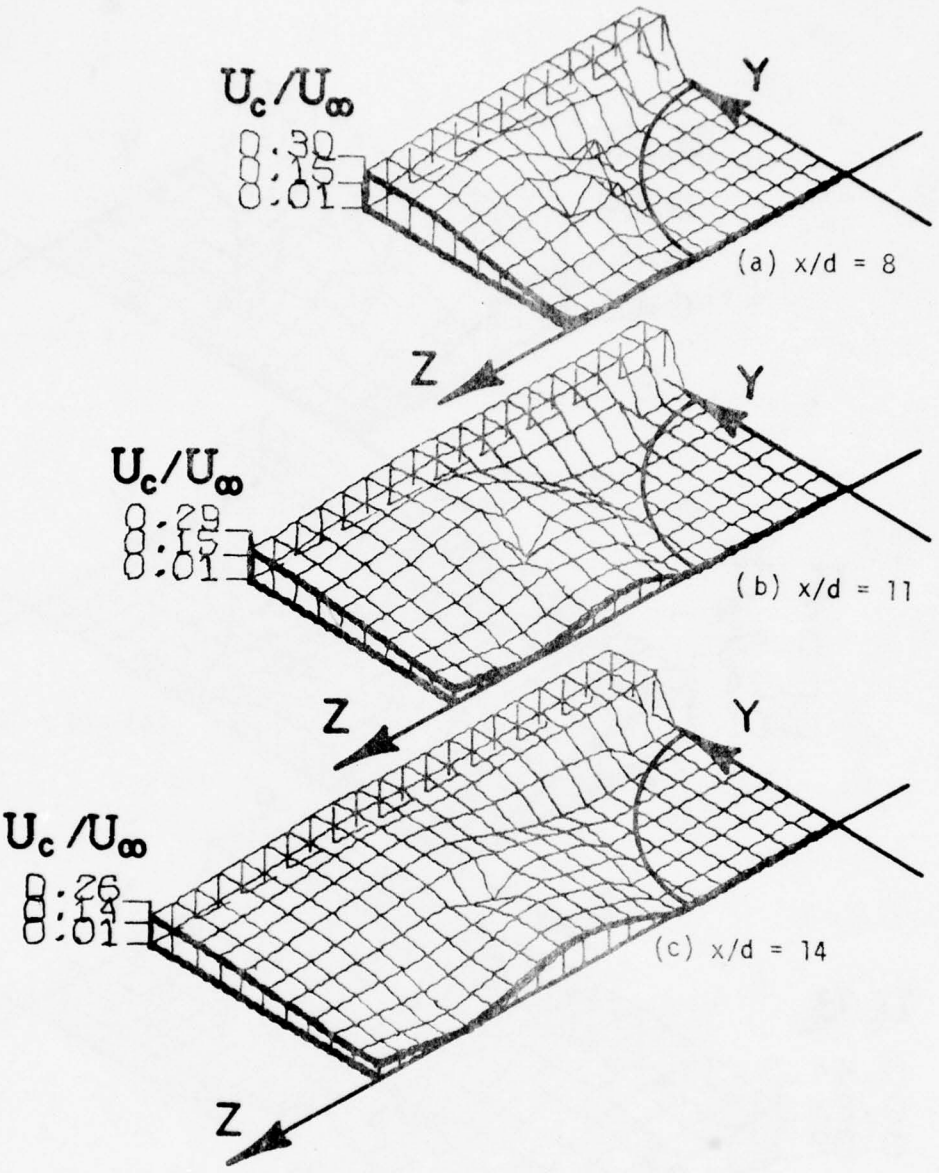


Figure 66. Magnitude of Cross-Flow Velocity for $M_\infty = 2.$, $R_d = 1.75 \times 10^6$ and $\alpha_b = 10°$.

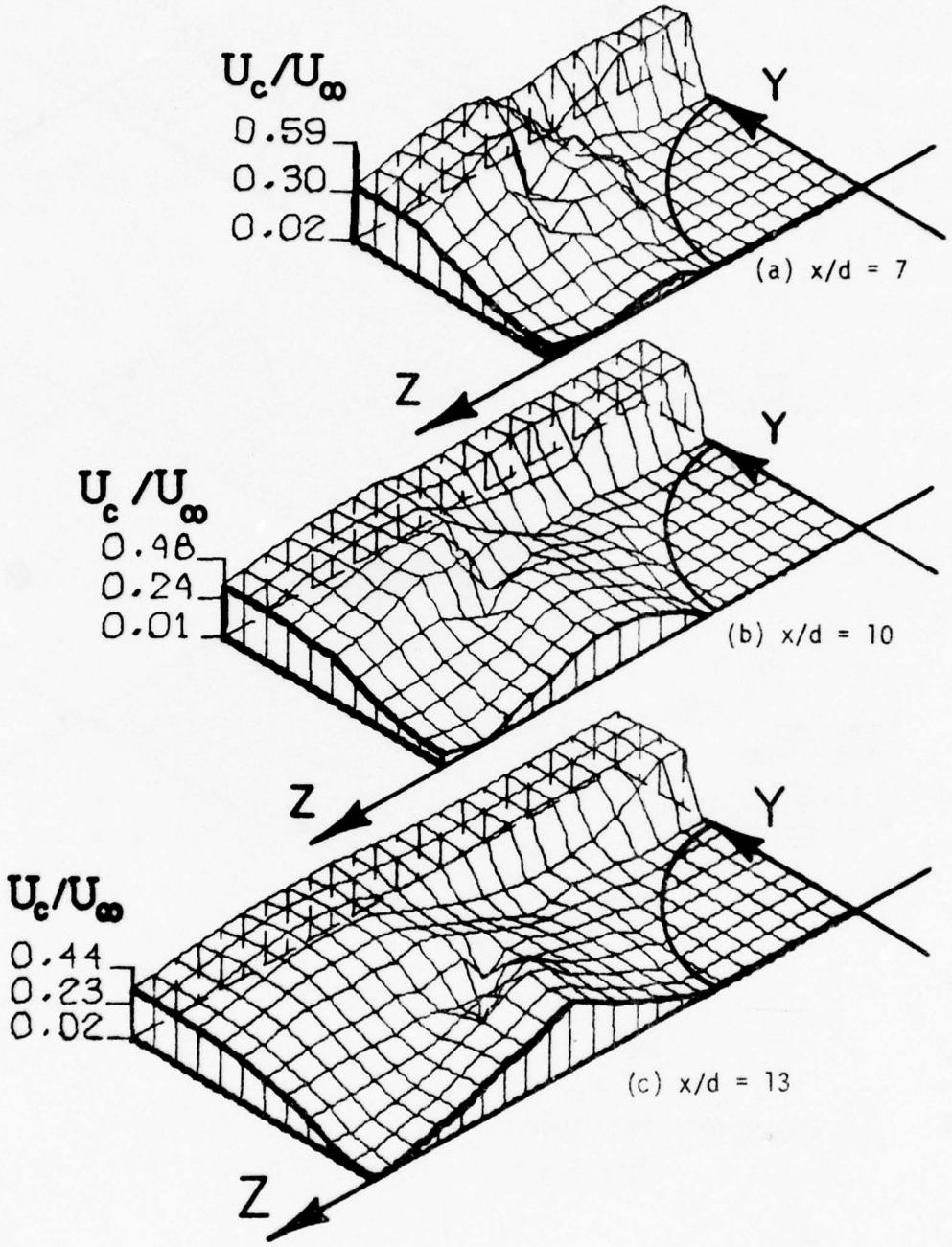


Figure 67. Magnitude of Cross-Flow Velocity for $M_\infty = 2.$, $R_d = 1.75 \times 10^6$ and $\alpha_b = 15°$.

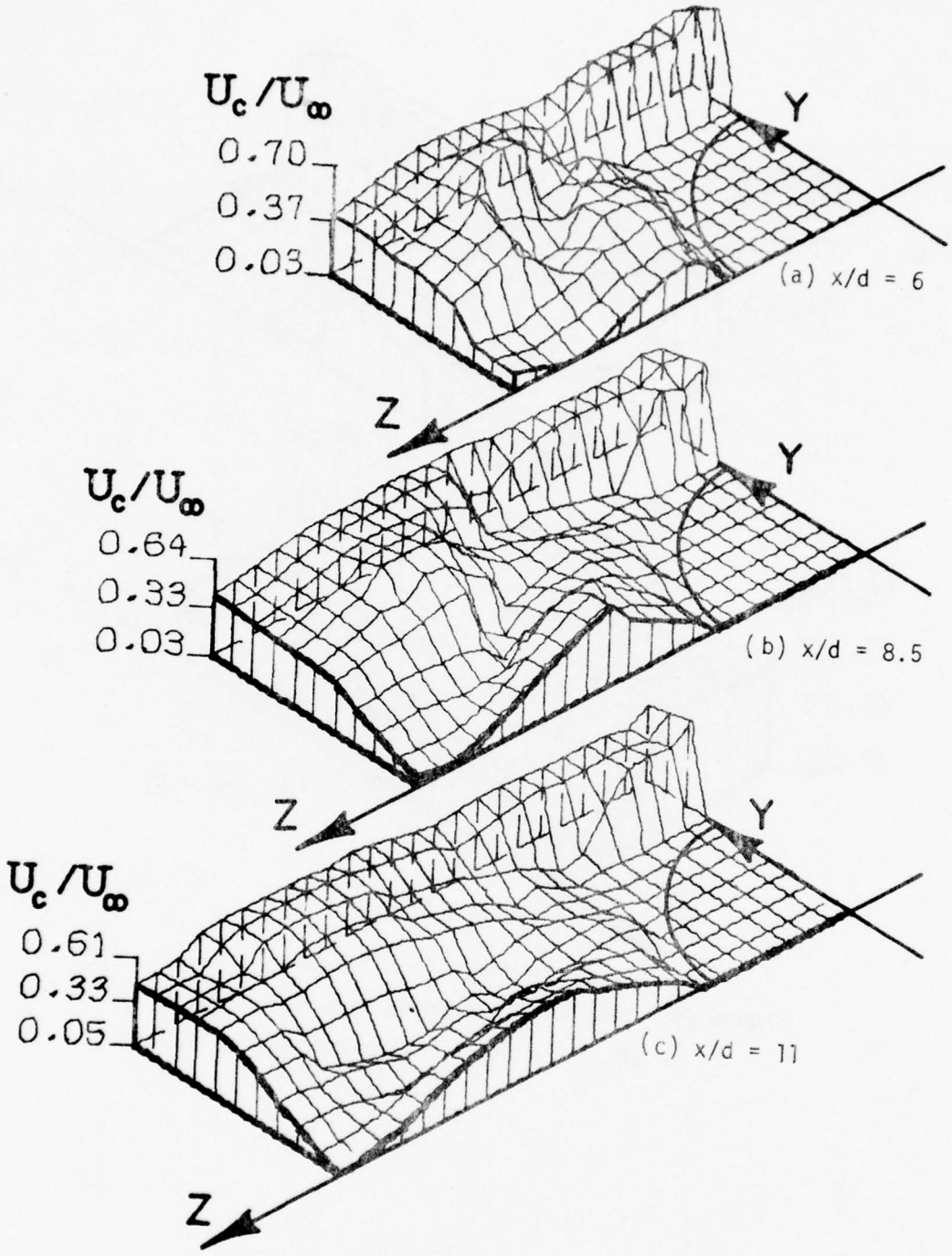


Figure 68. Magnitude of Cross-Flow Velocity for $M_\infty = 2.$, $R_d = 1.75 \times 10^6$ and $\alpha_b = 20°$.

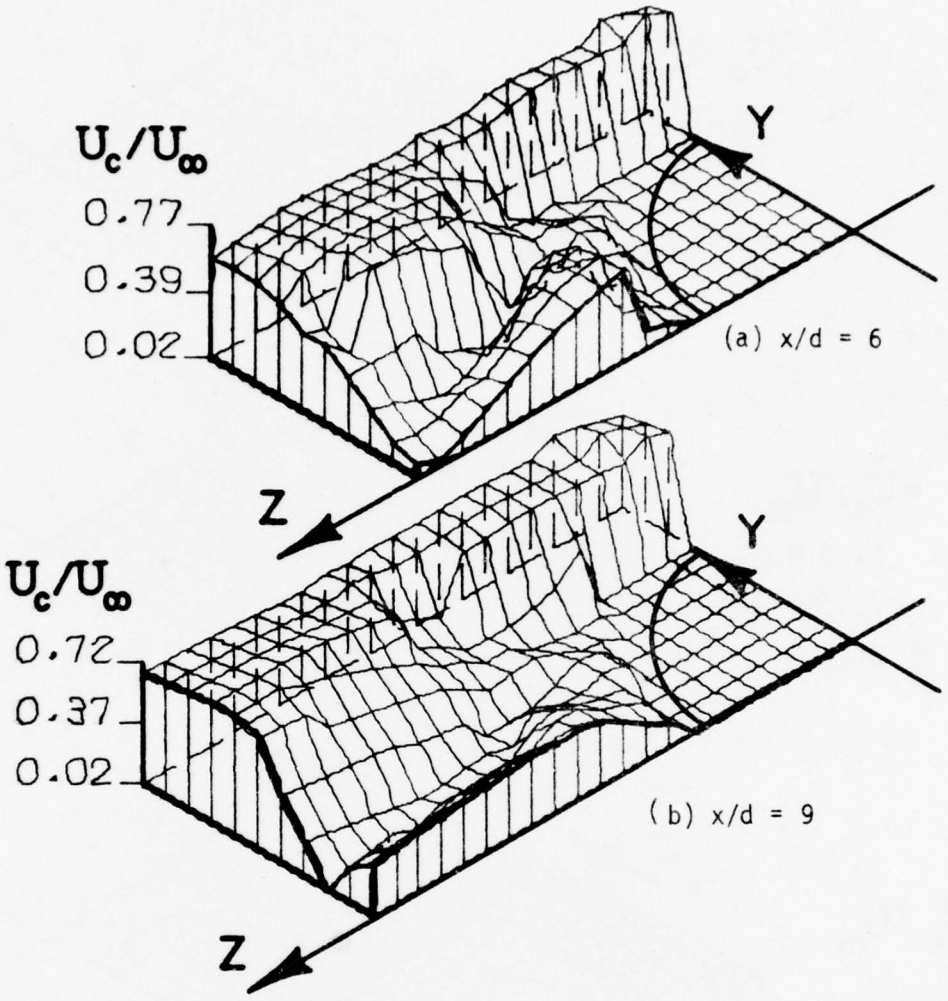


Figure 69. Magnitude of Cross-Flow Velocity for $M_\infty = 2.$, $R_d = 1.75 \times 10^6$ and $\alpha_b = 25°$.

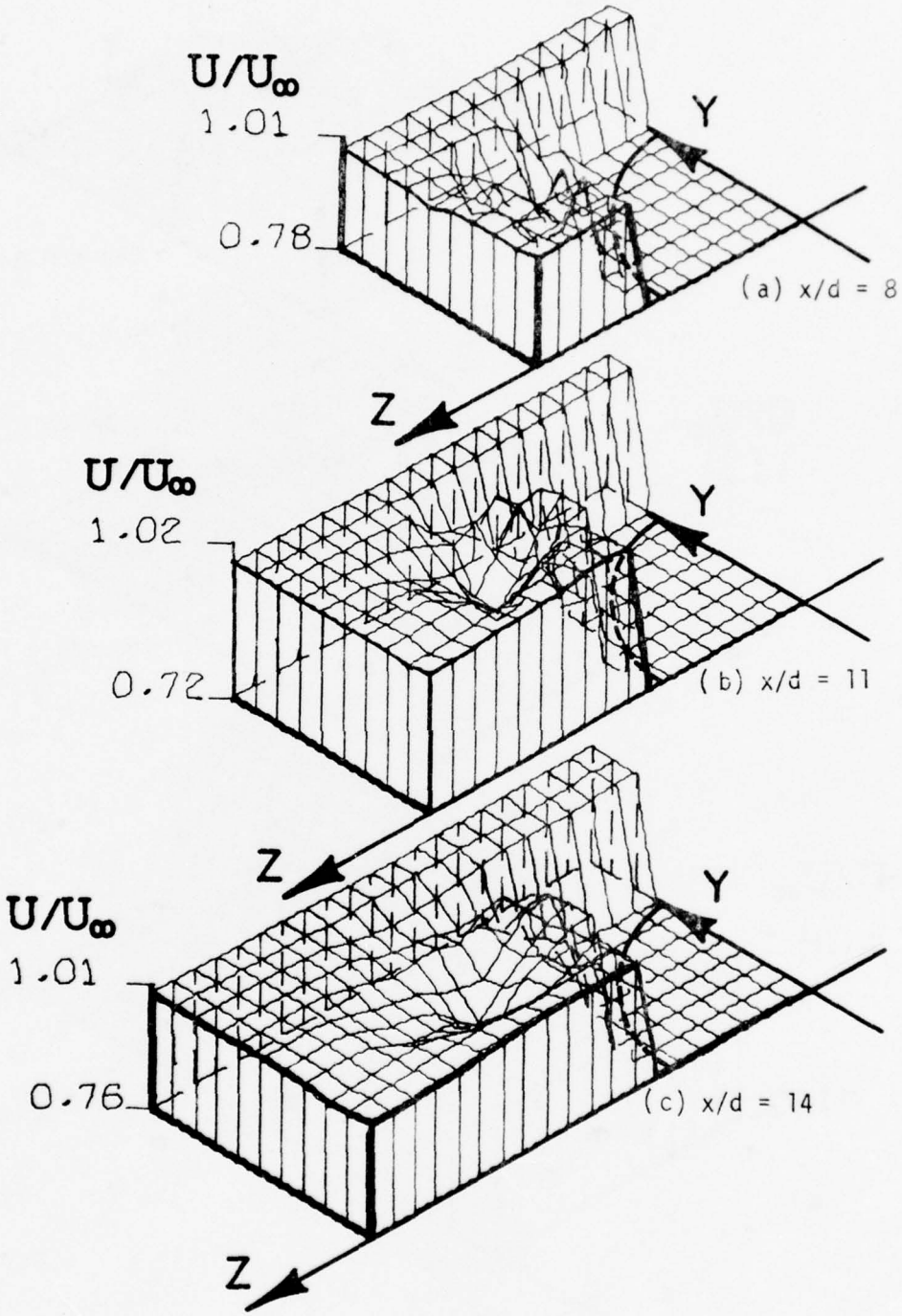


Figure 70. Axial Velocity in Cross-Flow Plane for $M_\infty = 2.$, $R_d = 1.75 \times 10^6$ and $\alpha_b = 10°$.

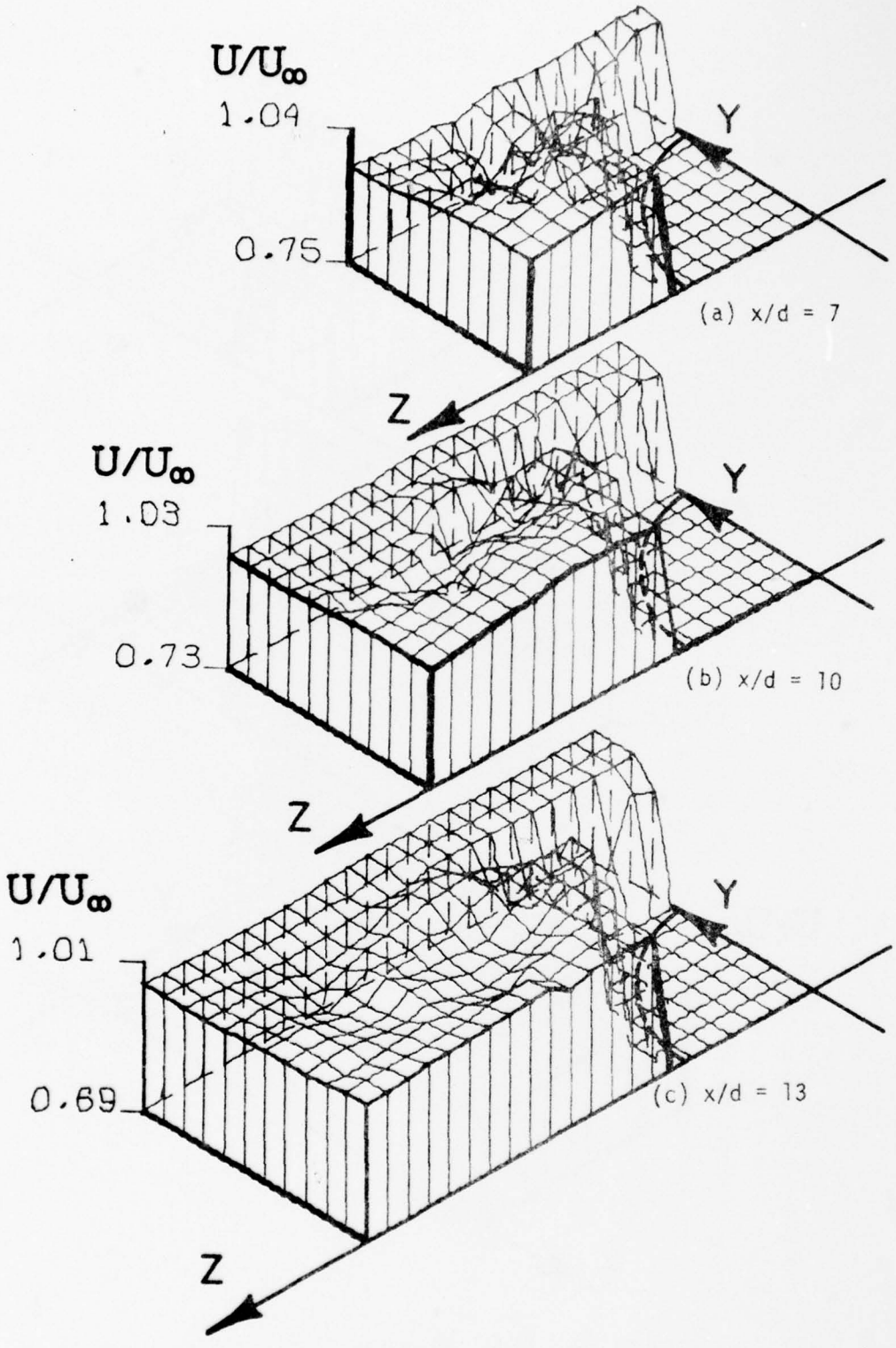


Figure 71. Axial Velocity in Cross-Flow Plane for $M_\infty = 2.$, $R_d = 1.75 \times 10^6$ and $\alpha_b = 15°$.

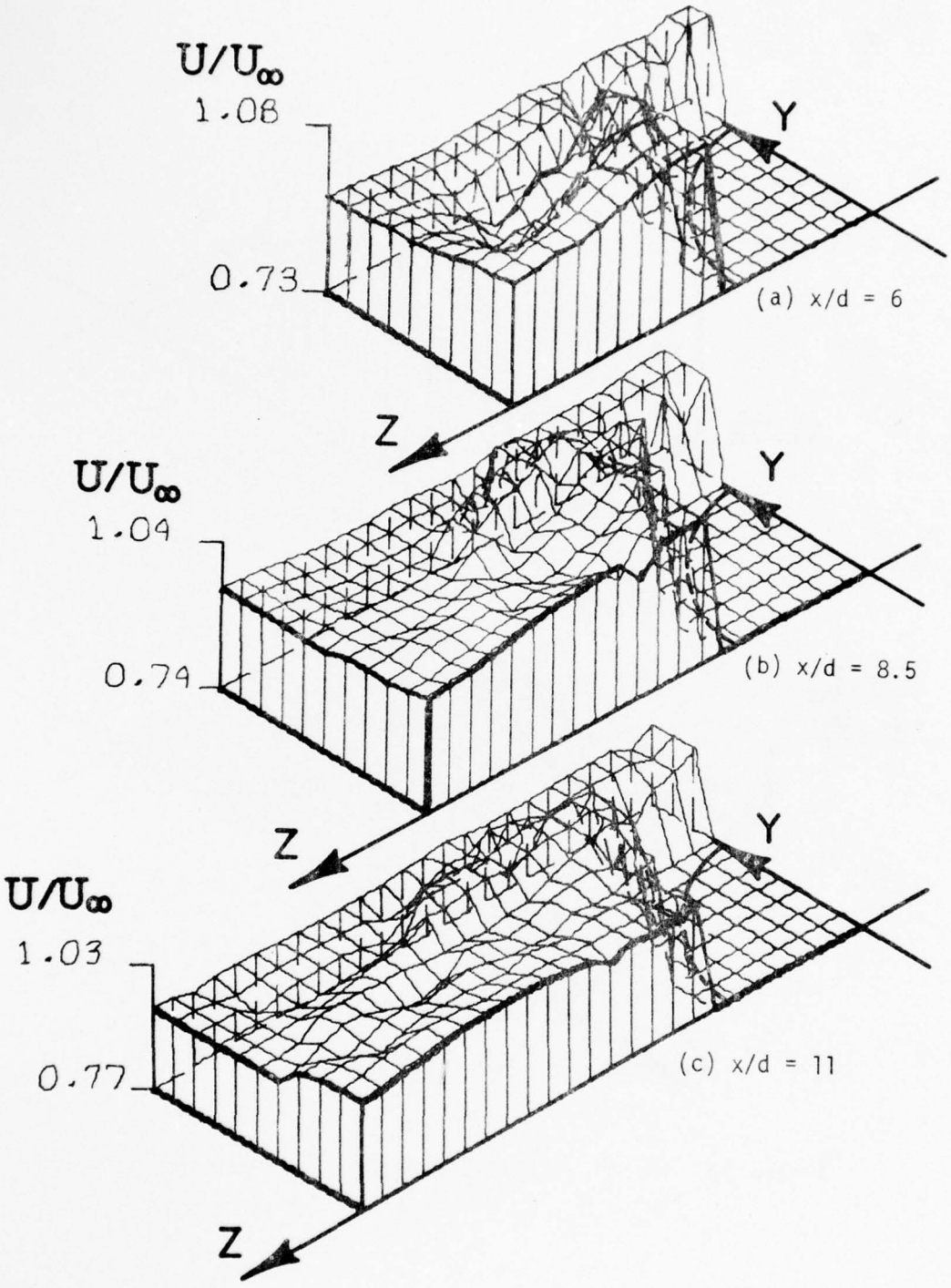


Figure 72. Axial Velocity in Cross-Flow Plane for $M_\infty = 2.$, $R_d = 1.75 \times 10^6$ and $\alpha_b = 20°$.

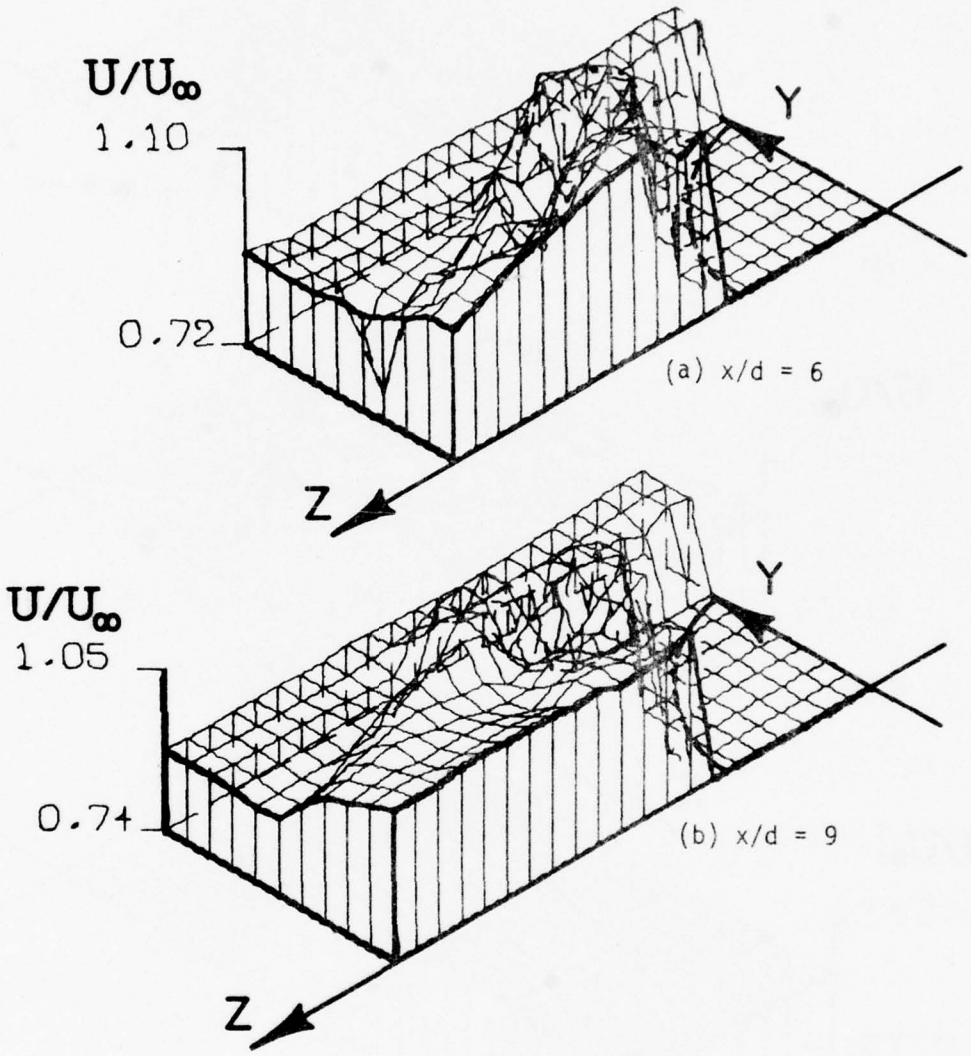


Figure 73. Axial Velocity in Cross-Flow Plane for $M_\infty = 2.$, $R_d = 1.75 \times 10^6$ and $\alpha_b = 25°$.

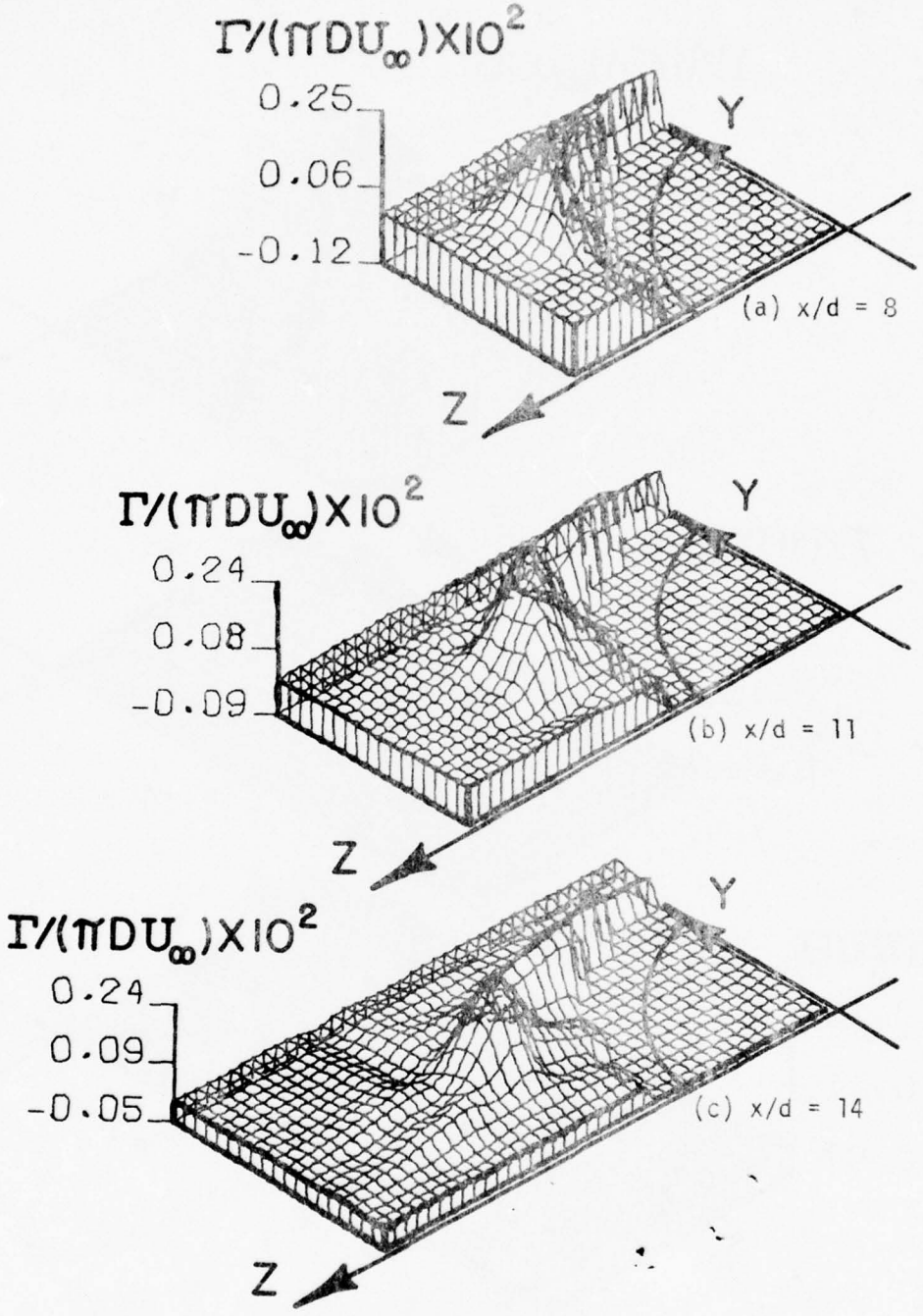


Figure 74. Local Circulation in Cross-Flow Plane for $M_\infty = 2.$, $R_d = 1.75 \times 10^6$ and $\alpha_b = 10°$.

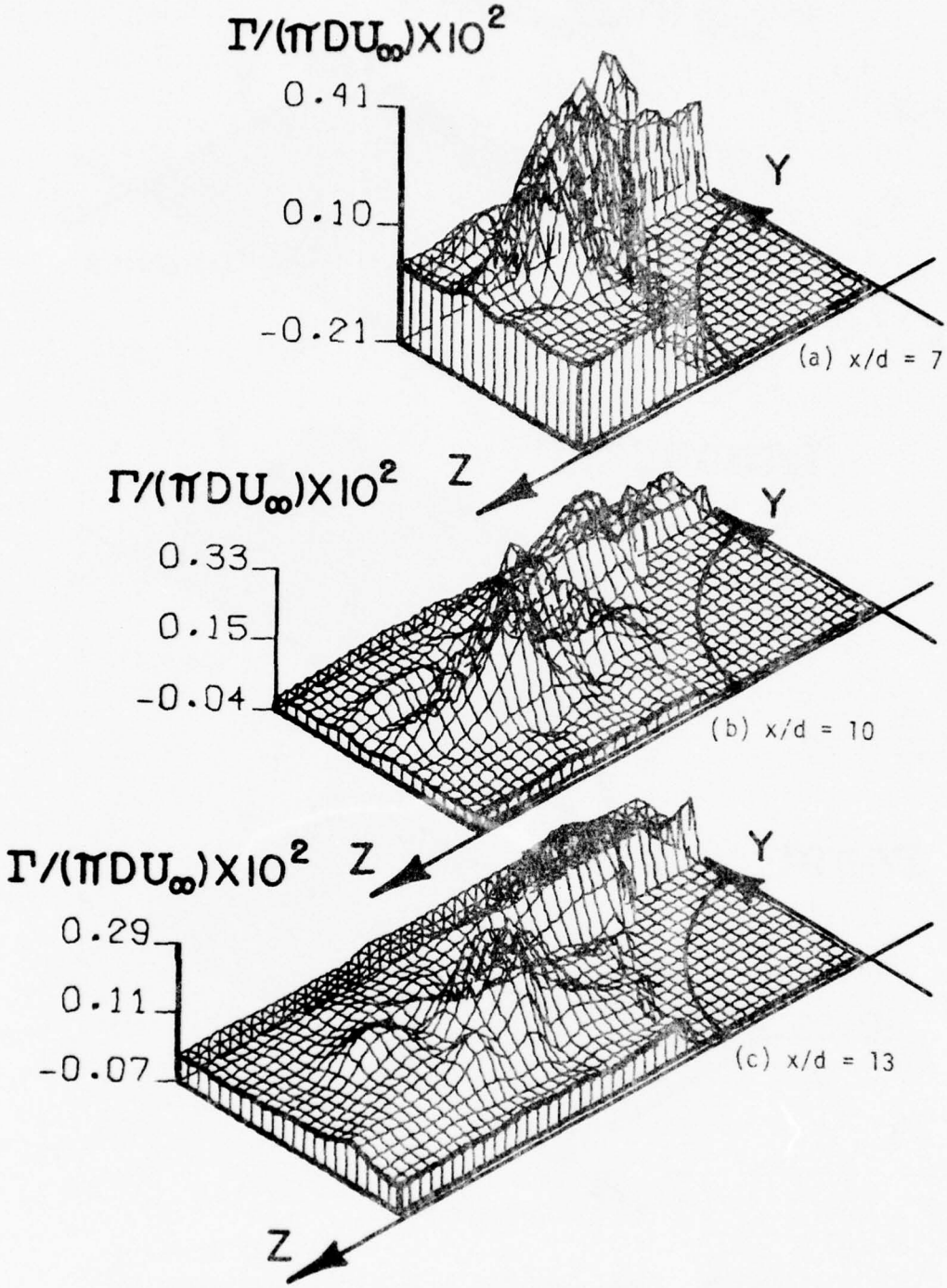


Figure 75. Local Circulation in Cross-Flow Plane for $M_\infty = 2.$, $R_d = 1.75 \times 10^6$ and $\alpha_b = 15°$.

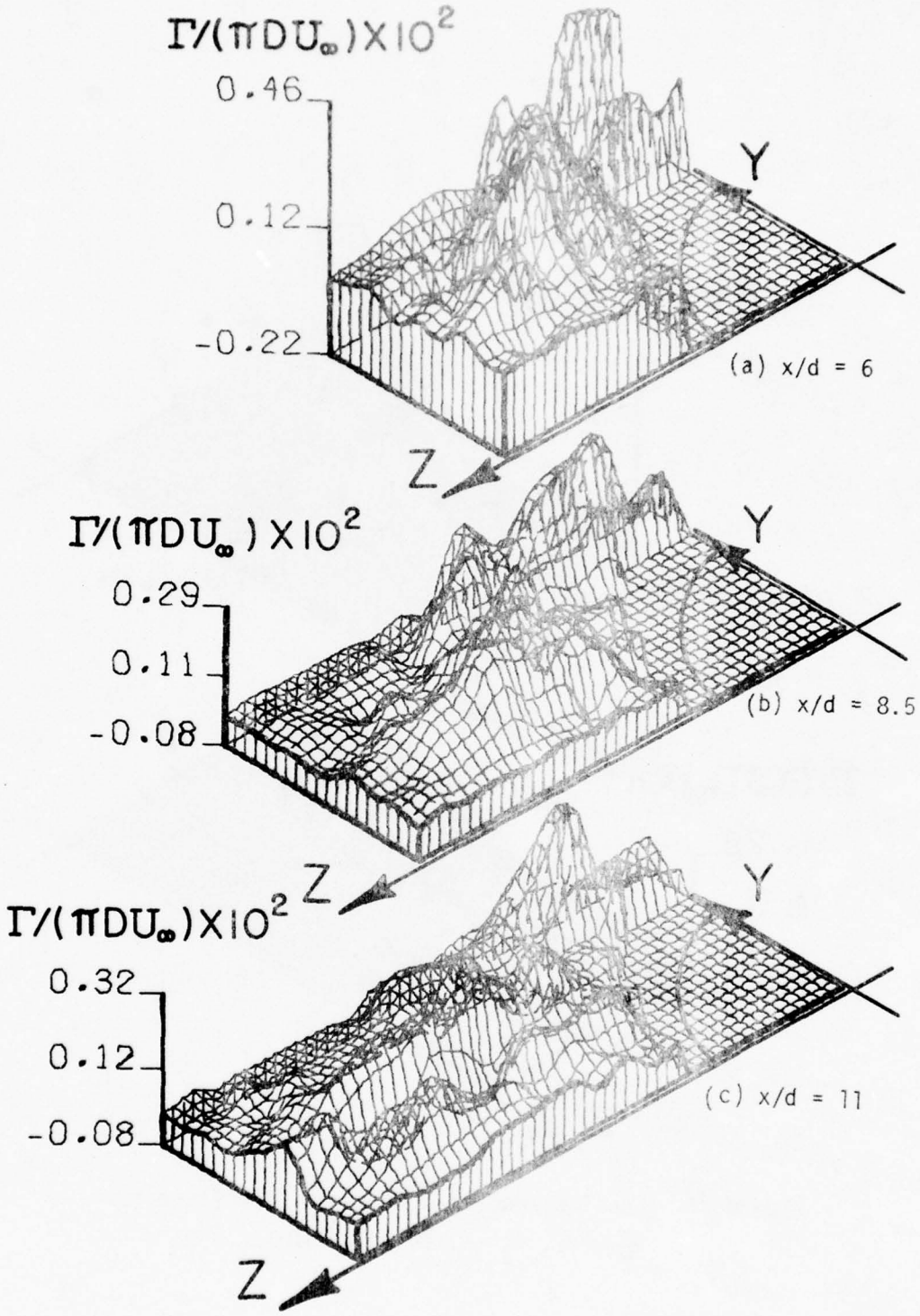


Figure 76. Local Circulation in Cross-Flow Plane for $M_\infty = 2.$, $R_d = 1.75 \times 10^6$ and $\alpha_b = 20°$.

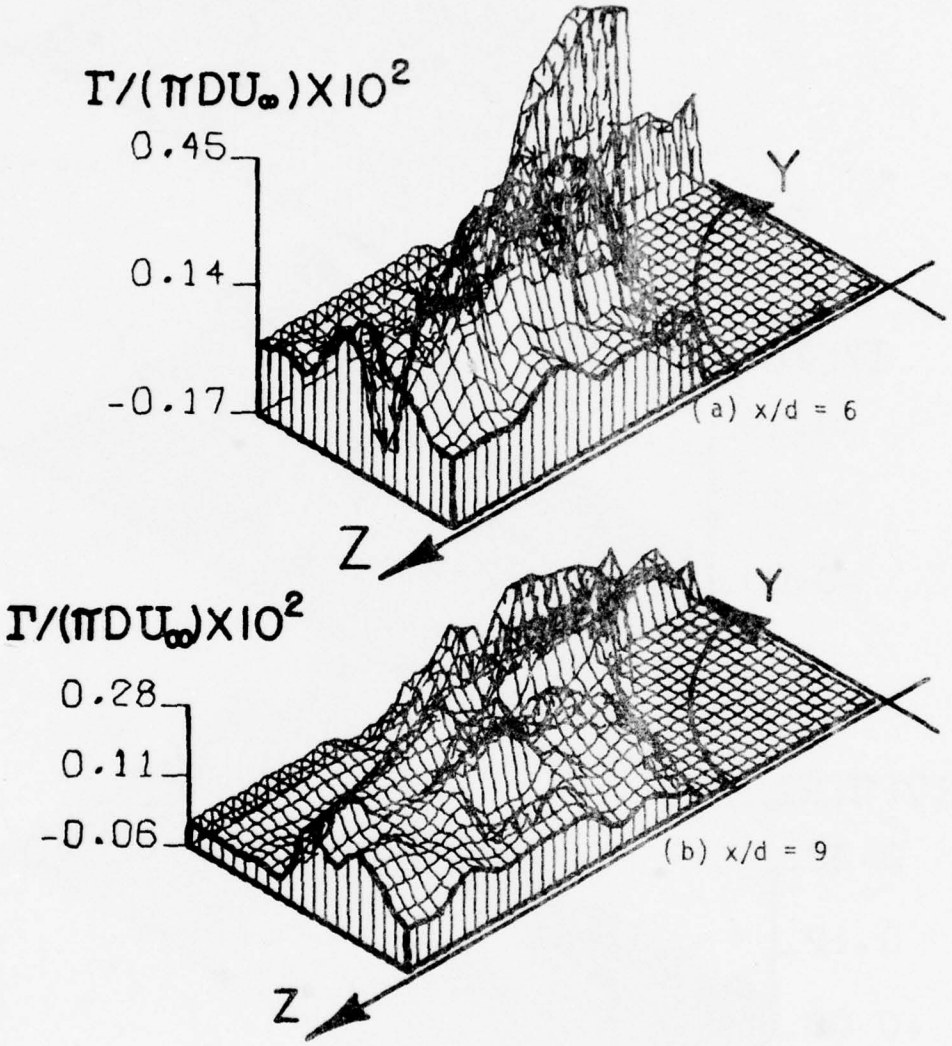


Figure 77. Local Circulation in Cross-Flow Plane for $M_\infty = 2.$, $R_d = 1.75 \times 10^6$ and $\alpha_b = 25°$.

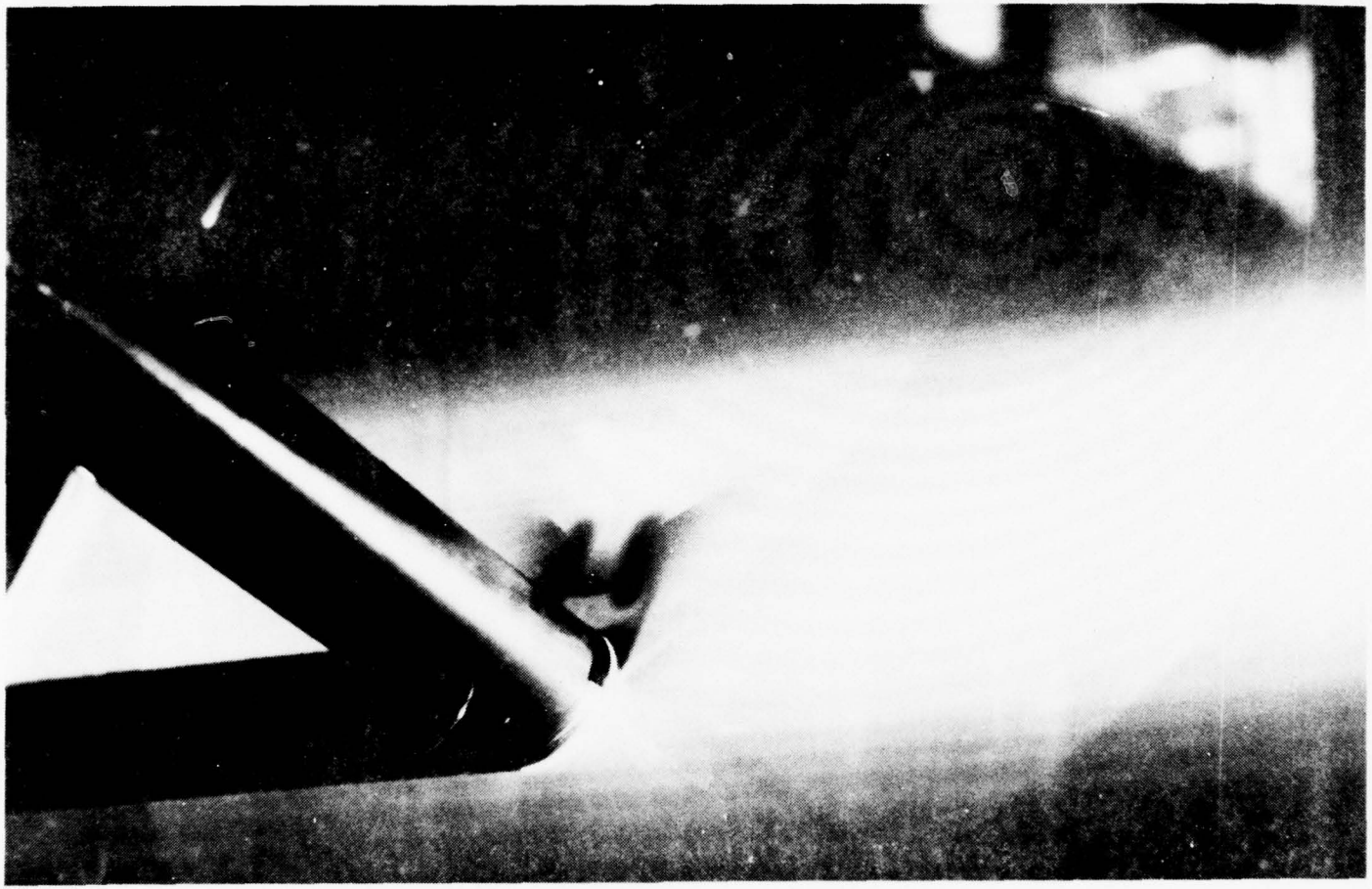


Figure 78. Vapor Screen Photograph for $M_\infty = 2.0$, $R_d = 1.58 \times 10^6$, $\alpha_b = 25°$, and $x/d = 6$

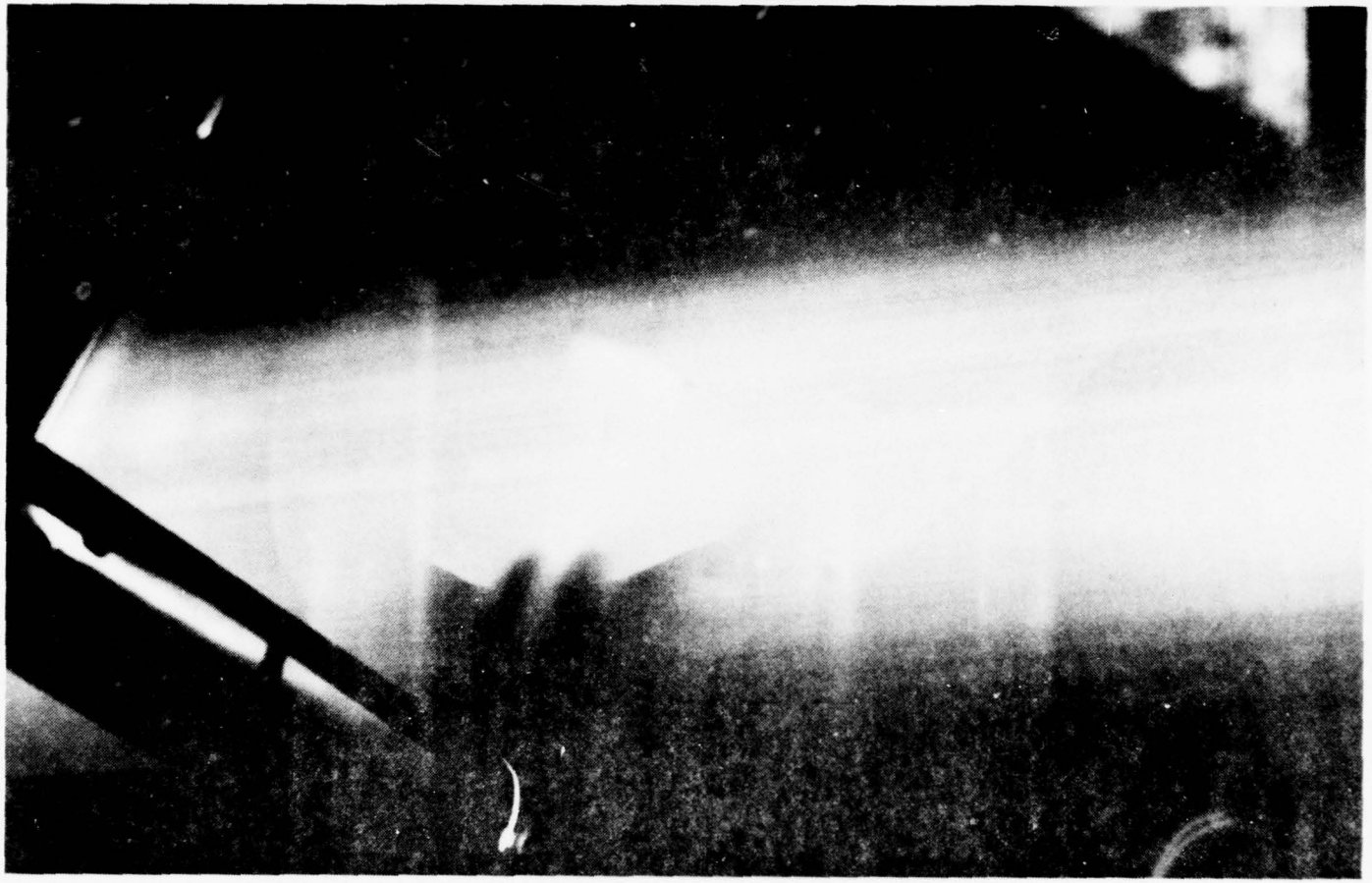
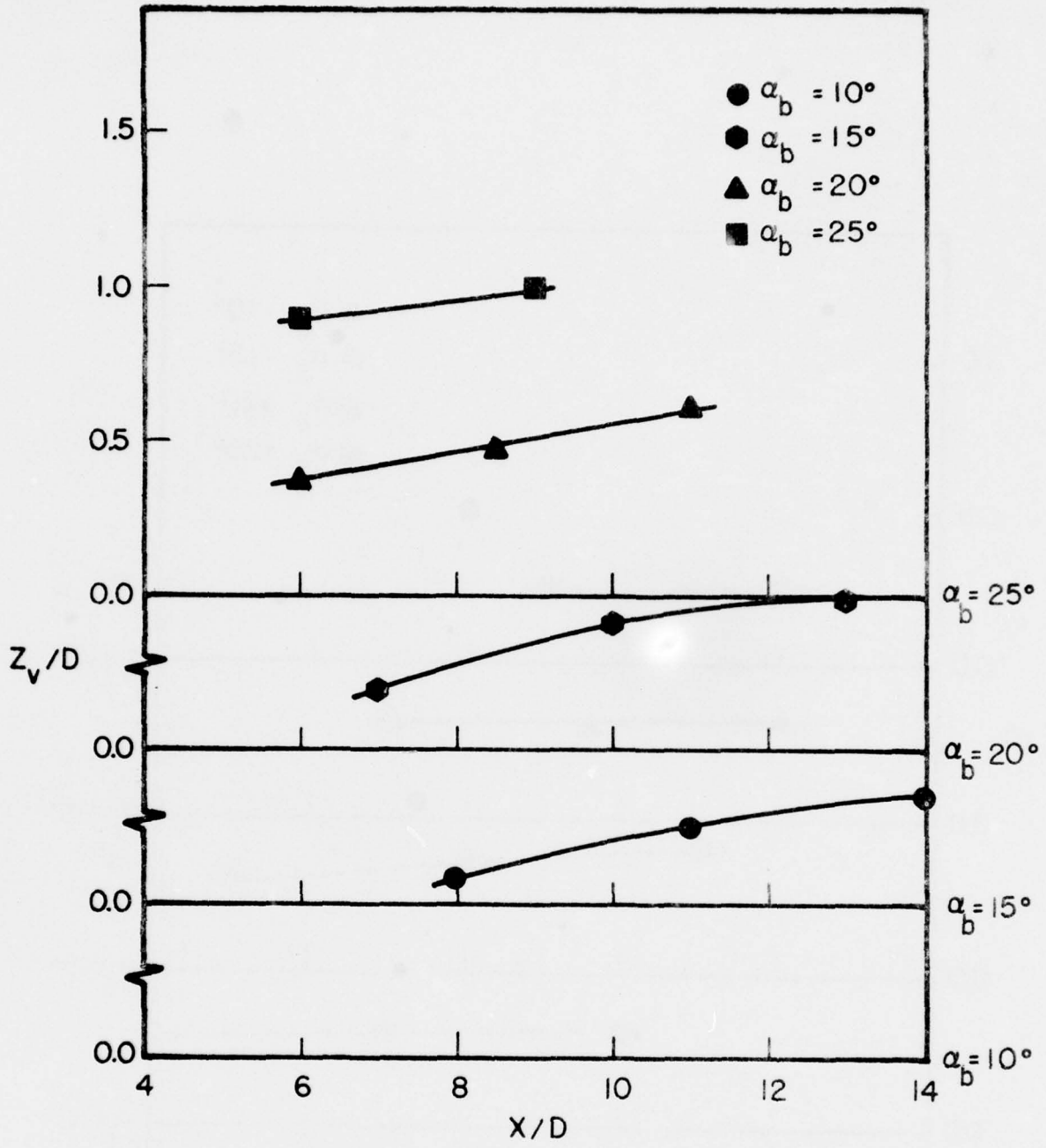
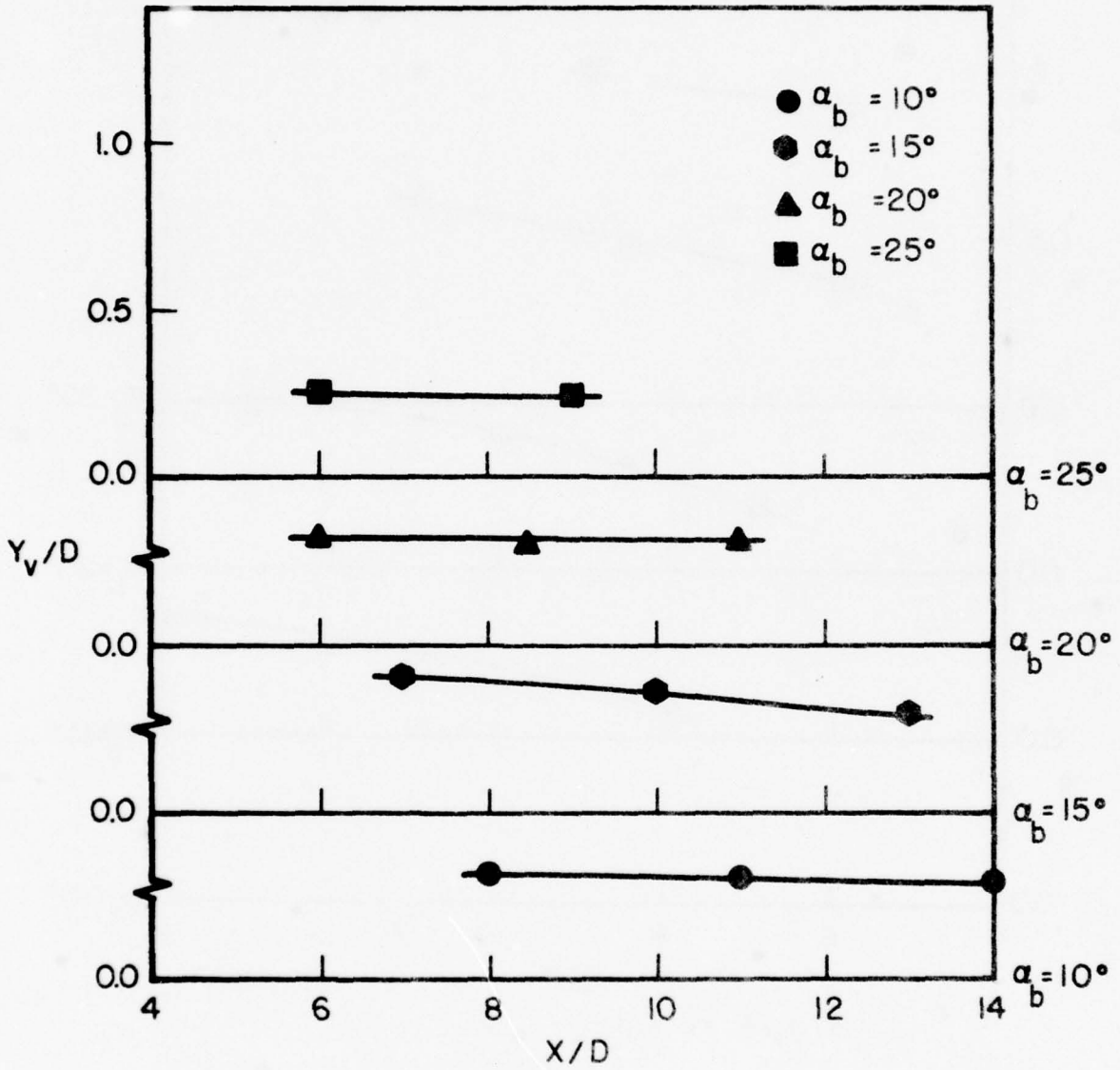


Figure 79. Vapor Screen Photograph for $M_\infty = 2.0$, $R_d = 1.58 \times 10^6$, $\alpha_b = 25°$ and $x/d = 9$



(a) z_v/d vs x/d

Figure 80. Vortex Center Location in the Cross-Flow Plane for M_∞ = 2. and R_d = 1.75 x 10^6



(b) y_v/d vs x/d

Figure 80. Vortex Center Location in the Cross-Flow Location for M_∞ = 2. and R_d = 1.75 x 10^6 (Concluded)

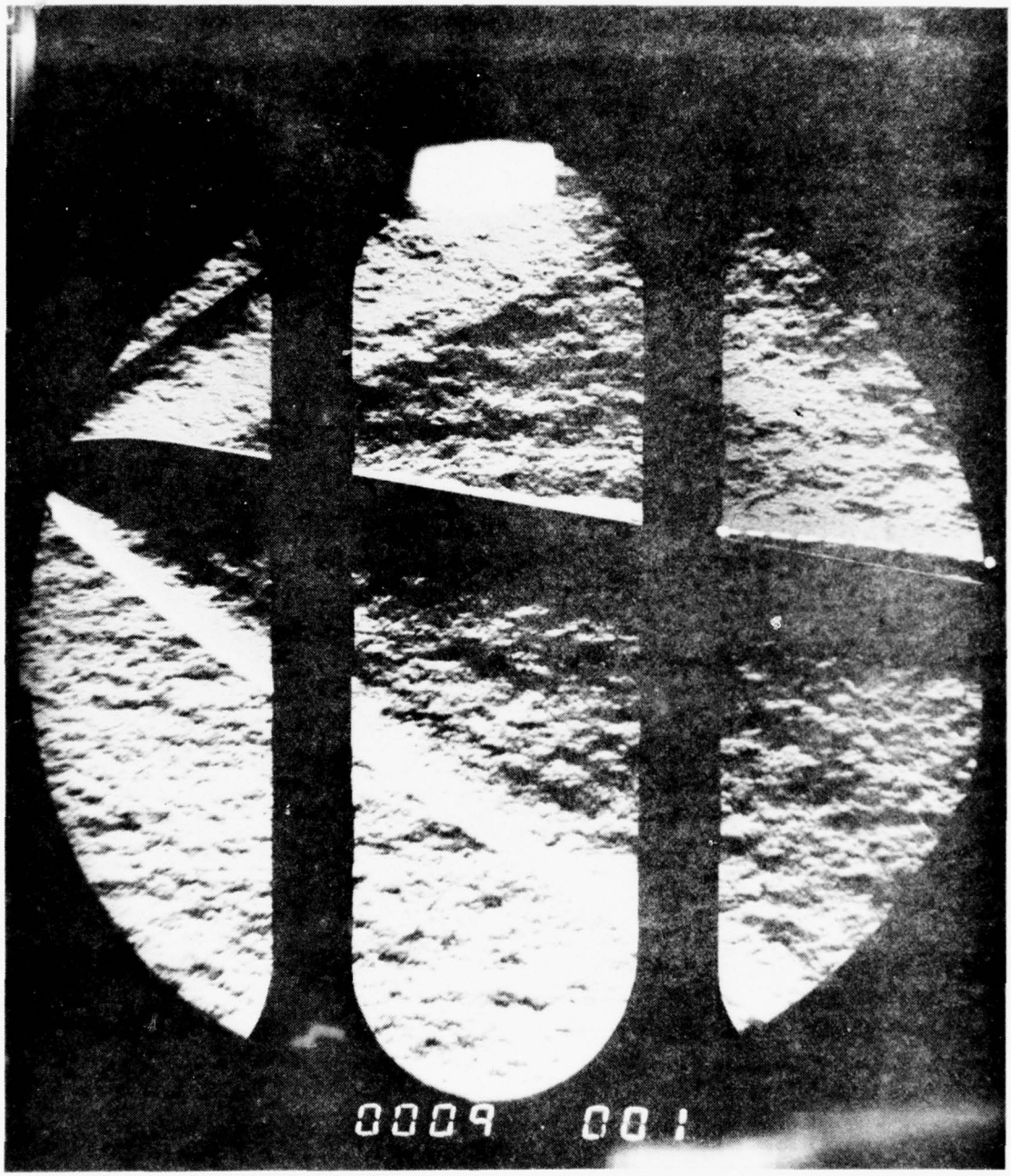


Figure 81. Schlieren Photograph for M_∞ = 2.0, R_d = 1.75 x 10^6 and α_b = 10°

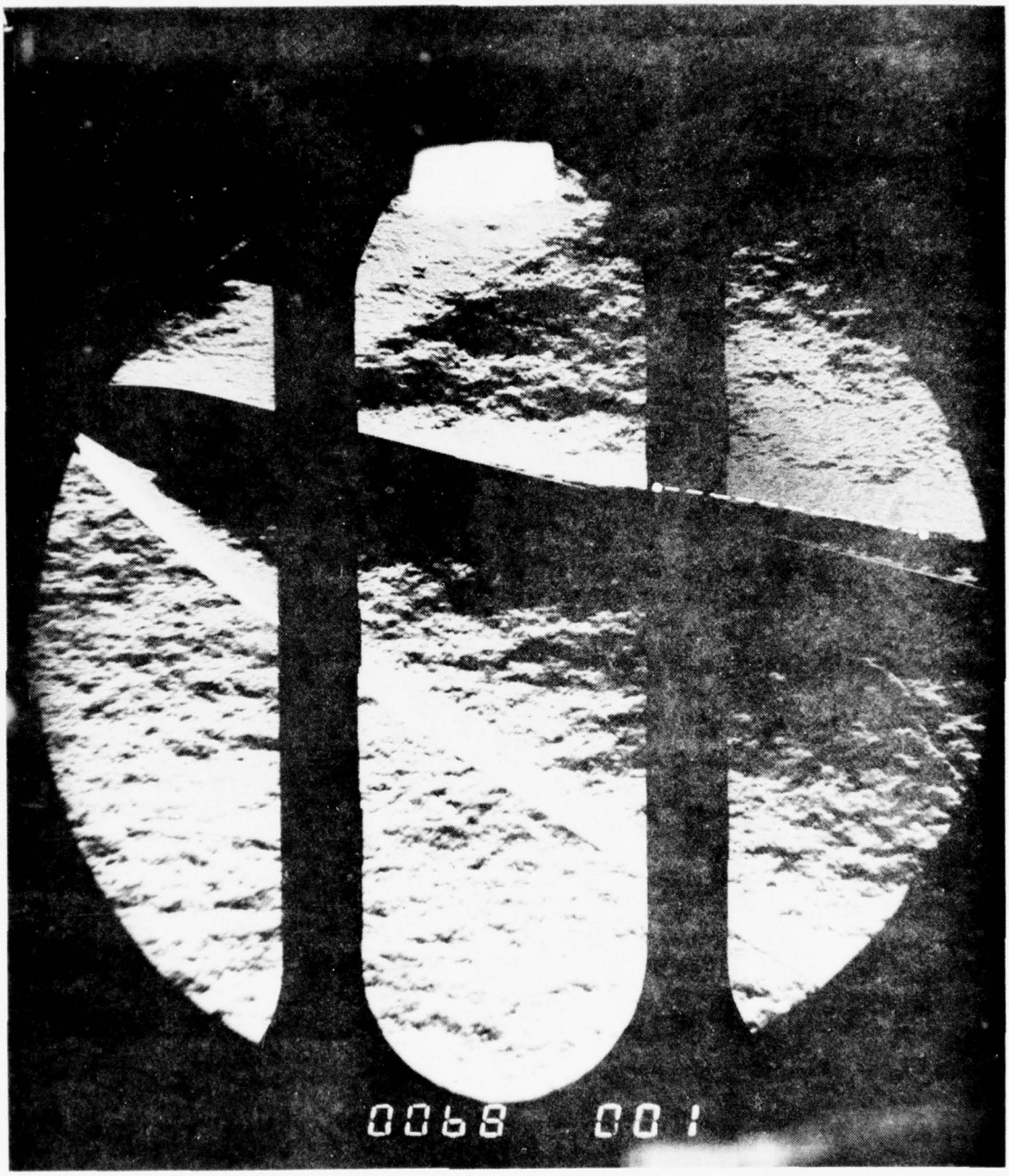


Figure 82. Schlieren Photograph for $M_\infty = 2.0$, $R_d = 1.75 \times 10^6$ and $\alpha_b = 15°$

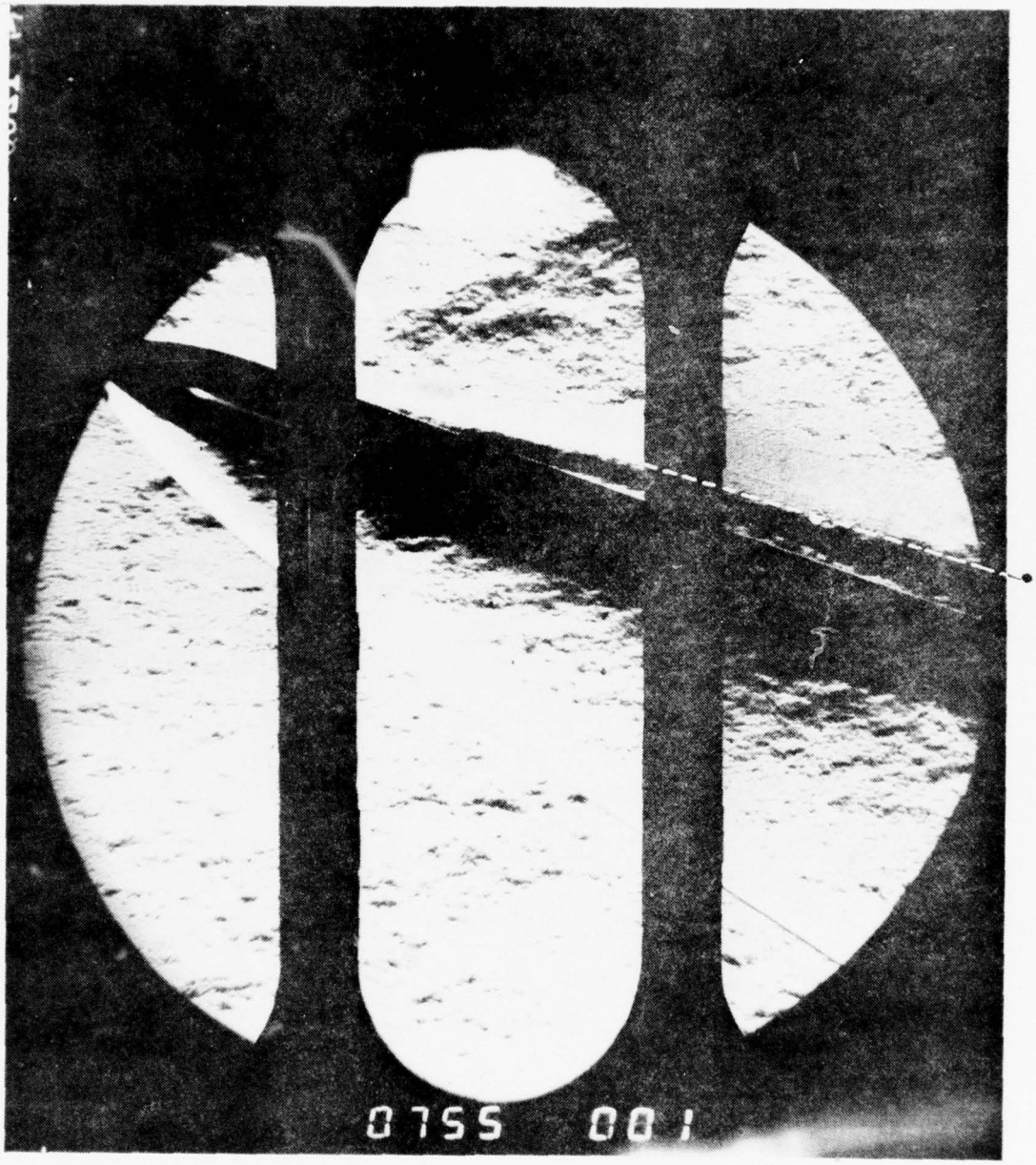


Figure 83. Schlieren Photograph for $M_\infty = 2.0$, $R_d = 1.75 \times 10^6$ and $\alpha_b = 20°$

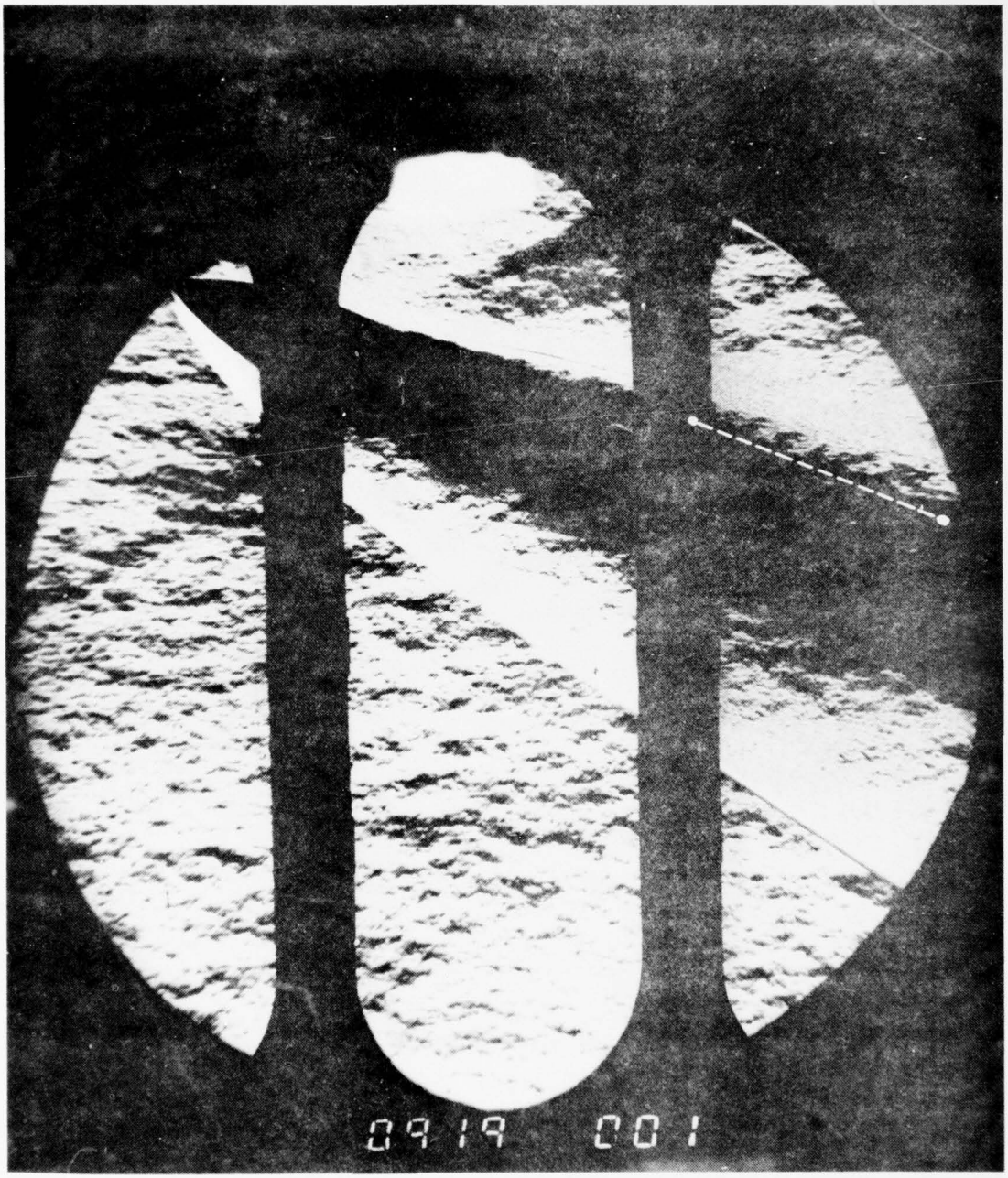


Figure 84. Schlieren Photograph for $M_\infty = 2.0$, $R_d = 1.75 \times 10^6$ and $\alpha_b = 25°$

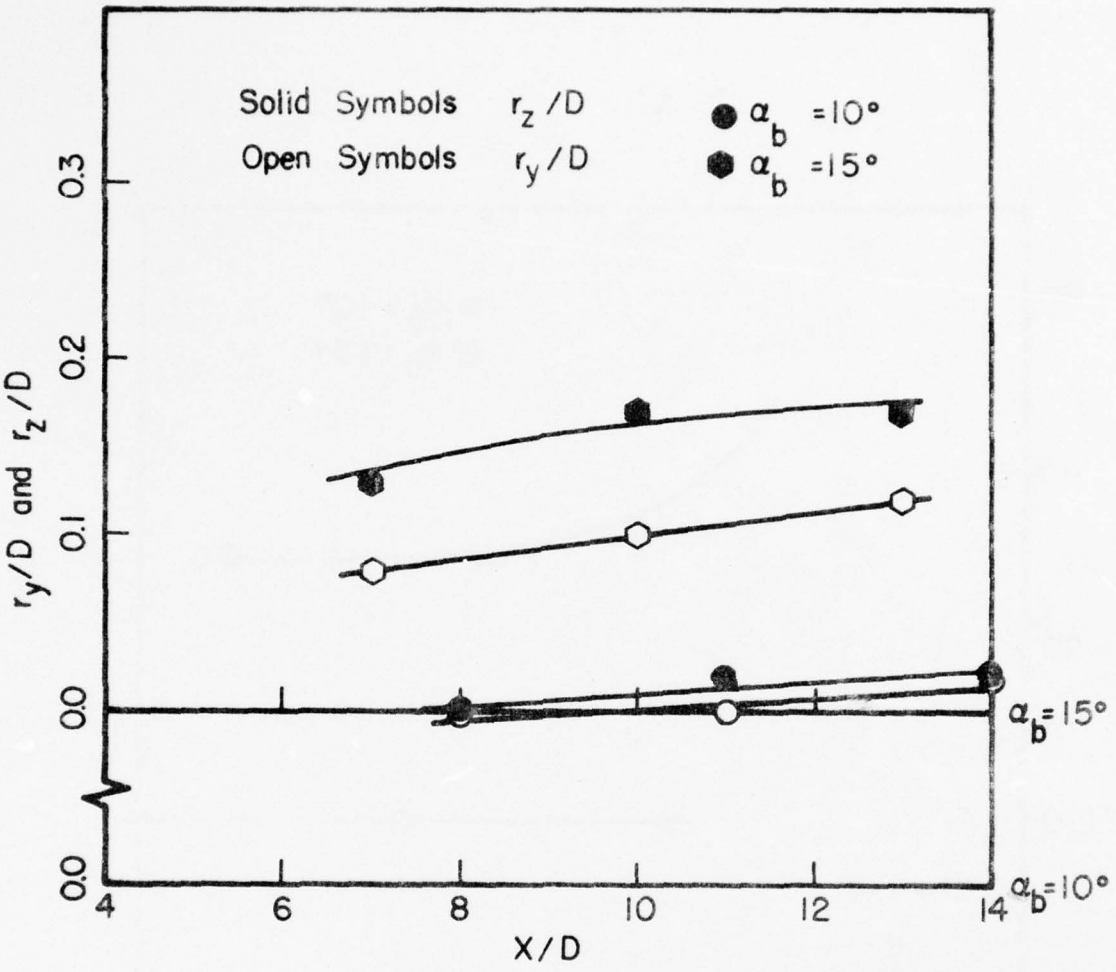


Figure 85. Vortex Core Radii for
M_∞ = 2. and R_d = 1.75 x 10^6

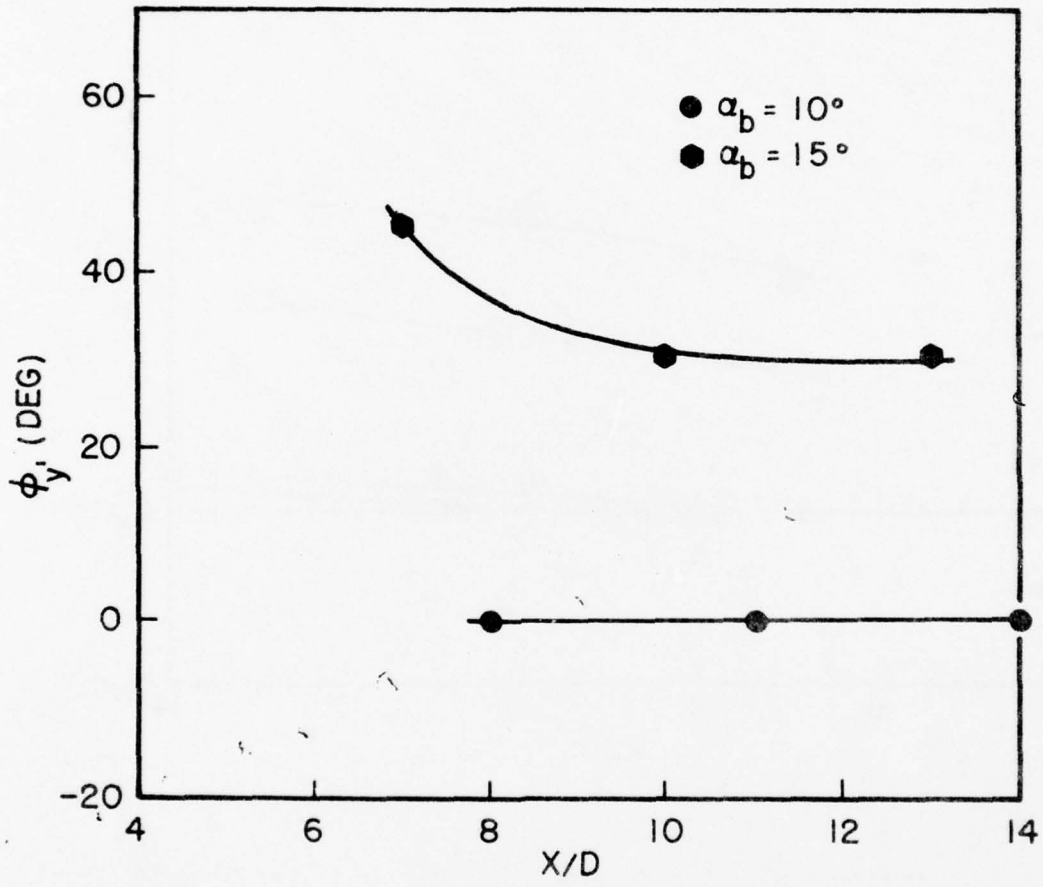


Figure 86. Angular Orientation of Vortex Core for M_∞ = 2. and R_d = 1.75 x 10^6

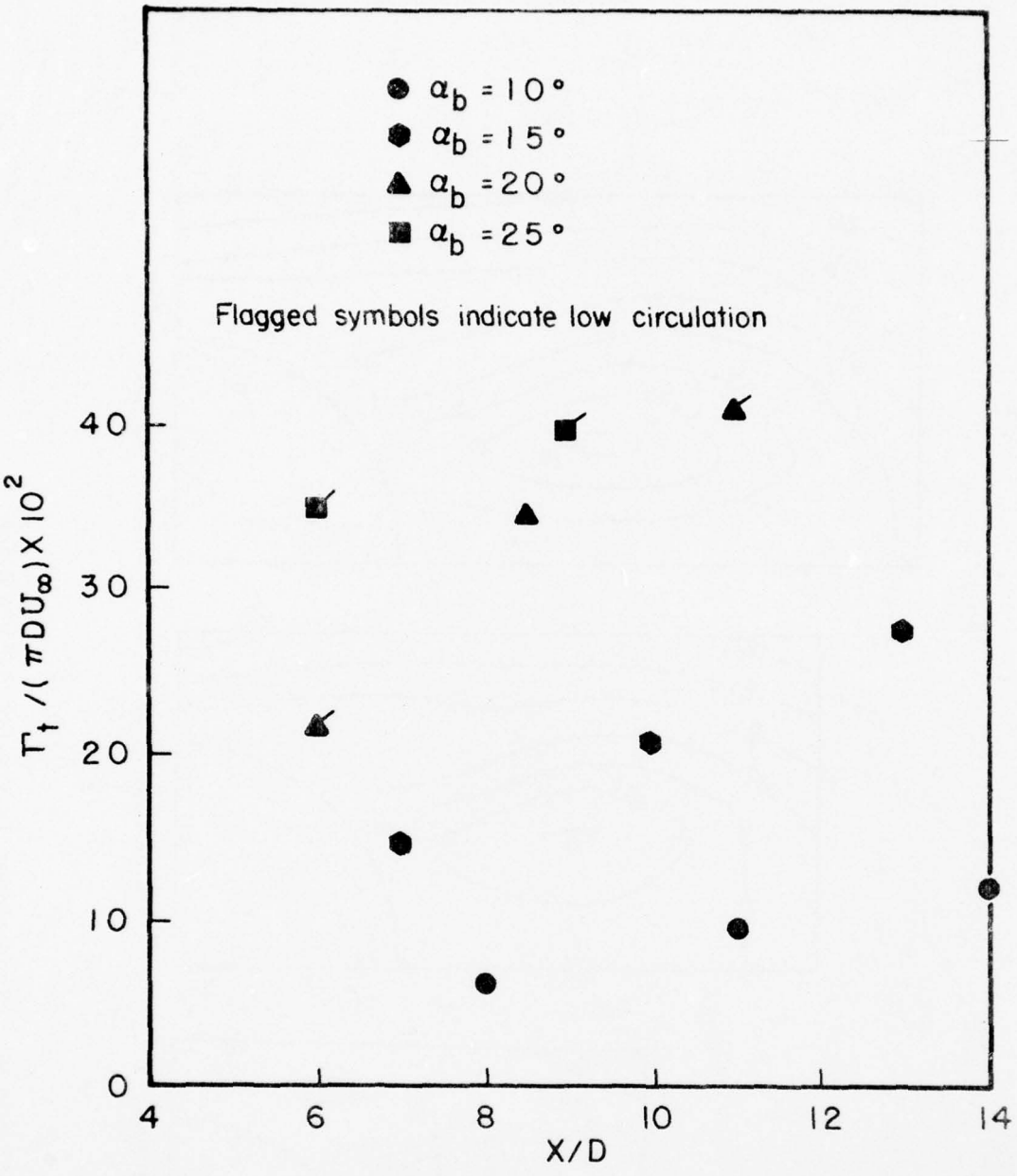


Figure 87. Total Circulation in the Survey Grids for $M_\infty = 2.$ and $R_d = 1.75 \times 10^6$

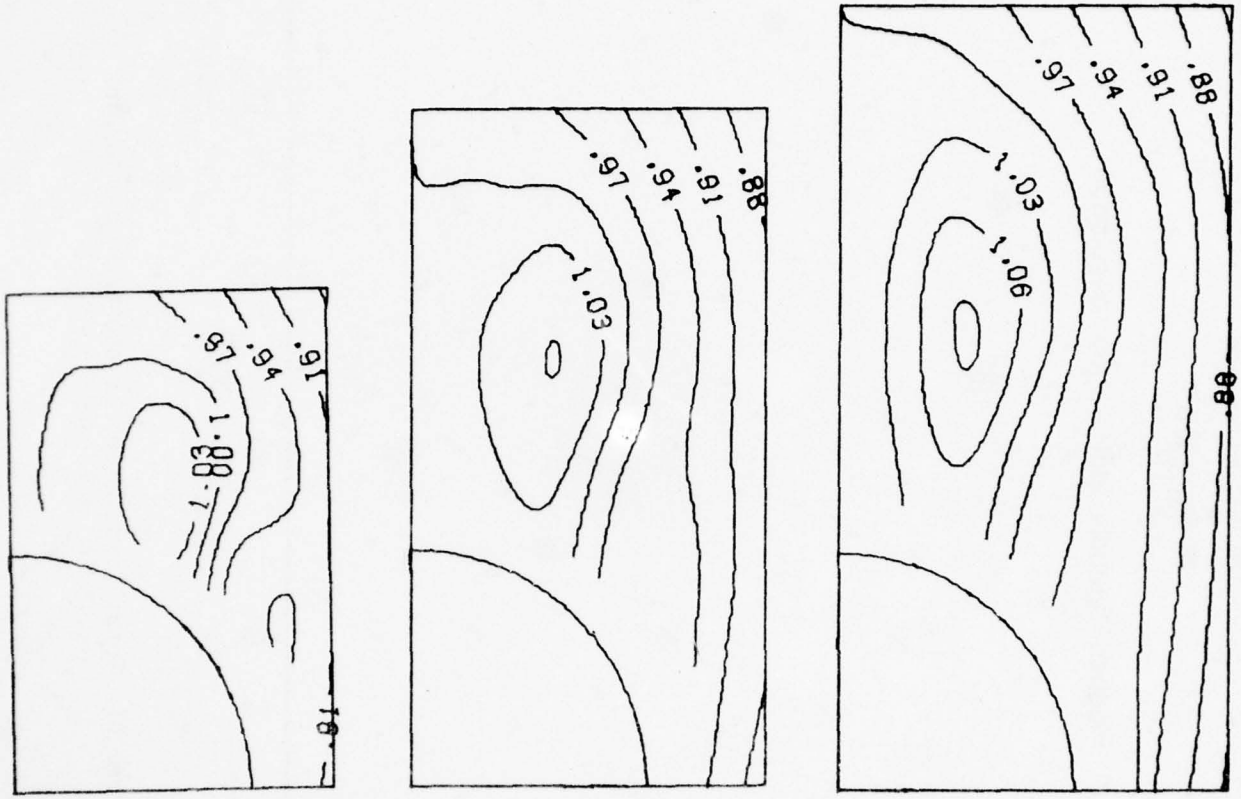
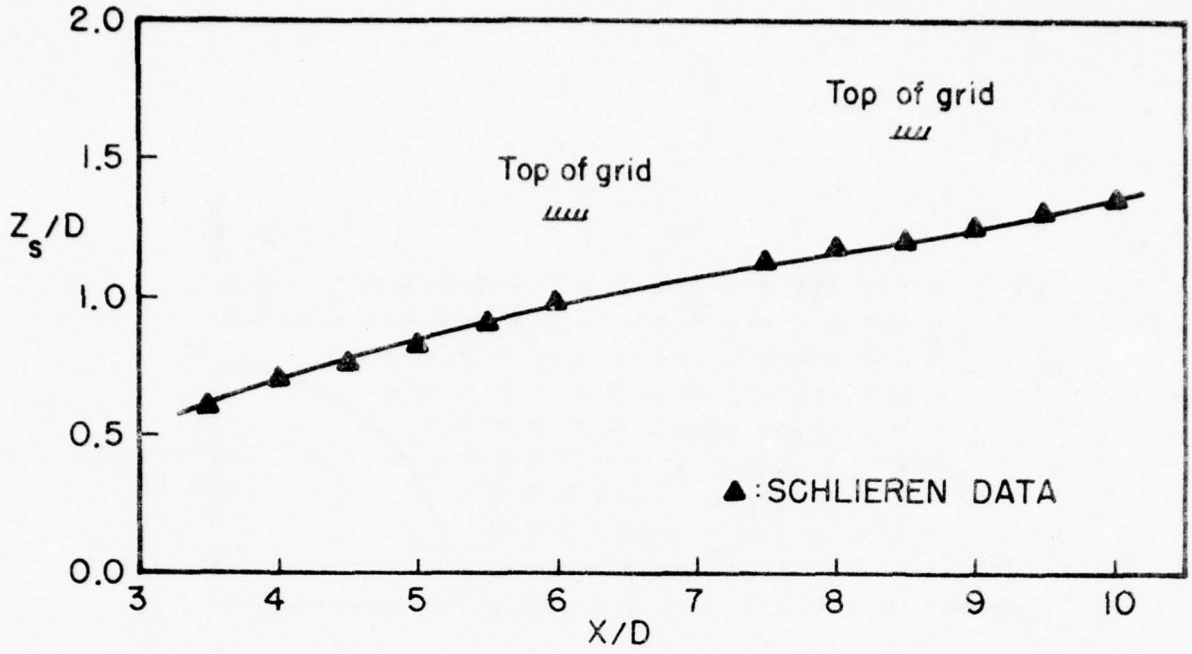
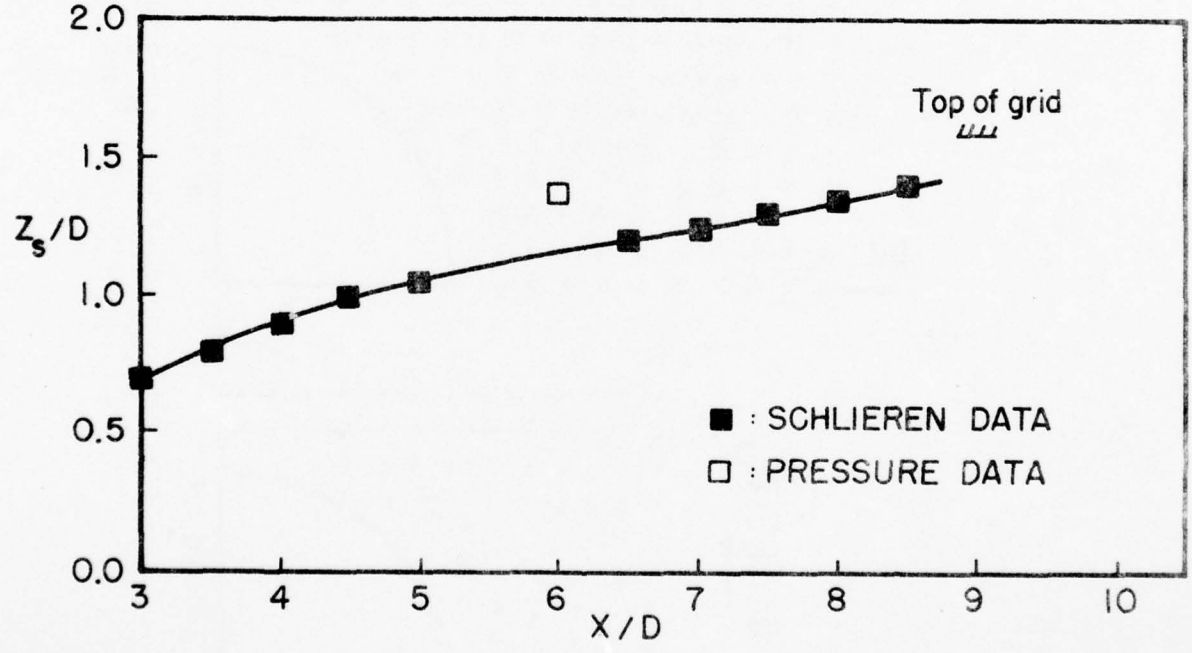


Figure 88. Streamlines in the Cross-Flow Plane for $M_\infty = 2.$, $R = 1.75 \times 10^6$ and $\alpha_b = 15°$



(a) $\alpha_b = 20°$



(b) $\alpha_b = 25°$

Figure 89. z-Coordinate of Secondary Nose Vortex for $M_\infty = 2.$ and $R_d = 1.75 \times 10^6$

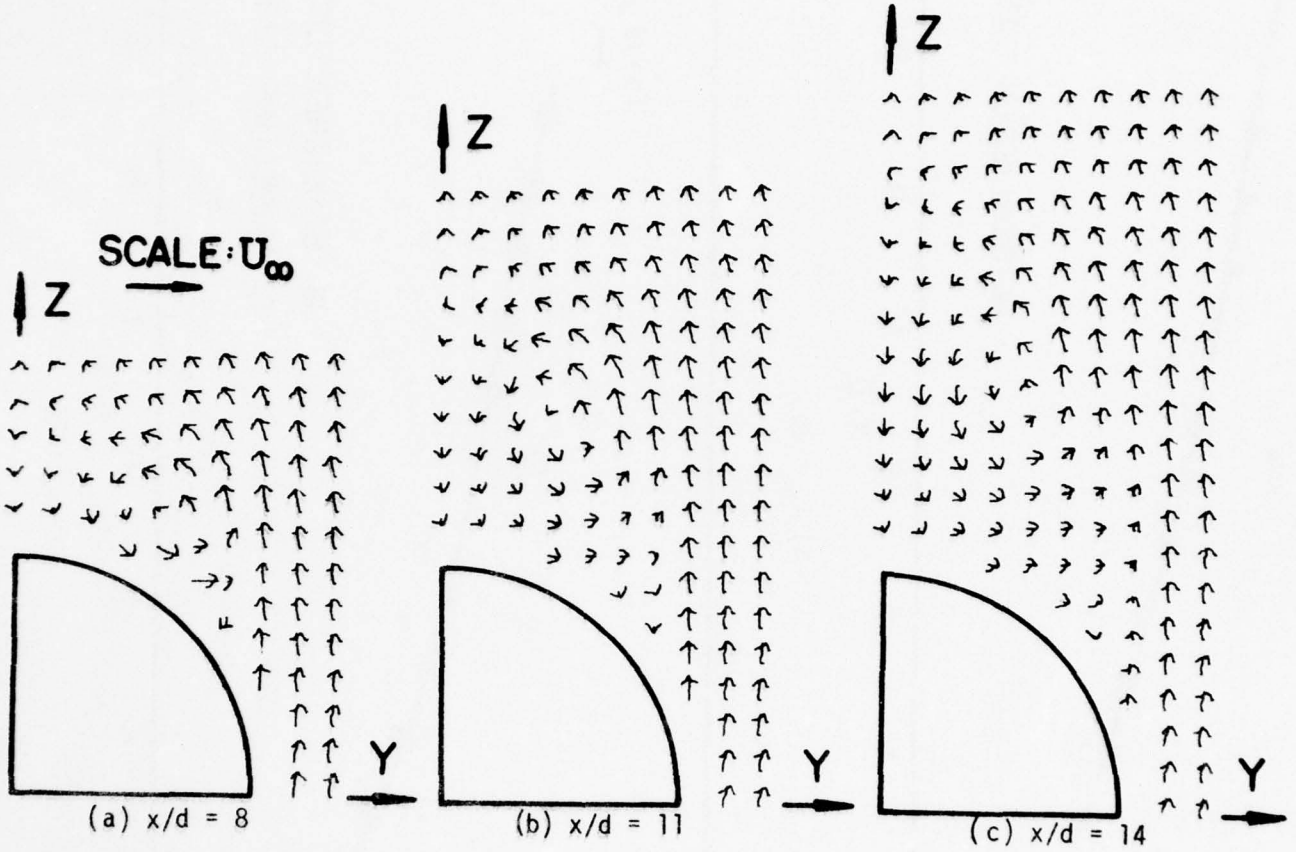


Figure 90. Cross-Flow Plane Vector Plot for $M_\infty = 3.01$, $R_d = 1.70 \times 10^6$ and $\alpha_b = 10°$.

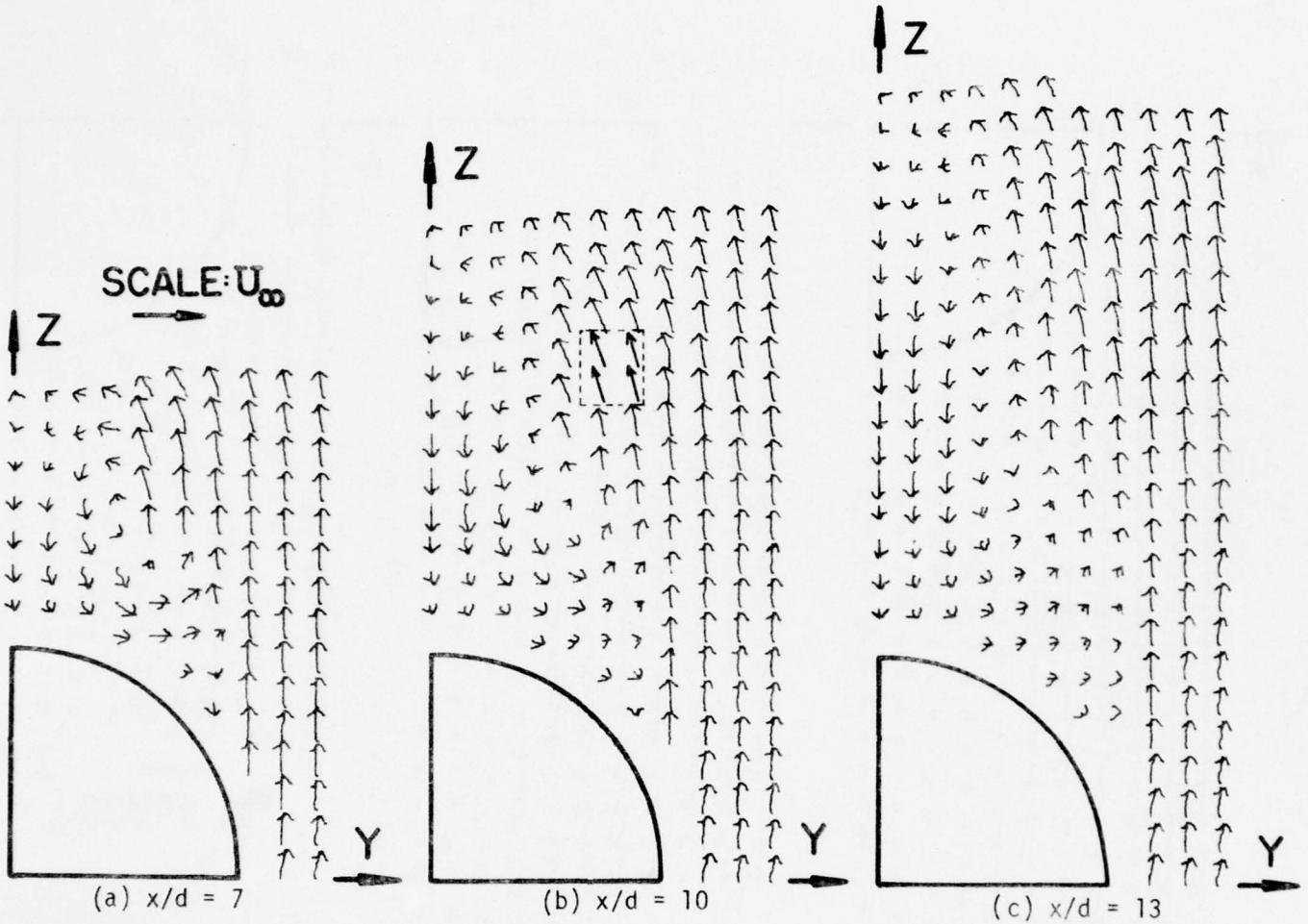


Figure 91. Cross-Flow Plane Vector Plot for $M_\infty = 3.01$, $R_d = 1.70 \times 10^6$ and $\alpha_b = 15°$.

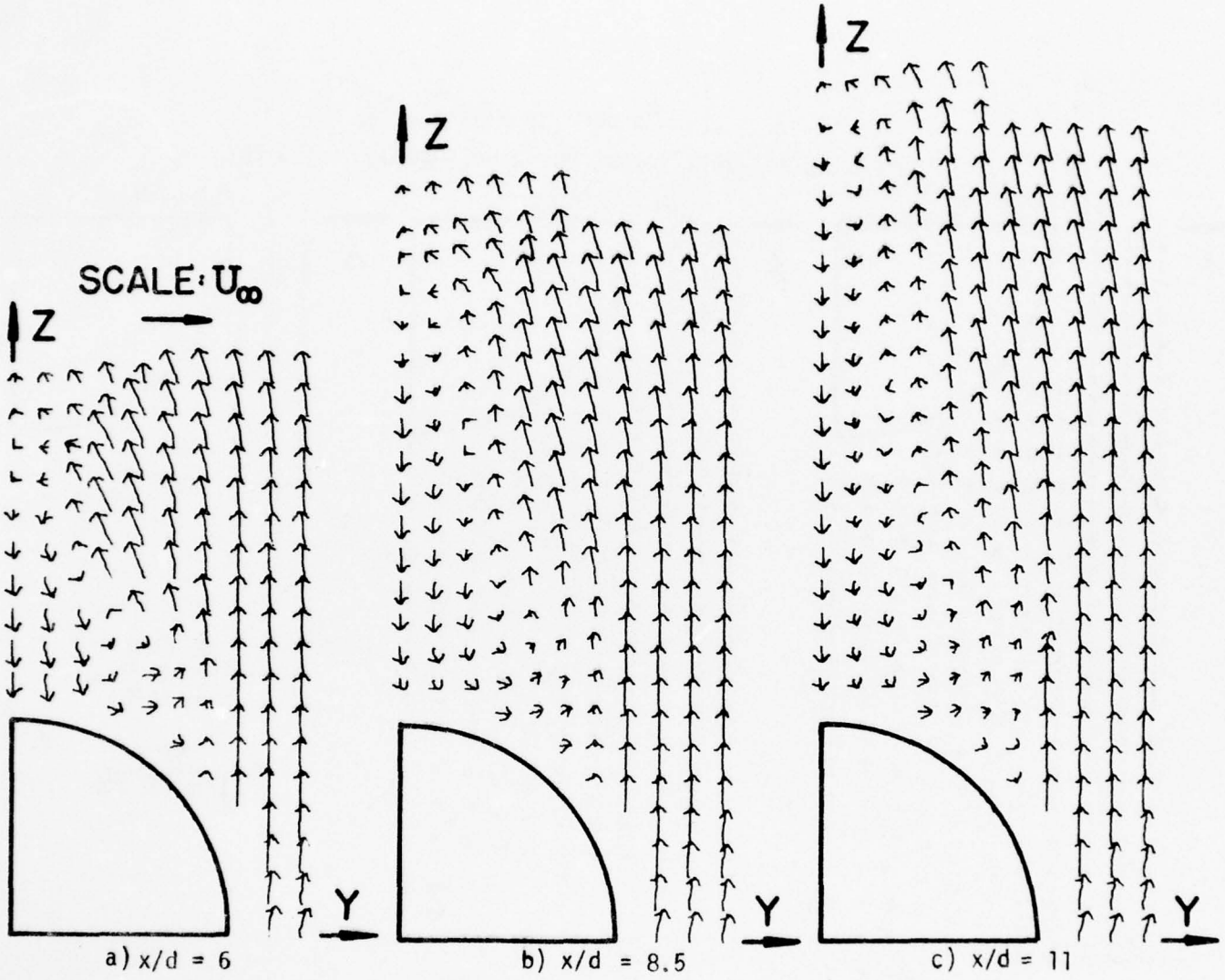
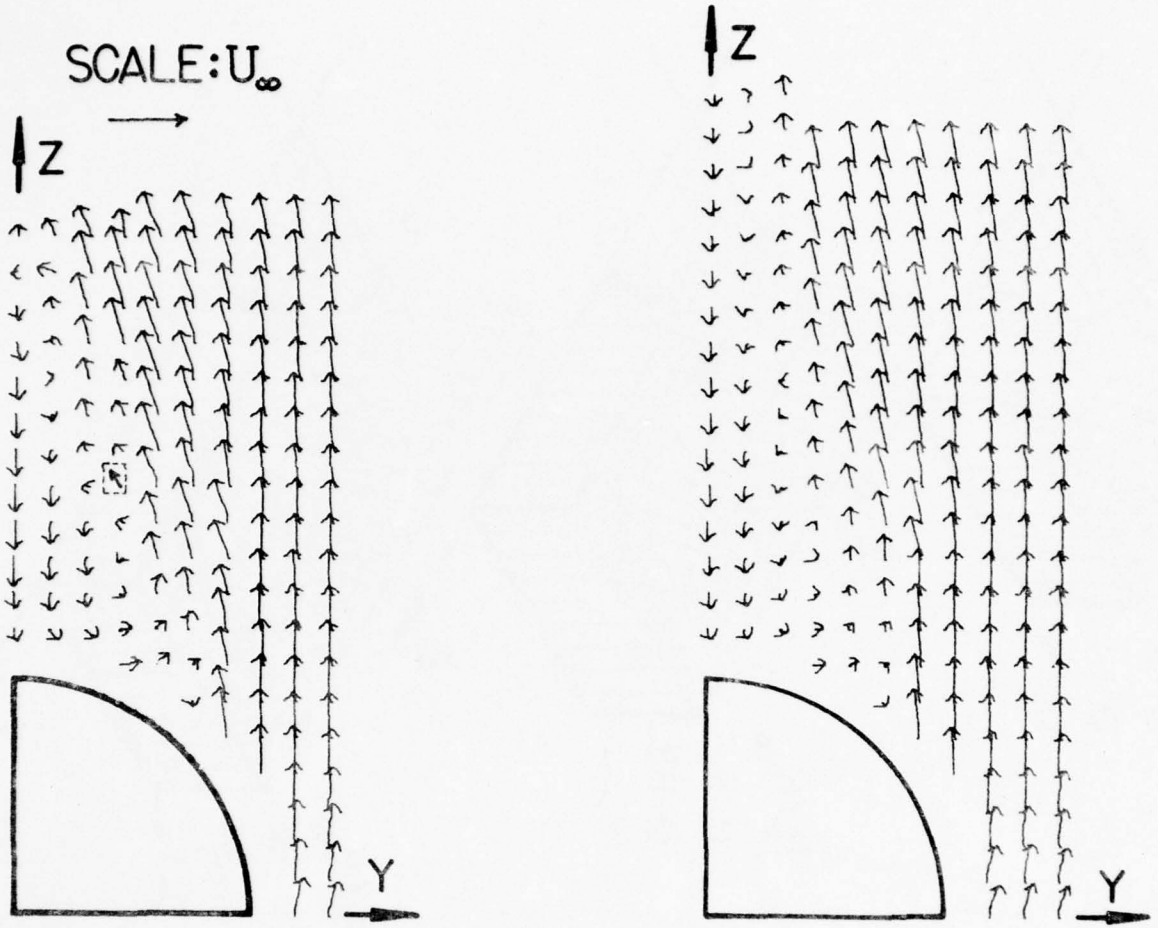


Figure 92. Cross-Flow Plane Vector Plot for $M_\infty = 3.01$, $R_d = 1.70 \times 10^6$ and $\alpha_b = 20°$.



(a) x/d = 6.

(b) x/d = 9.

Figure 93. Cross-Flow Plane Vector Plot for M_∞ = 3.01, R_d = 1.70 x 10^6 and α_b = 25°.

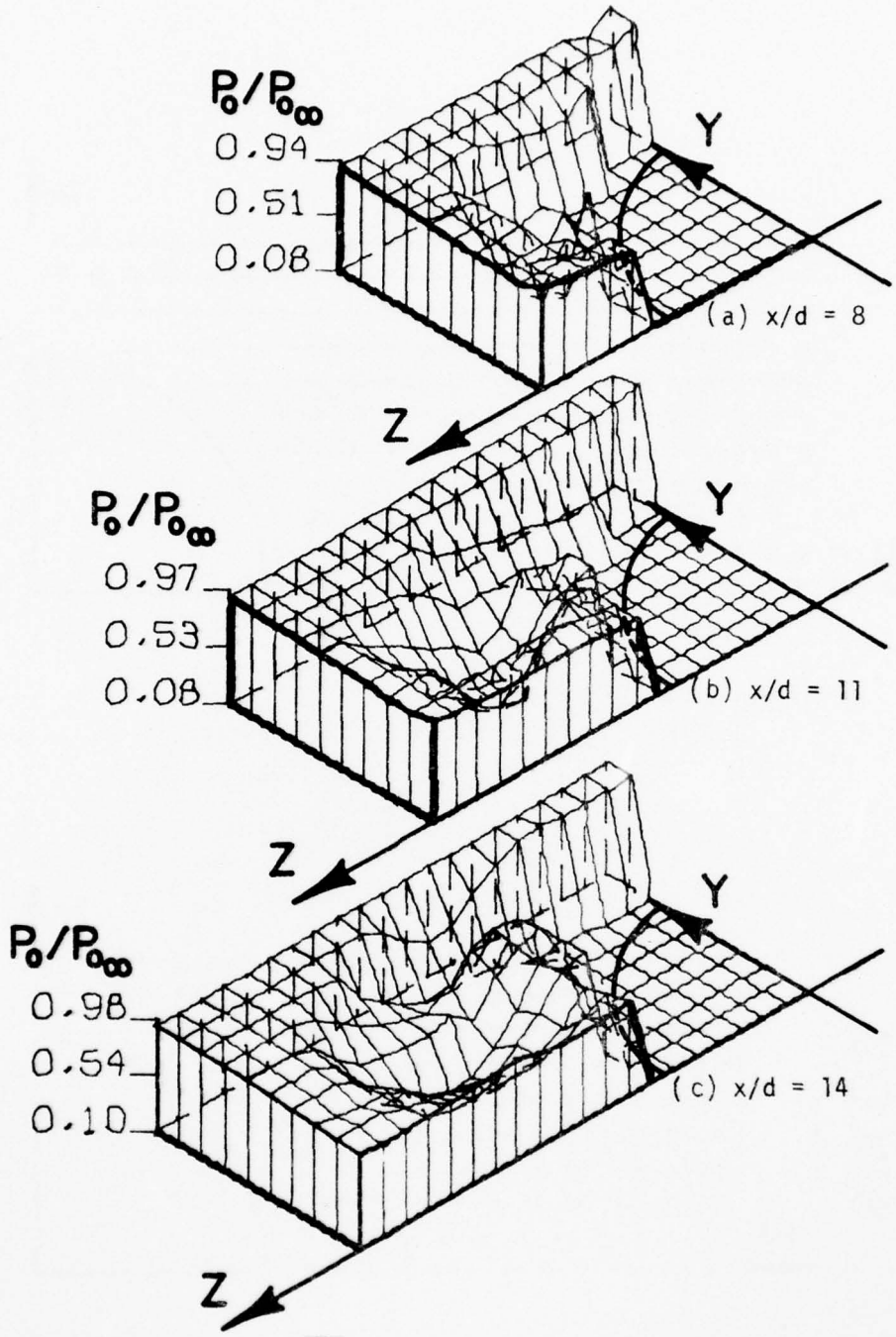


Figure 94. Total Pressure in Cross-Flow Plane for $M_\infty = 3.01$, $R_d = 1.70 \times 10^6$ and $\alpha_b = 10°$.

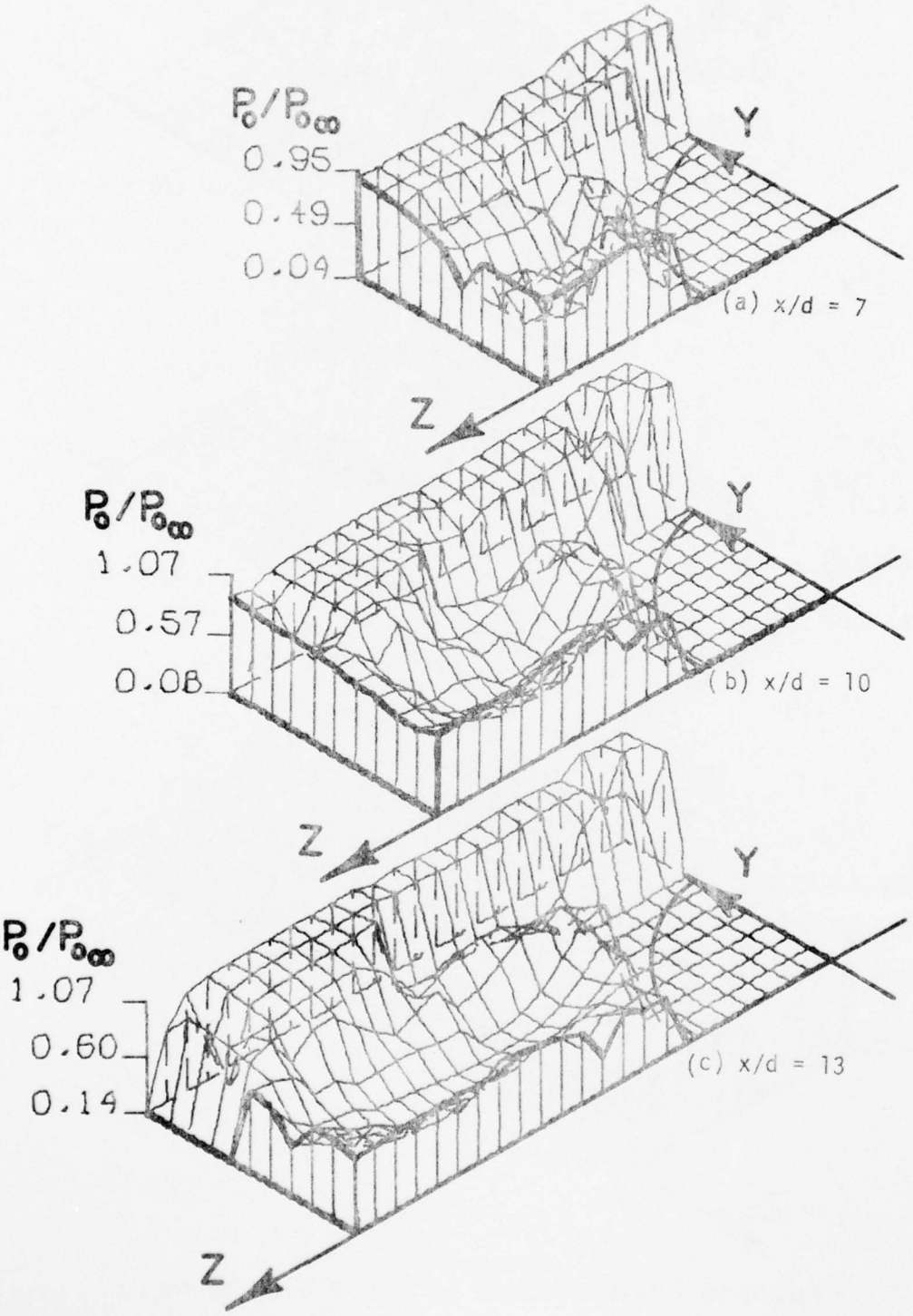


Figure 95. Total Pressure in Cross-Flow Plane for $M_\infty = 3.01$, $R_d = 1.70 \times 10^6$ and $\alpha_b = 15°$.

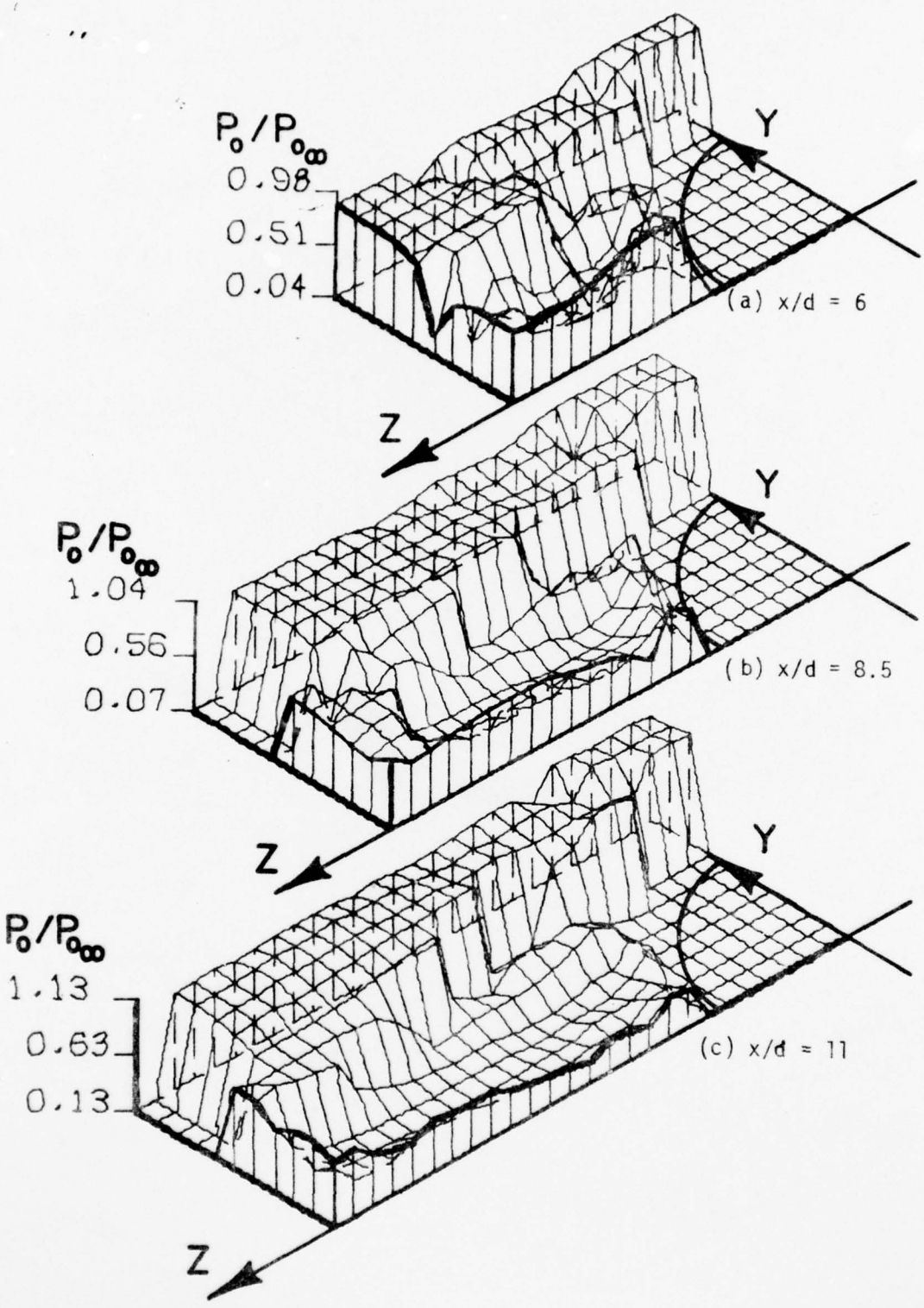


Figure 96. Total Pressure in Cross-Flow Plane for $M_\infty = 3.01$, $R_d = 1.70 \times 10^6$ and $\alpha_b = 20°$.

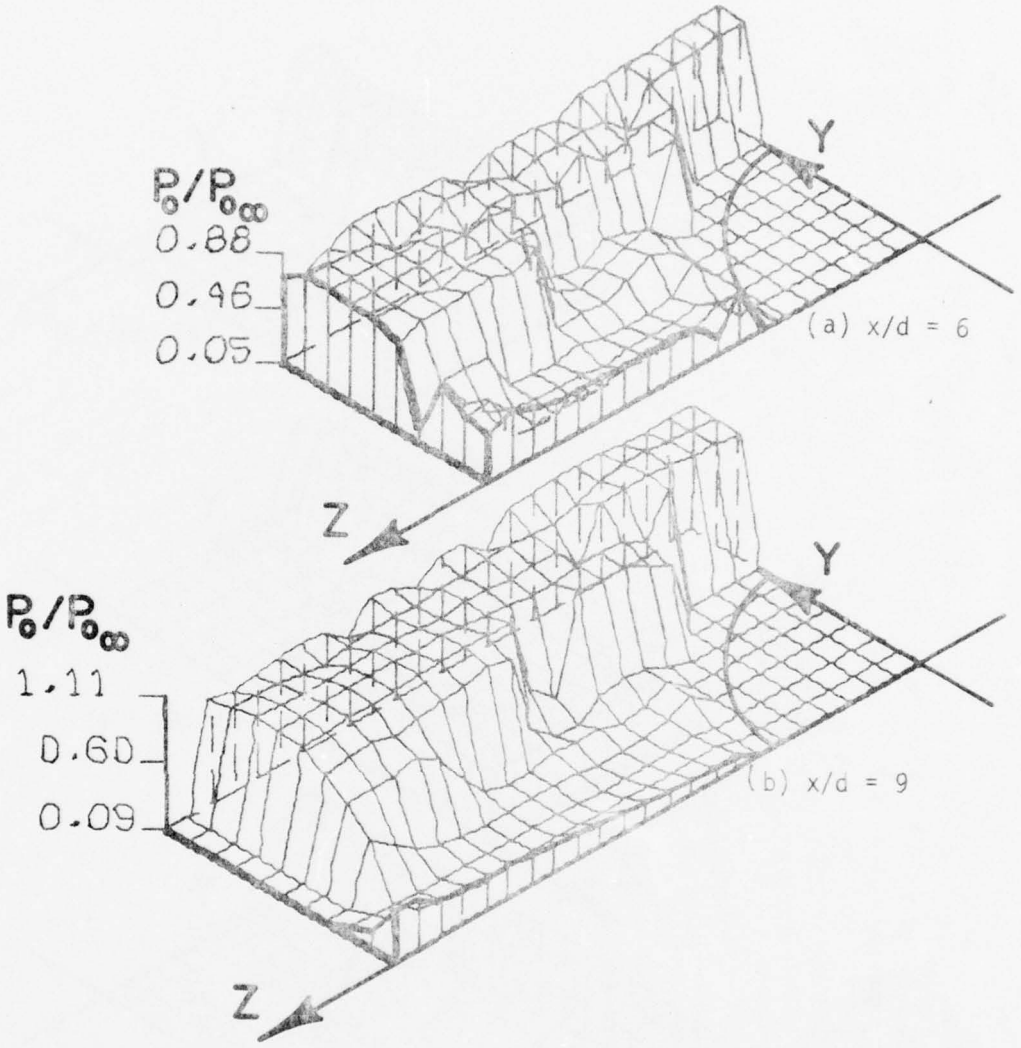


Figure 97. Total Pressure in Cross-Flow Plane for $M_\infty = 3.01$, $R_d = 1.70 \times 10^6$ and $\alpha_b = 25°$.

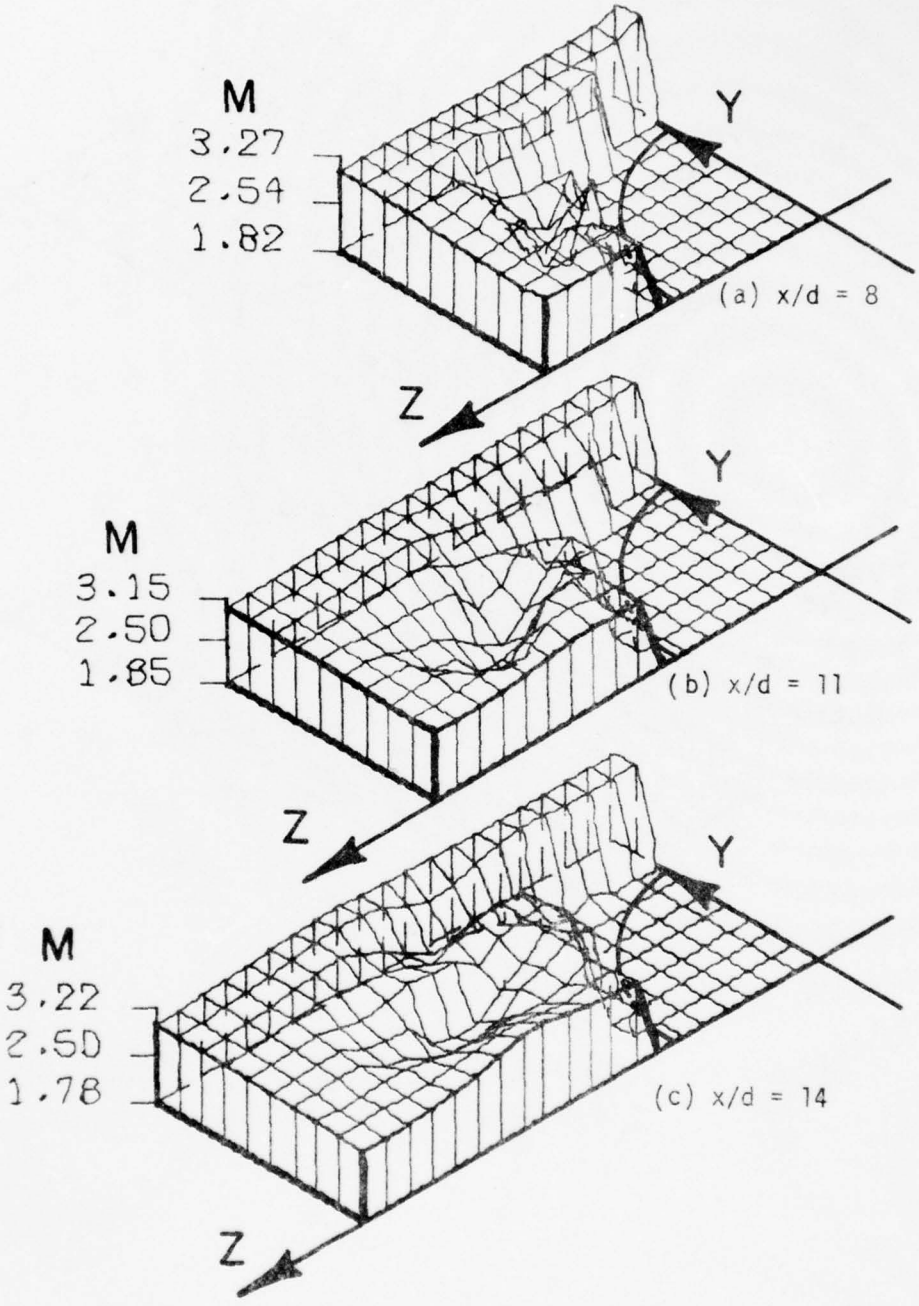
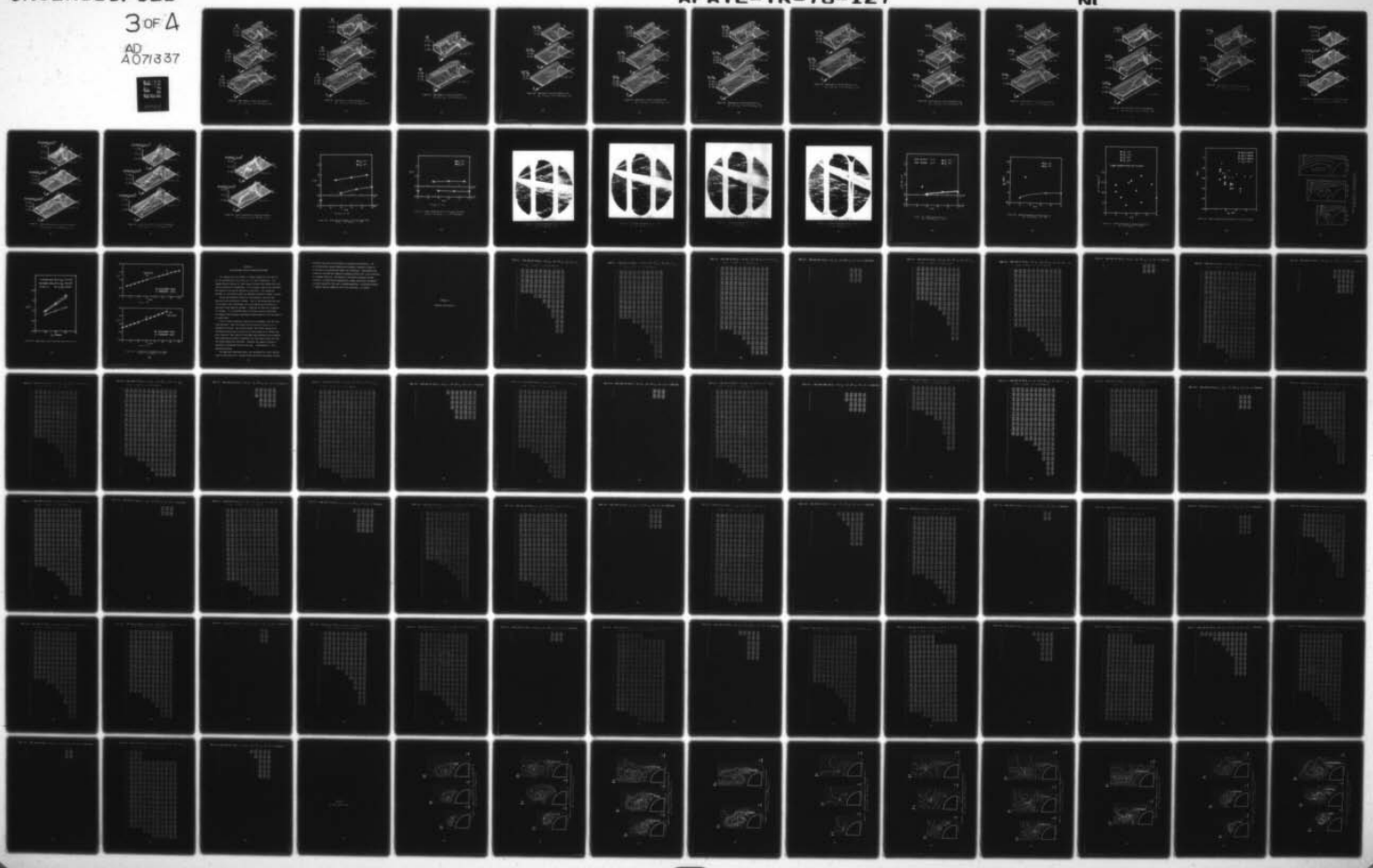


Figure 98. Mach Number in Cross-Flow Plane for $M_\infty = 3.01$, $R_d = 1.70 \times 10^6$ and $\alpha_b = 10°$.

AD-A071 337 TEXAS UNIV AT AUSTIN DEPT OF MECHANICAL ENGINEERING F/G 16/2
SUPERSONIC FLOW MEASUREMENTS IN THE BODY VORTEX WAKE OF AN OGIV--ETC(U)
NOV 78 W L OBERKAMPF, T J BARTEL F08635-77-C-0049

UNCLASSIFIED AFATL-TR-78-127 NL

3 OF 4
AD A071337



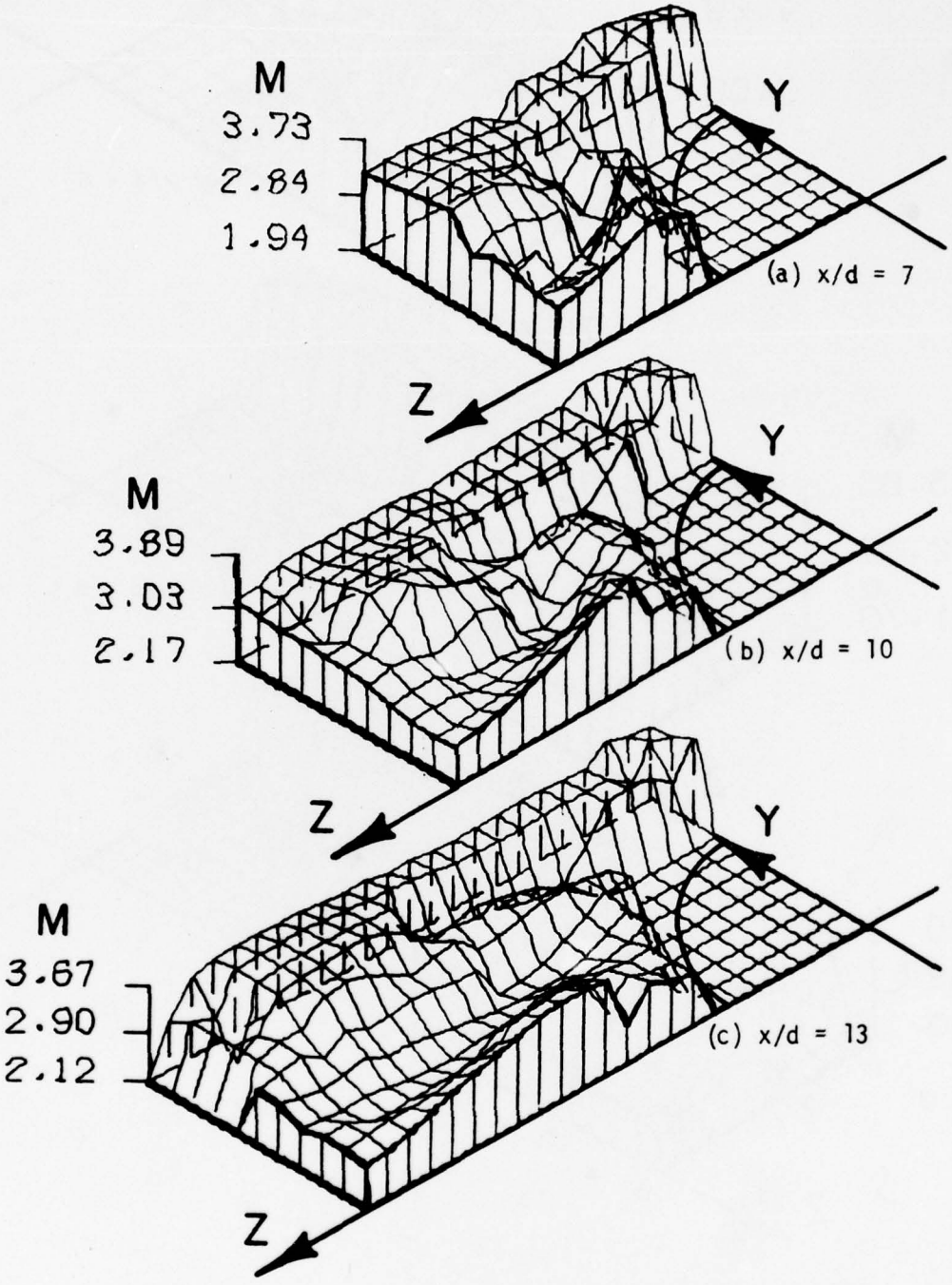


Figure 99. Mach Number in Cross-Flow Plane for $M_\infty = 3.01$, $R_d = 1.70 \times 10^6$ and $\alpha_b = 15°$.

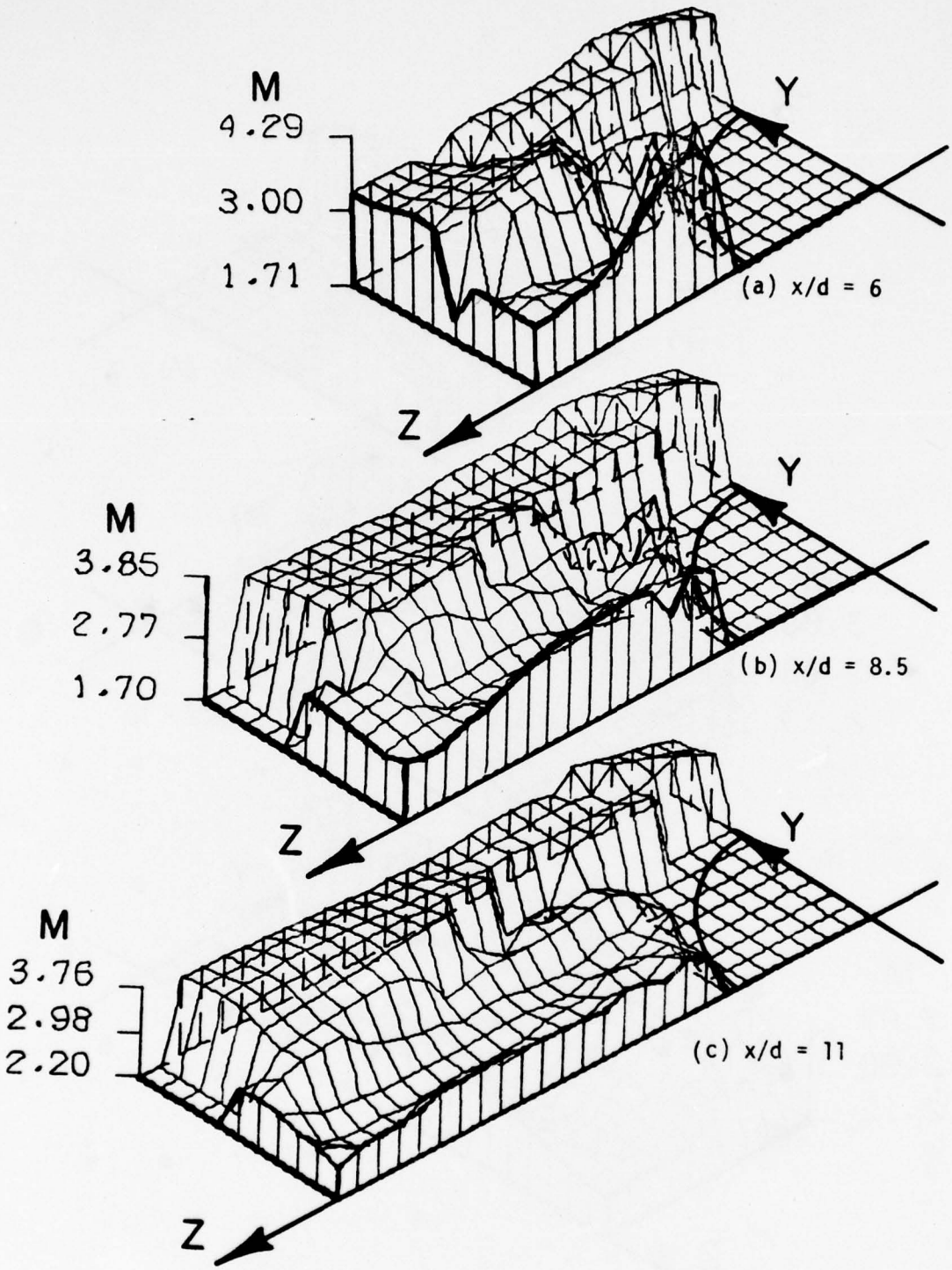


Figure 100. Mach Number in Cross-Flow Plane for $M_\infty = 3.01$, $R_d = 1.70 \times 10^6$ and $\alpha_b = 20°$.

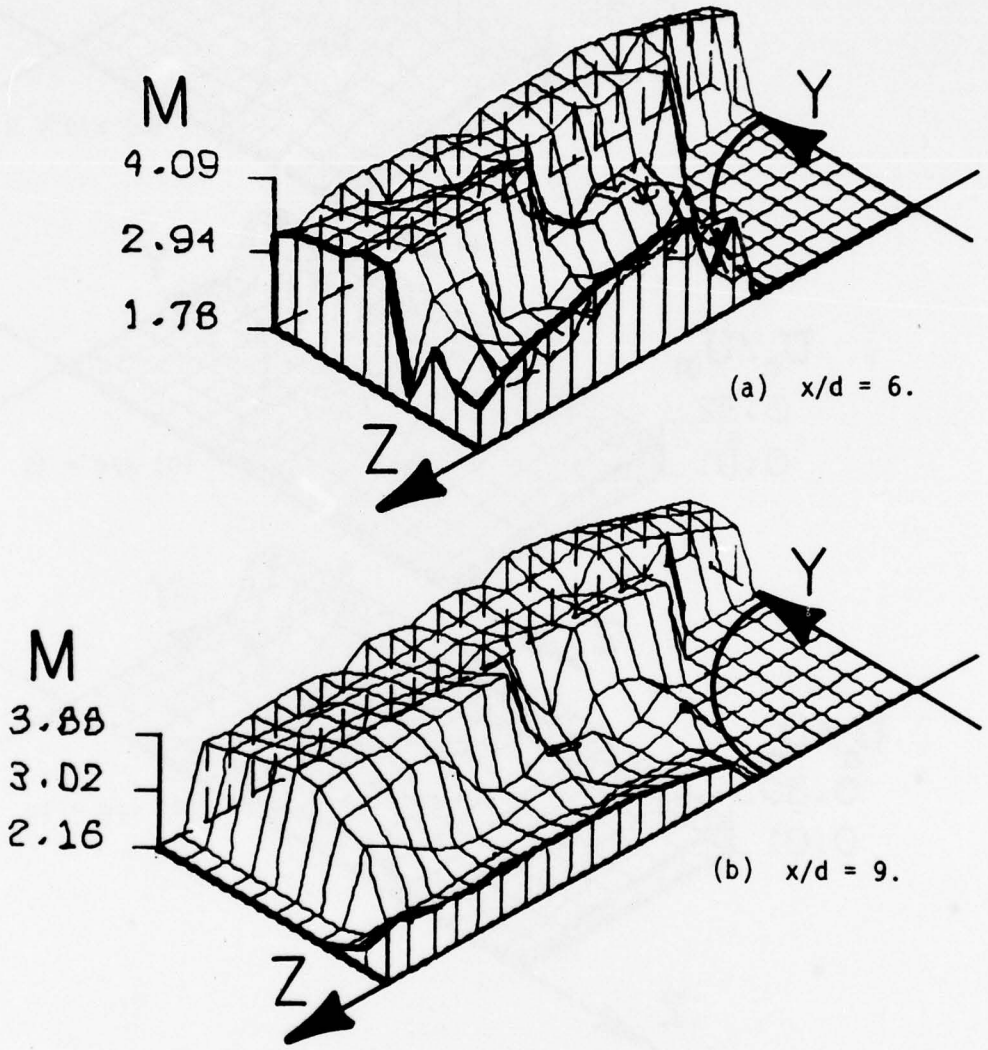


Figure 101. Mach Number in Cross-Flow Plane for $M_\infty = 3.01$, $R_d = 1.70 \times 10^6$ and $\alpha_b = 25°$.

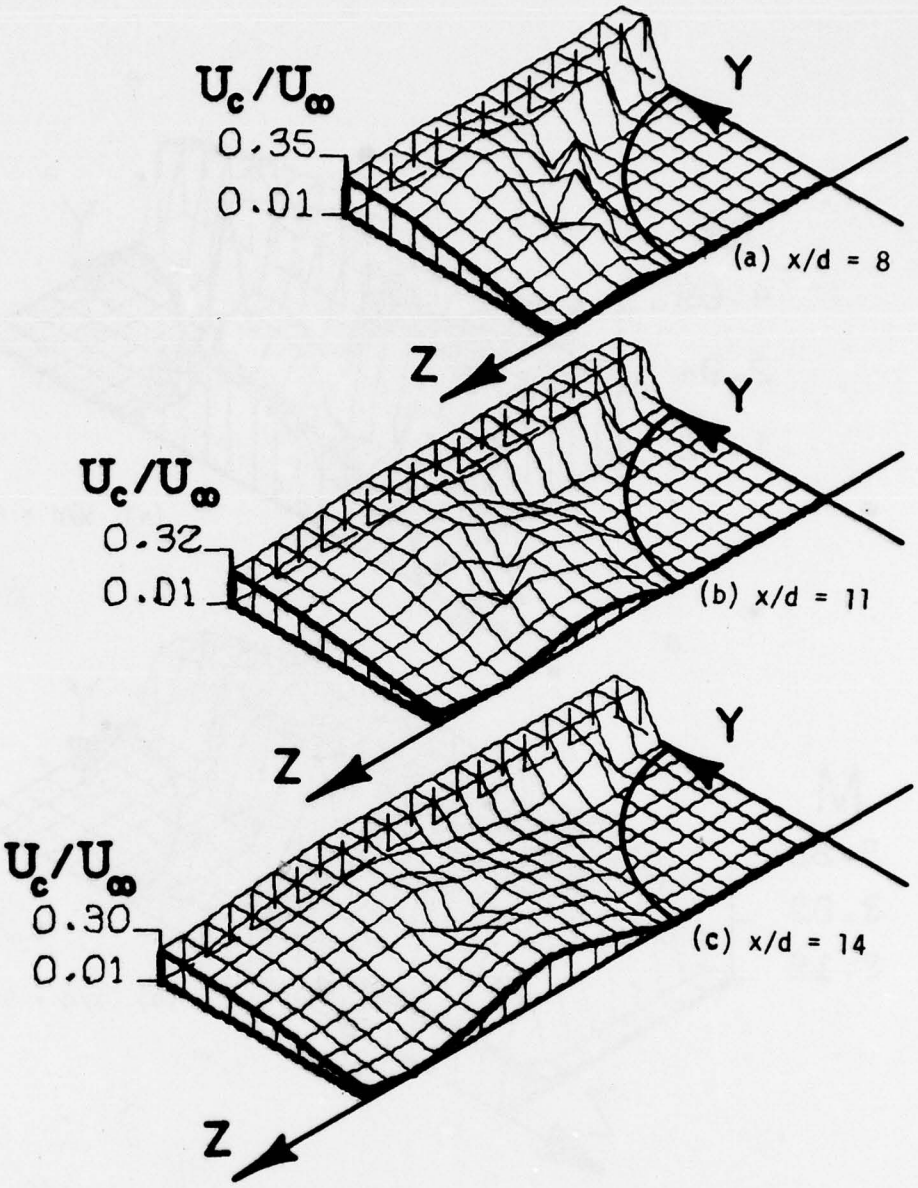


Figure 102. Magnitude of Cross-Flow Velocity for $M_\infty = 3.01$, $R_d = 1.70 \times 10^6$ and $\alpha_b = 10°$.

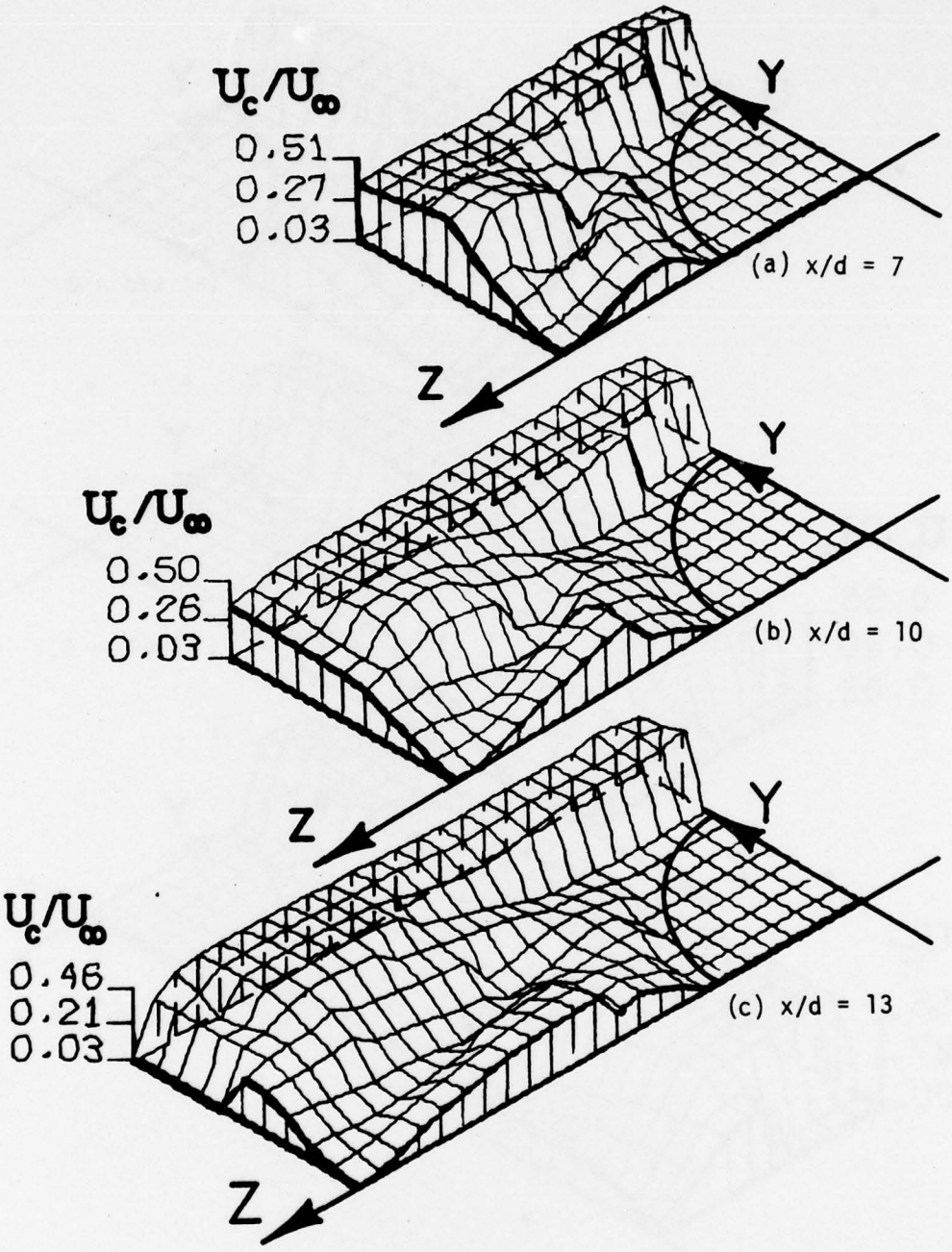


Figure 103. Magnitude of Cross-Flow Velocity for $M_\infty = 3.01$, $R_d = 1.70 \times 10^6$ and $\alpha_b = 15°$.

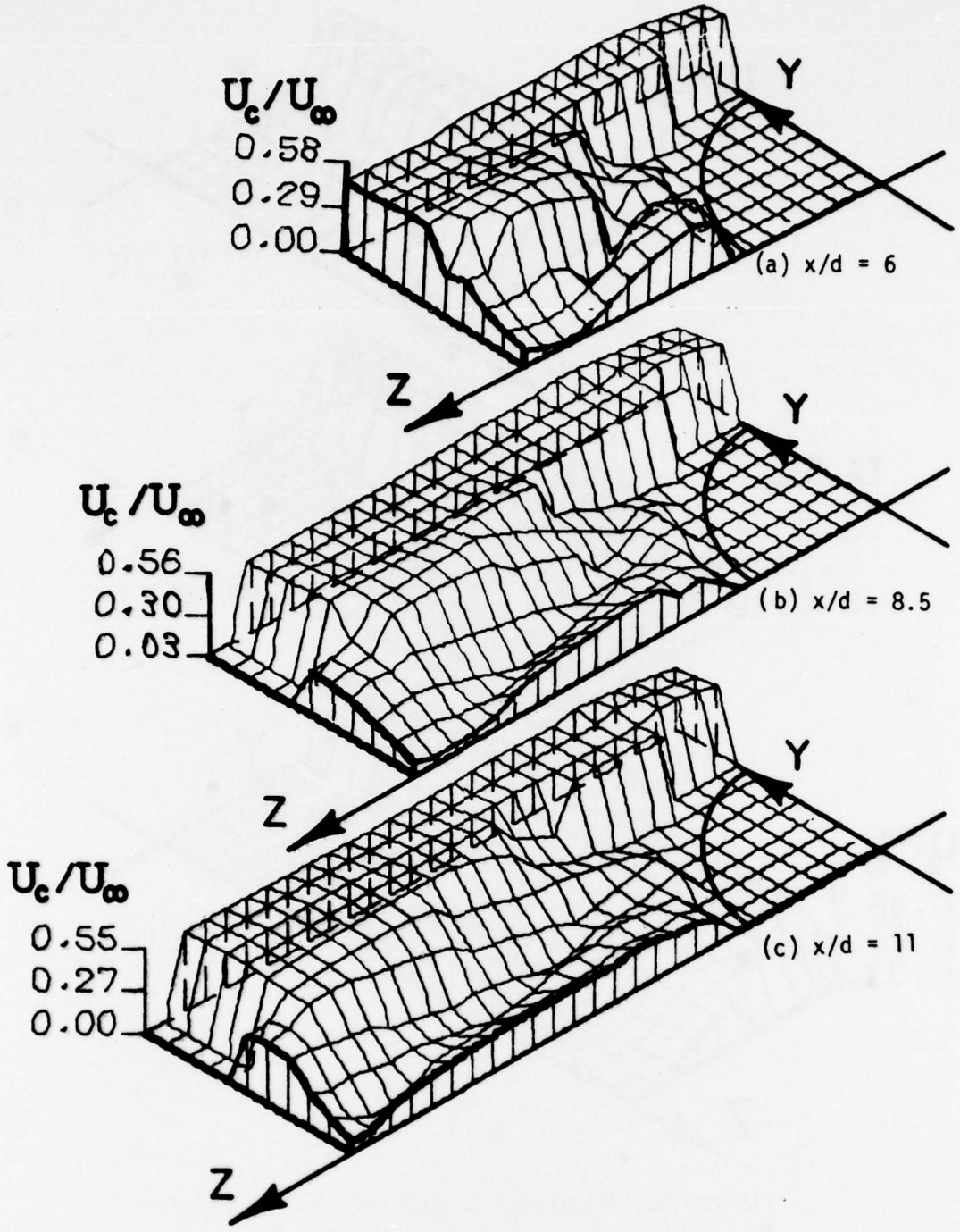


Figure 104. Magnitude of Cross-Flow Velocity for $M_\infty = 3.01$, $R_d = 1.70 \times 10^6$ and $\alpha_b = 20°$.

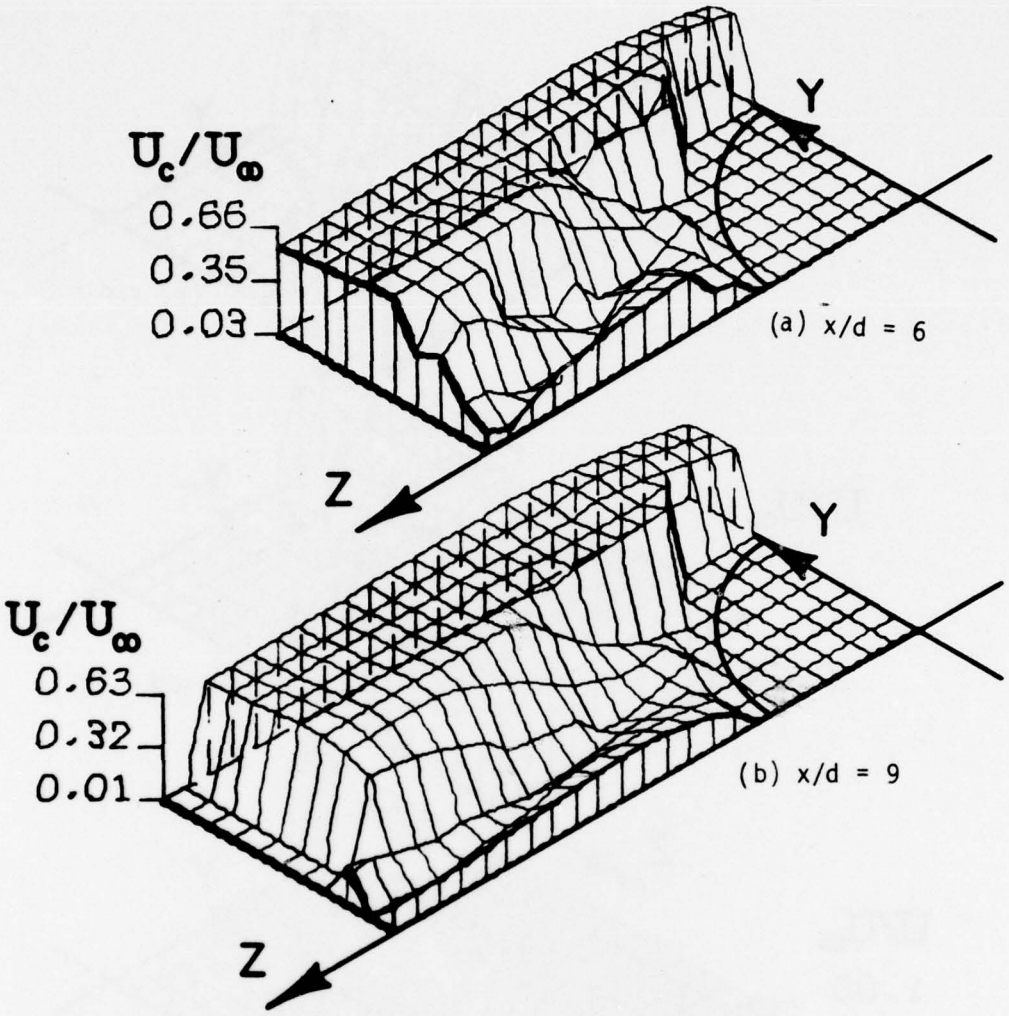


Figure 105. Magnitude of Cross-Flow Velocity for $M_\infty = 3.01$, $R_d = 1.70 \times 10^6$ and $\alpha_b = 25°$.

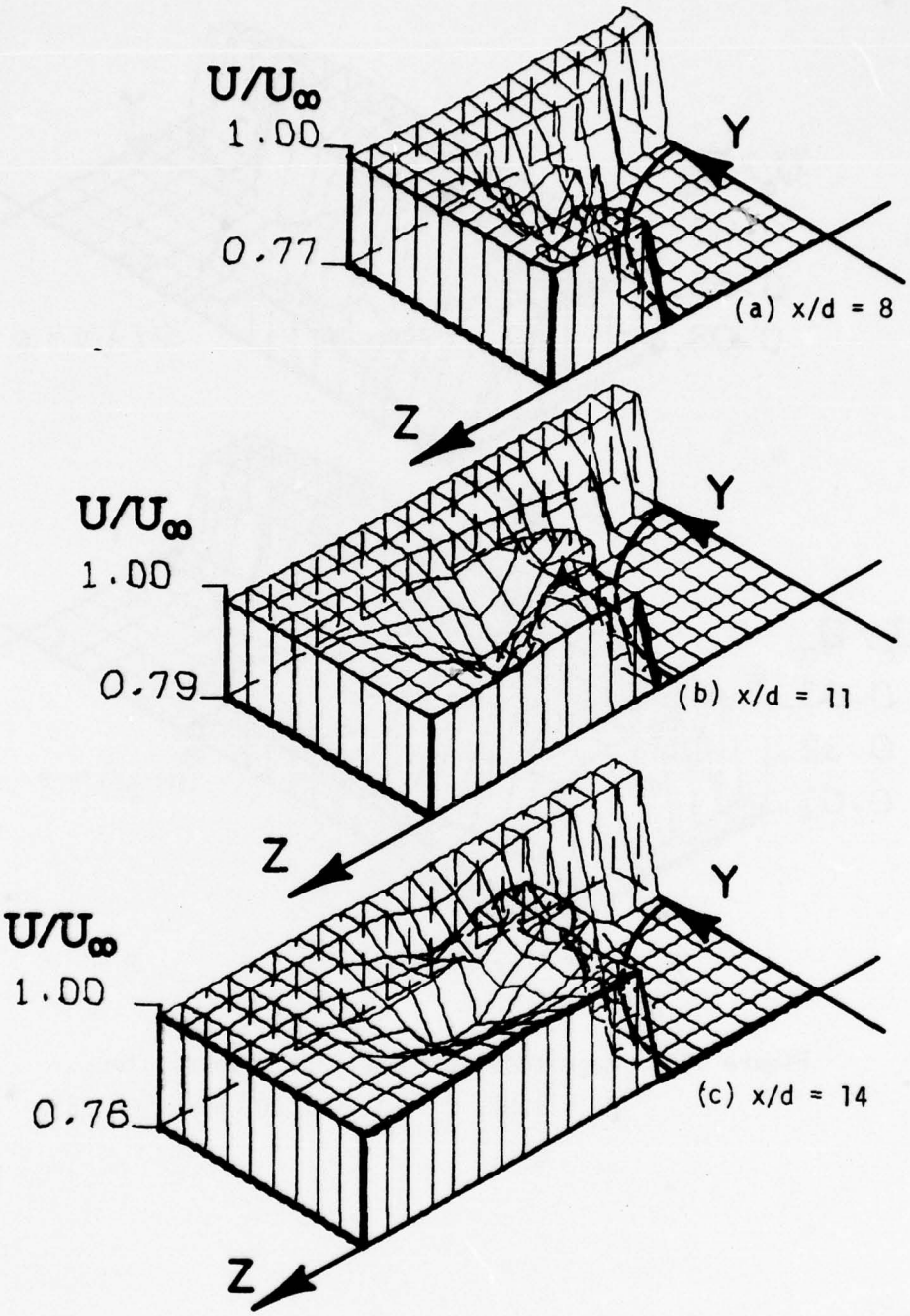


Figure 106. Axial Velocity in Cross-Flow Plane for $M_\infty = 3.01$, $R_d = 1.70 \times 10^6$ and $\alpha_b = 10°$.

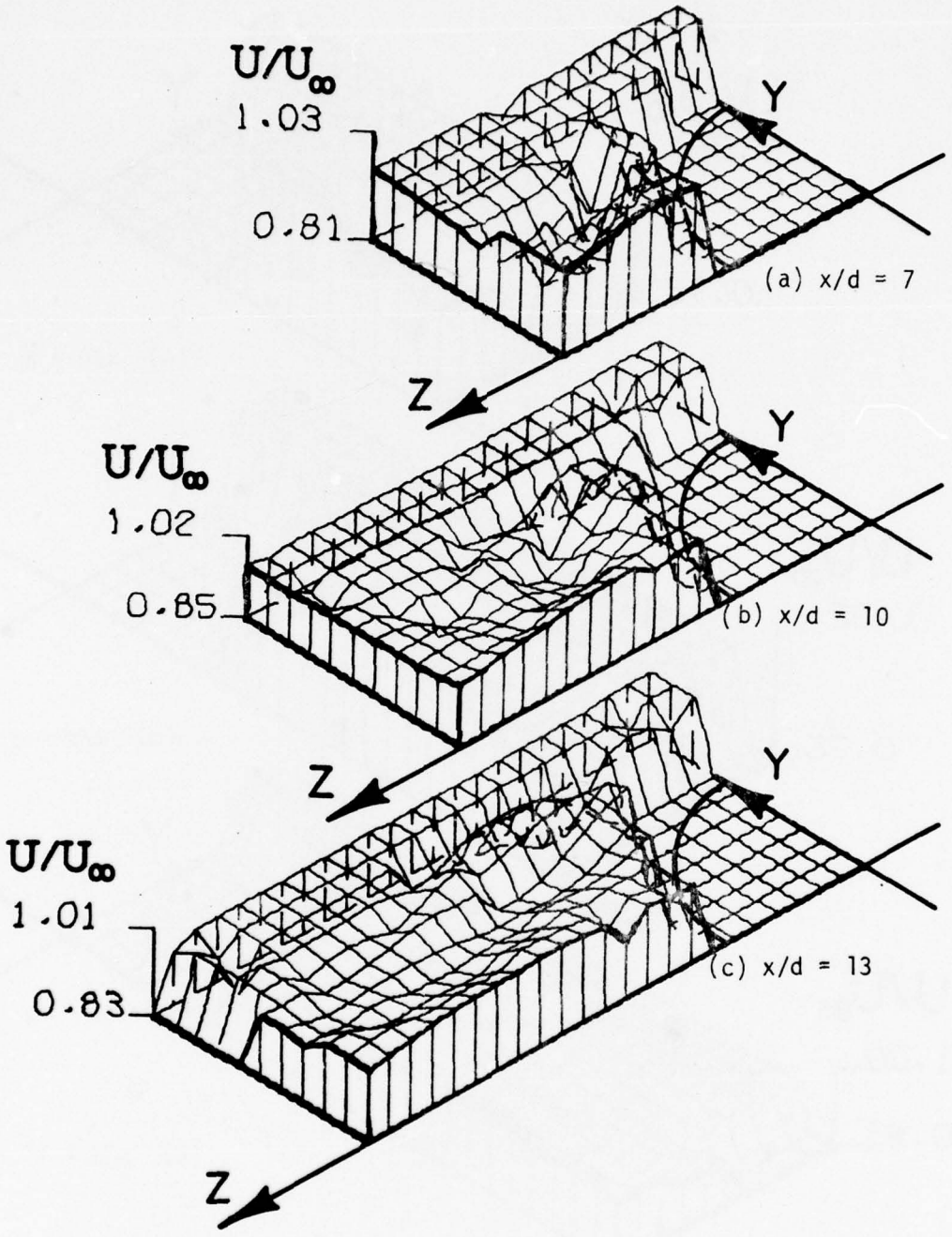


Figure 107. Axial Velocity in Cross-Flow Plane for $M_\infty = 3.01$, $R_d = 1.70 \times 10^6$ and $\alpha_b = 15°$.

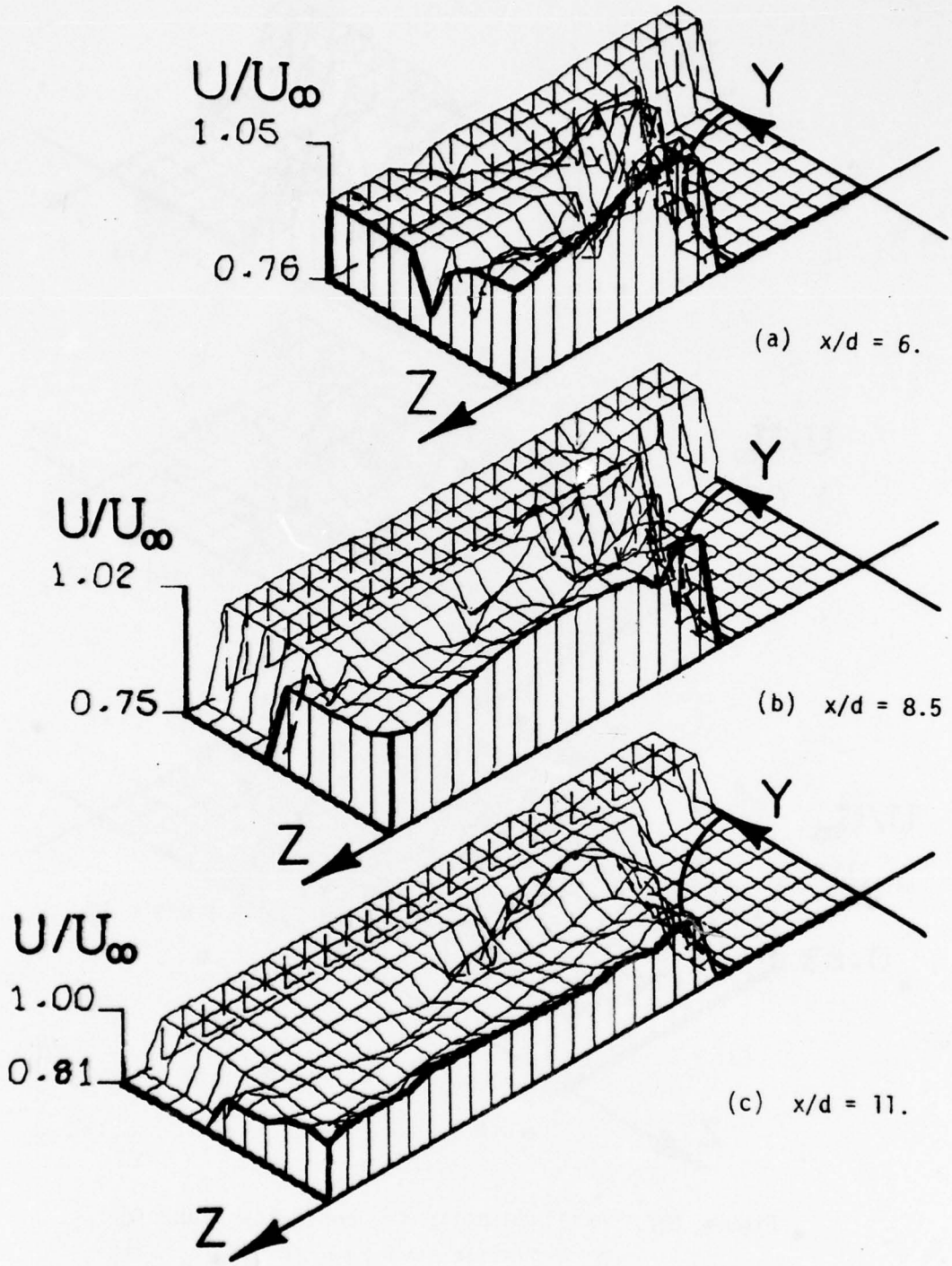


Figure 108. Axial Velocity in Cross-Flow Plane for $M_\infty = 3.01$, $R_d = 1.70 \times 10^6$ and $\alpha_b = 20°$.

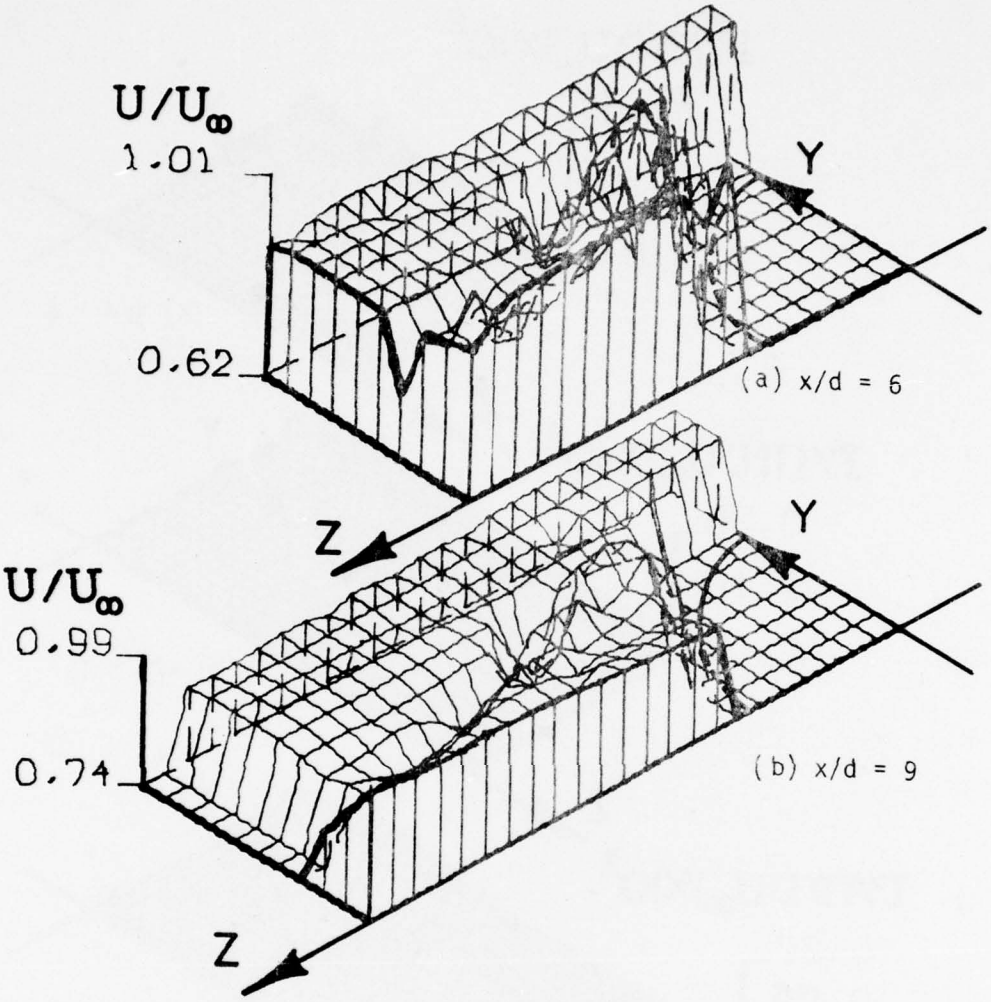


Figure 109. Axial Velocity in Cross-Flow Plane for $M_\infty = 3.01$, $R_d = 1.70 \times 10^6$ and $\alpha_b = 25°$.

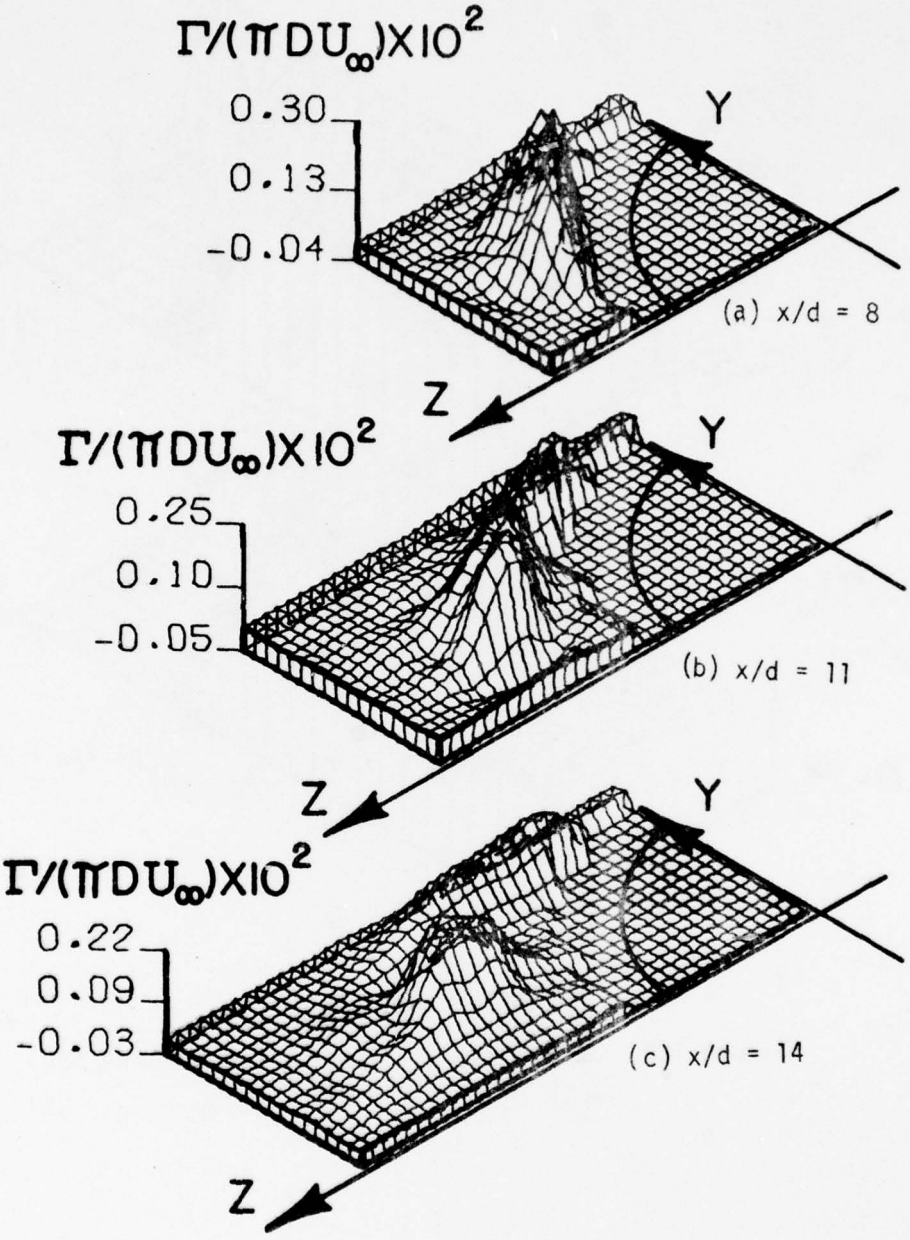


Figure 110. Local Circulation in Cross-Flow Plane for $M_\infty = 3.01$, $R_d = 1.70 \times 10^6$ and $\alpha_b = 10°$.

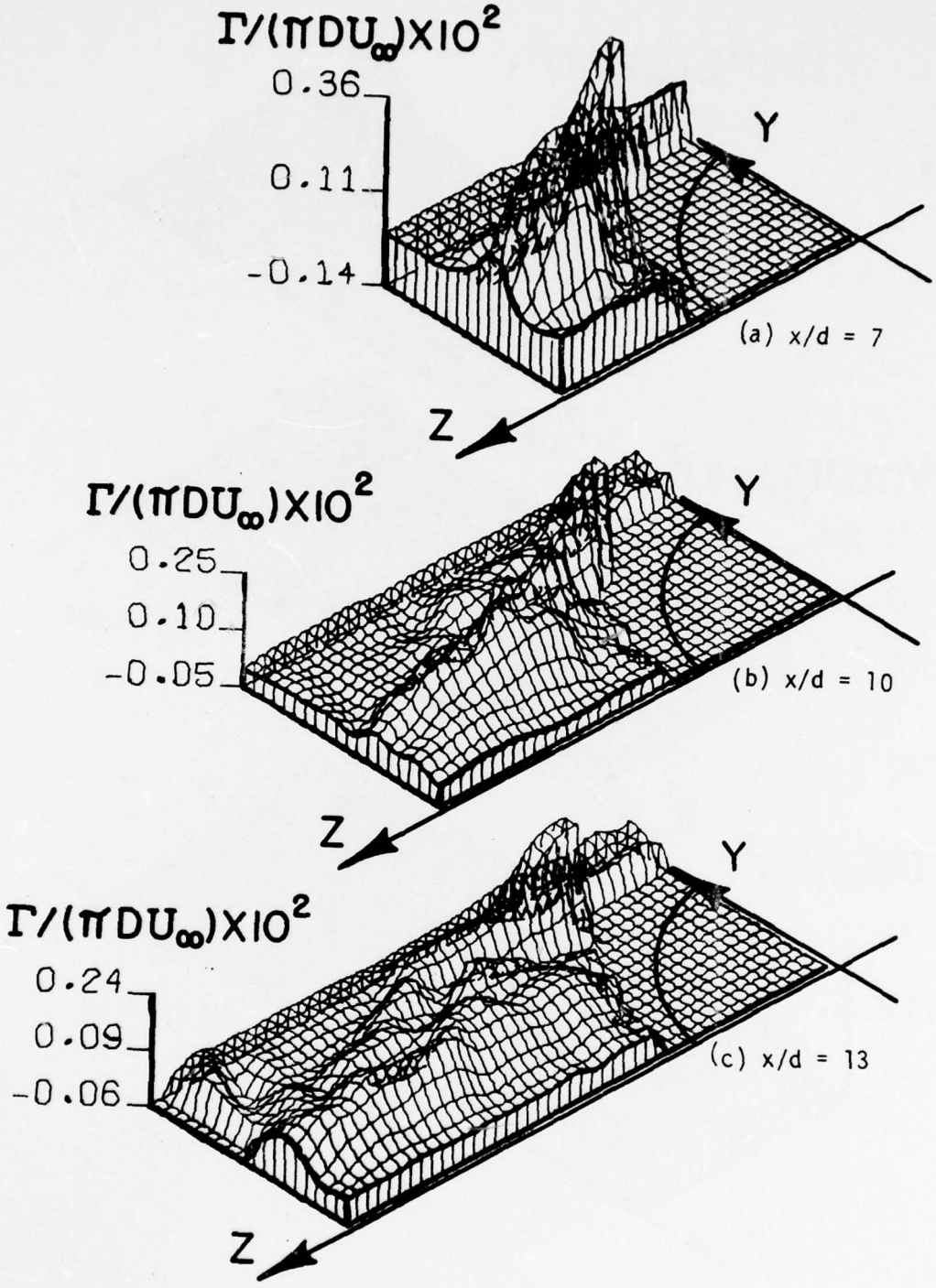


Figure 111. Local Circulation in Cross-Flow Plane for $M_\infty = 3.01$, $R_d = 1.70 \times 10^6$ and $\alpha_b = 15°$.

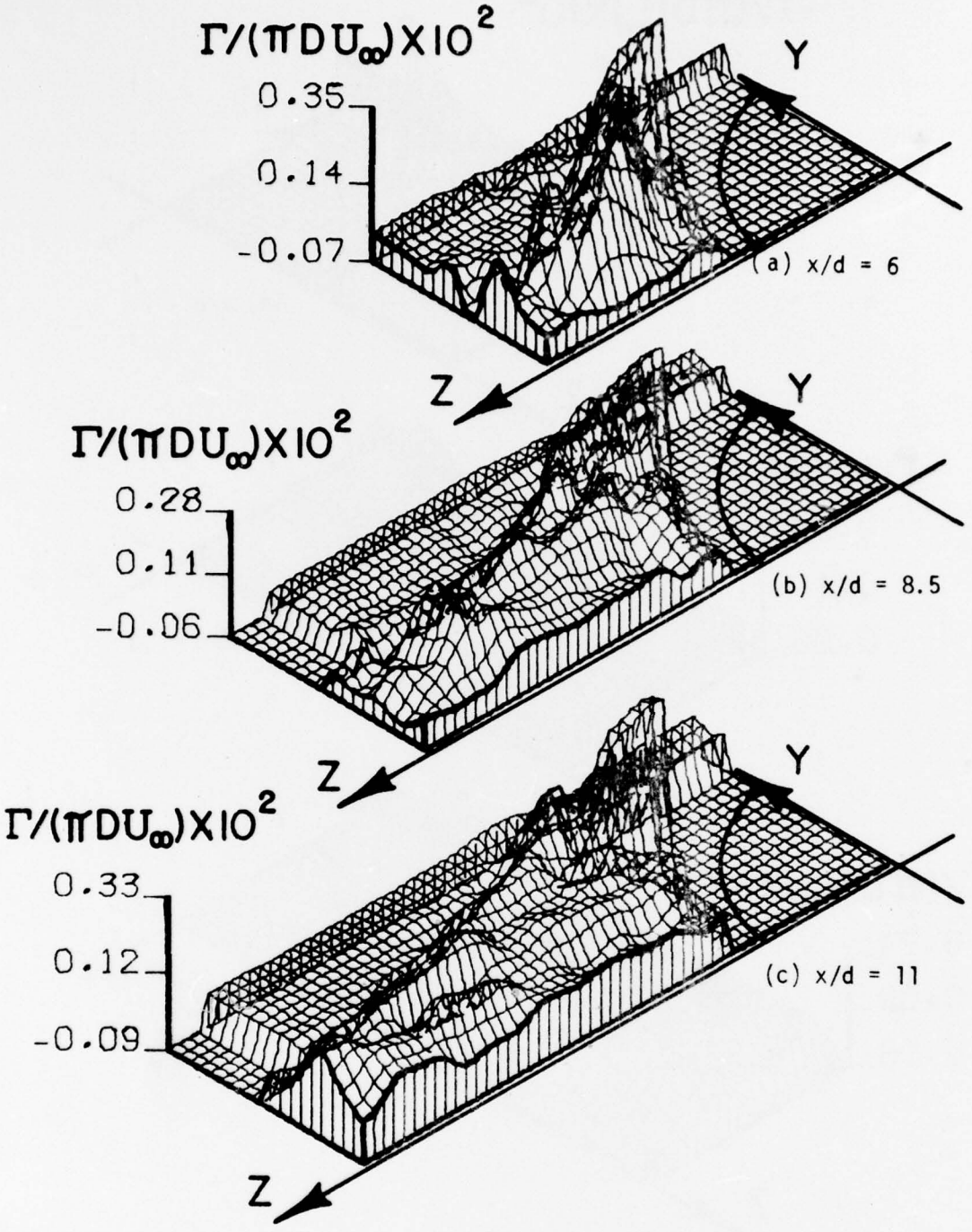


Figure 112. Local Circulation in Cross-Flow Plane for $M_\infty = 3.01$, $R_d = 1.70 \times 10^6$ and $\alpha_b = 20°$.

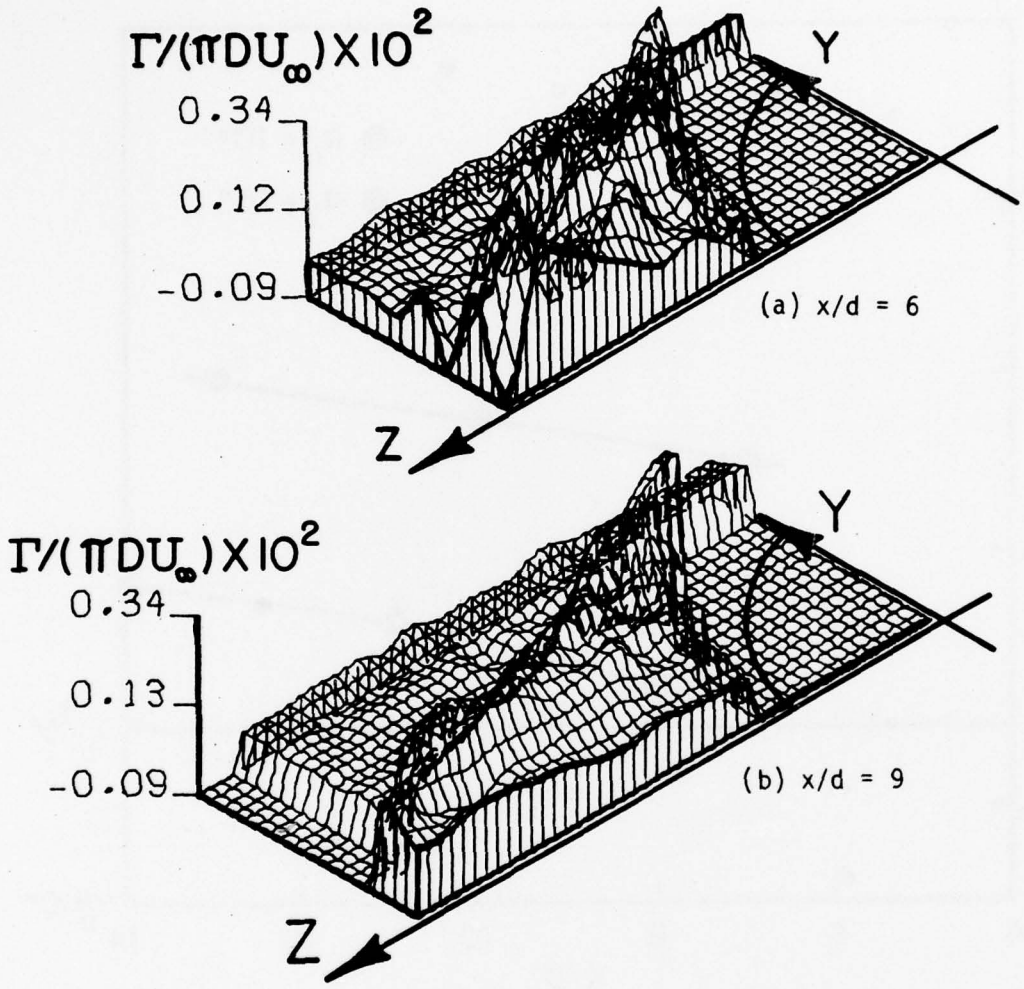
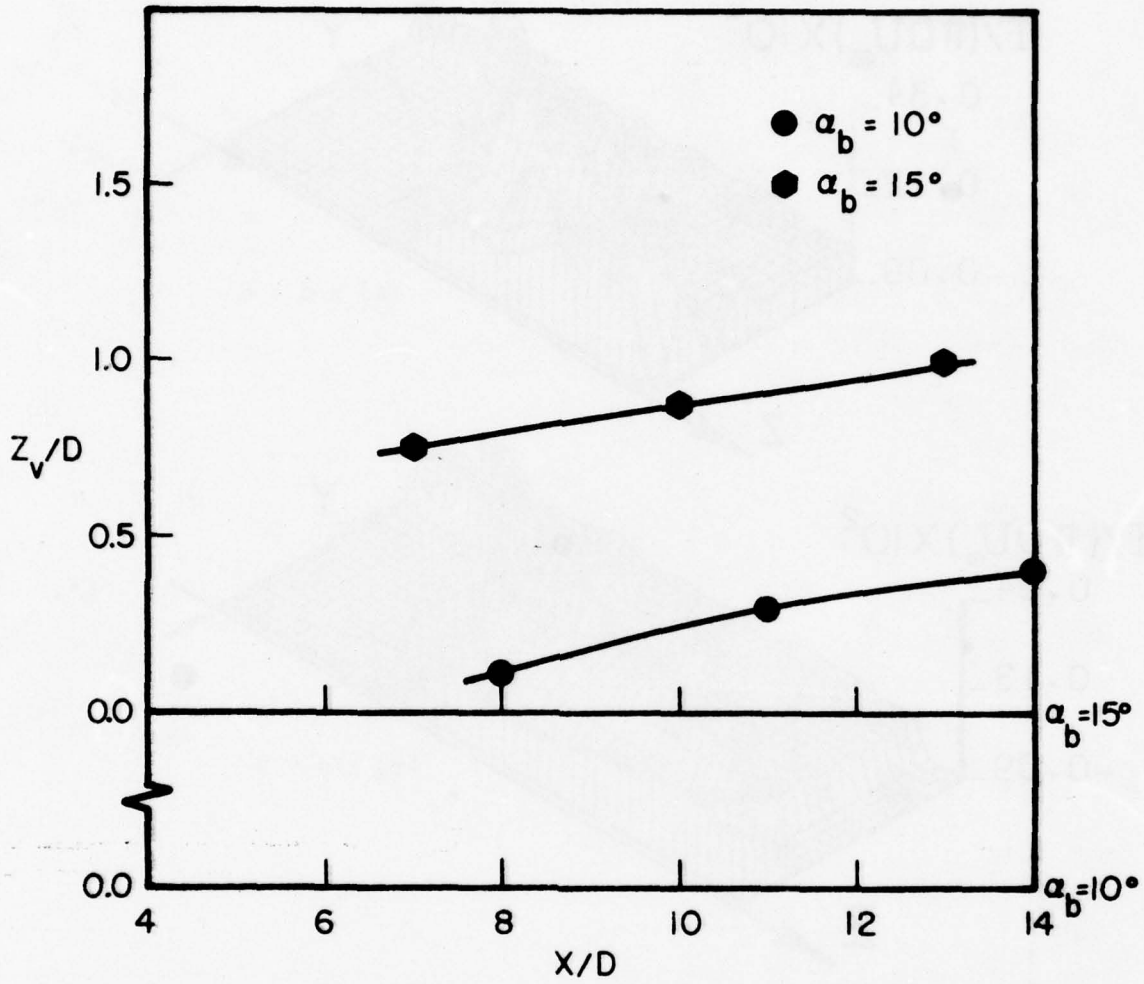
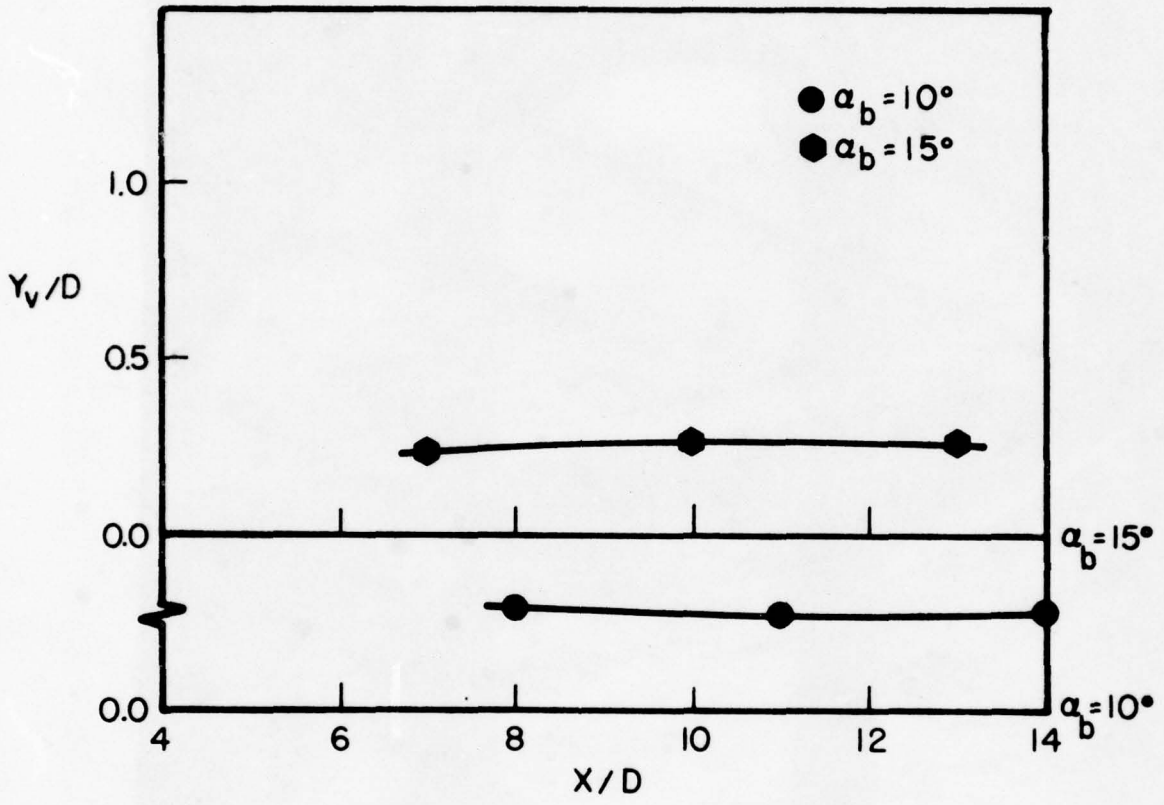


Figure 113. Local Circulation in Cross-Flow Plane for $M_\infty = 3.01$, $R_d = 1.70 \times 10^6$ and $\alpha_b = 25°$.



(a) z_v/d vs x/d

Figure 114. Vortex Center Location in the Cross-Flow Plane for M_∞ = 3.01 and R_d = 1.7 x 10^6



(b) y_v/d vs x/d

Figure 114. Vortex Center Location in the Cross-Flow Plane for $M_\infty = 3.01$ and $R_d = 1.7 \times 10^6$ (Concluded)



Figure 115. Schlieren Photograph for $M_\infty = 3.01$, $R_d = 1.7 \times 10^6$ and $\alpha_b = 10°$



Figure 116. Schlieren Photograph for M_∞ = 3.01, R_d = 1.7 x 10^6 and α_b = 15°



Figure 117. Schlieren Photograph for $M_\infty = 3.01$, $R_d = 1.7 \times 10^6$ and $\alpha_b = 20°$

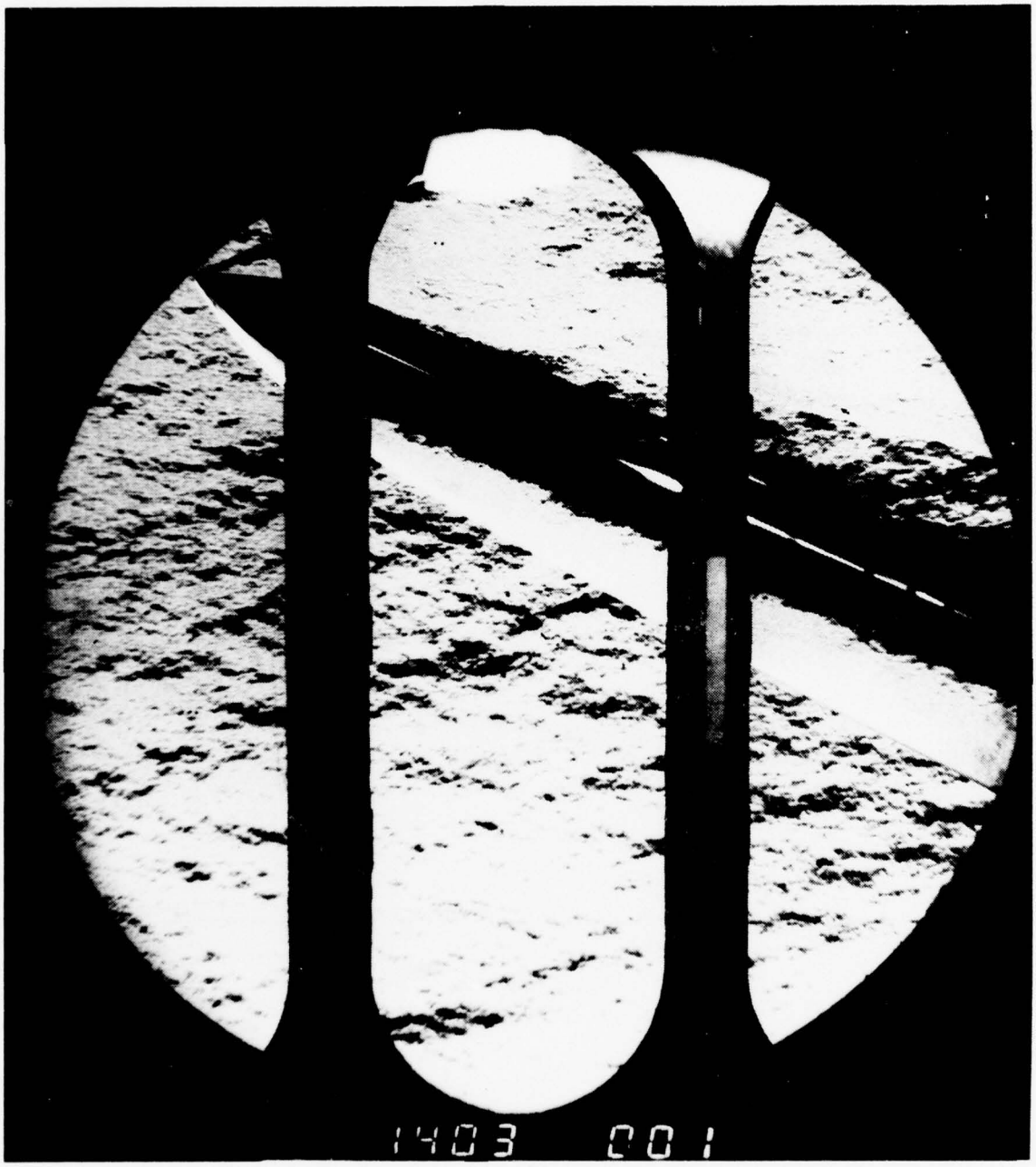


Figure 118. Schlieren Photograph for M_∞ = 3.01, R_d = 1.7 x 10^6 and α_b = 25°

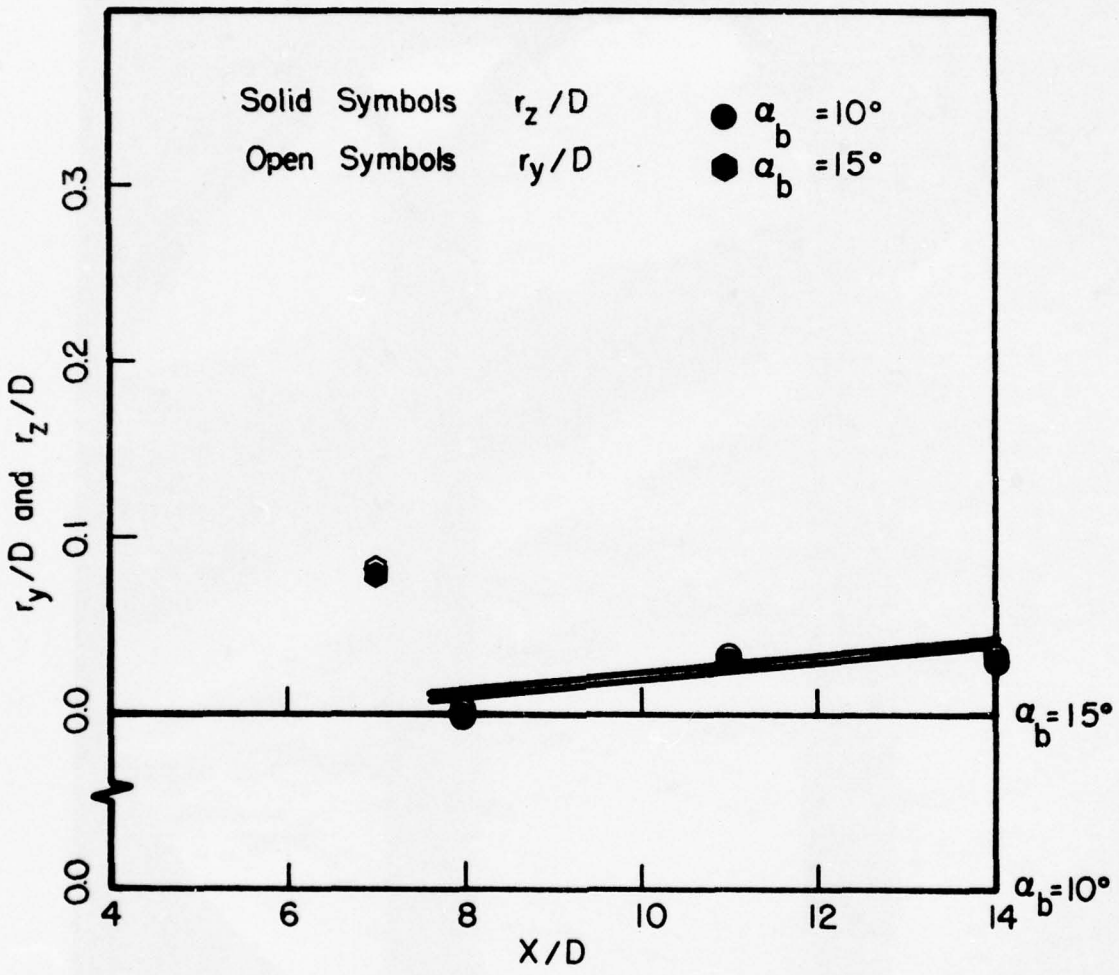


Figure 119. Vortex Core Radii for $M_\infty = 3.01$ and $R_d = 1.7 \times 10^6$

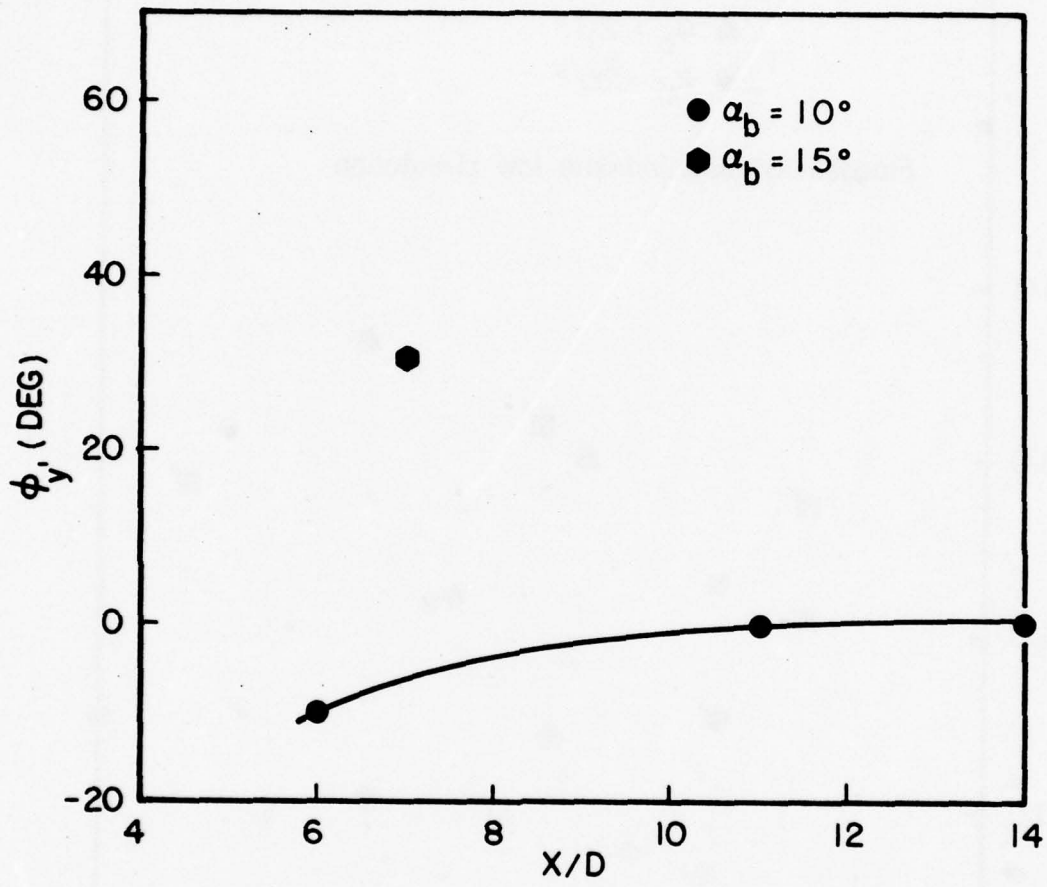


Figure 120. Angular Orientation of Vortex Core for M_∞ = 3.01 and R_d = 1.7 x 10^6

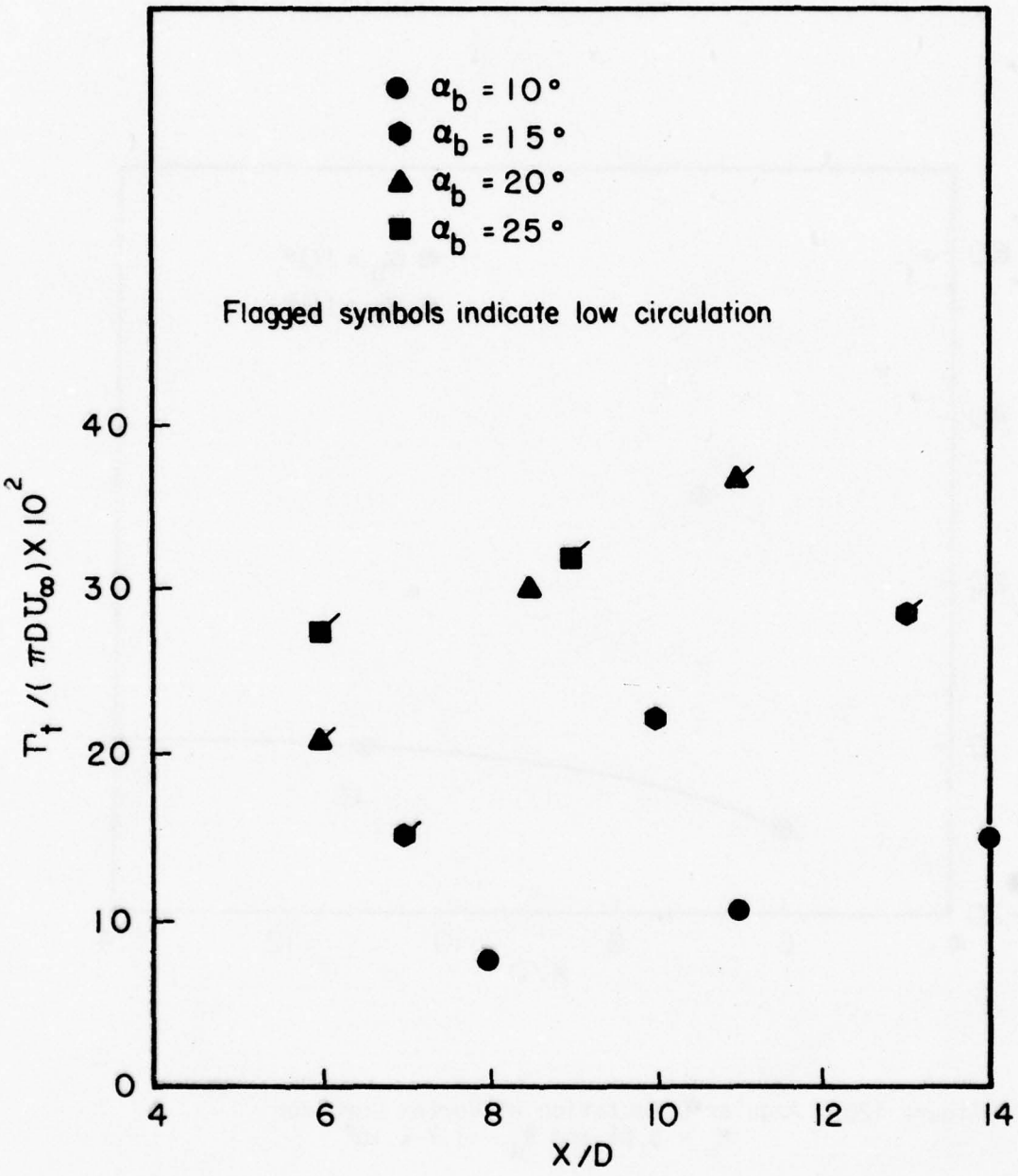


Figure 121. Total Circulation in the Survey Grids for $M_\infty = 3.01$ and $R_d = 1.7 \times 10^6$

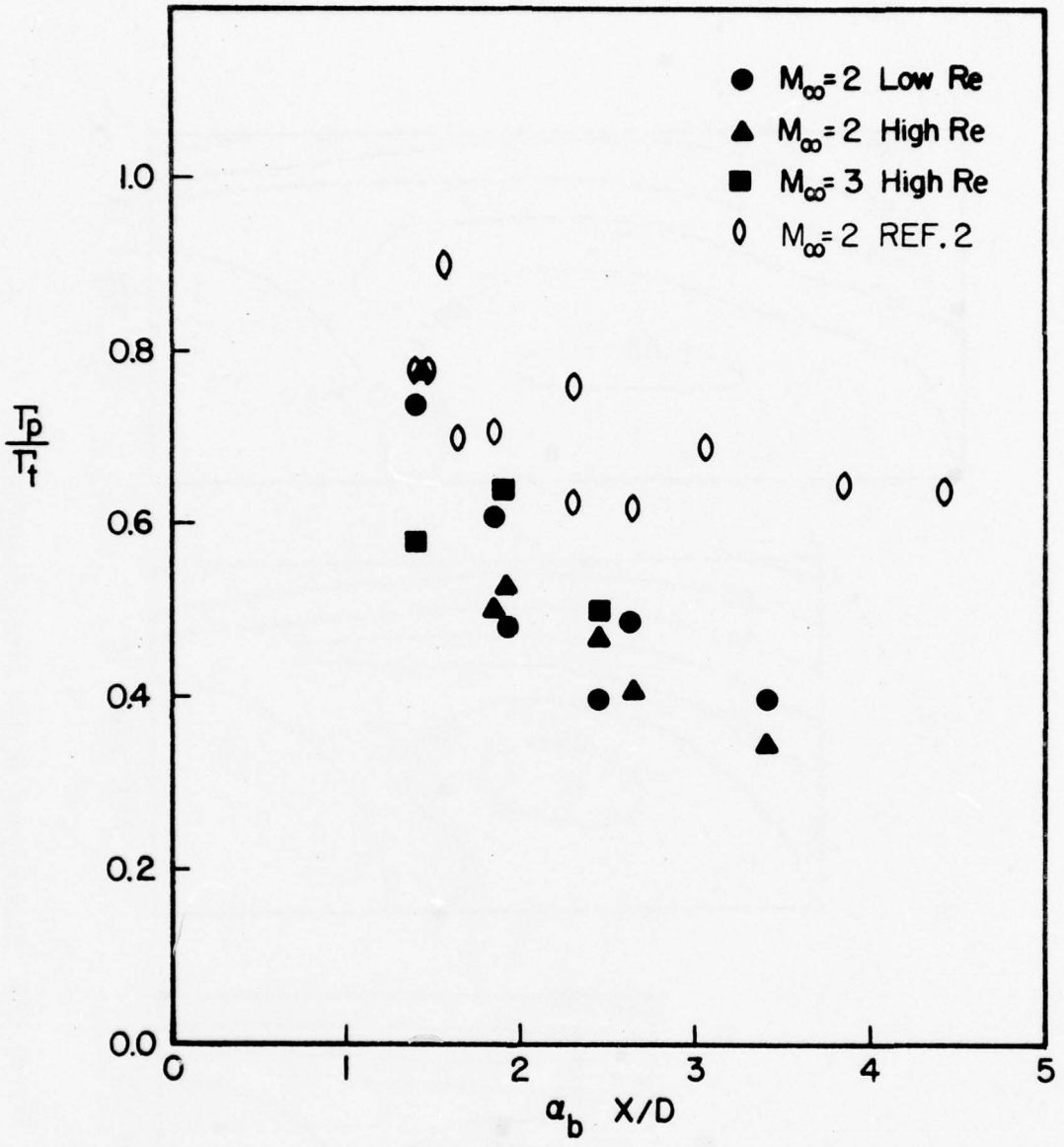


Figure 122. Ratio of Body Vortex Circulation to Total Circulation

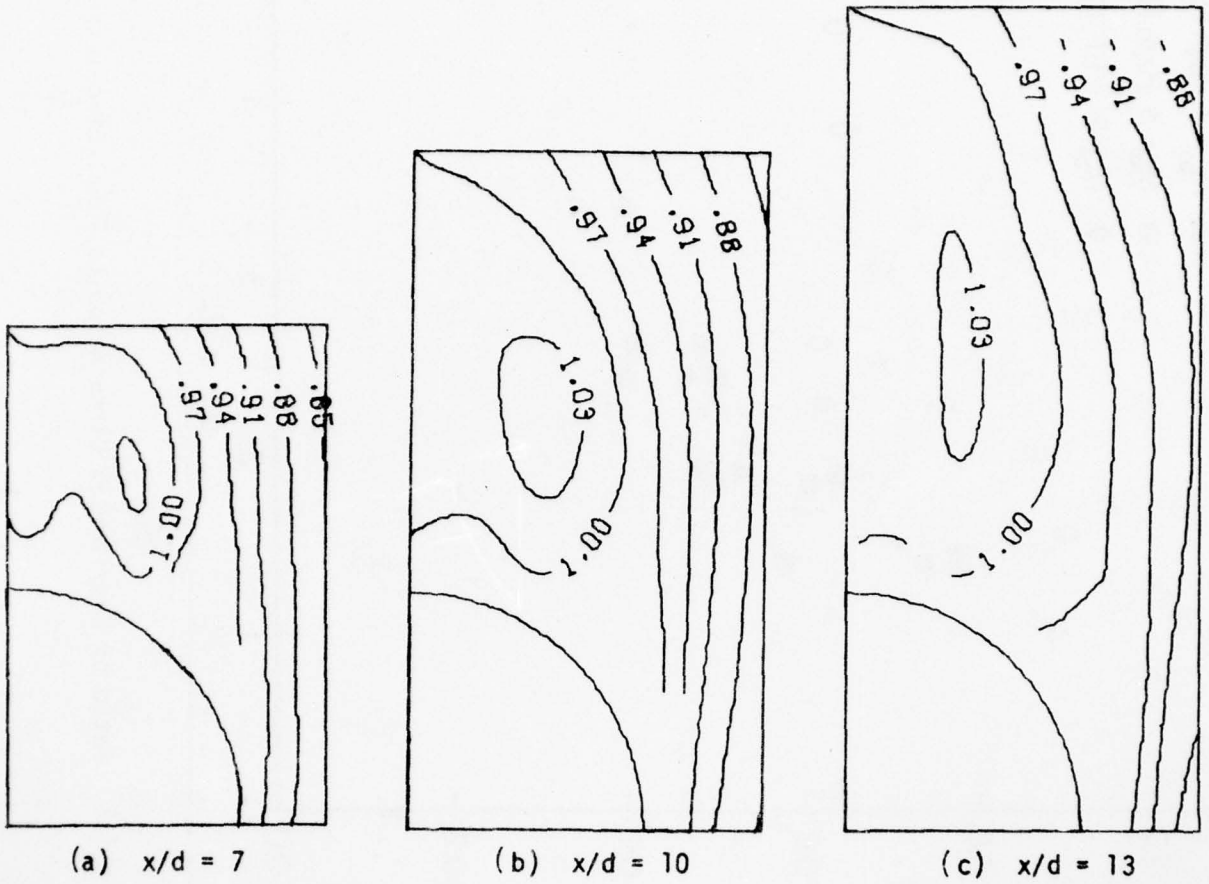


Figure 123. Streamlines in the Cross-Flow Plane for $M_\infty = 3.01$, $R_d = 1.7 \times 10^6$ and $\alpha_b = 15°$

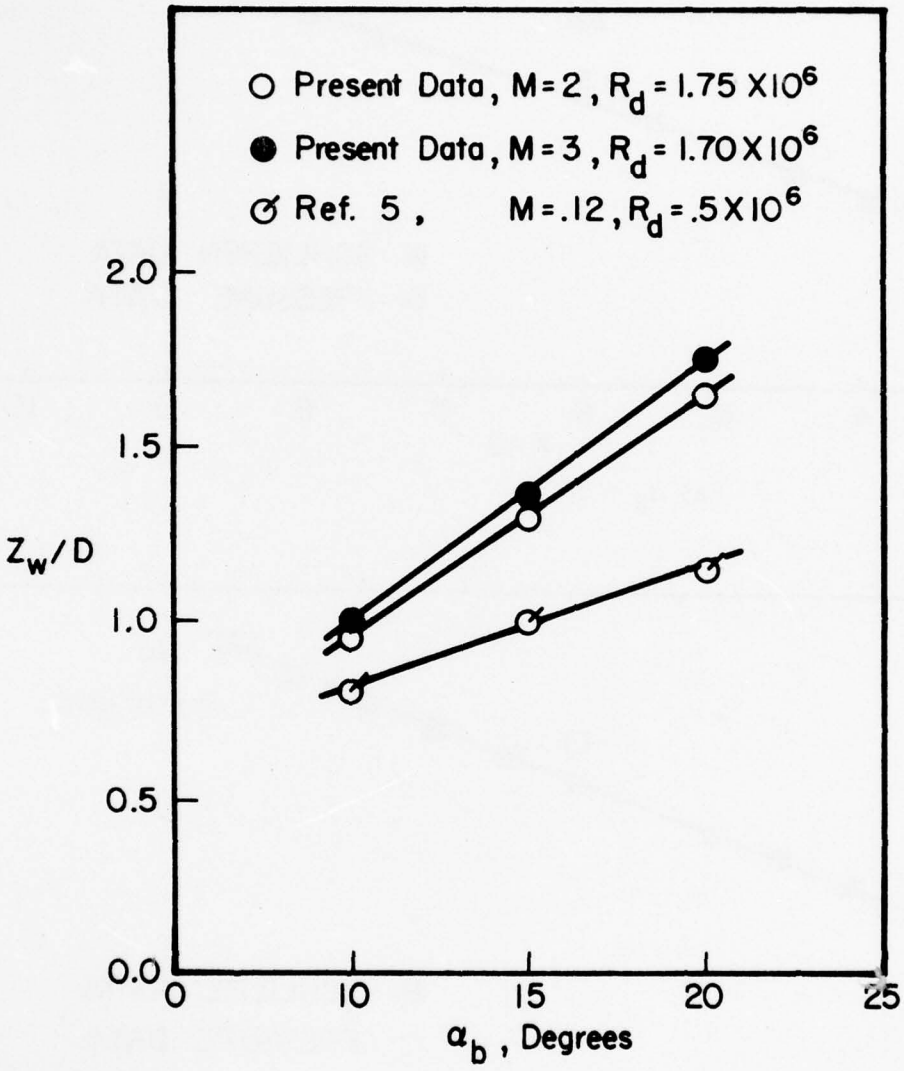
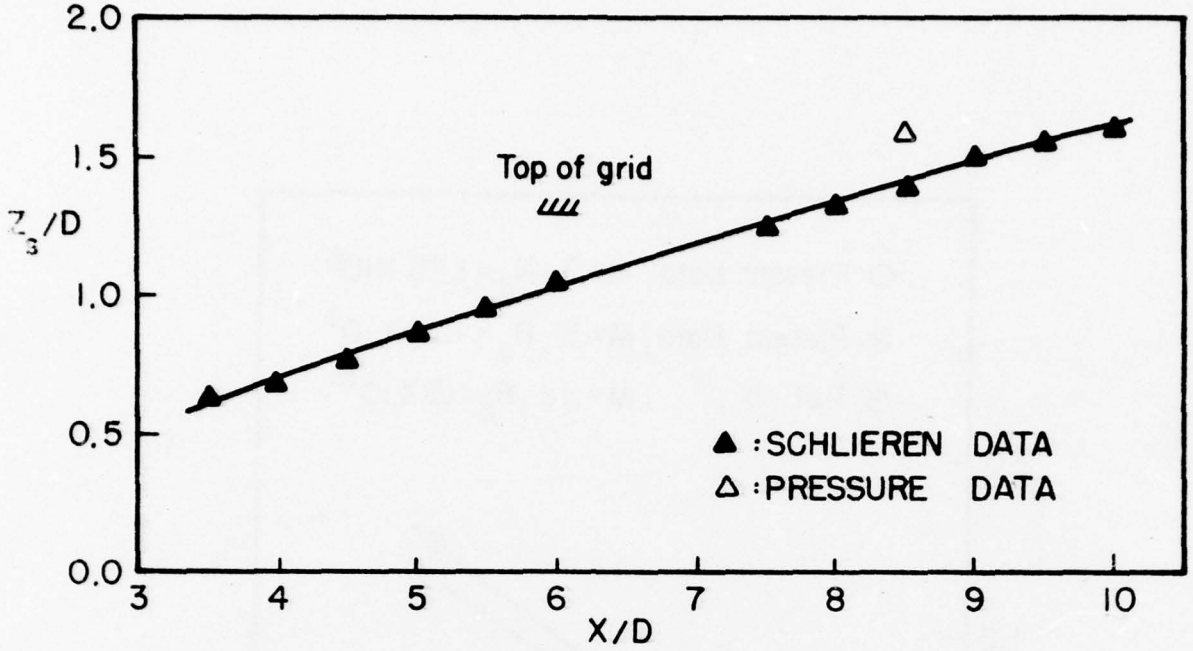
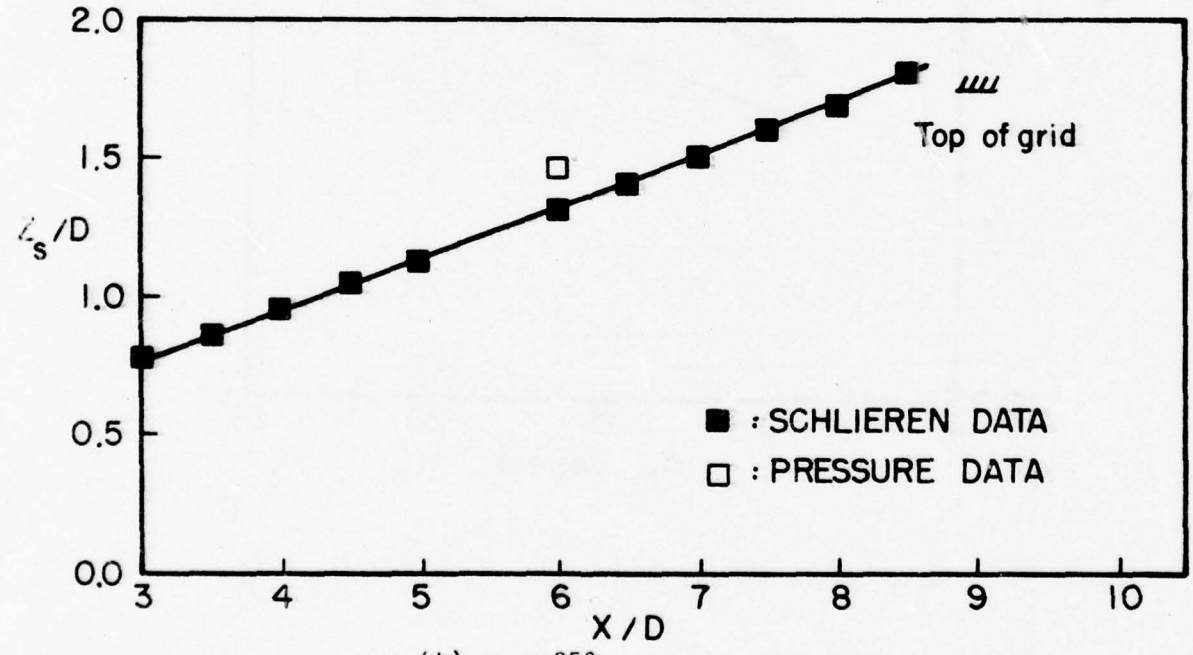


Figure 124. Wake Height in the Cross-Flow Plane for x/d = 10



(a) $\alpha_b = 20°$



(b) $\alpha_b = 25°$

Figure 125. z-Coordinate of Secondary Nose Vortex for $M_\infty = 3.01$ and $R_d = 1.7 \times 10^6$

APPENDIX A

TWO-DIMENSIONAL SURFACE CONSTRUCTION SOFTWARE

This appendix describes SPLPAK, a software package which was used for all the two dimension (2-D) surface fits for this investigation. This package contains routines for least squares fitting a multi-dimensional cubic spline to arbitrarily located data. It also contains routines for evaluating the function or its partial derivative at any point. This package was provided by the National Center for Atmospheric Research, Boulder, Colorado.

One of the exceptional features of this package is that the input data points can be arbitrarily located. That is, the present data were used at the actual y and z coordinates, not at the nominal grid location as is required by other numerical packages. SPLPAK was utilized only to generate 2-D surfaces. It is conceivable that 3-D surfaces could be constructed, but computer time and memory requirements become prohibitive with the quantity of present data.

The 2-D surface dimensions, required to be rectangular, were the cross-plane data grid. Thus, the surface contained data void regions, e.g., a quandrant of the body. Due to these regions, the fitting instead of the interpolation option was utilized with the spline nodes at the nominal data point locations. Many numerical experiments were performed on the parameters which controlled the extent of smoothing; the final values chosen such that the fitting effects were minimized. Therefore, the numerical surface is essentially interpolated from the final data. See Reference 21 for a complete discussion.

The numerically generated surface was represented as a basis function value at each nodal point. Function values and partial derivatives could be

obtained at any point on the surface by evaluating these functions. The partial derivative feature allowed cubic polynomial integration schemes to be utilized in circulation and stream line calculations. Approximately 300 seconds on a CDC 6600 were required to generate surfaces for v and w velocities for a medium sized grid. The function or derivative evaluation time was negligible. As there were 33 survey grids, roughly three hours of computer time were required for the v and w surface generations. An equivalent amount of computer time was needed for all of the circulation, Γ, surfaces.

APPENDIX B

TABULATED FINAL DATA SET

TABLE B-1. FINAL DATA SET FOR $M_\infty = 1.95$, $R_d = .48 \times 10^6$, $\alpha_b = 10°$, $x/d = 8$

M2M2G1

P -- PO/POINF M -- MACH NUMBER U,V,W -- 3-D VELOCITY COMPONENTS/UINF

		1	2	3	4	5	6	7	8	9	10
P	13	0.9425	0.9220	0.9303	0.9308	0.9390	0.9423	0.9445	0.9316	0.9472	0.9513
M		1.8716	1.8604	1.8705	1.8774	1.8891	1.9003	1.9103	1.9028	1.9158	1.9220
U		0.9791	0.9781	0.9712	0.9702	0.9703	0.9709	0.9711	0.9680	0.9715	0.9734
V		-0.0198	-0.0455	-0.0645	-0.0776	-0.0801	-0.0736	-0.0718	-0.0628	-0.0545	-0.0454
W		0.0496	0.0612	0.0754	0.0997	0.1272	0.1510	0.1688	0.1767	0.1823	0.1847
P	12	0.9325	0.9297	0.9230	0.9113	0.9227	0.9333	0.9450	0.9512	0.9433	0.9341
M		1.8689	1.8729	1.8742	1.8743	1.8888	1.9009	1.9167	1.9198	1.9140	1.9141
U		0.9750	0.9748	0.9723	0.9677	0.9673	0.9672	0.9694	0.9702	0.9687	0.9642
V		-0.0224	-0.0569	-0.0885	-0.1104	-0.1092	-0.0918	-0.0814	-0.0660	-0.0567	-0.0452
W		0.0214	0.0302	0.0458	0.0820	0.1276	0.1649	0.1847	0.1914	0.1932	0.1940
P	11	0.9163	0.9286	0.8677	0.8035	0.8553	0.9376	0.9516	0.9606	0.9479	0.9618
M		1.8627	1.8835	1.8561	1.8250	1.8688	1.9250	1.9318	1.9301	1.9190	1.9270
U		0.9735	0.9788	0.9654	0.9486	0.9549	0.9685	0.9685	0.9697	0.9674	0.9710
V		-0.0229	-0.0646	-0.1110	-0.1497	-0.1441	-0.1107	-0.0862	-0.0657	-0.0548	-0.0428
W		-0.0071	-0.0103	-0.0064	0.0561	0.1389	0.1873	0.2094	0.2091	0.2075	0.2046
P	10	0.9171	0.9004	0.6001	0.5484	0.6429	0.8498	0.9322	0.9430	0.9577	0.9560
M		1.8677	1.8660	1.6450	1.6186	1.7262	1.8962	1.9338	1.9274	1.9291	1.9220
U		0.9748	0.9727	0.8960	0.8790	0.9035	0.9519	0.9631	0.9654	0.9677	0.9675
V		-0.0187	-0.0415	-0.0771	-0.1512	-0.1536	-0.1202	-0.0822	-0.0617	-0.0502	-0.0379
W		-0.0259	-0.0484	-0.0640	0.0286	0.1568	0.2185	0.2376	0.2264	0.2208	0.2146
P	9	0.9190	0.9253	0.5744	0.4285	0.5276	0.6968	0.9233	0.9433	0.9316	0.9474
M		1.8698	1.9049	1.6474	1.4921	1.6304	1.7823	1.9346	1.9347	1.9167	1.9189
U		0.9755	0.9843	0.8955	0.8444	0.8764	0.9149	0.9604	0.9649	0.9622	0.9651
V		-0.0088	0.0154	0.0681	0.0123	-0.0636	-0.0840	-0.0830	-0.0499	-0.0433	-0.0330
W		-0.0294	-0.0668	-0.0885	-0.0107	0.1769	0.2350	0.2544	0.2400	0.2295	0.2221
P	8				0.6222	0.5823	0.5474	0.8885	0.9471	0.9568	0.9546
M					1.7097	1.6554	1.6455	1.9080	1.9379	1.9364	1.9274
U					0.9121	0.8950	0.8749	0.9542	0.9654	0.9670	0.9666
V					0.1476	0.0813	-0.0104	-0.0441	-0.0376	-0.0337	-0.0276
W					0.0162	0.1096	0.1971	0.2508	0.2441	0.2364	0.2282
P	7						0.5191	0.8942	0.9552	0.9485	0.9615
M							1.5153	1.9108	1.9446	1.9336	1.9367
U							0.8477	0.9582	0.9672	0.9654	0.9682
V							0.0110	-0.0421	-0.0284	-0.0262	-0.0212
W							0.0994	0.2387	0.2460	0.2399	0.2332
P	6							0.8372	0.9524	0.9533	0.9583
M								1.8717	1.9454	1.9387	1.9375
U								0.9476	0.9670	0.9663	0.9675
V								-0.0508	-0.0245	-0.0195	-0.0159
W								0.2305	0.2483	0.2433	0.2375
P	5								0.9642	0.9642	0.9664
M									1.9547	1.9484	1.9465
U									0.9687	0.9681	0.9692
V									-0.0194	-0.0140	-0.0097
W									0.2529	0.2481	0.2418
P	4								0.9300	0.9574	0.9639
M									1.9377	1.9523	1.9486
U									0.9619	0.9677	0.9689
V									-0.0151	-0.0063	-0.0029
W									0.2593	0.2548	0.2458
P	3									0.9544	0.9501
M										1.9586	1.9430
U										0.9677	0.9660
V										-0.0002	0.0056
W										0.2620	0.2506
P	2									0.9468	0.9481
M										1.9577	1.9435
U										0.9652	0.9651
V										0.0143	0.0173
W										0.2694	0.2539
P	1									0.9328	0.9479
M										1.9510	1.9406
U										0.9620	0.9742
V										0.0240	0.0244
W										0.2727	0.2608

TABLE B-2. FINAL DATA SET FOR $M_\infty = 1.95$, $R_d = .48 \times 10^6$, $\alpha_b = 10°$, $x/d = 11$

M2R262

P -- P0/P0INF M -- MACH NUMBER U,V,W -- 3-D VELOCITY COMPONENTS/U1NF

		1	2	3	4	5	6	7	8	9	10
P	18	0.9352	0.9409	0.9393	0.9371	0.9381	0.9334	0.9583	0.9617	0.9583	0.9556
M		1.8793	1.8775	1.8747	1.8726	1.8746	1.8758	1.8876	1.8934	1.8918	1.8898
U		0.9725	0.9730	0.9708	0.9682	0.9674	0.9659	0.9677	0.9682	0.9670	0.9656
V		-0.0069	-0.0185	-0.0370	-0.0434	-0.0475	-0.0515	-0.0457	-0.0428	-0.0421	-0.0386
W		0.0940	0.1009	0.1083	0.1224	0.1317	0.1434	0.1571	0.1654	0.1700	0.1753
P	17	0.9422	0.9342	0.9368	0.9370	0.9434	0.9451	0.9467	0.9506	0.9559	0.9618
M		1.8784	1.8698	1.8711	1.8745	1.8809	1.8899	1.8853	1.8902	1.8945	1.8985
U		0.9747	0.9718	0.9701	0.9685	0.9685	0.9688	0.9656	0.9661	0.9667	0.9671
V		-0.0185	-0.0275	-0.0500	-0.0565	-0.0562	-0.0622	-0.0547	-0.0493	-0.0478	-0.0423
W		0.0764	0.0861	0.0991	0.1194	0.1337	0.1485	0.1630	0.1702	0.1749	0.1805
P	16	0.9228	0.9434	0.9425	0.9430	0.9335	0.9543	0.9580	0.9502	0.9498	0.9478
M		1.8582	1.8743	1.8779	1.8831	1.8793	1.9008	1.9009	1.8974	1.8961	1.8934
U		0.9708	0.9744	0.9723	0.9701	0.9663	0.9700	0.9681	0.9663	0.9654	0.9644
V		-0.0174	-0.0347	-0.0678	-0.0769	-0.0775	-0.0770	-0.0634	-0.0563	-0.0519	-0.0460
W		0.0542	0.0650	0.0869	0.1160	0.1365	0.1560	0.1727	0.1791	0.1834	0.1859
P	15	0.9242	0.9211	0.9257	0.9324	0.9380	0.9454	0.9403	0.9552	0.9607	0.9612
M		1.8580	1.8573	1.8717	1.8846	1.8906	1.9008	1.8950	1.9085	1.9117	1.9087
U		0.9718	0.9698	0.9696	0.9683	0.9667	0.9662	0.9630	0.9670	0.9676	0.9670
V		-0.0239	-0.0565	-0.0946	-0.1044	-0.1002	-0.0929	-0.0733	-0.0618	-0.0551	-0.0468
W		0.0253	0.0376	0.0677	0.1136	0.1431	0.1698	0.1866	0.1919	0.1953	0.1962
P	14	0.9306	0.9240	0.8476	0.8501	0.8955	0.9420	0.9497	0.9547	0.9676	0.9574
M		1.8672	1.8668	1.8334	1.8436	1.8805	1.9116	1.9098	1.9132	1.9213	1.9078
U		0.9746	0.9723	0.9559	0.9520	0.9583	0.9640	0.9635	0.9652	0.9682	0.9643
V		-0.0311	-0.0732	-0.1250	-0.1357	-0.1278	-0.1088	-0.0788	-0.0650	-0.0551	-0.0469
W		-0.0184	-0.0024	0.0343	0.1101	0.1559	0.1907	0.2045	0.2064	0.2067	0.2078
P	13	0.9249	0.8731	0.6742	0.6977	0.7592	0.8556	0.9328	0.9524	0.9574	0.9573
M		1.8789	1.8577	1.7110	1.7388	1.7970	1.8675	1.9070	1.9156	1.9080	1.8933
U		0.9764	0.9571	0.9150	0.9156	0.9277	0.9448	0.9576	0.9626	0.9608	0.9567
V		-0.0335	-0.0790	-0.1330	-0.1411	-0.1328	-0.1148	-0.0797	-0.0625	-0.0558	-0.0474
W		-0.0602	-0.0622	0.0060	0.1185	0.1733	0.2133	0.2267	0.2221	0.2216	0.2215
P	12	0.9301	0.7705	0.5831	0.6275	0.6889	0.7383	0.9383	0.9518	0.9448	0.9749
M		1.9066	1.8057	1.6630	1.7176	1.7620	1.7842	1.9193	1.9078	1.8890	1.9068
U		0.9815	0.9460	0.9011	0.9077	0.9131	0.9163	0.9575	0.9562	0.9523	0.9598
V		-0.0214	-0.0473	-0.1059	-0.1257	-0.1066	-0.0897	-0.0711	-0.0586	-0.0526	-0.0438
W		-0.1037	-0.1128	-0.0351	0.1392	0.2042	0.2297	0.2454	0.2398	0.2333	0.2268
P	11	0.9134	0.7204	0.5372	0.4846	0.6265	0.6967	0.8767	0.9365	0.9587	0.9496
M		1.9168	1.7835	1.6278	1.5741	1.7184	1.7415	1.8764	1.8868	1.8984	1.8892
U		0.9822	0.9387	0.8913	0.8691	0.9010	0.9058	0.9430	0.9475	0.9538	0.9535
V		0.0012	0.0098	0.0063	-0.0316	-0.0512	-0.0367	-0.0545	-0.0471	-0.0434	-0.0367
W		-0.1261	-0.1370	-0.0859	0.1034	0.2124	0.2283	0.2536	0.2505	0.2409	0.2318
P	10	0.9112	0.7793	0.6015	0.5479	0.6679	0.6888	0.8277	0.9413	0.9515	0.9515
M		1.9076	1.8270	1.6840	1.6187	1.7293	1.7133	1.8139	1.8862	1.8934	1.8946
U		0.9814	0.9537	0.9079	0.8829	0.9123	0.9048	0.9250	0.9479	0.9523	0.9548
V		0.0217	0.0663	0.1056	0.0964	0.0429	0.0110	-0.0346	-0.0322	-0.0339	-0.0312
W		-0.1070	-0.1135	-0.0490	0.0852	0.1796	0.1936	0.2489	0.2506	0.2420	0.2341
P	9	0.9133	0.8732	0.7765	0.7361	0.7986	0.6416	0.8573	0.9509	0.9656	0.9645
M		1.8961	1.8801	1.8169	1.7747	1.8109	1.6232	1.8226	1.8855	1.9009	1.9056
U		0.9812	0.9735	0.9508	0.9347	0.9463	0.8824	0.9315	0.9489	0.9551	0.9583
V		0.0358	0.0826	0.1278	0.1274	0.0830	0.0244	-0.0247	-0.0205	-0.0262	-0.0260
W		-0.0647	-0.0644	-0.0148	0.0692	0.1205	0.1406	0.2359	0.2473	0.2415	0.2343
P	8				0.8659	0.7111	0.5468	0.8878	0.9557	0.9365	0.9564
M					1.8514	1.7034	1.4901	1.8490	1.8919	1.8754	1.9003
U					0.9646	0.9187	0.8342	0.9428	0.9528	0.9474	0.9567
V					0.0974	0.0653	0.0019	-0.0260	-0.0185	-0.0205	-0.0220
W					0.0395	0.0435	0.0874	0.2246	0.2401	0.2406	0.2346
P	7						0.4536	0.8958	0.9594	0.9627	0.9487
M							1.3434	1.8602	1.9021	1.9025	1.8918
U							0.7802	0.9459	0.9564	0.9565	0.9538
V							-0.0278	-0.0333	-0.0194	-0.0187	-0.0168
W							0.0672	0.2259	0.2382	0.2383	0.2361
P	6							0.8920	0.9629	0.9675	0.9535
M								1.8632	1.9087	1.9138	1.9000
U								0.9451	0.9577	0.9594	0.9560
V								-0.0371	-0.0197	-0.0178	-0.0133
W								0.2324	0.2412	0.2411	0.2375
P	5								0.9566	0.9716	0.9554
M									1.9118	1.9216	1.9081
U									0.9575	0.9607	0.9579
V									-0.0206	-0.0155	-0.0090
W									0.2457	0.2455	0.2405
P	4								0.9584	0.9517	0.9509
M									1.9231	1.9139	1.9070
U									0.9585	0.9569	0.9566
V									-0.0201	-0.0131	-0.0033
W									0.2552	0.2511	0.2441
P	3									0.9695	0.9662
M										1.9358	1.9239
U										0.9610	0.9604
V										-0.0056	0.0034
W										0.2610	0.2495
P	2									0.9601	0.9726
M										1.9381	1.9352
U										0.9594	0.9626
V										0.0056	0.0135
W										0.2696	0.2540
P	1									0.9549	0.9660
M										1.9396	1.9334
U										0.9586	0.9617
V										0.0219	0.0263
W										0.2732	0.2544

TABLE B-3. FINAL DATA SET FOR M_∞ = 1.95, R_d = .48 x 10^6, α_b = 10°, x/d = 14

428263

P -- P0/P0INF M -- MACH NUMBER U,V,W -- 3-D VELOCITY COMPONENTS/U1NF

		1	2	3	4	5	6	7	8	9	10	11
P	21	0.9113	0.9330	0.9305	0.9355	0.9418	0.9485	0.9543	0.9565	0.9760	0.9541	0.9628
M		1.8653	1.8657	1.8644	1.8764	1.8813	1.8979	1.9010	1.8983	1.9133	1.9014	1.9082
U		0.9697	0.9687	0.9673	0.9694	0.9698	0.9728	0.9725	0.9708	0.9748	0.9706	0.9723
V		0.0066	-0.0123	-0.0253	-0.0429	-0.0468	-0.0506	-0.0465	-0.0407	-0.0384	-0.0353	-0.0300
W		0.0978	0.1079	0.1145	0.1218	0.1299	0.1428	0.1525	0.1594	0.1637	0.1676	0.1709
P	20	0.9181	0.9396	0.9428	0.9382	0.9495	0.9617	0.9529	0.9578	0.9501	0.9691	0.9576
M		1.8558	1.8623	1.8677	1.8816	1.8897	1.9100	1.9035	1.9035	1.8978	1.9109	1.9033
U		0.9678	0.9689	0.9693	0.9711	0.9719	0.9759	0.9725	0.9718	0.9696	0.9727	0.9701
V		-0.0045	-0.0200	-0.0330	-0.0535	-0.0571	-0.0593	-0.0547	-0.0470	-0.0449	-0.0383	-0.0323
W		0.0871	0.0946	0.1036	0.1170	0.1291	0.1438	0.1545	0.1617	0.1650	0.1714	0.1747
P	19	0.9340	0.9425	0.9266	0.9560	0.9555	0.9782	0.9651	0.9610	0.9470	0.9548	0.9603
M		1.8593	1.8640	1.8551	1.8988	1.9025	1.9267	1.9156	1.9096	1.9006	1.9063	1.9067
U		0.9703	0.9708	0.9662	0.9760	0.9748	0.9796	0.9751	0.9727	0.9695	0.9708	0.9706
V		-0.0181	-0.0305	-0.0471	-0.0685	-0.0713	-0.0705	-0.0617	-0.0529	-0.0509	-0.0427	-0.0348
W		0.0681	0.0754	0.0897	0.1124	0.1292	0.1478	0.1590	0.1656	0.1687	0.1731	0.1768
P	18	0.9327	0.9291	0.9238	0.9182	0.9269	0.9420	0.9615	0.9684	0.9637	0.9551	0.9693
M		1.8588	1.8583	1.8582	1.8799	1.8926	1.9163	1.9178	1.9200	1.9165	1.9102	1.9179
U		0.9717	0.9702	0.9677	0.9691	0.9699	0.9724	0.9738	0.9743	0.9731	0.9710	0.9733
V		-0.0184	-0.0455	-0.0670	-0.0875	-0.0879	-0.0827	-0.0689	-0.0584	-0.0537	-0.0453	-0.0369
W		0.0382	0.0473	0.0689	0.1090	0.1336	0.1562	0.1675	0.1723	0.1746	0.1780	0.1806
P	17	0.9326	0.9284	0.8465	0.8372	0.8772	0.9407	0.9737	0.9719	0.9687	0.9667	0.9614
M		1.8640	1.8678	1.8127	1.8264	1.8698	1.9180	1.9342	1.9278	1.9251	1.9215	1.9157
U		0.9740	0.9737	0.9536	0.9517	0.9611	0.9720	0.9765	0.9749	0.9741	0.9734	0.9720
V		-0.0219	-0.0568	-0.0808	-0.0954	-0.0993	-0.0905	-0.0729	-0.0613	-0.0571	-0.0467	-0.0374
W		0.0018	0.0121	0.0459	0.1076	0.1380	0.1681	0.1784	0.1815	0.1823	0.1833	0.1835
P	16	0.9416	0.8561	0.7648	0.7614	0.8189	0.9021	0.9526	0.9568	0.9542	0.9636	0.9658
M		1.8810	1.8255	1.7535	1.7719	1.8328	1.9016	1.9275	1.9250	1.9202	1.9228	1.9217
U		0.9784	0.9602	0.9349	0.9335	0.9483	0.9644	0.9716	0.9719	0.9711	0.9727	0.9729
V		-0.0242	-0.0564	-0.0788	-0.0957	-0.0997	-0.0939	-0.0755	-0.0618	-0.0566	-0.0458	-0.0370
W		-0.0384	-0.0251	0.0357	0.1110	0.1451	0.1809	0.1929	0.1925	0.1905	0.1895	0.1883
P	15	0.9136	0.7640	0.7159	0.7291	0.7639	0.8427	0.9532	0.9659	0.9538	0.9580	0.9642
M		1.8640	1.7657	1.7238	1.7572	1.7983	1.8673	1.9368	1.9362	1.9254	1.9168	1.9227
U		0.9762	0.9393	0.9247	0.9271	0.9347	0.9514	0.9718	0.9731	0.9708	0.9698	0.9725
V		-0.0253	-0.0567	-0.0869	-0.1011	-0.0985	-0.0914	-0.0730	-0.0587	-0.0532	-0.0435	-0.0360
W		-0.0867	-0.0596	0.0188	0.1182	0.1605	0.1935	0.2064	0.2041	0.2008	0.1956	0.1921
P	14	0.9183	0.7041	0.6703	0.6733	0.7166	0.7911	0.9334	0.9685	0.9486	0.9517	0.9596
M		1.9181	1.7360	1.7187	1.7292	1.7689	1.8354	1.9374	1.9495	1.9254	1.9204	1.9220
U		0.9793	0.9261	0.9222	0.9194	0.9236	0.9412	0.9786	0.9752	0.9693	0.9699	0.9716
V		-0.0173	-0.0564	-0.0950	-0.1085	-0.0892	-0.0799	-0.0681	-0.0571	-0.0475	-0.0384	-0.0327
W		-0.1313	-0.0991	-0.0173	0.0962	0.1734	0.1962	0.2145	0.2132	0.2092	0.2013	0.1964
P	13	0.8919	0.6919	0.5613	0.5683	0.7187	0.7616	0.8993	0.9614	0.9606	0.9493	0.9565
M		1.9191	1.7627	1.6516	1.6586	1.7992	1.8177	1.9187	1.9495	1.9366	1.9204	1.9212
U		0.9769	0.9296	0.8994	0.8953	0.9308	0.9341	0.9634	0.9737	0.9717	0.9691	0.9707
V		-0.0035	-0.0244	-0.0711	-0.0850	-0.0671	-0.0576	-0.0558	-0.0471	-0.0378	-0.0325	-0.0279
W		-0.1656	-0.1500	-0.0565	0.1134	0.1973	0.2126	0.2245	0.2224	0.2157	0.2061	0.2005
P	12	0.8792	0.6787	0.5276	0.5547	0.7048	0.7286	0.9054	0.9603	0.9730	0.9651	0.9761
M		1.9246	1.7694	1.6367	1.6609	1.7930	1.7862	1.9266	1.9501	1.9448	1.9326	1.9373
U		0.9732	0.9301	0.8928	0.8980	0.9304	0.9259	0.9665	0.9734	0.9738	0.9725	0.9749
V		0.0159	0.0285	0.0445	0.0118	-0.0147	-0.0228	-0.0381	-0.0341	-0.0286	-0.0249	-0.0221
W		-0.1732	-0.1599	-0.0681	0.1285	0.2002	0.2093	0.2254	0.2268	0.2187	0.2086	0.2039
P	11	0.8799	0.7248	0.6041	0.5920	0.6989	0.7304	0.7707	0.9623	0.9651	0.9598	0.9755
M		1.9139	1.7984	1.6952	1.6771	1.7606	1.7782	1.8028	1.9506	1.9398	1.9306	1.9384
U		0.9780	0.9425	0.9119	0.9072	0.9264	0.9295	0.9338	0.9742	0.9727	0.9716	0.9758
V		0.0320	0.0735	0.1077	0.0902	0.0428	0.0108	-0.0173	-0.0233	-0.0213	-0.0189	-0.0179
W		-0.1456	-0.1247	-0.0408	0.0473	0.1596	0.1808	0.1991	0.2254	0.2176	0.2105	0.2058
P	10	0.8947	0.8060	0.7133	0.7100	0.7954	0.6999	0.7341	0.9571	0.9781	0.9606	0.9793
M		1.8935	1.8477	1.7783	1.7696	1.8258	1.7329	1.7582	1.9429	1.9426	1.9302	1.9415
U		0.9772	0.9618	0.9395	0.9374	0.9537	0.9218	0.9232	0.9729	0.9739	0.9716	0.9757
V		0.0442	0.0875	0.1178	0.1093	0.0696	0.0266	-0.0129	-0.0156	-0.0156	-0.0144	-0.0136
W		-0.0947	-0.0810	-0.0191	0.0303	0.1078	0.1352	0.1788	0.2216	0.2165	0.2102	0.2071
P	9	0.9117	0.8878	0.8497	0.8607	0.8266	0.6430	0.6816	0.9646	0.9513	0.9614	0.9516
M		1.8837	1.8853	1.8743	1.8816	1.8406	1.6619	1.6974	1.9440	1.9276	1.9313	1.9225
U		0.9778	0.9763	0.9717	0.9740	0.9629	0.9032	0.9065	0.9743	0.9699	0.9718	0.9699
V		0.0430	0.0833	0.1052	0.1027	0.0698	0.0259	-0.0193	-0.0116	-0.0129	-0.0107	-0.0102
W		-0.0537	-0.0424	-0.0095	0.0187	0.0535	0.0853	0.1555	0.2172	0.2144	0.2116	0.2075
P	8				0.9027	0.6938	0.5416	0.6175	0.9632	0.9587	0.9672	0.9672
M					1.9011	1.7137	1.5299	1.6188	1.9403	1.9332	1.9368	1.9343
U					0.9821	0.9238	0.8579	0.8810	0.9734	0.9715	0.9733	0.9733
V					0.0822	0.0557	0.0099	-0.0283	-0.0097	-0.0108	-0.0082	-0.0073
W					-0.0013	0.0007	0.0441	0.1383	0.2161	0.2152	0.2118	0.2085
P	7						0.4616	0.5264	0.9650	0.9768	0.9720	0.9729
M							1.4051	1.4943	1.9418	1.9457	1.9405	1.9388
U							0.8094	0.8359	0.9731	0.9751	0.9743	0.9744
V							0.0072	-0.0298	-0.0078	-0.0081	-0.0058	-0.0042
W							0.0133	0.1227	0.2194	0.2160	0.2126	0.2100
P	6							0.4461	0.9627	0.9618	0.9691	0.9785
M								1.3397	1.9372	1.9346	1.9384	1.9415
U								0.7737	0.9716	0.9715	0.9734	0.9750
V								-0.0232	-0.0045	-0.0060	-0.0033	-0.0012
W								0.1108	0.2203	0.2172	0.2137	0.2105
P	5								0.9695	0.9746	0.9523	0.9709
M									1.9420	1.9449	1.9285	1.9389
U									0.9729	0.9741	0.9701	0.9739
V									-0.0026	-0.0030	-0.0011	0.0014
W									0.2209	0.2193	0.2154	0.2122
P	4								0.9576	0.9461	0.9822	0.9632
M									1.9348	1.9272	1.9516	1.9338
U									0.9699	0.9683	0.9761	0.9719
V									-0.0013	-0.0018	0.0038	0.0053
W									0.2244	0.2217	0.2195	0.2143

TABLE B-3. FINAL DATA SET FOR $M_\infty = 1.95$, $R_d = .48 \times 10^6$, $\alpha_b = 10°$, x/d = 14 (CONCLUDED)

P	3		
N			
U			
V			
W			
		0.9671	0.9793	0.9674
		1.9503	1.9536	1.9404
		0.9734	0.9758	0.9733
		0.0010	0.0076	0.0103
		0.2295	0.2234	0.2170
P	2		
N			
U			
V			
W			
		0.9791	0.9708	0.9689
		1.9653	1.9502	1.9431
		0.9758	0.9739	0.9735
		0.0073	0.0139	0.0159
		0.2378	0.2269	0.2190
P	1		
N			
U			
V			
W			
		0.9578	0.9750	0.9782
		1.9581	1.9562	1.9499
		0.9720	0.9750	0.9754
		0.0183	0.0228	0.0237
		0.2444	0.2292	0.2191

TABLE B-4. FINAL DATA SET FOR $M_\infty = 1.95$, $R_d = .48 \times 10^6$, $\alpha_b = 15°$, x/d = 7

42R26A

P -- P0/P0INF M -- MACH NUMBER U,V,W -- 3-D VELOCITY COMPONENTS/U1NF

		1	2	3	4	5	6	7	8	9	10
P	15	0.9123	0.9092	0.9143	0.9285	0.9429	0.9498	0.9444	0.9474	0.9374	0.9550
M		1.8771	1.8767	1.8897	1.8820	1.9114	1.9290	1.9398	1.9490	1.9463	1.9622
U		0.9754	0.9741	0.9744	0.9655	0.9665	0.9657	0.9623	0.9595	0.9550	0.9571
V		-0.0087	-0.0379	-0.0809	-0.1197	-0.1450	-0.1527	-0.1558	-0.1415	-0.1297	-0.1143
W		0.0740	0.0803	0.0925	0.1160	0.1489	0.1783	0.2093	0.2424	0.2627	0.2794
P	14	0.8997	0.9191	0.9263	0.9268	0.9279	0.9472	0.9429	0.9429	0.9481	0.9419
M		1.8765	1.8911	1.9115	1.8959	1.9241	1.9545	1.9675	1.9692	1.9733	1.9688
U		0.9731	0.9803	0.9820	0.9688	0.9662	0.9674	0.9621	0.9564	0.9546	0.9518
V		-0.0184	-0.0465	-0.0983	-0.1494	-0.1823	-0.1891	-0.1902	-0.1669	-0.1478	-0.1258
W		0.0411	0.0460	0.0580	0.0859	0.1341	0.1760	0.2201	0.2617	0.2835	0.2986
P	13	0.9097	0.9101	0.9337	0.9114	0.9319	0.9342	0.9298	0.9286	0.9523	0.9467
M		1.9003	1.9019	1.9406	1.9228	1.9739	1.9941	2.0046	1.9957	2.0046	1.9934
U		0.9852	0.9843	0.9902	0.9723	0.9704	0.9655	0.9569	0.9495	0.9514	0.9490
V		-0.0120	-0.0533	-0.1184	-0.1924	-0.2442	-0.2480	-0.2359	-0.1955	-0.1650	-0.1357
W		0.0028	0.0050	0.0086	0.0409	0.1120	0.1783	0.2453	0.2945	0.3150	0.3257
P	12	0.9189	0.9143	0.9323	0.8891	0.8182	0.8791	0.8870	0.9383	0.9364	0.9317
M		1.9257	1.9323	1.9817	1.9936	2.0290	2.0815	2.0713	2.0603	2.0370	2.0096
U		0.9920	0.9926	0.9990	0.9794	0.9666	0.9655	0.9470	0.9452	0.9427	0.9409
V		-0.0104	-0.0522	-0.1288	-0.2491	-0.3270	-0.3281	-0.2932	-0.2223	-0.1770	-0.1373
W		-0.0390	-0.0417	-0.0625	-0.0474	0.0647	0.1866	0.2937	0.3465	0.3604	0.3698
P	11	0.9100	0.9172	0.9077	0.5572	0.4624	0.5513	0.6282	0.9056	0.9608	0.9483
M		1.9532	1.9673	2.0233	1.8481	1.8241	1.9464	1.9873	2.1317	2.1039	2.0522
U		0.9980	1.0006	1.0053	0.9413	0.9264	0.9330	0.9114	0.9369	0.9409	0.9396
V		-0.0070	-0.0358	-0.0893	-0.1750	-0.2544	-0.2949	-0.2908	-0.2345	-0.1746	-0.1284
W		-0.0760	-0.0868	-0.1532	-0.1511	0.0451	0.2012	0.3260	0.4116	0.4138	0.3989
P	10	0.9097	0.9188	0.9265	0.6779	0.4018	0.4128	0.4403	0.6746	0.9572	0.9384
M		1.9739	1.9956	2.0491	2.0004	1.8316	1.8762	1.8913	2.0508	2.1354	2.0619
U		1.0028	1.0069	1.0124	0.9837	0.9559	0.9510	0.9144	0.9058	0.9303	0.9310
V		0.0026	J0.0034	J0.0041	0.0086	J0.0963	J0.1966	J0.2194	J0.1911	J0.1419	J0.1024
W		-0.0914	-0.1128	-0.1632	-0.2478	-0.0909	0.1310	0.2857	0.4489	0.4675	0.4321
P	9	0.8920	0.9055	0.9257	0.7492	0.4251	0.3213	0.3480	0.6005	0.9609	0.9527
M		1.9695	2.0013	2.0629	2.0822	1.8679	1.8060	1.8381	1.9662	2.1381	2.0674
U		1.0025	1.0082	1.0155	0.9920	0.9387	0.9520	0.9263	0.9027	0.9326	0.9287
V		0.0152	0.0425	0.0803	0.1707	0.1898	0.0757	-0.0565	-0.0797	-0.0935	-0.0615
W		-0.0780	-0.1067	-0.1633	-0.2487	-0.1853	-0.0431	0.2688	0.4336	0.4766	0.4483
P	8				0.9238	0.7929	0.4040	0.3963	0.5835	0.9096	0.9602
M					2.1925	2.2099	1.8737	1.8020	1.9273	2.0551	2.0425
U					1.0173	0.9988	0.9073	0.9077	0.9219	0.9263	0.9276
V					0.2444	0.3358	0.3543	0.2417	0.0535	-0.0346	-0.0172
W					-0.2001	-0.1830	-0.0794	0.1707	0.3660	0.4481	0.4384
P	7						0.8555	0.7979	0.6869	0.9135	0.9570
M							2.1613	2.0798	1.8831	1.9978	2.0046
U							0.9886	0.9755	0.9425	0.9298	0.9286
V							0.3703	0.3457	0.1858	0.0021	0.0133
W							-0.0609	0.0518	0.1895	0.4038	0.4112
P	6							0.4604	0.6421	0.9271	0.9514
M								1.6843	1.7797	1.9048	1.9756
U								0.9049	0.9431	0.9308	0.9297
V								0.0945	0.0805	0.0101	0.0248
W								-0.1010	0.0419	0.3769	0.3871
P	5								0.5100	0.9038	0.9432
M									1.6405	1.9484	1.9517
U									0.8981	0.9273	0.9284
V									-0.0396	0.0220	0.0301
W									0.0430	0.3724	0.3717
P	4								0.4927	0.9337	0.9517
M									1.6444	2.0197	1.9839
U									0.8835	0.9408	0.9336
V									-0.0045	0.0515	0.0365
W									0.1788	0.3903	0.3830
P	3									0.9464	0.9088
M										2.0257	1.9493
U										0.9437	0.9253
V										0.0646	0.0441
W										0.3857	0.3761
P	2									0.9247	0.9219
M										2.0067	1.9716
U										0.9401	0.9351
V										0.0804	0.0551
W										0.3774	0.3675
P	1									0.9451	0.9499
M										2.0130	2.0097
U										0.9452	0.9467
V										0.0892	0.0813
W										0.3673	0.3627

TABLE B-5. FINAL DATA SET FOR $M_\infty = 1.95$, $R_d = .48 \times 10^6$, $\alpha_b = 15°$, $x/d = 10$

M2R2G5

P -- P0/P0INF M -- MACH NUMBER U,V,W -- 3-D VELOCITY COMPONENTS/U1NF

		1	2	3	4	5	6	7	8	9	10	11
P	20	0.9114	0.9345	0.9336	0.9398	0.9357	0.9114	0.9197	0.9372	0.9444	0.9593	0.9490
M		1.8427	1.8624	1.8726	1.8883	1.8978	1.8907	1.8901	1.9254	1.9349	1.9475	1.9389
U		0.9658	0.9700	0.9693	0.9691	0.9638	0.9535	0.9469	0.9498	0.9483	0.9502	0.9479
V		-0.0222	-0.0533	-0.0869	-0.1153	-0.1457	-0.1589	-0.1412	-0.1399	-0.1270	-0.1102	-0.0983
W		0.0586	0.0664	0.0845	0.1062	0.1383	0.1749	0.2196	0.2529	0.2762	0.2891	0.2922
P	19	0.9255	0.9403	0.9475	0.9319	0.8406	0.8092	0.8429	0.9003	0.9232	0.9465	0.9693
M		1.8649	1.8773	1.8931	1.8978	1.8578	1.8433	1.8618	1.9221	1.9384	1.9513	1.9630
U		0.9748	0.9757	0.9761	0.9712	0.9495	0.9350	0.9330	0.9423	0.9430	0.9448	0.9485
V		-0.0262	-0.0647	-0.1075	-0.1441	-0.1713	-0.1797	-0.1545	-0.1497	-0.1339	-0.1154	-0.1026
W		0.0190	0.0312	0.0470	0.0724	0.1203	0.1734	0.2310	0.2707	0.2934	0.3078	0.3121
P	18	0.9202	0.9452	0.9345	0.8505	0.7456	0.7382	0.7962	0.8466	0.9157	0.9357	0.9561
M		1.8792	1.9016	1.9102	1.8768	1.8200	1.8298	1.8711	1.9154	1.9566	1.9599	1.9650
U		0.9782	0.9828	0.9798	0.9629	0.9322	0.9213	0.9258	0.9318	0.9406	0.9404	0.9427
V		-0.0298	-0.0744	-0.1287	-0.1695	-0.2020	-0.2091	-0.1720	-0.1580	-0.1364	-0.1169	-0.1023
W		-0.0211	-0.0132	-0.0023	0.0287	0.1131	0.1894	0.2582	0.2940	0.3171	0.3283	0.3311
P	17	0.9342	0.9424	0.8896	0.7290	0.6770	0.6958	0.7760	0.8172	0.8862	0.9317	0.9520
M		1.9213	1.9319	1.9290	1.8391	1.8330	1.8640	1.9165	1.9346	1.9633	1.9719	1.9727
U		0.9884	0.9891	0.9811	0.9444	0.9255	0.9163	0.9237	0.9240	0.9331	0.9374	0.9397
V		-0.0308	-0.0796	-0.1415	-0.2042	-0.2512	-0.2481	-0.1937	-0.1647	-0.1356	-0.1111	-0.0956
W		-0.0726	-0.0697	-0.0717	-0.0235	0.1035	0.2189	0.2994	0.3320	0.3445	0.3488	0.3479
P	16	0.9385	0.9461	0.8181	0.6234	0.5698	0.6081	0.7400	0.8081	0.8842	0.9329	0.9412
M		1.9682	1.9877	1.9519	1.8577	1.8591	1.8988	1.9650	1.9745	1.9887	1.9830	1.9703
U		0.9972	0.9992	0.9794	0.9419	0.9299	0.9119	0.9154	0.9200	0.9306	0.9349	0.9347
V		-0.0295	-0.0755	-0.1302	-0.2184	-0.2678	-0.2558	-0.1984	-0.1612	-0.1257	-0.1004	-0.0833
W		-0.1241	-0.1334	-0.1586	-0.1018	0.0986	0.2701	0.3625	0.3765	0.3748	0.3675	0.3621
P	15	0.9328	0.9406	0.8672	0.5888	0.4234	0.5115	0.7048	0.7676	0.8619	0.9179	0.9390
M		2.0039	2.0273	2.0458	1.9023	1.8224	1.9152	1.9993	1.9871	1.9990	1.9899	1.9722
U		1.0098	1.0050	1.0002	0.9548	0.9398	0.9183	0.9100	0.9102	0.9244	0.9306	0.9289
V		-0.0110	-0.0437	-0.0726	-0.1201	-0.1828	-0.1967	-0.1594	-0.1335	-0.1051	-0.0824	-0.0707
W		-0.1712	-0.1801	-0.2217	-0.2144	0.0857	0.3125	0.4183	0.4185	0.4034	0.3875	0.3809
P	14	0.9218	0.9525	0.8520	0.5374	0.3384	0.4450	0.6926	0.7619	0.8592	0.9182	0.9430
M		2.0490	2.0931	2.0981	1.9243	1.7409	1.8958	2.0223	2.0116	2.0178	2.0056	2.0041
U		1.0070	1.0159	1.0058	0.9562	0.9317	0.9273	0.9148	0.9115	0.9242	0.9299	0.9336
V		-0.0042	-0.0143	-0.0069	-0.0028	-0.0415	-0.0924	-0.0906	-0.0844	-0.0728	-0.0604	-0.0522
W		-0.2061	-0.2212	-0.2685	-0.2659	0.0616	0.3157	0.4432	0.4444	0.4234	0.4046	0.3960
P	13	0.9155	0.9358	0.8683	0.5691	0.3824	0.3468	0.4688	0.7081	0.7535	0.8566	0.9230
M		2.0643	2.1011	2.1188	1.9594	1.7891	1.7238	1.8380	1.9930	1.9705	1.9932	2.0037
U		1.0106	1.0171	1.0116	0.9657	0.9406	0.9155	0.9016	0.9118	0.9063	0.9211	0.9302
V		0.0023	0.0148	0.0473	0.0897	0.0809	0.0372	0.0077	-0.0098	-0.0229	-0.0269	-0.0284
W		-0.2094	-0.2255	-0.2637	-0.2547	-0.1110	0.1530	0.3471	0.4397	0.4359	0.4193	0.4060
P	12	0.8778	0.9011	0.8652	0.6491	0.4805	0.4287	0.5527	0.7390	0.7469	0.8609	0.9334
M		1.9955	2.0282	2.0434	1.9385	1.8342	1.7585	1.8611	1.9692	1.9374	1.9857	2.0053
U		0.9995	1.0062	1.0045	0.9686	0.9424	0.9201	0.9218	0.9242	0.9091	0.9243	0.9331
V		0.0081	0.0373	0.0795	0.1444	0.1875	0.1555	0.1055	0.0557	0.0248	0.0037	-0.0056
W		-0.1650	-0.1762	-0.1953	-0.1852	-0.0881	0.2178	0.2943	0.3922	0.4069	0.4077	0.4015
P	11	0.8948	0.9133	0.9170	0.9049	0.7691	0.6198	0.6578	0.7483	0.7434	0.8616	0.9297
M		1.9681	1.9930	2.0165	2.0531	2.0039	1.8646	1.8585	1.9150	1.8949	1.9641	1.9905
U		0.9977	1.0034	1.0069	1.0111	0.9925	0.9500	0.9342	0.9308	0.9127	0.9262	0.9332
V		0.0098	0.0411	0.0787	0.1331	0.1878	0.1974	0.1540	0.0931	0.0517	0.0253	0.0138
W		-0.1226	-0.1276	-0.1354	-0.1374	-0.1034	0.0895	0.2224	0.3231	0.3630	0.3869	0.3903
P	10	0.9179	0.9176	0.9315	0.9282	0.8560	0.7655	0.8349	0.6876	0.7108	0.8948	0.9448
M		1.9728	1.9803	2.0041	2.0228	1.9869	1.9012	1.9431	1.8056	1.8284	1.9652	1.9850
U		1.0027	1.0037	1.0080	1.0091	0.9953	0.9652	0.9697	0.9154	0.9050	0.9342	0.9373
V		0.0139	0.0481	0.0841	0.1290	0.1688	0.1812	0.1584	0.0926	0.0535	0.0358	0.0279
W		-0.0871	-0.0886	-0.0899	-0.0835	-0.0477	0.0830	0.1741	0.2591	0.3252	0.3673	0.3755
P	9	0.9128	0.9084	0.9236	0.9272	0.9173	0.9043	0.8268	0.6366	0.7322	0.9122	0.9593
M		1.9635	1.9613	1.9815	1.9898	1.9768	1.9544	1.8914	1.7183	1.8194	1.9562	1.9791
U		1.0024	1.0007	1.0044	1.0041	0.9975	0.9875	0.9678	0.8963	0.9089	0.9373	0.9414
V		0.0152	0.0496	0.0821	0.1151	0.1432	0.1481	0.1216	0.0699	0.0488	0.0411	0.0338
W		-0.0523	-0.0522	-0.0508	-0.0393	-0.0075	0.0736	0.1190	0.2264	0.3059	0.3514	0.3598
P	8				0.9010	0.9085	0.8151	0.7029	0.6620	0.8309	0.9455	0.9592
M					1.9533	1.9492	1.8700	1.7676	1.7269	1.8817	1.9610	1.9666
U					0.9963	0.9937	0.9703	0.9362	0.9006	0.9297	0.9435	0.9427
V					0.0961	0.1094	0.0956	0.0759	0.0354	0.0422	0.0409	0.0337
W					-0.0102	0.0111	0.0457	0.0891	0.2291	0.3058	0.3385	0.3460
P	7						0.5922	0.5476	0.8074	0.9172	0.9418	0.9693
M							1.6504	1.5758	1.8544	1.9291	1.9464	1.9647
U							0.9030	0.8741	0.9356	0.9443	0.9426	0.9454
V							0.0290	0.0097	0.0010	0.0311	0.0341	0.0305
W							0.0090	0.0642	0.2607	0.3085	0.3290	0.3373
P	6							0.4978	0.9336	0.9582	0.9667	0.9706
M								1.5104	1.9527	1.9544	1.9581	1.9617
U								0.8488	0.9538	0.9490	0.9465	0.9461
V								-0.0502	-0.0171	0.0158	0.0259	0.0264
W								0.0476	0.3025	0.3189	0.3290	0.3331
P	5								0.9415	0.9621	0.9664	0.9680
M									1.9728	1.9692	1.9657	1.9573
U									0.9482	0.9485	0.9470	0.9440
V									-0.0153	0.0121	0.0199	0.0237
W									0.3376	0.3338	0.3347	0.3354
P	4								0.9560	0.9508	0.9591	0.9693
M									1.9885	1.9730	1.9731	1.9752
U									0.9477	0.9459	0.9461	0.9469
V									0.0031	0.0158	0.0208	0.0233
W									0.3523	0.3442	0.3433	0.3428
P	3									0.9531	0.9712	0.9689
M										1.9898	1.9890	1.9875
U										0.9463	0.9495	0.9470
V										0.0189	0.0223	0.0249
W										0.3567	0.3554	0.3524

TABLE B-5. FINAL DATA SET FOR $M_\infty = 1.95$, $R_d = .48 \times 10^6$, $\alpha_b = 15°$, x/d = 10 (CONCLUDED)

P	7			
M		0.9623	0.9549	0.9714
U		2.0262	2.0077	2.0002
V		0.9489	0.9469	0.9479
W		0.0241	0.0271	0.0312
		0.3778	0.3688	0.3599
P	1	0.9444	0.9647	0.9607
M		2.0413	2.0299	1.9958
U		0.9456	0.9490	0.9453
V		0.0429	0.0423	0.0422
W		0.3954	0.3787	0.3620

TABLE B-6. FINAL DATA SET FOR $M_\infty = 1.95$, $R_d = .48 \times 10^6$, $\alpha_b = 15°$, x/d = 13

P -- P0/P0INF M -- MACH NUMBER U,V,W -- 3-D VELOCITY COMPONENTS/U1NF

		1	2	3	4	5	6	7	8	9	10	11	12
P	23	0.9339	0.9041	0.8809	0.8396	0.8121	0.8117	0.8474	0.8934	0.9210	0.9325	0.9518	0.9619
M		1.8846	1.8789	1.8709	1.8596	1.8496	1.8468	1.8801	1.9018	1.9146	1.9235	1.9345	1.9395
U		0.9803	0.9770	0.9718	0.9629	0.9507	0.9402	0.9419	0.9406	0.9412	0.9429	0.9460	0.9486
V		-0.0215	-0.0583	-0.0919	-0.1254	-0.1381	-0.1384	-0.1375	-0.1256	-0.1127	-0.1046	-0.0927	-0.0788
W		-0.0879	-0.0024	0.0203	0.0597	0.1327	0.1888	0.2293	0.2668	0.2839	0.2905	0.2957	0.2964
P	22	0.9348	0.8874	0.8619	0.7621	0.7627	0.7958	0.8283	0.8623	0.8800	0.9154	0.9560	0.9743
M		1.9069	1.8902	1.8859	1.8268	1.8394	1.8606	1.8814	1.8944	1.9137	1.9250	1.9486	1.9541
U		0.9856	0.9789	0.9754	0.9518	0.9456	0.9400	0.9363	0.9329	0.9360	0.9383	0.9459	0.9496
V		-0.0233	-0.0651	-0.1017	-0.1391	-0.1500	-0.1435	-0.1394	-0.1244	-0.1091	-0.1021	-0.0894	-0.0752
W		-0.0531	-0.0479	-0.0238	0.0354	0.1327	0.2070	0.2519	0.2855	0.3012	0.3074	0.3107	0.3082
P	21	0.9333	0.8764	0.7996	0.7058	0.7439	0.7788	0.8238	0.8649	0.9072	0.9153	0.9480	0.9683
M		1.9382	1.9165	1.8762	1.8232	1.8656	1.8857	1.9111	1.9192	1.9398	1.9429	1.9536	1.9608
U		0.9910	0.9831	0.9691	0.9489	0.9504	0.9405	0.9377	0.9342	0.9388	0.9387	0.9433	0.9483
V		-0.0231	-0.0663	-0.1084	-0.1551	-0.1686	-0.1539	-0.1376	-0.1192	-0.1031	-0.0943	-0.0838	-0.0701
W		-0.1029	-0.0978	-0.0742	0.0051	0.1353	0.2323	0.2810	0.3081	0.3195	0.3254	0.3246	0.3194
P	20	0.9283	0.8513	0.7485	0.6388	0.6410	0.7396	0.8232	0.8708	0.9040	0.9246	0.9388	0.9668
M		1.9708	1.9417	1.8805	1.8267	1.8366	1.9129	1.9531	1.9563	1.9567	1.9651	1.9612	1.9679
U		0.9941	0.9839	0.9652	0.9486	0.9378	0.9377	0.9395	0.9379	0.9380	0.9404	0.9421	0.9475
V		-0.0216	-0.0601	-0.1033	-0.1582	-0.1886	-0.1683	-0.1372	-0.1077	-0.0936	-0.0835	-0.0727	-0.0620
W		-0.1527	-0.1533	-0.1294	-0.0421	0.1324	0.2658	0.3168	0.3353	0.3395	0.3426	0.3371	0.3299
P	19	0.9194	0.8484	0.6933	0.5375	0.4599	0.6402	0.8310	0.8855	0.9050	0.9297	0.9480	0.9677
M		2.0066	1.9820	1.8928	1.8060	1.7457	1.9076	2.0055	2.0023	1.9784	1.9828	1.9795	1.9667
U		0.9904	0.9876	0.9625	0.9437	0.9138	0.9188	0.9376	0.9431	0.9396	0.9414	0.9438	0.9447
V		-0.0136	-0.0415	-0.0881	-0.1385	-0.1739	-0.1629	-0.1177	-0.0895	-0.0787	-0.0703	-0.0600	-0.0530
W		-0.1994	-0.2036	-0.1795	-0.0648	0.1062	0.3230	0.3730	0.3643	0.3569	0.3576	0.3505	0.3382
P	18	0.9156	0.8145	0.6583	0.4428	0.3974	0.5771	0.8245	0.8702	0.9123	0.9287	0.9546	0.9668
M		2.0682	2.0152	1.9366	1.7728	1.7550	1.9049	2.0388	2.0211	2.0229	1.9921	1.9919	1.9833
U		1.0014	0.9862	0.9654	0.9372	0.9264	0.9099	0.9376	0.9424	0.9470	0.9409	0.9455	0.9482
V		-0.0087	-0.0388	-0.0818	-0.0682	-0.0982	-0.1126	-0.0870	-0.0651	-0.0562	-0.0527	-0.0467	-0.0419
W		-0.2448	-0.2540	-0.2418	-0.1027	0.1210	0.3648	0.4051	0.3854	0.3766	0.3691	0.3578	0.3441
P	17	0.9155	0.8049	0.6429	0.4137	0.3956	0.5775	0.8313	0.8750	0.9175	0.9394	0.9639	0.9776
M		2.1121	2.0637	1.9763	1.7770	1.7812	1.9363	2.0560	2.0289	2.0305	2.0135	1.9962	1.9912
U		1.0069	0.9906	0.9678	0.9406	0.9372	0.9185	0.9430	0.9449	0.9488	0.9468	0.9473	0.9510
V		0.0004	0.0067	0.0111	0.0230	0.0058	-0.0375	-0.0402	-0.0352	-0.0320	-0.0301	-0.0328	-0.0313
W		-0.2788	-0.2889	-0.2803	-0.1044	0.1422	0.3833	0.4118	0.3887	0.3806	0.3732	0.3582	0.3442
P	16	0.9182	0.8024	0.6580	0.4920	0.3884	0.5069	0.7026	0.8940	0.9192	0.9517	0.9601	0.9575
M		2.1418	2.0752	1.9775	1.8618	1.7163	1.8345	1.9684	2.0291	2.0190	2.0187	1.9915	1.9777
U		1.0147	0.9932	0.9675	0.9543	0.9218	0.9244	0.9335	0.9515	0.9494	0.9507	0.9480	0.9480
V		0.0116	0.0327	0.0515	0.0795	0.0588	0.0759	0.0299	-0.0047	-0.0092	-0.0115	-0.0187	-0.0216
W		-0.2899	-0.2893	-0.2778	-0.1755	0.0715	0.2664	0.3720	0.3743	0.3718	0.3683	0.3534	0.3418
P	15	0.8981	0.8036	0.6781	0.5351	0.4582	0.5993	0.7989	0.9030	0.9406	0.9783	0.9522	0.9695
M		2.0989	2.0417	1.9453	1.8344	1.7328	1.8487	1.9913	2.0055	2.0146	2.0252	1.9865	1.9874
U		1.0081	0.9932	0.9689	0.9472	0.9196	0.9333	0.9577	0.9537	0.9535	0.9561	0.9486	0.9515
V		0.0142	0.0471	0.0809	0.1377	0.1312	0.1178	0.0659	0.0132	0.0061	0.0027	-0.0073	-0.0152
W		-0.2682	-0.2526	-0.2282	-0.1231	0.0822	0.2327	0.3199	0.3498	0.3576	0.3593	0.3480	0.3408
P	14	0.8783	0.8089	0.7070	0.6067	0.5476	0.7289	0.8477	0.8521	0.8947	0.9594	0.9509	0.9664
M		2.0344	1.9900	1.9059	1.8234	1.7447	1.8892	1.9661	1.9629	1.9632	1.9989	1.9911	1.9877
U		1.0023	0.9909	0.9688	0.9486	0.9191	0.9579	0.9703	0.9595	0.9461	0.9529	0.9511	0.9523
V		0.0148	0.0529	0.0936	0.1522	0.1574	0.1109	0.0694	0.0492	0.0213	0.0157	0.0113	-0.0011
W		-0.2087	-0.1961	-0.1639	-0.0737	0.0803	0.1856	0.2511	0.2905	0.3349	0.3465	0.3451	0.3389
P	13	0.8899	0.8327	0.7845	0.6858	0.6447	0.6511	0.8577	0.8487	0.9347	0.9687	0.9578	0.9392
M		2.0088	1.9708	1.9408	1.8637	1.8106	1.7766	1.9386	1.9253	1.9736	1.9971	1.9918	1.9685
U		1.0029	0.9929	0.9843	0.9625	0.9457	0.9316	0.9750	0.9608	0.9540	0.9549	0.9530	0.9479
V		0.0157	0.0545	0.0830	0.1314	0.1483	0.1303	0.0745	0.0324	0.0187	0.0167	0.0131	0.0028
W		-0.1667	-0.1525	-0.1370	-0.0726	0.0187	0.1052	0.1927	0.2479	0.3213	0.3393	0.3401	0.3350
P	12	0.8730	0.8608	0.8320	0.7635	0.7389	0.7840	0.8592	0.8075	0.9349	0.9635	0.9705	0.9703
M		1.9702	1.9622	1.9458	1.8913	1.8497	1.8579	1.9154	1.8777	1.9828	1.9865	1.9984	1.9955
U		0.9979	0.9958	0.9911	0.9750	0.9626	0.9649	0.9791	0.9537	0.9524	0.9536	0.9563	0.9557
V		0.0154	0.0545	0.0795	0.1147	0.1156	0.0957	0.0422	0.0045	0.0074	0.0140	0.0138	0.0074
W		-0.1255	-0.1122	-0.0948	-0.0413	0.0247	0.0721	0.1391	0.2188	0.3168	0.3341	0.3365	0.3354
P	11	0.9098	0.8797	0.8584	0.8538	0.8494	0.8620	0.8039	0.7092	0.8971	0.9556	0.9704	0.9722
M		1.9736	1.9589	1.9448	1.9394	1.9128	1.9245	1.8813	1.7892	1.9378	1.9796	1.9971	2.0005
U		1.0037	0.9982	0.9938	0.9922	0.9854	0.9897	0.9743	0.9292	0.9433	0.9519	0.9564	0.9574
V		0.0169	0.0513	0.0709	0.0922	0.0835	0.0641	0.0182	-0.0112	-0.0003	0.0120	0.0129	0.0111
W		-0.0935	-0.0784	-0.0657	-0.0278	0.0139	0.0382	0.0997	0.2003	0.3210	0.3330	0.3353	0.3351
P	10	0.9104	0.9088	0.9110	0.8971	0.9040	0.8908	0.7149	0.6006	0.9077	0.9730	0.9592	0.9773
M		1.9668	1.9713	1.9726	1.9544	1.9431	1.9330	1.8129	1.6813	1.9504	1.9961	1.9891	2.0071
U		1.0029	1.0038	1.0036	0.9986	0.9963	0.9939	0.9556	0.8927	0.9436	0.9546	0.9541	0.9597
V		0.0171	0.0440	0.0593	0.0692	0.0579	0.0454	0.0172	-0.0111	0.0042	0.0145	0.0130	0.0141
W		-0.0594	-0.0532	-0.0477	-0.0240	-0.0032	0.0124	0.0685	0.1975	0.3314	0.3395	0.3348	0.3341
P	9	0.9198	0.9107	0.9132	0.9042	0.9145	0.8931	0.6563	0.5791	0.9173	0.9775	0.9675	0.9725
M		1.9682	1.9631	1.9611	1.9392	1.9393	1.9445	1.7581	1.6651	1.9583	2.0029	1.9988	2.0042
U		1.0046	1.0026	1.0016	0.9954	0.9957	0.9973	0.9386	0.8853	0.9434	0.9561	0.9563	0.9592
V		0.0180	0.0391	0.0490	0.0509	0.0474	0.0464	0.0315	0.0017	0.0133	0.0190	0.0179	0.0166
W		-0.0331	-0.0307	-0.0279	-0.0160	-0.0126	-0.0113	0.0494	0.2051	0.3386	0.3406	0.3368	0.3331
P	8				0.8963	0.8957	0.8654	0.7094	0.5798	0.9397	0.9688	0.9787	0.9879
M					1.9332	1.9425	1.9302	1.8122	1.6585	1.9682	1.9956	2.0076	2.0156
U					0.9937	0.9960	0.9923	0.9565	0.8830	0.9470	0.9547	0.9588	0.9621
V					0.0489	0.0525	0.0537	0.0515	0.0083	0.0192	0.0216	0.0210	0.0218
W					-0.0205	-0.0299	-0.0295	0.0119	0.2047	0.3368	0.3382	0.3369	0.3340
P	7						0.7306	0.6909	0.5839	0.9603	0.9735	0.9804	0.9850
M							1.8167	1.7869	1.6514	1.9769	1.9948	2.0042	2.0043
U							0.9569	0.9482	0.8824	0.9505	0.9555	0.9585	0.9593
V							0.0512	0.0557	-0.0005	0.0201	0.0225	0.0221	0.0257
W							-0.0461	-0.0049	0.1960	0.3343	0.3353	0.3348	0.3324
P	6							0.6132	0.5528	0.9664	0.9690	0.9804	0.9833
M								1.6933	1.6035	1.9850	1.9866	1.9996	1.9919
U								0.9172	0.8669	0.9531	0.9543	0.9579	0.9569
V								0.0390	-0.0092	0.0211	0.0232	0.0250	0.0241
W								-0.0291	0.1860	0.3338	0.3323	0.3323	0.3284

TABLE B-6. FINAL DATA SET FOR $M_\infty = 1.95$, $R_d = .48 \times 10^6$, $\alpha_b = 15°$, x/d = 13 (CONCLUDED)

P	5	0.5485	0.9630	0.9680	0.9790	0.9807
M		1.5984	1.9864	1.9823	1.9927	1.9992
U		0.8621	0.9528	0.9532	0.9568	0.9594
V		-0.0249	0.0249	0.0246	0.0268	0.0312
W		0.1974	0.3356	0.3310	0.3295	0.3270
P	4	0.5166	0.9671	0.9528	0.9699	0.9853
M		1.5389	1.9914	1.9886	1.9837	1.9989
U		0.8370	0.9525	0.9493	0.9545	0.9598
V		-0.0217	0.0312	0.0279	0.0301	0.0337
W		0.2073	0.3402	0.3300	0.3278	0.3253
P	3		0.9670	0.9636	0.9602	0.9704
M			1.9983	1.9827	1.9752	1.9860
U			0.9522	0.9522	0.9521	0.9567
V			0.0418	0.0350	0.0336	0.0368
W			0.3457	0.3332	0.3278	0.3228
P	2		0.9579	0.9553	0.9552	0.9728
M			1.9993	1.9880	1.9769	1.9883
U			0.9510	0.9520	0.9518	0.9577
V			0.0505	0.0443	0.0403	0.0411
W			0.3485	0.3371	0.3286	0.3215
P	1		0.9456	0.9585	0.9671	0.9694
M			2.0048	1.9993	1.9916	1.9912
U			0.9499	0.9533	0.9545	0.9578
V			0.0585	0.0559	0.0505	0.0468
W			0.3547	0.3414	0.3322	0.3229

TABLE B-7. FINAL DATA SET FOR $M_\infty = 1.95$, $R_d = .48 \times 10^6$, $\alpha_b = 20°$, x/d = 6

HPN207

P -- PO/POINF M -- MACH NUMBER U,V,W -- 3-D VELOCITY COMPONENTS/UINF

		1	2	3	4	5	6	7	8	9	10
P	18	0.9062	0.8931	0.8998	0.9176	0.9115	0.9234	0.9286	0.9014	0.9475	0.9354
M		1.8559	1.8543	1.8698	1.9005	1.9231	1.9465	1.9543	1.9136	1.9498	1.9367
U		0.9684	0.9597	0.9570	0.9554	0.9493	0.9452	0.9422	0.9232	0.9280	0.9236
V		-0.0195	-0.0557	-0.0896	-0.1121	-0.1511	-0.1506	-0.1427	-0.1445	-0.1260	-0.1164
W		0.1175	0.1383	0.1692	0.2135	0.2453	0.2863	0.3074	0.3243	0.3498	0.3561
P	17	0.8914	0.8803	0.9075	0.8984	0.8997	0.9162	0.9205	0.9195	0.9191	0.9420
M		1.8573	1.8544	1.8925	1.9105	1.9493	1.9770	1.9830	1.9815	1.9488	1.9628
U		0.9686	0.9632	0.9654	0.9554	0.9493	0.9434	0.9408	0.9325	0.9182	0.9217
V		-0.0281	-0.0758	-0.1221	-0.1489	-0.1909	-0.1841	-0.1762	-0.1544	-0.1408	-0.1295
W		0.0778	0.0994	0.1384	0.2047	0.2489	0.3028	0.3265	0.3532	0.3692	0.3758
P	16	0.8952	0.8956	0.8964	0.9136	0.9023	0.9080	0.9147	0.9178	0.9094	0.9397
M		1.8882	1.8938	1.9210	1.9660	2.0181	2.0279	2.0299	2.0241	1.9708	1.9892
U		0.9781	0.9769	0.9725	0.9649	0.9508	0.9399	0.9363	0.9295	0.9120	0.9173
V		-0.0411	-0.1032	-0.1693	-0.2001	-0.2499	-0.2196	-0.2096	-0.1723	-0.1537	-0.1409
W		0.0237	0.0445	0.0924	0.1954	0.2694	0.3363	0.3598	0.3860	0.3958	0.4019
P	15	0.8902	0.8941	0.9097	0.9164	0.8459	0.9090	0.9030	0.9163	0.9172	0.8990
M		1.8948	1.9220	1.9634	2.0685	2.1122	2.1217	2.0992	2.0900	2.0524	1.9963
U		0.9827	0.9851	0.9853	0.9745	0.9454	0.9354	0.9295	0.9244	0.9175	0.9044
V		-0.0398	-0.1146	-0.1891	-0.2848	-0.3198	-0.2608	-0.2286	-0.1913	-0.1404	-0.1488
W		-0.0173	-0.0107	0.0346	0.1916	0.3092	0.3921	0.4103	0.4340	0.4419	0.4321
P	14	0.9002	0.9066	0.8658	0.6905	0.6203	0.7971	0.8867	0.9256	0.9272	0.9424
M		1.9533	2.0087	2.0769	2.1000	2.1125	2.2356	2.2580	2.1899	2.1141	2.1035
U		0.9951	1.0012	1.0057	0.9769	0.9379	0.9189	0.9177	0.9169	0.9137	0.9178
V		-0.0440	-0.1299	-0.2305	-0.3114	-0.2987	-0.2441	-0.2598	-0.1958	-0.1410	-0.1233
W		-0.0990	-0.1202	-0.0871	0.1633	0.3504	0.4759	0.5090	0.5042	0.4677	0.4788
P	13	0.9163	0.8674	0.5929	0.5300	0.5029	0.7659	0.8840	0.9531	0.9623	0.9515
M		2.0596	2.1385	2.0304	2.1073	2.2548	2.4417	2.3954	2.2724	2.1652	2.1315
U		1.0119	1.0189	0.9983	0.9994	0.9445	0.9296	0.9144	0.9133	0.9159	0.9127
V		-0.0271	-0.0841	-0.1515	-0.2790	-0.2841	-0.2795	-0.2401	-0.1704	-0.1176	-0.1001
W		-0.1945	-0.2463	-0.1734	0.2113	0.4531	0.5627	0.5851	0.5594	0.5172	0.5090
P	12	0.9280	0.8503	0.4332	0.2925	0.4911	0.6276	0.7902	0.9562	0.9388	0.9361
M		2.1940	2.2385	2.0970	2.0547	2.3990	2.2955	2.3395	2.2780	2.1476	2.1212
U		1.0274	1.0239	1.0069	0.9975	0.9867	0.9296	0.9231	0.9114	0.9070	0.9034
V		0.0084	0.0053	-0.0062	-0.1923	-0.2309	-0.1832	-0.1848	-0.1314	-0.0845	-0.0711
W		-0.2824	-0.3322	-0.2632	0.1666	0.4559	0.5387	0.5688	0.5754	0.5300	0.5247
P	11	0.9019	0.8972	0.6012	0.2539	0.2032	0.4310	0.6880	0.9092	0.9324	0.9530
M		2.2747	2.3534	2.3015	1.9774	1.8702	2.1816	2.2789	2.2625	2.1619	2.1124
U		1.0334	1.0371	1.0137	0.9799	0.9658	0.9229	0.9060	0.9123	0.8998	0.9059
V		0.0520	0.0862	0.1442	0.1284	0.1079	-0.0746	-0.0657	-0.0897	-0.0578	-0.0417
W		-0.3267	-0.3654	-0.3774	-0.1982	0.0917	0.4204	0.4920	0.5751	0.5527	0.5190
P	10	0.8541	0.8623	0.5997	0.3305	0.2502	0.2731	0.5610	0.8532	0.9463	0.9520
M		2.2398	2.3112	2.2175	2.0544	1.9113	1.8639	2.0655	2.1631	2.1326	2.0915
U		1.0318	1.0356	0.9944	0.9619	0.9529	0.9304	0.9552	0.9132	0.8997	0.9043
V		0.0832	0.1434	0.2357	0.3056	0.2593	0.0812	0.0255	-0.0470	-0.0232	-0.0135
W		-0.2883	-0.3205	-0.3215	-0.2025	-0.0439	0.2771	0.3909	0.5320	0.5409	0.5121
P	9	0.8427	0.8650	0.6237	0.5112	0.4945	0.4980	0.7686	0.5693	0.8988	0.9499
M		2.1481	2.2211	2.2736	2.0712	2.0847	1.9850	2.1005	1.8627	2.1072	2.0625
U		1.0312	1.0366	1.0283	0.9468	0.9538	0.9545	1.0040	0.9254	0.8986	0.8966
V		0.1077	0.1756	0.2715	0.3900	0.4055	0.2989	0.1633	0.0500	-0.0063	0.0150
W		-0.1896	-0.2104	-0.2135	-0.1427	-0.0485	0.1411	0.2248	0.2991	0.5303	0.5045
P	8				0.7822	0.8137	0.8268	0.8468	0.4812	0.8903	0.9038
M					2.2027	2.2247	2.1546	2.0873	1.6984	2.0748	2.0133
U					1.0037	1.0118	1.0146	1.0213	0.9029	0.8936	0.8888
V					0.3540	0.3558	0.2888	0.1746	0.0561	0.0150	0.0389
W					-0.0861	-0.0336	0.0422	0.0666	0.1691	0.5216	0.4949
P	7						0.8124	0.7946	0.3718	0.8746	0.8972
M							2.1364	2.0470	1.5009	2.0821	2.0914
U							1.0144	1.0137	0.8445	0.8859	0.8909
V							0.2691	0.1511	0.0426	0.0417	0.0436
W							-0.0481	-0.0712	0.0632	0.5372	0.5334
P	6							0.6018	0.3024	0.8491	0.9260
M								1.9225	1.3775	2.1410	2.1385
U								0.9679	0.7928	0.8893	0.8979
V								0.0355	0.0064	0.0600	0.0494
W								-0.2141	0.0909	0.5593	0.5451
P	5								0.3035	0.9379	0.9467
M									1.4127	2.1724	2.1295
U									0.7910	0.8992	0.9031
V									0.0080	0.0745	0.0678
W									0.1880	0.5567	0.5300
P	4								0.3043	0.9331	0.9335
M									1.3673	2.1325	2.0946
U									0.7618	0.8994	0.9011
V									0.0217	0.0936	0.0845
W									0.2219	0.5338	0.5126
P	3								0.3207	0.9118	0.9336
M									1.3678	2.0952	2.0884
U									0.7271	0.8961	0.9034
V									0.0265	0.1080	0.0960
W									0.3176	0.5173	0.5032
P	2									0.9251	0.9457
M										2.1036	2.0984
U										0.9005	0.9063
V										0.1192	0.1039
W										0.5116	0.4972
P	1									0.9253	0.9305
M										2.0951	2.0750
U										0.9026	0.9078
V										0.1318	0.1142
W										0.5088	0.4837

TABLE B-8. FINAL DATA SET FOR $M_\infty = 1.95$, $R_d = .48 \times 10^6$, $\alpha_b = 20°$, $x/d = 8.5$

H29208

P -- P0/P0INF M -- MACH NUMBER U,V,W -- 1-D VELOCITY COMPONENTS/U1NF

		1	2	3	4	5	6	7	8	9	10	11	12
P	22	0.9088	0.9089	0.9137	0.9332	0.9277	0.9302	0.9398	0.9413	0.9453	0.9352	0.9415	0.9363
M		1.8147	1.8232	1.8536	1.8834	1.9105	1.9225	1.9341	1.9362	1.9490	1.9495	1.9751	1.9794
U		0.9548	0.9542	0.9563	0.9563	0.9458	0.9390	0.9394	0.9355	0.9337	0.9307	0.9338	0.9314
V		-0.0289	-0.0556	-0.0993	-0.1281	-0.1772	-0.1675	-0.1589	-0.1490	-0.1360	-0.1221	-0.1211	-0.1146
W		0.0841	0.1037	0.1358	0.1724	0.2256	0.2722	0.2882	0.3076	0.3303	0.3444	0.3576	0.3694
P	21	0.9093	0.9115	0.9276	0.9303	0.9285	0.9241	0.9355	0.9431	0.9302	0.9280	0.9349	0.9474
M		1.8299	1.8415	1.8866	1.9126	1.9624	1.9591	1.9671	1.9745	1.9649	1.9725	1.9971	2.0096
U		0.9623	0.9624	0.9669	0.9626	0.9495	0.9372	0.9367	0.9347	0.9275	0.9276	0.9303	0.9388
V		-0.0303	-0.0756	-0.1356	-0.1719	-0.2289	-0.2026	-0.1894	-0.1704	-0.1499	-0.1337	-0.1330	-0.1225
W		0.0392	0.0593	0.0963	0.1480	0.2309	0.2931	0.3109	0.3339	0.3549	0.3672	0.3797	0.3912
P	20	0.9195	0.9197	0.9354	0.9273	0.9320	0.9550	0.9623	0.9378	0.9223	0.9277	0.9456	0.9418
M		1.8573	1.8705	1.9324	1.9784	2.0337	2.0357	2.0516	2.0649	1.9966	2.0261	2.0465	2.0410
U		0.9712	0.9713	0.9768	0.9719	0.9622	0.9461	0.9360	0.9260	0.9236	0.9265	0.9289	0.9269
V		-0.0377	-0.0983	-0.1851	-0.2446	-0.2752	-0.2499	-0.2269	-0.1649	-0.1480	-0.1479	-0.1411	-0.1248
W		-0.0216	-0.0046	0.0373	0.1103	0.2155	0.3026	0.3613	0.3834	0.3899	0.4041	0.4152	0.4213
P	19	0.9219	0.9209	0.8679	0.7525	0.7260	0.8574	0.9340	0.9281	0.8996	0.9181	0.9355	0.9485
M		1.9019	1.9224	1.9798	1.9631	1.9904	2.0816	2.1146	2.0395	2.0402	2.0803	2.0929	2.0857
U		0.9808	0.9816	0.9863	0.9683	0.9495	0.9462	0.9337	0.9197	0.9173	0.9223	0.9239	0.9245
V		-0.0435	-0.1146	-0.2059	-0.2533	-0.2645	-0.2675	-0.2377	-0.1671	-0.1587	-0.1598	-0.1474	-0.1267
W		-0.0893	-0.0850	-0.0456	0.0771	0.2278	0.3285	0.4056	0.4212	0.4301	0.4448	0.4536	0.4542
P	18	0.9179	0.9274	0.6765	0.6243	0.6586	0.6844	0.8044	0.7758	0.9096	0.9486	0.9433	0.9380
M		1.9685	2.0269	1.9295	1.9363	2.0058	2.0424	2.0870	1.9949	2.2030	2.2022	2.1579	2.1059
U		0.9903	1.0005	0.9777	0.9727	0.9619	0.9461	0.9256	0.8907	0.9166	0.9208	0.9186	0.9156
V		-0.0415	-0.1028	-0.1550	-0.1920	-0.2072	-0.1830	-0.1865	-0.1484	-0.1905	-0.1702	-0.1438	-0.1189
W		-0.1681	-0.1804	-0.0900	0.0952	0.2527	0.3525	0.4315	0.4590	0.5136	0.5127	0.5018	0.4855
P	17	0.9416	0.8758	0.6267	0.6336	0.6933	0.7178	0.6165	0.9065	0.9165	0.9301	0.9503	0.9547
M		2.0781	2.0739	1.9817	2.0399	2.1352	2.1431	2.0136	2.3645	2.2938	2.2411	2.1973	2.1447
U		1.0043	1.0051	0.9948	1.0082	0.9946	0.9673	0.8993	0.9164	0.9124	0.9094	0.9132	0.9155
V		-0.0302	-0.0552	-0.1100	-0.1756	-0.2063	-0.1558	-0.1197	-0.1977	-0.1686	-0.1496	-0.1262	-0.1036
W		-0.2517	-0.2391	-0.1287	0.0646	0.2690	0.3851	0.4620	0.5858	0.5709	0.5574	0.5361	0.5103
P	16	0.9497	0.7893	0.6074	0.5335	0.6181	0.6247	0.6789	0.9046	0.9320	0.9453	0.9458	0.9693
M		2.1982	2.1159	2.0499	2.0736	2.1942	2.1787	2.3139	2.4033	2.3307	2.2730	2.2018	2.1593
U		1.0138	1.0011	1.0110	1.0232	1.0058	0.9535	0.9213	0.9206	0.9143	0.9085	0.9084	0.9148
V		-0.0161	-0.0133	-0.0738	-0.1514	-0.2094	-0.1407	-0.1676	-0.1716	-0.1381	-0.1223	-0.1026	-0.0833
W		-0.3270	-0.3020	-0.2021	-0.0189	0.2829	0.4455	0.5658	0.6032	0.5919	0.5798	0.5512	0.5231
P	15	0.9522	0.8683	0.6138	0.4596	0.3584	0.6307	0.7247	0.8249	0.9517	0.9509	0.9551	0.9379
M		2.3126	2.3087	2.1742	2.0778	1.9627	2.3477	2.3675	2.3339	2.3394	2.2755	2.2057	2.1305
U		1.0179	1.0173	1.0181	1.0224	0.9928	0.9633	0.9411	0.9141	0.9178	0.9078	0.9087	0.9062
V		0.0031	0.0162	-0.0127	-0.0578	-0.1166	-0.1575	-0.1406	-0.1375	-0.1090	-0.0897	-0.0752	-0.0599
W		-0.4003	-0.3993	-0.2970	-0.1551	0.0902	0.5110	0.5639	0.5937	0.5962	0.5878	0.5570	0.5261
P	14	0.9533	0.8757	0.5881	0.3775	0.2694	0.5847	0.7866	0.7601	0.7910	0.9479	0.9606	0.9680
M		2.4395	2.4414	2.2585	2.0602	1.8639	2.3242	2.3791	2.3437	2.2557	2.2769	2.2209	2.1674
U		1.0241	1.0242	1.0157	1.0093	0.9722	0.9710	0.9637	0.9578	0.9081	0.9076	0.9086	0.9097
V		0.0157	0.0426	0.0195	0.0330	-0.0329	-0.1272	-0.0983	-0.0996	-0.0807	-0.0585	-0.0399	-0.0332
W		-0.4572	-0.4561	-0.3685	-0.2078	0.0524	0.4931	0.5393	0.5335	0.5800	0.5927	0.5677	0.5413
P	13	0.9425	0.8696	0.5724	0.3599	0.3145	0.2562	0.8341	0.7998	0.7252	0.9263	0.9501	0.9562
M		2.5667	2.5602	2.3133	2.0681	2.0091	1.8348	2.3408	2.3039	2.1469	2.2195	2.1808	2.1444
U		1.0292	1.0261	1.0065	0.9998	1.0059	0.9521	0.9810	0.9741	0.9019	0.9030	0.9065	0.9093
V		0.0263	0.0627	0.0712	0.0723	0.0607	-0.0069	-0.0433	-0.0441	-0.0371	-0.0268	-0.0118	-0.0080
W		-0.5061	-0.5063	-0.4226	-0.2498	-0.1368	0.1578	0.4961	0.4912	0.5436	0.5768	0.5537	0.5312
P	12	0.9457	0.8479	0.6650	0.4303	0.3346	0.2718	0.7348	0.8319	0.7038	0.9477	0.9585	0.9688
M		2.7038	2.6360	2.4575	2.1716	2.0219	1.8466	2.2463	2.2244	2.0599	2.1856	2.1527	2.1288
U		1.0367	1.0260	1.0138	1.0116	1.0069	0.9548	0.9894	0.9839	0.9033	0.9075	0.9082	0.9122
V		0.0311	0.0667	0.0865	0.0925	0.0969	0.0607	-0.0007	0.0156	0.0006	0.0015	0.0108	0.0122
W		-0.5467	-0.5376	-0.4809	-0.3029	-0.1346	0.1523	0.4289	0.4278	0.4967	0.5546	0.5372	0.5188
P	11	0.7130	0.7458	0.6469	0.4717	0.3915	0.3581	0.5933	0.8344	0.6734	0.8314	0.9741	0.9516
M		2.0146	2.0797	2.1012	2.0787	2.0063	1.9049	2.0827	2.1818	1.9719	2.0759	2.1356	2.0976
U		0.9897	1.0020	1.0000	1.0019	0.9943	0.9606	0.9776	0.9958	0.9232	0.8986	0.9094	0.9073
V		0.0229	0.0552	0.1016	0.1748	0.1983	0.1752	0.1662	0.0922	0.0478	0.0216	0.0354	0.0356
W		-0.2392	-0.2580	-0.2741	-0.1971	-0.0669	0.1418	0.3035	0.3591	0.3977	0.5134	0.5254	0.5090
P	10	0.8340	0.8262	0.7415	0.5542	0.5340	0.5564	0.6774	0.8777	0.6381	0.8544	0.9648	0.9638
M		2.0536	2.0496	2.1215	2.0245	2.0141	2.0012	2.0573	2.1035	1.8644	2.0438	2.0916	2.0787
U		1.0114	1.0147	1.0125	0.9827	0.9800	0.9739	0.9767	1.0026	0.9116	0.9001	0.9082	0.9106
V		0.0371	0.0966	0.1763	0.2546	0.2764	0.2566	0.1672	0.1325	0.0545	0.0405	0.0502	0.0504
W		-0.1926	-0.2004	-0.2012	-0.1112	-0.0108	0.1236	0.2614	0.2532	0.3398	0.4918	0.5030	0.4912
P	9	0.8560	0.8657	0.8552	0.7587	0.7297	0.8075	0.8338	0.7701	0.5941	0.8971	0.9574	0.9588
M		2.0282	2.0781	2.1205	2.0944	2.0548	2.0936	2.0685	1.9533	1.7629	2.0327	2.0579	2.0508
U		1.0139	1.0204	1.0216	1.0007	0.9914	1.0021	0.9980	0.9793	0.8908	0.9035	0.9077	0.9098
V		0.0509	0.1212	0.1864	0.2740	0.2760	0.2595	0.2132	0.1048	0.0346	0.0488	0.0614	0.0599
W		-0.1200	-0.1301	-0.1326	-0.0737	0.0274	0.0991	0.1610	0.1785	0.3045	0.4783	0.4835	0.4756
P	8				0.8617	0.8727	0.8706	0.8178	0.6666	0.5566	0.9434	0.9674	0.9707
M					2.0935	2.0917	2.0787	2.0198	1.8382	1.6907	2.0375	2.0408	2.0383
U					1.0115	1.0131	1.0100	1.0003	0.9590	0.8675	0.9075	0.9097	0.9120
V					0.2389	0.2310	0.2213	0.1844	0.0661	0.0107	0.0556	0.0677	0.0681
W					-0.0333	0.0242	0.0635	0.0740	0.0974	0.2991	0.4728	0.4688	0.4628
P	7						0.5276	0.4979	0.5472	0.5497	0.9417	0.9509	0.9848
M							1.7496	1.6872	1.7258	1.6902	2.0232	2.0071	2.0240
U							0.9219	0.9114	0.9280	0.8493	0.9037	0.9068	0.9144
V							0.1670	0.0935	0.0189	0.0123	0.0698	0.0735	0.0749
W							0.0371	-0.0185	0.0523	0.3467	0.4695	0.4530	0.4481
P	6							0.4148	0.4562	0.6297	0.9487	0.9461	0.9600
M								1.5363	1.5761	1.8098	2.0333	2.0207	2.0219
U								0.8580	0.8765	0.8588	0.9049	0.9075	0.9116
V								-0.0688	0.0004	0.0563	0.0900	0.0853	0.0843
W								-0.0375	-0.0127	0.0189	0.4698	0.4581	0.4509
P	5								0.4685	0.8778	0.9644	0.9680	0.9688
M									1.5935	2.0242	2.0492	2.0506	2.0460
U									0.8779	0.9089	0.9120	0.9139	0.9138
V									0.0359	0.0977	0.0983	0.0906	0.0882
W									0.0878	0.4558	0.4640	0.4634	0.4605

TABLE B-8. FINAL DATA SET FOR $M_\infty = 1.95$, $R_d = .48 \times 10^6$, $\alpha_b = 20°$, x/d = 8.5 (CONCLUDED)

PITOT PRESSURE PROBE	4	0.4182	0.9455	0.9613	0.9623	0.9706
		1.4372	2.0374	2.0381	2.0398	2.0425
		0.8100	0.9222	0.9147	0.9135	0.9149
		-0.0106	0.0945	0.0911	0.0907	0.0904
		0.1432	0.4367	0.4533	0.4569	0.4558
PITOT PRESSURE PROBE	3	0.3607	0.9575	0.9721	0.9681	0.9823
		1.2871	2.0564	2.0403	2.0347	2.0417
		0.7266	0.9236	0.9170	0.9150	0.9179
		-0.0687	0.0847	0.0867	0.0914	0.0926
		0.2885	0.4479	0.4510	0.4505	0.4488
PITOT PRESSURE PROBE	2		0.9426	0.9577	0.9625	0.9606
			2.0673	2.0370	2.0295	2.0210
			0.9175	0.9133	0.9141	0.9136
			0.0899	0.0878	0.0940	0.0954
			0.4658	0.4561	0.4487	0.4438
PITOT PRESSURE PROBE	1		0.9546	0.9584	0.9732	0.9789
			2.1048	2.0516	2.0389	2.0279
			0.9164	0.9121	0.9148	0.9164
			0.1092	0.0987	0.1021	0.1032
			0.4856	0.4652	0.4512	0.4409

TABLE B-9. FINAL DATA SET FOR M_∞ = 1.95, R_d = .48 x 10^6, α_b = 20°, x/d = 11

H28209

P -- P0/PDINF M -- MACH NUMBER U+V+W -- 3-D VELOCITY COMPONENTS/UINF

		1	2	3	4	5	6	7	8	9	10	11	12	13
P	24	0.9324	0.9349	0.8254	0.7581	0.7410	0.8022	0.8914	0.9311	0.9362	0.9583	0.9652	0.9700	0.9407
M		1.8693	1.8761	1.8339	1.8067	1.8379	1.8962	1.9608	1.9771	1.9729	1.9799	1.9794	1.9691	1.9428
U		0.9735	0.9715	0.9534	0.9351	0.9252	0.9184	0.9160	0.9114	0.9076	0.9110	0.9135	0.9158	0.9121
V		-0.0385	-0.0973	-0.1482	-0.1724	-0.1857	-0.2047	-0.2061	-0.1895	-0.1763	-0.1510	-0.1351	-0.1150	-0.0986
W		-0.0567	-0.0548	0.0025	0.1007	0.2069	0.2879	0.3532	0.3862	0.3980	0.4057	0.4053	0.3994	0.3926
P	23	0.9447	0.8815	0.7395	0.7077	0.6888	0.6992	0.7681	0.8821	0.8939	0.9644	0.9326	0.9575	0.9566
M		1.9252	1.8931	1.8132	1.8081	1.8356	1.8520	1.9124	1.9889	1.9852	2.0110	1.9686	1.9902	1.9830
U		0.9849	0.9727	0.9507	0.9413	0.9307	0.9096	0.9007	0.9076	0.8996	0.9085	0.9041	0.9119	0.9136
V		-0.0358	-0.0841	-0.1182	-0.1428	-0.1623	-0.1830	-0.1925	-0.1861	-0.1732	-0.1486	-0.1244	-0.1118	-0.1010
W		-0.1189	-0.1156	-0.0225	0.0937	0.1985	0.2847	0.3599	0.4051	0.4256	0.4331	0.4219	0.4234	0.4174
P	22	0.9430	0.8567	0.7065	0.7044	0.6861	0.6806	0.6972	0.8267	0.8734	0.9484	0.9532	0.9627	0.9689
M		1.9721	1.9202	1.8371	1.8584	1.8670	1.8659	1.8859	1.9838	2.0021	2.0382	2.0292	2.0146	2.0077
U		0.9915	0.9758	0.9599	0.9580	0.9382	0.9140	0.8897	0.8998	0.8965	0.9047	0.9067	0.9110	0.9150
V		-0.0304	-0.0659	-0.0999	-0.1377	-0.1627	-0.1703	-0.1711	-0.1682	-0.1547	-0.1391	-0.1185	-0.1029	-0.0952
W		-0.1701	-0.1616	-0.0372	0.0947	0.2104	0.2929	0.3759	0.4263	0.4499	0.4613	0.4576	0.4434	0.4324
P	21	0.9293	0.8203	0.7065	0.6812	0.6569	0.6711	0.6858	0.7393	0.8323	0.9502	0.9650	0.9559	0.9432
M		2.0284	1.9526	1.9032	1.9067	1.9132	1.9136	1.9249	1.9651	2.0346	2.0700	2.0456	2.0123	2.0030
U		0.9946	0.9774	0.9777	0.9747	0.9483	0.9211	0.8960	0.8865	0.8948	0.9061	0.9072	0.9095	0.9104
V		-0.0250	-0.0520	-0.0984	-0.1479	-0.1773	-0.1573	-0.1267	-0.1292	-0.1278	-0.1195	-0.0988	-0.0878	-0.0856
W		-0.2252	-0.2086	-0.0837	0.0511	0.2182	0.3250	0.4080	0.4541	0.4811	0.4827	0.4710	0.4483	0.4410
P	20	0.9394	0.8103	0.6629	0.5716	0.5693	0.5305	0.6917	0.7297	0.8095	0.8895	0.8151	0.8745	0.9311
M		2.0979	2.0106	1.9388	1.8963	1.9425	1.9011	2.0237	2.0208	2.0217	2.0225	1.9575	2.0668	2.1256
U		1.0021	0.9834	0.9814	0.9742	0.9547	0.9265	0.9125	0.8983	0.8934	0.8983	0.8823	0.8990	0.9106
V		-0.0211	-0.0399	-0.0882	-0.1388	-0.1745	-0.1444	-0.0969	-0.0737	-0.0891	-0.0787	-0.0591	-0.0835	-0.0905
W		-0.2811	-0.2575	-0.1503	-0.0009	0.2317	0.3034	0.4475	0.4778	0.4848	0.4780	0.4716	0.5014	0.5113
P	19	0.9203	0.7941	0.6048	0.4395	0.4484	0.4598	0.6805	0.7086	0.7346	0.8503	0.9301	0.9647	0.9545
M		2.1607	2.0759	1.9689	1.8372	1.8840	1.9081	2.0704	2.0282	2.0296	2.1587	2.2134	2.2093	2.1771
U		1.0034	0.9869	0.9790	0.9622	0.9389	0.9216	0.9070	0.8915	0.8803	0.8948	0.9067	0.9091	0.9108
V		-0.0167	-0.0293	-0.0594	-0.0791	-0.1167	-0.0836	-0.0619	-0.0355	-0.0557	-0.0751	-0.0801	-0.0775	-0.0738
W		-0.3328	-0.3112	-0.2188	-0.0303	0.2568	0.3452	0.4919	0.4988	0.5173	0.5571	0.5728	0.5578	0.5400
P	18	0.9324	0.8063	0.6253	0.4435	0.3946	0.4395	0.6649	0.7107	0.7464	0.8432	0.9613	0.9426	0.9709
M		2.2574	2.1786	2.0565	1.8790	1.8391	1.9214	2.1208	2.1317	2.1550	2.1928	2.2306	2.1842	2.1806
U		1.0073	0.9946	0.9935	0.9712	0.9274	0.9227	0.9002	0.8866	0.8869	0.8957	0.9089	0.9065	0.9148
V		-0.0034	-0.0082	-0.0331	-0.0364	-0.0623	-0.0330	-0.0222	-0.0171	-0.0250	-0.0344	-0.0628	-0.0540	-0.0573
W		-0.3923	-0.3714	-0.2696	-0.1165	0.2648	0.3616	0.5343	0.5620	0.5723	0.5756	0.5697	0.5523	0.5369
P	17	0.9304	0.7932	0.5708	0.3994	0.3502	0.4489	0.6826	0.7440	0.7755	0.8673	0.9589	0.9679	0.9812
M		2.3401	2.2418	2.0417	1.8358	1.7606	1.9408	2.1539	2.1772	2.1796	2.2175	2.2143	2.1866	2.1713
U		1.0108	0.9970	0.9837	0.9591	0.9226	0.9247	0.9030	0.8961	0.8955	0.9075	0.9116	0.9133	0.9174
V		0.0020	0.0003	-0.0137	-0.0064	-0.0347	-0.0121	-0.0023	-0.0052	-0.0124	-0.0182	-0.0449	-0.0434	-0.0417
W		-0.4340	-0.4079	-0.2909	-0.1102	0.1831	0.3733	0.5466	0.5689	0.5707	0.5692	0.5595	0.5438	0.5292
P	16	0.9201	0.7634	0.5561	0.3829	0.3479	0.4746	0.6882	0.7626	0.8389	0.9233	0.9556	0.9438	0.9784
M		2.4052	2.2646	2.0421	1.8045	1.7393	1.9625	2.1333	2.1721	2.2109	2.2174	2.1907	2.1497	2.1504
U		1.0121	0.9936	0.9819	0.9504	0.9149	0.9276	0.9034	0.9023	0.9122	0.9164	0.9139	0.9114	0.9186
V		-0.0095	-0.0011	-0.0143	-0.0012	-0.0213	-0.0002	0.0133	0.0084	-0.0012	-0.0033	-0.0257	-0.0258	-0.0276
W		-0.4668	-0.4300	-0.2973	-0.0970	0.1873	0.3830	0.5356	0.5565	0.5587	0.5549	0.5458	0.5297	0.5174
P	15	0.8938	0.7476	0.5805	0.4265	0.3729	0.5399	0.7430	0.7819	0.8320	0.9246	0.9657	0.9734	0.9687
M		2.4245	2.2613	2.0662	1.8765	1.7663	2.0141	2.1556	2.1512	2.1832	2.2023	2.1919	2.1666	2.1388
U		1.0082	0.9909	0.9777	0.9677	0.9227	0.9422	0.9222	0.9094	0.9162	0.9211	0.9213	0.9206	0.9189
V		-0.0082	-0.0164	-0.0191	-0.0010	-0.0141	0.0124	0.0240	0.0183	-0.0034	-0.0027	-0.0026	-0.0041	-0.0047
W		-0.4842	-0.4339	-0.3315	-0.1419	0.1949	0.3859	0.5138	0.5342	0.5389	0.5399	0.5344	0.5230	0.5115
P	14	0.8486	0.8409	0.5596	0.4183	0.4095	0.5172	0.7675	0.8076	0.8999	0.9634	0.9754	0.9707	0.9688
M		1.9325	1.9852	1.9765	1.8276	1.8139	1.9356	2.1318	2.1335	2.1888	2.1889	2.1669	2.1380	2.1175
U		0.9506	0.9602	0.9690	0.9574	0.9518	0.9335	0.9363	0.9233	0.9318	0.9286	0.9248	0.9214	0.9202
V		-0.0142	-0.0163	-0.0059	0.0117	0.0391	0.0458	0.0449	0.0322	0.0024	0.0059	0.0078	0.0069	0.0059
W		-0.2933	-0.3132	-0.2763	-0.1015	0.1062	0.3436	0.4729	0.4997	0.5144	0.5200	0.5155	0.5065	0.4977
P	13	0.8938	0.7878	0.5746	0.4412	0.4815	0.6161	0.7853	0.8578	0.9166	0.9820	0.9785	0.9671	0.9608
M		2.1539	2.1152	1.9664	1.8110	1.8592	1.9824	2.0810	2.1148	2.1438	2.1586	2.1348	2.1102	2.0900
U		0.9993	0.9899	0.9727	0.9539	0.9610	0.9511	0.9467	0.9373	0.9341	0.9320	0.9267	0.9223	0.9195
V		0.0052	0.0276	0.0418	0.0442	0.0779	0.0751	0.0507	0.0273	0.0053	0.0113	0.0128	0.0131	0.0137
W		-0.3400	-0.3355	-0.2483	-0.0709	0.1292	0.3294	0.4190	0.4622	0.4858	0.4979	0.4949	0.4895	0.4829
P	12	0.8272	0.7602	0.6909	0.5407	0.5796	0.7114	0.7373	0.7790	0.9246	0.9814	0.9793	0.9847	0.9724
M		2.0718	2.0364	2.0091	1.8730	1.8991	1.9939	2.0867	2.0150	2.0978	2.1192	2.1085	2.1005	2.0797
U		0.9935	0.9858	0.9826	0.9653	0.9687	0.9668	0.9505	0.9400	0.9333	0.9313	0.9277	0.9262	0.9226
V		0.0179	0.0573	0.0772	0.0991	0.1254	0.1010	0.0583	0.0148	-0.0020	0.0111	0.0159	0.0171	0.0191
W		-0.2804	-0.2729	-0.2503	-0.1133	0.1263	0.2835	0.3547	0.3919	0.4612	0.4775	0.4782	0.4764	0.4713
P	11	0.8440	0.7920	0.7262	0.6283	0.7476	0.8040	0.7673	0.7242	0.9296	0.9913	0.9732	0.9899	0.9867
M		2.0109	1.9880	1.9448	1.8633	1.9704	1.9998	1.9663	1.9126	2.0862	2.1008	2.0830	2.0869	2.0761
U		0.9942	0.9884	0.9763	0.9619	0.9880	0.9858	0.9666	0.9308	0.9344	0.9338	0.9275	0.9282	0.9255
V		0.0270	0.0792	0.1064	0.1396	0.1569	0.1163	0.0546	-0.0071	-0.0044	0.0107	0.0127	0.0210	0.0241
W		-0.2142	-0.1989	-0.1779	-0.0627	0.1055	0.2083	0.2689	0.3341	0.4394	0.4617	0.4638	0.4645	0.4632
P	10	0.8343	0.8245	0.8025	0.7542	0.7438	0.7988	0.7185	0.6576	0.9114	0.9778	0.9839	0.9767	0.9636
M		1.9589	1.9462	1.9285	1.9198	1.9190	1.9484	1.8828	1.8197	2.0360	2.0734	2.0604	2.0623	2.0476
U		0.9916	0.9878	0.9807	0.9772	0.9755	0.9847	0.9637	0.9120	0.9271	0.9296	0.9247	0.9245	0.9211
V		0.0162	0.0736	0.1154	0.1592	0.1604	0.1164	0.0361	-0.0242	-0.0094	0.0061	0.0101	0.0202	0.0258
W		-0.1434	-0.1290	-0.1100	-0.0455	0.0688	0.1261	0.1742	0.2998	0.4355	0.4538	0.4558	0.4570	0.4547
P	9	0.8498	0.8446	0.8568	0.8620	0.8499	0.8280	0.6836	0.5999	0.9310	0.9750	0.9790	0.9659	0.9444
M		1.9325	1.9341	1.9531	1.9713	1.9720	1.9512	1.8479	1.7451	2.0429	2.0641	2.0635	2.0485	2.0583
U		0.9916	0.9902	0.9920	0.9961	0.9967	0.9963	0.9649	0.8943	0.9284	0.9258	0.9253	0.9217	0.9254
V		0.0156	0.0687	0.1112	0.1408	0.1389	0.1001	0.0402	-0.0349	-0.0134	0.0048	0.0148	0.0220	0.0281
W		-0.0797	-0.0743	-0.0728	-0.0395	0.0088	0.0405	0.0822	0.2744	0.4371	0.4560	0.4564	0.4542	0.4525
P	8				0.8518	0.8516	0.7825	0.6287	0.5571	0.9126	0.9633	0.9896	0.9863	0.9812
M					1.9655	1.9766	1.9378	1.7969	1.7086	2.0402	2.0609	2.0567	2.0640	2.0534
U					0.9966	1.0004	0.9921	0.9522	0.8904	0.9196	0.9185	0.9204	0.9242	0.9243
V					0.1404	0.1185	0.0875	0.0384	-0.0547	-0.0240	0.0038	0.0173	0.0272	0.0324
W					-0.0372	-0.0260	-0.0296	0.0141	0.2400	0.4530	0.4686	0.4620	0.4584	0.4514
P	7						0.6573	0.5610	0.4427	0.8040	0.9418	0.9866	0.9697	0.9667
M							1.8654	1.7565	1.6101	1.9949	2.0587	2.0570	2.0491	2.0374
U							0.9816	0.9371	0.8712	0.8918	0.9077	0.9161	0.9190	0.9203
V							0.0792	0.0387	-0.0299	-0.0365	0.0152	0.0260	0.0341	0.0373
W							-0.0830	-0.0498	0.1746	0.4796	0.4878	0.4703	0.4593	0.4491

TABLE B-9. FINAL DATA SET FOR $M_\infty = 1.95$, $R_d = .48 \times 10^6$, $\alpha_b = 20°$, x/d = 11 (CONCLUDED)

K-CNTR	K-CNTD						
6		0.5143	0.3992	0.7319	0.9668	0.9683	0.9880	0.9658
		1.7258	1.5736	1.9550	2.0797	2.0580	2.0555	2.0305
		0.9233	0.8644	0.8686	0.9100	0.9147	0.9224	0.9204
		0.0573	0.0448	0.0154	0.0446	0.0446	0.0469	0.0456
		-0.0910	0.1324	0.4982	0.4935	0.4722	0.4551	0.4438
5			0.4278	0.8978	0.9585	0.9842	0.9798	0.9771
			1.5573	2.0379	2.0426	2.0515	2.0407	2.0336
			0.8546	0.9038	0.9108	0.9187	0.9210	0.9231
			0.0896	0.0735	0.0692	0.0617	0.0574	0.0550
			0.1332	0.4777	0.4676	0.4584	0.4477	0.4391
4			0.4167	0.9531	0.9655	0.9512	0.9565	0.9801
			1.4405	2.0504	2.0534	2.0231	2.0126	2.0269
			0.8098	0.9183	0.9172	0.9165	0.9180	0.9244
			0.0172	0.0848	0.0807	0.0694	0.0638	0.0620
			0.1512	0.4549	0.4596	0.4440	0.4349	0.4310
3			0.3887	0.9496	0.9572	0.9612	0.9584	0.9687
			1.3693	2.0724	2.0657	2.0628	2.0579	2.0576
			0.7624	0.9158	0.9165	0.9184	0.9215	0.9251
			-0.0567	0.0764	0.0845	0.0821	0.0760	0.0710
			0.2165	0.4745	0.4678	0.4623	0.4546	0.4478
2				0.9406	0.9445	0.9450	0.9579	0.9728
				2.0845	2.0670	2.0632	2.0723	2.0730
				0.9114	0.9151	0.9176	0.9228	0.9262
				0.0973	0.0942	0.0880	0.0811	0.0790
				0.4861	0.4694	0.4635	0.4599	0.4537
1				0.9365	0.9325	0.9765	0.9464	0.9847
				2.1298	2.1037	2.1182	2.0711	2.0735
				0.9126	0.9166	0.9260	0.9207	0.9279
				0.1240	0.1047	0.0951	0.0904	0.0915
				0.5025	0.4856	0.4778	0.4616	0.4482

TABLE B-10. FINAL DATA SET FOR M_∞ = 1.95, R_d = .48 x 10^6, α_b = 25°, x/d = 6

M2R2G10

P -- P0/P0INF M -- MACH NUMBER U,V,W -- 3-D VELOCITY COMPONENTS/UINF

		1	2	3	4	5	6	7	8	9	10	11
P	20	0.8385	0.8648	0.8793	0.9027	0.8592	0.8986	0.9066	0.8969	0.8965	0.9188	0.9206
M		1.7763	1.8141	1.8797	1.9300	1.9279	1.9679	1.9808	2.0079	2.0532	2.0992	2.0984
U		0.9415	0.9459	0.9376	0.9312	0.9090	0.9046	0.9031	0.9008	0.8998	0.9000	0.8954
V		-0.0577	-0.1166	-0.2020	-0.2188	-0.2309	-0.2159	-0.1918	-0.1906	-0.1904	-0.1877	-0.1630
W		0.0765	0.1026	0.1964	0.2708	0.3277	0.3814	0.4067	0.4308	0.4616	0.4891	0.5057
P	19	0.8526	0.8733	0.8104	0.8235	0.8160	0.8719	0.8852	0.8408	0.8987	0.9196	0.9216
M		1.8434	1.8648	1.8950	1.9364	1.9600	1.9847	1.9969	2.1480	2.2049	2.1980	2.1555
U		0.9659	0.9638	0.9356	0.9188	0.8991	0.8995	0.8980	0.8886	0.8908	0.8932	0.8908
V		-0.0612	-0.1424	-0.2486	-0.2532	-0.2588	-0.2236	-0.2041	-0.2595	-0.2324	-0.2041	-0.1641
W		0.0041	0.0211	0.1743	0.2894	0.3611	0.4013	0.4232	0.5040	0.5419	0.5461	0.5427
P	18	0.8642	0.7965	0.6436	0.7908	0.8207	0.8678	0.8869	0.9143	0.9281	0.9408	0.9248
M		1.9270	1.8982	1.9171	2.0501	2.0575	2.0056	2.4247	2.3629	2.3658	2.2394	2.1788
U		0.9878	0.9696	0.9405	0.9264	0.8956	0.9208	0.8741	0.8723	0.8772	0.8793	0.8776
V		-0.0586	-0.1504	-0.2812	-0.3127	-0.2848	-0.2013	-0.3208	-0.2856	-0.2368	-0.1916	-0.1621
W		-0.0857	-0.0824	0.1309	0.3180	0.4221	0.3790	0.6197	0.6157	0.6061	0.5911	0.5763
P	17	0.8791	0.7199	0.5188	0.5417	0.4829	0.7707	0.9052	0.9160	0.9263	0.9486	0.9499
M		2.0699	2.0058	1.9449	1.9332	1.8192	2.4814	2.4881	2.3919	2.3217	2.2464	2.1975
U		1.0102	0.9928	0.9740	0.9186	0.8445	0.8648	0.8691	0.8644	0.8690	0.8735	0.8752
V		-0.0428	-0.0838	-0.1655	-0.2207	-0.1548	-0.3643	-0.3137	-0.2727	-0.2226	-0.1758	-0.1472
W		-0.1865	-0.1988	0.1448	0.3125	0.4299	0.6566	0.6533	0.6432	0.6294	0.6082	0.5914
P	16	0.8973	0.6690	0.4848	0.4770	0.4470	0.7714	0.9231	0.9470	0.9244	0.9006	0.9177
M		2.1779	2.0823	2.0147	2.0671	2.1392	2.5822	2.5744	2.4729	2.3550	2.2121	2.1676
U		1.0241	1.0007	1.0111	0.9979	0.8673	0.8505	0.8636	0.8617	0.8622	0.8602	0.8654
V		-0.0158	-0.0184	-0.1209	-0.1466	-0.2009	-0.3522	-0.2959	-0.2512	-0.2002	-0.1545	-0.1265
W		-0.2789	-0.2707	0.0143	0.2221	0.5601	0.6898	0.6972	0.6841	0.6587	0.6174	0.5972
P	15	0.9095	0.6401	0.3520	0.3310	0.4795	0.6635	0.9458	0.9800	0.9536	0.9619	0.9453
M		2.3268	2.2050	1.9579	1.9988	2.2988	2.5640	2.5965	2.4853	2.3980	2.3062	2.2234
U		1.0381	1.0071	0.9997	0.9936	0.9170	0.8742	0.8643	0.8626	0.8620	0.8649	0.8635
V		0.0041	0.0419	-0.0056	-0.0888	-0.1986	-0.3140	-0.2842	-0.2328	-0.1831	-0.1377	-0.1047
W		-0.3547	-0.3540	-0.0716	0.1819	0.5561	0.6723	0.7081	0.6936	0.6794	0.6529	0.6279
P	14	0.8932	0.6589	0.2855	0.2497	0.5493	0.5167	0.8504	0.9746	0.9581	0.9526	0.9584
M		2.4730	2.3567	1.9071	1.9025	2.4560	2.3879	2.5170	2.4523	2.3707	2.2687	2.2051
U		1.0458	1.0154	0.9767	0.9833	0.9804	0.8849	0.8577	0.8589	0.8584	0.8596	0.8628
V		0.0204	0.0828	0.0831	-0.0180	-0.1952	-0.2527	-0.2665	-0.2098	-0.1587	-0.1134	-0.0835
W		-0.4237	-0.4248	-0.1335	0.0707	0.5163	0.6217	0.6980	0.6944	0.6805	0.6500	0.6244
P	13	0.9184	0.7807	0.3719	0.2253	0.2016	0.5400	0.5420	0.6793	0.9651	0.9609	0.9336
M		2.6769	2.6104	2.1637	1.8444	1.7763	2.4503	2.3788	2.3577	2.3328	2.2353	2.1558
U		1.0602	1.0417	1.0000	0.9648	0.9342	0.9857	0.9163	0.8511	0.8564	0.8587	0.8574
V		0.0416	0.0967	0.1078	0.0344	-0.0625	-0.1767	-0.1875	-0.1963	-0.1297	-0.0882	-0.0604
W		-0.4837	-0.4906	-0.3283	-0.0726	0.1377	0.5101	0.5952	0.6751	0.6755	0.6418	0.6135
P	12	0.8999	0.8153	0.5981	0.3149	0.2024	0.3692	0.6246	0.5756	0.9599	0.9578	0.9493
M		2.8036	2.7605	2.5613	2.1516	1.8070	2.1911	2.4415	2.2131	2.2761	2.1888	2.1323
U		1.0629	1.0516	1.0266	1.0132	0.9561	0.9624	0.9893	0.9556	0.8530	0.8562	0.8589
V		0.0432	0.0959	0.1330	0.1064	0.0031	-0.1333	-0.1237	-0.1427	-0.0966	-0.0606	-0.0388
W		-0.5396	-0.5317	-0.4920	-0.2738	-0.0197	0.4359	0.5147	0.6270	0.6641	0.6292	0.6028
P	11	0.8464	0.8131	0.6049	0.3136	0.2067	0.3462	0.5904	0.5116	0.8180	0.9289	0.9335
M		2.9047	2.8582	2.6148	2.1281	1.8655	2.0908	2.2984	2.0515	2.2551	2.1817	2.1285
U		1.0644	1.0552	1.0268	0.9982	0.9721	0.9740	0.9904	0.9676	0.8513	0.8475	0.8525
V		0.0423	0.0837	0.1155	0.1029	0.0576	-0.0175	-0.0522	-0.0640	-0.0693	-0.0447	-0.0211
W		-0.5692	-0.5618	-0.5192	-0.3053	-0.0422	0.3618	0.4535	0.5488	0.6616	0.6393	0.6109
P	10	0.7002	0.7333	0.7102	0.4090	0.2435	0.5360	0.6743	0.4945	0.8041	0.8848	0.9280
M		2.1311	2.2008	2.2701	2.1366	1.8671	2.2118	2.2315	1.9250	2.1814	2.1076	2.1015
U		1.0325	1.0400	1.0416	1.0004	0.9594	1.0147	1.0133	0.8823	0.8519	0.8382	0.8510
V		0.0375	0.0831	0.1327	0.1913	0.1681	0.1535	0.0832	0.0015	-0.0277	-0.0180	-0.0003
W		-0.1854	-0.2246	-0.2692	-0.2598	-0.0467	0.3029	0.3483	0.4549	0.6343	0.6214	0.6013
P	9	0.7487	0.7308	0.7255	0.5488	0.3806	0.7826	0.7748	0.5881	0.8236	0.9255	0.8978
M		2.1160	2.1462	2.2064	2.1051	1.9252	2.2202	2.1856	1.9711	2.1445	2.1504	2.0886
U		1.0367	1.0350	1.0352	0.9924	0.9389	1.0354	1.0312	0.9666	0.8553	0.8551	0.8465
V		0.0569	0.1264	0.1916	0.2901	0.3223	0.2205	0.1182	0.0730	0.0027	0.0259	0.0075
W		-0.1254	-0.1510	-0.1838	-0.1367	0.0061	0.1692	0.2316	0.2693	0.6144	0.6167	0.6017
P	8				0.7624	0.7207	0.7569	0.7540	0.4786	0.8471	0.8912	0.9162
M					2.1983	2.1809	2.1599	2.0931	1.7680	2.1360	2.1377	2.1530
U					1.0303	1.0193	1.0252	1.0280	0.9323	0.8547	0.8523	0.8527
V					0.2673	0.2963	0.2447	0.1307	0.0644	0.0234	0.0360	-0.0056
W					-0.0692	-0.0017	0.0805	0.0845	0.1307	0.6112	0.6146	0.6217
P	7						0.6618	0.6241	0.3404	0.8702	0.9104	0.8939
M							2.0829	1.9784	1.4725	2.1613	2.1974	2.1202
U							1.0163	1.0045	0.8346	0.8539	0.8587	0.8459
V							0.2043	0.0716	0.0197	0.0383	0.0260	0.0019
W							-0.0298	-0.0483	0.0576	0.6224	0.6319	0.6167
P	6							0.4522	0.3060	0.9101	0.9411	0.8939
M								1.8008	1.4750	2.2206	2.2074	2.0990
U								0.9470	0.8268	0.8611	0.8660	0.8507
V								-0.0102	-0.0160	0.0377	0.0384	0.0201
W								-0.1175	0.1344	0.6376	0.6254	0.6002
P	5								0.3405	0.9244	0.9306	0.9360
M									1.5883	2.2100	2.1617	2.1312
U									0.8601	0.8629	0.8654	0.8662
V									0.0125	0.0553	0.0602	0.0577
W									0.1908	0.6294	0.6048	0.5902
P	4								0.3136	0.9309	0.9313	0.9504
M									1.4307	2.1746	2.1445	2.1323
U									0.8017	0.8670	0.8671	0.8701
V									-0.0026	0.0801	0.0740	0.0706
W									0.1723	0.6059	0.5931	0.5835
P	3									0.9216	0.9518	0.9417
M										2.1558	2.1533	2.1179
U										0.8656	0.8722	0.8701
V										0.0916	0.0853	0.0802
W										0.5979	0.5881	0.5756

TABLE B-10. FINAL DATA SET FOR $M_\infty = 1.95$, $R_d = .48 \times 10^6$, $\alpha_b = 25°$, x/d = 6 (CONCLUDED)

P	2		
M			
U		0.9199	0.9431	0.9178
V		2.1500	2.1350	2.1000
W		0.0858	0.0713	0.0683
		0.1028	0.0969	0.0980
		0.5932	0.5792	0.5682
P	1			
M		0.0958	0.0805	0.0823
U		2.1306	2.1785	2.1218
V		0.0625	0.0787	0.0792
W		0.1187	0.1019	0.1023
		0.5862	0.5871	0.5598

TABLE B-11. FINAL DATA SET FOR M_∞ = 1.95, R_d = .48 x 10^6, α_b = 25°, x/d = 9

M2R2G11

P -- P0/P0INF M -- MACH NUMBER U,V,W -- 3-D VELOCITY COMPONENTS/U1NF

		1	2	3	4	5	6	7	8	9	10	11	12
P	22	0.8554	0.7033	0.5381	0.4936	0.4778	0.5666	0.7498	0.8636	0.9019	0.9345	0.9388	0.9445
M		2.1496	2.0566	1.9390	1.9033	1.9047	1.9773	2.1763	2.3145	2.3571	2.3778	2.3420	2.2984
U		1.0086	0.9937	0.9937	0.9537	0.9482	0.8867	0.8498	0.8459	0.8525	0.8614	0.8631	0.8657
V		-0.0093	-0.0096	-0.0349	-0.0989	-0.0932	-0.0895	-0.1083	-0.1512	-0.1798	-0.1850	-0.1732	-0.1569
W		-0.3188	-0.2708	-0.0695	0.2307	0.2563	0.4707	0.6262	0.6775	0.6778	0.6725	0.6603	0.6444
P	21	0.8378	0.6909	0.5073	0.4508	0.4417	0.5514	0.7422	0.8688	0.9051	0.9299	0.9337	0.9458
M		2.2207	2.1169	1.9625	1.8961	1.9063	2.0485	2.2579	2.3856	2.4008	2.3748	2.3316	2.2899
U		1.0098	0.9971	0.9970	0.9563	0.9518	0.8907	0.8563	0.8489	0.8515	0.8596	0.8614	0.8643
V		-0.0015	0.0035	-0.0090	-0.0709	-0.0732	-0.0846	-0.1276	-0.1444	-0.1707	-0.1726	-0.1585	-0.1421
W		-0.3603	-0.3160	-0.1145	0.2206	0.2513	0.5057	0.6474	0.6995	0.6967	0.6770	0.6624	0.6463
P	20	0.8150	0.6652	0.4834	0.4198	0.4148	0.5577	0.6941	0.8971	0.9095	0.9353	0.9317	0.9389
M		2.2757	2.1492	1.9758	1.8934	1.9087	2.1050	2.2541	2.4182	2.4124	2.3926	2.3395	2.2732
U		1.0098	0.9945	0.9967	0.9602	0.9565	0.9073	0.8609	0.8535	0.8508	0.8584	0.8593	0.8621
V		0.0006	0.0075	0.0035	-0.0571	-0.0685	-0.0880	-0.1323	-0.1521	-0.1632	-0.1531	-0.1384	-0.1268
W		-0.3975	-0.3502	-0.1469	0.2035	0.2371	0.5067	0.6389	0.7045	0.7034	0.6895	0.6725	0.6459
P	19	0.8393	0.6136	0.4488	0.3597	0.4303	0.5509	0.6132	0.8652	0.9159	0.9312	0.9490	0.9492
M		2.3674	2.1463	1.9627	1.8343	1.9859	2.1280	2.2158	2.4274	2.4170	2.3719	2.3284	2.2863
U		1.0191	0.9942	0.9929	0.9640	0.9692	0.9267	0.8572	0.8532	0.8538	0.8518	0.8572	0.8593
V		0.0099	0.0087	0.0070	-0.0351	-0.0657	-0.0890	-0.1347	-0.1564	-0.1536	-0.1426	-0.1247	-0.1119
W		-0.4299	-0.3487	-0.1467	0.0252	0.2777	0.4832	0.6277	0.7071	0.7034	0.6926	0.6737	0.6575
P	18	0.8226	0.6105	0.4387	0.3360	0.3950	0.5408	0.5633	0.7863	0.9226	0.9261	0.9519	0.9501
M		2.4011	2.1842	1.9894	1.8246	1.9626	2.1507	2.1879	2.3833	2.4075	2.3442	2.3053	2.2627
U		1.0179	0.9957	0.9950	0.9612	0.9695	0.9426	0.8642	0.8488	0.8543	0.8504	0.8571	0.8589
V		0.0085	0.0006	0.0073	-0.0366	-0.0668	-0.0887	-0.1239	-0.1524	-0.1400	-0.1244	-0.1071	-0.0950
W		-0.4512	-0.3726	-0.1807	-0.0074	0.2507	0.4648	0.6084	0.6981	0.7024	0.6880	0.6683	0.6514
P	17	0.8158	0.6010	0.4250	0.3120	0.3669	0.5404	0.5529	0.7037	0.9364	0.9592	0.9642	0.9522
M		2.4273	2.2086	2.0075	1.8052	1.9435	2.1799	2.1920	2.3161	2.3957	2.3376	2.2845	2.2368
U		1.0173	0.9958	0.9950	0.9543	0.9678	0.9566	0.8799	0.8443	0.8561	0.8551	0.8593	0.8597
V		0.0012	-0.0065	0.0040	-0.0366	-0.0659	-0.0857	-0.1017	-0.1365	-0.1234	-0.1056	-0.0888	-0.0765
W		-0.4663	-0.3893	-0.2076	-0.0370	0.2348	0.4535	0.5915	0.6831	0.6993	0.6829	0.6603	0.6426
P	16	0.8028	0.6215	0.4218	0.3318	0.3415	0.5119	0.5941	0.6468	0.9458	0.9421	0.9410	0.9678
M		2.4327	2.2717	2.0435	1.8779	1.9153	2.1568	2.2348	2.2483	2.3769	2.2911	2.2365	2.2192
U		1.0138	1.0035	0.9999	0.9763	0.9641	0.9551	0.9037	0.8454	0.8598	0.8540	0.8577	0.8635
V		-0.0022	-0.0047	0.0028	-0.0159	-0.0595	-0.0782	-0.0762	-0.1045	-0.1027	-0.0814	-0.0652	-0.0577
W		-0.4764	-0.4107	-0.2316	-0.0635	0.2161	0.4443	0.5783	0.6619	0.6916	0.6705	0.6464	0.6323
P	15	0.7711	0.5870	0.4059	0.3177	0.3024	0.4896	0.6380	0.6441	0.9417	0.9615	0.9574	0.9662
M		2.4060	2.2454	2.0300	1.8735	1.8382	2.1329	2.2515	2.2093	2.3346	2.2710	2.2190	2.1911
U		1.0062	0.9990	0.9952	0.9742	0.9510	0.9567	0.9236	0.8556	0.8630	0.8602	0.8623	0.8651
V		-0.0060	-0.0086	0.0003	-0.0122	-0.0462	-0.0663	-0.0550	-0.0705	-0.0766	-0.0584	-0.0458	-0.0383
W		-0.4791	-0.4053	-0.2358	-0.0745	0.1645	0.4280	0.5562	0.6377	0.6758	0.6572	0.6348	0.6198
P	14	0.7621	0.5572	0.3831	0.3000	0.2953	0.4624	0.6763	0.7014	0.9475	0.9692	0.9824	0.9719
M		2.3648	2.1952	1.9820	1.8241	1.8076	2.1010	2.2385	2.2169	2.2917	2.2826	2.2394	2.1909
U		1.0028	0.9967	0.9859	0.9598	0.9451	0.9538	0.9360	0.8772	0.8688	0.8668	0.8667	0.8675
V		-0.0092	-0.0101	0.0046	-0.0013	-0.0234	-0.0479	-0.0379	-0.0456	-0.0469	-0.0269	-0.0192	-0.0130
W		-0.4652	-0.3777	-0.2156	-0.0611	0.1457	0.4165	0.5303	0.6131	0.6549	0.6551	0.6358	0.6173
P	13	0.8055	0.6494	0.4158	0.3131	0.3191	0.5188	0.6969	0.7356	0.7249	0.9819	0.9772	0.9709
M		2.2344	2.1495	1.9970	1.8414	1.8314	2.1089	2.1908	2.1833	2.1415	2.2374	2.1956	2.1556
U		1.0027	0.9930	0.9869	0.9643	0.9520	0.9658	0.9453	0.8914	0.8613	0.8734	0.8712	0.8691
V		0.0240	0.0326	0.0347	0.0282	0.0021	-0.0220	-0.0213	-0.0309	-0.0203	-0.0085	-0.0046	0.0004
W		-0.3860	-0.3531	-0.2281	-0.0688	0.1521	0.3955	0.4896	0.5781	0.6044	0.6286	0.6143	0.5998
P	12	0.8298	0.7154	0.5099	0.3716	0.3345	0.4304	0.6876	0.6783	0.8191	0.9594	0.9737	0.9792
M		2.3850	2.3069	2.1261	1.9159	1.8309	1.9468	2.1609	2.1000	2.1538	2.1940	2.1774	2.1495
U		1.0169	1.0136	1.0025	0.9764	0.9588	0.9520	0.9736	0.9308	0.8809	0.8748	0.8724	0.8707
V		0.0379	0.0728	0.0790	0.0740	0.0512	0.0299	0.0139	-0.0012	-0.0079	0.0024	0.0058	0.0120
W		-0.4432	-0.4010	-0.2908	-0.1455	0.0852	0.3014	0.4121	0.4674	0.5814	0.6085	0.6046	0.5946
P	11	0.7043	0.6443	0.5055	0.3976	0.4362	0.5465	0.7304	0.6563	0.8722	0.9612	0.9785	0.9814
M		2.1821	2.1848	2.0440	1.8961	1.9408	2.0225	2.1051	1.9963	2.1264	2.1530	2.1470	2.1106
U		1.0013	1.0005	0.9901	0.9722	0.9849	0.9802	0.9908	0.9323	0.8860	0.8751	0.8732	0.8685
V		0.0369	0.0745	0.0977	0.1112	0.1183	0.0910	0.0449	-0.0163	-0.0094	0.0048	0.0136	0.0191
W		-0.3539	-0.3521	-0.2530	-0.1035	0.1034	0.2694	0.3225	0.3965	0.5605	0.5898	0.5897	0.5797
P	10	0.7584	0.7100	0.5848	0.4798	0.6144	0.7026	0.7096	0.5502	0.8046	0.9578	0.9692	0.9543
M		2.0448	2.0609	1.9972	1.9040	2.0530	2.0863	2.0429	1.8401	2.0567	2.1357	2.1230	2.0927
U		1.0024	0.9997	0.9851	0.9671	1.0041	1.0078	0.9954	0.9287	0.8678	0.8695	0.8704	0.8669
V		0.0567	0.1193	0.1711	0.1913	0.2010	0.1531	0.0715	-0.0169	-0.0429	0.0077	0.0196	0.0263
W		-0.2148	-0.2228	-0.1661	-0.0324	0.1015	0.1955	0.2390	0.2683	0.5532	0.5902	0.5826	0.5733
P	9	0.7784	0.7802	0.7249	0.6989	0.7620	0.7621	0.7144	0.6481	0.6947	0.9531	0.9450	0.9365
M		1.9980	2.0384	2.0284	2.0381	2.0784	2.0695	2.0183	1.7067	1.9768	2.1328	2.1104	2.0946
U		1.0040	1.0069	0.9966	0.9947	1.0143	1.0173	1.0103	0.9094	0.8349	0.8628	0.8641	0.8635
V		0.0683	0.1337	0.2035	0.2448	0.2052	0.1604	0.0859	0.0168	-0.0353	0.0209	0.0273	0.0288
W		-0.1227	-0.1376	-0.1015	-0.0347	0.0459	0.0864	0.1061	0.1575	0.5633	0.5982	0.5857	0.5791
P	8				0.7785	0.7671	0.7484	0.6671	0.3753	0.6902	0.9520	0.9550	0.9462
M					2.0535	2.0617	2.0527	1.9851	1.5772	1.9826	2.1565	2.1461	2.1251
U					1.0077	1.0118	1.0160	1.0063	0.8707	0.8242	0.8585	0.8630	0.8634
V					0.2035	0.1996	0.1619	0.0871	0.0492	-0.0011	0.0423	0.0357	0.0329
W					-0.0472	-0.0136	0.0145	-0.0066	0.0928	0.5828	0.6138	0.6032	0.5934
P	7						0.6295	0.5908	0.3434	0.7638	0.9684	0.9619	0.9586
M							1.9479	1.9174	1.4923	2.0483	2.1752	2.1514	2.1229
U							0.9884	0.9838	0.8384	0.8315	0.8619	0.8634	0.8649
V							0.1343	0.0904	0.0504	0.0348	0.0570	0.0486	0.0461
W							-0.0500	-0.0693	0.0883	0.6030	0.6160	0.6041	0.5893
P	6							0.4841	0.3533	0.9179	0.9639	0.9420	0.9388
M								1.7717	1.4919	2.1483	2.1526	2.1193	2.0919
U								0.9365	0.8352	0.8596	0.8651	0.8630	0.8614
V								0.0782	0.0389	0.0623	0.0672	0.0597	0.0530
W								-0.0987	0.1185	0.6069	0.6005	0.5891	0.5794
P	5								0.3504	0.9467	0.9654	0.9699	0.9540
M									1.4721	2.1472	2.1217	2.1233	2.0835
U									0.8260	0.8662	0.8654	0.8693	0.8609
V									0.0219	0.0783	0.0741	0.0692	0.0570
W									0.1312	0.5979	0.5850	0.5806	0.5757

TABLE B-11. FINAL DATA SHEET FOR M_∞ = 1.95, R_d = .48 x 10^6, α_b = 25°, x/d = 9 (CONCLUDED)

4	0.2924	0.9208	0.9584	0.9365	0.9365
	1.2998	2.1264	2.1386	2.0924	2.0484
	0.7320	0.8632	0.8697	0.8653	0.8572
	-0.8114	0.0928	0.0815	0.0734	0.0627
	0.2208	0.5879	0.5856	0.5715	0.5634
3	0.2994	0.9489	0.9443	0.9448	0.9396
	1.3122	2.1633	2.1565	2.1206	2.0769
	0.6873	0.8658	0.8671	0.8625	0.8569
	-0.9331	0.0977	0.0894	0.0799	0.0742
	0.3457	0.6811	0.5964	0.5881	0.5764
2		0.9464	0.9269	0.9789	1.0020
		2.1798	2.1502	2.1511	2.1194
		0.8651	0.8660	0.8608	0.8646
		0.1116	0.0991	0.0816	0.0859
		0.6060	0.5936	0.6041	0.5836
1		0.9813	0.9976	1.0038	1.0051
		2.2547	2.1724	2.1067	2.0650
		0.8721	0.8687	0.8642	0.8658
		0.1110	0.1132	0.1077	0.1069
		0.6279	0.5971	0.5746	0.5518

TABLE B-12. FINAL DATA SET FOR $M_\infty = 2.$, $R_d = 1.75 \times 10^6$, $\alpha_b = 10°$, $x/d = 8$ M2R7G1

P -- P0/P0INF M -- MACH NUMBER U,V,W -- 3-D VELOCITY COMPONENTS/UINF

		1	2	3	4	5	6	7	8	9	10
P	13	0.9830	0.9479	0.9552	0.9565	0.9562	0.9273	0.9697	0.9749	0.9751	0.9831
M		1.9990	1.9726	1.9815	1.9837	1.9864	1.9398	2.0016	2.0088	2.0143	2.0231
U		0.9983	0.9908	0.9919	0.9898	0.9872	0.9683	0.9807	0.9811	0.9824	0.9850
V		0.0056	-0.0150	-0.0433	-0.0687	-0.0844	-0.1049	-0.1195	-0.1006	-0.0849	-0.0652
W		0.0533	0.0526	0.0622	0.0803	0.1040	0.1327	0.1575	0.1795	0.1888	0.1957
P	12	0.9830	0.9460	0.9514	0.9520	0.9531	0.9258	0.9660	0.9670	0.9730	0.9829
M		2.0055	1.9773	1.9885	1.9935	1.9973	1.9569	2.0164	2.0158	2.0214	2.0295
U		1.0042	0.9932	0.9948	0.9926	0.9885	0.9689	0.9767	0.9770	0.9798	0.9836
V		0.0058	-0.0188	-0.0548	-0.0917	-0.1171	-0.1402	-0.1487	-0.1125	-0.0904	-0.0664
W		0.0259	0.0242	0.0319	0.0520	0.0877	0.1323	0.1815	0.2041	0.2089	0.2106
P	11	0.9695	0.9417	0.9570	0.9515	0.9489	0.9410	0.9005	0.9640	0.9734	0.9744
M		2.0067	1.9872	2.0073	2.0192	2.0381	2.0251	2.0163	2.0323	2.0304	2.0285
U		1.0018	0.9962	1.0001	0.9977	0.9937	0.9804	0.9615	0.9718	0.9765	0.9801
V		0.0063	-0.0197	-0.0628	-0.1231	-0.1755	-0.1828	-0.1853	-0.1206	-0.0905	-0.0652
W		-0.0031	-0.0054	-0.0086	-0.0001	0.0534	0.1389	0.2242	0.2427	0.2348	0.2256
P	10	0.9688	0.9443	0.9512	0.7060	0.4832	0.5417	0.5302	0.9747	0.9686	0.9794
M		2.0171	2.0023	2.0180	1.8824	1.6773	1.7529	1.6994	2.0568	2.0314	2.0346
U		1.0044	1.0001	1.0023	0.9533	0.8803	0.8884	0.8563	0.9897	0.9726	0.9795
V		0.0038	-0.0102	-0.0421	-0.1064	-0.1874	-0.2181	-0.1604	-0.1060	-0.0790	-0.0581
W		-0.0255	-0.0307	-0.0593	-0.1143	-0.0116	0.1397	0.2546	0.2821	0.2551	0.2372
P	9	0.9800	0.9317	0.9364	0.4840	0.3251	0.3771	0.5506	0.9385	0.9725	0.9778
M		2.0343	2.0034	2.0320	1.6664	1.4666	1.5745	1.7510	2.0332	2.0306	2.0326
U		1.0090	1.0001	1.0043	0.8815	0.8215	0.8461	0.8896	0.9660	0.9728	0.9781
V		-0.0002	0.0121	0.0245	0.0463	-0.0324	-0.1018	-0.0212	-0.0741	-0.0580	-0.0474
W		-0.0286	-0.0403	-0.0925	-0.1553	-0.0308	0.1399	0.2518	0.2823	0.2592	0.2429
P	8				0.7364	0.3747	0.3689	0.5947	0.8858	0.9631	0.9759
M					1.9582	1.5498	1.5180	1.7316	1.9682	2.0148	2.0296
U					0.9605	0.8286	0.8273	0.9020	0.9589	0.9709	0.9770
V					0.1948	0.2065	0.0915	0.1257	-0.0567	-0.0425	-0.0384
W					-0.1268	-0.0304	0.1303	0.1186	0.2441	0.2524	0.2456
P	7						0.6846	0.3768	0.7325	0.9588	0.9790
M							1.7933	1.3850	1.8327	2.0107	2.0302
U							0.9007	0.7865	0.9212	0.9701	0.9767
V							0.2415	-0.0405	-0.0900	-0.0403	-0.0321
W							0.1053	-0.0598	0.2177	0.2514	0.2483
P	6								0.5336	0.9730	0.9894
M									1.6115	2.0266	2.0259
U									0.8447	0.9730	0.9748
V									-0.0927	-0.0359	-0.0263
W									0.2168	0.2584	0.2518
P	5								0.4647	0.9749	0.9806
M									1.5749	2.0280	2.0354
U									0.8378	0.9729	0.9769
V									-0.1162	-0.0280	-0.0201
W									0.1749	0.2612	0.2545
P	4								0.3779	0.9297	0.9774
M									1.4289	1.9919	2.0360
U									0.7831	0.9625	0.9766
V									-0.1278	-0.0256	-0.0143
W									0.1598	0.2617	0.2569
P	3									0.9481	0.9855
M										2.0367	2.0438
U										0.9733	0.9783
V										-0.0182	-0.0074
W										0.2696	0.2589
P	2									0.9711	0.9782
M										2.0837	2.0446
U										0.9816	0.9771
V										0.0098	0.0024
W										0.2867	0.2641
P	1									0.9674	0.9788
M										2.0917	2.0465
U										0.9815	0.9766
V										0.0332	0.0162
W										0.2926	0.2676

TABLE B-13. FINAL DATA SET FOR $M_\infty = 2.$, $R_d = 1.75 \times 10^6$, $\alpha_b = 10°$, $x/d = 11$

M2BTG2

P -- P0/P0INF M -- MACH NUMBER U,V,W -- 3-D VELOCITY COMPONENTS/U1NF

		1	2	3	4	5	6	7	8	9	10
P	18	0.9883	0.9689	0.9648	0.9701	0.9734	0.9825	0.9741	0.9773	0.9824	0.9869
M		1.9748	1.9540	1.9773	1.9816	1.9829	1.9879	1.9925	2.0013	2.0059	2.0075
U		0.9967	0.9831	0.9885	0.9879	0.9869	0.9867	0.9855	0.9857	0.9860	0.9858
V		0.0033	-0.0117	-0.0315	-0.0415	-0.0478	-0.0548	-0.0562	-0.0561	-0.0498	-0.0412
W		0.0813	0.0866	0.0958	0.1092	0.1195	0.1289	0.1464	0.1610	0.1689	0.1751
P	17	0.9884	0.9378	0.9714	0.9758	0.9735	0.9747	0.9773	0.9765	0.9857	0.9869
M		1.9800	1.9427	1.9851	1.9862	1.9848	1.9886	2.0023	2.0074	2.0128	2.0113
U		0.9922	0.9812	0.9918	0.9896	0.9872	0.9853	0.9862	0.9853	0.9861	0.9855
V		0.0041	-0.0148	-0.0436	-0.0568	-0.0628	-0.0713	-0.0694	-0.0653	-0.0573	-0.0468
W		0.0661	0.0702	0.0788	0.0907	0.1138	0.1334	0.1543	0.1706	0.1770	0.1815
P	16	0.9870	0.9447	0.9664	0.9668	0.9713	0.9774	0.9743	0.9767	0.9780	0.9853
M		1.9834	1.9460	1.9800	1.9852	1.9890	1.9978	2.0119	2.0186	2.0163	2.0168
U		0.9943	0.9833	0.9908	0.9898	0.9875	0.9852	0.9859	0.9849	0.9862	0.9851
V		0.0038	-0.0200	-0.0598	-0.0775	-0.0841	-0.0919	-0.0843	-0.0752	-0.0632	-0.0505
W		0.0451	0.0489	0.0603	0.0872	0.1079	0.1401	0.1657	0.1861	0.1905	0.1909
P	15	1.0008	0.9540	0.9448	0.9518	0.9459	0.9291	0.9642	0.9710	0.9846	0.9790
M		2.0055	1.9635	1.9928	1.9854	1.9821	1.9763	2.0131	2.0248	2.0283	2.0202
U		1.0014	0.9892	0.9941	0.9875	0.9826	0.9742	0.9815	0.9821	0.9843	0.9835
V		0.0034	-0.0262	-0.0824	-0.1102	-0.1180	-0.1202	-0.0991	-0.0811	-0.0652	-0.0508
W		0.0145	0.0187	0.0320	0.0678	0.1027	0.1524	0.1846	0.2063	0.2065	0.2031
P	14	0.9869	0.9516	0.8897	0.7826	0.7994	0.8044	0.9532	0.9802	0.9763	0.9858
M		2.0122	1.9807	1.9702	1.8969	1.9064	1.9228	2.0259	2.0409	2.0319	2.0304
U		1.0032	0.9939	0.9860	0.9588	0.9562	0.9517	0.9780	0.9811	0.9818	0.9838
V		0.0031	-0.0342	-0.1026	-0.1441	-0.1505	-0.1445	-0.1109	-0.0803	-0.0633	-0.0485
W		-0.0192	-0.0144	-0.0232	0.0381	0.1002	0.1711	0.2132	0.2312	0.2230	0.2159
P	13	0.9932	0.9660	0.6977	0.6347	0.6541	0.6882	0.8769	0.9702	0.9827	0.9807
M		2.0317	2.0128	1.8506	1.8227	1.8370	1.8802	2.0012	2.0461	2.0403	2.0288
U		1.0072	1.0013	0.9465	0.9299	0.9275	0.9274	0.9644	0.9780	0.9811	0.9809
V		0.0023	-0.0349	-0.1048	-0.1828	-0.1880	-0.1566	-0.1089	-0.0798	-0.0545	-0.0415
W		-0.0584	-0.0575	-0.0486	-0.0060	0.1053	0.2175	0.2423	0.2527	0.2382	0.2280
P	12	0.9826	0.9591	0.6892	0.4171	0.4497	0.5964	0.7731	0.9685	0.9883	0.9781
M		2.0483	2.0369	1.8173	1.6291	1.6853	1.8534	1.9407	2.0507	2.0456	2.0281
U		1.0077	1.0049	0.9303	0.8733	0.8822	0.9136	0.9438	0.9766	0.9804	0.9791
V		0.0050	-0.0207	-0.0537	-0.1184	-0.1607	-0.1156	-0.0797	-0.0492	-0.0306	-0.0320
W		-0.0881	-0.1004	-0.1635	-0.0597	0.1052	0.2613	0.2638	0.2680	0.2500	0.2365
P	11	1.0134	0.9612	0.8479	0.5028	0.3304	0.3727	0.6485	0.8945	0.9849	0.9786
M		2.1008	2.0676	2.0149	1.7504	1.5086	1.5775	1.8802	1.8503	2.0286	2.0339
U		1.0206	1.0106	0.9967	0.9081	0.8386	0.8461	0.9229	0.9209	0.9708	0.9773
V		0.0056	0.0045	0.0298	0.0440	0.0034	-0.0141	-0.0461	-0.0299	-0.0379	-0.0305
W		-0.1151	-0.1256	-0.1406	-0.1689	-0.0220	0.1776	0.2795	0.2561	0.2683	0.2505
P	10	1.0048	0.9708	0.9324	0.6095	0.4436	0.5205	0.7213	0.6224	0.9447	0.9853
M		2.1189	2.0874	2.0685	1.8316	1.6663	1.7449	1.9810	1.7478	2.0187	2.0355
U		1.0238	1.0161	1.0071	0.9322	0.8791	0.9008	0.9445	0.8986	0.9717	0.9787
V		0.0038	0.0254	0.0719	0.1612	0.1748	0.1419	0.0504	0.0002	-0.0186	-0.0175
W		-0.1098	-0.1208	-0.1345	-0.1207	-0.0028	0.1413	0.2223	0.2141	0.2565	0.2476
P	9	0.9857	0.9435	0.9523	0.8795	0.7174	0.8058	0.8234	0.5414	0.9711	0.9795
M		2.0855	2.0576	2.0577	2.0127	1.8969	1.9535	1.9423	1.6179	2.0227	2.0280
U		1.0205	1.0116	1.0095	0.9911	0.9529	0.9713	0.9715	0.8631	0.9758	0.9781
V		0.0027	0.0405	0.0788	0.1475	0.1827	0.1496	0.0906	-0.0067	-0.0094	-0.0097
W		-0.0724	-0.0820	-0.0800	-0.0545	0.0160	0.0899	0.1247	0.1678	0.2454	0.2424
P	8				0.9485	0.9456	0.8870	0.6533	0.4608	0.9684	0.9775
M					2.0276	2.0303	1.9822	1.7628	1.4841	2.0140	2.0257
U					1.0010	1.0002	0.9882	0.9261	0.8164	0.9746	0.9779
V					0.1120	0.1269	0.1127	0.0643	-0.0378	-0.0085	-0.0066
W					-0.0248	0.0139	0.0294	0.0238	0.1419	0.2404	0.2404
P	7						0.3292	0.4215	0.3919	0.9796	0.9877
M							1.2394	1.4324	1.3690	2.0244	2.0345
U							0.7272	0.8080	0.7686	0.9767	0.9800
V							-0.0047	-0.0023	-0.0610	-0.0085	-0.0052
W							-0.0051	-0.0414	0.1375	0.2437	0.2419
P	6							0.3426	0.3484	0.9796	0.9823
M								1.2149	1.2767	2.0280	2.0328
U								0.7158	0.7288	0.9771	0.9792
V								0.0088	-0.0620	-0.0042	-0.0028
W								-0.0212	0.1349	0.2464	0.2433
P	5								0.3392	0.9731	0.9861
M									1.3086	2.0250	2.0374
U									0.7397	0.9760	0.9800
V									-0.1084	0.0001	0.0000
W									0.1231	0.2476	0.2456
P	4								0.3332	0.9805	0.9859
M									1.2983	2.0337	2.0393
U									0.7327	0.9776	0.9796
V									-0.1160	0.0014	0.0038
W									0.1303	0.2509	0.2493
P	3									0.9884	0.9819
M										2.0520	2.0407
U										0.9801	0.9787
V										0.0015	0.0098
W										0.2608	0.2540
P	2									0.9877	0.9879
M										2.0679	2.0508
U										0.9799	0.9800
V										0.0126	0.0196
W										0.2773	0.2590
P	1									0.9859	0.9892
M										2.0776	2.0559
U										0.9803	0.9808
V										0.0345	0.0344
W										0.2834	0.2594

TABLE B-14. FINAL DATA SET FOR $M_\infty = 2.$, $R_d = 1.75 \times 10^6$, $\alpha_b = 10°$, x/d = 14

M2R763

P -- P0/P0INF M -- MACH NUMBER U,V,W -- 3-D VELOCITY COMPONENTS/U0INF

		1	2	3	4	5	6	7	8	9	10	11
P	21	0.9706	0.9546	0.9521	0.9758	0.9767	0.9823	0.9846	0.9816	0.9847	0.9841	0.9914
M		1.9659	1.9550	1.9389	1.9791	1.9864	2.0000	2.0026	2.0045	2.0086	2.0169	2.0200
U		0.9800	0.9828	0.9775	0.9869	0.9877	0.9900	0.9888	0.9881	0.9883	0.9901	0.9907
V		0.0024	-0.0059	-0.0233	-0.0383	-0.0426	-0.0490	-0.0473	-0.0446	-0.0448	-0.0422	-0.0357
W		0.0932	0.0938	0.0986	0.1139	0.1226	0.1323	0.1466	0.1553	0.1613	0.1654	0.1681
P	20	0.9572	0.9592	0.9574	0.9825	0.9775	0.9756	0.9795	0.9854	0.9852	0.9863	0.9915
M		1.9583	1.9613	1.9478	1.9866	1.9868	2.0005	2.0050	2.0123	2.0149	2.0223	2.0238
U		0.9852	0.9860	0.9812	0.9896	0.9878	0.9891	0.9884	0.9891	0.9888	0.9904	0.9910
V		0.0034	-0.0099	-0.0300	-0.0519	-0.0566	-0.0626	-0.0586	-0.0526	-0.0515	-0.0457	-0.0377
W		0.0732	0.0776	0.0841	0.1022	0.1169	0.1342	0.1498	0.1603	0.1670	0.1711	0.1725
P	19	0.9586	0.9639	0.9631	0.9733	0.9817	0.9799	0.9784	0.9848	0.9804	0.9910	0.9856
M		1.9606	1.9642	1.9581	1.9850	1.9986	2.0126	2.0150	2.0188	2.0197	2.0259	2.0218
U		0.9873	0.9882	0.9853	0.9891	0.9907	0.9906	0.9891	0.9890	0.9884	0.9901	0.9894
V		0.0058	-0.0139	-0.0410	-0.0691	-0.0753	-0.0800	-0.0719	-0.0619	-0.0579	-0.0485	-0.0391
W		0.0567	0.0568	0.0638	0.0922	0.1095	0.1388	0.1578	0.1687	0.1748	0.1777	0.1779
P	18	0.9522	0.9676	0.9671	0.9396	0.9460	0.9496	0.9744	0.9864	0.9908	0.9875	0.9830
M		1.9612	1.9722	1.9708	1.9693	1.9839	2.0055	2.0265	2.0273	2.0332	2.0265	2.0203
U		0.9887	0.9916	0.9898	0.9844	0.9853	0.9863	0.9896	0.9887	0.9898	0.9889	0.9873
V		0.0079	-0.0200	-0.0522	-0.0901	-0.0981	-0.0988	-0.0843	-0.0699	-0.0616	-0.0497	-0.0408
W		0.0265	0.0269	0.0366	0.0756	0.1025	0.1430	0.1680	0.1806	0.1866	0.1853	0.1865
P	17	0.9443	0.9632	0.9474	0.8347	0.8511	0.8733	0.9610	0.9786	0.9864	0.9819	0.9810
M		1.9680	1.9799	1.9725	1.9096	1.9325	1.9710	2.0314	2.0318	2.0376	2.0257	2.0224
U		0.9909	0.9940	0.9901	0.9668	0.9694	0.9741	0.9879	0.9870	0.9884	0.9864	0.9855
V		0.0093	-0.0264	-0.0656	-0.1034	-0.1124	-0.1104	-0.0928	-0.0757	-0.0626	-0.0501	-0.0435
W		-0.0095	-0.0080	-0.0005	0.0599	0.0987	0.1507	0.1812	0.1939	0.1997	0.1968	0.1981
P	16	0.9699	0.9634	0.8905	0.7362	0.7557	0.7904	0.8986	0.9688	0.9739	0.9825	0.9849
M		1.9937	1.9914	1.9476	1.8513	1.8770	1.9262	2.0063	2.0370	2.0356	2.0352	2.0292
U		0.9984	0.9960	0.9819	0.9485	0.9516	0.9592	0.9779	0.9853	0.9848	0.9857	0.9856
V		0.0094	-0.0329	-0.0733	-0.1144	-0.1203	-0.1151	-0.0947	-0.0769	-0.0606	-0.0502	-0.0417
W		-0.0428	-0.0457	-0.0328	0.0474	0.1004	0.1621	0.1958	0.2089	0.2148	0.2127	0.2071
P	15	0.9734	0.9485	0.7942	0.6828	0.7083	0.7379	0.8325	0.9539	0.9788	0.9891	0.9910
M		2.0234	2.0086	1.9038	1.8428	1.8682	1.9117	1.9768	2.0469	2.0440	2.0419	2.0362
U		1.0022	0.9973	0.9864	0.9433	0.9456	0.9503	0.9665	0.9846	0.9834	0.9853	0.9861
V		0.0068	-0.0316	-0.0738	-0.1392	-0.1377	-0.1116	-0.0871	-0.0685	-0.0568	-0.0451	-0.0365
W		-0.0927	-0.0957	-0.0784	0.0284	0.1087	0.1858	0.2129	0.2272	0.2324	0.2243	0.2150
P	14	0.9712	0.9385	0.7290	0.6321	0.6006	0.6879	0.7460	0.8175	0.8732	0.9723	0.9880
M		2.0559	2.0391	1.8892	1.8291	1.8121	1.8864	1.9250	1.9742	2.0051	2.0402	2.0424
U		1.0054	0.9999	0.9864	0.9372	0.9283	0.9418	0.9504	0.9622	0.9688	0.9799	0.9839
V		0.0062	-0.0227	-0.0692	-0.1269	-0.1686	-0.1413	-0.1017	-0.0876	-0.0645	-0.0564	-0.0437
W		-0.1410	-0.1460	-0.1327	-0.0835	0.0423	0.1691	0.2100	0.2281	0.2453	0.2424	0.2311
P	13	0.9721	0.9093	0.6850	0.4901	0.3969	0.5694	0.7448	0.7734	0.8319	0.9735	0.9867
M		2.0899	2.0581	1.9000	1.7400	1.6289	1.8291	1.9522	1.9521	1.9701	2.0490	2.0411
U		1.0084	0.9981	0.9516	0.9061	0.8752	0.9185	0.9546	0.9536	0.9589	0.9817	0.9829
V		0.0036	-0.0031	-0.0293	-0.0533	-0.1154	-0.1172	-0.0717	-0.0601	-0.0419	-0.0364	-0.0332
W		-0.1792	-0.1891	-0.1925	-0.1573	0.0269	0.2113	0.2385	0.2451	0.2492	0.2487	0.2355
P	12	0.9668	0.8951	0.6659	0.4632	0.3544	0.5210	0.7527	0.7487	0.8185	0.9807	0.9853
M		2.0952	2.0587	1.9020	1.7240	1.5734	1.7844	1.9572	1.9266	1.9478	2.0532	2.0354
U		1.0086	0.9966	0.9494	0.9003	0.8682	0.9065	0.9567	0.9478	0.9550	0.9840	0.9821
V		0.0008	0.0211	0.0379	0.0815	0.0539	-0.0040	-0.0134	-0.0240	-0.0205	-0.0159	-0.0227
W		-0.1852	-0.1962	-0.2043	-0.1473	0.0467	0.2317	0.2383	0.2443	0.2413	0.2465	0.2332
P	11	0.9658	0.9195	0.7043	0.6672	0.4933	0.5095	0.6846	0.7199	0.8242	0.9832	0.9783
M		2.0781	2.0590	1.9135	1.8943	1.7436	1.7348	1.8742	1.8722	1.9384	2.0442	2.0246
U		1.0085	1.0012	0.9576	0.9522	0.9083	0.8994	0.9433	0.9369	0.9560	0.9834	0.9804
V		-0.0011	0.0404	0.0875	0.1034	0.1599	0.1108	0.0744	0.0622	-0.0123	-0.0040	-0.0136
W		-0.1604	-0.1684	-0.1626	-0.1505	-0.0178	0.1555	0.1817	0.2226	0.2267	0.2391	0.2287
P	10	0.9680	0.9428	0.7930	0.7619	0.6618	0.6756	0.8199	0.6846	0.8361	0.9908	0.9838
M		2.0584	2.0482	1.9501	1.9377	1.8625	1.8629	1.9526	1.8125	1.9407	2.0450	2.0297
U		1.0091	1.0048	0.9752	0.9713	0.9468	0.9453	0.9757	0.9246	0.9588	0.9850	0.9818
V		-0.0020	0.0479	0.1017	0.1174	0.1586	0.1387	0.0875	0.0075	-0.0152	0.0007	-0.0054
W		-0.1186	-0.1211	-0.1031	-0.0887	-0.0001	0.0948	0.1176	0.1928	0.2171	0.2333	0.2288
P	9	0.9669	0.9526	0.9229	0.8998	0.8427	0.8632	0.8825	0.6193	0.8733	0.9887	0.9865
M		2.0387	2.0337	2.0246	2.0160	1.9785	1.9838	1.9769	1.7266	1.9687	2.0418	2.0354
U		1.0083	1.0054	1.0009	0.9977	0.9848	0.9868	0.9884	0.9006	0.9668	0.9848	0.9834
V		-0.0022	0.0477	0.0931	0.1068	0.1347	0.1171	0.0748	-0.0029	-0.0217	0.0024	0.0005
W		-0.0689	-0.0735	-0.0558	-0.0404	0.0060	0.0589	0.0599	0.1713	0.2176	0.2308	0.2291
P	8				0.9480	0.9428	0.9149	0.6899	0.5465	0.9129	1.0019	0.9974
M					2.0339	2.0302	2.0033	1.8101	1.6307	1.9985	2.0506	2.0469
U					1.0051	1.0033	0.9967	0.9423	0.8693	0.9736	0.9870	0.9864
V					0.0889	0.1001	0.0892	0.0527	-0.0183	-0.0228	0.0027	0.0048
W					-0.0245	0.0019	0.0239	-0.0002	0.1583	0.2252	0.2315	0.2297
P	7						0.5271	0.4235	0.4770	0.9543	0.9968	0.9901
M							1.5903	1.4345	1.5288	2.0316	2.0474	2.0430
U							0.8672	0.8092	0.8318	0.9814	0.9860	0.9855
V							0.0805	0.0245	-0.0249	-0.0221	0.0047	0.0087
W							-0.0010	-0.0257	0.1549	0.2321	0.2323	0.2292
P	6							0.3788	0.4326	0.9589	0.9951	0.9916
M								1.3170	1.4614	2.0350	2.0427	2.0483
U								0.7611	0.8084	0.9815	0.9848	0.9867
V								-0.0116	-0.0362	-0.0184	0.0085	0.0102
W								-0.0071	0.1477	0.2359	0.2315	0.2299
P	5								0.3809	0.9634	0.9904	0.9972
M									1.3597	2.0379	2.0485	2.0579
U									0.7673	0.9815	0.9853	0.9890
V									-0.0304	-0.0046	0.0105	0.0120
W									0.1333	0.2401	0.2341	0.2314
P	4								0.3485	0.9655	0.9907	0.9954
M									1.3425	2.0250	2.0591	2.0630
U									0.7632	0.9779	0.9877	0.9899
V									-0.0561	0.0136	0.0137	0.0153
W									0.1022	0.2397	0.2383	0.2332

TABLE B-14. FINAL DATA SET FOR $M_\infty = 2.$, $R_d = 1.75 \times 10^6$, $\alpha_b = 10°$, x/d = 14 (CONCLUDED)

M	3			
U		0.9779	0.9989	1.0087
V		2.0413	2.0724	2.0735
W		0.9821	0.9903	0.9917
		0.0150	0.0153	0.0208
		0.2408	0.2423	0.2373
M	2			
U		0.9894	1.0024	0.9919
V		2.0760	2.0794	2.0672
W		0.9883	0.9912	0.9902
		0.0094	0.0204	0.0274
		0.2546	0.2460	0.2360
M	1			
U		0.9937	0.9934	1.0085
V		2.0850	2.0683	2.0741
W		0.9889	0.9888	0.9928
		0.0247	0.0323	0.0356
		0.2605	0.2421	0.2317

TABLE B-15. FINAL DATA SET FOR $M_\infty = 2.$, $R_d = 1.75 \times 10^6$, $\alpha_b = 15°$, $x/d = 7$

M.ARTGA

P -- P0/P0INF M -- MACH NUMBER U,V,W -- 3-D VELOCITY COMPONENTS/U1INF

		1	2	3	4	5	6	7	8	9	10
P	15	0.9385	0.9283	0.9418	0.9396	0.9530	0.9509	0.9617	0.9624	0.9606	0.9613
M		1.9771	1.9706	1.9948	1.9908	2.0197	2.0255	2.0756	2.0622	2.0568	2.0415
U		0.9965	0.9885	0.9931	0.9875	0.9839	0.9776	0.9685	0.9612	0.9585	0.9563
V		0.0088	-0.0141	-0.0619	-0.0954	-0.1447	-0.1549	-0.1816	-0.1491	-0.1531	-0.1210
W		0.0782	0.0795	0.0833	0.1034	0.1480	0.1854	0.2641	0.2968	0.2985	0.3062
P	14	0.9259	0.9227	0.9392	0.9298	0.9426	0.9528	0.9432	0.9649	0.9562	0.9571
M		1.9822	1.9776	2.0096	2.0074	2.0458	2.0669	2.1340	2.1070	2.0966	2.0617
U		0.9934	0.9925	0.9986	0.9928	0.9864	0.9795	0.9603	0.9554	0.9507	0.9509
V		0.0096	-0.0185	-0.0753	-0.1190	-0.1953	-0.2104	-0.2339	-0.1704	-0.1753	-0.1294
W		0.0471	0.0459	0.0490	0.0680	0.1190	0.1818	0.3092	0.3410	0.3436	0.3360
P	13	0.9239	0.9254	0.9467	0.9529	0.9469	0.9417	0.7504	0.9478	0.9472	0.9551
M		2.0033	2.0022	2.0437	2.0702	2.1568	2.1727	2.1385	2.1717	2.1635	2.0942
U		1.0008	1.0003	1.0085	1.0082	1.0003	0.9860	0.9275	0.9515	0.9463	0.9455
V		0.0194	-0.0229	-0.0835	-0.1480	-0.2813	-0.3045	-0.2547	-0.1736	-0.1822	-0.1252
W		0.0115	0.0109	-0.0025	0.0097	0.0675	0.1665	0.3870	0.3957	0.3991	0.3766
P	12	0.9231	0.9231	0.9434	0.9523	0.5558	0.5104	0.6063	0.8112	0.8087	0.9509
M		2.0284	2.0318	2.0843	2.1414	2.0906	2.0773	2.1443	2.1419	2.1251	2.1436
U		1.0074	1.0081	1.0178	1.0221	0.9696	0.9392	0.8812	0.9294	0.9261	0.9443
V		0.0090	-0.0225	-0.0789	-0.1598	-0.3221	-0.3794	-0.1759	-0.1167	-0.1251	-0.1031
W		-0.0272	-0.0214	-0.0627	-0.0766	-0.0747	0.1271	0.5290	0.4464	0.4409	0.4186
P	11	0.9227	0.9261	0.9498	0.9090	0.2300	0.2048	0.7004	0.8104	0.7861	0.9519
M		2.0685	2.0658	2.1386	2.2173	1.7863	1.7561	2.3187	2.1953	2.1889	2.1765
U		1.0147	1.0155	1.0281	1.0323	0.9211	0.8846	0.9038	0.9327	0.9230	0.9463
V		0.0050	-0.0160	-0.0432	-0.1086	-0.1259	-0.1929	-0.0367	-0.0358	-0.0478	-0.0487
W		-0.0642	-0.0681	-0.1267	-0.1951	-0.1108	0.1489	0.5846	0.4628	0.4967	0.4436
P	10	0.9163	0.9274	0.9479	0.9634	0.7276	0.3142	0.2257	0.2734	0.5584	0.8204
M		2.0848	2.0973	2.1181	2.1702	2.2018	1.9696	1.8718	1.8076	2.1356	2.1603
U		1.0193	1.0222	1.0267	1.0337	1.0166	0.9705	0.9481	0.8278	0.8535	0.9315
V		-0.0033	-0.0025	-0.0174	-0.0374	-0.0556	-0.0856	0.0724	0.0452	-0.0043	-0.0124
W		-0.0860	-0.0902	-0.0982	-0.1464	-0.2667	-0.1840	0.1514	0.4493	0.5872	0.4673
P	9	0.9256	0.9226	0.9368	0.9516	0.9622	0.5808	0.3073	0.6082	0.7681	0.8637
M		2.1054	2.1087	2.1312	2.1941	2.2590	2.1391	1.8694	2.0713	2.1175	2.1100
U		1.0252	1.0254	1.0294	1.0357	1.0398	0.9891	0.8927	0.9115	0.9326	0.9481
V		-0.0143	0.0163	0.0182	0.0495	0.0938	0.1555	0.2709	0.1999	0.1385	0.0229
W		-0.0780	-0.0852	-0.1051	-0.1691	-0.2158	-0.2696	0.1415	0.4101	0.4181	0.4005
P	8				0.9439	0.9261	0.8054	0.8760	0.6552	0.6543	0.9393
M					2.2043	2.2252	2.1928	2.1839	1.8798	1.8710	2.0869
U					1.0350	1.0304	1.0070	0.9840	0.9303	0.9349	0.9589
V					0.1302	0.1792	0.2530	0.3290	0.2098	0.0510	0.0091
W					-0.1444	-0.1587	-0.1579	0.1479	0.1493	0.2236	0.3593
P	7						0.9188	0.3194	0.3713	0.5045	0.9416
M							2.1768	1.3540	1.5123	1.6773	2.0827
U							1.0169	0.7585	0.8354	0.8851	0.9530
V							0.2332	0.1668	-0.0540	-0.1073	-0.0181
W							-0.0803	0.0228	-0.0734	0.1234	0.3647
P	6							0.3000	0.3339	0.3528	0.9456
M								1.2938	1.4789	1.5186	2.1242
U								0.7441	0.8170	0.8054	0.9508
V								-0.0127	-0.0570	-0.0160	-0.0092
W								0.0546	-0.1182	0.2475	0.4039
P	5								0.3314	0.3513	0.9356
M									1.3820	1.4546	2.1318
U									0.7845	0.7686	0.9497
V									0.0762	0.0104	0.0263
W									0.0235	0.2796	0.4107
P	4									0.7386	0.9540
M										1.9947	2.1559
U										0.9154	0.9572
V										0.0047	0.0101
W										0.3987	0.4071
P	3									0.8727	0.9567
M										2.0356	2.1358
U										0.9265	0.9592
V										0.0471	0.0419
W										0.3897	0.3894
P	2									0.9485	0.9804
M										2.1672	2.1740
U										0.9597	0.9666
V										0.0513	0.0548
W										0.4076	0.3949
P	1									0.9326	0.9701
M										2.1851	2.1618
U										0.9581	0.9643
V										0.0684	0.0723
W										0.4202	0.3898

TABLE B-16. FINAL DATA SET FOR M_∞ = 2., R_d = 1.75 x 10^6, α_b = 15°, x/d = 10

#28705

P -- P0/P0INF M -- MACH NUMBER U,V,W -- 3-D VELOCITY COMPONENTS/U1NF

		1	2	3	4	5	6	7	8	9	10	11
P	20	0.9392	0.9471	0.9517	0.9506	0.9618	0.9505	0.9676	0.9662	0.9738	0.9772	0.9806
M		1.9409	1.9477	1.9616	1.9719	2.0070	2.0465	2.0301	2.0465	2.0604	2.0645	2.0625
U		0.9802	0.9816	0.9829	0.9814	0.9809	0.9746	0.9706	0.9662	0.9672	0.9669	0.9676
V		0.0029	-0.0260	-0.0648	-0.0920	-0.1363	-0.1834	-0.1438	-0.1354	-0.1207	-0.1018	-0.0983
W		0.0770	0.0798	0.0909	0.1125	0.1522	0.2051	0.2322	0.2714	0.2883	0.3001	0.2972
P	19	0.9388	0.9506	0.9510	0.9319	0.9519	0.8045	0.9574	0.9428	0.9731	0.9789	0.9801
M		1.9547	1.9631	1.9760	1.9731	2.0305	1.9960	2.0591	2.0774	2.0920	2.0896	2.0826
U		0.9864	0.9880	0.9884	0.9815	0.9831	0.9517	0.9690	0.9606	0.9637	0.9649	0.9658
V		-0.0026	-0.0370	-0.0821	-0.1176	-0.1779	-0.2176	-0.1773	-0.1558	-0.1303	-0.1032	-0.0992
W		0.0490	0.0425	0.0542	0.0879	0.1367	0.2116	0.2490	0.3089	0.3231	0.3274	0.3203
P	18	0.9474	0.9639	0.9120	0.9189	0.8408	0.7157	0.8330	0.8766	0.9548	0.9789	0.9784
M		1.9830	1.9948	1.9760	1.9927	2.0161	1.9928	2.0321	2.0863	2.1207	2.1107	2.1009
U		0.9952	0.9975	0.9882	0.9856	0.9726	0.9411	0.9507	0.9504	0.9591	0.9620	0.9633
V		-0.0048	-0.0455	-0.0998	-0.1471	-0.2225	-0.2086	-0.1922	-0.1539	-0.1297	-0.0983	-0.0975
W		-0.0054	-0.0043	0.0112	0.0548	0.1162	0.2584	0.2775	0.3466	0.3588	0.3537	0.3429
P	17	0.9483	0.9555	0.9005	0.9091	0.6584	0.6942	0.7586	0.8292	0.9385	0.9857	0.9835
M		2.0143	2.0242	2.0128	2.0397	1.9404	2.0780	2.0403	2.1089	2.1499	2.1347	2.1233
U		1.0020	1.0036	0.9959	0.9957	0.9466	0.9430	0.9383	0.9446	0.9558	0.9604	0.9626
V		-0.0084	-0.0494	-0.1152	-0.1743	-0.2365	-0.2097	-0.1714	-0.1303	-0.1136	-0.0858	-0.0846
W		-0.0616	-0.0609	-0.0437	0.0005	0.1203	0.3307	0.3353	0.3872	0.3928	0.3782	0.3649
P	16	0.9510	0.9479	0.8775	0.8024	0.5299	0.5663	0.7089	0.8230	0.9265	0.9763	0.9734
M		2.0627	2.0730	2.0670	2.0553	1.9642	2.0976	2.1465	2.1445	2.1603	2.1409	2.1298
U		1.0094	1.0112	1.0049	0.9961	0.9507	0.9214	0.9490	0.9447	0.9527	0.9573	0.9591
V		-0.0099	-0.0478	-0.1165	-0.1782	-0.2574	-0.1678	-0.1454	-0.0965	-0.0835	-0.0626	-0.0653
W		-0.1241	-0.1236	-0.1154	-0.0804	0.0991	0.4197	0.3986	0.4198	0.4142	0.3947	0.3823
P	15	0.9554	0.9588	0.8902	0.8610	0.2895	0.4880	0.7985	0.8394	0.9286	0.9693	0.9786
M		2.0813	2.1034	2.0792	2.1183	1.7910	2.0735	2.2515	2.1699	2.1656	2.1421	2.1421
U		1.0105	1.0159	1.0062	1.0124	0.9146	0.9324	0.9562	0.9487	0.9528	0.9557	0.9597
V		0.0061	-0.0304	-0.0753	-0.1360	-0.1747	-0.1967	-0.1085	-0.0509	-0.0494	-0.0385	-0.0432
W		-0.1529	-0.1528	-0.1585	-0.1437	0.1108	0.3636	0.4546	0.4343	0.4228	0.4023	0.3921
P	14	0.9820	0.9668	0.8799	0.7618	0.2226	0.4190	0.8414	0.8441	0.9442	0.9708	0.9917
M		2.1786	2.1889	2.1702	2.1591	1.7419	2.1361	2.3256	2.1496	2.1623	2.1372	2.1489
U		1.0250	1.0266	1.0177	1.0110	0.9103	0.9310	0.9696	0.9512	0.9556	0.9566	0.9621
V		0.0019	-0.0208	-0.0508	-0.0928	-0.0424	-0.1028	-0.0345	-0.0052	-0.0167	-0.0165	-0.0231
W		-0.2123	-0.2163	-0.2304	-0.2343	0.1388	0.4430	0.4774	0.4194	0.4170	0.3986	0.3927
P	13	0.9761	0.9533	0.8434	0.6894	0.4748	0.2812	0.2264	0.8901	0.8873	0.8554	0.9349
M		2.2390	2.2440	2.2294	2.2093	2.1009	1.8632	1.7161	2.2581	2.2352	2.1332	2.1423
U		1.0389	1.0305	1.0201	1.0087	0.9861	0.9470	0.8931	0.9835	0.9771	0.9528	0.9545
V		-0.0011	-0.0029	-0.0088	-0.0240	-0.0091	0.0253	0.0318	0.0668	0.0299	-0.0051	-0.0169
W		-0.2582	-0.2589	-0.2844	-0.3057	-0.2872	-0.1565	0.1880	0.4053	0.4111	0.4053	0.4067
P	12	0.9353	0.9407	0.8349	0.6451	0.4455	0.3242	0.3416	0.9120	0.8664	0.8713	0.9745
M		2.2143	2.2370	2.2362	2.1735	2.0359	1.8612	1.8123	2.1496	2.1302	2.0989	2.1284
U		1.0261	1.0290	1.0206	0.9973	0.9700	0.9460	0.9052	0.9945	0.9784	0.9574	0.9645
V		-0.0041	0.0156	0.0375	0.0603	0.0967	0.1393	0.1606	0.0840	0.0569	0.0121	0.0026
W		-0.2432	-0.2578	-0.2865	-0.3079	-0.2637	-0.0807	0.2166	0.2907	0.3317	0.3703	0.3731
P	11	0.9573	0.9517	0.8920	0.8191	0.6399	0.4731	0.6198	0.8373	0.8013	0.9153	0.9836
M		2.2169	2.2278	2.2232	2.2068	2.0841	1.8705	1.9592	2.0234	2.0127	2.0873	2.1162
U		1.0311	1.0322	1.0268	1.0199	0.9878	0.9375	0.9509	0.9859	0.9678	0.9623	0.9656
V		0.0041	0.0193	0.0550	0.0734	0.1041	0.2176	0.2051	0.0521	0.0313	0.0071	0.0006
W		-0.2284	-0.2346	-0.2474	-0.2540	-0.2438	0.0098	0.1758	0.1957	0.2635	0.3487	0.3615
P	10	0.9285	0.9163	0.8912	0.8490	0.7147	0.7168	0.8876	0.6950	0.7081	0.9516	0.9835
M		2.1529	2.1516	2.1524	2.1231	2.0323	1.9689	2.0657	1.8731	1.8952	2.0862	2.1034
U		1.0258	1.0243	1.0229	1.0148	0.9887	0.9721	1.0022	0.9559	0.9420	0.9627	0.9628
V		0.0113	0.0282	0.0674	0.0901	0.1406	0.1885	0.1451	0.0040	-0.0210	-0.0072	-0.0026
W		-0.1732	-0.1781	-0.1767	-0.1698	-0.1436	0.0469	0.1031	0.1182	0.2299	0.3468	0.3597
P	9	0.9294	0.9144	0.9170	0.9125	0.8669	0.9288	0.9394	0.5159	0.5165	0.9595	0.9843
M		2.1021	2.1006	2.1072	2.1071	2.0811	2.0690	2.0600	1.6806	1.6775	2.0914	2.1007
U		1.0211	1.0204	1.0207	1.0195	1.0097	1.0098	1.0107	0.9606	0.8749	0.9579	0.9592
V		0.0122	0.0261	0.0685	0.0924	0.1407	0.1313	0.0923	0.0009	-0.0566	-0.0198	-0.0004
W		-0.1128	-0.1133	-0.1084	-0.1017	-0.0713	0.0289	0.0534	0.0346	0.2042	0.3633	0.3670
P	8				0.9408	0.9315	0.9434	0.9289	0.4366	0.3768	0.9622	0.9823
M					2.0966	2.0872	2.0642	2.0519	1.5972	1.4806	2.1079	2.0994
U					1.0212	1.0174	1.0128	1.0111	0.8713	0.8043	0.9540	0.9563
V					0.0826	0.1075	0.0961	0.0754	0.0323	-0.0417	-0.0112	0.0117
W					-0.0540	-0.0326	0.0138	0.0222	-0.0006	0.1928	0.3854	0.3733
P	7						0.7271	0.7384	0.4124	0.3336	0.9716	0.9686
M							1.9098	1.9264	1.5500	1.3927	2.1257	2.0915
U							0.9702	0.9761	0.8535	0.7736	0.9539	0.9539
V							0.0845	0.0631	0.0424	0.0085	0.0113	0.0278
W							-0.0226	-0.0411	-0.0042	0.1744	0.3975	0.3732
P	6							0.3809	0.3831	0.3189	0.9780	0.9880
M								1.4310	1.4609	1.3173	2.1144	2.1024
U								0.8070	0.8194	0.7391	0.9560	0.9582
V								0.0331	0.0347	0.0288	0.0449	0.0395
W								-0.0378	0.0209	0.1805	0.3823	0.3688
P	5								0.3017	0.7126	0.9845	0.9840
M									1.2395	1.8725	2.1039	2.0945
U									0.7771	0.8978	0.9604	0.9587
V									-0.0104	0.0090	0.0514	0.0455
W									0.0030	0.3483	0.3626	0.3611
P	4									0.9210	0.9894	1.0011
M										2.0121	2.1071	2.1085
U										0.9322	0.9616	0.9629
V										0.0758	0.0517	0.0495
W										0.3633	0.3617	0.3597
P	3									0.9508	0.9951	0.9872
M										2.0476	2.1116	2.0762
U										0.9447	0.9621	0.9558
V										0.0743	0.0557	0.0616
W										0.3581	0.3633	0.3526

TABLE B-16. FINAL DATA SET FOR $M_\infty = 2.$, $R_d = 1.75 \times 10^6$, $\alpha_b = 15°$, x/d = 10 (CONCLUDED)

0.9907	0.9468	0.9833
2.1204	2.0699	2.1152
0.9590	0.9518	0.9632
0.0556	0.0698	0.0568
0.3776	0.3570	0.3628
0.9220	0.9942	1.0015
2.0797	2.1401	2.1276
0.9467	0.9634	0.9651
0.0809	0.0696	0.0686
0.3751	0.3779	0.3646

TABLE B-17. FINAL DATA SET FOR $M_\infty = 2.$, $R_d = 1.75 \times 10^6$, $\alpha_b = 15°$, x/d = 13

P -- P0/P0INF M -- MACH NUMBER U,V,W -- 3-D VELOCITY COMPONENTS/U1INF

		1	2	3	4	5	6	7	8	9	10	11	12
P	23	0.9538	0.9451	0.9344	0.9011	0.9501	0.9750	0.9815	0.9808	0.9830	0.9811	0.9859	0.9974
M		1.9479	1.9485	1.9492	1.9420	1.9860	2.0069	2.0302	2.0291	2.0369	2.0444	2.0534	2.0604
U		0.9850	0.9844	0.9766	0.9711	0.9762	0.9732	0.9715	0.9661	0.9665	0.9665	0.9658	0.9685
V		-0.0022	-0.0387	-0.0685	-0.1099	-0.1231	-0.1255	-0.1295	-0.1253	-0.1155	-0.1205	-0.1049	-0.0860
W		0.0244	0.0249	0.0409	0.1111	0.1637	0.2023	0.2368	0.2590	0.2772	0.2822	0.2926	0.2964
P	22	0.9500	0.9454	0.8733	0.9040	0.9419	0.9713	0.9735	0.9726	0.9815	0.9874	0.9965	0.9900
M		1.9573	1.9579	1.9072	1.9638	1.9976	2.0239	2.0506	2.0486	2.0552	2.0675	2.0703	2.0632
U		0.9877	0.9872	0.9707	0.9779	0.9768	0.9745	0.9709	0.9641	0.9625	0.9634	0.9648	0.9650
V		-0.0040	-0.0413	-0.0720	-0.1267	-0.1466	-0.1514	-0.1545	-0.1446	-0.1277	-0.1312	-0.1099	-0.0867
W		-0.0207	-0.0139	0.0130	0.0862	0.1517	0.2019	0.2478	0.2764	0.2959	0.3026	0.3091	0.3099
P	21	0.9485	0.9226	0.8427	0.8690	0.8894	0.9425	0.9486	0.9774	0.9880	0.9819	0.9897	0.9979
M		1.9763	1.9639	1.9094	1.9736	1.9979	2.0426	2.0800	2.0912	2.0858	2.0897	2.0837	2.0877
U		0.9913	0.9875	0.9707	0.9809	0.9754	0.9743	0.9688	0.9654	0.9620	0.9590	0.9612	0.9648
V		-0.0055	-0.0424	-0.0780	-0.1429	-0.1727	-0.1840	-0.1883	-0.1643	-0.1393	-0.1380	-0.1120	-0.0881
W		-0.0635	-0.0535	-0.0214	0.0514	0.1329	0.2011	0.2642	0.3014	0.3195	0.3319	0.3367	0.3306
P	20	0.9567	0.9053	0.8431	0.7731	0.7574	0.7971	0.8012	0.9475	0.9778	0.9753	0.9933	0.9939
M		2.0112	1.9817	1.9459	1.9520	1.9566	2.0018	2.0489	2.1379	2.1175	2.1205	2.1164	2.0983
U		0.9971	0.9891	0.9790	0.9737	0.9630	0.9589	0.9501	0.9642	0.9584	0.9549	0.9606	0.9612
V		-0.0077	-0.0458	-0.0874	-0.1578	-0.1940	-0.2134	-0.2130	-0.1814	-0.1436	-0.1386	-0.1100	-0.0832
W		-0.1089	-0.0967	-0.0599	0.0083	0.1029	0.1895	0.2808	0.3346	0.3531	0.3665	0.3583	0.3503
P	19	0.9529	0.8795	0.8443	0.6883	0.6607	0.6768	0.6470	0.7840	0.9452	0.9356	0.9883	0.9956
M		2.0301	1.9811	1.9485	1.9309	1.9218	1.9562	1.9788	2.0789	2.1579	2.1486	2.1415	2.1150
U		0.9985	0.9856	0.9834	0.9658	0.9537	0.9488	0.9302	0.9389	0.9554	0.9503	0.9573	0.9602
V		-0.0092	-0.0450	-0.0966	-0.1685	-0.1930	-0.2104	-0.1660	-0.1608	-0.1344	-0.1242	-0.0977	-0.0720
W		-0.1396	-0.1266	-0.0771	0.0017	0.0950	0.1758	0.3088	0.3686	0.3926	0.4020	0.3879	0.3677
P	18	0.9544	0.8759	0.8085	0.5919	0.5814	0.5984	0.6682	0.6992	0.7835	0.8875	0.9806	0.9973
M		2.0802	2.0304	2.0035	1.9225	1.9168	1.9484	2.0560	2.0512	2.1013	2.1630	2.1676	2.1374
U		1.0017	0.9900	0.9858	0.9620	0.9549	0.9473	0.9566	0.9306	0.9339	0.9468	0.9555	0.9598
V		-0.0112	-0.0495	-0.1051	-0.1751	-0.1705	-0.1635	-0.1120	-0.1127	-0.1190	-0.0904	-0.0728	-0.0545
W		-0.2010	-0.1852	-0.1385	-0.0141	0.1105	0.2143	0.3214	0.3867	0.4110	0.4279	0.4145	0.3874
P	17	0.9507	0.8569	0.7239	0.5229	0.5793	0.6424	0.7111	0.7271	0.7551	0.8610	0.9830	0.9942
M		2.1429	2.0891	2.0193	1.9756	2.0302	2.0815	2.1463	2.1116	2.1060	2.1569	2.1827	2.1448
U		1.0038	0.9912	0.9761	0.9744	0.9832	0.9804	0.9737	0.9492	0.9361	0.9452	0.9567	0.9591
V		-0.0124	-0.0489	-0.1092	-0.1909	-0.1706	-0.1341	-0.0656	-0.0578	-0.0698	-0.0495	-0.0430	-0.0342
W		-0.2636	-0.2524	-0.2143	-0.0212	0.1448	0.2556	0.3558	0.3953	0.4202	0.4344	0.4251	0.3963
P	16	0.9596	0.9109	0.7281	0.5768	0.5460	0.4359	0.6107	0.7809	0.7727	0.8636	0.9840	0.9998
M		2.1815	2.1481	2.0720	1.9825	1.9787	1.9682	2.1165	2.1832	2.1326	2.1536	2.1775	2.1460
U		1.0067	0.9997	0.9755	0.9618	0.9731	0.9598	0.9734	0.9659	0.9457	0.9485	0.9582	0.9607
V		-0.0020	-0.0347	-0.0428	-0.1592	-0.1977	-0.1452	-0.1010	-0.0123	-0.0226	-0.0120	-0.0148	-0.0145
W		-0.2895	-0.2816	-0.2844	-0.1999	-0.0455	0.2000	0.3247	0.4063	0.4205	0.4278	0.4206	0.3944
P	15	0.9589	0.9124	0.6655	0.4513	0.3581	0.3710	0.5051	0.8195	0.8022	0.8941	0.9931	0.9917
M		2.2784	2.2434	2.1224	1.9821	1.8947	1.9702	2.1565	2.1756	2.1304	2.1495	2.1767	2.1364
U		1.0093	1.0024	0.9634	0.9482	0.9576	0.9494	0.9696	0.9729	0.9539	0.9552	0.9621	0.9615
V		-0.0087	-0.0225	-0.0403	-0.0894	-0.1418	-0.0512	-0.0304	0.0261	0.0153	0.0132	0.0121	0.0046
W		-0.3567	-0.3512	-0.3697	-0.2880	-0.0573	0.2818	0.3783	0.3834	0.4006	0.4100	0.4110	0.3863
P	14	0.9707	0.9165	0.6334	0.3759	0.2723	0.4170	0.6426	0.7398	0.8109	0.8094	0.8810	1.0038
M		2.4007	2.3629	2.1919	1.9601	1.8102	1.9803	2.1368	2.1331	2.1497	2.0759	2.1169	2.1785
U		1.0135	1.0057	0.9546	0.9389	0.9436	0.9489	0.9724	0.9810	0.9832	0.9571	0.9563	0.9682
V		-0.0153	-0.0054	0.0138	0.0146	-0.0166	0.0716	0.0542	0.0899	0.0586	0.0367	0.0217	0.0198
W		-0.4211	-0.4189	-0.4373	-0.3098	-0.0089	0.2888	0.3541	0.3186	0.3325	0.3524	0.3854	0.3973
P	13	0.7834	0.7591	0.7713	0.5414	0.3716	0.3082	0.5619	0.8324	0.8595	0.8021	0.9266	1.0078
M		2.1721	2.1845	2.2448	2.0895	1.9410	1.8214	2.0250	2.1080	2.1140	2.0321	2.1173	2.1581
U		0.9846	0.9809	0.9853	0.9472	0.9488	0.9412	0.9627	0.9931	0.9901	0.9537	0.9634	0.9700
V		-0.0090	0.0099	0.0110	0.0448	0.0665	0.1057	0.1496	0.1083	0.0731	0.0355	0.0288	0.0293
W		-0.3585	-0.3695	-0.3981	-0.3869	-0.2493	-0.0193	0.2543	0.2463	0.2763	0.3269	0.3669	0.3785
P	12	0.9023	0.8545	0.8313	0.6152	0.4462	0.4517	0.7490	0.8669	0.8767	0.8367	0.9757	1.0047
M		2.1390	2.1080	2.1125	2.0062	1.8827	1.8672	2.0539	2.0460	2.0768	2.0336	2.1220	2.1359
U		1.0013	0.9923	0.9899	0.9594	0.9408	0.9391	0.9867	0.9960	0.9939	0.9579	0.9701	0.9709
V		-0.0161	0.0312	0.0405	0.1192	0.1716	0.2033	0.1661	0.0923	0.0641	0.0296	0.0317	0.0315
W		-0.2689	-0.2703	-0.2820	-0.2623	-0.1370	0.0334	0.1691	0.1891	0.2237	0.3165	0.3523	0.3602
P	11	0.9167	0.8966	0.8904	0.7264	0.6387	0.6988	0.8521	0.8870	0.8164	0.9180	0.9941	1.0023
M		2.0943	2.0865	2.0975	1.9940	1.9198	1.9818	2.0534	2.0449	2.0004	2.0729	2.1175	2.1195
U		1.0046	1.0023	1.0031	0.9760	0.9579	0.9750	0.9998	1.0006	0.9839	0.9685	0.9725	0.9714
V		-0.0162	0.0410	0.0569	0.1404	0.1869	0.1973	0.1308	0.0451	0.0402	0.0214	0.0310	0.0296
W		-0.2048	-0.2023	-0.2088	-0.1561	-0.0486	0.0191	0.1122	0.1388	0.1747	0.3184	0.3423	0.3470
P	10	0.9247	0.9125	0.9109	0.8551	0.8221	0.8412	0.8835	0.8381	0.7067	0.9704	0.9992	0.9938
M		2.0558	2.0440	2.0530	2.0206	2.0174	2.0260	2.0387	1.9948	1.8835	2.0961	2.1111	2.1079
U		1.0054	1.0030	1.0040	0.9948	0.9927	0.9968	1.0027	0.9944	0.9566	0.9728	0.9727	0.9704
V		-0.0157	0.0380	0.0522	0.1183	0.1530	0.1436	0.0967	0.0375	0.0047	0.0140	0.0253	0.0243
W		-0.1402	-0.1299	-0.1354	-0.0879	-0.0291	0.0128	0.0813	0.0830	0.1366	0.3255	0.3370	0.3408
P	9	0.9279	0.9288	0.9229	0.9123	0.8938	0.8939	0.9182	0.7243	0.5556	0.9919	0.9922	1.0043
M		2.0289	2.0288	2.0309	2.0383	2.0370	2.0359	2.0517	1.9096	1.7260	2.1092	2.1033	2.1085
U		1.0038	1.0041	1.0042	1.0044	1.0035	1.0041	1.0104	0.9737	0.9096	0.9722	0.9704	0.9717
V		-0.0141	0.0308	0.0435	0.0952	0.1142	0.1069	0.0701	0.0210	-0.0157	0.0116	0.0223	0.0290
W		-0.0896	-0.0827	-0.0824	-0.0568	-0.0182	0.0121	0.0506	0.0191	0.1059	0.3378	0.3377	0.3376
P	8				0.9175	0.9117	0.9089	0.9080	0.5969	0.4256	0.9950	0.9970	0.9979
M					2.0307	2.0339	2.0349	2.0357	1.7933	1.5448	2.1140	2.1075	2.1033
U					1.0049	1.0052	1.0061	1.0064	0.9374	0.8485	0.9691	0.9699	0.9704
V					0.0777	0.0909	0.0838	0.0694	0.0259	-0.0102	0.0210	0.0262	0.0310
W					-0.0319	-0.0085	0.0116	0.0456	-0.0378	0.0832	0.3497	0.3421	0.3371
P	7						0.9282	0.9074	0.4825	0.3703	0.9908	0.9921	0.9818
M							2.0512	2.0491	1.6471	1.4447	2.1111	2.1056	2.0897
U							1.0117	1.0116	0.8886	0.8101	0.9677	0.9688	0.9666
V							0.0673	0.0582	0.0295	0.0123	0.0364	0.0341	0.0331
W							0.0068	0.0151	-0.0674	0.0793	0.3502	0.3430	0.3371
P	6							0.6323	0.4508	0.3644	0.9907	0.9871	0.9879
M								1.8334	1.5984	1.4249	2.1076	2.1008	2.0860
U								0.9491	0.8498	0.8067	0.9682	0.9681	0.9652
V								0.0517	0.0198	0.0123	0.0450	0.0400	0.0346
W								-0.0308	-0.0518	0.0928	0.3450	0.3407	0.3377

TABLE B-17. FINAL DATA SET FOR $M_\infty = 2.$, $R_d = 1.75 \times 10^6$, $\alpha_b = 15°$, x/d = 13 (CONCLUDED)

EXPD PANEL	5				
		0.4071	0.3263	0.9821	0.9889	0.9879
		1.4213	1.3038	2.1017	2.0983	2.0831
		0.8028	0.7472	0.9673	0.9672	0.9640
		0.0455	-0.0145	0.0478	0.0428	0.0383
		-0.0297	0.1112	0.3427	0.3410	0.3385
EXPD PANEL	4					
			0.3068	0.9931	0.9788	0.9943
			1.2110	2.1118	2.0896	2.0906
			0.6926	0.9693	0.9638	0.9653
			-0.0494	0.0494	0.0428	0.0420
			0.1676	0.3447	0.3431	0.3405
EXPD PANEL	3					
			0.4249	0.9911	0.9887	0.9965
			1.5229	2.1144	2.0979	2.0929
			0.8015	0.9685	0.9650	0.9653
			-0.0738	0.0502	0.0452	0.0459
			0.2553	0.3488	0.3464	0.3418
EXPD PANEL	2					
			0.7892	0.9857	0.9976	0.9935
			1.9886	2.1124	2.1075	2.0929
			0.9298	0.9662	0.9667	0.9651
			-0.0330	0.0511	0.0506	0.0515
			0.3578	0.3534	0.3485	0.3415
EXPD PANEL	1					
			0.8389	0.9896	0.9906	1.0017
			1.9289	2.1293	2.1118	2.0997
			0.9119	0.9675	0.9668	0.9672
			0.1219	0.0601	0.0591	0.0584
			0.3370	0.3610	0.3501	0.3398

TABLE B-18. FINAL DATA SET FOR $M_\infty = 2.$, $R_d = 1.75 \times 10^6$, $\alpha_b = 20°$, $x/d = 6$

424767

P -- P0/P0INF M -- MACH NUMBER U,V,W -- S-D VELOCITY COMPONENTS/U1NF

		1	2	3	4	5	6	7	8	9	10
P	18	0.9560	0.9111	0.9161	0.9326	0.9355	0.9379	0.9456	0.9435	0.9453	0.9421
M		1.9816	1.9480	1.9573	2.0437	2.0627	2.0684	2.0595	2.0638	2.0718	2.0548
U		0.9857	0.9754	0.9743	0.9606	0.9504	0.9419	0.9453	0.9340	0.9323	0.9323
V		0.0008	-0.0339	-0.0663	-0.2076	-0.2018	-0.1774	-0.1670	-0.1373	-0.1234	-0.1263
W		0.1344	0.1355	0.1500	0.2436	0.2993	0.3448	0.3336	0.3793	0.3937	0.3808
P	17	0.9350	0.9222	0.9261	0.9099	0.9235	0.9459	0.9410	0.9415	0.9574	0.9512
M		1.9817	1.9730	1.9833	2.1132	2.1264	2.1254	2.0996	2.1138	2.1181	2.1016
U		0.9902	0.9868	0.9858	0.9555	0.9421	0.9352	0.9377	0.9287	0.9286	0.9294
V		-0.0009	-0.0404	-0.0801	-0.2835	-0.2552	-0.2086	-0.2004	-0.1570	-0.1332	-0.1369
W		0.0966	0.0974	0.1118	0.2611	0.3402	0.3871	0.3672	0.4180	0.4291	0.4150
P	16	0.9425	0.9253	0.9276	0.6466	0.7886	0.8389	0.9208	0.9400	0.9533	0.9481
M		2.0133	2.0032	2.0096	2.0726	2.1610	2.1101	2.1485	2.1880	2.1664	2.1478
U		1.0026	0.9985	0.9961	0.9246	0.9243	0.9118	0.9261	0.9209	0.9215	0.9242
V		-0.0014	-0.0463	-0.0967	-0.3157	-0.2805	-0.2081	-0.2239	-0.1697	-0.1336	-0.1445
W		0.0477	0.0519	0.0613	0.2919	0.3918	0.4303	0.4156	0.4729	0.4716	0.4524
P	15	0.9167	0.9300	0.9273	0.4337	0.5205	0.8011	0.7672	0.9554	0.9716	0.9658
M		2.0016	2.0176	2.0303	2.1171	2.0998	2.4051	2.2786	2.3035	2.2380	2.2263
U		1.0001	0.9995	0.9937	0.9036	0.8752	0.9054	0.8996	0.9142	0.9196	0.9210
V		-0.0140	-0.0963	-0.1597	-0.3317	-0.2170	-0.2301	-0.2464	-0.1569	-0.1164	-0.1331
W		0.0227	0.0372	0.0610	0.3701	0.4913	0.5780	0.5256	0.5460	0.5166	0.5052
P	14	0.9160	0.9293	0.9461	0.4461	0.2033	0.2161	0.5309	0.7505	0.9755	0.9644
M		2.0418	2.0733	2.1284	1.9343	1.6956	1.8349	2.3558	2.4295	2.2633	2.2599
U		1.0103	1.0133	1.0143	0.9161	0.8640	0.8582	0.8656	0.8901	0.9170	0.9138
V		-0.0180	-0.1054	-0.1966	-0.2240	-0.2116	-0.3007	-0.2712	-0.2173	-0.0428	-0.1001
W		-0.0447	-0.0472	-0.0461	-0.0217	-0.1739	0.2800	0.6015	0.6154	0.5393	0.5403
P	13	0.9264	0.9478	0.9335	0.4006	0.1226	0.1545	0.4100	0.8079	0.9703	0.9588
M		2.1145	2.1816	2.2979	1.8542	1.6258	1.8932	2.3553	2.5138	2.2381	2.2439
U		1.0241	1.0347	1.0446	0.9377	0.8694	0.8986	0.8291	0.9040	0.9169	0.9107
V		-0.0177	-0.0803	-0.1662	-0.0804	-0.0280	-0.1293	-0.2158	-0.1351	-0.0428	-0.0577
W		-0.1147	-0.1385	-0.1921	-0.2463	-0.1467	0.3395	0.6705	0.6485	0.5324	0.5443
P	12	0.9424	0.9588	0.7313	0.3995	0.1274	0.1560	0.4052	0.8146	0.9590	0.9702
M		2.2229	2.3158	2.3375	2.0286	1.6629	1.8863	2.3194	2.4549	2.1917	2.2173
U		1.0425	1.0533	1.0352	0.9636	0.8789	0.9284	0.8416	0.9171	0.9174	0.9163
V		-0.0103	-0.0431	-0.0409	0.0189	0.0987	-0.0208	-0.0992	-0.0364	-0.0090	-0.0223
W		-0.1771	-0.2305	-0.3188	-0.3141	-0.1380	0.2704	0.6694	0.6224	0.5106	0.5248
P	11	0.9460	0.9676	1.0090	0.5121	0.2549	0.1892	0.1386	0.7724	0.8970	0.9683
M		2.3286	2.3640	2.5257	2.3687	2.0098	1.8134	1.7480	2.2218	2.2410	2.1883
U		1.0565	1.0621	1.0790	1.0203	0.9298	0.9203	0.8916	0.9286	0.9248	0.9194
V		0.0015	-0.0054	0.0094	0.0589	0.1626	0.1871	-0.0032	0.0460	0.0108	0.0051
W		-0.2333	-0.2437	-0.3117	-0.3811	-0.3382	-0.1040	0.2417	0.5034	0.5217	0.5054
P	10	0.9279	0.9568	0.9694	0.7116	0.4974	0.5085	0.1903	0.7573	0.9318	0.9653
M		2.3883	2.4474	2.6159	2.4474	2.1775	2.1670	1.7429	2.0660	2.1611	2.1465
U		1.0636	1.0768	1.0808	1.0397	0.9893	0.9772	0.8794	0.9318	0.9276	0.9214
V		0.0163	0.0422	0.0983	0.1777	0.2981	0.3671	0.1432	0.0397	0.0207	0.0122
W		-0.2544	-0.2792	-0.3498	-0.3489	-0.2489	0.0038	0.2379	0.3844	0.4752	0.4794
P	9	0.8943	0.9072	0.8887	0.8915	0.9099	0.9125	0.4545	0.6640	0.8215	0.9393
M		2.3380	2.4000	2.4874	2.4453	2.4125	2.2760	1.8881	1.9173	2.0513	2.1170
U		1.0635	1.0678	1.0686	1.0592	1.0593	1.0271	0.8883	0.9443	0.9384	0.9285
V		0.0337	0.0825	0.1698	0.2573	0.3445	0.2976	0.3005	0.1307	-0.0056	0.0139
W		-0.2032	-0.2397	-0.2715	-0.1911	-0.0403	0.0384	0.2391	0.2111	0.3841	0.4485
P	8				0.6332	0.8756	0.7924	0.8361	0.4444	0.8482	0.9376
M					2.0138	2.2431	2.1551	2.1301	1.6618	2.0624	2.1028
U					0.9708	1.0221	1.0078	0.9961	0.8935	0.9266	0.9248
V					0.2476	0.2864	0.2511	0.2457	-0.0400	-0.0652	-0.0047
W					-0.0613	-0.0429	-0.0696	0.1336	-0.0261	0.4139	0.4480
P	7						0.2622	0.2847	0.2844	0.6208	0.8528
M							1.2673	1.4007	1.3899	1.9921	2.1222
U							0.7310	0.7929	0.7809	0.8546	0.9088
V							-0.0328	0.0505	-0.0551	-0.0428	0.0013
W							0.1078	-0.0541	-0.1192	0.5133	0.4903
P	6							0.2821	0.2702	0.7493	0.9007
M								1.4471	1.4492	2.1494	2.2523
U								0.8115	0.8154	0.8789	0.9244
V								-0.0563	-0.0215	-0.0347	0.0101
W								-0.0497	-0.0172	0.5497	0.5278
P	5								0.3221	0.9052	0.9571
M									1.5305	2.2689	2.2373
U									0.8451	0.9103	0.9249
V									0.0527	-0.0141	0.0225
W									0.0303	0.5589	0.5193
P	4									0.9193	0.8978
M										2.2527	2.1814
U										0.9062	0.9174
V										0.0327	0.0437
W										0.5545	0.5037
P	3									0.8259	0.8222
M										2.1174	2.2482
U										0.8754	0.9043
V										0.1067	0.0259
W										0.5339	0.5504
P	2									1.0326	1.0041
M										2.5963	2.3423
U										0.9298	0.9295
V										0.0113	0.0542
W										0.6535	0.5566
P	1									1.0269	0.9998
M										2.4471	2.2593
U										0.9313	0.9267
V										0.0404	0.0442
W										0.6937	0.5605

TABLE B-19. FINAL DATA SET FOR $M_\infty = 2.$, $R_d = 1.75 \times 10^6$, $\alpha_b = 20°$, x/d = 8.5

M287GA

P -- P0/P0INF M -- MACH NUMBER U,V,W -- 3-D VELOCITY COMPONENTS/U1NF

		1	2	3	4	5	6	7	8	9	10	11
P	22	0.9284	0.8892	0.8779	0.9194	0.9434	0.9313	0.9297	0.9642	0.9637	0.9676	0.9723
M		1.9293	1.9014	1.9104	1.9614	2.0458	2.0305	2.0246	2.0619	2.0760	2.0893	2.0998
U		0.9740	0.9640	0.9558	0.9579	0.9561	0.9430	0.9422	0.9666	0.9457	0.9468	0.9450
V		-0.0436	-0.0890	-0.1242	-0.1454	-0.1821	-0.1767	-0.1756	-0.1633	-0.1499	-0.1341	-0.1195
W		0.0664	0.0840	0.1429	0.1791	0.2792	0.3104	0.3083	0.3335	0.3533	0.3718	0.3834
P	21	0.9184	0.8409	0.8603	0.9109	0.9293	0.9477	0.9404	0.9344	0.9602	0.9664	0.9687
M		1.9352	1.8940	1.9285	1.9860	2.0945	2.1169	2.1019	2.0809	2.1035	2.1118	2.1188
U		0.9804	0.9637	0.9622	0.9622	0.9560	0.9506	0.9486	0.9383	0.9417	0.9415	0.9409
V		-0.0478	-0.0976	-0.1442	-0.1749	-0.2129	-0.1934	-0.1915	-0.1846	-0.1683	-0.1462	-0.1285
W		0.0050	0.0425	0.1145	0.1889	0.3038	0.3498	0.3449	0.3602	0.3757	0.3911	0.4032
P	20	0.9303	0.8688	0.8684	0.8910	0.8391	0.9148	0.9401	0.9689	0.9678	0.9697	0.9773
M		1.9475	1.9244	2.0020	2.0373	2.1008	2.1600	2.1902	2.1679	2.1502	2.1455	2.1485
U		0.9845	0.9746	0.9816	0.9706	0.9499	0.9458	0.9457	0.9383	0.9350	0.9348	0.9364
V		-0.0314	-0.0870	-0.1716	-0.2056	-0.2388	-0.2226	-0.2049	-0.1735	-0.1560	-0.1429	-0.1227
W		-0.0183	0.0097	0.0903	0.1905	0.3090	0.3769	0.4066	0.4239	0.4279	0.4294	0.4338
P	19	0.9345	0.8296	0.7325	0.7575	0.6823	0.8790	0.9398	0.9060	0.9481	0.9556	0.9717
M		1.9964	1.9412	1.9905	2.0441	2.0878	2.2616	2.2478	2.1971	2.1962	2.1943	2.1890
U		0.9948	0.9778	0.9819	0.9731	0.9417	0.9447	0.9405	0.9260	0.9261	0.9273	0.9301
V		-0.0319	-0.0918	-0.1716	-0.2174	-0.2259	-0.2414	-0.1959	-0.1723	-0.1514	-0.1406	-0.1188
W		-0.0853	-0.0506	0.0350	0.1739	0.3319	0.4325	0.4561	0.4669	0.4735	0.4735	0.4711
P	18	0.9225	0.7993	0.5817	0.5983	0.5934	0.7594	0.9531	0.9529	0.9352	0.9460	0.9642
M		2.0647	2.0044	1.9691	2.0178	2.1601	2.2334	2.5116	2.3754	2.2491	2.2277	2.2066
U		1.0043	0.9895	0.9799	0.9711	0.9504	0.9420	0.9329	0.9260	0.9171	0.9191	0.9236
V		-0.0273	-0.0844	-0.1497	-0.1929	-0.2136	-0.2124	-0.2125	-0.1669	-0.1438	-0.1320	-0.1074
W		-0.1615	-0.1259	-0.0103	0.1722	0.3703	0.4372	0.5828	0.5547	0.5195	0.5086	0.4956
P	17	0.9201	0.7478	0.4622	0.4842	0.5142	0.7021	0.9842	0.9934	0.9709	0.9575	0.9687
M		2.1667	2.0845	1.9996	2.0442	2.2529	2.4700	2.5678	2.4264	2.3174	2.2567	2.2228
U		1.0144	0.9980	0.9877	0.9852	0.9564	0.9379	0.9355	0.9271	0.9211	0.9151	0.9187
V		-0.0186	-0.0637	-0.1271	-0.1841	-0.1850	-0.2230	-0.1961	-0.1423	-0.1147	-0.1124	-0.0910
W		-0.2451	-0.2146	-0.0895	0.1735	0.4295	0.5542	0.6051	0.5804	0.5511	0.5341	0.5158
P	16	0.9150	0.6788	0.3089	0.3283	0.4849	0.6347	0.9485	0.9913	0.9799	0.9736	0.9788
M		2.2893	2.1717	1.9118	2.0086	2.3486	2.4482	2.5455	2.4085	2.3152	2.2820	2.2226
U		1.0223	0.9961	0.9595	0.9786	0.9756	0.9461	0.9383	0.9234	0.9201	0.9191	0.9170
V		-0.0059	-0.0249	-0.0354	-0.1454	-0.1832	-0.2024	-0.1801	-0.1193	-0.0887	-0.0839	-0.0736
W		-0.3262	-0.3152	-0.1480	0.1611	0.4414	0.5302	0.5976	0.5844	0.5564	0.5441	0.5215
P	15	0.8874	0.6168	0.4407	0.2860	0.2192	0.4641	0.8067	0.9903	0.9793	0.9719	0.9737
M		2.4063	2.2735	2.1342	1.8955	1.8779	2.3310	2.4219	2.3775	2.2927	2.2636	2.2000
U		1.0252	0.9954	0.9789	0.9665	0.9492	0.9834	0.9339	0.9196	0.9180	0.9163	0.9135
V		0.0127	0.0166	0.0124	-0.0603	-0.0776	-0.1687	-0.1552	-0.0962	-0.0646	-0.0590	-0.0571
W		-0.3953	-0.3906	-0.3377	-0.0553	0.1535	0.4197	0.5642	0.5822	0.5534	0.5437	0.5187
P	14	0.9088	0.6052	0.4176	0.2164	0.2021	0.3795	0.6028	0.6049	0.8102	0.9951	0.9865
M		2.5776	2.3985	2.1923	1.8433	1.8320	2.1871	2.2530	2.2565	2.3172	2.3389	2.2776
U		1.0320	0.9922	0.9662	0.9455	0.9476	0.9853	0.9749	0.9759	0.9248	0.9234	0.9216
V		0.0353	0.0657	0.0704	0.0193	0.0110	-0.0997	-0.0570	-0.0640	-0.1138	-0.0726	-0.0518
W		-0.4684	-0.4637	-0.4054	-0.1262	0.0755	0.3456	0.4240	0.4228	0.5449	0.5636	0.5419
P	13	0.9191	0.6238	0.4228	0.2281	0.2444	0.2019	0.6713	0.6797	0.6182	0.9895	0.9930
M		2.7269	2.5084	2.2406	1.8930	1.9279	1.8027	2.2222	2.2253	2.0969	2.3003	2.2534
U		1.0355	0.9944	0.9586	0.9432	0.9608	0.9345	1.0068	1.0083	0.8985	0.9182	0.9187
V		0.0477	0.0842	0.0948	0.0867	0.0843	0.0035	0.0340	0.0362	-0.0742	-0.0491	-0.0301
W		-0.5204	-0.5078	-0.4465	-0.2069	-0.1710	0.1143	0.3212	0.3188	0.4900	0.5581	0.5374
P	12	0.5512	0.4623	0.5294	0.2956	0.3411	0.2609	0.7557	0.7523	0.5031	0.9829	0.9789
M		2.1853	2.0542	2.3447	2.0253	2.0420	1.8817	2.1914	2.1881	1.9113	2.2672	2.2127
U		0.9808	0.9544	0.9840	0.9653	0.9812	0.9524	1.0229	1.0228	0.8761	0.9141	0.9134
V		0.0420	0.0872	0.0827	0.1122	0.1899	0.1412	0.0966	0.0906	-0.0219	-0.0239	-0.0080
W		-0.3680	-0.3336	-0.4508	-0.2637	-0.1557	0.0759	0.2160	0.2152	0.4265	0.5517	0.5280
P	11	0.8485	0.7718	0.6588	0.3932	0.3343	0.3273	0.8062	0.7791	0.8034	0.4345	0.9340
M		2.3038	2.2852	2.2592	2.0569	2.0014	1.9636	2.2409	2.2101	2.1846	1.7722	2.2176
U		1.0350	1.0254	1.0114	0.9723	0.9714	0.9643	1.0403	1.0323	1.0306	0.8677	0.9082
V		0.0309	0.0844	0.1357	0.2131	0.2141	0.2141	0.2054	0.1222	0.1019	0.0147	-0.0124
W		-0.2941	-0.3016	-0.3087	-0.2013	-0.1067	0.0128	0.0549	0.1771	0.1619	0.3387	0.5392
P	10	0.8644	0.8364	0.7738	0.5985	0.5776	0.6118	0.5079	0.8710	0.8101	0.4318	0.9406
M		2.2430	2.2467	2.2359	2.1188	2.1281	2.1376	2.0434	2.2052	2.1317	1.7179	2.1999
U		1.0388	1.0370	1.0298	0.9965	0.9982	1.0053	0.9803	1.0407	1.0257	0.8616	0.9096
V		0.0491	0.0990	0.1566	0.2413	0.2631	0.2522	0.2053	0.1274	0.1008	0.0419	0.0179
W		-0.2187	-0.2124	-0.1995	-0.1150	-0.0611	0.0068	0.1443	0.1005	0.0957	0.3017	0.5282
P	9	0.8655	0.8692	0.8844	0.8815	0.8082	0.8370	0.7779	0.8861	0.6499	0.5685	1.0010
M		2.1871	2.2006	2.2077	2.2249	2.2017	2.1992	2.1802	2.1713	2.0154	1.8418	2.1794
U		1.0382	1.0391	1.0421	1.0430	1.0308	1.0344	1.0278	1.0375	0.9876	0.8627	0.9219
V		0.0411	0.0945	0.0788	0.1356	0.2080	0.1901	0.1917	0.1116	0.1008	0.0066	0.0521
W		-0.1431	-0.1354	-0.1358	-0.1144	-0.0421	-0.0090	0.0583	0.0564	0.1518	0.4064	0.4935
P	8				0.9035	0.8637	0.8796	0.8838	0.8214	0.6489	0.7903	0.9596
M					2.2054	2.1919	2.1717	2.1894	2.0973	1.9708	2.0664	2.1592
U					1.0440	1.0356	1.0352	1.0384	1.0218	0.9814	0.9047	0.9188
V					0.1210	0.1703	0.1430	0.1493	0.0920	0.0943	0.0241	0.0634
W					-0.0692	-0.0313	-0.0072	0.0274	0.0198	0.1079	0.4661	0.4874
P	7						0.8813	0.8984	0.5644	0.5588	0.9625	0.9608
M							2.1371	2.1647	1.8370	1.8377	2.2012	2.1677
U							1.0301	1.0358	0.9503	0.9467	0.9268	0.9211
V							0.1139	0.1229	0.0464	0.0716	0.0455	0.0641
W							0.0029	0.0213	-0.0182	0.0750	0.4963	0.4873
P	6							0.7981	0.4431	0.4012	0.9748	0.9837
M								2.1021	1.6811	1.5850	2.2004	2.1807
U								1.0213	0.8935	0.8449	0.9234	0.9251
V								0.1117	-0.0040	0.0146	0.0717	0.0704
W								-0.0035	-0.0827	0.0560	0.4988	0.4858
P	5								0.3846	0.3150	0.9707	0.9745
M									1.5865	1.4472	2.1819	2.1574
U									0.8648	0.8146	0.9228	0.9235
V									-0.0043	0.0204	0.0873	0.0819
W									-0.0740	-0.0145	0.4881	0.4746

TABLE B-19. FINAL DATA SET FOR M_∞ = 2., R_d = 1.75 x 10^6, α_b = 20°, x/d = 8.5 (CONCLUDED)

		0.3437	0.9738	0.9644
		1.4544	2.1781	2.1462
		0.7365	0.9255	0.9234
		-0.0373	0.0978	0.0971
		0.3535	0.4788	0.4656
	1			
		1.0651	1.0071	0.9813
		2.3328	2.1884	2.1570
		0.9421	0.9324	0.9304
		0.0028	0.1083	0.1000
		0.5339	0.4686	0.4571
	2			
		0.7957	0.9669	1.0167
		1.9384	2.3303	2.3185
		0.8617	0.9363	0.9375
		0.2105	0.0827	0.0850
		0.4225	0.5366	0.5288
	1			
		1.0293	1.0253	1.0156
		2.3895	2.3081	2.2472
		0.9342	0.9380	0.9391
		0.1214	0.1180	0.1106
		0.5587	0.5166	0.4862

TABLE B-20. FINAL DATA SET FOR M_∞ = 2., R_d = 1.75 x 10^6, α_b = 20°, x/d = 11

M2R7G9

P -- PG/POINF M -- MACH NUMBER U,V,W -- 3-D VELOCITY COMPONENTS/UINF

		1	2	3	4	5	6	7	8	9	10	11
P	25	0.9322	0.9548	0.9637	0.9685	0.9739	0.9795	0.9397	0.9576	0.9651	0.9744	0.9712
M		1.9634	1.9844	2.0094	2.0225	1.9852	2.0757	2.1227	2.1140	2.1243	2.1159	2.1063
U		0.9886	0.9899	0.9871	0.9756	0.9332	0.9336	0.9325	0.9317	0.9323	0.9340	0.9348
V		-0.0452	-0.0991	-0.1599	-0.2077	-0.2081	-0.2082	-0.1791	-0.1497	-0.1368	-0.1197	-0.1129
W		0.0096	0.0391	0.0721	0.1307	0.2785	0.3556	0.4061	0.4141	0.4237	0.4198	0.4139
P	24	0.9348	0.9579	0.9408	0.8878	0.6712	0.7671	0.9226	0.9641	0.9677	0.9796	0.9808
M		1.9855	2.0106	2.0284	2.0292	2.0022	2.0648	2.1452	2.1438	2.1391	2.1254	2.1222
U		0.9944	0.9970	0.9919	0.9767	0.9428	0.9321	0.9315	0.9309	0.9304	0.9330	0.9354
V		-0.0493	-0.1085	-0.1753	-0.2271	-0.1798	-0.1864	-0.1768	-0.1491	-0.1345	-0.1155	-0.1097
W		-0.0239	0.0051	0.0337	0.1030	0.2855	0.3634	0.4236	0.4345	0.4378	0.4292	0.4234
P	23	0.9366	0.9410	0.7971	0.6597	0.6749	0.7167	0.8763	0.9816	0.9891	0.9284	0.8851
M		2.0357	2.0620	2.0044	1.9286	2.0634	2.0748	2.1644	2.1827	2.1483	2.0762	2.1084
U		1.0043	1.0082	0.9869	0.9558	0.9618	0.9361	0.9305	0.9308	0.9305	0.9225	0.9204
V		-0.0588	-0.1101	-0.1643	-0.2007	-0.1522	-0.1555	-0.1614	-0.1409	-0.1217	-0.1015	-0.1100
W		-0.0920	-0.0733	-0.0384	0.0769	0.2941	0.3748	0.4432	0.4601	0.4465	0.4248	0.4469
P	22	0.9387	0.9423	0.8929	0.8114	0.5592	0.6339	0.7181	0.8734	0.7770	0.8795	0.9677
M		2.0626	2.0894	1.9213	1.9656	1.9830	2.0674	2.1162	2.1774	2.0395	2.2524	2.3094
U		1.0079	1.0132	0.9883	0.9654	0.9782	0.9714	0.9362	0.9278	0.8988	0.9154	0.9285
V		-0.0374	-0.0838	-0.1339	-0.1585	-0.1320	-0.1490	-0.1397	-0.1385	-0.0964	-0.1346	-0.1291
W		-0.1387	-0.1229	-0.0038	0.1557	0.1272	0.2667	0.4087	0.4639	0.4525	0.5264	0.5316
P	21	0.9377	0.9039	0.5535	0.5962	0.4686	0.5606	0.6770	0.7493	0.8945	0.9604	0.9883
M		2.1467	2.1532	1.9574	2.0195	1.9365	2.0667	2.1262	2.1362	2.3628	2.4043	2.3463
U		1.0136	1.0200	0.9833	0.9864	0.9733	0.9727	0.9387	0.9136	0.9152	0.9223	0.9286
V		-0.0285	-0.0582	-0.0955	-0.1280	-0.1061	-0.1348	-0.1052	-0.0985	-0.1258	-0.1370	-0.1136
W		-0.2071	-0.1974	-0.0116	0.1468	0.0761	0.2687	0.4197	0.4799	0.5776	0.5806	0.5513
P	20	0.9357	0.8369	0.5238	0.5135	0.3773	0.4950	0.6689	0.7555	0.9205	0.9720	0.9917
M		2.2369	2.1879	1.9960	2.0075	1.8642	2.0660	2.2090	2.2814	2.4312	2.4318	2.3502
U		1.0230	1.0165	0.9959	0.9894	0.9566	0.9714	0.9453	0.9186	0.9214	0.9237	0.9267
V		-0.0157	-0.0282	-0.0633	-0.1038	-0.0785	-0.1102	-0.0881	-0.1072	-0.1249	-0.1222	-0.0974
W		-0.2784	-0.2578	-0.0445	0.1263	0.0364	0.2835	0.4583	0.5407	0.5952	0.5925	0.5591
P	19	0.9136	0.7942	0.4724	0.4090	0.3164	0.4473	0.6721	0.7231	0.8990	0.9826	0.9826
M		2.3140	2.2335	1.9960	1.9332	1.8016	2.0520	2.2646	2.3018	2.4304	2.4367	2.3352
U		1.0248	1.0148	0.9968	0.9738	0.9390	0.9665	0.9549	0.9189	0.9223	0.9248	0.9228
V		-0.0046	-0.0088	-0.0313	-0.0689	-0.0600	-0.0915	-0.0815	-0.1079	-0.1163	-0.1065	-0.0779
W		-0.3362	-0.3064	-0.0845	0.0971	0.0166	0.2934	0.4698	0.5443	0.5953	0.5957	0.5623
P	18	0.9119	0.6672	0.4973	0.4911	0.2892	0.4273	0.6861	0.6877	0.8683	0.9925	0.9848
M		2.3820	2.1897	2.0325	2.0304	1.7774	2.0528	2.2988	2.2822	2.4059	2.4290	2.3172
U		1.0282	1.0060	0.9981	0.9996	0.9320	0.9684	0.9684	0.9201	0.9229	0.9248	0.9213
V		0.0073	0.0046	-0.0156	-0.0261	-0.0448	-0.0807	-0.0756	-0.1007	-0.1083	-0.0898	-0.0590
W		-0.3724	-0.2989	-0.1469	-0.1298	-0.0047	0.2912	0.4612	0.5397	0.5863	0.5955	0.5592
P	17	0.8826	0.6644	0.4545	0.4483	0.2966	0.3792	0.7108	0.6447	0.7848	0.9837	0.9910
M		2.4388	2.2515	2.0283	2.0305	1.8055	1.9760	2.3267	2.2359	2.3264	2.3972	2.2970
U		1.0275	1.0116	0.9919	0.9938	0.9399	0.9585	0.9844	0.9208	0.9137	0.9211	0.9207
V		0.0123	0.0120	0.0024	-0.0096	-0.0265	-0.0861	-0.0665	-0.0905	-0.0985	-0.0726	-0.0395
W		-0.4081	-0.3304	-0.1784	-0.1705	-0.0623	0.2521	0.4430	0.5184	0.5700	0.5911	0.5532
P	16	0.8518	0.6302	0.4287	0.4116	0.3909	0.3606	0.7312	0.5973	0.6924	0.9785	0.9953
M		2.4760	2.2674	2.0313	2.0169	1.9913	1.9532	2.3381	2.1714	2.2223	2.3649	2.2762
U		1.0249	1.0101	0.9878	0.9849	0.9865	0.9553	1.0013	0.9228	0.8993	0.9187	0.9202
V		0.0114	0.0116	0.0083	-0.0023	-0.0079	-0.0483	-0.0466	-0.0696	-0.0767	-0.0514	-0.0208
W		-0.4345	-0.3466	-0.2036	-0.1982	-0.1481	0.2424	0.4128	0.4853	0.5509	0.5842	0.5430
P	15	0.7992	0.6180	0.5449	0.3526	0.3622	0.3546	0.6205	0.7611	0.5899	0.7257	0.9867
M		2.4646	2.2826	2.1995	1.9367	1.9666	1.9428	2.2373	2.3164	2.1163	2.1979	2.3215
U		1.0174	1.0098	1.0040	0.9728	0.9771	0.9553	0.9964	1.0087	0.9275	0.8940	0.9200
V		0.0027	0.0052	-0.0004	0.0010	-0.0025	-0.0146	-0.0090	0.0013	-0.0127	-0.0453	-0.0254
W		-0.4477	-0.3584	-0.3139	-0.1342	-0.1628	0.2348	0.3624	0.3839	0.4502	0.5517	0.5657
P	14	0.7629	0.5812	0.5144	0.3413	0.3267	0.3106	0.6687	0.8218	0.6573	0.7367	0.9847
M		2.4399	2.2476	2.1725	1.9265	1.8817	1.8585	2.2273	2.2929	2.1152	2.1521	2.2749
U		1.0125	1.0035	0.9977	0.9706	0.9611	0.9488	1.0027	1.0153	0.9437	0.8976	0.9204
V		-0.0127	-0.0046	-0.0067	0.0052	0.0263	0.0093	0.0418	0.0459	0.0424	0.0026	0.0029
W		-0.4444	-0.3518	-0.3116	-0.1286	-0.0915	0.1375	0.3368	0.3470	0.4126	0.5257	0.5453
P	13	0.6539	0.6448	0.4806	0.3397	0.3567	0.3526	0.7664	0.8517	0.7021	0.8387	0.9963
M		2.1966	2.2502	2.0926	1.9076	1.9121	1.9072	2.2165	2.2215	2.0745	2.1760	2.2360
U		0.9843	1.0012	0.9884	0.9661	0.9700	0.9594	1.0111	1.0097	0.9451	0.9195	0.9263
V		-0.0167	-0.0191	0.0035	0.0234	0.0802	0.0705	0.0862	0.0882	0.0604	0.0327	0.0252
W		-0.3686	-0.3596	-0.2706	-0.1173	-0.0546	0.1489	0.2921	0.3059	0.3793	0.4974	0.5161
P	12	0.8204	0.6813	0.6045	0.4195	0.4498	0.4080	0.6991	0.7447	0.7159	0.9557	0.9865
M		2.2362	2.1891	2.1652	2.0203	2.0111	1.9463	2.1310	2.1570	2.0208	2.2002	2.1882
U		1.0054	1.0019	1.0029	0.9901	0.9879	0.9620	1.0011	1.0026	0.9406	0.9399	0.9284
V		0.0169	0.0361	0.0274	0.0500	0.1114	0.1079	0.1322	0.1030	0.0385	0.0333	0.0322
W		-0.3375	-0.3098	-0.2869	-0.1686	-0.1338	0.1812	0.2262	0.2621	0.3540	0.4715	0.4876
P	11	0.7485	0.6669	0.5986	0.4312	0.5468	0.5524	0.8112	0.8357	0.8266	0.7874	0.9725
M		2.1301	2.1208	2.1211	1.9844	2.0520	2.0299	2.1169	2.1268	2.1973	2.0505	2.1750
U		0.9955	0.9969	0.9990	0.9818	0.9960	0.9821	1.0112	1.0120	1.0108	0.9349	0.9354
V		0.0423	0.0831	0.0866	0.1155	0.1744	0.1626	0.1254	0.0946	0.0727	-0.0064	0.0143
W		-0.2785	-0.2544	-0.2453	-0.1182	-0.0788	0.1598	0.1585	0.1887	0.2799	0.3921	0.4674
P	10	0.7872	0.7630	0.6373	0.5071	0.6724	0.7176	0.8657	0.8672	0.8403	0.8816	0.9789
M		2.0823	2.1050	2.0751	1.9942	2.0796	2.0805	2.1093	2.1058	2.1296	1.9465	2.1737
U		0.9994	1.0031	0.9949	0.9788	1.0019	1.0017	1.0211	1.0208	1.0033	0.8958	0.9285
V		0.0068	0.0775	0.1438	0.1843	0.1939	0.1676	0.0963	0.0663	0.0777	-0.0588	0.0045
W		-0.2147	-0.2119	-0.1747	-0.0690	-0.0456	0.1119	0.0865	0.1058	0.2391	0.4050	0.4807
P	9	0.7898	0.7649	0.7328	0.6751	0.6293	0.8324	0.8446	0.8746	0.7884	0.5571	0.9806
M		2.0703	2.0591	2.0739	2.0617	2.0206	2.1100	2.1110	2.1194	2.0387	1.8461	2.1784
U		1.0078	1.0023	1.0012	0.9959	0.9848	1.0178	1.0172	1.0160	0.9892	0.8404	0.9265
V		0.0105	0.0426	0.1415	0.1914	0.2021	0.1391	0.1243	0.0903	0.0476	-0.0445	0.0170
W		-0.1598	-0.1388	-0.1345	-0.0735	0.0260	0.0676	0.0961	0.1581	0.2014	0.4515	0.4981
P	8				0.7656	0.7537	0.8806	0.8972	0.8796	0.8510	0.6628	1.0059
M					2.0852	2.0610	2.1298	2.1258	2.1666	1.9233	1.9653	2.1766
U					1.0008	1.0018	1.0278	1.0274	1.0225	0.9685	0.8634	0.9225
V					0.1797	0.1721	0.1141	0.0994	0.0575	-0.0164	0.0698	0.0461
W					-0.0445	0.0173	0.0297	0.0512	0.0877	0.1365	0.4730	0.4906

TABLE B-20. FINAL DATA SET FOR $M_\infty = 2.$, $R_d = 1.75 \times 10^6$, $\alpha_b = 20°$, x/d = 11 (CONCLUDED)

PHUVW	7	0.7417	0.7867	0.8017	0.4490	0.9801
		2.0225	2.0553	2.0706	1.7287	2.1566
		1.0014	1.0114	1.0181	0.9153	0.9222
		0.0972	0.0864	0.0460	0.0119	0.0678
		-0.0152	0.0019	0.0117	0.0607	0.4786
PHUVW	6		0.3196	0.6116	0.3830	0.9845
			1.3765	1.9087	1.5909	2.1535
			0.7845	0.9717	0.8636	0.9270
			0.0521	0.0448	0.0622	0.0717
			-0.0129	-0.0471	0.0806	0.4671
PHUVW	5			0.4603	0.3929	0.9851
				1.6976	1.4919	2.1598
				0.9051	0.7662	0.9312
				0.0186	-0.0609	0.0679
				-0.0528	0.3197	0.4629
PHUVW	4				0.6477	0.9813
					1.9277	2.1626
					0.8473	0.9275
					0.0024	0.0753
					0.4913	0.4706
PHUVW	3				0.9412	0.9833
					2.1281	2.1553
					0.9005	0.9257
					0.1086	0.0938
					0.4966	0.4667
PHUVW	2				0.9490	0.9005
					2.1158	2.0544
					0.9125	0.9123
					0.1422	0.1044
					0.4583	0.4311
PHUVW	1				1.0541	1.0356
					2.4424	2.3374
					0.9380	0.9367
					0.1158	0.1180
					0.5752	0.5324

TABLE B-21. FINAL DATA SET FOR $M_\infty = 2.$, $R_d = 1.75 \times 10^6$, $\alpha_b = 25°$, x/d = 6

M2R7G10

P -- P0/PGINF M -- MACH NUMBER U,V,W -- 3-D VELOCITY COMPONENTS/UINF

		1	2	3	4	5	6	7	8	9	10
P	20	0.8790	0.8950	0.7248	0.7367	0.8720	0.8944	0.8502	0.8947	0.9461	0.9593
M		1.9125	1.9344	1.9206	1.9631	2.0630	2.0652	2.2022	2.2798	2.3102	2.2832
U		0.9708	0.9726	0.9446	0.9215	0.9041	0.9092	0.8953	0.8949	0.8982	0.8990
V		-0.0298	-0.0920	-0.2122	-0.2340	-0.1846	-0.1816	-0.2302	-0.2386	-0.2044	-0.1731
W		0.0851	0.0929	0.1336	0.2713	0.4279	0.4196	0.5033	0.5377	0.5597	0.5570
P	19	0.8900	0.9037	0.5566	0.5819	0.3966	0.4778	0.9425	0.9279	0.9602	0.9592
M		1.9718	1.9960	1.8861	1.9547	1.4155	1.7139	2.4415	2.4169	2.3717	2.3121
U		0.9913	0.9931	0.9441	0.9168	0.7227	0.8143	0.8882	0.8848	0.8910	0.8911
V		-0.0384	-0.1074	-0.1983	-0.2364	0.0150	-0.0989	-0.2479	-0.2398	-0.1985	-0.1651
W		0.0084	0.0055	0.0690	0.2796	0.3481	0.3998	0.6110	0.6099	0.5983	0.5842
P	18	0.9018	0.8720	0.5024	0.5399	0.8450	0.9061	0.9502	0.9536	0.9186	0.9083
M		2.0688	2.0863	1.9893	2.0731	2.7084	2.7541	2.5687	2.5501	2.3778	2.2875
U		1.0139	1.0152	0.9853	0.9555	0.8716	0.8752	0.8841	0.8850	0.8788	0.8759
V		-0.0339	-0.0870	-0.1491	-0.1875	-0.2854	-0.2851	-0.2177	-0.2047	-0.1779	-0.1506
W		-0.0851	-0.0947	0.0122	0.3031	0.7048	0.7133	0.6716	0.6685	0.6245	0.6005
P	17	0.9213	0.7671	0.3403	0.3165	0.8329	0.9573	0.9654	0.9393	0.9382	0.9615
M		2.1992	2.1419	1.9160	2.0193	2.7236	2.7890	2.6282	2.5309	2.4377	2.3677
U		1.0365	1.0182	0.9706	0.9279	0.8839	0.8822	0.8835	0.8799	0.8781	0.8802
V		-0.0299	-0.0404	-0.0504	-0.1409	-0.2551	-0.2629	-0.2095	-0.1947	-0.1607	-0.1343
W		-0.1773	-0.1953	-0.0899	0.3604	0.7056	0.7227	0.6934	0.6748	0.6520	0.6297
P	16	0.9362	0.5590	0.4627	0.3241	0.7596	0.9445	0.9928	0.9614	0.9530	0.9427
M		2.3147	2.1088	2.1265	1.9946	2.6690	2.7820	2.6361	2.5356	2.4348	2.3475
U		1.0497	1.0072	1.0241	0.9785	0.8966	0.8892	0.8864	0.8822	0.8810	0.8787
V		-0.0184	-0.0329	-0.0262	-0.1138	-0.2371	-0.2454	-0.1860	-0.1644	-0.1326	-0.1143
W		-0.2489	-0.2087	-0.1381	0.1633	0.6797	0.7184	0.6987	0.6786	0.6533	0.6282
P	15	0.9061	0.5265	0.3751	0.1869	0.6152	0.8869	0.9820	0.9748	0.9659	0.9538
M		2.4737	2.2551	2.1196	1.7443	2.5465	2.7201	2.5901	2.5167	2.4176	2.3264
U		1.0608	1.0207	1.0045	0.9111	0.9298	0.8993	0.8862	0.8845	0.8825	0.8794
V		0.0329	0.0553	0.0629	-0.0409	-0.1897	-0.2229	-0.1577	-0.1390	-0.1071	-0.0857
W		-0.3345	-0.2996	-0.2276	0.1394	0.6082	0.6959	0.6921	0.6751	0.6499	0.6236
P	14	0.9401	0.4901	0.3453	0.1540	0.6950	0.7795	0.9807	0.9561	0.9716	0.9660
M		2.6597	2.3345	2.1312	1.6586	2.6204	2.5845	2.5346	2.4588	2.3844	2.3099
U		1.0763	1.0143	0.9836	0.8930	0.9759	0.9080	0.8888	0.8812	0.8840	0.8834
V		0.0608	0.1090	0.0998	0.0207	-0.1704	-0.1877	-0.1263	-0.1088	-0.0788	-0.0563
W		-0.3953	-0.3642	-0.3060	0.0275	0.5663	0.6535	0.6779	0.6657	0.6400	0.6149
P	13	0.9442	0.9643	0.6685	0.1425	0.1862	0.6949	0.7302	0.8620	0.9747	0.9628
M		2.8350	2.9065	2.6237	1.6094	1.8120	2.5757	2.4716	2.4054	2.3405	2.2707
U		1.0883	1.0920	1.0505	0.8745	0.8909	0.9708	0.8880	0.8713	0.8859	0.8833
V		0.0304	0.0874	0.1145	0.0054	-0.1103	-0.1542	-0.1640	-0.1701	-0.0514	-0.0335
W		-0.4491	-0.4620	-0.4311	-0.0549	0.2932	0.5628	0.6495	0.6473	0.6236	0.6008
P	12	0.9404	0.9631	0.8577	0.3736	0.1404	0.3233	0.3612	0.6120	0.9706	0.9734
M		3.0074	3.0534	2.9255	2.3031	1.6148	2.6794	2.0498	2.2808	2.2855	2.2383
U		1.0952	1.0973	1.0848	1.0043	0.8734	0.9214	0.9177	0.8798	0.8858	0.8856
V		0.0385	0.0866	0.1131	0.0989	-0.0300	-0.1180	-0.1124	-0.1227	-0.0251	-0.0130
W		-0.4986	-0.5029	-0.4803	-0.3740	0.0865	0.4249	0.4153	0.5898	0.6035	0.5846
P	11	0.9277	0.8775	0.8141	0.3975	0.1555	0.3819	0.5244	0.5361	0.7987	0.9503
M		3.1554	3.0882	2.9567	2.3387	1.6558	2.0845	2.1496	2.0689	2.2755	2.3066
U		1.1001	1.0932	1.0790	1.0043	0.8896	0.9597	0.9826	0.8787	0.8728	0.8802
V		0.0297	0.0750	0.0933	0.0749	0.0366	0.0199	0.0690	-0.0675	-0.0755	-0.0430
W		-0.5355	-0.5248	-0.5082	-0.4015	0.0644	0.3532	0.3324	0.5110	0.6142	0.6191
P	10	0.7028	0.7117	0.7542	0.4488	0.2067	0.2073	0.8284	0.4558	0.7938	0.9521
M		2.2050	2.2033	2.3018	2.1666	1.7786	1.7113	2.2789	1.8691	2.1995	2.2485
U		1.0476	1.0448	1.0556	1.0066	0.9235	0.8775	1.0429	0.8642	0.8716	0.8807
V		0.0007	0.0489	0.0820	0.1598	0.1380	0.0507	0.1623	-0.0303	-0.0477	-0.0161
W		-0.1144	-0.1199	-0.1912	-0.2253	-0.0096	0.2420	0.1798	0.4216	0.5869	0.5961
P	9	0.8207	0.7401	0.6948	0.6782	0.4437	0.4977	0.7840	0.6348	0.8329	0.9186
M		2.2864	2.2222	2.1700	2.2293	2.0256	2.0784	2.2429	2.0871	2.2020	2.2129
U		1.0690	1.0521	1.0331	1.0329	0.9636	0.9794	1.0392	1.0129	0.8713	0.8748
V		0.0080	0.0546	0.1082	0.2151	0.2887	0.2185	0.0970	0.0681	-0.0224	0.0045
W		-0.0857	-0.0903	-0.1104	-0.0919	0.0475	0.1894	0.1977	0.1299	0.5900	0.5899
P	8				0.8669	0.8398	0.8425	0.6587	0.4542	0.8699	0.9098
M					2.3147	2.3132	2.2914	2.1069	1.8622	2.2663	2.2936
U					1.0624	1.0525	1.0497	1.0239	0.9589	0.8706	0.8712
V					0.1866	0.2302	0.2072	0.0496	0.0388	-0.0084	-0.0040
W					-0.0204	0.0477	0.0871	0.0431	-0.0205	0.6182	0.6282
P	7						0.3783	0.4589	0.2984	0.9157	0.9513
M							1.7719	1.9061	1.5868	2.3595	2.3450
U							0.9170	0.9697	0.8640	0.8740	0.8784
V							0.1628	0.0309	-0.0039	-0.0091	-0.0012
W							-0.0218	-0.0757	-0.0837	0.6491	0.6378
P	6							0.3166	0.2755	0.9643	0.9545
M								1.6780	1.5660	2.3962	2.3198
U								0.8941	0.8603	0.8809	0.8794
V								-0.0155	0.0034	0.0057	0.0193
W								-0.1041	-0.0147	0.6531	0.6266
P	5								0.3193	0.9360	0.9425
M									1.4657	2.3358	2.2922
U									0.8954	0.8754	0.8793
V									0.0347	0.0322	0.0351
W									-0.0005	0.6378	0.6152
P	4									0.9243	0.9030
M										2.3193	2.2745
U										0.8740	0.8828
V										0.0520	0.0545
W										0.6282	0.6015
P	3									0.9024	1.0066
M										2.3128	2.5236
U										0.8851	0.8886
V										0.0744	0.0927
W										0.6115	0.6863

TABLE B-21. FINAL DATA SET FOR M_∞ = 2., R_d = 1.75 x 10^6, α_b = 25°, x/d = 6 (CONCLUDED)

P	/	1.0204 1.0006
M		2.6103 2.4093
U		0.8873 0.8891
V		0.0100 0.0482
W		0.7144 0.6449
P	1	0.9848 0.9859
M		2.4206 2.2945
U		0.8845 0.8840
V		0.0722 0.0938
W		0.6531 0.6031

TABLE B-22. FINAL DATA SET FOR $M_\infty = 2.$, $R_d = 1.75 \times 10^6$, $\alpha_b = 25°$, x/d = 9

M2R7G11

P -- P0/P0INF M -- MACH NUMBER U,V,W -- 3-D VELOCITY COMPONENTS/UINF

		1	2	3	4	5	6	7	8	9	10	11
P	22	0.8184	0.8356	0.4681	0.4331	0.4810	0.8215	0.9240	0.9594	0.9964	0.9910	0.9833
M		2.2764	2.1275	1.9663	1.9977	2.0592	2.4368	2.5463	2.5788	2.5355	2.4675	2.4116
U		1.0221	1.0093	0.9903	0.9742	0.9329	0.8848	0.8789	0.8854	0.8904	0.8893	0.8882
V		0.0141	0.0172	0.0021	-0.0462	-0.0773	-0.1290	-0.1550	-0.1652	-0.1426	-0.1212	-0.1040
W		-0.3186	-0.2236	-0.0224	0.2183	0.3952	0.6496	0.6883	0.6879	0.6726	0.6556	0.6405
P	21	0.8000	0.8227	0.4521	0.4175	0.4672	0.7505	0.9403	0.9842	0.9913	0.9957	0.9833
M		2.3143	2.1631	1.9905	2.0159	2.0821	2.4169	2.5811	2.5935	2.5131	2.4498	2.3912
U		1.0230	1.0127	0.9958	0.9843	0.9475	0.8860	0.8816	0.8875	0.8885	0.8885	0.8871
V		0.0117	0.0161	0.0091	-0.0526	-0.0787	-0.1349	-0.1574	-0.1592	-0.1298	-0.1077	-0.0906
W		-0.3420	-0.2488	-0.0544	0.1928	0.3754	0.6396	0.6952	0.6911	0.6705	0.6531	0.6366
P	20	0.7827	0.8019	0.4317	0.3942	0.4561	0.6696	0.9580	0.9865	1.0030	0.9831	0.9760
M		2.3393	2.1850	2.0079	2.0178	2.1042	2.3776	2.6081	2.5863	2.4948	2.4143	2.3610
U		1.0230	1.0126	0.9986	0.9897	0.9611	0.8874	0.8850	0.8863	0.8886	0.8855	0.8848
V		0.0080	0.0130	0.0088	-0.0573	-0.0794	-0.1380	-0.1571	-0.1488	-0.1149	-0.0908	-0.0741
W		-0.3594	-0.2712	-0.0842	0.1646	0.3560	0.6224	0.6992	0.6928	0.6670	0.6471	0.6307
P	19	0.8078	0.4985	0.3862	0.3823	0.4535	0.5016	0.6973	0.9629	0.9967	0.9888	0.9824
M		2.3951	2.1061	1.9651	2.0247	2.1222	2.2097	2.4245	2.6096	2.4743	2.3969	2.3510
U		1.0328	1.0049	0.9896	0.9972	0.9717	0.9285	0.8839	0.8879	0.8883	0.8851	0.8864
V		0.0100	0.0210	-0.0095	-0.0514	-0.0788	-0.0976	-0.1547	-0.1598	-0.1015	-0.0783	-0.0626
W		-0.3680	-0.2181	-0.0314	0.1390	0.3402	0.4900	0.6407	0.6953	0.6627	0.6430	0.6259
P	18	0.8039	0.4917	0.3706	0.3433	0.4398	0.5230	0.5949	0.9545	1.0074	0.9845	0.9862
M		2.4278	2.1393	1.9788	1.9951	2.1422	2.2631	2.3297	2.5925	2.4469	2.3624	2.3175
U		1.0341	1.0059	0.9906	0.9917	0.9834	0.9587	0.8828	0.8908	0.8887	0.8840	0.8850
V		0.0097	0.0188	-0.0041	-0.0488	-0.0766	-0.0875	-0.1434	-0.1503	-0.0936	-0.0692	-0.0453
W		-0.3847	-0.2511	-0.0833	0.1074	0.3222	0.4601	0.6092	0.6886	0.6552	0.6336	0.6164
P	17	0.7687	0.4899	0.3607	0.3030	0.4148	0.5429	0.5234	0.9121	0.9988	0.9869	0.9950
M		2.4374	2.1751	2.0060	1.9439	2.1352	2.3020	2.2423	2.5451	2.4021	2.3296	2.2931
U		1.0312	1.0058	0.9923	0.9796	0.9875	0.9829	0.8900	0.8938	0.8871	0.8833	0.8859
V		0.0117	0.0176	0.0024	-0.0455	-0.0718	-0.0755	-0.1195	-0.1379	-0.0835	-0.0613	-0.0291
W		-0.3979	-0.2862	-0.1362	0.0805	0.3046	0.4311	0.5673	0.6723	0.6438	0.6239	0.6063
P	16	0.7644	0.4694	0.3326	0.2978	0.3920	0.5625	0.4831	0.8358	0.9884	0.9877	0.9784
M		2.4710	2.1929	1.9968	1.9305	2.0388	2.3175	2.1763	2.4745	2.3540	2.2965	2.2521
U		1.0326	1.0087	0.9904	0.9756	0.9786	1.0001	0.9042	0.8922	0.8840	0.8834	0.8837
V		0.0133	0.0168	-0.0053	-0.0151	-0.0581	-0.0554	-0.0747	-0.1191	-0.0605	-0.0222	-0.0120
W		-0.4129	-0.2921	-0.1276	-0.0944	0.2456	0.4023	0.5202	0.6545	0.6322	0.6116	0.5933
P	15	0.7356	0.4393	0.3045	0.2755	0.3165	0.5764	0.5073	0.7317	0.9854	0.9778	0.9680
M		2.4762	2.1775	1.9588	1.8921	1.9859	2.3035	2.1639	2.3565	2.3226	2.2677	2.2299
U		1.0296	1.0023	0.9777	0.9613	0.9640	1.0100	0.9325	0.8825	0.8820	0.8810	0.8817
V		0.0151	0.0202	0.0034	-0.0020	-0.0362	-0.0284	-0.0281	-0.0885	-0.0151	-0.0032	0.0043
W		-0.4232	-0.3003	-0.1448	-0.1216	0.2278	0.3708	0.4666	0.6304	0.6241	0.6038	0.5870
P	14	0.6930	0.4143	0.2841	0.2683	0.3203	0.6203	0.5492	0.7035	0.9646	1.0069	1.0003
M		2.4252	2.1450	1.9125	1.8707	1.9636	2.2839	2.1326	2.2775	2.2737	2.3855	2.3157
U		1.0228	0.9956	0.9645	0.9544	0.9669	1.0171	0.9511	0.8803	0.8781	0.8844	0.8892
V		0.0191	0.0271	0.0201	0.0164	-0.0014	0.0102	0.0149	-0.0443	0.0081	-0.0230	-0.0088
W		-0.4118	-0.2930	-0.1414	-0.1237	0.2118	0.3381	0.4087	0.6069	0.6105	0.6372	0.6112
P	13	0.7131	0.6073	0.3684	0.2600	0.2572	0.5304	0.7317	0.6720	0.5484	0.9911	0.9869
M		2.4662	2.3649	2.0709	1.8556	1.8047	2.1609	2.2802	2.2782	2.1199	2.3218	2.2766
U		1.0278	1.0230	0.9876	0.9537	0.9393	1.0083	1.0227	1.0140	0.9423	0.8668	0.8862
V		0.0309	0.0356	0.0363	0.0284	0.0367	0.0715	0.0487	0.0258	0.0083	0.0036	0.0076
W		-0.4213	-0.3744	-0.2493	-0.0844	0.0618	0.2546	0.3142	0.3424	0.4207	0.6171	0.5998
P	12	0.6136	0.5948	0.4530	0.3543	0.2675	0.3158	0.7000	0.7312	0.5294	0.8214	0.9809
M		2.3150	2.3572	2.1893	2.0295	1.8472	1.8827	2.2212	2.2329	2.0063	2.2187	2.2829
U		1.0047	1.0207	1.0069	0.9865	0.9526	0.9483	1.0216	1.0224	0.9344	0.8738	0.8805
V		0.0151	0.0344	0.0442	0.0451	0.0396	0.0546	0.1002	0.0625	0.0178	-0.0190	0.0082
W		-0.3800	-0.3758	-0.2921	-0.2028	-0.0606	0.1764	0.2526	0.2724	0.3607	0.5938	0.6106
P	11	0.6651	0.5670	0.4408	0.3573	0.2876	0.4418	0.7577	0.7348	0.4598	0.9018	0.9699
M		2.2506	2.1497	2.0965	1.9801	1.8382	2.0183	2.1775	2.1621	1.8674	2.2451	2.2537
U		1.0191	1.0086	0.9951	0.9790	0.9493	0.9834	1.0295	1.0257	0.9080	0.8622	0.8796
V		0.0582	0.0469	0.0570	0.0676	0.0735	0.1147	0.1144	0.0689	-0.0014	-0.0023	0.0167
W		-0.3004	-0.2950	-0.2434	-0.1608	-0.0290	0.1731	0.1489	0.1740	0.2472	0.5927	0.5999
P	10	0.6910	0.6020	0.4599	0.4199	0.3647	0.6641	0.7627	0.3221	0.9662	0.9336	0.9700
M		2.1588	2.1665	2.0462	1.9980	1.8951	2.1635	2.1929	1.5644	2.2890	2.2663	2.2514
U		1.0185	1.0125	0.9906	0.9862	0.9607	1.0201	1.0323	0.8412	0.8974	0.8782	0.8782
V		0.0972	0.1029	0.1089	0.1245	0.1318	0.1638	0.1119	-0.0023	0.0267	0.0022	0.0221
W		-0.1969	-0.2319	-0.1798	-0.1041	0.0172	0.1432	0.1577	0.1783	0.5879	0.6073	0.6008
P	9	0.8201	0.7131	0.5881	0.6173	0.5775	0.7725	0.7100	0.2667	0.9715	0.9618	0.9592
M		2.2018	2.1583	2.0815	2.1382	2.0845	2.1804	2.1146	1.4336	2.2886	2.3035	2.2537
U		1.0417	1.0240	1.0034	1.0159	1.0028	1.0341	1.0247	0.7893	0.8929	0.8764	0.8751
V		0.1651	0.1415	0.1745	0.2011	0.1973	0.1476	0.0861	0.0105	0.0251	0.0202	0.0303
W		-0.1069	-0.1292	-0.0850	-0.0471	0.0410	0.0741	0.0695	0.1799	0.5944	0.6244	0.6060
P	8				0.8214	0.7718	0.7167	0.6996	0.2557	0.9643	0.9654	0.9736
M					2.2540	2.1918	2.1142	2.1091	1.3930	2.2966	2.3189	2.2743
U					1.0470	1.0346	1.0248	1.0256	0.7666	0.8862	0.8790	0.8779
V					0.1920	0.1772	0.1059	0.0625	0.0076	0.0376	0.0474	0.0419
W					-0.0286	0.0245	0.0261	0.0588	0.2032	0.6068	0.6254	0.6096
P	7						0.6416	0.6214	0.2534	0.9668	0.9840	0.9761
M							2.0570	2.0430	1.3643	2.3033	2.3051	2.2669
U							1.0111	1.0100	0.7384	0.8847	0.8818	0.8800
V							0.0421	0.0601	-0.0001	0.0540	0.0634	0.0550
W							-0.0227	-0.0023	0.2551	0.6104	0.6145	0.6025
P	6							0.4641	0.2457	0.9644	0.9823	0.9786
M								1.8867	1.4883	2.2916	2.2916	2.2565
U								0.9561	0.7362	0.8859	0.8851	0.8824
V								0.0581	-0.0031	0.0674	0.0714	0.0667
W								-0.0523	0.1856	0.6028	0.6013	0.5934
P	5									0.9716	0.9860	0.9873
M										2.2821	2.2887	2.2549
U										0.8894	0.8866	0.8843
V										0.0780	0.0805	0.0778
W										0.5922	0.5984	0.5885

TABLE B-22. FINAL DATA SET FOR M_∞ = 2., R_d = 1.75 x 10^6, α_b = 25°, x/d = 9 (CONCLUDED)

0.9814	0.9816	0.9951	
2.2815	2.2788	2.4360	
0.8914	0.8872	0.8868	
0.0475	0.0404	0.0292	
0.5877	0.5924	0.6566	
			3
0.8244	1.0554	1.0223	
2.1611	2.5179	2.3736	
0.8701	0.8932	0.8913	
0.1126	0.0441	0.0673	
0.5630	0.6768	0.6270	
			2
1.0388	1.0604	1.0300	
2.4766	2.3985	2.2926	
0.9004	0.8958	0.8949	
0.0628	0.0957	0.0995	
0.6519	0.6263	0.5851	
			1
1.0067	1.0331	1.0162	
2.3292	2.2617	2.1938	
0.8939	0.8932	0.8939	
0.1082	0.1343	0.1294	
0.6001	0.5662	0.5364	

TABLE B-23. FINAL DATA SET FOR $M_\infty = 3.01$, $R_d = 1.70 \times 10^6$, $\alpha_b = 10°$, x/d = 8

M1R761

P -- P0/P0INF M -- MACH NUMBER U,V,W -- 3-D VELOCITY COMPONENTS/U0INF

		1	2	3	4	5	6	7	8	9	10
P	13	0.8640	0.7927	0.8108	0.8123	0.8214	0.8386	0.8512	0.8552	0.8725	0.8957
M		2.9455	2.8915	2.9164	2.9284	2.9475	2.9734	3.0196	3.0201	3.0347	3.0489
U		0.9916	0.9862	0.9855	0.9837	0.9826	0.9817	0.9804	0.9791	0.9767	0.9808
V		-0.0016	-0.0277	-0.0554	-0.0748	-0.0902	-0.0911	-0.1025	-0.0867	-0.0746	-0.0607
W		0.0343	0.0424	0.0559	0.0797	0.1062	0.1384	0.1722	0.1904	0.2013	0.2077
P	12	0.8269	0.7904	0.8103	0.8143	0.8188	0.8268	0.8323	0.8410	0.8678	0.8806
M		2.9289	2.9105	2.9428	2.9699	2.9946	3.0132	3.0586	3.0445	3.0614	3.0542
U		0.9901	0.9872	0.9840	0.9876	0.9850	0.9812	0.9774	0.9756	0.9774	0.9736
V		-0.0024	-0.0346	-0.0720	-0.1107	-0.1302	-0.1273	-0.1273	-0.0993	-0.0747	-0.0614
W		0.0076	0.0123	0.0219	0.0523	0.0962	0.1474	0.1998	0.2182	0.2246	0.2253
P	11	0.8008	0.7864	0.8011	0.8347	0.8290	0.8187	0.8019	0.8416	0.8667	0.8748
M		2.9288	2.9319	2.9772	3.1240	3.1894	3.1247	3.1319	3.1115	3.0962	3.0857
U		0.9900	0.9897	0.9921	0.9953	0.9972	0.9824	0.9709	0.9723	0.9746	0.9773
V		-0.0019	-0.0336	-0.0843	-0.1656	-0.2053	-0.1781	-0.1586	-0.1058	-0.0744	-0.0572
W		-0.0186	-0.0216	-0.0277	-0.0096	0.0627	0.1719	0.2581	0.2586	0.2529	0.2433
P	10	0.7936	0.7689	0.7472	0.1607	0.1569	0.2494	0.4234	0.8526	0.8656	0.8855
M		2.9498	2.9659	3.0203	2.2124	2.2858	2.5361	2.8335	3.1793	3.1131	3.0867
U		0.9920	0.9906	0.9933	0.8598	0.8686	0.8870	0.9143	0.9679	0.9782	0.9743
V		0.0047	-0.0133	-0.0455	-0.1279	-0.1876	-0.2278	-0.1802	-0.0931	-0.0657	-0.0449
W		-0.0378	-0.0555	-0.1174	-0.1101	0.0583	0.1859	0.2966	0.3046	0.2798	0.2578
P	9	0.7518	0.7578	0.5687	0.1004	0.0852	0.1200	0.2231	0.8597	0.8640	0.8808
M		2.9301	2.9566	2.8864	2.0324	2.0246	2.2109	2.4554	3.2191	3.1067	3.0766
U		0.9893	0.9908	0.9672	0.8286	0.8351	0.8510	0.8636	0.9668	0.9677	0.9723
V		0.0095	0.0278	0.0808	0.0616	-0.0349	-0.1249	-0.0945	-0.0666	-0.0377	-0.0275
W		-0.0442	-0.0688	-0.1671	-0.1085	0.0230	0.1656	0.3059	0.3282	0.2906	0.2633
P	8				0.8072	0.2203	0.0813	0.2321	0.7665	0.8608	0.8870
M					3.1682	2.5235	1.9855	2.3404	3.0842	3.0656	3.0689
U					0.9993	0.8899	0.8145	0.8703	0.9623	0.9666	0.9721
V					0.1447	0.2469	0.1436	0.0649	-0.0264	-0.0101	-0.0122
W					-0.1278	-0.1282	-0.0082	0.2216	0.3007	0.2801	0.2619
P	7						0.3487	0.2865	0.7320	0.8436	0.8692
M							2.6841	2.3177	2.9607	3.0171	3.0391
U							0.9108	0.8942	0.9620	0.9654	0.9695
V							0.2941	0.0637	-0.0146	-0.0012	-0.0033
W							0.0109	0.0080	0.2497	0.2040	0.2587
P	6							0.1203	0.6771	0.8252	0.8672
M								1.8177	2.9655	3.0173	3.0437
U								0.7713	0.9563	0.9636	0.9687
V								-0.0862	-0.0545	-0.0028	0.0019
W								-0.1230	0.2682	0.2706	0.2635
P	5								0.6687	0.8645	0.8951
M									3.0522	3.0879	3.0740
U									0.9560	0.9678	0.9709
V									-0.0467	0.0071	0.0106
W									0.3124	0.2853	0.2686
P	4								0.8194	0.8629	0.8801
M									3.1757	3.0739	3.0526
U									0.9704	0.9671	0.9686
V									-0.0207	0.0221	0.0217
W									0.3088	0.2813	0.2671
P	3									0.8638	0.8873
M										3.0716	3.0625
U										0.9668	0.9690
V										0.0330	0.0315
W										0.2802	0.2688
P	2									0.8180	0.8055
M										3.0551	3.0408
U										0.9643	0.9651
V										0.0425	0.0224
W										0.2807	0.2447
P	1									0.9285	0.9416
M										3.2718	3.2122
U										0.9752	0.9764
V										0.0345	0.0374
W										0.3244	0.2991

TABLE B-24. FINAL DATA SET FOR $M_\infty = 3.01$, $R_d = 1.70 \times 10^6$, $\alpha_b = 10°$, x/d = 11

P -- P0/P0INF M -- MACH NUMBER U,V,W -- 3-D VELOCITY COMPONENTS/U1NF

		1	2	3	4	5	6	7	8	9	10
P	18	0.8615	0.8269	0.8295	0.8562	0.8855	0.8700	0.8901	0.8907	0.8965	0.9044
M		2.8879	2.8641	2.8770	2.9119	2.9286	2.9489	2.9705	2.9725	2.9783	2.9854
U		0.9825	0.9786	0.9785	0.9801	0.9798	0.9789	0.9792	0.9779	0.9777	0.9778
V		-0.0024	-0.0201	-0.0468	-0.0617	-0.0693	-0.0769	-0.0710	-0.0667	-0.0613	-0.0531
W		0.0696	0.0787	0.0887	0.1086	0.1244	0.1438	0.1634	0.1743	0.1811	0.1876
P	17	0.8256	0.8248	0.8402	0.8572	0.8671	0.8632	0.8737	0.8910	0.8986	0.9093
M		2.8640	2.8688	2.8869	2.9265	2.9476	2.9658	2.9741	2.9886	2.9953	3.0015
U		0.9806	0.9803	0.9815	0.9814	0.9809	0.9785	0.9766	0.9768	0.9771	0.9776
V		-0.0055	-0.0279	-0.0643	-0.0835	-0.0914	-0.0984	-0.0848	-0.0766	-0.0680	-0.0577
W		0.0503	0.0600	0.0709	0.0981	0.1204	0.1496	0.1749	0.1869	0.1927	0.1973
P	16	0.8124	0.8202	0.8492	0.7479	0.7052	0.7270	0.8636	0.8891	0.8876	0.8987
M		2.8660	2.8783	2.9283	2.8814	2.8558	2.8952	3.0025	3.0111	2.9994	3.0026
U		0.9818	0.9824	0.9853	0.9754	0.9676	0.9654	0.9754	0.9753	0.9742	0.9752
V		-0.0096	-0.0385	-0.0875	-0.1107	-0.1199	-0.1212	-0.0991	-0.0844	-0.0719	-0.0595
W		0.0245	0.0355	0.0428	0.0702	0.1074	0.1594	0.1922	0.2046	0.2079	0.2090
P	15	0.8018	0.8279	0.8297	0.4531	0.5115	0.6342	0.8317	0.8711	0.8939	0.9031
M		2.8780	2.9082	2.7848	2.6045	2.6969	2.8764	3.0256	3.0265	3.0275	3.0250
U		0.9836	0.9863	0.9657	0.9311	0.9390	0.9547	0.9717	0.9721	0.9736	0.9746
V		-0.0133	-0.0503	-0.1036	-0.1500	-0.1531	-0.1444	-0.1093	-0.0870	-0.0723	-0.0589
W		-0.0069	0.0020	-0.0141	0.0632	0.1206	0.1869	0.2181	0.2264	0.2257	0.2241
P	14	0.8047	0.8345	0.3806	0.3396	0.4075	0.5259	0.8006	0.8726	0.8880	0.8994
M		2.9190	2.9542	2.5435	2.5625	2.6723	2.8547	3.0647	3.0686	3.0498	3.0429
U		0.9878	0.9908	0.9222	0.9142	0.9436	0.9389	0.9677	0.9707	0.9716	0.9733
V		-0.0151	-0.0556	-0.1318	-0.2096	-0.2006	-0.1630	-0.1138	-0.0844	-0.0687	-0.0550
W		-0.0446	-0.0421	-0.0862	0.0363	0.1434	0.2314	0.2517	0.2536	0.2462	0.2397
P	13	0.8075	0.8536	0.2492	0.1340	0.2117	0.4098	0.7356	0.8788	0.8839	0.9045
M		2.9744	3.0386	2.4239	2.2002	2.4632	2.8186	3.0867	3.1176	3.0751	3.0654
U		0.9922	0.9981	0.8924	0.8606	0.8863	0.9213	0.9623	0.9698	0.9698	0.9726
V		-0.0118	-0.0447	-0.0519	-0.1501	-0.1934	-0.1486	-0.1047	-0.0723	-0.0586	-0.0466
W		-0.0828	-0.0925	-0.1985	0.0129	0.1668	0.2855	0.2841	0.2811	0.2667	0.2544
P	12	0.8025	0.8500	0.2223	0.0866	0.1109	0.3380	0.6042	0.8898	0.8971	0.9170
M		3.0210	3.1076	2.3966	2.0065	2.1616	2.7655	2.9934	3.1470	3.0959	3.0815
U		0.9954	1.0026	0.8812	0.8318	0.8485	0.9145	0.9482	0.9698	0.9701	0.9731
V		-0.0021	-0.0121	0.0731	-0.0072	-0.0933	-0.0967	-0.0770	-0.0520	-0.0414	-0.0353
W		-0.1081	-0.1311	-0.2185	-0.0155	0.1451	0.3046	0.3018	0.2965	0.2775	0.2616
P	11	0.7901	0.8288	0.6686	0.1653	0.0836	0.1802	0.4227	0.7315	0.9098	0.9060
M		3.0460	3.1254	3.0812	2.2976	1.9605	2.3366	2.7711	3.0497	3.1274	3.0797
U		0.9974	1.0036	0.9902	0.8685	0.8177	0.8693	0.9247	0.9598	0.9708	0.9709
V		0.0111	0.0250	0.0894	0.1512	0.0737	-0.0043	-0.0222	-0.0362	-0.0256	-0.0240
W		-0.1161	-0.1366	-0.1672	-0.1407	0.0220	0.2330	0.2902	0.2945	0.2898	0.2699
P	10	0.7615	0.7817	0.7976	0.3789	0.1835	0.2821	0.4364	0.6709	0.9000	0.9111
M		3.0036	3.0554	3.1269	2.6993	2.3004	2.4706	2.6951	2.9469	3.0927	3.0754
U		0.9949	0.9983	1.0023	0.9361	0.8707	0.9032	0.9338	0.9549	0.9700	0.9715
V		0.0218	0.0478	0.0981	0.1810	0.1995	0.1073	0.0427	-0.0214	-0.0104	-0.0126
W		-0.0953	-0.1079	-0.1137	-0.1065	-0.0023	0.1605	0.2140	0.2693	0.2796	0.2670
P	9	0.7699	0.7775	0.7899	0.6842	0.4522	0.6318	0.4113	0.6266	0.8998	0.9241
M		2.9973	3.0277	3.0723	2.9988	2.7154	2.8946	2.5825	2.8714	3.0710	3.0779
U		0.9961	0.9978	0.9999	0.9860	0.9455	0.9738	0.9328	0.9504	0.9703	0.9728
V		0.0287	0.0592	0.1004	0.1493	0.1753	0.1288	0.0683	-0.0247	-0.0032	-0.0048
W		-0.0628	-0.0712	-0.0672	-0.0528	0.0003	0.0840	0.1099	0.2494	0.2697	0.2636
P	8				0.7499	0.7536	0.5636	0.2855	0.5751	0.9009	0.9251
M					3.0074	3.0061	2.7777	2.3234	2.8076	3.0663	3.0745
U					0.9925	0.9911	0.9656	0.8959	0.9420	0.9707	0.9728
V					0.1176	0.1296	0.0968	0.0498	-0.0359	-0.0013	0.0001
W					-0.0644	0.0039	0.0034	0.0236	0.2469	0.2661	0.2620
P	7						0.1750	0.1728	0.5548	0.9035	0.9273
M							2.0436	2.0233	2.8136	3.0759	3.0788
U							0.8381	0.8353	0.9345	0.9710	0.9730
V							0.0309	0.0141	-0.0437	0.0004	0.0043
W							-0.0536	-0.0253	0.2581	0.2691	0.2632
P	6							0.1266	0.4901	0.9001	0.9333
M								1.8471	2.7524	3.0839	3.0878
U								0.7926	0.9273	0.9702	0.9732
V								-0.0007	-0.0483	0.0061	0.0102
W								-0.0346	0.2694	0.2753	0.2654
P	5								0.4367	0.9170	0.9377
M									2.6906	3.1046	3.0933
U									0.9153	0.9713	0.9732
V									-0.0463	0.0164	0.0146
W									0.2793	0.2794	0.2678
P	4								0.4981	0.9147	0.9333
M									2.7970	3.0962	3.0846
U									0.9271	0.9708	0.9726
V									-0.0357	0.0240	0.0283
W									0.2931	0.2767	0.2656
P	1									0.9012	0.9339
M										3.0866	3.0898
U										0.9701	0.9731
V										0.0410	0.0369
W										0.2740	0.2651
P	2									0.9117	0.9324
M										3.0925	3.1002
U										0.9721	0.9752
V										0.0449	0.0442
W										0.2677	0.2606
P	1									0.9094	0.9314
M										3.1168	3.1231
U										0.9704	0.9729
V										0.0600	0.0568
W										0.2611	0.2582

TABLE B-25. FINAL DATA SET FOR M_∞ = 3.01, R_d = 1.70 x 10^6, α_b = 10°, x/d = 14 M3R7G3

P -- P0/P0INF M -- MACH NUMBER U,V,W -- 3-D VELOCITY COMPONENTS/U1NF

		1	2	3	4	5	6	7	8	9	10
P	21	0.8331	0.8641	0.8659	0.8666	0.8869	0.9096	0.9108	0.9203	0.9178	0.9257
M		2.8415	2.8580	2.8825	2.8922	2.9149	2.9490	2.9546	2.9641	2.9673	2.9806
U		0.9743	0.9787	0.9805	0.9787	0.9795	0.9813	0.9798	0.9793	0.9788	0.9795
V		0.0006	-0.0226	-0.0394	-0.0558	-0.0627	-0.0694	-0.0672	-0.0614	-0.0601	-0.0525
W		0.0576	0.0653	0.0768	0.1019	0.1164	0.1329	0.1488	0.1621	0.1676	0.1758
P	20	0.8132	0.8544	0.8293	0.8742	0.8897	0.9053	0.9154	0.9275	0.9275	0.9191
M		2.8308	2.8740	2.8624	2.9156	2.9354	2.9644	2.9792	2.9905	2.9949	2.9938
U		0.9769	0.9817	0.9784	0.9812	0.9812	0.9813	0.9808	0.9805	0.9800	0.9790
V		-0.0036	-0.0327	-0.0547	-0.0743	-0.0805	-0.0861	-0.0803	-0.0727	-0.0689	-0.0590
W		0.0347	0.0443	0.0587	0.0936	0.1133	0.1368	0.1559	0.1695	0.1767	0.1849
P	19	0.8165	0.8561	0.8029	0.8765	0.8942	0.8997	0.9057	0.9211	0.9238	0.9315
M		2.8491	2.8940	2.8614	2.9429	2.9684	2.9935	3.0013	3.0136	3.0174	3.0269
U		0.9799	0.9848	0.9782	0.9837	0.9832	0.9814	0.9798	0.9799	0.9796	0.9803
V		-0.0088	-0.0407	-0.0709	-0.0974	-0.1043	-0.1075	-0.0951	-0.0835	-0.0768	-0.0649
W		0.0065	0.0163	0.0390	0.0824	0.1115	0.1464	0.1701	0.1835	0.1903	0.1972
P	18	0.8198	0.7865	0.7987	0.7930	0.8098	0.8429	0.9119	0.9204	0.9234	0.9328
M		2.8750	2.8641	2.8943	2.9347	2.9635	3.0108	3.0542	3.0499	3.0509	3.0558
U		0.9830	0.9805	0.9819	0.9810	0.9795	0.9784	0.9807	0.9795	0.9793	0.9801
V		-0.0117	-0.0488	-0.0877	-0.1258	-0.1342	-0.1311	-0.1091	-0.0918	-0.0829	-0.0685
W		-0.0244	-0.0198	0.0076	0.0614	0.1068	0.1606	0.1916	0.2037	0.2092	0.2129
P	17	0.8305	0.7418	0.7204	0.5195	0.5602	0.6546	0.8853	0.9314	0.9195	0.9240
M		2.9264	2.8725	2.8891	2.7278	2.7926	2.9160	3.0831	3.1064	3.0834	3.0733
U		0.9876	0.9795	0.9800	0.9528	0.9555	0.9628	0.9781	0.9801	0.9783	0.9785
V		-0.0132	-0.0550	-0.0942	-0.1345	-0.1432	-0.1370	-0.1168	-0.0963	-0.0845	-0.0687
W		-0.0654	-0.0628	-0.0362	0.0465	0.1099	0.1775	0.2159	0.2286	0.2300	0.2289
P	16	0.8383	0.7236	0.5895	0.3927	0.4461	0.5220	0.7471	0.9118	0.9275	0.9472
M		2.9887	2.9090	2.8148	2.6469	2.7364	2.8480	3.0571	3.1482	3.1320	3.1234
U		0.9915	0.9812	0.9686	0.9394	0.9443	0.9494	0.9701	0.9788	0.9785	0.9802
V		-0.0121	-0.0512	-0.0869	-0.1484	-0.1496	-0.1300	-0.1133	-0.0944	-0.0816	-0.0663
W		-0.0992	-0.1002	-0.0755	0.0331	0.1284	0.2046	0.2388	0.2539	0.2527	0.2466
P	15	0.8534	0.6783	0.4514	0.2229	0.3299	0.4946	0.6235	0.8899	0.9395	0.9446
M		3.0809	2.9595	2.7413	2.4536	2.6960	2.9189	3.0071	3.1976	3.1851	3.1415
U		0.9973	0.9811	0.9533	0.9085	0.9318	0.9508	0.9593	0.9787	0.9791	0.9789
V		-0.0083	-0.0367	-0.0759	-0.1495	-0.1652	-0.1173	-0.1008	-0.0869	-0.0727	-0.0579
W		-0.1487	-0.1549	-0.1317	-0.0051	0.1546	0.2454	0.2624	0.2773	0.2748	0.2614
P	14	0.8691	0.6269	0.3747	0.1641	0.1393	0.4604	0.5361	0.6344	0.9296	0.9567
M		3.1969	3.0094	2.7437	2.3402	2.2800	3.0011	2.9624	3.0363	3.2181	3.1765
U		1.0022	0.9781	0.9440	0.8879	0.8766	0.9528	0.9520	0.9587	0.9793	0.9795
V		-0.0033	-0.0119	-0.0338	-0.0485	-0.1245	-0.0896	-0.0730	-0.0771	-0.0622	-0.0492
W		-0.1938	-0.2073	-0.2005	-0.1431	0.0846	0.2864	0.2774	0.2847	0.2893	0.2756
P	13	0.8185	0.5713	0.3364	0.1421	0.1017	0.4462	0.4698	0.5162	0.9251	0.9590
M		3.2070	3.0129	2.7503	2.3109	2.1590	2.9526	2.8435	2.8861	3.2176	3.1721
U		0.9995	0.9722	0.9367	0.8804	0.8622	0.9564	0.9467	0.9459	0.9802	0.9797
V		0.0055	0.0169	0.0212	0.0399	-0.0236	-0.0301	-0.0339	-0.0546	-0.0498	-0.0348
W		-0.2127	-0.2348	-0.2374	-0.1575	0.0697	0.2659	0.2481	0.2683	0.2884	0.2785
P	12	0.7846	0.5561	0.3484	0.1877	0.1217	0.5108	0.4081	0.3840	0.8431	0.9552
M		3.1352	2.9535	2.7292	2.4123	2.2091	2.9278	2.6883	2.6476	3.1462	3.1521
U		0.9963	0.9695	0.9368	0.8964	0.8690	0.9688	0.9390	0.9237	0.9746	0.9773
V		0.0146	0.0486	0.0754	0.1182	0.0846	0.0543	0.0089	-0.0281	-0.0427	-0.0208
W		-0.1892	-0.2101	-0.2126	-0.1312	0.0650	0.1966	0.1882	0.2275	0.2818	0.2770
P	11	0.7834	0.5942	0.3947	0.3811	0.2497	0.3802	0.5291	0.3011	0.6706	0.9479
M		3.0668	2.9153	2.6969	2.7072	2.5046	2.6685	2.8660	2.4502	2.9727	3.1323
U		0.9956	0.9731	0.9404	0.9429	0.9132	0.9369	0.9674	0.9029	0.9563	0.9756
V		0.0223	0.0681	0.1106	0.1307	0.1722	0.1472	0.0831	0.0084	-0.0333	-0.0071
W		-0.1465	-0.1595	-0.1517	-0.1277	0.0043	0.1110	0.1482	0.1774	0.2746	0.2759
P	10	0.7980	0.6906	0.5114	0.5241	0.4426	0.6095	0.7046	0.2960	0.5652	0.9499
M		3.0351	2.9555	2.7881	2.8189	2.7317	2.9136	2.9079	2.4046	2.8397	3.1220
U		0.9971	0.9852	0.9591	0.9445	0.9503	0.9778	0.9910	0.9012	0.9411	0.9752
V		0.0255	0.0717	0.1190	0.1309	0.1618	0.1323	0.0960	0.0429	-0.0161	0.0064
W		-0.1046	-0.1059	-0.0905	-0.0718	0.0094	0.0549	0.0770	0.1373	0.2684	0.2733
P	9	0.8230	0.7719	0.7136	0.7410	0.7101	0.7445	0.7835	0.3049	0.5941	0.9590
M		3.0238	2.9958	2.9626	3.0011	2.9854	3.0086	3.0285	2.3904	2.8541	3.1164
U		0.9994	0.9942	0.9876	0.9925	0.9890	0.9931	0.9979	0.9015	0.9454	0.9763
V		0.0275	0.0663	0.1035	0.1072	0.1266	0.1109	0.0854	0.0574	-0.0015	0.0191
W		-0.0699	-0.0623	-0.0488	-0.0374	0.0044	0.0340	0.0358	0.1041	0.2599	0.2664
P	8				0.7928	0.7870	0.7841	0.7458	0.2745	0.7530	0.9487
M					3.0220	3.0178	3.0153	2.9789	2.2925	2.9970	3.0926
U					0.9971	0.9962	0.9964	0.9932	0.8867	0.9454	0.9758
V					0.0895	0.0967	0.0908	0.0776	0.0504	0.0040	0.0270
W					-0.0251	-0.0035	0.0130	0.0120	0.0801	0.2548	0.2572
P	7						0.4638	0.2996	0.2013	0.8674	0.9444
M							2.6803	2.3638	2.0848	3.0836	3.0846
U							0.9535	0.9034	0.8464	0.9756	0.9759
V							0.0721	0.0475	0.0209	0.0044	0.0313
W							-0.0243	-0.0255	0.0692	0.2554	0.2527
P	6							0.1614	0.1452	0.9559	0.9521
M								1.9794	1.8886	3.1508	3.0893
U								0.8256	0.7992	0.9818	0.9768
V								-0.0021	0.0059	0.0150	0.0354
W								-0.0155	0.0841	0.2608	0.2508
P	5								0.1231	0.9751	0.9488
M									1.7784	3.1415	3.0856
U									0.7450	0.9809	0.9768
V									0.0142	0.0370	0.0410
W									0.1261	0.2580	0.2484
P	4								0.1569	0.9476	0.9588
M									1.9467	3.0462	3.0017
U									0.7971	0.9775	0.9782
V									-0.0113	0.0513	0.0454
W									0.1834	0.2683	0.2447

TABLE B-25. FINAL DATA SET FOR M_∞ = 3.01, R_d = 1.70 x 10^6, α_b = 10°, x/d = 14 (CONCLUDED)

P	3		
M		0.9492	0.9650
U		3.0912	3.0939
V		0.9783	0.9793
W		0.0533	0.0490
		0.2427	0.2408
P	2		
M		0.9443	0.9634
U		3.0869	3.0896
V		0.9784	0.9796
W		0.0555	0.0519
		0.2397	0.2368
P	1		
M		0.9676	0.9703
U		3.1098	3.0953
V		0.9810	0.9808
W		0.0601	0.0564
		0.2389	0.2337

TABLE B-26. FINAL DATA SET FOR $M_\infty = 3.01$, $R_d = 1.70 \times 10^6$, $\alpha_b = 15°$, x/d = 7 M3R7G4

P -- P0/P0INF M -- MACH NUMBER U,V,W -- 3-D VELOCITY COMPONENTS/U1NF

		1	2	3	4	5	6	7	8	9	10
P	15	0.7540	0.7417	0.7443	0.7646	0.4528	0.6952	0.7702	0.8270	0.8528	0.8706
M		2.8839	2.8648	2.9685	3.0727	2.8784	3.4024	3.3560	3.2804	3.2261	3.1835
U		0.9841	0.9825	0.9844	0.9813	0.9278	0.9398	0.9421	0.9478	0.9508	0.9526
V		-0.0075	-0.0529	-0.1401	-0.2032	-0.1845	-0.2088	-0.1716	-0.1221	-0.0961	-0.0774
W		0.0263	0.0370	0.0366	0.1014	0.2702	0.3961	0.3972	0.3824	0.3675	0.3547
P	14	0.7578	0.7467	0.7174	0.2727	0.2724	0.5872	0.7041	0.8744	0.8617	0.8754
M		2.9542	2.9614	3.1794	2.7218	3.0677	3.4686	3.4189	3.3777	3.2601	3.1998
U		0.9929	0.9922	1.0048	0.9299	0.8722	0.9257	0.9332	0.9492	0.9491	0.9514
V		-0.0102	-0.0593	-0.1521	-0.2459	-0.2172	-0.1757	-0.1522	-0.1014	-0.0794	-0.0626
W		-0.0256	-0.0213	-0.0746	0.0427	0.4534	0.4545	0.4392	0.4095	0.3851	0.3655
P	13	0.7745	0.7812	0.2066	0.0522	0.2196	0.5676	0.6858	0.8672	0.8648	0.8836
M		3.0770	3.1239	2.5804	2.0434	3.0629	3.4523	3.4322	3.3767	3.2708	3.2169
U		1.0040	1.0073	0.9141	0.8292	0.8645	0.9253	0.9347	0.9489	0.9484	0.9511
V		-0.0084	-0.0495	-0.0627	-0.1272	-0.1959	-0.1305	-0.1081	-0.0715	-0.0565	-0.0457
W		-0.0867	-0.0945	-0.2164	0.0487	0.4761	0.4691	0.4517	0.4209	0.3937	0.3736
P	12	0.8042	0.8137	0.1116	0.0394	0.1775	0.5221	0.6713	0.8413	0.8584	0.8690
M		3.2540	3.3351	2.3460	1.9896	2.8916	3.2590	3.2896	3.2828	3.2188	3.1721
U		1.0157	1.0201	0.8589	0.8262	0.8673	0.9257	0.9381	0.9467	0.9490	0.9502
V		-0.0005	-0.0157	0.0558	-0.0228	-0.1422	-0.0771	-0.0596	-0.0404	-0.0340	-0.0293
W		-0.1501	-0.1722	-0.2688	0.0502	0.4457	0.4385	0.4216	0.4026	0.3807	0.3647
P	11	0.8212	0.8599	0.1102	0.0440	0.2356	0.4740	0.6994	0.8276	0.8522	0.8524
M		3.4454	3.5850	2.3990	2.0421	2.8772	2.9714	3.1723	3.1811	3.1415	3.1237
U		1.0245	1.0301	0.8552	0.8384	0.9040	0.9296	0.9463	0.9484	0.9499	0.9492
V		0.0104	0.0273	0.1351	0.0483	-0.0404	-0.0099	-0.0314	-0.0181	-0.0178	-0.0170
W		-0.2057	-0.2354	-0.2843	-0.0229	0.3855	0.3558	0.3745	0.3727	0.3631	0.3533
P	10	0.7339	0.7091	0.7667	0.1056	0.0460	0.5166	0.4475	0.7392	0.8240	0.8439
M		3.3895	3.4614	3.7327	2.4730	1.9843	2.8775	2.7492	3.1092	3.1102	3.1040
U		1.0203	1.0187	1.0260	0.8779	0.8216	0.9557	0.9246	0.9451	0.9475	0.9487
V		0.0229	0.0705	0.1096	0.1429	0.0302	0.1047	-0.0327	-0.0205	-0.0113	-0.0101
W		-0.1992	-0.2287	-0.2783	-0.2505	0.0882	0.2079	0.2793	0.3596	0.3539	0.3487
P	9	0.7079	0.6494	0.6435	0.1827	0.1047	0.1215	0.2718	0.7707	0.8062	0.6024
M		3.2331	3.2244	3.3346	2.5670	2.3069	2.1920	2.3956	3.0682	3.0659	2.8575
U		1.0164	1.0095	1.0099	0.8917	0.8649	0.8271	0.8727	0.9454	0.9454	0.9187
V		0.0332	0.0929	0.1413	0.2394	0.2281	0.2194	-0.0782	-0.0286	-0.0109	-0.0078
W		-0.1248	-0.1424	-0.1752	-0.1721	-0.0037	0.1682	0.2483	0.3448	0.3452	0.3442
P	8				0.6130	0.4687	0.5898	0.4979	0.7436	0.8127	0.8678
M					3.0428	3.2648	3.0032	2.8179	3.0846	3.2691	3.2828
U					0.9865	0.9927	0.9764	0.9461	0.9402	0.9433	0.9501
V					0.1832	0.2656	0.1940	0.1042	-0.0286	-0.0312	-0.0272
W					-0.0312	0.0204	0.0863	0.0902	0.3646	0.4079	0.3957
P	7						0.1057	0.2179	0.7577	0.8390	0.8437
M							1.9394	2.3718	3.2768	3.2758	3.2375
U							0.8104	0.9031	0.9363	0.9451	0.9479
V							0.0966	0.0219	-0.0347	-0.0163	-0.0141
W							-0.0119	-0.0744	0.4254	0.4063	0.3898
P	6							0.1330	0.8676	0.8024	0.8364
M								2.1475	3.4179	3.2198	3.2326
U								0.8523	0.9477	0.9414	0.9479
V								-0.0224	-0.0341	-0.0023	-0.0048
W								-0.1330	0.4330	0.4009	0.3888
P	5								0.8988	0.7986	0.9245
M									3.4460	3.2297	3.4795
U									0.9508	0.9416	0.9545
V									-0.0206	0.0089	-0.0284
W									0.4331	0.4029	0.4317
P	4								0.8876	0.8619	0.9492
M									3.4435	3.4854	3.4423
U									0.9488	0.9483	0.9558
V									-0.0037	-0.0236	-0.0025
W									0.4373	0.4466	0.4217
P	3									0.9429	0.9403
M										3.5009	3.3542
U										0.9537	0.9549
V										0.0062	0.0222
W										0.4389	0.4025
P	2									0.9283	0.9153
M										3.3774	3.2446
U										0.9523	0.9523
V										0.0381	0.0466
W										0.4130	0.3784
P	1									0.9155	0.9227
M										3.2491	3.1687
U										0.9514	0.9528
V										0.0674	0.0679
W										0.3786	0.3515

TABLE B-27. FINAL DATA SET FOR M_∞ = 3.01, R_d = 1.70 x 10^6, α_b = 15°, x/d = 10 M3R70S

P -- P0/P0INF M -- MACH NUMBER U,V,W -- 3-D VELOCITY COMPONENTS/UINF

		1	2	3	4	5	6	7	8	9	10	11
P	20	0.7535	0.7000	0.6973	0.7636	0.7675	0.8127	0.8368	0.8456	0.8357	0.8673	0.8910
M		2.7886	2.7590	2.7823	2.8637	2.9869	3.0279	3.0508	3.0673	3.0652	3.1132	3.1300
U		0.9769	0.9644	0.9599	0.9619	0.9577	0.9576	0.9568	0.9563	0.9534	0.9547	0.9560
V		-0.0236	-0.0640	-0.0984	-0.1134	-0.1450	-0.1323	-0.1202	-0.1171	-0.1098	-0.0998	-0.0946
W		0.0373	0.0491	0.1081	0.1609	0.2374	0.2640	0.2821	0.2918	0.3029	0.3198	0.3234
P	19	0.7640	0.6326	0.6718	0.7355	0.7538	0.8147	0.7972	0.5740	0.6609	0.8261	0.8459
M		2.8390	2.7417	2.8194	2.8993	3.0887	3.0839	3.0697	2.8527	3.0055	3.1797	3.1759
U		0.9782	0.9627	0.9656	0.9638	0.9577	0.9584	0.9540	0.9197	0.9293	0.9473	0.9486
V		-0.0261	-0.0714	-0.1189	-0.1413	-0.1669	-0.1383	-0.1301	-0.1261	-0.1228	-0.1045	-0.0961
W		-0.0134	0.0084	0.0788	0.1558	0.2704	0.2820	0.2946	0.3156	0.3469	0.3606	0.3585
P	18	0.7708	0.5896	0.5509	0.6124	0.5653	0.6322	0.9370	0.9393	0.9254	0.9125	0.9106
M		2.9195	2.7841	2.8079	2.9201	3.0177	3.1399	3.6396	3.5535	3.4375	3.3227	3.2886
U		0.9862	0.9679	0.9672	0.9665	0.9465	0.9325	0.9532	0.9533	0.9522	0.9516	0.9509
V		-0.0219	-0.0668	-0.1164	-0.1619	-0.1501	-0.1864	-0.1684	-0.1473	-0.1233	-0.0960	-0.0875
W		-0.0714	-0.0464	0.0257	0.1336	0.2889	0.4089	0.4356	0.4257	0.4105	0.3916	0.3865
P	17	0.7681	0.5157	0.3744	0.3384	0.2830	0.8665	0.9572	0.9641	0.9514	0.9252	0.9359
M		3.0232	2.8094	2.6780	2.6667	2.8785	3.8082	3.6842	3.5856	3.4651	3.3371	3.3146
U		0.9931	0.9683	0.9527	0.9390	0.8971	0.9517	0.9517	0.9524	0.9521	0.9505	0.9511
V		-0.0141	-0.0452	-0.0802	-0.1291	-0.1564	-0.2041	-0.1601	-0.1353	-0.1093	-0.0826	-0.0746
W		-0.1291	-0.1023	-0.0191	0.1134	0.3722	0.4546	0.4502	0.4381	0.4210	0.4010	0.3955
P	16	0.7688	0.4198	0.2891	0.2484	0.2612	0.6475	0.8952	0.9725	0.9537	0.9176	0.9247
M		3.1572	2.8672	2.6462	2.5964	2.9871	3.5563	3.6390	3.5908	3.4575	3.3176	3.2890
U		0.9992	0.9602	0.9472	0.9339	0.9109	0.9341	0.9487	0.9504	0.9500	0.9487	0.9488
V		-0.0063	-0.0242	-0.0598	-0.0952	-0.1638	-0.1791	-0.1460	-0.1208	-0.0919	-0.0680	-0.0604
W		-0.1874	-0.1638	-0.0679	0.0986	0.3715	0.4664	0.4521	0.4478	0.4280	0.4030	0.3969
P	15	0.8468	0.5345	0.2813	0.2167	0.3020	0.4753	0.7546	0.9754	0.9538	0.9460	0.9399
M		3.3284	3.0672	2.7367	2.6136	3.1614	3.3911	3.4438	3.5614	3.4202	3.3220	3.2864
U		1.0083	0.9804	0.9518	0.9420	0.9426	0.9414	0.9399	0.9487	0.9488	0.9502	0.9491
V		-0.0089	-0.0018	-0.0329	-0.0814	-0.1519	-0.1472	-0.1189	-0.1041	-0.0730	-0.0505	-0.0446
W		-0.2293	-0.2285	-0.1539	0.0450	0.3505	0.4479	0.4382	0.4497	0.4261	0.4033	0.3974
P	14	0.8792	0.5339	0.2138	0.1505	0.2459	0.3857	0.3506	0.9856	0.9552	0.9246	0.9400
M		3.5353	3.2449	2.7257	2.5557	3.0403	3.2391	3.0031	3.5294	3.3749	3.2644	3.2529
U		1.0144	0.9832	0.9381	0.9356	0.9443	0.9560	0.9065	0.9492	0.9486	0.9472	0.9489
V		0.0041	0.0214	0.0134	-0.0595	-0.1332	-0.0993	-0.0946	-0.0841	-0.0513	-0.0341	-0.0290
W		-0.2817	-0.2916	-0.2177	0.0084	0.3126	0.3567	0.4096	0.4466	0.4195	0.3973	0.3907
P	13	0.9026	0.5581	0.1999	0.1055	0.0910	0.2184	0.2694	0.4175	0.8396	0.9374	0.9409
M		3.7437	3.4411	2.8064	2.6433	2.3940	2.8311	2.9001	2.9956	3.3857	3.3270	3.2675
U		1.0183	0.9877	0.9336	0.9173	0.9032	0.9279	0.9245	0.9038	0.9393	0.9446	0.9469
V		0.0088	0.0405	0.0571	-0.0093	-0.0548	-0.0606	-0.0946	-0.0755	-0.0582	-0.0307	-0.0229
W		-0.3269	-0.3376	-0.2728	-0.0548	0.0999	0.3016	0.3312	0.4171	0.4414	0.4193	0.3997
P	12	0.8972	0.6205	0.2117	0.0929	0.0807	0.2796	0.2785	0.3408	0.7756	0.9321	0.9307
M		3.8947	3.6503	2.8912	2.3944	2.2952	2.8541	2.8707	2.7479	3.2629	3.2654	3.2094
U		1.0187	0.9968	0.9338	0.9037	0.8901	0.9446	0.9298	0.8942	0.9374	0.9447	0.9462
V		0.0108	0.0461	0.0747	0.0476	0.0430	0.0486	-0.0412	-0.0257	-0.0310	-0.0109	-0.0081
W		-0.3596	-0.3642	-0.3057	-0.1032	0.0456	0.2589	0.3155	0.3651	0.4197	0.4049	0.3866
U	11	0.5927	0.6076	0.3551	0.2450	0.1139	0.1301	0.3546	0.2967	0.7421	0.8586	0.8891
M		3.1056	3.1984	2.9673	2.8848	2.4604	2.3703	2.8574	2.5568	3.1485	3.1334	3.1253
U		0.9918	0.9988	0.9644	0.9543	0.9091	0.8824	0.9473	0.8843	0.9356	0.9393	0.9434
V		0.0220	0.0471	0.0936	0.1310	0.1216	0.0832	0.0599	0.0057	-0.0082	0.0074	0.0056
W		-0.1945	-0.2061	-0.2257	-0.2041	-0.0929	0.1884	0.2482	0.3120	0.3950	0.3820	0.3694
P	10	0.6658	0.6452	0.5137	0.3858	0.2175	0.3544	0.5803	0.2607	0.8391	0.8945	0.9068
M		3.1432	3.1966	3.1099	2.9988	2.6989	2.7803	3.0197	2.4147	3.2074	3.1890	3.1809
U		1.0029	1.0048	0.9888	0.9726	0.9345	0.9475	0.9856	0.8699	0.9431	0.9429	0.9447
V		0.0296	0.0462	0.1281	0.1747	0.2055	0.1677	0.1033	0.0057	0.0061	0.0211	0.0145
W		-0.1540	-0.1675	-0.1698	-0.1444	-0.0688	0.1283	0.1421	0.2805	0.3935	0.3883	0.3821
P	9	0.6853	0.6737	0.6688	0.6643	0.5203	0.6445	0.6855	0.2470	0.8885	0.8916	0.8946
M		3.1045	3.1182	3.1538	3.1940	3.0542	3.0477	3.0639	2.3649	3.2173	3.1820	3.1732
U		1.0059	1.0049	1.0052	1.0057	0.9858	0.9946	1.0002	0.8580	0.9452	0.9438	0.9444
V		0.0349	0.0655	0.1146	0.1523	0.1962	0.1267	0.0852	-0.0127	0.0172	0.0255	0.0187
W		-0.0937	-0.1039	-0.0961	-0.0822	-0.0290	0.0599	0.0704	0.2882	0.3908	0.3841	0.3803
P	8				0.6674	0.6638	0.6840	0.5928	0.2484	0.8656	0.8860	0.9031
M					3.1100	3.1076	3.0584	2.9657	2.3805	3.1886	3.1938	3.1997
U					1.0038	1.0022	1.0005	0.9917	0.8497	0.9412	0.9438	0.9459
V					0.1181	0.1340	0.0973	0.0718	-0.0271	0.0267	0.0276	0.0214
W					-0.0369	-0.0103	0.0295	0.0263	0.3189	0.3920	0.3871	0.3840
P	7						0.3901	0.3075	0.2926	0.8672	0.9130	0.9253
M							2.7211	2.5377	2.5201	3.2023	3.2309	3.2211
U							0.9588	0.9333	0.8585	0.9402	0.9463	0.9482
V							0.0786	0.0405	-0.0355	0.0319	0.0311	0.0292
W							-0.0281	-0.0303	0.3605	0.3977	0.3910	0.3838
P	6							0.1696	0.4406	0.8984	0.9267	0.9244
M								2.1718	2.8508	3.2311	3.2272	3.2074
U								0.8655	0.8953	0.9432	0.9476	0.9484
V								-0.0031	-0.0387	0.0374	0.0389	0.0371
W								-0.0656	0.3972	0.3979	0.3861	0.3789
P	5								0.7590	0.9160	0.9287	0.9353
M									3.2847	3.2286	3.2171	3.2082
U									0.9376	0.9466	0.9494	0.9498
V									-0.0279	0.0479	0.0466	0.0434
W									0.4249	0.3879	0.3775	0.3749
P	4									0.9121	0.9672	0.9627
M										3.2177	3.2137	3.2062
U										0.9468	0.9055	0.9534
V										0.0575	0.0610	0.0191
W										0.3832	0.3572	0.4140
P	1									0.6210	1.0413	1.0170
M										2.9774	3.4544	3.3734
U										0.9155	0.9592	0.9568
V										0.0582	0.0349	0.0387
W										0.3882	0.4151	0.4015

TABLE B-27. FINAL DATA SET FOR M_∞ = 3.01, R_d = 1.70 x 10^6, α_b = 15°, x/d = 10 (CONCLUDED)

P	2	1.0687	1.0361	0.9905
M		3.4900	3.3548	3.2715
U		0.9602	0.9594	0.9550
V		0.0489	0.0581	0.0572
W		0.4194	0.3882	0.3775
P	1	1.0367	1.0277	0.9948
M		3.3347	3.2498	3.1970
U		0.9587	0.9590	0.9556
V		0.0792	0.0803	0.0743
W		0.3811	0.3565	0.3514

TABLE B-28. FINAL DATA SET FOR $M_\infty = 3.01$, $R_d = 1.70 \times 10^6$, $\alpha_b = 15°$, x/d = 13

P -- P0/P0INF M -- MACH NUMBER U/V/W -- 3-D VELOCITY COMPONENTS/U1NF

		1	2	3	4	5	6	7	8	9	10	11
P	24	0.7548	0.8239	0.8231	0.5583	0.7642	0.8268					
M		2.7974	2.8689	2.8877	2.7746	2.9887	3.0176					
U		0.9727	0.9801	0.9783	0.9471	0.9577	0.9574					
V		-0.0216	-0.0591	-0.0941	-0.1565	-0.1554	-0.1271					
W		0.0140	0.0364	0.0657	0.1392	0.2315	0.2625					
P	23	0.7751	0.8052	0.7167	0.4877	0.5556	0.8024	0.8599	0.8985	0.9242	0.9276	0.7132
M		2.8677	2.9210	2.8927	2.7445	2.8833	3.0977	3.0962	3.0941	3.0903	3.0871	2.8895
U		0.9813	0.9863	0.9791	0.9462	0.9436	0.9547	0.9571	0.9607	0.9613	0.9611	0.9373
V		-0.0281	-0.0723	-0.1129	-0.1435	-0.1410	-0.1362	-0.1093	-0.0913	-0.0860	-0.0866	-0.0770
W		-0.0358	-0.0207	0.0034	0.1298	0.2444	0.3005	0.3033	0.2968	0.2950	0.2944	0.2936
P	22	0.7811	0.7454	0.4670	0.3801	0.4285	0.7356	0.9313	0.8825	0.3753	0.6030	0.9350
M		2.9559	2.9741	2.7132	2.6816	2.8195	3.1567	3.1837	3.0687	2.4275	2.9569	3.3811
U		0.9891	0.9905	0.9570	0.9416	0.9361	0.9555	0.9615	0.9609	0.8720	0.9256	0.9584
V		-0.0239	-0.0576	-0.0848	-0.1086	-0.1154	-0.1232	-0.0982	-0.0721	-0.0517	-0.1061	-0.1150
W		-0.0982	-0.0841	-0.0341	0.1301	0.2513	0.3222	0.3242	0.2916	0.2766	0.3454	0.3845
P	21	0.7941	0.6211	0.3660	0.3381	0.3952	0.5022	0.6656	0.8900	0.9244	0.9600	0.9757
M		3.0778	2.9568	2.6545	2.7188	2.8622	2.9334	3.1740	3.5341	3.5499	3.5543	3.4915
U		0.9968	0.9834	0.9490	0.9502	0.9383	0.9290	0.9308	0.9508	0.9546	0.9570	0.9588
V		-0.0162	-0.0301	-0.0585	-0.0915	-0.0924	-0.0777	-0.0823	-0.1138	-0.1190	-0.1147	-0.1024
W		-0.1479	-0.1386	-0.0611	0.1204	0.2733	0.3353	0.4049	0.4372	0.4308	0.4275	0.4132
P	20	0.8010	0.5335	0.3268	0.2677	0.3733	0.5158	0.8291	0.9251	0.9564	0.9949	0.9844
M		3.2086	2.9613	2.6850	2.6702	2.9318	3.1529	3.4955	3.5888	3.5864	3.5906	3.5043
U		1.0022	0.9769	0.9522	0.9468	0.9406	0.9344	0.9480	0.9538	0.9565	0.9591	0.9567
V		-0.0061	-0.0082	-0.0351	-0.0635	-0.0720	-0.0869	-0.1025	-0.1109	-0.1103	-0.1042	-0.0867
W		-0.2004	-0.1841	-0.0924	0.1082	0.3019	0.3897	0.4382	0.4426	0.4364	0.4331	0.4191
P	19	0.8063	0.5689	0.2996	0.2274	0.2673	0.3858	0.8413	0.9386	0.9674	0.9960	0.9900
M		3.2996	3.0736	2.7005	2.5944	2.7652	3.0026	3.5658	3.6124	3.5876	3.5741	3.4946
U		1.0047	0.9835	0.9533	0.9343	0.9446	0.9407	0.9526	0.9545	0.9573	0.9585	0.9589
V		0.0018	0.0073	-0.0162	-0.0539	-0.0575	-0.0705	-0.1089	-0.1051	-0.1016	-0.0934	-0.0773
W		-0.2323	-0.2178	-0.1075	0.1208	0.2868	0.3292	0.4410	0.4471	0.4370	0.4335	0.4191
P	18	0.7926	0.5352	0.2700	0.2029	0.2490	0.3802	0.6729	0.9515	0.9812	1.0073	0.9868
M		3.4052	3.1311	2.7017	2.5656	2.7483	3.0234	3.4420	3.6523	3.5903	3.5710	3.4704
U		1.0055	0.9819	0.9498	0.9322	0.9463	0.9498	0.9464	0.9568	0.9573	0.9593	0.9581
V		0.0059	0.0184	0.0046	-0.0439	-0.0570	-0.0679	-0.1143	-0.1084	-0.0900	-0.0810	-0.0645
W		-0.2709	-0.2517	-0.1370	0.1050	0.1873	0.3104	0.4273	0.4490	0.4401	0.4335	0.4176
P	17	0.7757	0.5164	0.2561	0.1860	0.2227	0.3912	0.5162	0.9473	0.9967	1.0024	1.0007
M		3.4957	3.1868	2.7170	2.5432	2.7001	3.0744	3.2538	3.6620	3.5743	3.5335	3.4556
U		1.0053	0.9814	0.9483	0.9308	0.9431	0.9627	0.9325	0.9596	0.9583	0.9583	0.9593
V		0.0073	0.0205	0.0133	-0.0410	-0.0547	-0.0623	-0.1111	-0.1083	-0.0782	-0.0678	-0.0506
W		-0.3010	-0.2762	-0.1605	0.0851	0.1678	0.2904	0.4148	0.4468	0.4370	0.4304	0.4137
P	16	0.8381	0.6861	0.3579	0.1937	0.1964	0.3701	0.3897	0.8278	1.0026	1.0078	0.9879
M		3.6187	3.4550	2.9747	2.5815	2.6306	3.0486	3.0517	3.5517	3.5430	3.4987	3.4061
U		1.0123	1.0020	0.9655	0.9393	0.9383	0.9672	0.9480	0.9546	0.9581	0.9585	0.9579
V		0.0046	0.0146	0.0172	0.0007	-0.0446	-0.0559	-0.0580	-0.1030	-0.0648	-0.0538	-0.0368
W		-0.3136	-0.2994	-0.2432	-0.0662	0.1362	0.2656	0.3281	0.4354	0.4332	0.4245	0.4070
P	15	0.8097	0.6658	0.3556	0.1898	0.1704	0.3368	0.4704	0.6457	1.0342	1.0111	0.9970
M		3.6670	3.4931	3.0068	2.5977	2.5545	2.9823	3.1666	3.3391	3.5172	3.4504	3.3679
U		1.0104	1.0008	0.9671	0.9400	0.9292	0.9428	0.9713	0.9432	0.9601	0.9581	0.9584
V		0.0030	0.0089	0.0115	0.0028	-0.0325	-0.0455	-0.0385	-0.0895	-0.0495	-0.0375	-0.0224
W		-0.3321	-0.3148	-0.2528	-0.0882	0.1188	0.2535	0.3005	0.4168	0.4254	0.4165	0.3976
P	14	0.7693	0.6282	0.3588	0.1833	0.1556	0.3321	0.5534	0.3942	0.3520	1.0110	1.0058
M		3.6720	3.4819	3.0393	2.5846	2.4923	2.9484	3.2281	3.0011	2.8275	3.4466	3.3703
U		1.0069	0.9971	0.9704	0.9365	0.9206	0.9621	0.9872	0.9494	0.8961	0.9583	0.9586
V		0.0062	0.0000	0.0012	0.0045	-0.0106	-0.0236	-0.0134	-0.0290	-0.0638	-0.0274	-0.0156
W		-0.3438	-0.3233	-0.2552	-0.1025	0.1108	0.2430	0.2719	0.3093	0.3844	0.4159	0.3980
P	13	0.7124	0.5795	0.4390	0.2339	0.1517	0.1371	0.3217	0.4838	0.3184	0.9804	0.9499
M		3.6171	3.4130	3.1937	2.7585	2.4760	2.3779	2.8788	3.0897	2.7151	3.3871	3.2806
U		1.0010	0.9913	0.9827	0.9556	0.9237	0.9047	0.9532	0.9731	0.8946	0.9557	0.9546
V		-0.0041	-0.0129	-0.0048	0.0140	0.0108	-0.0003	-0.0106	0.0079	-0.0228	-0.0071	-0.0018
W		-0.3476	-0.3210	-0.2752	-0.1521	-0.0284	0.0718	0.2436	0.2674	0.3521	0.4091	0.3852
P	12	0.4140	0.3701	0.3835	0.2380	0.1520	0.1410	0.3652	0.5912	0.3236	0.9809	0.9861
M		2.4986	2.7514	2.9272	2.7301	2.4521	2.3716	2.9049	3.1627	2.8624	3.3333	3.2923
U		0.9440	0.9460	0.9689	0.9547	0.9198	0.9026	0.9616	0.9919	0.8971	0.9570	0.9578
V		0.0077	-0.0017	0.0137	0.0301	0.0326	0.0284	0.0303	0.0346	0.0022	0.0115	0.0137
W		-0.1703	-0.1994	-0.2627	-0.1309	-0.0127	0.0783	0.2210	0.2226	0.3245	0.3928	0.3799
P	11	0.6813	0.5682	0.4408	0.2475	0.1710	0.1782	0.4752	0.6181	0.3260	0.9804	0.9886
M		3.1740	3.1065	3.0080	2.6939	2.4677	2.4662	2.9864	3.0962	2.5918	3.2648	3.2432
U		0.9950	0.9871	0.9800	0.9503	0.9262	0.9152	0.9776	0.9930	0.8930	0.9566	0.9572
V		0.0146	0.0389	0.0624	0.0742	0.0722	0.0716	0.0675	0.0505	0.0067	0.0228	0.0226
W		-0.2168	-0.2153	-0.1874	-0.1009	0.0120	0.0950	0.1845	0.1767	0.3034	0.3751	0.3674
P	10	0.6084	0.5210	0.4672	0.3140	0.2378	0.2683	0.6124	0.6028	0.3255	0.9544	0.9540
M		3.0205	2.9476	2.9392	2.7468	2.5752	2.6371	3.0525	3.0101	2.5417	3.2382	3.2166
U		0.9874	0.9773	0.9767	0.9560	0.9320	0.9382	0.9930	0.9905	0.8874	0.9567	0.9562
V		0.0206	0.0414	0.0946	0.1227	0.1220	0.1179	0.0882	0.0499	-0.0095	0.0265	0.0279
W		-0.1647	-0.1614	-0.1416	-0.0667	0.0352	0.0935	0.1269	0.1284	0.2954	0.3673	0.3622
P	9	0.6136	0.5473	0.5271	0.4322	0.3788	0.4408	0.6843	0.5138	0.2739	0.9484	0.9498
M		2.9644	2.9038	2.9364	2.8395	2.7514	2.8449	3.0672	2.8842	2.4153	3.2329	3.2165
U		0.9884	0.9789	0.9806	0.9668	0.9536	0.9666	1.0009	0.9807	0.8606	0.9552	0.9554
V		0.0247	0.0723	0.1114	0.1489	0.1530	0.1409	0.0824	0.0445	-0.0321	0.0295	0.0319
W		-0.1072	-0.1035	-0.0906	-0.0333	0.0419	0.0715	0.0483	0.0750	0.3064	0.3694	0.3638
P	M				0.5816	0.5751	0.6456	0.6887	0.3702	0.2313	0.9395	0.9597
M					2.9575	2.9532	3.0377	3.0428	2.6842	2.3218	3.2338	3.2360
U					0.9838	0.9829	0.9946	0.9981	0.9559	0.8318	0.9532	0.9562
V					0.1334	0.1407	0.1265	0.0942	0.0461	-0.0335	0.0366	0.0364
W					-0.0150	0.0241	0.0356	0.0517	0.0153	0.3348	0.3741	0.3671
P	7						0.4962	0.5670	0.2347	0.2458	0.9492	0.9708
M							3.1025	2.9828	2.3998	2.3700	3.2466	3.2650
U							1.0051	0.9930	0.9083	0.8309	0.9539	0.9571
V							0.1054	0.0862	0.0477	-0.0208	0.0451	0.0424
W							-0.0021	-0.0084	-0.0122	0.3608	0.3749	0.3666

TABLE B-28. FINAL DATA SET FOR M_∞ = 3.01, R_d = 1.70 x 10^6, α_b = 15°, x/d = 13 (CONCLUDED)

6	0.1577	0.1648	0.3954	0.9660	0.9731
	2.1736	2.1526	2.6963	3.2473	3.2310
	0.8564	0.8629	0.8771	0.9562	0.9577
	0.0437	0.0420	-0.0064	0.0533	0.0497
	-0.0255	-0.0044	0.3876	0.3681	0.3600
5			0.8530	0.9589	0.9590
			3.2446	3.2254	3.2059
			0.9475	0.9564	0.9568
			0.0281	0.0601	0.0558
			0.3919	0.3604	0.3541
4			0.9779	0.9530	0.9333
			3.2905	3.2143	3.1806
			0.9577	0.9562	0.9555
			0.0605	0.0659	0.0625
			0.3761	0.3565	0.3489
3			0.9367	0.6632	1.0546
			3.2353	2.9808	3.4274
			0.9530	0.9258	0.9649
			0.0760	0.0683	0.0456
			0.3691	0.3623	0.3942
2			0.6426	1.0701	1.6312
			2.9707	3.4365	3.3273
			0.9219	0.9659	0.9636
			0.0856	0.0609	0.0641
			0.3654	0.3920	0.3694
1			1.0687	1.0486	1.0355
			3.4989	3.3197	3.2551
			0.9627	0.9644	0.9642
			0.0720	0.0830	0.0805
			0.4121	0.3612	0.3437

TABLE B-29. FINAL DATA SET FOR M_∞ = 3.01, R_d = 1.70 x 10^6, α_b = 20°, x/d = 6 M30767

P -- PO/POINF M -- MACH NUMBER U,V,W -- 3-D VELOCITY COMPONENTS/UINF

		1	2	3	4	5	6	7	8	9	10
P	18	0.6605	0.6564	0.6702	0.5927	0.2163	0.7531	0.8338	0.8513	0.8462	0.8561
M		2.7455	2.7624	2.8080	2.7890	2.0859	3.4493	3.5115	3.3938	3.3006	3.2812
U		0.9597	0.9573	0.9540	0.9240	0.8065	0.9200	0.9238	0.9246	0.9231	0.9226
V		-0.0133	-0.0728	-0.1150	-0.1135	-0.0262	-0.1920	-0.1726	-0.1335	-0.1072	-0.0951
W		0.1090	0.1259	0.1625	0.2792	0.2663	0.4576	0.4700	0.4576	0.4472	0.4467
P	17	0.6644	0.6738	0.5168	0.1704	0.8631	0.8476	0.8556	0.8441	0.8450	0.8590
M		2.7742	2.8604	2.6976	2.1002	3.8214	3.6235	3.5631	3.3985	3.3025	3.2869
U		0.9683	0.9759	0.9412	0.8022	0.9233	0.9221	0.9221	0.9209	0.9208	0.9206
V		-0.0190	-0.0820	-0.1131	-0.0657	-0.2328	-0.1892	-0.1652	-0.1237	-0.0962	-0.0857
W		0.0534	0.0647	0.1454	0.2821	0.4994	0.4876	0.4856	0.4687	0.4549	0.4538
P	16	0.6528	0.4983	0.3757	0.6162	0.8840	0.8599	0.8589	0.8408	0.8499	0.8470
M		2.8760	2.7546	2.6977	3.7307	3.8950	3.6593	3.5753	3.3889	3.2927	3.2607
U		0.9831	0.9631	0.9410	0.9000	0.9208	0.9198	0.9195	0.9186	0.9196	0.9177
V		-0.0192	-0.0891	-0.1756	-0.2702	-0.2288	-0.1801	-0.1535	-0.1101	-0.0826	-0.0729
W		-0.0284	-0.0004	0.0596	0.5087	0.5167	0.5015	0.4965	0.4746	0.4578	0.4560
P	15	0.6649	0.5012	0.1548	0.5573	0.9154	0.8783	0.8704	0.8388	0.8413	0.8455
M		2.8848	2.7761	2.5096	3.7658	3.9673	3.6842	3.5761	3.3619	3.2605	3.2382
U		0.9836	0.9647	0.8945	0.8999	0.9199	0.9187	0.9182	0.9171	0.9174	0.9165
V		-0.0265	-0.0965	-0.1119	-0.2735	-0.2248	-0.1684	-0.1397	-0.0915	-0.0662	-0.0581
W		-0.0347	-0.0341	0.2290	0.5126	0.5301	0.5117	0.5030	0.4758	0.4577	0.4555
P	14	0.7179	0.3383	0.0944	0.3000	0.9781	0.8987	0.8814	0.8449	0.8145	0.6394
M		3.1171	2.7945	2.3940	3.3105	4.0599	3.6834	3.5532	3.3326	3.1994	2.9777
U		1.0051	0.9590	0.8897	0.8760	0.9236	0.9188	0.9177	0.9166	0.9136	0.8905
V		-0.0137	-0.0227	-0.0802	-0.2497	-0.2224	-0.1524	-0.1219	-0.0733	-0.0489	-0.0338
W		-0.1189	-0.1611	0.1758	0.4858	0.5368	0.5163	0.5045	0.4740	0.4535	0.4451
P	13	0.8008	0.2425	0.0544	0.2401	0.9505	0.9133	0.8519	0.8111	0.5283	0.7779
M		3.4577	2.7677	2.1150	3.1457	4.0828	3.6522	3.4646	3.2434	2.8604	3.2956
U		1.0264	0.9389	0.8550	0.8872	0.9320	0.9189	0.9143	0.9119	0.8746	0.9116
V		0.0126	0.0711	-0.0117	-0.2071	-0.2256	-0.1313	-0.0971	-0.0526	-0.0144	-0.0749
W		-0.2014	-0.2287	0.0408	0.4482	0.5237	0.5168	0.5001	0.4664	0.4450	0.4755
P	12	0.8677	0.2490	0.0547	0.3390	0.5497	0.8985	0.8357	0.6582	0.8215	0.8388
M		3.8037	2.9491	2.0256	3.4385	3.5864	3.5678	3.3751	3.0291	3.3604	3.3666
U		1.0400	0.9448	0.8344	0.9452	0.9192	0.9169	0.9124	0.8924	0.9161	0.9165
V		0.0342	0.1132	0.0323	-0.1964	-0.2001	-0.1074	-0.0701	-0.0217	-0.0733	-0.0702
W		-0.2654	-0.2827	-0.0474	0.4012	0.4821	0.5119	0.4910	0.4557	0.4807	0.4816
P	11	0.8827	0.7843	0.1537	0.0439	0.0816	0.2414	0.6636	0.6649	0.8168	0.8196
M		4.0796	4.0306	2.8311	1.9781	2.3325	2.9903	3.3750	3.0748	3.3795	3.3278
U		1.0460	1.0394	0.9340	0.8254	0.8448	0.9255	0.9051	0.8919	0.9123	0.9139
V		0.0495	0.0859	0.1212	-0.0018	-0.1502	-0.1157	-0.1021	-0.0216	-0.0665	-0.0569
W		-0.3125	-0.3145	-0.2622	0.0024	0.2692	0.3542	0.5024	0.4680	0.4925	0.4804
P	10	0.8581	0.8226	0.1976	0.0455	0.0442	0.3202	0.4393	0.6514	0.8331	0.7909
M		4.2860	4.2621	3.0850	2.0823	1.9918	2.9868	2.9863	3.1732	3.3780	3.2934
U		1.0472	1.0437	0.9498	0.8439	0.8240	0.9605	0.8777	0.8903	0.9133	0.9108
V		0.0389	0.0821	0.1183	0.0493	0.0774	0.0397	-0.0833	-0.0416	-0.0532	-0.0474
W		-0.3489	-0.3477	-0.3181	-0.0788	-0.0406	0.2653	0.4660	0.4926	0.4920	0.4801
P	9	0.3799	0.7051	0.1675	0.0500	0.1444	0.4962	0.1557	0.6666	0.7992	0.7772
M		3.5455	4.2636	2.8529	2.0570	2.6265	3.0641	2.2760	3.2305	3.3685	3.2920
U		1.0060	1.0387	0.9385	0.8343	0.9178	0.9025	0.8533	0.8905	0.9071	0.9066
V		0.0289	0.0734	0.0881	0.0815	0.2389	0.1376	0.0056	-0.0431	-0.0483	-0.0422
W		-0.3120	-0.3644	-0.2699	-0.0927	0.0186	0.0931	0.2480	0.5044	0.5021	0.4881
P	8				0.6446	0.5892	0.4432	0.1084	0.7483	0.7812	0.7640
M					3.3616	3.2855	2.9890	2.0190	3.3520	3.3266	3.2928
U					1.0226	1.0107	0.9801	0.8266	0.8992	0.9051	0.9059
V					0.1671	0.1971	0.1246	0.0361	-0.0409	-0.0325	-0.0350
W					-0.0475	0.0187	0.1376	0.1115	0.5136	0.4986	0.4901
P	7						0.3055	0.0644	0.7617	0.7609	0.7503
M							2.7904	1.7274	3.3447	3.3036	3.3624
U							0.9654	0.7604	0.9005	0.9028	0.9050
V							0.1063	-0.0000	-0.0246	-0.0238	-0.0545
W							-0.0427	0.0416	0.5109	0.4987	0.5041
P	6							0.0580	0.7280	0.7027	0.8791
M								1.7138	3.2958	3.2543	3.4882
U								0.7570	0.8974	0.8984	0.9155
V								0.0067	-0.0121	-0.0164	-0.0436
W								0.0344	0.5072	0.4967	0.5098
P	5								0.7106	0.8774	0.8897
M									3.2890	3.5781	3.4322
U									0.8961	0.9148	0.9155
V									-0.0057	-0.0477	-0.0178
W									0.5082	0.5263	0.5010
P	4									0.9315	0.9109
M										3.5484	3.3693
U										0.9189	0.9174
V										-0.0156	0.0121
W										0.5160	0.4854
P	3									0.9281	0.8997
M										3.4346	3.2558
U										0.9190	0.9170
V										0.0172	0.0403
W										0.4949	0.4603
P	2									0.8826	0.8885
M										3.2592	3.1398
U										0.9154	0.9161
V										0.0527	0.0673
W										0.4631	0.4311
P	1									0.8695	0.8848
M										3.1113	3.0314
U										0.9144	0.9161
V										0.0857	0.0913
W										0.4241	0.3969

TABLE B-30 FINAL DATA SET FOR M_∞ = 3.01, R_d = 1.70 x 10^6, α_b = 20°, x/d = 8.5

M3R7GP

P -- P0/P0INF M -- MACH NUMBER U,V,W -- 3-D VELOCITY COMPONENTS/UINF

		1	2	3	4	5	6	7	8	9	10	11
P	24	0.6750	0.5723	0.6060	0.6479	0.6856	0.7206					
M		2.7381	2.6390	2.6927	2.7623	2.8219	2.8671					
U		0.9585	0.9354	0.9350	0.9302	0.9310	0.9317					
V		-0.0180	-0.0381	-0.0578	-0.0867	-0.0773	-0.0723					
W		0.1089	0.1641	0.2021	0.2544	0.2840	0.3026					
P	23	0.5610	0.6424	0.6819	0.6720	0.6953	0.7224					
M		2.6204	2.7617	2.8385	2.8688	2.8679	2.8900					
U		0.9457	0.9552	0.9481	0.9244	0.9281	0.9315					
V		-0.0283	-0.1130	-0.1501	-0.1367	-0.0927	-0.0745					
W		0.0636	0.1104	0.1902	0.3035	0.3087	0.3122					
P	22	0.5667	0.6488	0.6932	0.6957	0.7035	0.3003	0.8692	0.9375	0.9409	0.9229	0.9333
M		2.6682	2.7902	2.8810	2.8879	2.8727	2.4865	3.7008	3.7055	3.6323	3.5326	3.4594
U		0.9511	0.9606	0.9527	0.9362	0.9249	0.8475	0.9236	0.9293	0.9303	0.9296	0.9307
V		-0.0484	-0.1239	-0.1677	-0.1402	-0.0859	-0.0977	-0.1813	-0.1619	-0.1430	-0.1220	-0.1048
W		0.0555	0.0826	0.1809	0.2723	0.3218	0.3608	0.5009	0.4978	0.4893	0.4784	0.4662
P	21	0.6008	0.4453	0.3610	0.6942	0.5559	0.8487	0.9140	0.9446	0.9459	0.9476	0.9239
M		2.8333	2.7671	2.7232	3.1270	3.2099	3.7094	3.7617	3.7121	3.6317	3.5444	3.4390
U		0.9755	0.9631	0.9360	0.9478	0.8849	0.9200	0.9247	0.9282	0.9293	0.9303	0.9289
V		-0.0473	-0.1036	-0.1689	-0.1847	-0.1373	-0.1847	-0.1768	-0.1549	-0.1351	-0.1128	-0.0952
W		-0.0496	-0.0219	0.1494	0.3071	0.4928	0.5076	0.5102	0.5031	0.4934	0.4815	0.4677
P	20	0.6221	0.4064	0.1834	0.2230	0.6924	0.7106	0.9336	0.9191	0.9062	0.9115	0.9123
M		2.8905	2.7756	2.6490	2.5883	3.4196	3.5506	3.7607	3.5989	3.5074	3.4604	3.3851
U		0.9806	0.9658	0.9081	0.8899	0.8999	0.9035	0.9261	0.9276	0.9273	0.9279	0.9282
V		-0.0168	-0.0692	-0.0320	-0.0761	-0.1243	-0.1732	-0.1702	-0.1298	-0.1098	-0.0953	-0.0792
W		-0.0948	-0.0598	0.1643	0.3017	0.5117	0.5147	0.5099	0.4922	0.4812	0.4741	0.4612
P	19	0.6388	0.2695	0.1717	0.1884	0.6665	0.7738	0.9366	0.9305	0.9114	0.9066	0.9226
M		3.1057	2.6130	2.4755	2.5385	3.4666	3.6692	3.7531	3.5893	3.4897	3.4345	3.3771
U		0.9967	0.9438	0.9163	0.8912	0.9045	0.9104	0.9244	0.9276	0.9265	0.9263	0.9285
V		0.0099	0.0094	-0.0162	-0.0640	-0.1373	-0.1659	-0.1627	-0.1205	-0.1000	-0.0838	-0.0671
W		-0.1691	-0.0707	0.1211	0.2747	0.5088	0.5246	0.5141	0.4931	0.4814	0.4742	0.4607
P	18	0.6329	0.2573	0.1645	0.1750	0.5044	0.7975	0.9381	0.9162	0.9003	0.9240	0.9018
M		3.2534	2.6608	2.4931	2.5407	3.3253	3.7179	3.7395	3.5480	3.4503	3.4236	3.3333
U		1.0042	0.9478	0.9246	0.9016	0.8954	0.9114	0.9231	0.9248	0.9242	0.9269	0.9255
V		0.0217	0.0367	-0.0133	-0.0541	-0.1467	-0.1636	-0.1545	-0.1093	-0.0886	-0.0729	-0.0558
W		-0.2122	-0.0996	0.0701	0.2414	0.4953	0.5312	0.5169	0.4934	0.4805	0.4727	0.4590
P	17	0.6347	0.2706	0.1513	0.1721	0.3212	0.8408	0.8890	0.9116	0.8930	0.9153	0.8995
M		3.3660	2.7684	2.4911	2.5917	3.0531	3.7910	3.6783	3.5139	3.4134	3.3867	3.3103
U		1.0096	0.9587	0.9266	0.9186	0.8725	0.9144	0.9186	0.9225	0.9218	0.9246	0.9238
V		0.0194	0.0370	-0.0183	-0.0576	-0.1465	-0.1614	-0.1411	-0.0965	-0.0754	-0.0604	-0.0441
W		-0.2388	-0.1364	0.0213	0.2061	0.4769	0.5377	0.5191	0.4942	0.4800	0.4713	0.4586
P	16	0.6256	0.2645	0.1344	0.1693	0.2200	0.8557	0.9234	0.9076	0.8930	0.9058	0.8771
M		3.4341	2.8257	2.4670	2.6005	2.8351	3.8475	3.7046	3.4733	3.3798	3.3488	3.2710
U		1.0147	0.9619	0.9224	0.9266	0.8579	0.9182	0.9197	0.9198	0.9198	0.9217	0.9198
V		0.0143	0.0287	-0.0230	-0.0597	-0.1356	-0.1620	-0.1242	-0.0822	-0.0625	-0.0483	-0.0338
W		-0.2571	-0.1677	-0.0248	0.1736	0.4498	0.5392	0.5255	0.4944	0.4791	0.4705	0.4588
P	15	0.5712	0.2392	0.1492	0.1400	0.2271	0.2682	0.9443	0.8902	0.8806	0.8767	0.8214
M		3.4385	2.8272	2.4918	2.5795	2.9319	3.0170	3.6880	3.4094	3.3268	3.2873	3.2092
U		1.0077	0.9598	0.9243	0.9265	0.9232	0.8644	0.9199	0.9161	0.9163	0.9168	0.9128
V		0.0187	0.0254	-0.0012	-0.0652	-0.0962	-0.1513	-0.1084	-0.0665	-0.0470	-0.0356	-0.0238
W		-0.2736	-0.1810	-0.0724	0.1532	0.3459	0.4812	0.5260	0.4913	0.4768	0.4681	0.4592
P	14	0.5369	0.2252	0.1446	0.1060	0.2256	0.2180	0.9533	0.9095	0.8774	0.9013	0.8438
M		3.4617	2.8629	2.5556	2.4477	2.9519	2.8574	3.7564	3.5733	3.3710	3.3100	3.2412
U		1.0044	0.9595	0.9309	0.9312	0.9362	0.8723	0.9183	0.9129	0.9114	0.9158	0.9120
V		0.0173	0.0203	-0.0025	-0.0571	-0.0944	-0.1140	-0.1082	-0.0748	-0.0538	-0.0302	-0.0241
W		-0.2932	-0.2071	-0.1115	0.1114	0.3174	0.4343	0.5394	0.5255	0.4941	0.4754	0.4681
P	13	0.5037	0.2044	0.1343	0.0780	0.1664	0.2461	0.9402	0.9160	0.8865	0.8679	0.8627
M		3.4830	2.8600	2.5704	2.2575	2.7295	2.8896	3.7287	3.5244	3.3516	3.2654	3.2827
U		1.0045	0.9557	0.9283	0.8822	0.9221	0.9007	0.9216	0.9126	0.9133	0.9123	0.9133
V		0.0163	0.0162	-0.0013	-0.0260	-0.0739	-0.0644	-0.0986	-0.0548	-0.0333	-0.0221	-0.0282
W		-0.3094	-0.2224	-0.1467	0.0658	0.2700	0.3728	0.5313	0.5203	0.4886	0.4730	0.4744
P	12	0.4289	0.1769	0.1485	0.0970	0.1593	0.3311	0.8477	0.8859	0.8637	0.8446	0.9152
M		3.3887	2.7659	2.8401	2.4002	2.6446	2.9977	3.5938	3.4257	3.3007	3.2581	3.3342
U		0.9925	0.9437	0.9543	0.9092	0.9239	0.9515	0.9191	0.9098	0.9110	0.9098	0.9173
V		0.0143	0.0166	0.0193	-0.0006	-0.0182	-0.0123	-0.0854	-0.0316	-0.0183	-0.0223	-0.0283
W		-0.3096	-0.2185	-0.2166	-0.0643	0.2259	0.3028	0.5165	0.5095	0.4831	0.4761	0.4776
P	11	0.3005	0.2352	0.1723	0.0895	0.0732	0.3736	0.3960	0.8914	0.8476	0.8406	0.8863
M		2.7901	2.8215	2.7279	2.3425	2.1898	3.0163	3.0387	3.4227	3.3192	3.2734	3.3176
U		0.9503	0.9520	0.9459	0.8981	0.8694	0.9728	0.9708	0.9120	0.9075	0.9089	0.9132
V		0.0112	0.0209	0.0322	0.0331	0.0070	0.0314	0.0235	-0.0219	-0.0122	-0.0108	-0.0248
W		-0.2042	-0.2156	-0.1804	-0.0655	0.0610	0.2327	0.2523	0.5053	0.4937	0.4815	0.4823
P	10	0.6541	0.3192	0.1862	0.0942	0.0837	0.4513	0.1435	0.8400	0.8188	0.8317	0.8766
M		3.4681	3.0294	2.7313	2.3074	2.2271	2.9945	2.1845	3.3404	3.2720	3.2866	3.2990
U		1.0208	0.9775	0.9473	0.8897	0.8748	0.9849	0.8412	0.9074	0.9048	0.9078	0.9111
V		0.0359	0.0789	0.0848	0.0796	0.0693	0.0894	0.0316	-0.0103	-0.0040	-0.0124	-0.0209
W		-0.2300	-0.2070	-0.1567	-0.0496	0.0529	0.1352	0.2220	0.4982	0.4890	0.4864	0.4824
P	9	0.5488	0.3775	0.3874	0.2397	0.1399	0.3643	0.1101	0.8197	0.8063	0.8662	0.8502
M		3.1774	2.9608	3.0484	2.7937	2.4164	2.7640	1.9732	3.3188	3.2768	3.3329	3.2674
U		1.0090	0.9793	0.9867	0.9544	0.8981	0.9651	0.8110	0.9053	0.9041	0.9103	0.9092
V		0.0481	0.1166	0.1517	0.1766	0.1539	0.0759	0.0348	-0.0039	-0.0027	-0.0108	-0.0130
W		-0.1322	-0.1245	-0.1110	-0.0585	0.0758	0.0278	0.1429	0.4979	0.4914	0.4914	0.4796
P	8				0.4909	0.3705	0.4241	0.0781	0.8266	0.8341	0.8826	0.8777
M					3.1144	2.8836	2.9273	1.7443	3.3538	3.3376	3.3397	3.3124
U					0.9953	0.9652	0.9749	0.7594	0.9057	0.9067	0.9120	0.9133
V					0.1807	0.1840	0.1380	0.0127	-0.0048	-0.0039	-0.0027	-0.0031
W					-0.0254	0.0538	0.0814	0.1012	0.5041	0.4991	0.4896	0.4818
P	7						0.4942	0.0484	0.8703	0.8622	0.8858	0.9515
M							3.0785	1.7007	3.4172	3.3583	3.3247	3.5014
U							1.0016	0.7504	0.9088	0.9083	0.9103	0.9172
V							0.1127	-0.0039	-0.0046	0.0024	0.0024	-0.0286
W							-0.0003	0.0746	0.5105	0.5001	0.4898	0.5102

TABLE B-30. FINAL DATA SET FOR M_∞ = 3.01, R_d = 1.70 x 10^6, α_b = 20°, x/d = 8.5 (CONCLUDED)

P	6	0.0698	0.8486	0.8444	0.6105	0.9806
M		1.7261	3.3620	3.3370	3.0639	3.4673
U		0.7583	0.9064	0.9062	0.8836	0.9189
V		0.0137	0.0059	0.0091	-0.0007	-0.0071
W		0.0654	0.5082	0.4997	0.4815	0.5015
P	5		0.8317	0.8202	0.9896	0.9857
M			3.3626	3.3281	3.5510	3.3983
U			0.9051	0.9047	0.9182	0.9195
V			0.0155	0.0144	-0.0105	0.0137
W			0.5066	0.5005	0.5178	0.4872
P	4			0.9372	0.9900	0.9784
M				3.5972	3.4576	3.3100
U				0.9123	0.9184	0.9189
V				-0.0165	0.0166	0.0351
W				0.5355	0.5006	0.4690
P	3			1.0448	0.9927	0.9920
M				3.5892	3.3532	3.2354
U				0.9197	0.9191	0.9208
V				0.0167	0.0451	0.0601
W				0.5214	0.4769	0.4459
P	2			1.0341	0.9943	0.9822
M				3.4306	3.2437	3.1381
U				0.9207	0.9205	0.9209
V				0.0559	0.0744	0.0809
W				0.4882	0.4462	0.4179
P	1			0.9870	0.9813	0.9804
M				3.2316	3.1196	3.0495
U				0.9193	0.9209	0.9215
V				0.0922	0.0987	0.0984
W				0.4425	0.4092	0.3878

TABLE B-31. FINAL DATA SET FOR M_∞ = 3.01, R = 1.70 x 10^6, α_b = 20°, x/d = 11

M38769

P -- P0/P0INF M -- MACH NUMBER U,V,W -- 3-D VELOCITY COMPONENTS/UINF

		1	2	3	4	5	6	7	8	9	10	11
P	27	0.6863	0.7828	0.7692	0.6861	0.8284	0.8479					
M		2.7240	2.8698	2.9035	3.0339	3.0694	3.0234					
U		0.9600	0.9722	0.9611	0.9339	0.9296	0.9308					
V		-0.0388	-0.1194	-0.1622	-0.1668	-0.1362	-0.1011					
W		0.0584	0.0794	0.1550	0.3249	0.3421	0.3558					
P	26	0.7293	0.4561	0.3214	0.4298	0.8680	0.7846					
M		2.9163	2.7169	2.5648	2.8737	3.2379	2.9971					
U		0.9865	0.9596	0.9252	0.9185	0.9369	0.9217					
V		-0.0239	-0.0636	-0.1101	-0.1090	-0.1079	-0.0785					
W		-0.0600	-0.0175	0.1168	0.3333	0.4016	0.3759					
P	25	0.5696	0.2515	0.2284	0.2887	0.8197	0.8032	0.8138	0.8965	0.9377	0.9641	0.9678
M		2.9469	2.4661	2.4494	2.6836	3.3751	3.3604	3.4479	3.6121	3.6283	3.6012	3.5429
U		0.9819	0.9228	0.9017	0.9034	0.9136	0.9070	0.9108	0.9201	0.9230	0.9258	0.9266
V		0.0075	-0.0087	-0.0550	-0.0645	-0.0862	-0.0911	-0.1114	-0.1364	-0.1403	-0.1282	-0.1140
W		-0.1438	-0.0005	0.1740	0.3092	0.4862	0.4946	0.5005	0.5067	0.5047	0.4965	0.4881
P	24	0.5132	0.2337	0.2042	0.2522	0.7916	0.8055	0.8244	0.9294	0.9652	0.9565	0.9746
M		2.9750	2.4753	2.4310	2.6330	3.4029	3.4046	3.4956	3.6577	3.6621	3.5865	3.5404
U		0.9791	0.9240	0.9035	0.9015	0.9146	0.9073	0.9111	0.9221	0.9245	0.9245	0.9265
V		0.0152	0.0105	-0.0279	-0.0587	-0.0919	-0.0939	-0.1160	-0.1361	-0.1352	-0.1207	-0.1067
W		-0.1813	-0.0270	0.1532	0.2925	0.4887	0.5023	0.5076	0.5107	0.5075	0.4983	0.4894
P	23	0.4822	0.2309	0.1965	0.2264	0.7627	0.8121	0.8263	0.9477	0.9579	0.9705	0.9880
M		2.9845	2.5108	2.4487	2.5893	3.4303	3.4544	3.5300	3.6841	3.6567	3.5914	3.5391
U		0.9769	0.9286	0.9108	0.9017	0.9177	0.9078	0.9104	0.9226	0.9230	0.9249	0.9267
V		0.0127	0.0126	-0.0195	-0.0551	-0.0990	-0.0975	-0.1180	-0.1322	-0.1284	-0.1127	-0.0988
W		-0.1985	-0.0543	0.1273	0.2699	0.4869	0.5099	0.5145	0.5152	0.5100	0.5002	0.4905
P	22	0.5443	0.3243	0.1833	0.1968	0.4577	0.8098	0.8289	0.9107	0.9871	0.9853	0.9580
M		3.1500	2.7484	2.3982	2.5216	3.1086	3.4887	3.5505	3.6580	3.7061	3.6324	3.4920
U		0.9939	0.9568	0.9005	0.9109	0.9043	0.9072	0.9085	0.9167	0.9240	0.9247	0.9245
V		0.0095	0.0181	-0.0274	-0.0421	-0.0944	-0.0994	-0.1168	-0.1283	-0.1268	-0.1106	-0.0886
W		-0.2099	-0.1343	0.1358	0.1932	0.4428	0.5169	0.5217	0.5224	0.5176	0.5081	0.4878
P	21	0.5481	0.3122	0.1767	0.1878	0.3510	0.7934	0.8509	0.9285	0.9857	1.0012	0.9651
M		3.1299	2.7608	2.4076	2.5160	2.9525	3.5159	3.5991	3.6751	3.6926	3.6262	3.4765
U		0.9901	0.9572	0.9062	0.9152	0.8936	0.9079	0.9103	0.9177	0.9234	0.9254	0.9246
V		0.0082	0.0158	-0.0235	-0.0382	-0.0943	-0.1059	-0.1176	-0.1242	-0.1192	-0.1026	-0.0788
W		-0.2169	-0.1434	0.1066	0.1670	0.4228	0.5191	0.5265	0.5244	0.5183	0.5075	0.4865
P	20	0.5343	0.2900	0.1786	0.1829	0.2779	0.7718	0.8657	0.9474	0.9839	0.9901	0.9758
M		3.1417	2.7472	2.4039	2.5289	2.8220	3.5516	3.6300	3.6872	3.6696	3.5929	3.4504
U		0.9900	0.9553	0.9173	0.9224	0.8857	0.9112	0.9108	0.9184	0.9227	0.9244	0.9252
V		0.0108	0.0171	-0.0198	-0.0345	-0.0905	-0.1143	-0.1168	-0.1186	-0.1103	-0.0931	-0.0673
W		-0.2202	-0.1434	0.0780	0.1379	0.4008	0.5176	0.5308	0.5263	0.5178	0.5053	0.4839
P	19	0.5301	0.2825	0.1758	0.1729	0.2330	0.6371	0.9053	0.9641	0.9999	0.9906	0.9759
M		3.1823	2.7653	2.4817	2.5206	2.7337	3.4567	3.6804	3.6913	3.6591	3.5644	3.4332
U		0.9920	0.9560	0.9241	0.9258	0.8875	0.9069	0.9141	0.9192	0.9237	0.9242	0.9253
V		0.0124	0.0190	-0.0142	-0.0302	-0.0802	-0.1215	-0.1147	-0.1109	-0.1011	-0.0828	-0.0563
W		-0.2339	-0.1552	0.0490	0.1025	0.3683	0.5067	0.5335	0.5272	0.5162	0.5026	0.4798
P	18	0.4513	0.2202	0.1667	0.1777	0.2173	0.4478	0.9281	0.9831	1.0046	1.0262	0.9752
M		3.1193	2.6263	2.4397	2.5195	2.7137	3.2256	3.7063	3.6905	3.6321	3.5643	3.4041
U		0.9862	0.9411	0.9183	0.9245	0.8992	0.8917	0.9157	0.9207	0.9237	0.9266	0.9250
V		0.0254	0.0254	-0.0100	-0.0284	-0.0683	-0.1215	-0.1112	-0.1012	-0.0910	-0.0721	-0.0447
W		-0.2277	-0.1154	-0.0022	0.1121	0.3333	0.4882	0.5356	0.5265	0.5137	0.4998	0.4758
P	17	0.4176	0.2179	0.1639	0.1721	0.1843	0.2232	0.9637	0.9976	0.9966	0.9910	0.9687
M		3.1123	2.6622	2.4619	2.5351	2.5640	2.7376	3.7395	3.6766	3.5886	3.4950	3.3694
U		0.9840	0.9452	0.9217	0.9299	0.9102	0.8852	0.9190	0.9215	0.9229	0.9237	0.9242
V		0.0262	0.0261	-0.0067	-0.0255	-0.0425	-0.0771	-0.1069	-0.0911	-0.0786	-0.0588	-0.0340
W		-0.2335	-0.1262	-0.0291	0.0867	0.2263	0.3760	0.5358	0.5248	0.5099	0.4945	0.4712
P	16	0.3811	0.2134	0.1616	0.1656	0.1883	0.2377	0.9805	0.9935	0.9847	0.9897	0.9638
M		3.0916	2.6925	2.4886	2.5477	2.6132	2.8055	3.7596	3.6400	3.5421	3.4566	3.3227
U		0.9813	0.9489	0.9252	0.9339	0.9243	0.9090	0.9226	0.9209	0.9220	0.9233	0.9218
V		0.0265	0.0236	-0.0045	-0.0234	-0.0377	-0.0626	-0.1042	-0.0794	-0.0644	-0.0455	-0.0234
W		-0.2351	-0.1321	-0.0513	0.0620	0.2002	0.3446	0.5332	0.5218	0.5053	0.4893	0.4667
P	15	0.3554	0.2006	0.1829	0.1535	0.1826	0.2731	0.3567	1.0039	0.9969	0.9892	0.9677
M		3.0825	2.6836	2.6223	2.5455	2.6174	2.9142	3.0299	3.6627	3.5609	3.4493	3.3643
U		0.9798	0.9478	0.9414	0.9358	0.9293	0.9363	0.8684	0.9220	0.9217	0.9220	0.9219
V		0.0250	0.0216	0.0073	-0.0096	-0.0367	-0.0491	-0.1106	-0.0732	-0.0562	-0.0355	-0.0192
W		-0.2371	-0.1326	-0.1108	0.0151	0.1793	0.3127	0.4882	0.5245	0.5101	0.4912	0.4754
P	14	0.3162	0.1918	0.1841	0.1392	0.1455	0.2603	0.2415	1.0222	1.0052	0.9707	0.9431
M		3.0195	2.6799	2.6554	2.4976	2.5144	2.8780	2.7279	3.6447	3.5286	3.4013	3.3289
U		0.9736	0.9461	0.9438	0.9281	0.9217	0.9472	0.8469	0.9228	0.9220	0.9205	0.9199
V		0.0249	0.0207	0.0092	-0.0015	-0.0236	-0.0382	-0.0909	-0.0600	-0.0393	-0.0215	-0.0121
W		-0.2320	-0.1301	-0.1307	0.0003	0.1285	0.2629	0.4502	0.5218	0.5054	0.4856	0.4722
P	13	0.4018	0.2390	0.1777	0.1302	0.1383	0.2608	0.1870	1.0227	0.9662	0.9510	0.9311
M		3.2014	2.8444	2.6361	2.4527	2.4804	2.8698	2.5074	3.6136	3.4566	3.3611	3.3186
U		0.9876	0.9609	0.9404	0.9204	0.9184	0.9531	0.8403	0.9231	0.9188	0.9193	0.9190
V		0.0281	0.0301	0.0153	0.0158	-0.0006	-0.0237	-0.0529	-0.0464	-0.0224	-0.0101	-0.0079
W		-0.2588	-0.1868	-0.1339	-0.0107	0.1126	0.2379	0.3943	0.5176	0.4983	0.4802	0.4719
P	12	0.3772	0.2306	0.2500	0.1557	0.1324	0.2793	0.3550	0.1802	0.9635	0.9335	0.9374
M		3.1328	2.8621	2.8757	2.5602	2.4453	2.8808	2.9624	2.4588	3.4126	3.3374	3.3359
U		0.9836	0.9573	0.9658	0.9340	0.9183	0.9569	0.9614	0.8528	0.9192	0.9184	0.9198
V		0.0302	0.0353	0.0368	0.0365	0.0344	-0.0073	0.0243	-0.0362	-0.0073	-0.0021	-0.0066
W		-0.2442	-0.1746	-0.1810	-0.0819	0.0273	0.2296	0.2526	0.3476	0.4906	0.4770	0.4740
P	11	0.3388	0.2272	0.2435	0.1548	0.1546	0.3140	0.3958	0.1802	0.9814	0.9643	0.9581
M		2.9726	2.7438	2.8052	2.5263	2.5114	2.9000	2.9462	2.4528	3.4678	3.3888	3.3735
U		0.9740	0.9533	0.9602	0.9288	0.9235	0.9672	0.9729	0.8755	0.9210	0.9210	0.9217
V		0.0349	0.0469	0.0485	0.0567	0.0664	0.0239	0.0520	0.0086	-0.0056	0.0046	-0.0012
W		-0.2029	-0.1471	-0.1571	-0.0860	0.0301	0.1489	0.1883	0.2865	0.4979	0.4826	0.4781
P	10	0.4830	0.3633	0.2519	0.1496	0.2145	0.3874	0.3726	0.1741	0.9693	0.9338	0.9775
M		3.1782	2.9955	2.7822	2.5376	2.4719	2.9720	2.8174	2.3244	3.4031	3.3628	3.4030
U		0.9964	0.9813	0.9659	0.9360	0.9285	0.9803	0.9669	0.8499	0.9191	0.9195	0.9240
V		0.0189	0.0515	0.0728	0.0824	0.1065	0.0476	0.0642	0.0367	0.0086	0.0037	0.0067
W		-0.2082	-0.1760	-0.1293	-0.0636	0.0399	0.1592	0.1141	0.2197	0.4891	0.4802	0.4797

TABLE 31. FINAL DATA SET FOR M_∞ = 3.01, R_d = 1.70 x 10^6, α_b = 20°, x/d = 11 (CONCLUDED)

P	9	0.4592	0.3753	0.3112	0.2448	0.2154	0.4831	0.4085	0.8087	0.9296	0.9508	0.9932
M		3.0118	2.9062	2.8180	2.6973	2.5955	3.0318	2.9810	3.3955	3.3765	3.3909	3.4084
U		0.9984	0.9777	0.9662	0.9508	0.9344	0.9918	0.9797	0.9134	0.9188	0.9218	0.9256
V		0.0210	0.0778	0.1033	0.1227	0.1187	0.1005	0.0689	-0.0275	0.0151	0.0088	0.0064
W		-0.1380	-0.1132	-0.0902	-0.0248	0.0688	0.1067	0.0946	0.4974	0.4840	0.4815	0.4776
P	8				0.4134	0.3858	0.3865	0.3303	0.8564	0.9138	0.9735	0.9766
M					2.9442	2.8813	2.8321	2.7370	3.4546	3.3733	3.4065	3.3846
U					0.9786	0.9705	0.9724	0.9626	0.9153	0.9176	0.9242	0.9250
V					0.1631	0.1542	0.0939	0.0568	-0.0242	0.0174	0.0140	0.0124
W					-0.0011	0.0534	0.0392	0.0277	0.5052	0.4856	0.4797	0.4738
P	7						0.1486	0.2172	1.0584	0.9345	0.9538	0.8685
M							2.2010	2.4656	3.6228	3.3941	3.3828	3.2983
U							0.8724	0.9217	0.9300	0.9204	0.9236	0.9193
V							0.0442	0.0362	-0.0099	0.0226	0.0198	0.0181
W							-0.0163	-0.0249	0.5087	0.4842	0.4759	0.4667
P	6							0.1537	1.0797	0.9225	0.8808	1.0964
M								2.2456	3.6006	3.3816	3.3337	3.6150
U								0.8814	0.9327	0.9214	0.9208	0.9333
V								0.0249	0.0055	0.0284	0.0255	-0.0078
W								-0.0422	0.5000	0.4796	0.4710	0.5013
P	5								1.0235	0.9042	1.1048	1.0854
M									3.5387	3.3818	3.6755	3.5261
U									0.9285	0.9203	0.9337	0.9329
V									0.0201	0.0333	-0.0064	0.0162
W									0.4966	0.4814	0.5107	0.4860
P	4									0.8602	1.0754	1.0544
M										3.4843	3.5478	3.4090
U										0.9162	0.9322	0.9317
V										0.0063	0.0235	0.0404
W										0.5096	0.4911	0.4641
P	3									1.1258	1.0756	1.0705
M										3.6647	3.4331	3.3297
U										0.9347	0.9336	0.9339
V										0.0244	0.0544	0.0639
W										0.5056	0.4638	0.4396
P	2									1.1265	1.0776	1.0786
M										3.5010	3.3202	3.2414
U										0.9367	0.9347	0.9354
V										0.0687	0.0816	0.0854
W										0.4691	0.4327	0.4113
P	1									1.0991	1.0593	1.0404
M										3.3235	3.1907	3.1162
U										0.9369	0.9344	0.9325
V										0.1037	0.1064	0.1033
W										0.4239	0.3954	0.3797

TABLE 32. FINAL DATA SET FOR $M_\infty = 3.01$, $R_d = 1.70 \times 10^6$, $\alpha_b = 25°$, $x/d = 6$

M3P7G10

P -- P0/P0INF M -- MACH NUMBER U,V,W -- 3-D VELOCITY COMPONENTS/U1NF

		1	2	3	4	5	6	7	8	9	10
P	20	0.4041	0.4469	0.5998	0.1481	0.7141	0.7932	0.7902	0.8140	0.8127	0.7080
M		2.4185	2.4963	2.9063	1.9866	3.7236	3.7569	3.5443	3.5045	3.4158	3.2199
U		0.6038	0.8974	0.8914	0.7438	0.8775	0.8802	0.8812	0.8826	0.8823	0.8688
V		-0.0398	-0.1016	-0.1706	-0.0650	-0.2333	-0.2099	-0.1590	-0.1351	-0.1127	-0.0919
W		0.1370	0.2132	0.3888	0.3566	0.5623	0.5720	0.5552	0.5529	0.5434	0.5327
P	19	0.4918	0.4767	0.3381	0.4053	0.7895	0.7821	0.7921	0.8104	0.8063	0.6209
M		2.7109	2.9718	2.9977	3.2543	3.8658	3.7592	3.5461	3.4930	3.3991	3.1137
U		0.9567	0.9712	0.8392	0.8234	0.8792	0.8768	0.8791	0.8804	0.8803	0.8588
V		-0.0491	-0.2081	-0.1658	-0.2026	-0.2309	-0.2053	-0.1499	-0.1264	-0.1036	-0.0417
W		-0.0195	0.0685	0.5151	0.5789	0.5802	0.5791	0.5613	0.5566	0.5455	0.5288
P	18	0.4188	0.0981	0.1693	0.4120	0.7808	0.7943	0.7990	0.8053	0.7918	0.7117
M		2.9298	2.1335	2.5923	3.2869	3.8749	3.7849	3.5467	3.4716	3.3694	3.2827
U		0.9770	0.8500	0.8202	0.8220	0.8756	0.8756	0.8779	0.8784	0.8773	0.8728
V		0.0203	-0.0338	-0.1438	-0.1954	-0.2270	-0.1991	-0.1399	-0.1160	-0.0935	-0.0945
W		-0.1578	0.1257	0.4431	0.5891	0.5883	0.5866	0.5658	0.5584	0.5468	0.5378
P	17	0.3752	0.0770	0.1142	0.3886	0.7939	0.7184	0.7906	0.7866	0.7673	0.8015
M		3.0399	2.0363	2.3944	3.2630	3.9042	3.7678	3.6406	3.4249	3.3279	3.4122
U		0.9760	0.8348	0.8310	0.8218	0.8741	0.8652	0.8721	0.8753	0.8737	0.8814
V		0.0586	0.0152	-0.1057	-0.1958	-0.2230	-0.2110	-0.1538	-0.1026	-0.0834	-0.0998
W		-0.2260	0.0800	0.3567	0.5851	0.5956	0.5955	0.5853	0.5581	0.5468	0.5467
P	16	0.3680	0.0809	0.0896	0.0947	0.8105	0.7744	0.8201	0.7896	0.6184	0.8067
M		3.1561	2.1466	2.2127	2.3338	3.9326	3.8505	3.6511	3.4048	3.1273	3.4107
U		0.9810	0.8620	0.8337	0.8581	0.8734	0.8663	0.8741	0.8746	0.8552	0.8808
V		0.0390	0.0346	-0.0712	-0.0980	-0.2186	-0.2025	-0.1396	-0.0900	-0.0663	-0.0921
W		-0.2635	0.0043	0.2603	0.2912	0.6018	0.6074	0.5873	0.5579	0.5395	0.5488
P	15	0.3738	0.0878	0.0880	0.0807	0.7371	0.7795	0.8262	0.7748	0.7021	0.7840
M		3.3047	2.2885	2.2695	2.2978	3.9014	3.8500	3.6257	3.3587	3.3033	3.3763
U		0.9881	0.8872	0.8643	0.8691	0.8646	0.8646	0.8740	0.8727	0.8684	0.8773
V		0.0196	0.0226	-0.0629	-0.0989	-0.2194	-0.1927	-0.1232	-0.0758	-0.0645	-0.0837
W		-0.2962	-0.0797	0.1909	0.1790	0.6103	0.6130	0.5875	0.5549	0.5505	0.5496
P	14	0.3577	0.0914	0.0823	0.0590	0.8371	0.7931	0.8555	0.6172	0.7890	0.7728
M		3.3638	2.4023	2.3255	2.1641	4.0929	3.8450	3.6145	3.1440	3.4237	3.3558
U		0.9869	0.8971	0.8907	0.8576	0.8744	0.8639	0.8759	0.8538	0.8763	0.8756
V		0.0081	0.0132	-0.0587	-0.0839	-0.2275	-0.1806	-0.1047	-0.0563	-0.0881	-0.0761
W		-0.3197	-0.1628	0.0979	0.0499	0.6154	0.6171	0.5867	0.5463	0.5587	0.5498
P	13	0.3646	0.1300	0.0467	0.1162	0.1375	0.7601	0.8347	0.7380	0.7799	0.7590
M		3.4375	2.7453	2.1118	2.4661	2.7319	3.8213	3.5767	3.4183	3.3980	3.3390
U		0.9930	0.9344	0.8527	0.8509	0.7960	0.8668	0.8719	0.8625	0.8747	0.8732
V		0.0052	0.0157	-0.0658	-0.1250	-0.2081	-0.1816	-0.0944	-0.0877	-0.0786	-0.0701
W		-0.3230	-0.2442	0.0156	0.2027	0.5024	0.6097	0.5888	0.5790	0.5582	0.5513
P	12	0.3716	0.1269	0.0940	0.0573	0.1558	0.2126	0.1966	0.7381	0.7491	0.6232
M		3.5407	2.8011	2.5816	2.2309	2.8697	2.8158	2.5948	3.3678	3.3520	3.1733
U		0.9940	0.9342	0.9247	0.8767	0.8985	0.7852	0.7437	0.8629	0.8707	0.8580
V		0.0079	0.0102	0.0045	-0.0682	-0.1461	-0.1948	-0.2076	-0.0671	-0.0695	-0.0598
W		-0.3483	-0.2741	-0.1778	0.0284	0.3700	0.5453	0.5426	0.5726	0.5577	0.5451
P	11	0.3488	0.1161	0.0893	0.0473	0.1289	0.1292	0.1252	0.6604	0.6567	0.7421
M		3.6312	2.7403	2.5971	2.1751	2.6907	2.3942	2.2883	3.2511	3.3016	3.3673
U		0.9893	0.9220	0.9179	0.8667	0.8992	0.7742	0.7223	0.8568	0.8572	0.8665
V		0.0064	0.0063	0.0152	-0.0262	-0.0941	-0.1330	-0.1922	-0.0527	-0.0775	-0.0730
W		-0.3591	-0.2853	-0.2199	-0.0520	0.3171	0.4602	0.4843	0.5627	0.5684	0.5664
P	10	0.1715	0.1237	0.0867	0.0452	0.2064	0.1730	0.0982	0.6071	0.7240	0.7429
M		2.4956	2.5485	2.4890	2.1028	2.8108	2.7241	2.0520	3.2368	3.4045	3.3646
U		0.9091	0.9123	0.9116	0.8513	0.9435	0.9031	0.7430	0.8501	0.8622	0.8660
V		0.0047	0.0207	0.0377	0.0498	0.0474	-0.0724	-0.1212	-0.0632	-0.0784	-0.0669
W		-0.1888	-0.2100	-0.1623	-0.0342	0.2410	0.3260	0.3777	0.5691	0.5787	0.5675
P	9	0.4376	0.2255	0.1215	0.0702	0.2958	0.2454	0.2180	0.7579	0.7266	0.7481
M		3.1762	2.8495	2.5710	2.2835	2.8523	2.8230	2.4371	3.4161	3.3932	3.3807
U		1.0064	0.9616	0.9228	0.8781	0.9659	0.9471	0.7490	0.8648	0.8626	0.8680
V		0.0440	0.1248	0.1598	0.1450	0.1304	0.0323	-0.1236	-0.0363	-0.0662	-0.0547
W		-0.1514	-0.1419	-0.0959	0.0134	0.1060	0.2356	0.5160	0.5807	0.5776	0.5681
P	8				0.2324	0.2166	0.2979	0.1587	0.6069	0.7299	0.7064
M					2.8279	2.6897	2.8511	2.1623	3.2428	3.3928	3.3841
U					0.9494	0.9317	0.9735	0.7609	0.8441	0.8627	0.8611
V					0.2275	0.1790	0.0864	-0.1231	-0.0458	-0.0592	-0.0746
W					0.0425	0.1322	0.0757	0.4934	0.5777	0.5781	0.5773
P	7						0.1189	0.0926	0.6427	0.7020	0.8131
M							2.2442	1.7839	3.3236	3.3610	3.4827
U							0.8802	0.6215	0.8418	0.8598	0.8693
V							0.0100	-0.1283	-0.0542	-0.0528	-0.0621
W							-0.0620	0.4482	0.5973	0.5777	0.5825
P	6							0.6985	0.7041	0.5402	0.8095
M								3.5484	3.4136	3.1412	3.4083
U								0.8398	0.8490	0.8407	0.8685
V								-0.0886	-0.0464	-0.0565	-0.0395
W								0.6306	0.6024	0.5495	0.5736
P	5								0.7085	0.8033	0.8411
M									3.4245	3.5421	3.3601
U									0.8502	0.8640	0.8722
V									-0.0494	-0.0594	-0.0109
W									0.6033	0.5997	0.5611
P	4									0.8403	0.8301
M										3.4808	3.2526
U										0.8677	0.8709
V										-0.0263	0.0176
W										0.5874	0.5432
P	3									0.8451	0.8638
M										3.3546	3.1819
U										0.8686	0.8762
V										0.0134	0.0442
W										0.5696	0.5185

TABLE B-32. FINAL DATA SET FOR M_∞ = 3.01, R_d = 1.70 x 10^b, α_b = 25°, x/d = 6 (CONCLUDED)

P	?		
I		0.8673	0.8771
T		3.2264	3.0809
O		0.8743	0.8781
T		0.0561	0.0800
A		0.5300	0.4888
L			
P	?	0.8676	0.8835
I		3.0712	2.9665
T		0.8764	0.8799
O		0.0466	0.1064
T		0.4867	0.4517
A			
L			

TABLE B-33. FINAL DATA SET FOR $M_\infty = 3.01$, $R_d = 1.70 \times 10^6$, $\alpha_b = 25°$, $x/d = 9$

M3R7611

P -- P0/PINF M -- MACH NUMBER U,V,W -- 3-D VELOCITY COMPONENTS/UINF

		1	2	3	4	5	6	7	8	9	10	11
P	24	0.4790	0.2206	0.1675								
M		2.9997	2.4660	2.2794								
U		0.9876	0.9223	0.8570								
V		0.0219	0.0292	-0.0230								
W		-0.1474	0.0087	0.2365								
P	23	0.4640	0.2186	0.1524								
M		3.0384	2.5086	2.2597								
U		0.9900	0.9293	0.8617								
V		0.0169	0.0270	-0.0182								
W		-0.1618	-0.0203	0.2032								
P	22	0.3485	0.1906	0.1377	0.5176	0.6945	0.8197	0.9334	0.9386	0.9508	0.9085	0.8705
M		2.8991	2.4852	2.3007	3.2200	3.4044	3.7186	3.7565	3.6712	3.5717	3.4460	3.3569
U		0.9738	0.9260	0.8790	0.8755	0.8611	0.8755	0.8850	0.8859	0.8886	0.8849	0.8816
V		0.0187	0.0097	-0.0378	-0.1064	-0.1050	-0.1635	-0.1493	-0.1294	-0.1076	-0.0872	-0.0710
W		-0.1570	-0.0099	0.1550	0.5188	0.5760	0.5886	0.5834	0.5748	0.5600	0.5490	0.5410
P	21	0.3233	0.1697	0.1279	0.3808	0.6997	0.8569	0.9303	0.9386	0.9408	0.9047	0.8319
M		2.8944	2.4461	2.2904	3.0404	3.4584	3.7653	3.7401	3.6557	3.5443	3.4326	3.3244
U		0.9711	0.9193	0.8826	0.8634	0.8622	0.8774	0.8842	0.8853	0.8875	0.8843	0.8776
V		0.0024	-0.0005	-0.0388	-0.1129	-0.1136	-0.1624	-0.1422	-0.1222	-0.0996	-0.0792	-0.0659
W		-0.1696	-0.0148	0.1187	0.4989	0.5814	0.5925	0.5841	0.5751	0.5590	0.5488	0.5422
P	20	0.3017	0.1645	0.1218	0.2612	0.6957	0.8672	0.9595	0.9497	0.9260	0.8906	0.8546
M		2.8835	2.4700	2.2953	2.8118	3.5052	3.7814	3.7558	3.6466	3.5112	3.4086	3.3686
U		0.9680	0.9225	0.8877	0.8439	0.8636	0.8772	0.8856	0.8857	0.8855	0.8827	0.8800
V		-0.0036	-0.0085	-0.0399	-0.1165	-0.1232	-0.1608	-0.1356	-0.1139	-0.0909	-0.0713	-0.0647
W		-0.1789	-0.0430	0.0818	0.4742	0.5868	0.5956	0.5858	0.5748	0.5583	0.5484	0.5458
P	19	0.3291	0.1523	0.1229	0.1822	0.7415	0.8075	0.9463	0.9651	0.9291	0.8649	0.8886
M		2.9779	2.4205	2.3394	2.5813	3.6552	3.7285	3.7788	3.6895	3.6217	3.3847	3.4169
U		0.9768	0.9122	0.8939	0.8279	0.8749	0.8710	0.8826	0.8845	0.8822	0.8804	0.8830
V		0.0019	-0.0149	-0.0391	-0.1117	-0.1358	-0.1541	-0.1344	-0.1102	-0.1019	-0.0654	-0.0734
W		-0.1954	-0.0706	0.1019	0.4344	0.5876	0.5992	0.5936	0.5835	0.5787	0.5485	0.5490
P	18	0.3011	0.1468	0.1226	0.1369	0.6394	0.8555	0.9567	0.9601	0.9319	0.8347	0.8973
M		2.9437	2.4453	2.3809	2.4347	3.6084	3.7921	3.7753	3.6612	3.5974	3.3585	3.4242
U		0.9703	0.9149	0.9040	0.8280	0.8718	0.8738	0.8828	0.8836	0.8815	0.8780	0.8840
V		0.0009	-0.0177	-0.0395	-0.0980	-0.1524	-0.1521	-0.1266	-0.1014	-0.0915	-0.0605	-0.0707
W		-0.2061	-0.0886	0.0757	0.3829	0.5814	0.6041	0.5946	0.5824	0.5778	0.5483	0.5491
P	17	0.2846	0.1433	0.1212	0.1215	0.3881	0.8641	0.9790	0.9666	0.9496	0.8709	0.8787
M		2.9435	2.4731	2.4135	2.4032	3.2411	3.8030	3.7725	3.6398	3.5917	3.4125	3.4031
U		0.9675	0.9177	0.9117	0.8456	0.8485	0.8735	0.8838	0.8839	0.8824	0.8813	0.8822
V		-0.0004	-0.0190	-0.0394	-0.0823	-0.1613	-0.1479	-0.1166	-0.0914	-0.0823	-0.0650	-0.0652
W		-0.2189	-0.1067	0.0485	0.3315	0.5526	0.6070	0.5948	0.5805	0.5770	0.5521	0.5490
P	16	0.2797	0.1498	0.1228	0.1228	0.1856	0.8847	0.9736	0.9421	0.9438	0.8903	0.7432
M		2.9462	2.5476	2.4468	2.4257	2.6996	3.8222	3.7401	3.5855	3.5584	3.4323	3.2664
U		0.9646	0.9221	0.9189	0.8877	0.8087	0.8746	0.8828	0.8820	0.8818	0.8827	0.8699
V		-0.0006	-0.0149	-0.0340	-0.0570	-0.1471	-0.1431	-0.1063	-0.0811	-0.0722	-0.0656	-0.0491
W		-0.2328	-0.1618	-0.0037	0.2182	0.4948	0.6089	0.5939	0.5770	0.5742	0.5531	0.5456
P	15	0.2546	0.1436	0.1161	0.1336	0.1341	0.9357	0.9783	0.9574	0.9266	0.9000	0.9439
M		2.9497	2.5461	2.4400	2.5279	2.5198	3.8800	3.7087	3.5699	3.5156	3.4368	3.5308
U		0.9608	0.9182	0.9174	0.9101	0.8107	0.8798	0.8832	0.8833	0.8803	0.8838	0.8883
V		-0.0008	-0.0145	-0.0337	-0.0566	-0.1233	-0.1412	-0.0952	-0.0701	-0.0623	-0.0618	-0.0813
W		-0.2454	-0.1812	-0.0286	0.1977	0.4424	0.6090	0.5909	0.5740	0.5710	0.5527	0.5585
P	14	0.2342	0.1343	0.1055	0.1351	0.1330	0.8894	0.9710	0.9245	0.8994	0.8854	0.9234
M		2.9153	2.5148	2.4051	2.5627	2.5392	3.8676	3.6656	3.5113	3.4694	3.4551	3.4724
U		0.9551	0.9110	0.9106	0.9203	0.8504	0.8785	0.8824	0.8807	0.8782	0.8789	0.8826
V		-0.0006	-0.0131	-0.0329	-0.0580	-0.0899	-0.1460	-0.0832	-0.0591	-0.0539	-0.0588	-0.0578
W		-0.2546	-0.1911	-0.0452	0.1756	0.3780	0.6083	0.5878	0.5700	0.5677	0.5637	0.5609
P	13	0.2179	0.1548	0.0896	0.1229	0.1803	0.2573	0.9657	0.9079	0.9251	0.9144	0.8360
M		2.8858	2.6772	2.3035	2.5314	2.7654	2.8442	3.6861	3.6862	3.5502	3.4914	3.3874
U		0.9506	0.9379	0.8810	0.9185	0.9208	0.7919	0.8810	0.8752	0.8753	0.8813	0.8767
V		0.0089	0.0061	-0.0159	-0.0521	-0.0612	-0.1506	-0.0764	-0.0989	-0.0644	-0.0577	-0.0538
W		-0.2569	-0.1858	-0.0699	0.1592	0.2946	0.5561	0.5936	0.5988	0.5778	0.5660	0.5569
P	12	0.1992	0.1407	0.1023	0.0860	0.1611	0.1097	0.3615	0.8908	0.9166	0.9075	0.9519
M		2.8127	2.6072	2.3984	2.2576	2.6583	2.2591	2.9678	3.6290	3.5172	3.4961	3.5227
U		0.9441	0.9269	0.9064	0.8845	0.9292	0.7694	0.8007	0.8734	0.8792	0.8801	0.8845
V		0.0075	0.0171	0.0046	0.0111	-0.0362	-0.0989	-0.1409	-0.0849	-0.0524	-0.0530	-0.0541
W		-0.2441	-0.1864	-0.0933	0.0311	0.2100	0.4268	0.5736	0.5957	0.5740	0.5692	0.5665
P	11	0.1891	0.1390	0.0979	0.0895	0.1667	0.1012	0.1972	0.8586	0.8909	0.9354	0.9496
M		2.7547	2.5871	2.3529	2.3127	2.6302	2.1581	2.4777	3.5603	3.4901	3.5289	3.5204
U		0.9407	0.9256	0.8986	0.8954	0.9333	0.8026	0.7413	0.8701	0.8779	0.8818	0.8851
V		0.0214	0.0365	0.0308	0.0150	0.0073	-0.0303	-0.1415	-0.0727	-0.0458	-0.0520	-0.0487
W		-0.2238	-0.1739	-0.0925	-0.0075	0.1721	0.3214	0.5346	0.5921	0.5722	0.5718	0.5656
P	10	0.1795	0.1481	0.1027	0.0993	0.1054	0.2270	0.9116	0.8566	0.9103	0.9430	0.8071
M		2.6781	2.5593	2.3554	2.3387	2.3038	2.7891	3.5663	3.4713	3.4898	3.5302	3.4088
U		0.9368	0.9240	0.8981	0.8987	0.8861	0.9472	0.8767	0.8755	0.8807	0.8832	0.8754
V		0.0350	0.0558	0.0586	0.0555	0.0123	0.0151	-0.0475	-0.0413	-0.0423	-0.0462	-0.0570
W		-0.1887	-0.1520	-0.0789	-0.0070	0.1175	0.2176	0.5858	0.5732	0.5682	0.5704	0.5616
P	9	0.1800	0.1492	0.1190	0.1318	0.1354	0.2582	0.9017	0.8920	0.8962	0.9287	1.0211
M		2.5770	2.5142	2.3848	2.4567	2.4162	2.7992	3.5850	3.5182	3.4756	3.5155	3.6475
U		0.9318	0.9215	0.9025	0.9157	0.9069	0.9627	0.8753	0.8788	0.8805	0.8832	0.8896
V		0.0585	0.0830	0.0947	0.1009	0.0675	0.0464	-0.0520	-0.0395	-0.0375	-0.0419	-0.0625
W		-0.1885	-0.1624	-0.0486	-0.0027	0.0940	0.1355	0.5903	0.5757	0.5665	0.5684	0.5768
P	8				0.2189	0.2242	0.2292	0.9023	0.8967	0.7063	0.9115	1.0423
M					2.6901	2.4934	2.6598	3.6290	3.5157	3.2873	3.5172	3.6082
U					0.9485	0.9483	0.9500	0.8727	0.8805	0.8653	0.8858	0.8919
V					0.1445	0.1247	0.0458	-0.0611	-0.0332	-0.0358	-0.0346	-0.0432
W					0.0019	0.0622	0.0494	0.5998	0.5732	0.5576	0.5652	0.5691
P	7						0.1393	0.8046	0.8845	1.0883	0.9675	1.0587
M							2.3189	3.5496	3.5064	3.7434	3.6386	3.5553
U							0.8949	0.8601	0.8806	0.8942	0.8852	0.8937
V							0.0619	-0.0684	-0.0298	-0.0539	-0.0588	-0.0218
W							-0.0376	0.6054	0.5717	0.5642	0.5827	0.5592

TABLE B-33. FINAL DATA SET FOR M_∞ = 3.01, R_d = 1.70 x 10^6, α_b = 25°, x/d = 9 (CONCLUDED)

P	6				
U		0.7134	0.7955	1.0989	1.0439	1.0572
V		3.4884	3.4310	3.6679	3.6418	3.4730
E		0.8432	0.8741	0.8953	0.8909	0.8943
		-0.0762	-0.0253	-0.0279	-0.0361	0.0020
		0.6189	0.5698	0.5737	0.5762	0.5452
P	5					
U			1.0678	1.1092	1.0775	1.0623
V			3.8118	3.5750	3.5770	3.3902
E			0.8920	0.8974	0.8944	0.8954
			-0.0542	-0.0011	-0.0063	0.0278
			0.5967	0.5570	0.5621	0.5281
P	4					
U				1.0887	1.0876	1.0305
V				3.4368	3.4716	3.2624
E				0.8973	0.8962	0.8932
				0.0303	0.0272	0.0542
				0.5331	0.5412	0.5051
P	3					
U				1.0511	1.0533	1.0223
V				3.2744	3.3153	3.1560
E				0.8968	0.8945	0.8940
				0.0646	0.0615	0.0784
				0.5000	0.5126	0.4774
P	2					
U				1.0486	1.0421	1.0318
V				3.1397	3.1736	3.0644
E				0.8971	0.8959	0.8964
				0.0969	0.0927	0.1003
				0.4642	0.4752	0.4463
P	1					
U				1.0186	1.0288	1.0279
V				2.9858	3.0336	2.9608
E				0.8958	0.8960	0.8965
				0.1245	0.1187	0.1197
				0.4200	0.4343	0.4126

APPENDIX C

P_o and U_c CONTOUR PLOTS

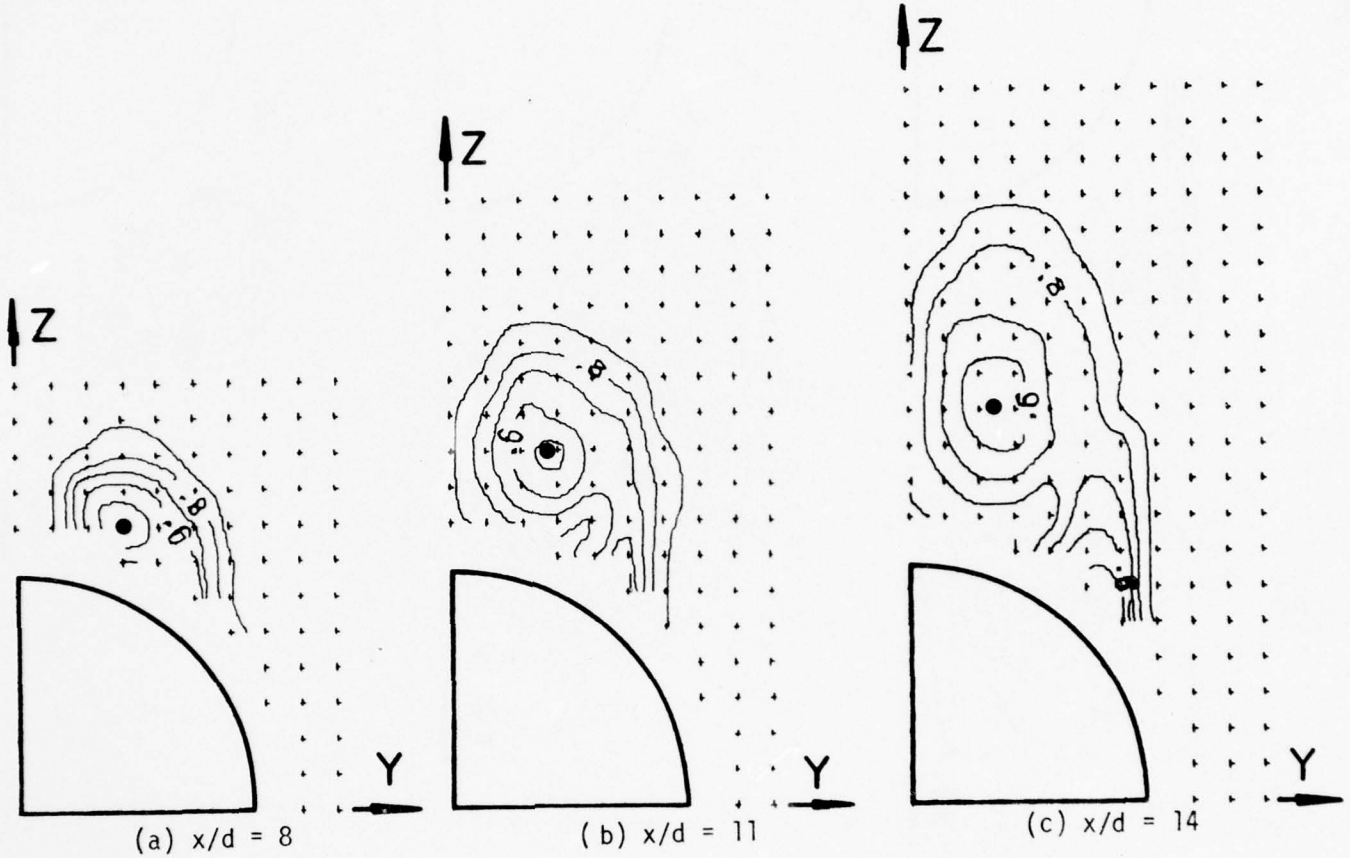
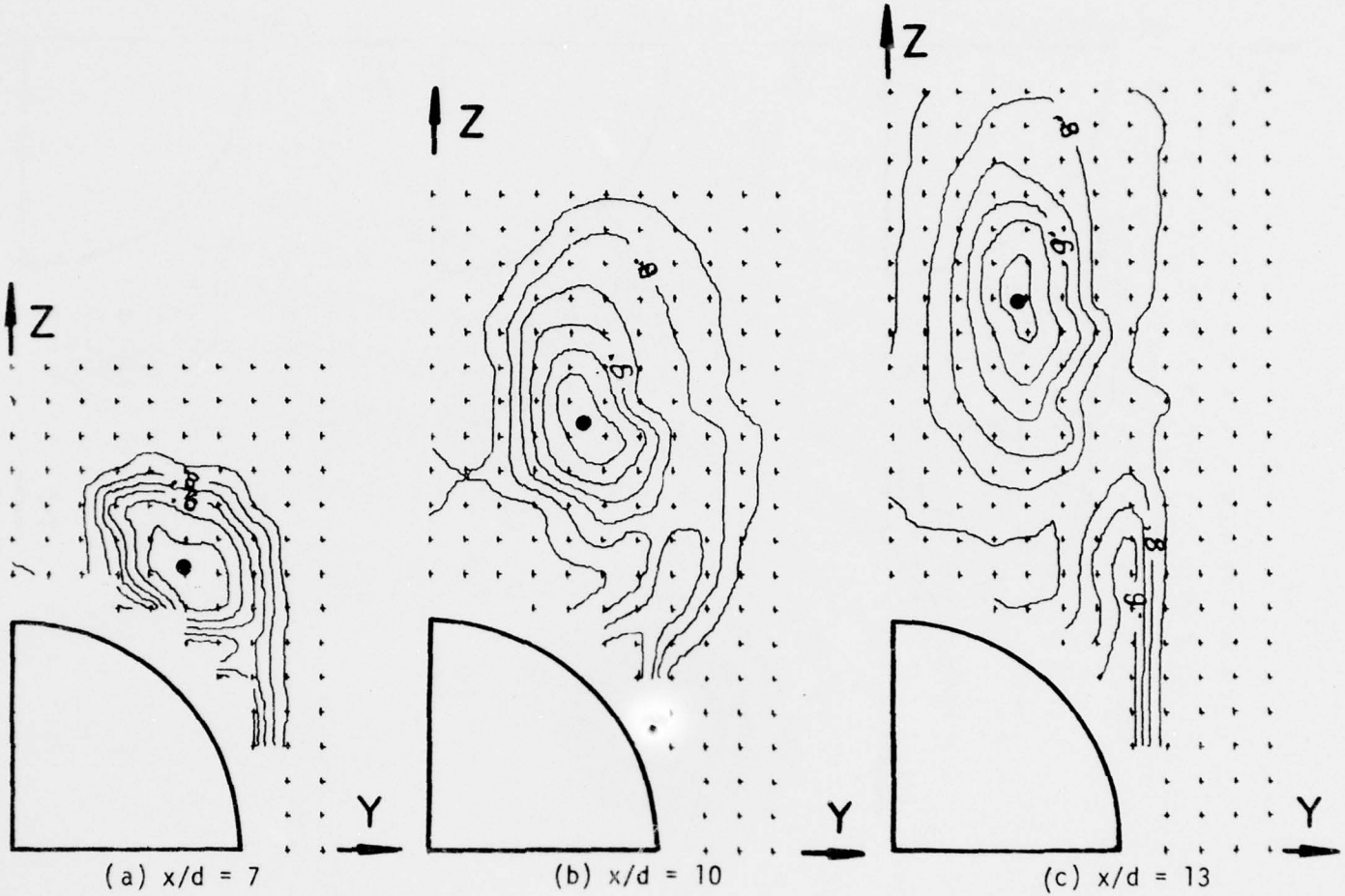
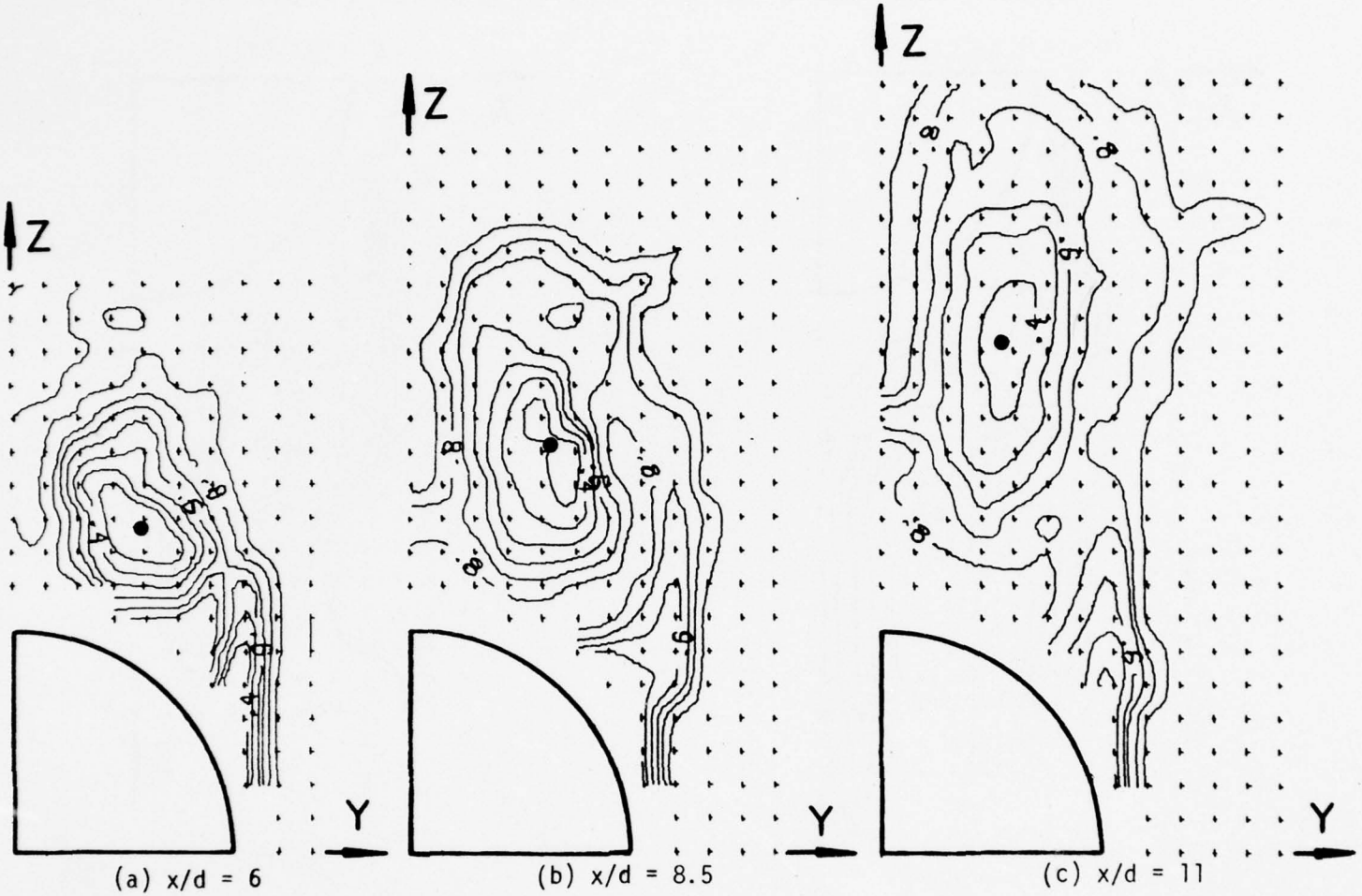


Figure C-1. Contours of Total Pressure in Cross-Flow Plane for $M_\infty = 1.95$, $R_d = .48 \times 10^6$ and $\alpha_b = 10°$.



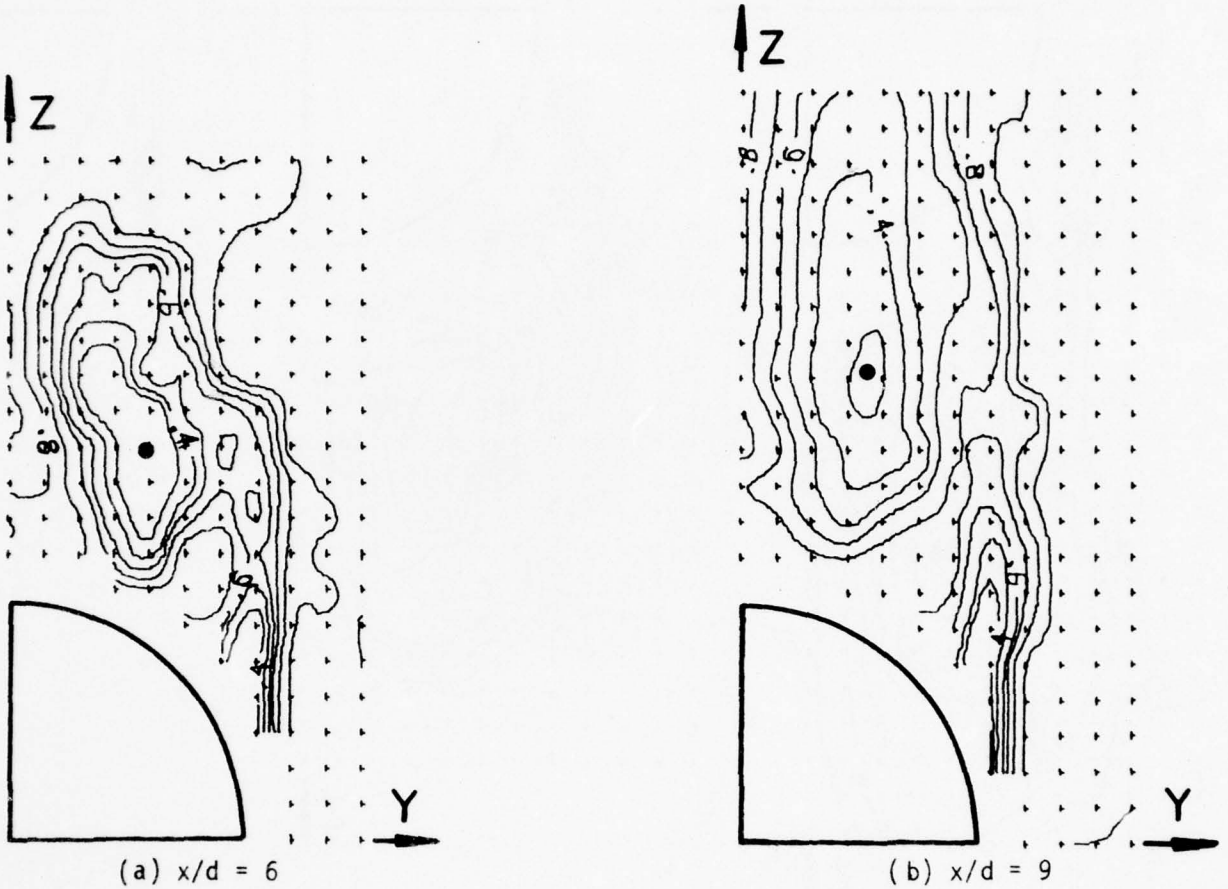
(a) x/d = 7 (b) x/d = 10 (c) x/d = 13

Figure C-2. Contours of Total Pressure in Cross-Flow Plane for $M_\infty = 1.95$, $R_d = .48 \times 10^6$ and $\alpha_b = 15°$.



(a) x/d = 6 (b) x/d = 8.5 (c) x/d = 11

Figure C-3. Contours of Total Pressure in Cross-Flow Plane for $M_\infty = 1.95$, $R_d = .48 \times 10^6$ and $\alpha_b = 20°$.



(a) x/d = 6 (b) x/d = 9

Figure C-4. Contours of Total Pressure in Cross-Flow Plane for $M_\infty = 1.95$, $R_d = .48 \times 10^6$ and $\alpha_b = 25°$.

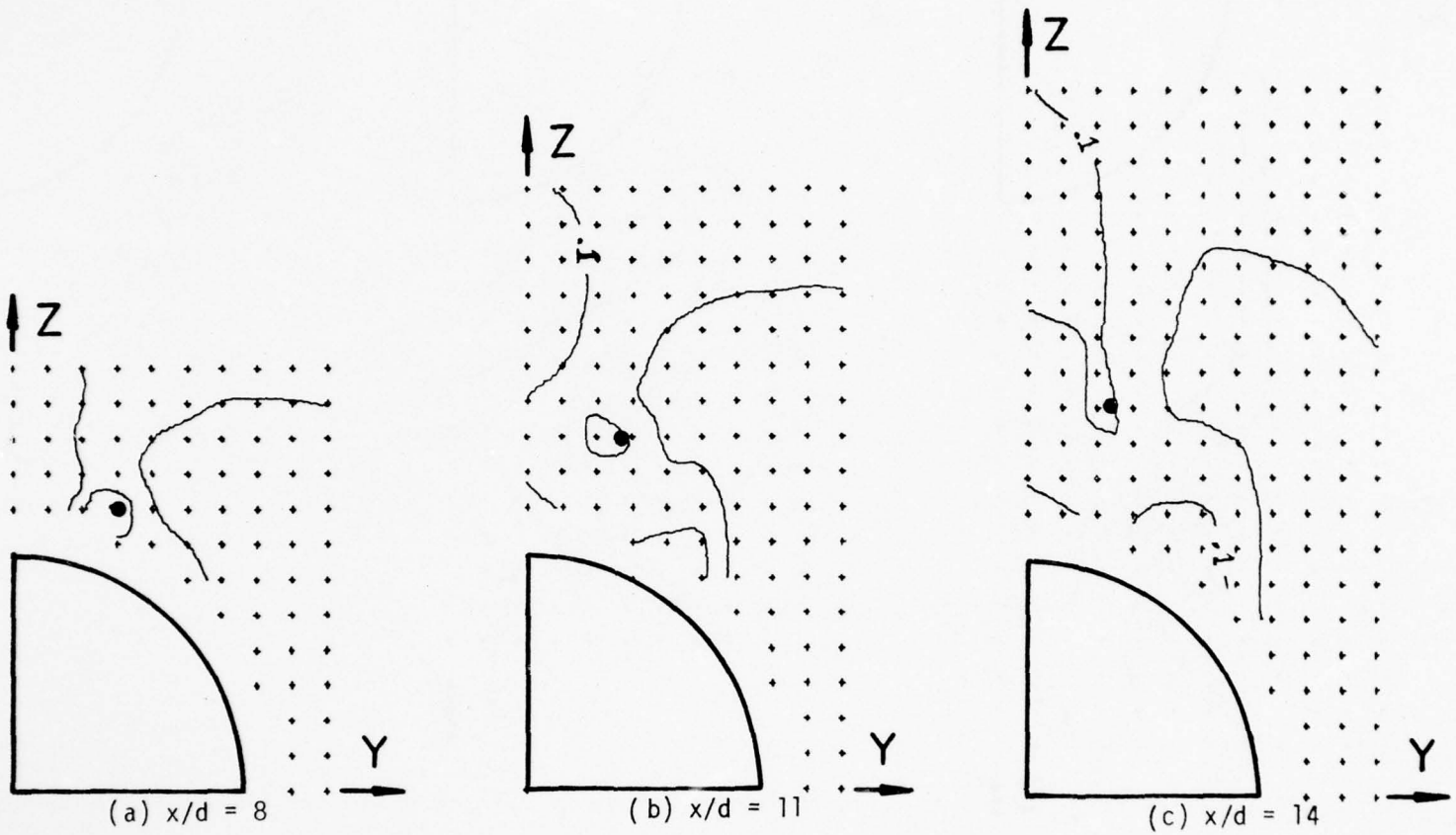


Figure C-5. Contours of Magnitude of Cross-Flow Velocity for $M_\infty = 1.95$, $R_d = .48 \times 10^6$ and $\alpha_b = 10°$.

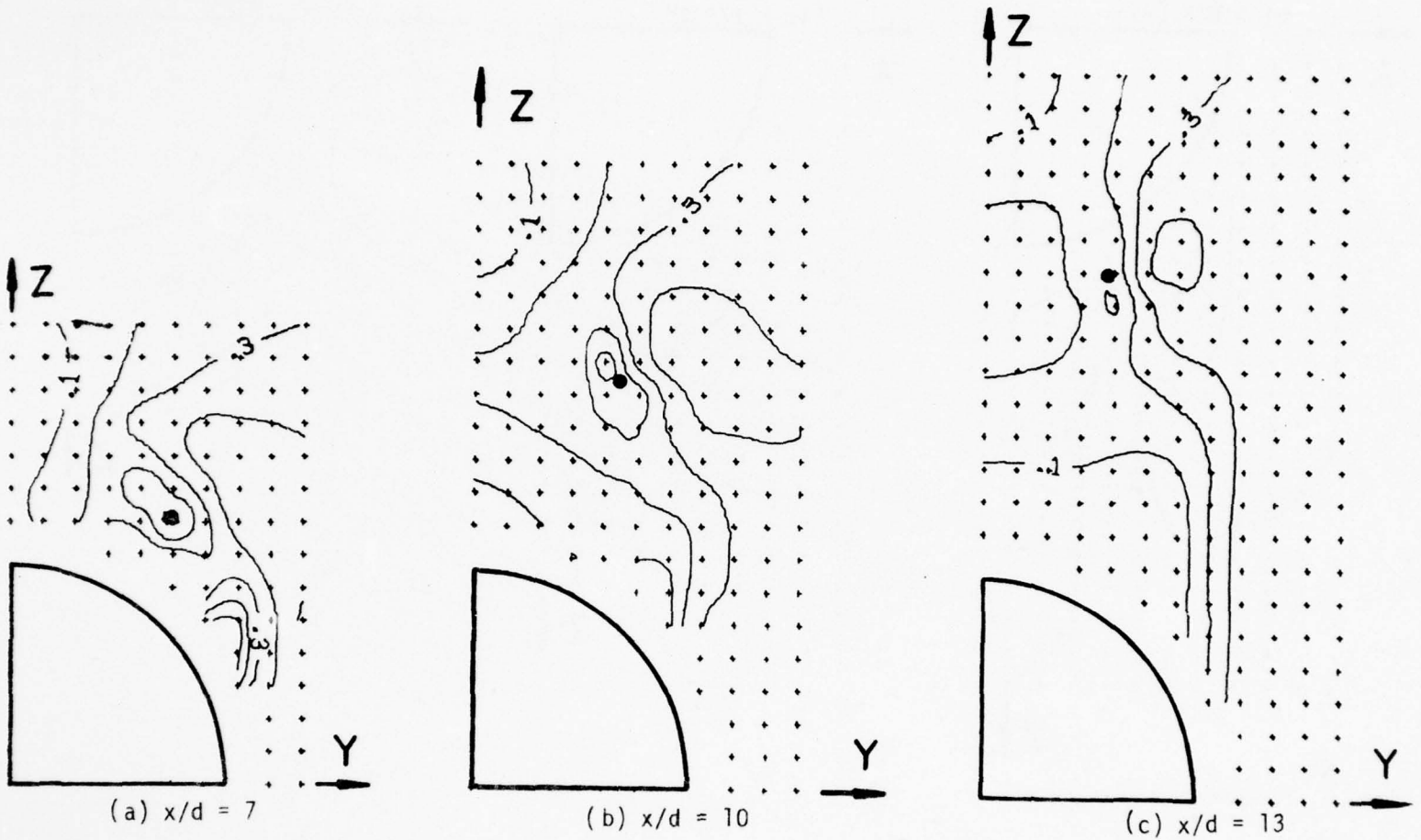


Figure C-6. Contours of Magnitude of Cross-Flow Velocity for $M_\infty = 1.95$, $R_d = .48 \times 10^6$ and $\alpha_b = 15°$.

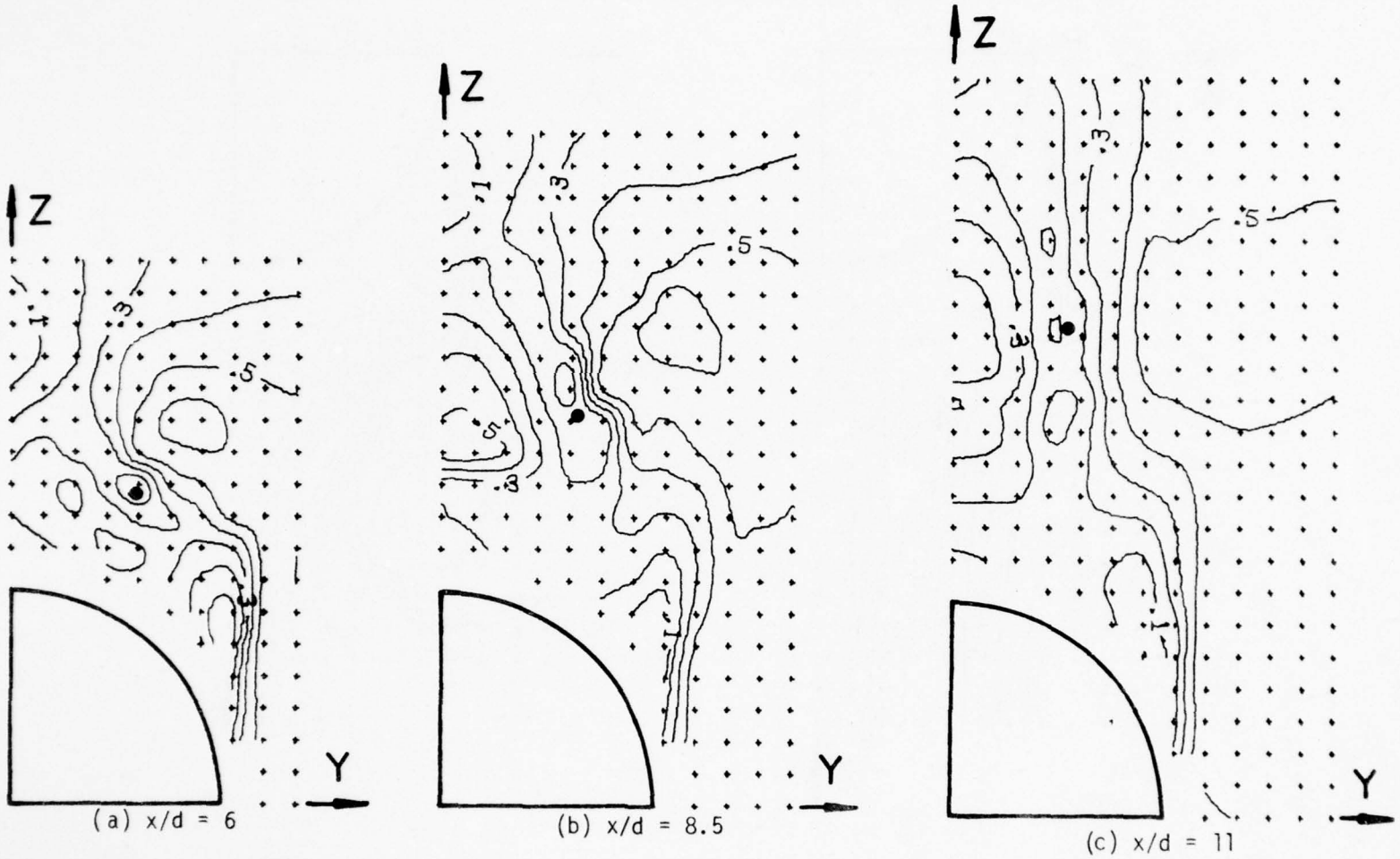
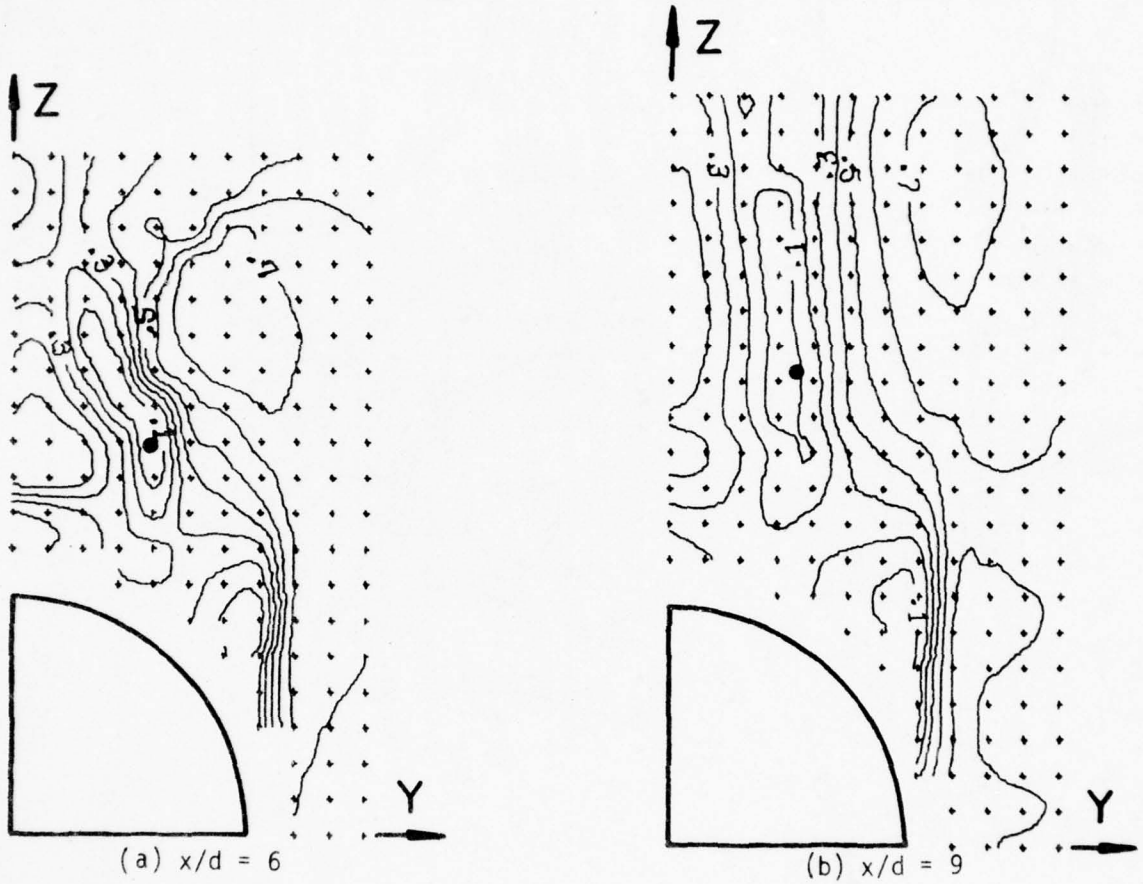


Figure C-7. Contours of Magnitude of Cross-Flow Velocity for $M_\infty = 1.95$, $R_d = .48 \times 10^6$ and $\alpha_b = 20°$.



(a) x/d = 6 (b) x/d = 9

Figure C-8. Contours of Magnitude of Cross-Flow Velocity for $M_\infty = 1.95$, $R_d = .48 \times 10^6$ and $\alpha_b = 25°$.

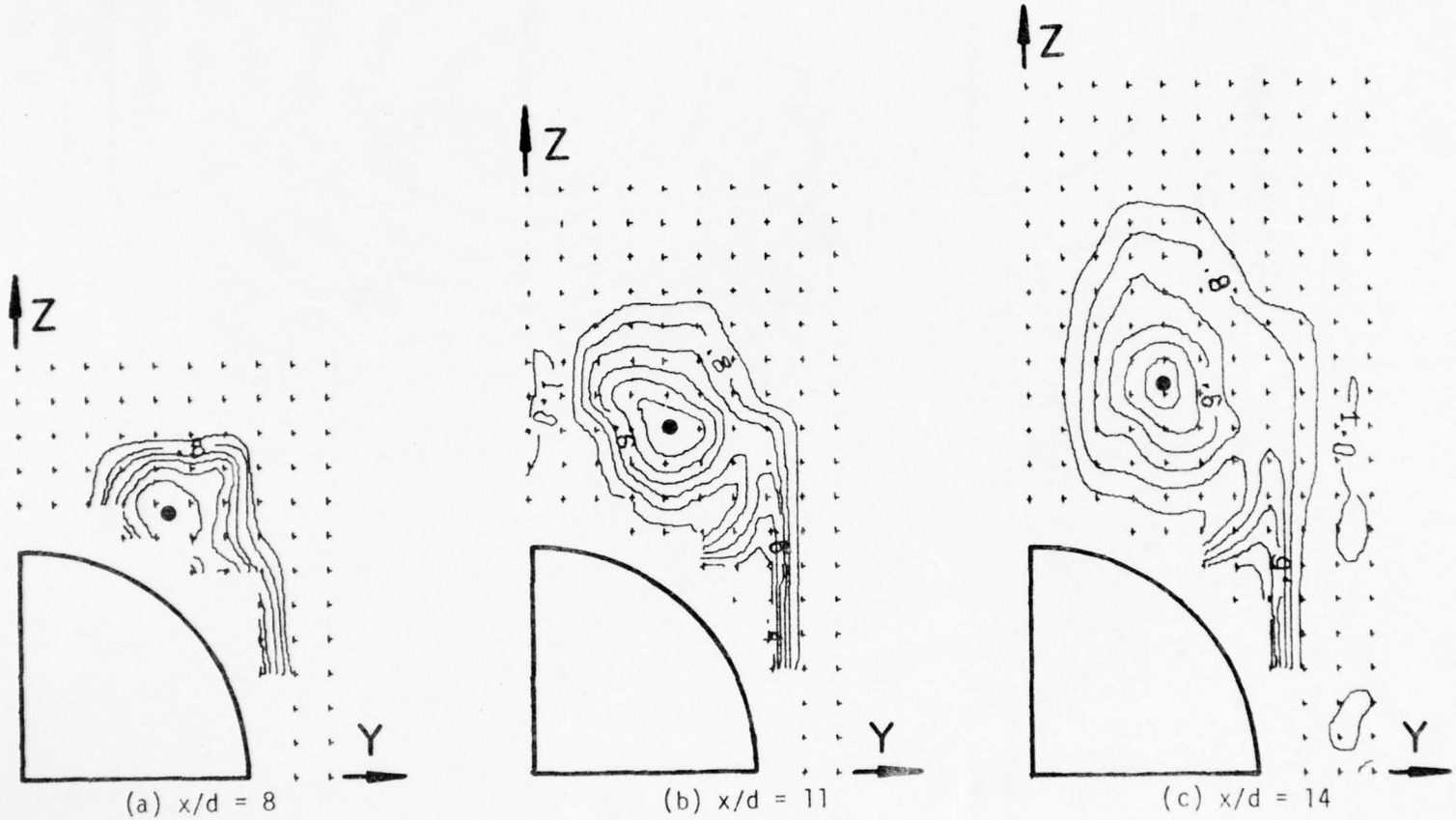


Figure C-9. Contours of Total Pressure in Cross-Flow Plane for $M_\infty = 2.$, $R_d = 1.75 \times 10^6$ and $\alpha_b = 10°$.

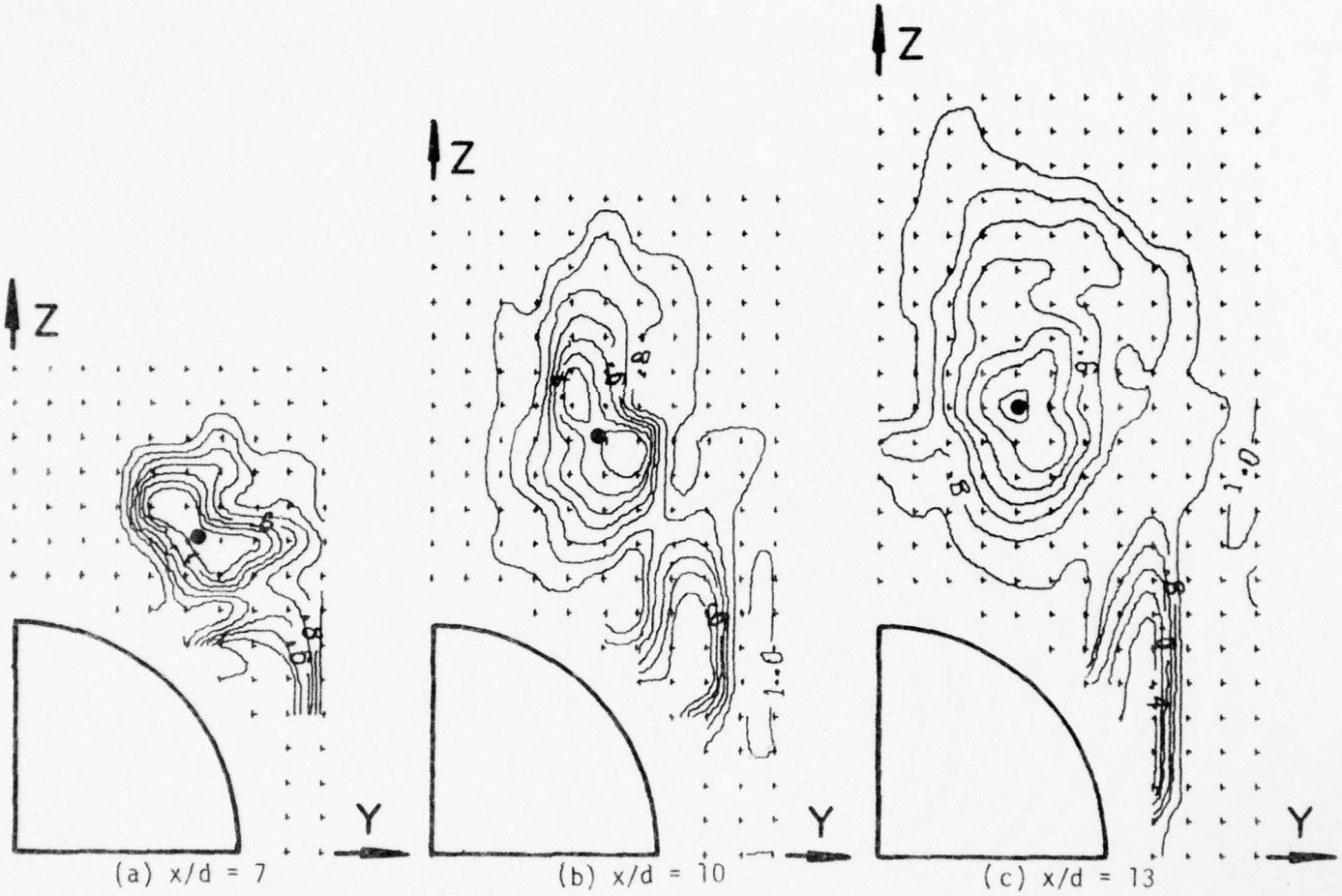
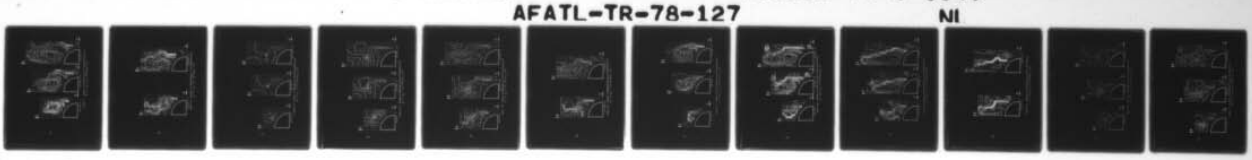


Figure C-10. Contours of Total Pressure in Cross-Flow Plane for $M_\infty = 2.$, $R_d = 1.75 \times 10^6$ and $\alpha_b = 15°$.

AD-A071 337 TEXAS UNIV AT AUSTIN DEPT OF MECHANICAL ENGINEERING F/G 16/2
SUPERSONIC FLOW MEASUREMENTS IN THE BODY VORTEX WAKE OF AN OGIV--ETC(U)
NOV 78 W L OBERKAMPF, T J BARTEL F08635-77-C-0049

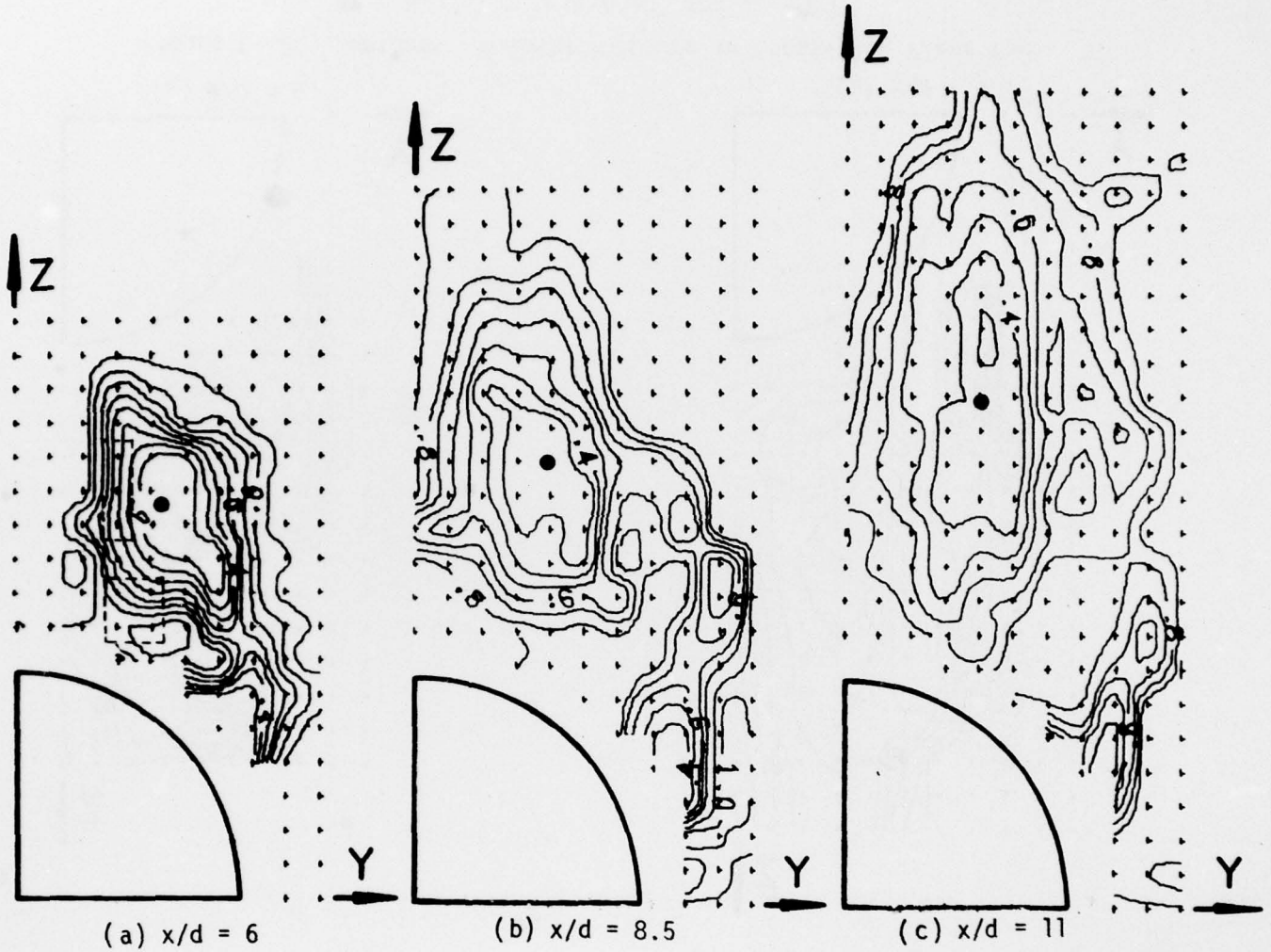
UNCLASSIFIED AFATL-TR-78-127 NL

4 OF 4
AD A071337



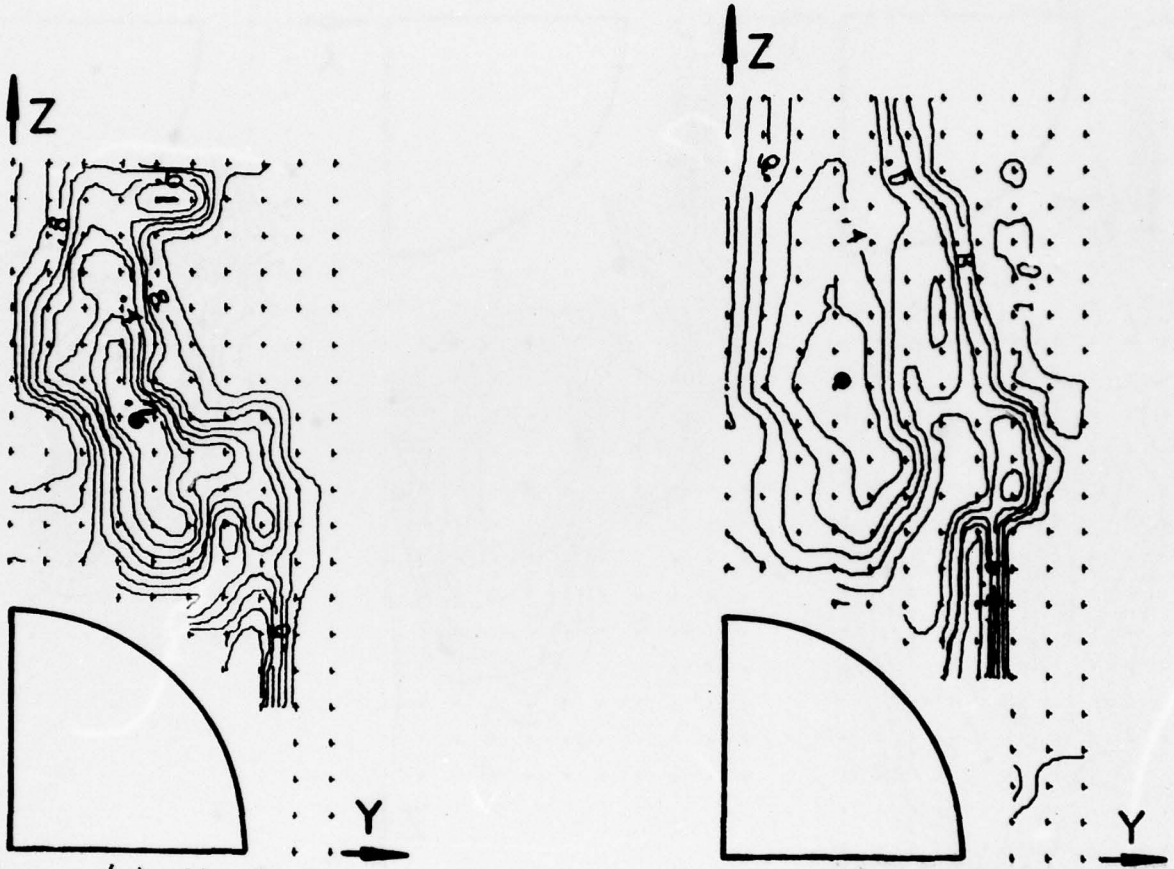


END
DATE FILMED
8 -79
DDC



(a) x/d = 6 (b) x/d = 8.5 (c) x/d = 11

Figure C-11. Contours of Total Pressure in Cross-Flow Plane for $M_\infty = 2.$, $R_d = 1.75 \times 10^6$ and $\alpha_b = 20°$.



(a) x/d = 6 (b) x/d = 9

Figure C-12. Contours of Total Pressure in Cross-Flow Plane for $M_\infty = 2.$, $R_d = 1.75 \times 10^6$ and $\alpha_b = 25°$.

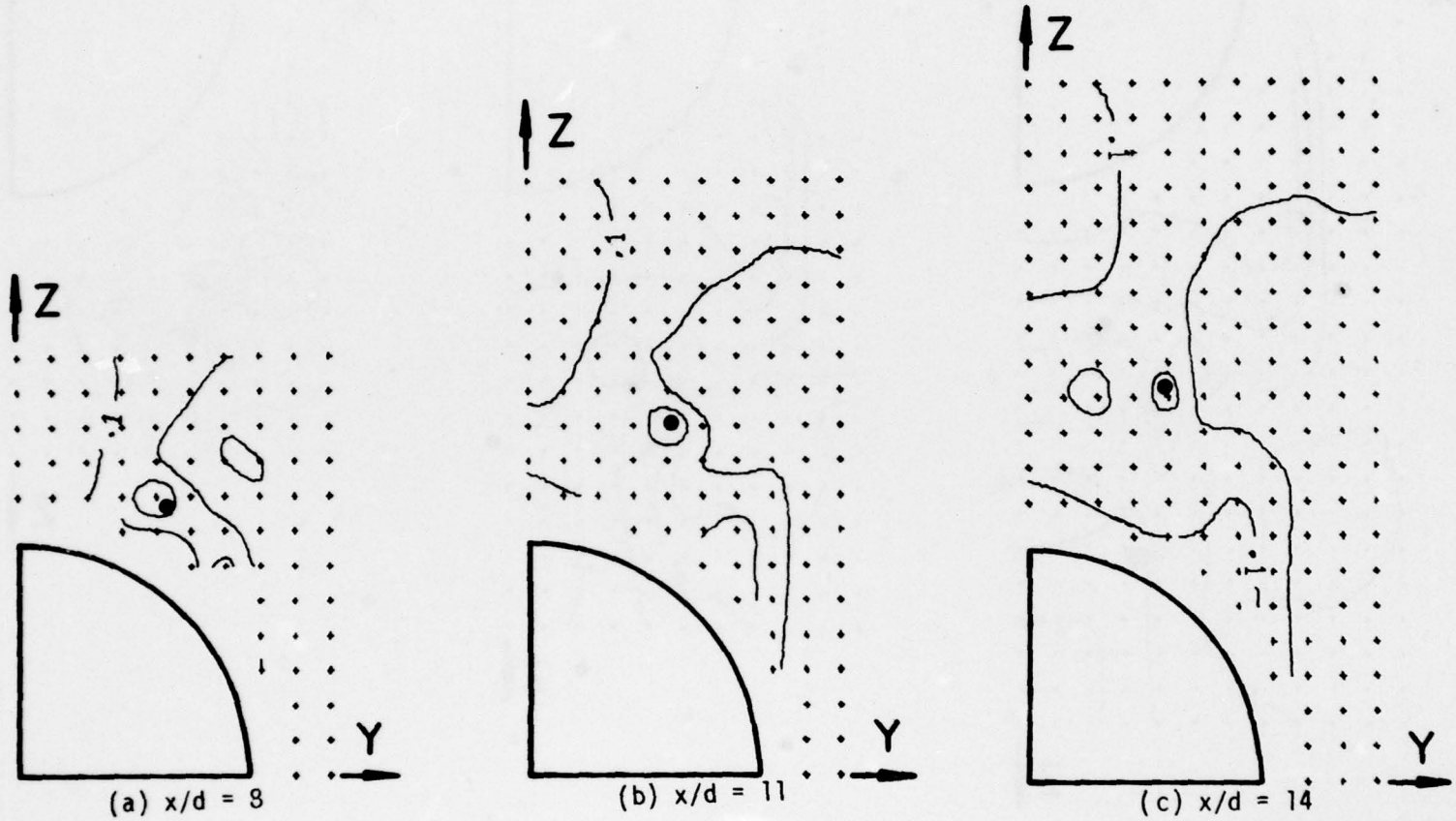


Figure C-13. Contours of Magnitude of Cross-Flow Velocity for $M_\infty = 2.$, $R_d = 1.75 \times 10^6$ and $\alpha_b = 10°$.

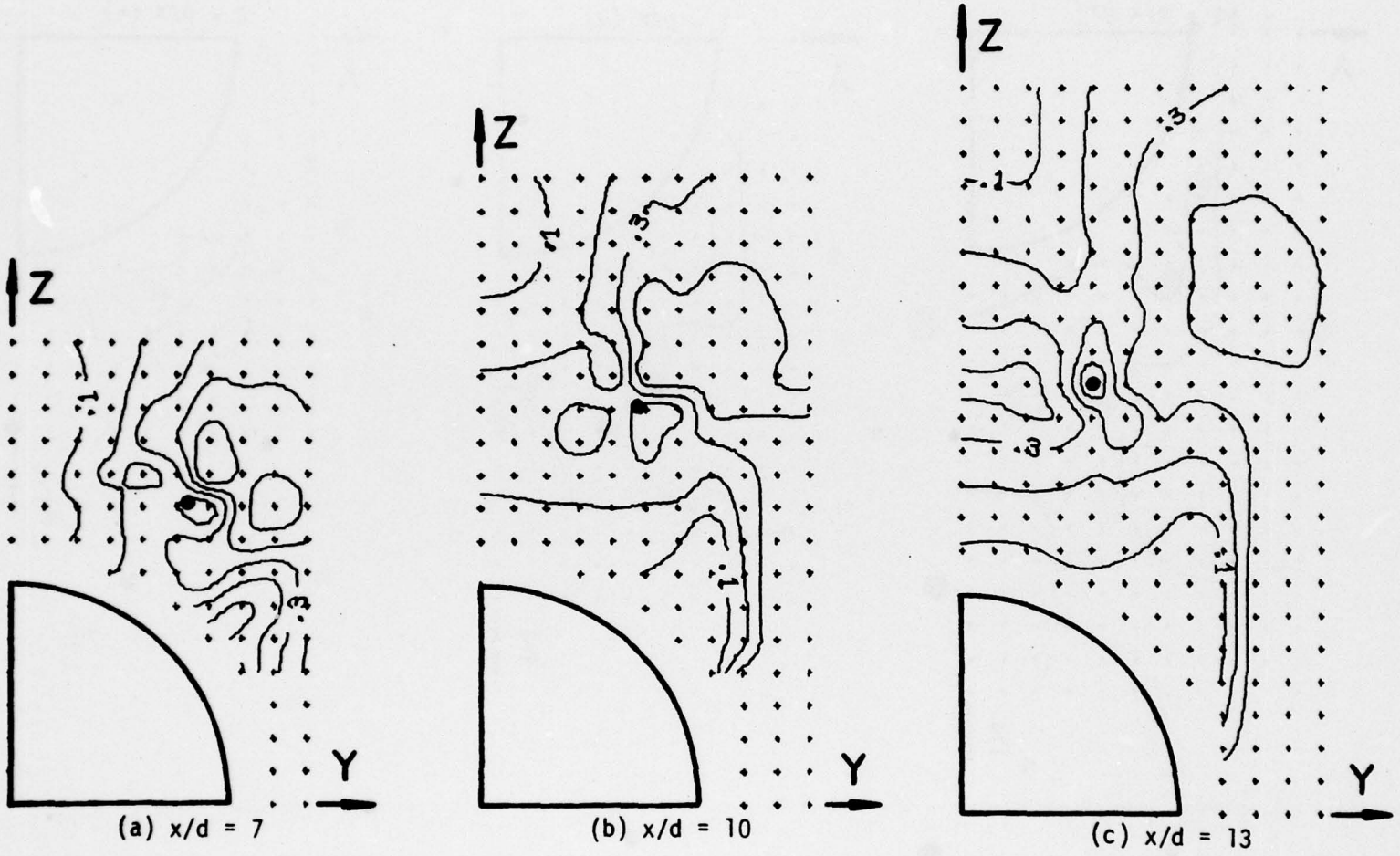
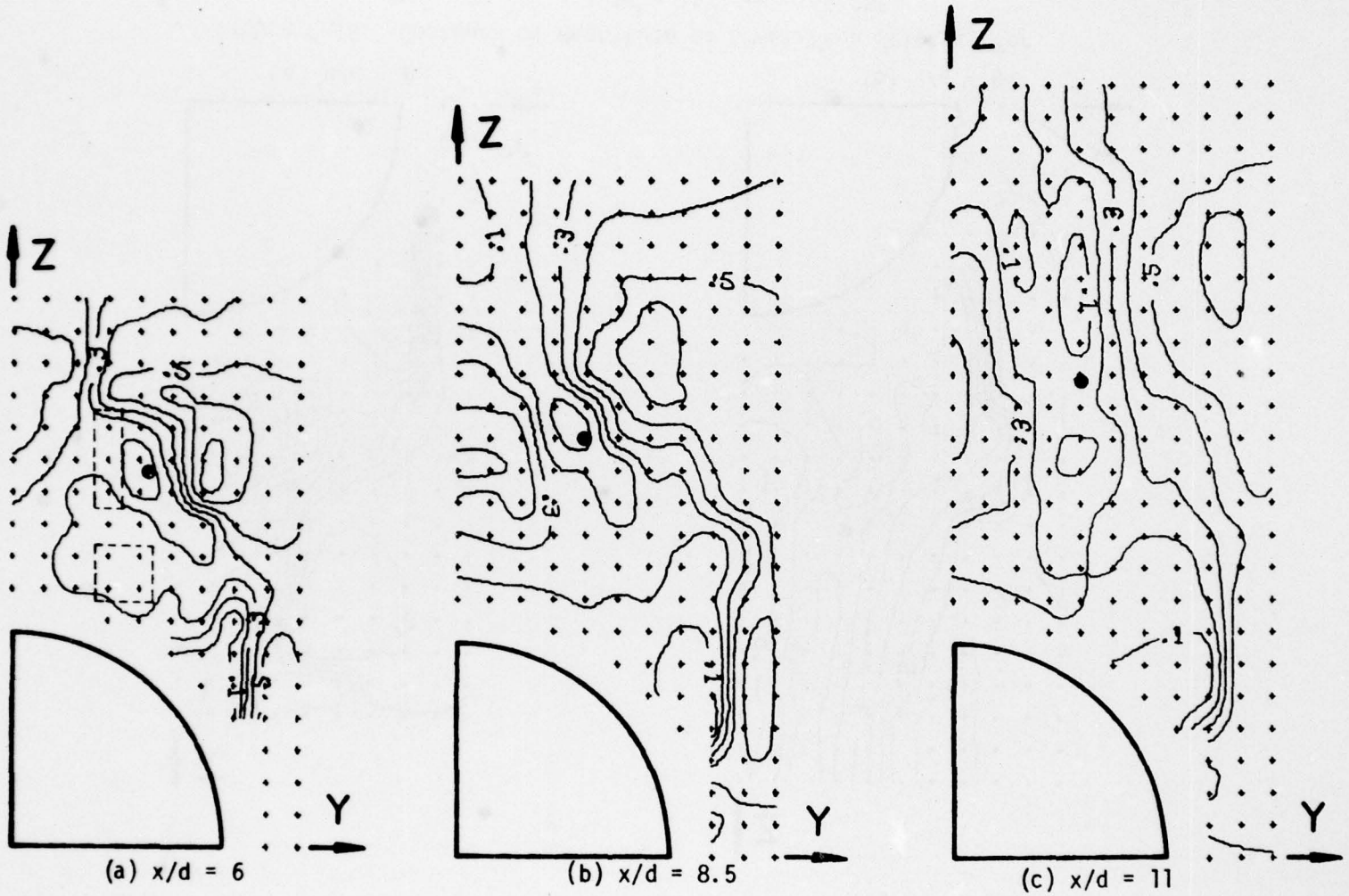
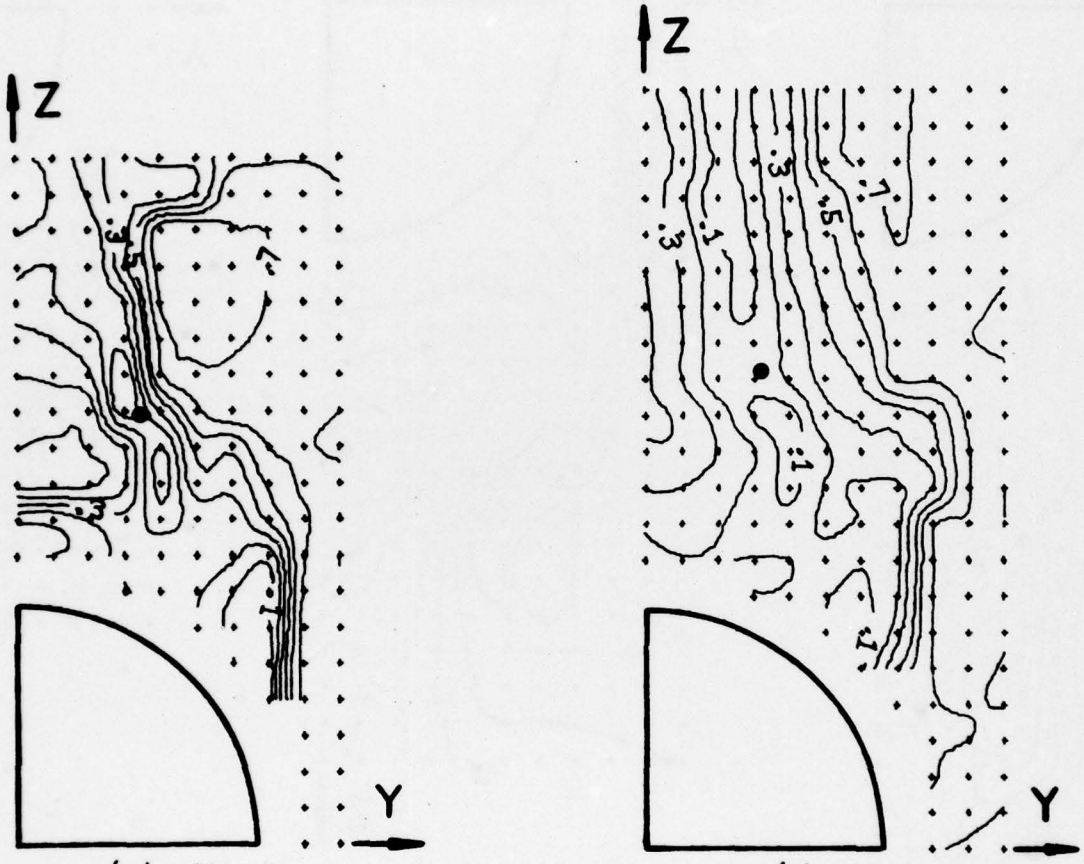


Figure C-14. Contours of Magnitude of Cross-Flow Velocity for $M_\infty = 2.$, $R_d = 1.75 \times 10^6$ and $\alpha_b = 15°$.



(a) x/d = 6 (b) x/d = 8.5 (c) x/d = 11

Figure C-15. Contours of Magnitude of Cross-Flow Velocity for $M_\infty = 2.$, $R_d = 1.75 \times 10^6$ and $\alpha_b = 20°$.



(a) x/d = 6 (b) x/d = 9

Figure C-16. Contours of Magnitude of Cross-Flow Velocity for $M_\infty = 2.$, $R_d = 1.75 \times 10^6$ and $\alpha_b = 25°$.

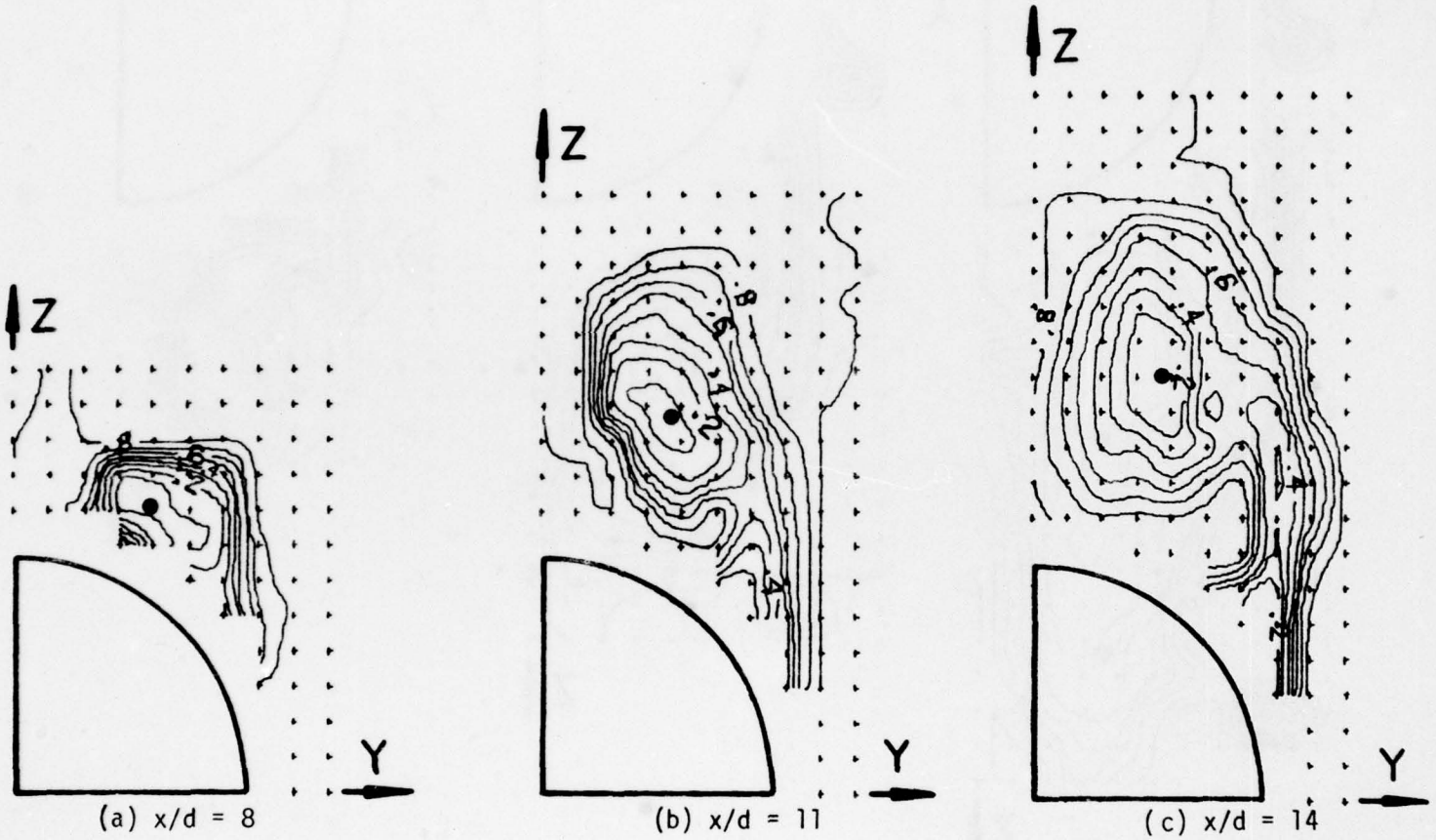
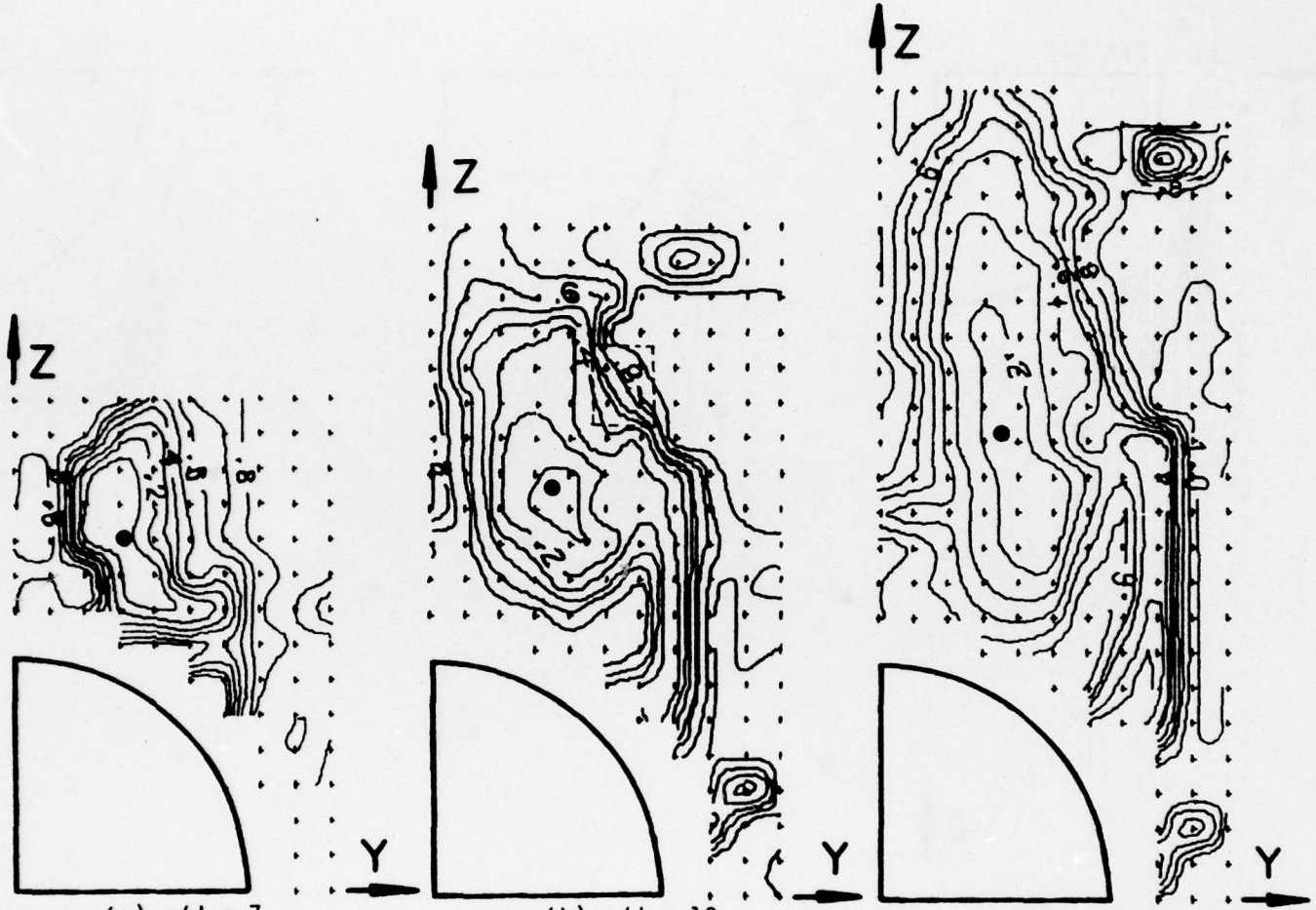


Figure C-17. Contours of Total Pressure in Cross-Flow Plane for $M_\infty = 3.01$, $R_d = 1.70 \times 10^6$ and $_b = 10°$.



(a) x/d = 7 (b) x/d = 10 (c) x/d = 13

Figure C-18. Contours of Total Pressure in Cross-Flow Plane for $M_\infty = 3.01$, $R_d = 1.70 \times 10^6$ and $\alpha_b = 15°$.

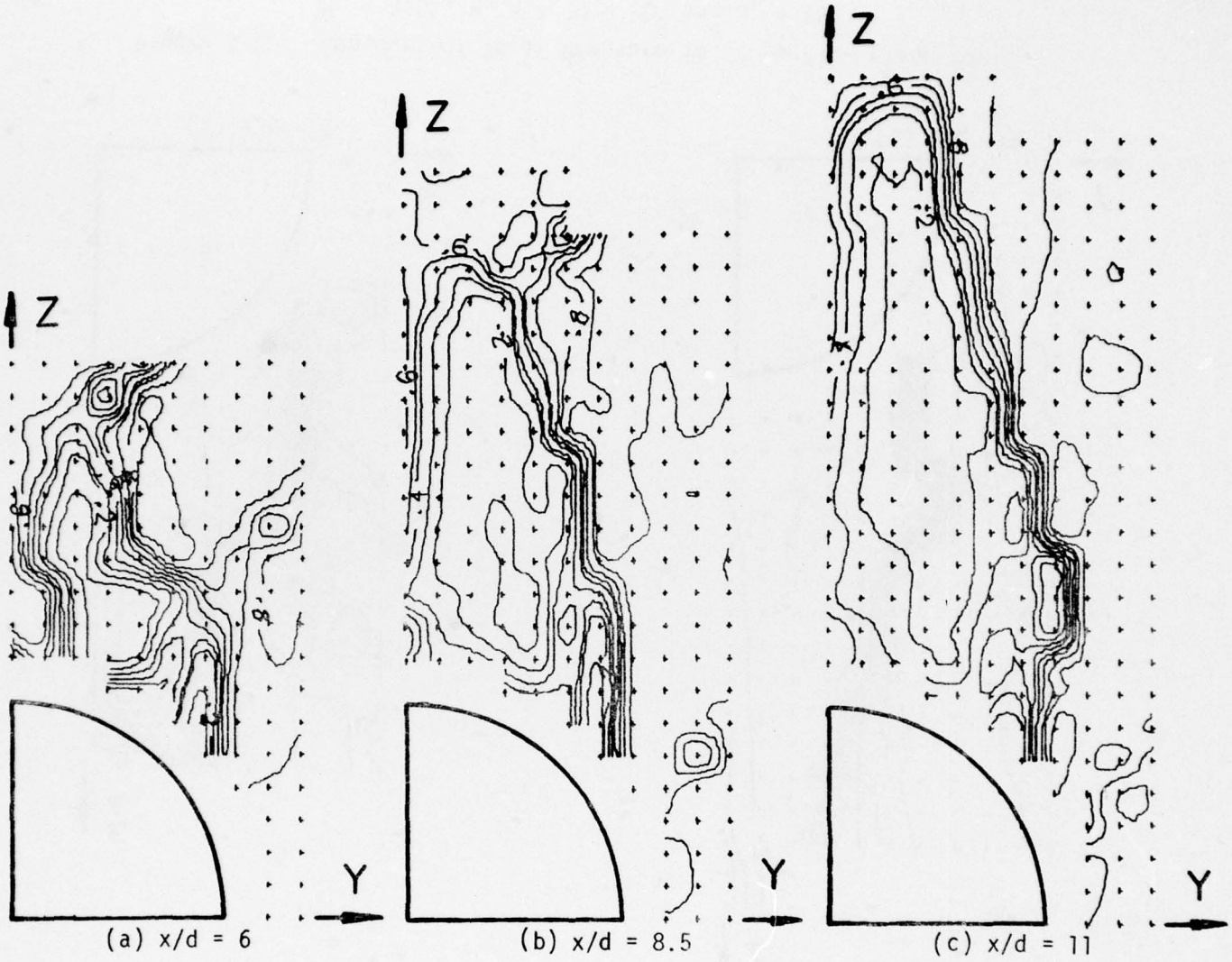


Figure C-19. Contours of Total Pressure in Cross-Flow Plane for $M_\infty = 3.01$, $R_d = 1.70 \times 10^6$ and $\alpha_b = 20°$.

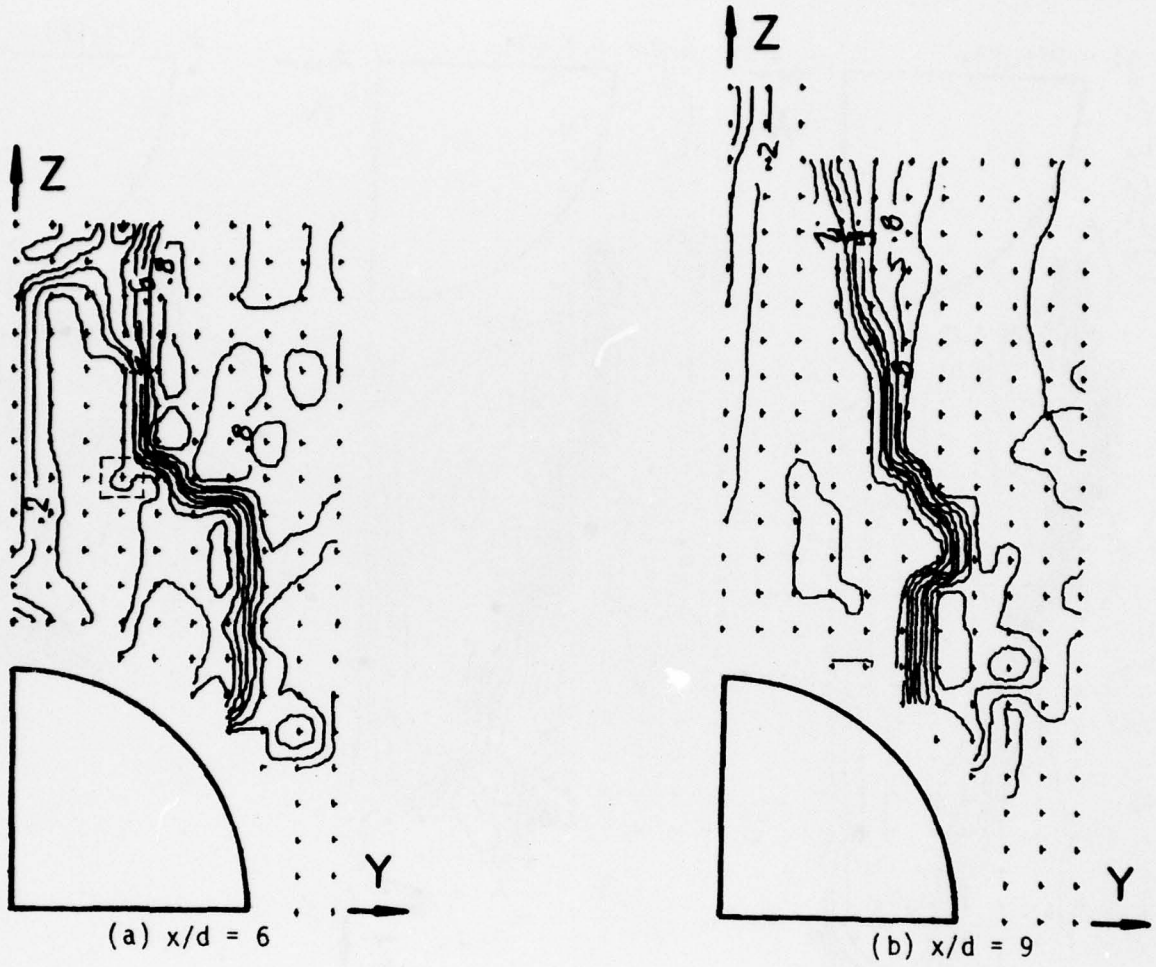


Figure C-20. Contours of Total Pressure in Cross-Flow Plane for $M_\infty = 3.01$, $R_d = 1.70 \times 10^6$ and $\alpha_b = 25°$

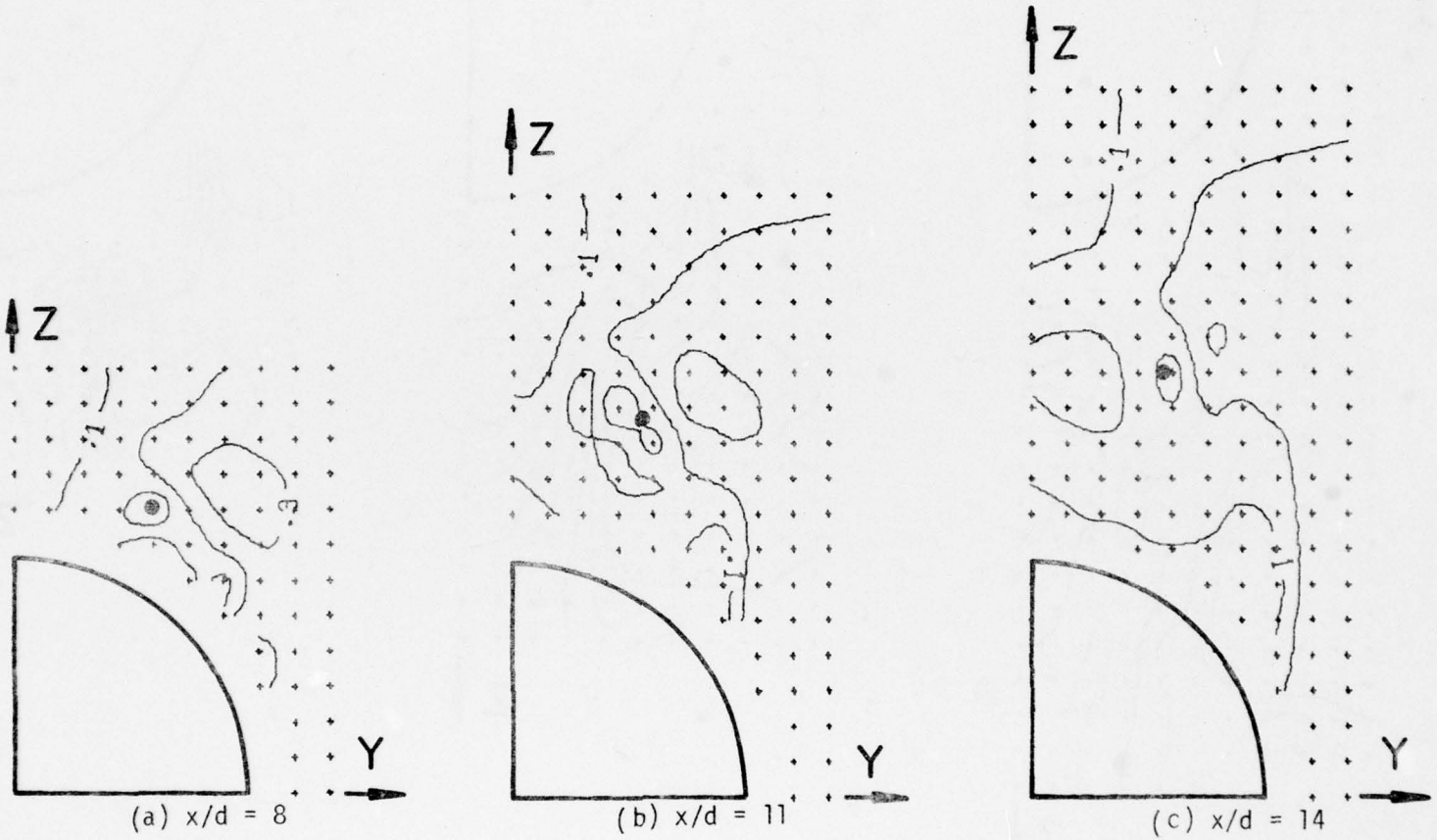


Figure C-21. Contours of Magnitude of Cross-Flow Velocity for $M_\infty = 3.01$, $R_d = 1.70 \times 10^6$ and $\alpha_b = 10°$.

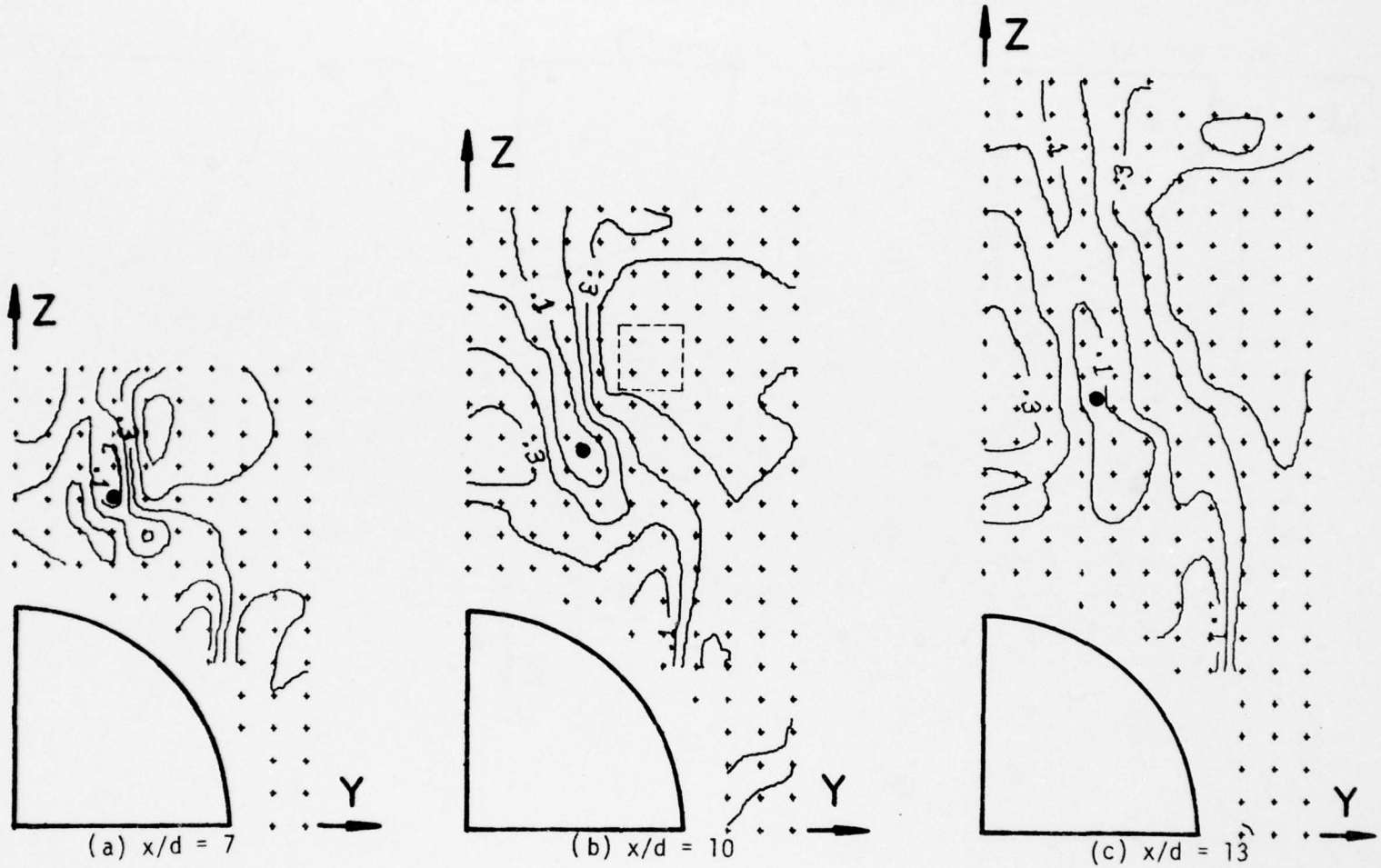
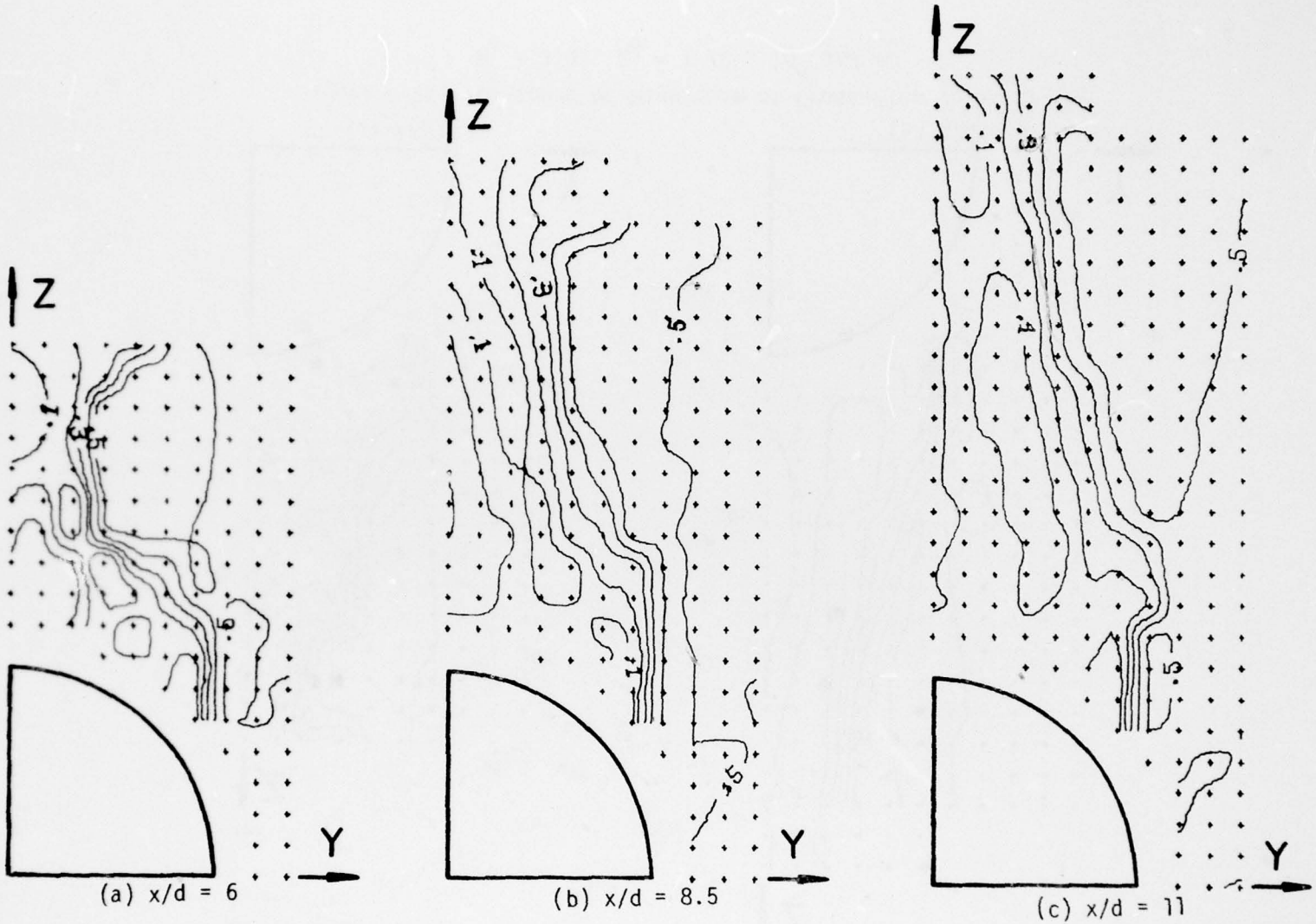


Figure C-22. Contours of Magnitude of Cross-Flow Velocity for $M_\infty = 3.01$, $R_d = 1.70 \times 10^6$ and $\alpha_b = 15°$.



(a) x/d = 6 (b) x/d = 8.5 (c) x/d = 11

Figure C-23. Contours of Magnitude of Cross-Flow Velocity for $M_\infty = 3.01$, $R_d = 1.70 \times 10^6$ and $\alpha_b = 20°$.

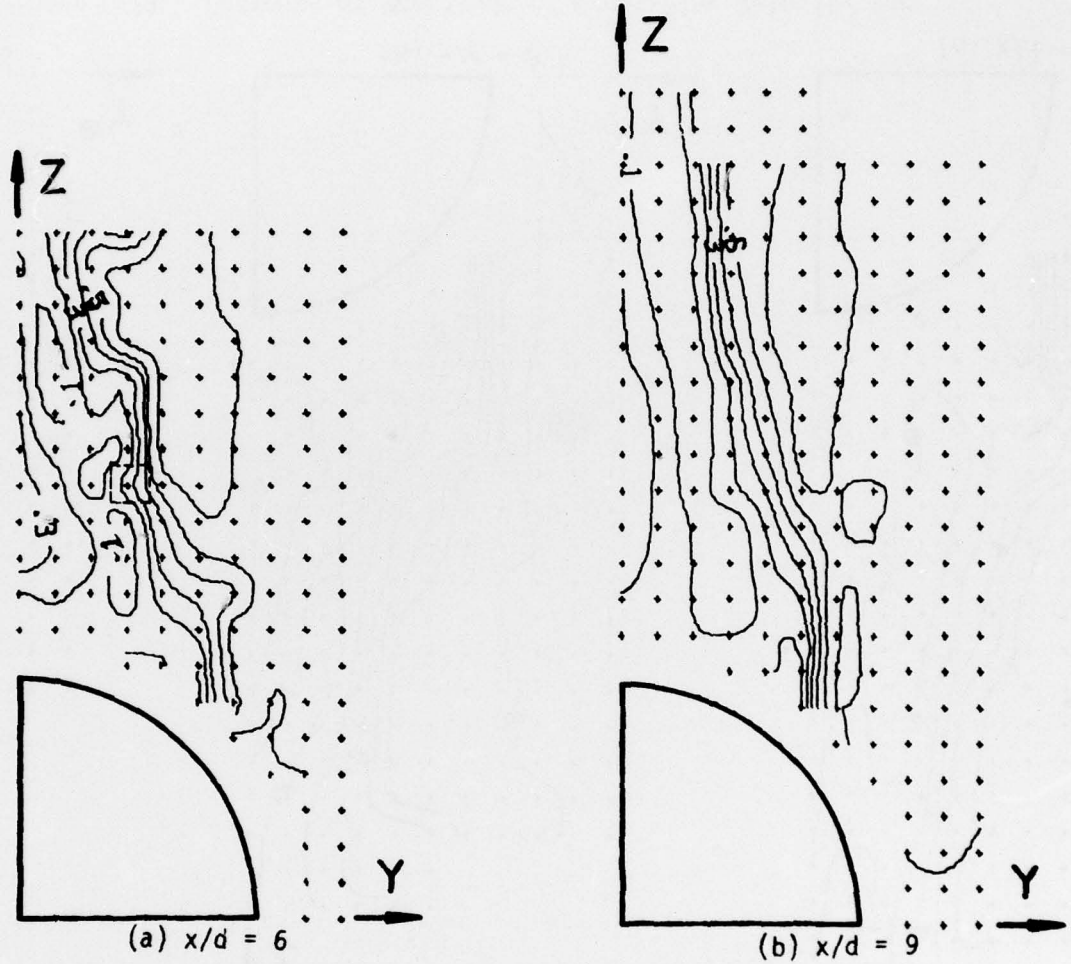


Figure C-24. Contours of Magnitude of Cross-Flow Velocity for $M_\infty = 3.01$, $R_d = 1.70 \times 10^6$ and $\alpha_b = 25°$.